Arthritis & Rheumatology

An Official Journal of the American College of Rheumatology
www.arthritisrheum.org and wileyonlinelibrary.com

Cover design: Todd Machen

This journal is printed on acid-free paper.

Arthritis & Rheumatology

An Official Journal of the American College of Rheumatology
www.arthritisrheum.org and wileyonlinelibrary.com

VOLUME 78 • May 2026 • NO. 5

Cover image: The cover image (from Jin et al; pages 1062–1075) features a multiplex immunohistochemical staining of synovial tissue from a patient with rheumatoid arthritis presenting inflammatory hyperplastic synovium. Markers include FAPα (green), PDPN (pink), NRP2 (red), THY1 (yellow), and DAPI (blue). Notably, distinct colocalization of NRP2 with THY1 (appearing as orange regions) is observed in this inflammatory tissue, indicating that NRP2 expression primarily localizes to THY1-positive areas within the sublining layer under inflammatory conditions.

In this Issue

Highlights from this issue of *A&R* | By Lara C. Pullen, PhD

TAOK3 as a Biomarker for Bone Destruction and Potential Therapeutic Target in RA

Despite significant advances in the treatment of rheumatoid arthritis (RA), bone destruction in active RA remains a major clinical challenge. Advances in plasma proteomics offer new insights into the molecular mechanisms underlying different RA stages and may help identify novel therapeutic targets. **In this issue, Xin et al. (p. 1045)** report that TAOK3, a serine/threonine kinase in the TAO kinase family, is found in the lining and sublining layers of RA synovium and is a potential biomarker for bone destruction in active RA. It modulates key signaling pathways, including MAPK, JNK/SAPK, and Hippo, and thus could serve as a therapeutic target for precision monitoring and intervention.

p. 1045

Using mass spectrometry for proteomic analysis on plasma samples from 160 patients with active or remitted RA and 40 healthy controls, the investigators identified 506 plasma proteins with significantly different expression between active RA and remission. Proteins significantly elevated in patients with active RA included TAOK3, CRP, SAA1, and SAA2. TAOK3 levels were positively associated with Sharp scores, and high TAOK3 expression was associated with increased relapse frequency relative to low TAOK3 expression. In addition, combining analysis of TAOK3 and CRP improved diagnostic accuracy for RA compared with CRP alone.

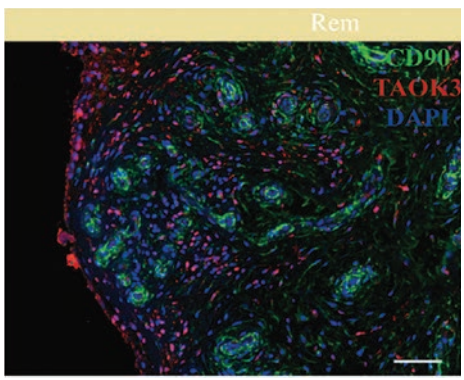

Figure 4C. Multiplex immunohistochemistry shows that CD90+TAOK3+ FLSs are distributed in both the lining and sublining areas of the synovial tissue.

Treatment of fibroblast-like synoviocytes (FLSs) with lipopolysaccharide or tumor necrosis factor markedly increased intracellular TAOK3 protein levels, whereas no significant changes were detected when the cells were stimulated with culture supernatants. Functional studies also revealed that TAOK3 knockdown suppressed the tumor-like phenotype of FLSs and downregulated matrix metalloproteinases 1/2/3 and cathepsin K, whereas TAOK3 overexpression promoted pannus cell–mediated bone erosion, a phenotype mitigated by a TAOK3-targeted inhibitor. Moreover, inhibition of TAOK3 had therapeutic effects in a collagen-induced arthritis mouse model. Taken together, the results demonstrate that TAOK3 plays a critical role in promoting the pathogenic phenotype and bone-invasive behavior of synovial cells and may be a useful therapeutic target.

Dose-Related Benefits and Risks of Hydroxychloroquine in SLE

As ophthalmic examination methods have advanced, an increased detection rate of hydroxychloroquine (HCQ) retinopathy has attracted considerable attention. HCQ use, longer duration of use, and cumulative dose all increase the risk of retinal toxicity; however, a focus on reducing HCQ exposure in patients with systemic lupus erythematosus (SLE) may affect disease management.

p. 1114

In this issue, Li et al. (p. 1114) report that they found no dose-related difference in the risk of HCQ retinopathy among patients with SLE aged younger than 45 years. Moreover, in patients with SLE, higher-dose HCQ (≥400 mg/day) improves effectiveness while reducing the risk of coronary artery disease (CAD) and venous thromboembolism (VTE) compared with lower-dose HCQ (<400 mg/day), indicating that different HCQ doses have distinct therapeutic effects.

Using Taiwan's Nationwide Health Insurance Research Database, the researchers were able to evaluate a large number of people for the relatively rare outcome of HCQ retinopathy. The database included 878 (3.8%) patients on higher-dose HCQ and 22,405 (96.2%) on lower-dose HCQ. When the investigators performed inverse probability weighting, they found that higher-dose HCQ was associated with an approximately 15% reduction in the risk of CAD and a 60% reduction in the risk of VTE. They identified no dose-related differences in the risk of ischemic stroke, end-stage renal disease, or malignancy over a mean follow-up of six years. There was an increased risk of HCQ retinopathy among SLE patients aged ≥45 years receiving higher-dose HCQ (HR 1.87, 95% CI 1.45-2.42). Despite earlier suggestions that antimalarials may have antineoplastic properties, the current study did not show evidence of this. The authors conclude that their findings underscore the need to weigh the benefits and risks of optimal HCQ dosing in managing SLE.

Transcriptomic Stratification of Antiphospholipid Syndrome

Previous use of whole-blood RNA sequencing to analyze transcriptomic profiles of patients with antiphospholipid syndrome (APS) have identified marked changes in gene expression compared with healthy controls, particularly in interferon-regulated genes. p. 1124 **In this issue, Ambati et al. (p. 1124)** describe four endotypes of patients with APS or persistent positive antiphospholipid antibody (aPL). Their pathway-informed stratification of patients into biologically distinct clusters, each with diverse immune activation patterns and clinical features, represents a step toward personalized medicine for APS.

The investigators performed whole-blood RNA sequencing on 174 aPL-positive patients, including those with primary APS (n=102), secondary APS (n=29), and aPL-positivity without classifiable APS (n=43). By integrating the sequencing data with unsupervised machine learning and immune cell deconvolution, they were able to achieve a level of stratification that would not have been possible through clinical or serological data alone. Patients in Cluster 1 had upregulated ribosomal and metabolic pathways and downregulated mTOR, NETosis, and Hippo/IL-6 signaling. Patients in Cluster 2 demonstrated modest enrichment in mRNA processing and amino acid metabolism, whereas those in Cluster 3 showed biosynthetic suppression with mild Hippo/IL-6 activation. Cluster 4 exhibited the opposite pattern of Cluster 1, with strong upregulation of mTOR, NETosis, and Hippo/IL-6 signaling. Patients in Cluster 4 also had distinct clinical features compared with the other clusters, including higher anticardiolipin and anti–β_2-glycoprotein I positivity, elevated neutrophil counts, and increased urine protein-to-creatinine ratios.

The results reinforce the role of neutrophil-driven inflammation in a subset of APS patients and further implicate NETs in disease pathogenesis. In their discussion, the authors suggest that the upregulation of Hippo/IL-6 signaling seen in Cluster 4 also expands the understanding of pathophysiology beyond NETosis to a potential role of APS-associated immune remodeling, particularly in the context of myeloid cell activation and inflammation. The results also highlight the relationship between immune cell composition and the molecular heterogeneity of APS and suggest that nonthrombotic APS manifestations are associated with distinct gene expression profiles.

Journal Club

A monthly feature designed to facilitate discussion on research methods in rheumatology.

Decision Tree Analysis as a Preliminary Evidence-Based Tool for Identifying SURF in Children

Papa et al. *Arthritis Rheumatol.* 2026;78:1166–1175.

Syndrome of undifferentiated recurrent fever (SURF) represents a growing clinical challenge in pediatric autoinflammatory disease. Patients with recurrent fever are frequently encountered in practice but the conditions causing it remain poorly classified, limiting comparability across studies and the development of targeted therapies. Establishing evidence-based classification criteria is therefore essential to improve cohort homogeneity for clinical and translational research. In this study, we investigated SURF in children, defined as a heterogeneous group of patients with periodic inflammatory flares who do not meet criteria for hereditary recurrent fevers (HRF) or periodic fever, aphthosis, pharyngitis, and adenitis (PFAPA) syndrome and lack a definitive genetic diagnosis.

We analyzed 112 pediatric SURF patients followed at a single tertiary referral center and compared them with well-characterized disease controls (HRF and PFAPA) from the Eurofever registry. Using a decision tree approach, we developed classification models integrating clinical features with and without genetic test results, then compared their performance with logistic regression models. Decision trees were chosen because they are data-driven, transparent, and easily interpretable, making them particularly suitable for clinical application. Models incorporating genetic data showed the highest accuracy, but clinically based decision trees still achieved good discriminative performance and high specificity. External validation in an independent, multicenter cohort confirmed the robustness of the decision tree approach. Overall, our findings demonstrated that decision tree analysis can identify key clinical variables associated with SURF and provide a practical, evidence-based tool for classifying patients, particularly when genetic testing is unavailable or pending.

Questions

1. **What is currently known about SURF, and how does this study advance the conceptualization of SURF as a distinct clinical entity?**
2. **How does the decision tree approach compare with traditional regression-based methods for developing classification criteria in autoinflammatory diseases?**
3. **How might the inclusion or exclusion of genetic testing influence both classification accuracy and real-world applicability?**
4. **What alternative methods (e.g., machine learning models, expert consensus) could have been considered, and how might they have affected the findings?**

Transcriptomic Stratification of Antiphospholipid Syndrome

Previous use of whole-blood RNA sequencing to analyze transcriptomic profiles of patients with antiphospholipid syndrome (APS) have identified marked changes in gene expression compared with healthy controls, particularly in interferon-regulated genes. p. 1124 **In this issue, Ambati et al. (p. 1124)** describe four endotypes of patients with APS or persistent positive antiphospholipid antibody (aPL). Their pathway-informed stratification of patients into biologically distinct clusters, each with diverse immune activation patterns and clinical features, represents a step toward personalized medicine for APS.

The investigators performed whole-blood RNA sequencing on 174 aPL-positive patients, including those with primary APS (n=102), secondary APS (n=29), and aPL-positivity without classifiable APS (n=43). By integrating the sequencing data with unsupervised machine learning and immune cell deconvolution, they were able to achieve a level of stratification that would not have been possible through clinical or serological data alone. Patients in Cluster 1 had upregulated ribosomal and metabolic pathways and downregulated mTOR, NETosis, and Hippo/IL-6 signaling. Patients in Cluster 2 demonstrated modest enrichment in mRNA processing and amino acid metabolism, whereas those in Cluster 3 showed biosynthetic suppression with mild Hippo/IL-6 activation. Cluster 4 exhibited the opposite pattern of Cluster 1, with strong upregulation of mTOR, NETosis, and Hippo/IL-6 signaling. Patients in Cluster 4 also had distinct clinical features compared with the other clusters, including higher anticardiolipin and anti–β_2-glycoprotein I positivity, elevated neutrophil counts, and increased urine protein-to-creatinine ratios.

The results reinforce the role of neutrophil-driven inflammation in a subset of APS patients and further implicate NETs in disease pathogenesis. In their discussion, the authors suggest that the upregulation of Hippo/IL-6 signaling seen in Cluster 4 also expands the understanding of pathophysiology beyond NETosis to a potential role of APS-associated immune remodeling, particularly in the context of myeloid cell activation and inflammation. The results also highlight the relationship between immune cell composition and the molecular heterogeneity of APS and suggest that nonthrombotic APS manifestations are associated with distinct gene expression profiles.

Journal Club

A monthly feature designed to facilitate discussion on research methods in rheumatology.

Decision Tree Analysis as a Preliminary Evidence-Based Tool for Identifying SURF in Children

Papa et al. *Arthritis Rheumatol.* 2026;78:1166–1175.

Syndrome of undifferentiated recurrent fever (SURF) represents a growing clinical challenge in pediatric autoinflammatory disease. Patients with recurrent fever are frequently encountered in practice but the conditions causing it remain poorly classified, limiting comparability across studies and the development of targeted therapies. Establishing evidence-based classification criteria is therefore essential to improve cohort homogeneity for clinical and translational research. In this study, we investigated SURF in children, defined as a heterogeneous group of patients with periodic inflammatory flares who do not meet criteria for hereditary recurrent fevers (HRF) or periodic fever, aphthosis, pharyngitis, and adenitis (PFAPA) syndrome and lack a definitive genetic diagnosis.

We analyzed 112 pediatric SURF patients followed at a single tertiary referral center and compared them with well-characterized disease controls (HRF and PFAPA) from the Eurofever registry. Using a decision tree approach, we developed classification models integrating clinical features with and without genetic test results, then compared their performance with logistic regression models. Decision trees were chosen because they are data-driven, transparent, and easily interpretable, making them particularly suitable for clinical application. Models incorporating genetic data showed the highest accuracy, but clinically based decision trees still achieved good discriminative performance and high specificity. External validation in an independent, multicenter cohort confirmed the robustness of the decision tree approach. Overall, our findings demonstrated that decision tree analysis can identify key clinical variables associated with SURF and provide a practical, evidence-based tool for classifying patients, particularly when genetic testing is unavailable or pending.

Questions

1. **What is currently known about SURF, and how does this study advance the conceptualization of SURF as a distinct clinical entity?**
2. **How does the decision tree approach compare with traditional regression-based methods for developing classification criteria in autoinflammatory diseases?**
3. **How might the inclusion or exclusion of genetic testing influence both classification accuracy and real-world applicability?**
4. **What alternative methods (e.g., machine learning models, expert consensus) could have been considered, and how might they have affected the findings?**

Clinical Connections

Romosozumab and Denosumab Combination Therapy After Denosumab in Postmenopausal Osteoporosis

Adami et al. *Arthritis Rheumatol.* 2026;78:1176–1183.

CORRESPONDENCE
Giovanni Adami, MD, PhD; giovanni.adami@univr.it

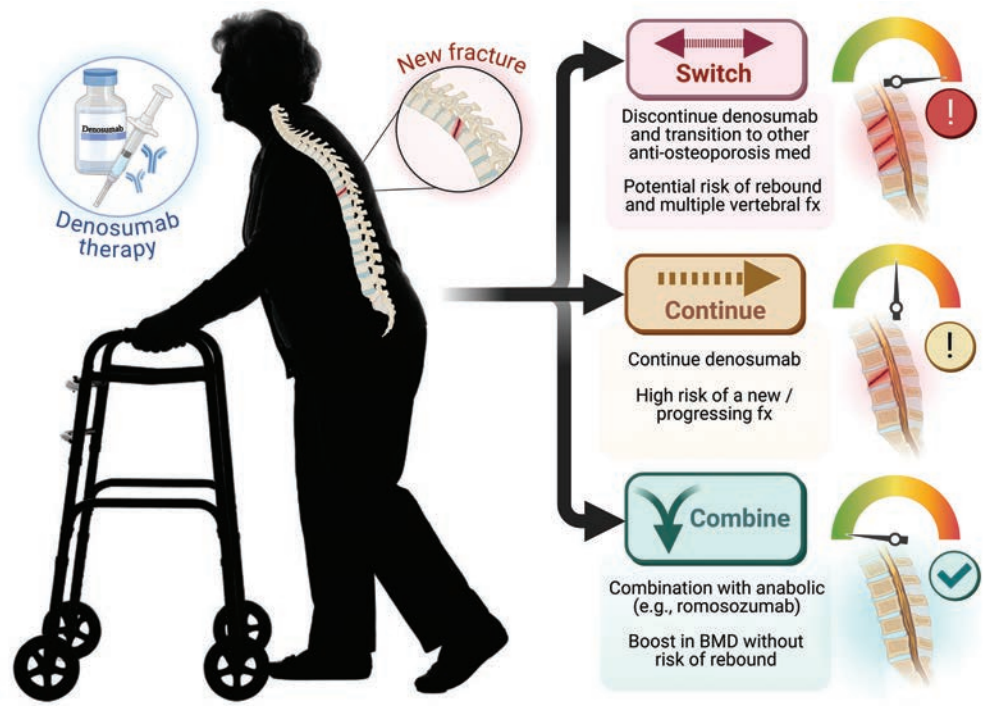

KEY POINTS

- Romosozumab stimulated new bone formation even in patients whose bone turnover was strongly suppressed by long-term denosumab.
- The combination of stimulated bone formation without increasing bone resorption suggests a favorable balance for improving bone strength.
- Combination romosozumab and denosumab therapy may represent a new option for patients with severe osteoporosis who continue to have fractures or lose bone despite denosumab therapy.

SUMMARY

Osteoporosis treatments, including denosumab, are not 100% effective, leaving patients vulnerable to fractures despite ongoing therapy. In this study, Adami et al. explored whether adding romosozumab to long-term denosumab treatment could further strengthen bone.

Romosozumab successfully stimulated new bone formation even when denosumab was continued, leading to meaningful gains in bone density, especially at the lumbar spine. Adding romosozumab to ongoing denosumab increased spine bone density by ~6% in 12 months, compared with minimal additional gains with denosumab alone. Importantly, this combined approach appeared to preserve the bone-building (modeling) benefits of romosozumab without triggering potentially harmful denosumab discontinuation rebound effect, a key concern of long-term denosumab treatment. The findings suggest that combining anabolic and antiresorptive therapies may offer a promising strategy for patients with severe osteoporosis who do not have adequate response to standard treatment. Larger studies are needed to confirm long-term benefits and fracture prevention.

Risk Factors for Relapse in AAV After Induction of Remission With Rituximab

Romich et al. *Arthritis Rheumatol.* 2026;78:1134–1144.

CORRESPONDENCE
Ellen Romich, MD, MSCE: ellen.romich@pennmedicine.upenn.edu

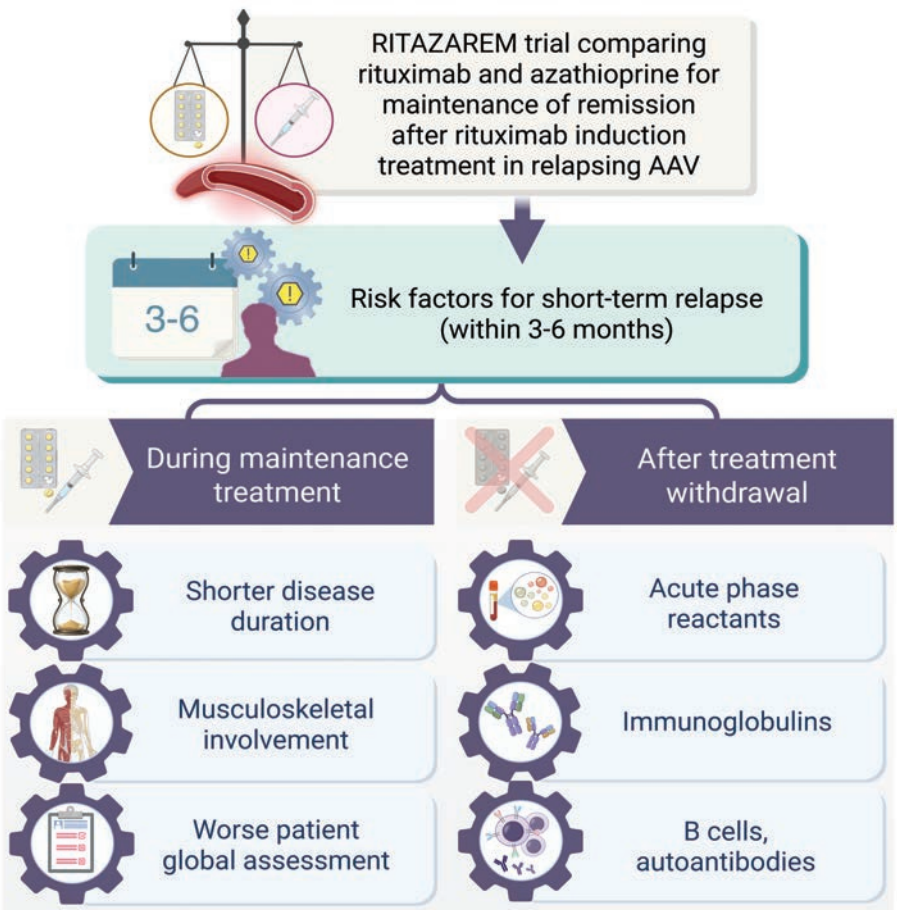

KEY POINTS

- Risk factors for relapse in AAV differ according to treatment phase, and withdrawal of maintenance treatment is associated with a high-risk period for relapse.
- Laboratory measures of immune reconstitution and inflammation (*e.g.*, acute phase reactants, autoantibodies, B cells, immunoglobulins) are associated with short-term relapse risk after withdrawal of treatment.
- Monitoring of laboratory tests at regular intervals may help identify patients with AAV at risk for relapse after withdrawal of treatment.

SUMMARY

Relapses in ANCA-associated vasculitis (AAV) are common during maintenance treatment and after treatment is discontinued. The RITAZAREM clinical trial compared rituximab and azathioprine for maintenance treatment after induction of remission with rituximab in relapsing AAV and demonstrated that rituximab is superior to azathioprine for maintaining remission.

Using data from the RITAZAREM trial, Romich et al. evaluated risk factors for short-term relapse (*i.e.*, within three to six months) during maintenance treatment and after withdrawal of treatment among 170 patients with AAV. Risk factors differed depending on the phase of treatment. During maintenance treatment, shorter disease duration, musculoskeletal involvement and worse patient global assessment were associated within increased likelihood of relapse. After withdrawal of treatment, higher markers of inflammation and immune reconstitution were associated with increased likelihood of relapse. These results highlight that withdrawal of treatment presents a high-risk time for relapse. Monitoring of laboratory tests at regular intervals may help to identify patients with AAV at risk for relapse.

Arthritis & Rheumatology
Vol. 78, No. 5, May 2026, pp 1017–1021
DOI 10.1002/art.70064

American College of Rheumatology
Empowering Rheumatology Professionals

ACR Presidential Address: The American College of Rheumatology in 2025 – The Strength, Resilience, and Importance of Our Rheumatology Community

Carol A. Langford

Introduction

It is my great pleasure to welcome all of you to Chicago and to the American College of Rheumatology (ACR) Convergence 2025. Whether you are here at this opening session in person or listening to this on demand, the ACR welcomes each of you as we come together at ACR Convergence to learn, share, and celebrate the latest advances in rheumatology.

I want to begin by thanking our Annual Meeting Planning Committee (AMPC), led by Dr Gregory Gardner, for their hard work and dedication. They have developed an outstanding program, with wide-ranging content, innovative formats, and networking options that are designed to meet your professional goals.

Our annual meeting holds a special place for me, as it is where I was first introduced to the ACR. While presentations of the latest science and education represent the foundation of this conference, what keeps me returning every year is the community within rheumatology that is brought together by the ACR. As we open ACR Convergence 2025, it is important, though, that we begin by reflecting on our past year.

The ACR guiding principles and 2025

For many of you, 2025 has represented a period of challenges and uncertainties. During times of challenge, the messages of our professional organizations take on even greater significance. The ACR remains steadfast in upholding its guiding principles (Figure 1), as seen through its mission, which is to empower rheumatology professionals to excel in their specialty, and through unwavering support for its core values. These speak to the necessity of innovation and collaboration in the advancement of rheumatology, the importance of inclusion that recognizes the dignity and belonging of every person and the value of their perspective, and that holds fast to the true meaning of community. It is through this path of respect for science and for each individual that the ACR demonstrates its commitment to the specialty of rheumatology.

In November 2024, when I had the honor of becoming the 88th President of the ACR, I spoke to the membership of my goal to shine a light on the three mission areas of education, research, and our connections as a community. Little did I know then how important these would become in 2025 and how the ACR's role in supporting these missions would take on a much deeper meaning.

ACR education

Much of my time as an ACR volunteer focused on education such that it was only natural that this would represent one of my focus areas. The rapid advancement of discoveries that benefit patients is one of many rewarding aspects of rheumatology. With these advancements, though, comes the responsibility and privilege of lifelong learning. During this year, I made it a goal to engage in every aspect of the ACR's educational portfolio in support of this vital mission. Through its spectrum of offerings, I saw firsthand how the ACR and Association of Rheumatology Professionals (ARP) provide learning opportunities that allow each person to choose the method and content that addresses their individual needs and preferences. These educational options are delivered through our ACR and ARP journals and publications (*Arthritis & Rheumatology*, *Arthritis Care & Research*, *ACR Open Rheumatology*, and *The Rheumatologist*), podcasts, webinars, and virtual and face-to-face meetings.

Our meetings include differing locations and topics through our Winter Rheumatology Symposium in Colorado; the Pediatric Rheumatology Symposium (PRYSM), which in 2026 will celebrate the 50th anniversary of the first meeting of pediatric

Presented at the American College of Rheumatology Convergence 2025, Chicago, IL, October 25, 2025.
Department of Rheumatic and Immunologic Diseases and Center for Vasculitis Care and Research, Cleveland Clinic, Cleveland, Ohio.
Author disclosures are available at https://onlinelibrary.wiley.com/doi/10.1002/art.70064.

Address correspondence via email to Carol A. Langford, MD, MHS, at langfoc@ccf.org.
Submitted for publication December 16, 2025; accepted December 30, 2025.

Figure 1. Guiding principles of the American College of Rheumatology.

rheumatology; and the State-of-the-Art Clinical Symposium (SOTA) held here in Illinois, all of which culminate at the end of our year here at ACR Convergence. Through this wide range of programs, the ACR and ARP strive to be the place where you choose to come to enhance your professional knowledge.

Practice innovation. One aspect recognized by our committees and meeting planners is that education at ACR Convergence is best defined broadly, covering a wide range of topics impactful to every career path. This year saw the launch of the Practice Innovation Summit, a novel advanced programming session designed to provide clinicians, office managers, and interprofessional team members in practice settings with strategies and expert insights to thrive in today's health care landscape. During the 2025 meeting, you will see exciting new program innovations such as this, combined with familiar aspects of ACR Convergence we know and love, including our plenaries, poster hall, and Meet the Professor sessions.

Artificial/augmented intelligence. Another aspect of ACR Convergence, well recognized by our AMPC, is that it needs to include discussion of areas that have emerged in recent times that will impact our field. 2025 saw a dramatic expansion of artificial/augmented intelligence in medicine and health care management, which will continue to grow in the years ahead. This brings exciting opportunities for accelerating research, developing new educational models, and improving efficiencies in clinical practice. With this, though, comes a responsibility to guide its use toward enhancing what must always remain at the core of the practice of medicine, which is individualized and compassionate care delivered by the provider in making shared decisions with their patient. Maintaining our understanding about this rapidly developing tool provides the most reliable way to ensure it is used in a manner that strengthens and enhances well-reasoned, humanistic medical care.

Addressing medical misinformation. The importance of education has also risen to the forefront in 2025 as we face an environment that has increasingly been filled with medical misinformation that places the safety of our patients at risk. The commitment our rheumatology community has consistently demonstrated toward maintaining evidence-based knowledge and then sharing this knowledge with their patients and others represents an empowering strategy in dispelling inaccuracy and enhancing trust.

Threats to research and barriers to the delivery of care

This evidence base comes to us as a direct result of research, which was the second ACR mission area I sought to focus on during this year. No matter your individual career path, research is critical to each and every one of us because research represents the source of advances that benefit our patients.

2025 has seen many developments that threaten the pace of scientific discovery through impacts on our academic institutions, federal organizations, medical publications, funding levels, and what lines of investigation that funding may be directed toward.

One of the greatest concerns is for our investigators, both those currently engaged in research and the next generation, who represent the future of our field. It is essential to rheumatology that the light of innovation and scientific curiosity be enabled to shine brightly without threat of being dimmed or extinguished.

During this same time, we have also seen barriers placed on the ability of dedicated clinicians to bring those research findings to the care of their patients. This continuum of the pursuit and application of knowledge that improves health represents the very best of humanity that all of us must strive to protect.

The ACR stands side-by-side with investigators and practitioners in driving forth the importance of research and the effective delivery of medical innovations to the care of people with rheumatic disease. This message has been advanced by the ACR through many different avenues.

ACR advocacy. The ACR is extremely fortunate to have a skilled and experienced advocacy team. Their impact has never been more apparent than in 2025, and I want to express my thanks to our advocacy and communications volunteer and staff members for their efforts toward ensuring that the voice of rheumatology is heard throughout all federal, state, and local levels. The ACR has a Washington, DC, office that allows us to be at the forefront of emerging policy decisions and executive actions, to attend briefings, and to request meetings with our legislators and their staff (https://rheumatology.org/about-acr-advocacy).

Since the beginning of 2025, the ACR has engaged in issuing over 120 op-eds, letters, media mentions, comments, and public statements (as of September 22, 2025). These have been released by the ACR both as a single organization and in coalition partnerships with other medical associations and state societies, advocating for issues important to rheumatology. The ACR's positions on critical issues are guided and reinforced by our ACR Health Policy Statements developed by our Government Affairs Committee, which are reviewed annually and can be updated at any time to address a newly emerging issue (https://rheumatology.org/policy-position-statements). Key policy areas include expanding patient access to rheumatology care, removing barriers to treatment, and increasing support for rheumatology research and training.

In May 2025, the ACR held our annual Advocates for Arthritis meeting in Washington, DC. Over 100 ACR, ARP, and patient delegates attended 123 meetings with bipartisan lawmakers and their staff from 27 states. In these meetings, the ACR brought forward vital messages to our nation's leaders in support of National Institutes of Health–funded research, preserving access to care for Medicare patients, opposing cuts to Medicaid, and urging pharmacy benefit manager reform to lower prescription drug costs and increase access to treatments for patients. During the year, the ACR Executive Committee also met with the US Food and Drug Administration Commissioner and the Deputy Administrator of the Centers for Medicare & Medicaid Services.

As a result of these collective efforts, we have seen a number of successes where the voice of rheumatology has brought about meaningful change. Throughout this time, the ACR advocacy and communications teams have worked hard to keep our membership informed through biweekly messages, as well as postings on the ACR website and social media. We appreciate, though, that there remain challenges that many of you and your colleagues, fellows, and patients continue to face at both state and federal levels. Please be assured that the ACR's advocacy efforts remain steady and ongoing to address the concerns of our membership and patients.

In addition to the actions of our advocacy team, the message of one remains powerful and there are many ways you can individually make a difference. Through the Legislative Action Center, the ACR provides easy ways to contact your legislators about rheumatology issues that matter to you. You can volunteer for ACR advocacy committees; join us in Washington, DC, at our 2026 advocacy event; and support RheumPAC. You can schedule time to speak to the ACR's advocacy team to discuss health care policy issues of concern to you. At ACR Convergence, you will also see signs around the convention center highlighting the ACR's advocacy on current issues and ways in which you can help.

Rheumatology Research Foundation. Another way that you can sustain research growth is through partnership with the Rheumatology Research Foundation, celebrating its 40th anniversary in 2025. The Foundation provides funding that increases the rheumatology workforce and enhances research through project grants and investigator career development awards. As one of largest private funders of rheumatology research, the Foundation's role in accelerating discovery and protecting the future of rheumatology has never been more critical. I hope that you will pursue learning more about our Foundation and join the ACR and me in supporting its vital mission (https://www.rheumresearch.org).

Our rheumatology community

My third and final focus area was directed toward enhancing connections between the ACR and its members. The ACR is your community. It has continued to grow and is now over 10,200 members strong.

Whether you are a clinician in practice; a clinical, translational, or basic science investigator; a clinician educator; a fellow; a Master; or a rheumatology professional, you are an essential part of that community who is recognized and respected by the ACR (Figure 2). All of us stand together with one shared goal, which is to improve the lives of those with rheumatic disease.

Having a thriving rheumatology workforce is necessary to achieve that goal. Protecting our workforce means not only growing the number of new rheumatologists and rheumatology professionals but maintaining and supporting those who are already in

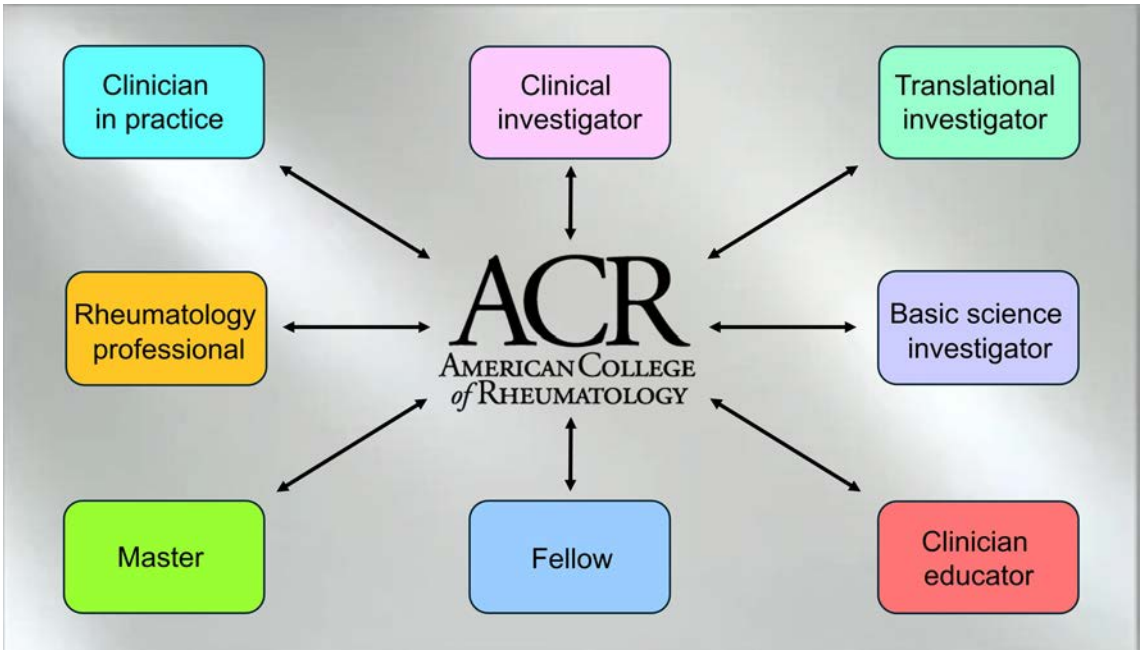

Figure 2. The American College of Rheumatology reflects the many disciplines within rheumatology that together represent one unified community.

our field. Burnout and other forms of occupational distress represent a growing threat in medicine and can affect anyone.[1–3] In addition to its potential to reduce our rheumatology workforce, occupational distress is important because of its negative effect on the individual experiencing it. When you are part of a community, it means caring about the well-being of those who are within it. It is for these reasons that the ACR chose to invite as our speaker, Dr Tait Shanafelt, a practicing hematologist-oncologist at Stanford University and an internationally recognized thought leader in system approaches to enhance clinician well-being and the impact of burnout in health care, and I am looking forward to his discussion later in this opening session.

An important part of each member's connection to the ACR is in seeing their individual objectives and priorities reflected through the ACR's commitment to our mission. Although this was an aspect of the ACR I had long appreciated, I gained a much deeper understanding of these important links through the President's Corner, which appeared in *The Rheumatologist* (https://www.the-rheumatologist.org/category/professional-topics/presidents-perspective). Each of these articles focused on a different aspect of the College and I am grateful to the many ACR, ARP, and Foundation staff and volunteers who helped me review these articles and for the encouragement of Physician Editor Dr Bharat Kumar in making this possible.

The meaning and impact of these connections between the ACR and its member community also became clear from discussions held during the past year with the ACR Board of Directors. At the beginning of each meeting, Board members shared their individual "mission moments," a time meaningful to them when they saw in action the ACR's mission to empower rheumatology professionals to excel in their specialty. This easily became my favorite part of the meeting, and by the end of the year, seeing how these moments cut across every aspect of the ACR and reflected each discipline within our membership was truly inspiring.

These moments occurred as a direct result of ACR volunteers and staff working together. Providing care to people with vasculitis and participating in the ACR have been the greatest privileges of my career. Being a volunteer with the ACR over the past 31 years has enriched my life. It has allowed me to get to know amazing people I would have never had the opportunity to meet, it enabled me to gain skills I would not have had the chance to learn, and it provided me with an additional way to contribute to this specialty that I care about so deeply. I would encourage all of you to volunteer with the ACR, ARP, or Rheumatology Research Foundation, as your voice is welcomed and needed.

No goals are achieved alone

I have many to thank for the past year. I am grateful to have served under remarkable ACR Past Presidents Drs Kenneth Saag, Douglas White, and Deborah Dyett Desir. I have had the honor of working with fantastic colleagues within the committees and Board of Directors, all of whom have exemplified the true meaning of dedication. I particularly wish to recognize and thank our 2025 Executive Committee: ARP President Dr Adam Goode,

Foundation President Dr Liana Fraenkel, and our ACR leaders Drs William Harvey, Anne Bass, and Angus Worthing. Their experience, guidance, and wisdom were deeply appreciated and essential in 2025.

None of what the ACR achieves, though, would be possible without our incredible staff, all of whom are deeply committed to the ACR and its mission. I wish to express my personal thanks to our Executive Vice President Mr Steven Echard and our entire staff team for everything they do for the ACR, its members, and the patients we serve.

As a child of the 1970s, the song "Dream On" by Aerosmith spoke to me of the future hopes of dreams coming true. Reaching our goals, though, takes a great deal more than dreams. It takes hard work, the strength to learn from those times when things don't go your way, humility and appreciation for when they do, and the recognition that those dreams were cultivated, supported, and made possible by the actions of others. My standing here would never have occurred were it not for mentors present at every stage of my career who not only taught me rheumatology and clinical research but who most importantly believed in me. These have included Dr James Louie (medical school); Dr Timothy Laing (residency); Drs Rex McCallum, E. William St. Clair, and David Pisetsky (fellowship); Drs Anthony Fauci and Michael Sneller (National Institutes of Health); and Dr Gary Hoffman (Cleveland Clinic). The vital role these physicians played in my life serves as a valuable reminder that mentorship must continue to be sustained, encouraged, and celebrated for its essential place in passing forward both the science and art of medicine.

I also wish to thank my many accomplished collaborators within vasculitis and my own rheumatology family at Cleveland Clinic, particularly my Chair, Dr Abby Abelson. The wonderful people in these communities have sustained me not only during this year but throughout my clinical and research career. There is really nothing better than working together with those you respect who are not just colleagues but also friends.

None of this would, of course, have been possible without my family. My dear late parents, who immigrated here from England, raised me to believe that anything could be possible if I just tried. They taught me the importance of service to others and that the joy of life is not in its accomplishments but in its journey. Finally, I would not be here without the support of my husband, Dr Matthew Bunyard, whom I met during fellowship. His belief is what sustains me, and the greatest blessing I was ever given was in having him by my side to share life with.

Looking ahead with optimism

ACR Convergence is where rheumatology meets. In between hearing the latest research advances and attending educational sessions, I hope you will take the opportunity to spend time with mentors, fellows, colleagues, and friends, as celebrating these connections is what makes ACR Convergence special. This meeting is more than just a conference—it is a place where all are welcomed and encouraged to engage and to grow.

Our collective commitment to serving people with rheumatic disease fills me with optimism for the years to come. The contributions each of us makes will allow rheumatology to face any challenge through our unity, strength, and resilience. It is in that spirit that I welcome each of you to ACR Convergence 2025, where we meet as one community looking ahead with confidence toward the exciting future of rheumatology.

AUTHOR CONTRIBUTIONS

Dr Langford contributed to at least one of the following manuscript preparation roles: conceptualization AND/OR methodology, software, investigation, formal analysis, data curation, visualization, and validation AND drafting or reviewing/editing the final draft. As corresponding author, Dr Langford confirms that she has provided the final approval of the version to be published and takes responsibility for the affirmations regarding article submission (eg, not under consideration by another journal), the integrity of the data presented, and the statements regarding compliance with institutional review board/Declaration of Helsinki requirements.

REFERENCES

1. Shanafelt TD, West CP, Sinsky C, et al. Changes in burnout and satisfaction with work-life integration in physicians and the general US working population between 2011 and 2023. Mayo Clin Proc 2025;100(7):1142–1158. doi:https://doi.org/10.1016/j.mayocp.2024.11.031
2. Sinsky CA, Brown RL, Rotenstein L, et al. Association of work control with burnout and career intentions among U.S. physicians: a multi-institution study. Ann Intern Med 2025;178(1):20–28. doi:https://doi.org/10.7326/ANNALS-24-00884
3. West CP, Dyrbye LN, Shanafelt TD. Physician burnout: contributors, consequences and solutions. J Intern Med 2018;283(6):516–529. doi:https://doi.org/10.1111/joim.12752

American College of Rheumatology
Empowering Rheumatology Professionals

Arthritis & Rheumatology
Vol. 78, No. 5, May 2026, pp 1022–1024
DOI 10.1002/art.70049

EDITORIAL

Getting It Right for Our Patients

Marie Hudson, MD, MPH[1] and Daniel H. Solomon, MD, MPH[2]

Immune checkpoint inhibitors (ICIs) have transformed cancer care, offering long-term remissions or durable disease control in patients with cancers that were once considered fatal. In a subset of patients, these responses have been likened to "functional cures." ICIs work by blocking receptors that normally down-regulate immune cells. The resulting up-regulation of immune cells by ICIs results in powerful antitumor immunity. However, these treatments are not specific to tumor cells. Instead, they modulate the immune system broadly, which can lead to off-target immune-related adverse events (irAEs) affecting normal tissue. Given this broad immune stimulation, the use of ICIs in patients with pre-existing autoimmune diseases has been the subject of some controversy. These patients were generally excluded from randomized clinical trials of ICIs for a number of reasons, including the risk of inducing flares of the underlying disease, subjecting them to higher risks of irAEs given their underlying autoimmune dysregulation, inferior efficacy in those requiring baseline immunosuppression, and possible medication interactions. However, numerous retrospective studies have provided real-world evidence showing that these additional risks are manageable.[1] The general consensus is that pre-existing autoimmune diseases are not a contraindication to treatment with an ICI. The question has now shifted to whether glucocorticoids as well as other immunosuppressants used to treat pre-existing autoimmune disease may blunt the efficacy of the ICI.

In this issue of *Arthritis and Rheumatology*, Jannat-Khah et al[2] ask the question, "Are glucocorticoids associated with worse survival among rheumatoid arthritis patients with lung cancer treated with immune checkpoint inhibitors?". They identified patients with rheumatoid arthritis (RA) from a large Medicare claims database who were treated with an ICI for stage IV (metastatic) non–small cell lung cancer (NSCLC). Their primary exposure was oral glucocorticoids (excluding dexamethasone) within 91 days of ICI initiation. The primary outcome was overall survival. Of the 663 patients included in the study, mean age was 75 years, 87% were White, 65% were women, and 368 (46%) patients were exposed to glucocorticoids (median prednisone-equivalent dose was 6.6 mg/day; interquartile range [IQR] 3.3–12.3). Using statistical methods that account for immortal time bias, they found that glucocorticoid use was not associated with a reduction in survival. In a Cox proportional hazards model with time-varying exposure windows, the risk of survival was identical between patients who were not exposed to glucocorticoids and those exposed to <4.9 mg/day, 5 to 9.9 mg/day, and ≥10 mg/day (all three doses were associated with hazard ratios of survival of 1.00 and confidence intervals of 1.00–1.00 compared with no glucocorticoids). Similarly, in a 91-day landmark analysis, the hazard ratio of glucocorticoid exposure (in 5-mg increments) was 1.01 (95% confidence interval 0.93–1.10). These alternative models, including adjustments for dose, support the conclusion that low-dose glucocorticoids are not associated with a reduction in survival in patients with RA with NSCLC treated with an ICI. Of note, in a sensitivity analysis including 116 additional patients exposed to dexamethasone in the same time window, dexamethasone use (vs nonuse) was associated with a significantly increased risk of death (hazard ratio 1.48; 95% confidence interval 1.09–2.02). The authors concluded that exposure to glucocorticoids (other than dexamethasone) at the time of ICI initiation and at dosages used to treat RA had a negligible effect on survival in patients with RA with stage IV NSCLC.

Other studies that have examined the impact of glucocorticoids at the time of ICI initiation had considerable limitations, including small heterogenous samples and confounding by indication (by lumping different types of glucocorticoids that may have different indications and associations with outcomes).[3] This study overcomes these limitations by including a large sample of patients with the same pre-existing autoimmune disease and cancer type and stage. In addition, although the indication for glucocorticoids is difficult to attribute with certainty, it is plausible that the low median dose and exclusion of dexamethasone were to treat RA and not cancer-related indications.

[1]Jewish General Hospital, McGill University, Montreal, Quebec, Canada; [2]Brigham and Women's Hospital, Harvard Medical School, Boston, Massachusetts.

Author disclosures are available at https://onlinelibrary.wiley.com/doi/10.1002/art.70049.

Address correspondence via email to Marie Hudson, MD, MPH, at marie.hudson@mcgill.ca.

Submitted for publication October 21, 2025; accepted in revised form November 26, 2025.

Recommendations for the management of immunosuppression at the time of ICI initiation in patients with pre-existing inflammatory arthritis have recently been developed using the Grading of Recommendations Assessment, Development, and Evaluation approach by the Canadian Research Group of Rheumatology in Immuno-Oncology (CanRIO).[4,5] However, the level of evidence supporting the recommendations was low or very low, and the strength of the recommendations were correspondingly weak. Nevertheless, the panel formulated a Good Practice Statement to the effect that "Glucocorticoids should be tapered to the lowest effective dose possible, ideally to <10 mg prednisone equivalent daily." The study results from Jannat-Khah et al[2] suggest that low-dose glucocorticoids (prednisone-equivalent dose of 6.6 mg/day; IQR 3.3–12.3) are not associated with worse survival in patients with RA with lung cancer treated with ICI and provide data-driven evidence in support of the CanRIO statement.

The question posed by Jannat-Khah et al[2] is very important, and the results may influence the practice of physicians caring for patients with RA who develop cancer and require ICIs. They may be comforted by the idea that low-dose glucocorticoids are "safe." However, perhaps the more relevant question is whether there ever is a safe dose of glucocorticoids. Getting the answer to this question right is of particular importance in the setting of ICIs. This question led us to consider whether the methods used in this article were the most appropriate and, therefore, the results robust. A major challenge of observational real-world evidence studies is correctly assessing the effects of exposure on outcome. Immortal time bias occurs when an exposure is defined after follow-up begins and during which time an outcome cannot occur, thereby creating a false survival advantage in the exposed group.

In this article, landmark analyses and time-dependent Cox proportional models were used as alternative methods to address the concern of immortal time bias. However, these methods are not without their own limitations. In a landmark analysis, a specific time point called "the landmark" is chosen after the start of the study, exposure is defined among patients who are event-free as of the landmark, and follow-up starts from that point forward. While mitigating immortal time bias, one of the limitations of a landmark analysis is that it excludes patients who had an event before the landmark time, potentially introducing selection bias. As can be seen from Table 1 and Figure 1, the landmark analysis excluded almost one-third of the study population.[2] Could the association between glucocorticoid exposure and early death be different than what is reported with the landmark analysis? A time-dependent Cox proportional hazards model is an alternative method that has the advantage of including all the subjects. It addresses immortal time bias by allowing exposure status to vary over time instead of fixing it at the start of the study. Although this alternative model has the benefit of generalizability by including all of the study cohort and addresses immortal time bias by including a time-dependent exposure variable, it is still susceptible to other time-related biases, including time-dependent confounding. For example, irAEs (which by definition occur after the start of the study, defined as ICI initiation) could be associated with both the exposure (glucocorticoids) and outcome (survival). In addition, irAEs are associated with better survival.[6] Thus, if glucocorticoids were started to treat irAEs rather than RA, the presence of an irAE could cancel out the negative effect of glucocorticoids on survival. The rates of irAEs in the study population are not reported in the study, but a recent systematic review reported rates of any grade irAE of 40.0% (37.3%–42.7%) and high grade of 19.7% (15.8%–23.7%) in real-world settings.[7] Alternative methods for observational real-world evidence studies that address time-varying biases and emulate randomized clinical trials, such as incident and prevalent new-user designs, exist and could be considered in future studies.[8,9]

Finally, the report by Jannat-Khah et al[2] nicely addresses a narrow yet important question, but it raises the question of whether baseline treatment of RA with disease-modifying antirheumatic drugs (DMARDs), including biologics, is better or worse than glucocorticoids. On this specific question, the CanRIO guidelines conditionally recommend considering de-escalating immunosuppression in patients with preexisting RA, particularly in those who have low disease activity or inactive disease[4]; this was based on low evidence. Unfortunately, the Jannat-Khah et al[2] dataset could not address this question as <5% of the patients were exposed to DMARDs in the first three months after ICI initiation (Table 1). This finding may speak to the fact that clinicians might be uncomfortable with baseline immunosuppression in patients with pre-existing autoimmune disease initiating ICI treatment and thus prefer glucocorticoids. However, preclinical studies suggest that biologics such as anti-tumor necrosis factor inhibitors or anti-interleukin-6 inhibitors may in fact enhance the antitumor effect of ICIs,[10,11] and there are ongoing trials designed to test the safety and efficacy of combining these biologics and ICIs in patients without RA (eg, ClinicalTrials.gov ID NCT03293784 and NCT03999749). In addition, two studies reported that JAK inhibition in patients also without RA enhanced checkpoint blockade in NSCLC[12] and Hodgkin lymphoma.[13] Jannat-Khah et al[2] have contributed to the evidence base for managing ICIs in rheumatic diseases, but many questions remain unanswered. The onus is on the research community to get it right for our patients with RA.

AUTHOR CONTRIBUTIONS

All authors contributed to at least one of the following manuscript preparation roles: conceptualization AND/OR methodology, software, investigation, formal analysis, data curation, visualization, and validation AND drafting or reviewing/editing the final draft. As corresponding author, Dr Hudson confirms that all authors have provided the final approval of the version to be published, and takes responsibility for the affirmations regarding article submission (eg, not under consideration by another journal), the integrity of the data presented, and the

statements regarding compliance with institutional review board/Declaration of Helsinki requirements.

REFERENCES

1. Lopez-Olivo MA, Kachira JJ, Abdel-Wahab N, et al. A systematic review and meta-analysis of observational studies and uncontrolled trials reporting on the use of checkpoint blockers in patients with cancer and pre-existing autoimmune disease. Eur J Cancer 2024;207:114148. doi:https://doi.org/10.1016/j.ejca.2024.114148
2. Jannat-Khah D, Curtis JR, Xie F, et al. Are glucocorticoids associated with worse survival among patients with rheumatoid arthritis and lung cancer treated with immune checkpoint inhibitors? Arthritis Rheumatol 2026;78(5):1038–1044. doi:https://doi.org/10.1002/art.43445
3. Bruera S, Suarez-Almazor ME. The effects of glucocorticoids and immunosuppressants on cancer outcomes in checkpoint inhibitor therapy. Front Oncol 2022;12:928390. doi:https://doi.org/10.3389/fonc.2022.928390
4. Ye C, Nikolic RPA, Choi M, et al. Canadian Rheumatology Association/Canadian Research Group of Rheumatology in Immuno-Oncology living guidelines for baseline immunosuppression in individuals with preexisting rheumatic diseases initiating immune checkpoint inhibitors. Part 1: preexisting inflammatory arthritides. J Rheumatol 2025;52(12):1207–1217. doi:https://doi.org/10.3899/jrheum.2025-0481
5. Ye C, Nikolic RPA, Choi M, et al. Canadian Rheumatology Association/Canadian Research Group of Rheumatology in Immuno-Oncology living guidelines for baseline immunosuppression in individuals with preexisting rheumatic diseases initiating immune checkpoint inhibitors. Part 2: preexisting systemic autoimmune rheumatic diseases. J Rheumatol 2025;52(12):1218–1230. doi:https://doi.org/10.3899/jrheum.2025-0482
6. Wolchok JD, Chiarion-Sileni V, Rutkowski P, et al; CheckMate 067 Investigators. Final, 10-year outcomes with nivolumab plus ipilimumab in advanced melanoma. N Engl J Med 2025;392(1):11–22. doi:https://doi.org/10.1056/NEJMoa2407417
7. Jayathilaka B, Mian F, Franchini F, et al. Cancer and treatment specific incidence rates of immune-related adverse events induced by immune checkpoint inhibitors: a systematic review. Br J Cancer 2025;132(1):51–57. doi:https://doi.org/10.1038/s41416-024-02887-1
8. Yu OHY, Suissa S. Metformin and cancer: solutions to a real-world evidence failure. Diabetes Care 2023;46(5):904–912. doi:https://doi.org/10.2337/dci22-0047
9. Suissa K, Dell'Aniello S, Comin E, et al. Glucosamine and cancer incidence in osteoarthritis: a prevalent new-user cohort design. Arthritis Care Res (Hoboken) 2024;76(11):1493–1500. doi:https://doi.org/10.1002/acr.25399
10. Perez-Ruiz E, Minute L, Otano I, et al. Prophylactic TNF blockade uncouples efficacy and toxicity in dual CTLA-4 and PD-1 immunotherapy. Nature 2019;569(7756):428–432. doi:https://doi.org/10.1038/s41586-019-1162-y
11. Hailemichael Y, Johnson DH, Abdel-Wahab N, et al. Interleukin-6 blockade abrogates immunotherapy toxicity and promotes tumor immunity. Cancer Cell 2022;40(5):509–523.e6. doi:https://doi.org/10.1016/j.ccell.2022.04.004
12. Mathew D, Marmarelis ME, Foley C, et al. Combined JAK inhibition and PD-1 immunotherapy for non-small cell lung cancer patients. Science 2024;384(6702):eadf1329. doi:https://doi.org/10.1126/science.adf1329
13. Zak J, Pratumchai I, Marro BS, et al. JAK inhibition enhances checkpoint blockade immunotherapy in patients with Hodgkin lymphoma. Science 2024;384(6702):eade8520. doi:https://doi.org/10.1126/science.ade8520

Arthritis & Rheumatology
Vol. 78, No. 5, May 2026, pp 1025–1028
DOI 10.1002/art.70063

American College of Rheumatology
Empowering Rheumatology Professionals

EDITORIAL

Where You Live Shouldn't Dictate Your Care: Multilateral Strategies Are Needed for National and Regional Equity in Psoriatic Arthritis Treatment

Jihwan Hwang,[1] Ashira Blazer,[2] and Irene Blanco[3]

The cross-sectional study by Banbury et al in the April issue of *Arthritis & Rheumatology*, entitled, "Where we live matters: varied disease burden and treatment in psoriatic arthritis in the United States" used the Rheumatology Informatics System for Effectiveness (RISE) registry to assess the clinical characteristics, social deprivation, insurance coverage, and medication use among patients with psoriatic arthritis (PsA) across different regions of the United States.[1] This article reveals disparities in PsA care at a time when new therapies and medications are continuously being developed. To ensure equitable outcomes for vulnerable populations, it is critical that advanced therapies be distributed effectively across regions, practice settings, and insurance types, especially as current legislation may lead to millions of Americans losing health insurance coverage.[2]

Overall, Banbury et al found the cohort was composed of a higher proportion of women (58%) than men. Women with PsA were more likely to have high disease activity (HDA) and high multimorbidity compared to men yet were less likely to receive biologic disease modifying antirheumatic drugs (bDMARDs). In addition, Black patients with PsA, those with Medicare or Medicaid, and those who clustered within Medicaid-serving provider practices all had greater odds of HDA. Regionally, patients residing in the South and the Midwest had greater odds of HDA compared to those in the West and Northeast. When controlling for age and sex, patients in the Northeast had the lowest odds of HDA compared to the other regions. The authors also found regional differences in treatment practices. The Midwest had the lowest use of bDMARD therapy but the highest use of glucocorticoids and conventional synthetic DMARDs. Patients seen in RISE practices in the South and the Midwest had overall higher socioeconomic deprivation, as measured by the Area Deprivation Index (ADI), which may have contributed to decreased access to bDMARD therapy. Likewise, authors identified access to care challenges in the subset of patients with PsA receiving Medicaid and living in high ADI areas. Among 198 RISE sites, only 14 practices were shown to provide care for half of all Medicaid-insured patients with PsA in this registry, and only 20 practices were shown to care for half of all patients with PsA with high social deprivation. Although this study was likely underpowered to detect differences in treatment across specific ethnic and racial groups within the geographic regions studied, it captures a detailed overview of these disparities in the US.

The RISE registry currently reports on the practices of over 1,000 rheumatology providers, representing a comprehensive view of treatment strategies across the US.[3] Notably, the authors were the first to report important regional differences in PsA disease activity and treatment patterns in the context of the ADI. This aids in understanding the role of adverse social determinants of health in PsA treatment disparities. By incorporating neighborhood-level indices, this study shifts the focus from individual health behaviors to broader community-level factors that may be systematic and policy driven. An inherent limitation to the use of RISE is that most rheumatology practices that participate in the registry are in private and community practice settings.[4] This may lead to a selection bias for patients who are more likely to be insured. Therefore, there may be an underrepresentation of patients with PsA that are on public insurance plans, such as Medicare and Medicaid. This is likely reflected in the fact that so few of the RISE practices care for the large majority of such patients. Moreover, the registry cannot currently assess differences in time to DMARD use, time to diagnosis, or chronicity of disease. These nuances could identify important temporal relationships between disease onset and DMARD administration across the regions. Similarly, this study only assesses distance

Dr Blazer's work was supported by the National Institute of Allergy and Infectious Diseases, NIH (grant K23-AI-163359), a Career Development Award from the Lupus Research Alliance, and the University of Maryland FIRST program (grant U54CA272205).

[1]Icahn School of Medicine at Mount Sinai, New York, New York; [2]University of Maryland School of Medicine, Baltimore, Maryland; [3]Feinberg School of Medicine, Northwestern University, Chicago, Illinois.

Author disclosures are available at https://onlinelibrary.wiley.com/doi/10.1002/art.70063.

Address correspondence via email to Irene Blanco, MD, MS, at irene.blanco@northwestern.edu.

Submitted for publication November 13, 2025; accepted in revised form January 13, 2026.

from a patient's address to the practice, but it does not account for population density, practice size, or rural versus urban setting. These factors could further influence treatment patterns, as delivery of bDMARDs may be more challenging in rural settings. Lastly, the choice to dichotomize continuous variables such as ADI could have limited clinical inferences across the spectrum of socioeconomic status.

In the US, the average annual incidence of PsA cases was estimated to be 8.5 per 100,000 between 2000 and 2017, with a point prevalence of 181.8 per 100,000 in 2015 and an increasing incidence in women.[5] Despite the increasing prevalence and more severe presentations of PsA among women, authors found a concerning trend toward decreased bDMARD prescriptions among this population.[6] Likewise, the authors showed higher odds of HDA among Black patients compared to White patients. The literature supports delayed treatment initiation and significantly longer time to DMARD therapy among Black patients newly diagnosed with PsA.[7] Similar ethnic, racial, and regional disparities in outcomes are also observed in patients with systemic lupus erythematosus (SLE). Black/African American patients with SLE have significantly greater disease severity, multimorbidity, and mortality rates compared to White patients. Racial and ethnic minority patients with SLE also disproportionately reside in disadvantaged neighborhoods, as measured by the ADI, which is notably a risk factor for poor retention in care.[8] Patients with SLE living in the Northeast were also shown to be more likely to receive immunosuppressive therapy than those residing in the South. Given the parallels between SLE and this study's findings in patients with PsA, similar challenges may influence treatment outcomes across multiple systemic autoimmune rheumatic disease populations.

In a 2021 Medicare and Medicaid database study, the prevalence of PsA was found to be 320 per 100,000 persons for Medicare enrollees and 132 per 100,000 persons for Medicaid enrollees.[9] The 63% of patients enrolled in commercial insurance, the 38% of those enrolled in Medicaid, and the 21% of those enrolled in Medicare were prescribed biologic or targeted-synthetic DMARDs. Therefore, congruent with the findings presented by Banbury et al, access to these medications remains an unmet need for many patients due to limited insurance coverage and costs, among other factors.[10] Numerous variables have been shown to perpetuate inequitable access to care; however, this study adds regional variations as a potential factor. This phenomenon may be attributed to a myriad of issues such as closure of local pharmacies, delivery limitations for bDMARDs in rural areas, or differences in Medicaid expansion across regions and states. However, even regional differences may be mitigated by insurance status. For example, a study of US veterans with rheumatoid arthritis showed smaller variations in bDMARD use between rural and urban dwelling patients. This is likely due to the more homogenous insurance coverage by the Veterans Affairs system compared to other payers.[11]

The 2018 ACR guidelines on PsA management stress the importance of early identification and initiation of therapy for improving long-term outcomes.[12] Notably, the recommendations focus on immunomodulatory agents, such as DMARDs, for long-term management rather than addressing acute symptoms through intra-articular injections or systemic glucocorticoids. Similarly, in treatment-naive patients with active PsA, the use of tumor necrosis factor inhibitors is recommended over oral small molecules as a first-line option, especially in severe presentations. In addition, given the chronic and heterogenous nature of PsA, the use of bDMARDs and, more importantly, the individualization of PsA therapy is important. This necessity for personalized treatment plans emphasizes the importance of addressing regional medication access challenges in PsA care.

Although the RISE registry highlights regional differences in the distance traveled to clinical rheumatology practices, regional differences in pharmacy access may also contribute to differences in bDMARD prescribing practices. Approximately 15.8 million people (4.7%) in the US live in pharmacy deserts, encompassing both rural and urban settings.[13] Prior studies have illustrated these pharmacy deserts and their impact on observed disparities in treatment patterns. For example, the higher prevalence of pharmacy deserts in the Midwest and South were significantly associated with COVID-19 deaths during the pandemic (Figure 1).[14] Moreover, neighborhood-level indices, like the ADI or the Social Vulnerability Index (SVI), may be used as tools to identify neighborhoods with disparities in PsA detection, treatment, and management. Greater socioeconomic disadvantage as measured by the SVI has been shown to be associated with lower screening rates for various conditions including cancer.[15] Therefore, beyond provider practice settings, disparities in pharmacy access, social vulnerability, and screening may underlie the regional differences in access to medications.

This study effectively identifies disparities and regional variations in treatment patterns in the US and offers a timely emphasis on the importance of addressing systemic barriers to care in PsA treatment. Systemic factors such as access to rheumatology practices and social deprivation are major drivers of care differences. Although systemic factors that influence geographic differences in prescribing patterns are critical to inform policy, individual-level provider/patient interactions can also impact disparities in care. This study highlights the importance of considering PsA across genders and racial and geographic groups for differences in treatment culture. Efforts to address these disparities will require interventions that encompass both individual and community-wide factors. Leveraging continuing medical education opportunities by national and regional rheumatology societies could ensure more uniform, evidence-based long-term PsA management and improved outcomes. Likewise, future studies investigating variables such as time to diagnosis and time to DMARD may be beneficial to provide a holistic assessment of treatment variations and equip individual providers with useful metrics to

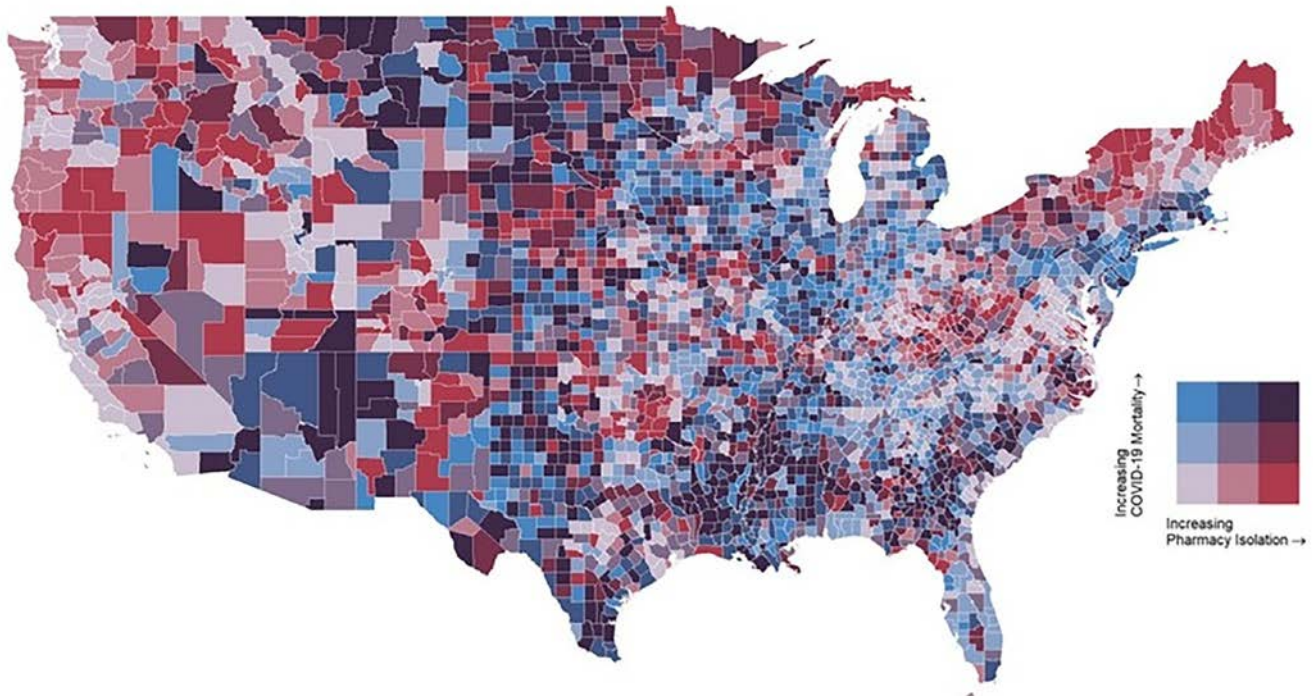

Figure 1. Bivariate map of county-level COVID-19 mortality rates and pharmacy isolation index. Tertiles of cumulative mortality rates per 100,000 persons through December 31, 2020, and pharmacy isolation index are visualized.[14]

mitigate disparities within their own practice. All in all, the data presented by Banbury et al underscore the national and regional disparities faced by patients with PsA. It will be through integrative and multilateral approaches that we achieve equitable care for this patient population.

No original data were shared in this editorial. Data for the figure can be downloaded from the US Census Bureau.

AUTHOR CONTRIBUTIONS

All authors contributed to at least one of the following manuscript preparation roles: conceptualization AND/OR methodology, software, investigation, formal analysis, data curation, visualization, and validation AND drafting or reviewing/editing the final draft. As corresponding author, Dr Blanco confirms that all authors have provided the final approval of the version to be published and takes responsibility for the affirmations regarding article submission (eg, not under consideration by another journal), the integrity of the data presented, and the statements regarding compliance with institutional review board/Declaration of Helsinki requirements.

REFERENCES

1. Banbury B, Dowell S, Jenkins C, et al. Where we live matters: varied disease burden and treatment patterns in psoriatic arthritis in the United States. Arthritis Rheumatol 2026;78(4):861–869. doi:https://doi.org/10.1002/art.43377
2. An act to provide for reconciliation pursuant to title II of H. Con. Res. 14. HR 1, 119th Cong (2025–2026). https://www.congress.gov/bill/119th-congress/house-bill/1/text
3. American College of Rheumatology. RISE FAQs. Accessed October 19, 2025. https://rheumatology.org/rise-faqs
4. Hammam N, Izadi Z, Li J, et al. The relationship between electronic health record system and performance on quality measures in the American College of Rheumatology's Rheumatology Informatics System for Effectiveness (RISE) Registry: observational study. JMIR Med Inform 2021;9(11):e31186.
5. Karmacharya P, Crowson CS, Bekele D, et al. The epidemiology of psoriatic arthritis over five decades: a population-based study. Arthritis Rheumatol 2021;73(10):1878–1885.
6. Lubrano E, Scriffignano S, Fatica M, et al. Psoriatic arthritis in males and females: differences and similarities. Rheumatol Ther 2023;10(3):589–599.
7. Lin I, Krupsky K, Way N, et al. Patient-reported and economic racial and ethnic disparities in patients with psoriatic arthritis: results from the National Health and Wellness Survey. Rheumatol Ther 2024;11(6):1569–1590.
8. Buie J, McMillan E, Kirby J, et al. Disparities in lupus and the role of social determinants of health: current state of knowledge and directions for future research. ACR Open Rheumatol 2023;5(9):454–464.
9. Ogdie A, Matthias W, Thielen RJ, et al. Racial differences in prevalence and treatment for psoriatic arthritis and ankylosing spondylitis by insurance coverage in the USA. Rheumatol Ther 2021;8(4):1725–1739.
10. Kamangar F, Isip L, Bhutani T, et al. How psoriasis patients perceive, obtain, and use biologic agents: survey from an academic medical center. J Dermatolog Treat 2013;24(1):13–24.
11. Naik A, Baraff A, Wysham KD, et al. Escalation to biologics after methotrexate among US veterans with rheumatoid arthritis grouped by rural versus urban areas. Arthritis Care Res (Hoboken) 2025;77(1):23–29.

12. Singh JA, Guyatt G, Ogdie A, et al. Special article: 2018 American College of Rheumatology/National Psoriasis Foundation guideline for the treatment of psoriatic arthritis. Arthritis Rheumatol 2019;71(1):5–32.
13. Wittenauer R, Shah PD, Bacci JL, et al. Locations and characteristics of pharmacy deserts in the United States: a geospatial study. Health Aff Sch 2024;2(4):qxae035.
14. US Census Bureau. Bivariate map of county-level COVID-19 mortality rates and pharmacy isolation index, United States, through December 31, 2020. Published 2021. Accessed 2025. https://catalog.data.gov/dataset/pharmacies
15. Hwang J, Risica PM, Lamy E, et al. Association between the social vulnerability index and breast, cervical, and colorectal cancer screening rates in Rhode Island. Cancer Causes Control 2024;35(8):1143–1149.

Arthritis & Rheumatology
Vol. 78, No. 5, May 2026, pp 1029–1031
DOI 10.1002/art.70062

American College of Rheumatology
Empowering Rheumatology Professionals

EDITORIAL

Optimizing Hydroxychloroquine in Lupus Treatment: Looking Beyond the 5-mg/kg Weight-Based Dosing Cutoff

April Jorge

Hydroxychloroquine (HCQ) remains the backbone of systemic lupus erythematosus (SLE) treatment today, 70 years after its initial US Food and Drug Administration approval, but the optimal dosing remains controversial. Due to its many benefits, including protection against lupus disease activity and flares, organ damage, cardiovascular and thrombotic events, pregnancy morbidity, and premature death, HCQ is strongly recommend in routine treatment of all people with SLE, unless contraindicated, and is generally continued indefinitely.[1] However, long-term HCQ use carries a well-recognized risk of HCQ retinopathy and a rare but increasingly recognized risk of cardiac toxicity,[2] and the risks increase with greater prolonged exposure to the medication. When considering the impact of HCQ dose, the risk of HCQ retinopathy is over three times higher with >5 mg/kg/day than with lower dosing, which has informed current ophthalmology and rheumatology guidelines on HCQ dosing.[3] In fact, there is a relatively linear association between higher weight-based dose and higher retinopathy risk rather than a safe dosing threshold.[4] Other factors that impact HCQ exposure, including kidney function, genetic polymorphisms in cytochrome P450 enzymes, and medication adherence, also influence toxicity risk. At the same time, observational studies in recent years have demonstrated that lower HCQ exposure—through either the intentional use of lower HCQ dosing or due to poor medication adherence—reduces the efficacy of HCQ in preventing SLE flares and related acute care use.[5–8] This presents a challenge for optimizing the use of HCQ to improve SLE outcomes and minimize toxicity. Two articles in this issue of *Arthritis & Rheumatology* provide useful insights into this challenging situation.

The first article of interest in this issue is by Li et al.[9] The authors address the impact of HCQ dose on other adverse outcomes aside from SLE flares and disease activity, including cardiovascular and thrombotic events, malignancy, and end-stage kidney disease. They conducted a retrospective observational study using a nationwide health insurance database in Taiwan to compare outcomes of patients prescribed an HCQ dose of ≥400 mg/day versus <400 mg/day. The key finding was a lower risk of coronary artery disease and venous thrombosis associated with dosing of ≥400 mg/day. No differences in the comparative risks of ischemic stroke, end-stage kidney disease, or malignancy were observed. Of note, a minority of patients (only 4%) received ≥400 mg/day dosing in this cohort, and the median dose in the primary "low dose" comparator group was 350 mg/day, still on the higher end of the typical dosing range (200–400 mg/day). They also compared ≥400 mg/day dosing with alternative thresholds of lower HCQ dosing, ≤300 and ≤200 mg/day, and their findings were similar. As this was an observational study using administrative health data, the possibility of misclassification and confounding by indication must be acknowledged, although the authors took steps to minimize potential bias by following the target trial emulation framework.[10]

Li et al[9] also found no difference, over a mean six years, in the risk of HCQ retinopathy according to HCQ dose. However, caution is warranted in interpreting this finding, as this HCQ retinopathy increases in frequency after more than 10 years of use, and their study had a limited follow-up time. In addition, diagnosis codes have limited accuracy in identifying cases of HCQ retinopathy.[11] Furthermore, prior studies that adjudicated outcomes of HCQ retinopathy and observed patients through longer periods have demonstrated a strong relationship between higher risk of HCQ retinopathy with higher dosing.[4] This study was also limited by the lack of data on body weight, so weight-based HCQ dosing could not be assessed or compared. Nonetheless, 400 mg/day exceeds 5 mg/kg dosing for the majority of people with SLE. Thus, this study adds to the growing body of evidence that greater HCQ exposure in a dose range that often exceeds the 5 mg/kg weight-based dosing threshold seems to improve the

Dr Jorge's work was supported by the National Institute of Arthritis and Musculoskeletal and Skin Diseases, NIH (grant K23-AR-079040), and the Rheumatology Research Foundation K Supplement.

[1]Division of Rheumatology, Inflammation, and Immunity, Massachusetts General Hospital, Mass General Brigham and Harvard Medical School, Boston.

Author disclosures are available at https://onlinelibrary.wiley.com/doi/10.1002/art.70062.

Address correspondence via email to April Jorge, MD, at amjorge@mgh.harvard.edu.

Submitted for publication November 14, 2025; accepted in revised form December 23, 2025.

efficacy of HCQ, including its cardiovascular and thrombotic benefits.

With increasing evidence that current guideline-recommended HCQ dosing[3] under 5 mg/kg may not be the optimal dose for all patients with SLE, HCQ blood level monitoring has been proposed as an alternative strategy to guide the safe use of HCQ. The preferred assays assess HCQ levels in whole blood, but serum levels are generally considered a reasonable alternative and can be interpreted with a conversion factor.[12] Trough levels are preferred to minimize variability, but random HCQ blood levels may also be used.[13] In recent years, multiple studies have identified very low HCQ levels (<200 ng/mL in whole blood or <106 mg/mL in serum) as a marker of severe nonadherence, and uncovering/addressing nonadherence is recognized as an increasingly accepted indication for HCQ blood level monitoring.[14,15] However, the potential use of HCQ blood levels to identify subtherapeutic and/or supratherapeutic HCQ dosing and to guide dose adjustments remains controversial. The recent American College of Rheumatology guidelines for the treatment of SLE did not provide consensus recommendations on the use of HCQ blood level monitoring but acknowledged the potential to inform HCQ dosing in the future, pending further evidence and wider availability of the laboratory testing.[1]

In the second article of interest in this issue of *Arthritis & Rheumatology*, Garg et al[16] sought to identify a target range for HCQ blood levels to maximize clinical efficacy while minimizing major toxicity. They combined data from multiple lupus cohorts from Wisconsin, France, and the international Systemic Lupus International Collaborating Clinics Inception Cohort to assess one-time HCQ blood levels (some cohorts used whole blood, whereas others used serum) in over 2,000 patients with SLE. They compared clinical information, including SLE disease activity scores (Systemic Lupus Erythematosus Disease Activity Index 2000 [SLEDAI-2K]) at the time of HCQ blood level assessment, and assessed HCQ toxicity outcomes over subsequent follow-up. They report a 5% risk of HCQ toxicity over variable follow-up periods, with most cases reported from retinopathy.

Using these data, Garg et al[16] identified and proposed an upper limit HCQ blood level threshold of 1,150 ng/mL, above which the risk of toxicity increases without additional observed benefit in controlling SLE disease activity. The authors found that HCQ blood levels above 1,150 ng/mL were associated with nearly double the risk of HCQ toxicity than lower blood levels, and dose-response curves demonstrated a greater increase in HCQ toxicity risk with HCQ blood levels above this threshold. The authors additionally found that higher HCQ blood levels were associated with lower baseline SLE disease activity scores (SLEDAI-2K) until the HCQ levels approached 1,150 ng/mL, above which there was not a further reduction in disease activity observed. Of note, this study did not assess the association between HCQ blood levels and the future risk of SLE flares or future disease activity scores, which limits the inference of causation.

A prior smaller study led by Dr Garg did demonstrate a lower risk of subsequent lupus-related acute care visits in patients with HCQ blood levels between 750 and 1,200 ng/mL than in patients with lower levels,[17] and several cross-sectional and cohort studies have similarly demonstrated associations between HCQ blood levels above 500 to 750 ng/mL and lower SLE disease activity scores.[13] Of additional importance in the current study, Garg and colleagues[16] demonstrated that 18% of patients who were prescribed weight-based HCQ dosing of ≤5 mg/kg had HCQ blood levels exceeding their proposed 1,150-ng/mL "supratherapeutic" threshold. As expected, the likelihood of supratherapeutic HCQ levels was higher among those with chronic kidney disease stage ≥3, given that the medication is partly cleared by the kidneys.

Based on the overall findings of their study, Garg et al[16] propose a rationale for the optimal therapeutic HCQ blood level ranging from 750 to 1,150 ng/mL for patients with SLE. The potential use of HCQ blood level monitoring to improve the personalized use of HCQ is increasingly compelling, and a safer and more effective approach to HCQ dosing could have a major impact on SLE care. However, there remains a lack of evidence as to whether changing the HCQ dose in response to HCQ blood levels either above or below the proposed therapeutic blood level range will lead to improved SLE outcomes. Future longitudinal studies are needed to determine whether HCQ blood levels can guide HCQ dose adjustments to improve SLE disease control, prevent toxicity, and prevent other adverse outcomes, including cardiovascular and thrombotic events.

AUTHOR CONTRIBUTIONS

Dr Jorge contributed to at least one of the following manuscript preparation roles: conceptualization AND/OR methodology, software, investigation, formal analysis, data curation, visualization, and validation AND drafting or reviewing/editing the final draft. As corresponding author, Dr Jorge confirms that she has provided the final approval of the version to be published and takes responsibility for the affirmations regarding article submission (eg, not under consideration by another journal), the integrity of the data presented, and the statements regarding compliance with institutional review board/Declaration of Helsinki requirements.

REFERENCES

1. Sammaritano LR, Askanase A, Bermas BL, et al. 2025 American College of Rheumatology (ACR) guideline for the treatment of systemic lupus erythematosus. Arthritis Rheumatol Published online November 4, 2025. doi:https://doi.org/10.1002/art.43452
2. DiGregorio H, Costenbader K, Garshick MS, et al. Antimalarial-mediated cardiotoxicity: evaluation and preliminary screening recommendations for patients on chronic therapy for autoimmune rheumatic diseases. American College of Cardiology Expert Analysis. February 18, 2025. https://www.acc.org/Latest-in-Cardiology/Articles/2025/02/14/16/19/Antimalarial-Mediated-Cardiotoxicity
3. Marmor MF, Kellner U, Lai TY, et al; American Academy of Ophthalmology. Recommendations on screening for chloroquine and hydroxychloroquine retinopathy (2016 revision). *Ophthalmology*

2016;123(6):1386–1394. doi:https://doi.org/10.1016/j.ophtha.2016.01.058

4. Jorge AM, Melles RB, Marmor MF, et al. Risk factors for hydroxychloroquine retinopathy and its subtypes. JAMA Netw Open 2024;7(5):e2410677. doi:https://doi.org/10.1001/jamanetworkopen.2024.10677
5. Jorge AM, Mancini C, Zhou B, et al. Hydroxychloroquine dose per ophthalmology guidelines and the risk of systemic lupus erythematosus flares. JAMA 2022;328(14):1458–1460. doi:https://doi.org/10.1001/jama.2022.13591
6. Nestor J, Choi H, Mancini C, et al. Hydroxychloroquine dose and hospitalizations for active lupus. Arthritis Rheumatol 2024;76(10):1512–1517. doi:https://doi.org/10.1002/art.42924
7. Feldman CH, Yazdany J, Guan H, et al. Medication nonadherence is associated with increased subsequent acute care utilization among Medicaid beneficiaries with systemic lupus erythematosus. Arthritis Care Res (Hoboken) 2015;67(12):1712–1721. doi:https://doi.org/10.1002/acr.22636
8. Almeida-Brasil CC, Hanly JG, Urowitz M, et al. Flares after hydroxychloroquine reduction or discontinuation: results from the Systemic Lupus International Collaborating Clinics (SLICC) inception cohort. Ann Rheum Dis 2022;81(3):370–378. doi:https://doi.org/10.1136/annrheumdis-2021-221295
9. Li BMH, Hung JH, Yang PC, et al. Weighing dose-related benefits and risks of hydroxychloroquine treatment in patients with systemic lupus erythematosus. Arthritis Rheumatol 2026;78(5):1114–1123. doi:https://doi.org/10.1002/art.70022
10. Hernán MA, Robins JM. Using big data to emulate a target trial when a randomized trial is not available. Am J Epidemiol 2016;183(8):758–764. doi:https://doi.org/10.1093/aje/kwv254
11. Chiu SY, Shaw JW, Luong TQ, et al. Coding patterns used by ophthalmologists for hydroxychloroquine retinal toxicity. Clin Ophthalmol 2018;12:2261–2265. doi:https://doi.org/10.2147/OPTH.S170789
12. Blanchet B, Jallouli M, Allard M, et al; PLUS Group. Hydroxychloroquine levels in patients with systemic lupus erythematosus: whole blood is preferable but serum levels also detect non-adherence. Arthritis Res Ther 2020;22(1):223. doi:10.1186/s13075-020-02291-z
13. Saleh ZF, Kahlenberg JM. Refining lupus management: a comprehensive review of HCQ blood levels. Rheumatol Adv Pract 2025;9(3):rkaf080. doi:https://doi.org/10.1093/rap/rkaf080
14. Durcan L, Clarke WA, Magder LS, et al. Hydroxychloroquine blood levels in systemic lupus erythematosus: clarifying dosing controversies and improving adherence. J Rheumatol 2015;42(11):2092–2097. doi:https://doi.org/10.3899/jrheum.150379
15. Nguyen Y, Blanchet B, Urowitz MB, et al. Association between severe nonadherence to hydroxychloroquine and systemic lupus erythematosus flares, damage, and mortality in 660 patients from the SLICC inception cohort. Arthritis Rheumatol 2023;75(12):2195–2206. doi:https://doi.org/10.1002/art.42645
16. Garg S, Blanchet B, Nguyen Y, et al. Defining optimally safe and effective blood levels of hydroxychloroquine in lupus: an important step toward precision drug monitoring. Arthritis Rheumatol 2026;78(5):1102–1113. doi:https://doi.org/10.1002/art.70010
17. Garg S, Astor BC, Saric C, et al. Therapeutic hydroxychloroquine blood levels are associated with fewer hospitalizations and possible reduction of health disparities in lupus. Arthritis Care Res (Hoboken) 2024;76(12):1606–1616. doi:https://doi.org/10.1002/acr.25422

Arthritis & Rheumatology
Vol. 78, No. 5, May 2026, pp 1032–1037
DOI 10.1002/art.43410

American College of Rheumatology
Empowering Rheumatology Professionals

NOTES FROM THE FIELD

National Mortality Databases to Assess Disease Burden in Systemic Autoimmune Diseases: A Valuable Resource But With Limitations

Ram Raj Singh

Introduction

Disease-specific mortality statistics are useful measures of disease burden. Population-based studies from a few US counties have reported mortality in systemic autoimmune diseases (SAIDs). However, due to substantial differences in the population structure of these counties as well as relatively small numbers of SAID deaths in these counties, it is difficult to extrapolate their findings to assess SAID national burden. In this regard, national mortality databases offer a large reference population, which is hard to assemble in individual SAIDs. However, two concerns are persistently raised regarding mortality databases for SAIDs: misclassification and underrecording. Although misclassification of SAIDs is common in health records and administrative databases, it appears to be rare on death certificates among decedents who did not have an SAID. However, SAIDs are underrecorded in death certificates. The underrecording of SAIDs does not differ by sex and race and ethnicity, but it is common in older adults who die of cardiovascular diseases, neoplasms, and chronic obstructive pulmonary disease. Underrecording of SAIDs may occur because it may be difficult to assign a specific SAID manifestation or treatment complication responsible for death. Furthermore, an SAID is commonly listed as a contributing, rather than as the underlying, cause of death on death certificates, which advocates using the multiple-causes-of-death database for SAIDs. Nevertheless, until we have large-scale prospective outcomes data, mortality data from the National Vital Statistics System offer valuable estimates of SAID national burden, which can be used for setting research priorities, health care policy planning, resource allocation, and precision public health.

The unmet need

SAIDs, such as systemic lupus erythematosus (SLE), systemic sclerosis (SSc), rheumatoid arthritis (RA), dermatopolymyositis (DPM), systemic vasculitis, and Sjogren disease, are chronic immune-inflammatory conditions with increasing prevalence.[1–4] With their onset at younger ages, SAIDs can incur substantial disease burden. Disease-specific mortality statistics are important measures of disease burden that can be used for setting research priorities, health care policy planning, resource allocation, and precision public health.

Most mortality reports on SAIDs are based on patient cohorts at referral centers,[5] but they do not capture changes in the incidence of these diseases over time and will not reflect the true burden of disease in the population. For example, it is well documented that Black persons experience worse morbidity and mortality from SSc.[6,7] However, in well-cared-for cohorts, such as the Scleroderma Lung Study cohort, time to death and survival were not different between Black and non-Black participants with SSc.[8]

A few studies have used population-based designs to quantitate mortality burden from SAIDs,[3,9–13] but they were limited to specific regions, specific patient populations, small samples, or relatively short durations (Table 1).[3,9,10,14] The racial and ethnic makeup of these counties/study populations was substantially different compared to the US population: White persons represented 85% of population in Olmsted County, Minnesota, from 1999 to 2018 as compared to 66% of the US population during the same time period; Asian persons represented 35% of the population in San Francisco County, California, versus 5% in the US population; Black persons represented 49% of the population in DeKalb and Fulton Counties, Georgia, versus 13% in the

Autoimmunity and Tolerance Laboratory, Division of Rheumatology, Department of Medicine, Department of Pathology and Laboratory Medicine, Molecular Toxicology Interdepartmental Program, and Jonsson Comprehensive Cancer Center, David Geffen School of Medicine, University of California, Los Angeles.

Additional supplementary information cited in this article can be found online in the Supporting Information section (https://acrjournals.onlinelibrary.wiley.com/doi/10.1002/art.43410).

Author disclosures and graphical abstract are available online at https://onlinelibrary.wiley.com/doi/10.1002/art.43410.

Address correspondence via email to Ram Raj Singh, MD, at rrsingh@mednet.ucla.edu.

Submitted for publication June 5, 2025; accepted in revised form September 29, 2025.

Table 1. Population structure in recent population-based studies on SLE mortality in the United States*

Location	DeKalb and Fulton Counties, GA[10]	Olmsted County, MN[3]	San Francisco County, CA[9]	Medicaid, 47 states[14]	Nationwide, 50 states and DC[18]
Duration	2002–2006	1999–2018	2007–2017	2000–2006	2000–2015
No. of SLE deaths	400	22	135	2,058	28,411
Population in the study period	7,451,017	2,816,126	9,125,648	1,226,467,530[a]	4,833,578,708
Population by race and ethnicity, %					
AI or AN[b]	0.2	0.3	0.3	1.1	0.8
Asian or PI[b]	4.5	5.7	35.4	3.3	5.0
Black[b]	49	5	6.1	22.7	12.7
Hispanic	7.4	3.9	15.1	26.9	15.4
White[b]	38.8	85.1	43.1	42.7	66.0
Population by age groups, %					
<44 y	69.2	62.4	60.2		61.8
45–64 y	22.6	24.9	25.6		25.1
>65 y	8.2	12.7	14.2		13.1

* AI, American Indian; AN, Alaska Native; CA, California; DC, District of Columbia; GA, Georgia; MN, Minnesota; PI, Pacific Islander; SLE, systemic lupus erythematosus.
[a] US population in the 18- to 65-year age group during the study period.
[b] Non-Hispanic.

US population; and Hispanic persons represented 27% of those on Medicaid versus 15% in the US population (Table 1). These limitations pose challenges in extrapolating their data to assess national disease burden.

Recognition of the need for large population-based data on SAIDs has led to the creation of databases such as the Rheumatology Informatics System for Effectiveness registry, which would be useful to assess SAID outcomes. In the meantime, a database maintained by the Centers for Disease Control and Prevention's (CDC) National Vital Statistics System provides a valuable resource to assess the national burden of SAIDs.

CDC's national mortality database

The CDC's database encompasses more than 99% of deaths of all US residents. Death certificates provide the *International Classification of Diseases* codes for the underlying or contributing cause of death (Supplemental Figure).[15] Information from death certificates can be used to assess disease-specific outcomes in an unbiased manner over a long time period in a large sample size. These data have been used to identify public health challenges and guide funding priorities. For example, to address the underdocumentation of maternal mortality, death certificates were changed in 2003.[16] The data obtained led to policy changes, such as expanding Medicaid coverage for women to a year after delivery.

For the mortality datasets to accurately capture disease burden, it is vital that primary physicians or nurse practitioners who usually fill death certificates have a clear understanding of the patient. However, some states allow individuals who have never interacted with the patient to sign the death certificate, which can lead to inaccuracy. Autopsies were performed to verify the accuracy of the cause of death in 40% to 60% of hospital deaths in the United States before 1970, but this rate has now gone below 5%.[17] Thus, difficulty to verify the accuracy of the coding on death certificates is a limitation of mortality datasets.

Changes in physicians' reporting/attributing a disease as a cause of death, the practice of recognizing a disease, and changes in diagnostic tools could influence trends in disease-specific mortality. Finally, data on clinical, laboratory, and socioenvironmental parameters are not available in mortality databases.

Assessing population-level mortality burden for SAIDs using national mortality databases

Population-level mortality statistics, such as the leading-causes-of-death ranking and mortality rates, serve as useful tools for assessing the relative burden of cause-specific mortality. For example, the cause-of-death ranking analysis revealed that SLE ranked among the top 10 leading causes of death in 15- to 24-year-old females.[18] Mortality databases have also been used to highlight persistent mortality burden in SAIDs over time.[6,7,15] Notably, the ratios of SLE or SSc mortality rates to all-cause mortality rates were higher in 2010s than in the 1970s.[7,15] However, there are at least two persistent concerns: (1) misclassification (ie, a specific disease recorded on the death certificate when the decedent did not have the disease) and (2) underrecording (ie, the decedent had the disease, but it was not recorded on the death certificate).

Is there a misclassification of SAIDs on death certificates?

In a chart review of patients in administrative billing and hospitalization databases, the specificity of SAID diagnoses ranged from 72.5% (lupus) to 96.4% (myositis).[19] However, unlike administrative databases, where possible and probable diagnoses are often recorded, death certificates usually have the most

proximate illness recorded as the cause of death. Due to a limited awareness about these diseases among primary physicians and hospitalists who often care for dying patients, SAIDs are unlikely to be perceived and recorded as a cause of death for decedents who did not have these diseases. In contrast, cardiovascular diseases are often perceived to be the illness at the time of death; hence, death certificates tend to overestimate cardiovascular disease mortality.[20] In a study designed to capture all patients with SLE, for the 731 decedents for whom SLE was recorded on the death certificate, only 2 (0.27%) had SLE erroneously recorded as a cause of death (when decedents did not have SLE).[21] Although studies are needed to determine the extent of SAID misclassification on death certificates, it is unlikely to influence SAID mortality assessments in a substantial way.

Underrecording of SAIDs on death certificates

Patients with SAIDs die prematurely of complications such as cardiovascular events, pulmonary complications, infections, cancer, and renal failure. These proximate causes of death may be perceived by physicians who care for the patients at the time of death to be unrelated to SAIDs, when in fact the SAID or the medications used for it predispose the patients to these causes of death.

In cohorts for which the extent of SAIDs not being recorded on death certificates could be deduced, the extent of underrecording for SLE varied from 32% to 59% (Table 2).Cardiovascular diseases, heart failure, pneumonia, neoplasms, and chronic obstructive pulmonary disease were among the most prevalent causes of death among individuals with SLE who had SLE absent from their death certificate.[21]

The age at death was higher among those for whom SLE was omitted on the death certificates than those who had SLE included in death certificates.[22,23] Decedents 60 to 79 years old at death were approximately 2.5 times as likely to have SLE missing from their death certificates compared with those aged <40 years.[21] The extent of SLE underrecording was even higher (64%) among those aged over 80 years.[21] Some proportions of these deaths in older adults could be due to causes unrelated to SLE. Thus, older age and diseases that are the leading causes of death in older adults are associated with the lack of recording of SLE on death certificates. As a corollary, younger decedents and those who had renal failure listed as a cause of death were less likely to have SLE absent from their death certificate compared to those without renal failure listed.[21] Likewise, younger age, a greater number of deformities, higher Sharp score, lower socioeconomic status, and a certified physician's signature on the death certificate were associated with recording RA on death certificates, whereas comorbidities were inversely associated with listing RA on the death certificate.[24]

Is there a selective underrecording of SAIDs on death certificates in certain subpopulations?

SAID outcomes differ by sex and race and ethnicity. For example, the SLE mortality risk was higher in females (odds ratio [OR] 5.3, 95% confidence interval [CI] 5.1–5.6) than males and in Black (OR 3.9, 95% CI 3.8–4.1) and Hispanic persons (OR 1.4, 95% CI 1.3–1.4) relative to White persons.[15] SSc mortality rates were also higher in females than males and in Black persons than in White persons.[7] Black persons had a 13-year lower median age at death and 5.1 times higher odds of premature death from SSc compared to White persons.[6] Such disparities are unlikely to be artifacts from underrecording or misclassification of cause of death because greater underreporting would lead to greater underestimation of mortality in the underprivileged groups, but we found the mortality to be higher, for example, in females and Black and Hispanic persons. Furthermore, in the Lupus in Minorities, Nature Versus Nurture (LUMINA) and Carolina Lupus Study (CLU) cohorts, no difference in education and poverty levels was found between SLE decedents who had lupus recorded on their death certificates and those who did not.[22]

To address the differential recording of SAIDs in death certificates, I tabulated SLE deaths by sex and race and ethnicity in the

Table 2. Underrecording of SLE on death certificates in the United States*

Location	Duration	No. of SLE deaths in the cohort	SLE recorded on death certificates[a]	SLE not recorded[b]	% not recorded
LUMINA and CLU cohorts[22,c]	1999–2004	76	46	30	39.5
Olmsted County, MN[3]	1999–2018	22	15	7	31.8
DeKalb and Fulton Counties, GA[10]	2002–2006	400	190	210	52.5
San Francisco County, CA[9]	2007–2017	135	55	80	59.3
Total	–	633	306	327	51.7

* CA, California; CDC, Centers for Disease Control and Prevention; CLU, Carolina Lupus Study; GA, Georgia; LUMINA, Lupus in Minorities, Nature Versus Nurture; MN, Minnesota; SLE, systemic lupus erythematosus.
[a] SLE death counts were obtained from the CDC WONDER database for the corresponding county and study period, except for the LUMINA and CLU cohorts, for which the information was extracted from the death certificates obtained from the Offices of Vital Statistics.
[b] Assuming that potential relocation in and out of the counties did not majorly affect SLE death counts.
[c] LUMINA is a multiethnic (Hispanic [Mexican or Puerto Rican ancestry], African American, or White race and ethnicity), multicenter (the University of Alabama at Birmingham, the University of Texas Health Science Center at Houston, and the University of Puerto Rico Medical Sciences Campus) cohort.

Table 3. Underrecording of SLE on death certificates by sex, race and ethnicity, and age in recent studies*

	DeKalb and Fulton Counties, GA[10,a] (2002–2006)		LUMINA and CLU cohorts[22] (1999–2004)		Medicaid (18–65 y)[14] (2000–2006)		Olmsted County, MN[3] (1999–2018)		San Francisco County, CA[9,a] (2007–2017)	
	Cohort	CDC	SLE recorded	Not recorded	Medicaid	CDC	Cohort	CDC	Cohort	CDC
SLE death count	400	190	46	30	2,058	9,402	22	15	135	53
Female sex, %	87	89	91	80	–	–	–	–	88	83
Race, %										
Asian	–	–	–	–	1	4	–	–	33	41
Black	81	84	63	53	51	41	–	–	31	15
Other	–	–	–	–	2	1	–	–	3	2
White	19	16	13	33	40	41	–	93	33	42
Hispanic ethnicity, %	–	–	22	13	6	13[b]	–	–	14	19
Race and sex, %										
Black female	72	75	–	–	–	–	–	–	–	–
White female	16	14	–	–	–	–	–	–	–	–
Age, %										
10–34 y	–	–	–	–	–	–	–	–	19	20
45–64 y	–	–	–	–	–	–	–	–	44	40
≥65 y	–	–	–	–	–	–	–	–	37	40

* SLE death counts reported in recent patient cohorts are tabulated by sex, race, ethnicity, and age ("Cohort"). SLE death counts were then obtained from the CDC WONDER database for the corresponding county/geographic location, age, and study duration ("CDC"). CA, California; CDC, Centers for Disease Control and Prevention; CLU, Carolina Lupus Study; GA, Georgia; LUMINA, Lupus in Minorities, Nature Versus Nurture; MN, Minnesota; SLE, systemic lupus erythematosus.
[a] Racial groups were not separated by Hispanic origin.
[b] $P < 0.001$, Fisher's exact test.

published population-based cohort studies and deduced the proportions of SLE deaths for the corresponding years, county/geographic region, and age from the CDC WONDER database. As shown in Table 3, the proportions of SLE deaths in females, Black persons, and Black females were similar or slightly higher in the CDC database than in the DeKalb and Fulton Counties cohort. There were also no statistically significant differences in the portions of SLE deaths in other cohorts versus the CDC database, except for an unusually low SLE death count in Hispanic persons on Medicaid (Table 3). These observations argue against differential underascertainment of SAID deaths by sex and race and ethnicity in national mortality databases in a substantial way.

Population-level mortality rates versus prevalence-adjusted mortality

Mortality rates measure disease burden in the general population but cannot distinguish whether differences in mortality rates are due to differences in the incidence/prevalence of disease or disease severity. This can be addressed by linking mortality data with prevalence data to estimate the mortality rate normalized for prevalence in a specific disease population (ie, case fatality rate).

For SLE, which is nine times more prevalent in females, the predicted annual mortality rate was only 5.3 times higher in females than males,[15] suggesting a relatively higher fatality rate in males with SLE. Consistently, when adjusted for prevalence, the case fatality rate was higher in males than females with SLE (RRS: unpublished observations). Likewise, in DPM, which is two to three times more common in females, the age-standardized mortality rate was only 1.6 times higher in females than males.[25] In SSc, which is four to seven times more prevalent in females, age-standardized mortality rates were only 1.9 to 3.5 times higher in females than males,[7] suggesting worse outcomes in males. Consistently, the median age at death was five years lower for males, and the risk of premature SSc death was higher for males than females (OR 1.8, 95% CI 1.6–2.0).[6] Hence, large population-based prevalence data are needed to address whether changes in SAID mortality rates are due to changing incidence/prevalence or SAID severity.

Underlying versus contributing causes of death in SAIDs

Cause of death is recorded as the underlying or a contributing cause on the death certificate. Because many patients with SAIDs die of complications of disease or of treatment, an SAID is likely to be listed as a contributing, rather than as the underlying, cause of death. For example, of 47,337 deaths from 1999 to 2020 in the United States, SLE was recorded as the underlying cause of death in 57% and as a contributing cause in 43%. These observations advocate using the multiple-causes-of-death database in SAID assessments.

Conclusions

The increasing prevalence of SAIDs calls for action to understand their population-level burden. National mortality databases offer a large reference population to assess disease burden.

Importantly, misclassification of SAIDs in death certificates appears to be rare among decedents who did not have an SAID. Furthermore, underrecording of SAIDs on death certificates, which is substantial, does not differ by sex and race and ethnicity and mostly occurs in older adults with comorbidities. Because an SAID is commonly listed as a contributing, rather than as the underlying, cause of death on death certificates, I suggest using the multiple-causes-of-death database in SAID assessments. Increasing awareness of the importance of death certificates, enhancing certifier-of-death training, timely audits of death certificates, increasing autopsies, and enhancing awareness about the multiorgan and varied complications of SAIDs at the time of death may reduce overall errors on death certificates and help improve SAID recording. Nevertheless, until we have large-scale prospective outcomes data, national mortality statistics offer valuable estimates of SAID burden. An unequal assignment of the national burden of disease may have implications for research and health care allocation of our limited public health dollars.

ACKNOWLEDGMENTS

This article builds on a large amount of work by my colleague Dr Eric Yen and many members of the Autoimmunity and Tolerance Laboratory, including Parmita Das, Margaret Essien, Laura Hernandez, Trennan Lange, Elizabeth Matz, KimNagn Nguyen, Elizabeth Park, Nathan Perez, Snehin Rajkumar, Rohan Sharma, Pranav Singamsetti, Devanshu Singh, and Meifang Wu. I am sincerely grateful to all of them. They have been supported by career development grants, internships, and preceptorships from the National Institutes of Health, Rheumatology Research Foundation, Lupus Foundation of America, American Cancer Society, and University of California, Los Angeles institutional funds.

AUTHOR CONTRIBUTIONS

Dr Singh contributed to at least one of the following manuscript preparation roles: conceptualization AND/OR methodology, software, investigation, formal analysis, data curation, visualization, and validation AND drafting or reviewing/editing the final draft. As corresponding author, Dr Singh confirms that he has provided the final approval of the version to be published and takes responsibility for the affirmations regarding article submission (eg, not under consideration by another journal), the integrity of the data presented, and the statements regarding compliance with institutional review board/Declaration of Helsinki requirements.

REFERENCES

1. Abend AH, He I, Bahroos N, et al. Estimation of prevalence of autoimmune diseases in the United States using electronic health record data. J Clin Invest 2024;135(4):e178722.
2. Miller FW. The increasing prevalence of autoimmunity and autoimmune diseases: an urgent call to action for improved understanding, diagnosis, treatment, and prevention. Curr Opin Immunol 2023;80:102266.
3. Duarte-García A, Hocaoglu M, Valenzuela-Almada M, et al. Rising incidence and prevalence of systemic lupus erythematosus: a population-based study over four decades. Ann Rheum Dis 2022;81(9):1260–1266.
4. Nguyen KP, Yen EY, Li N, Singh RR. The increasing prevalence of SLE, 2001-2011: United States nationwide population-based estimates [abstract]. Lupus Sci Med 2019;6(suppl 1):A127.
5. Elhai M, Meune C, Avouac J, et al. Trends in mortality in patients with systemic sclerosis over 40 years: a systematic review and meta-analysis of cohort studies. Rheumatology (Oxford) 2012;51(6):1017–1026.
6. Singh RR, Singh DR, Yen EY. Worsening premature death burden gap from systemic sclerosis in men and Black persons: a US nationwide population-based study. J Scleroderma Relat Disord 2023;8(1):20–26.
7. Yen EY, Singh DR, Singh RR. Trends in systemic sclerosis mortality over forty-eight years, 1968-2015: a US population-based study. Arthritis Care Res (Hoboken) 2021;73(10):1502–1510.
8. Volkmann ER, Steen V, Li N, et al. Racial disparities in systemic sclerosis: short- and long-term outcomes among African American participants of SLS I and II. ACR Open Rheumatol 2021;3(1):8–16.
9. Taylor T, Anastasiou C, Ja C, et al. Causes of death among individuals with systemic lupus erythematosus by race and ethnicity: a population-based study. Arthritis Care Res (Hoboken) 2023;75(1):61–68.
10. Lim SS, Helmick CG, Bao G, et al. Racial disparities in mortality associated with systemic lupus erythematosus - Fulton and DeKalb Counties, Georgia, 2002-2016. MMWR Morb Mortal Wkly Rep 2019;68(18):419–422.
11. Hocaoğlu M, Valenzuela-Almada MO, Dabit JY, et al. Incidence, prevalence, and mortality of lupus nephritis: a population-based study over four decades using the Lupus Midwest Network. Arthritis Rheumatol 2023;75(4):567–573.
12. Mayes MD, Lacey JV Jr, Beebe-Dimmer J, et al. Prevalence, incidence, survival, and disease characteristics of systemic sclerosis in a large US population. Arthritis Rheum 2003;48(8):2246–2255.
13. Gianfrancesco MA, Dall'Era M, Murphy LB, et al. Mortality among minority populations with systemic lupus erythematosus, including Asian and Hispanic/Latino persons - California, 2007-2017. MMWR Morb Mortal Wkly Rep 2021;70(7):236–239.
14. Gómez-Puerta JA, Barbhaiya M, Guan H, et al. Racial/ethnic variation in all-cause mortality among United States Medicaid recipients with systemic lupus erythematosus: a Hispanic and Asian paradox. Arthritis Rheumatol 2015;67(3):752–760.
15. Yen EY, Shaheen M, Woo JMP, et al. 46-year trends in systemic lupus erythematosus mortality in the United States, 1968 to 2013: a nationwide population-based study. Ann Intern Med 2017;167(11):777–785.
16. Rossen LM, Womack LS, Hoyert DL, et al. The impact of the pregnancy checkbox and misclassification on maternal mortality trends in the United States, 1999-2017. Vital Health Stat 3 2020;(44):1–61.
17. Hamza A. Declining rate of autopsies: implications for anatomic pathology residents. Autops Case Rep 2017;7(4):1–2.
18. Yen EY, Singh RR. Lupus-an unrecognized leading cause of death in young females: a population-based study using nationwide death certificates, 2000-2015. Arthritis Rheumatol 2018;70(8):1251–1255.
19. Bernatsky S, Linehan T, Hanly JG. The accuracy of administrative data diagnoses of systemic autoimmune rheumatic diseases. J Rheumatol 2011;38(8):1612–1616.
20. Coady SA, Sorlie PD, Cooper LS, et al. Validation of death certificate diagnosis for coronary heart disease: the Atherosclerosis Risk in Communities (ARIC) Study. J Clin Epidemiol 2001;54(1):40–50.
21. Falasinnu T, Rossides M, Chaichian Y, et al. Do death certificates underestimate the burden of rare diseases? the example of systemic lupus erythematosus mortality, Sweden, 2001-2013. Public Health Rep 2018;133(4):481–488.

22. Calvo-Alén J, Alarcón GS, Campbell R Jr, et al. Lack of recording of systemic lupus erythematosus in the death certificates of lupus patients. Rheumatology (Oxford) 2005;44(9):1186–1189.
23. Kaysen K, Drenkard C, Bao G, et al. Death certificates do not accurately identify SLE patients [abstract]. Arthritis Rheumatol 2017; 69(suppl 10). https://acrabstracts.org/abstract/death-certificates-do-not-accurately-identify-sle-patients/
24. Molina E, del Rincon I, Restrepo JF, et al. Mortality in rheumatoid arthritis (RA): factors associated with recording RA on death certificates. BMC Musculoskelet Disord 2015;16(1):277.
25. Matz E, Singh RR. Trends in dermatopolymyositis mortality, 1999-2022: a nationwide population-based study, United States. Arthritis Care Res (Hoboken) Published online July 14, 2025. doi: https://doi.org/10.1002/acr.25609

American College of Rheumatology
Empowering Rheumatology Professionals

Arthritis & Rheumatology
Vol. 78, No. 5, May 2026, pp 1038–1044
DOI 10.1002/art.43445

Are Glucocorticoids Associated With Worse Survival Among Patients With Rheumatoid Arthritis and Lung Cancer Treated With Immune Checkpoint Inhibitors?

Deanna Jannat-Khah,[1,2] Jeffrey R. Curtis,[3,4] Fenglong Xie,[4] Ashish Saxena,[5] and Anne R. Bass[1,2]

Objective. Glucocorticoids are commonly used for rheumatoid arthritis (RA) treatment and to palliate some malignancies, but it is unclear whether glucocorticoids attenuate the benefits of immune checkpoint inhibitor (ICI) cancer therapy. We examined the association between glucocorticoid use and survival among ICI-treated patients with RA and metastatic nonsmall cell lung cancer (mNSCLC).

Methods. A cohort of patients with RA enrolled in Medicare were identified based on the following: age ≥66 years, RA diagnosed before mNSCLC, and having initiated nivolumab, pembrolizumab, or atezolizumab (2015–2019, when approved only for mNSCLC). Landmark Kaplan-Meier curves and time-varying adjusted Cox models were used to examine the association between early glucocorticoid use (within 91 days after ICI initiation) and survival. Dexamethasone users were excluded from the primary analysis and included in a sensitivity analysis.

Results. We identified 663 ICI-treated patients with RA and mNSCLC, with a mean age of 75 years, 86.9% being White, 64.7% being female, and 363 (46%) receiving glucocorticoids. Among users, the median average prednisone equivalents was 6.59 mg/d (interquartile range 3.30, 12.31). In a time-varying Cox model, glucocorticoid use was not associated with survival. Additionally, in a 91-day landmark model, glucocorticoid dose was not associated with survival (hazard ratio 1.01; 95% confidence interval 0.93, 1.10).

Conclusion. Glucocorticoids, at the dosages used to treat ICI-treated patients with RA and mNSCLC, had a negligible effect on survival in the 91 days after ICI initiation.

INTRODUCTION

Patients with autoimmune diseases such as rheumatoid arthritis (RA) were excluded from oncology clinical trials of immune checkpoint inhibitors (ICIs)[1] for fear they would experience exacerbations of their autoimmune disease or excessive immune related adverse events (irAEs). As the use of ICIs for cancer becomes standard of care, however, more patients with RA are receiving ICIs. In fact, 5.9% of patients with nonsmall cell lung cancer (NSCLC) treated with ICIs have pre-existing RA.[2] It is estimated that about 14% of patients with lung cancer and an autoimmune disease receive concomitant glucocorticoid treatment for management of their underlying autoimmune disease,[1,3] and an important evidence gap is whether glucocorticoid use interferes with the efficacy of ICIs. There are only a few studies that have investigated concomitant glucocorticoid use among patients with pre-existing autoimmune disease on ICIs, and most are retrospective cohorts that include a mixture of cancers and/or a mixture of autoimmune diseases. Results from these studies are conflicting and encompass a wide range of glucocorticoid dosages given the heterogeneity of the autoimmune diseases they are being used to treat.[3–6] These inherent biases, including small sample size and inclusion of multiple autoimmune diseases and/or multiple cancers, lead to substantial heterogeneity in the populations studied and uncertain generalizability of these studies' results with poor precision.

Supported by the Hospital for Special Surgery's Department of Medicine Discovery Grant (to Dr Jannat-Khah), and analytic infrastructure for this analysis was supported by the National Institute of Arthritis and Musculoskeletal and Skin Diseases, NIH (P30-AR-072583 to Dr Curtis).

[1]Department of Medicine, Division of Rheumatology, Hospital for Special Surgery, New York, New York; [2]Department of Medicine, Division of Rheumatology, Weill Cornell Medicine, New York, New York; [3]Division of Clinical Immunology and Rheumatology, University of Alabama at Birmingham; [4]Foundation for Advancing Science, Technology, Education and Research, Birmingham, Alabama; [5]Department of Medicine, Division of Hematology and Medical Oncology, Weill Cornell Medicine, New York, New York.

Additional supplementary information cited in this article can be found online in the Supporting Information section (https://acrjournals.onlinelibrary.wiley.com/doi/10.1002/art.43445).

Author disclosures are available at https://onlinelibrary.wiley.com/doi/10.1002/art.43445.

Address correspondence via email to Deanna Jannat-Khah, DrPH, MSPH, at jannatkhahd@hss.edu.

Submitted for publication May 19, 2025; accepted in revised form October 10, 2025.

Currently, it is unknown whether glucocorticoid use among ICI-treated patients with RA and cancer could interfere with the benefits of ICIs as cancer therapies. Additionally, it is unknown what a "safe" daily dosage of glucocorticoid might be in ICI-treated patients with RA that would have limited or no impact on mortality. To address these unanswered questions, we investigated the association between glucocorticoid use after ICI initiation and overall survival in patients with a single autoimmune disease (RA) and a single cancer (NSCLC) in a large real-world data set.

PATIENTS AND METHODS

Study population. This retrospective cohort studied Medicare fee-for-service patients ≥66 years of age with two diagnoses made by an oncologist for a malignant neoplasm of lung and bronchus (*International Classification of Diseases, Ninth Revision* [ICD-9] 162.9, ICD-10 C34.X) and treated with an ICI. Specifically, patients had to have initiated treatment with nivolumab between March 4, 2015 and August 16, 2018, pembrolizumab between October 2, 2015 and April 11, 2019, or atezolizumab between October 18, 2015 and March 18, 2019. These periods reflect the US Food and Drug Administration (FDA) approval for ICI treatment for metastatic NSCLC (mNSCLC) and preceded the first FDA approval for stage III disease (May 2020) or for small cell lung cancer.[7,8] As there is no ICD-9 or ICD-10 code to indicate cancer stage or subtype in this data set, this restriction serves as an effective proxy for metastatic (stage IV) NSCLC, allowing us to homogenize cancer type and stage. Patients who initiated treatment with durvalumab (only approved for stage III disease) or cemiplimab, approved in 2021, were not included in the cohort. Additionally, patients were excluded if they had a history of other cancer types. All patients had at least one year of continuous enrollment in Medicare with part A, B, and D for one year prior and one year after ICI initiation, unless they died. Patients were followed through December 31, 2019 or until death. All available prior data were used to determine the line of therapy (ICI as first line vs prior receipt of chemotherapy, ie, second or later line of therapy). We excluded patients treated with dexamethasone from our primary analysis because dexamethasone is typically used for cancer palliation rather than RA or irAE treatment but included dexamethasone-treated patients in a sensitivity analysis.

Data source and definition of exposure. Fee-for-service Medicare claims from the Centers for Medicare and Medicaid Services (CMS) Chronic Conditions Data Warehouse that consisted of a 100% sample of patients with RA were used to create the analytic data set. Patients with RA were defined as having two Medicare claims at least 30 days apart associated with an ICD-9 or ICD-10 diagnosis code for RA (714.XX, M05.*, M06.*, except M06.1 and M06.4) from a rheumatologist and a claim for any disease-modifying antirheumatic drug (DMARD) before initiation of an ICI.[9] The accuracy of this definition exceeds 85%.[9] Allowable DMARDs included conventional synthetic DMARDs (methotrexate, leflunomide, hydroxychloroquine, sulfasalazine), biologic DMARDs (etanercept, adalimumab, infliximab, golimumab, certolizumab, tocilizumab, sarilumab, abatacept, rituximab), or targeted synthetic DMARDs (tofacitinib, upadacitinib, baricitinib). Oral glucocorticoid use during the 91 days before and after ICI initiation was calculated by determining the total cumulative dosage and dividing it by the number of days prescribed and then converted into the average daily prednisone equivalent dose. Patients who were on glucocorticoids before ICI initiation and continued them were included in the glucocorticoid group. A variable for any dexamethasone use (yes/no) during the 91 days after ICI initiation was created.

Covariates. Demographic variables such as age, sex, and race and ethnicity were included. An Elixhauser comorbidity score was calculated with an algorithm based on ICD-9 and ICD-10 codes in the 12 months before ICI initiation.[10] Chronic lung disease was defined using ICD-9 and ICD-10 codes for interstitial lung disease and chronic obstructive pulmonary disease. Additionally, the following cancer treatment characteristics were examined: radiation (yes/no) and chemotherapy procedures, kinase inhibitors, and antiangiogenic therapy (defined as chemotherapy yes/no). Healthcare Common Procedure Codes and National Drug Codes were used to identify cancer treatments, glucocorticoids, and DMARDs.

Primary outcome. Overall survival was the primary outcome. Recorded date of death from Medicare files was used to define death. In survival analyses, time was defined from ICI initiation to date of death or censoring (December 31, 2019).

Statistical methods. Frequencies, means, SDs, medians, and interquartile ranges (IQRs) were calculated via descriptive statistics. *P* values were calculated using χ^2 tests, *t*-tests, and Wilcoxon rank sum tests as appropriate. Kaplan–Meier curves were generated, and the log rank test was performed to determine if the Kaplan–Meier curves were different. We took two approaches to investigate the association between glucocorticoid use and overall survival. First, we investigated the association between glucocorticoid use in the first 91 days after ICI initiation and survival, using a time-varying adjusted Cox proportional hazard model. Second, we used a 91-day landmark Cox proportional hazard model. Landmark and time-varying adjusted Cox proportional hazard models were performed to allow for post-ICI characterization of glucocorticoid dose and to avoid immortal time bias. Immortal time bias occurs when patients are classified in treatment groups based on their future exposure. For the time-varying analysis, glucocorticoid use was evaluated in four different lagged time segments (–30 days to ICI initiation, 0–30 days after ICI

initiation, 31–60 days after ICI initiation, and 60–90 days after ICI initiation) and was allowed to vary over time. The data were set up so that there were four periods of time (four rows per person), and glucocorticoid use in the previous 30 days was included in the model as a categorized variable: none, 0 to 4.9 mg, 5 to 9.9 mg, and >10 mg. In this analysis, the primary outcome was survival within the first 91 days. We also analyzed overall survival over all time. In the landmark analysis, patients had to survive 91 days after ICI initiation to be included, at which time follow-up began. To be classified as a glucocorticoid user, they had to have a glucocorticoid prescription during the first 91-day period. Patients who had a dexamethasone prescription were excluded from the main analysis. A separate sensitivity landmark analysis was conducted that included dexamethasone users. Model covariates were selected based on subject matter expertise, and models controlled for age, race, sex, Hispanic ethnicity, year of ICI initiation, previous radiation treatment ever (yes or no), the modified Elixhauser comorbidity composite score (which removed RA, chronic obstructive pulmonary disease, and cancer), type of first- or second-line ICI treatment (using all available prior data), ICI monotherapy or ICI with concomitant chemotherapy, and chronic lung disease. Variables were removed from the model if they violated the proportional hazards assumption and were simultaneously not statistically significant.

Schoenfeld residuals were used to test the proportional hazard assumption. SAS version 9.4 (SAS Institute Inc) and Stata version 18.0 (StataCorp LLC) were used for analysis. An alpha of 0.05 was used to determine statistical significance. The institutional review board at the Hospital for Special Surgery determined that the study was exempt. The institutional review boards at the University of Alabama at Birmingham and at the Foundation for Advancing Science, Technology, Education and Research (FASTER) Medicine have approved this study. Data are available from CMS.

RESULTS

The cohort included 663 patients with RA and mNSCLC (after exclusion of 116 patients with RA treated with dexamethasone). Overall, the mean age was 75 (SD 7) years, 86.9% were White, and 64.7% were female. Despite all patients with RA having received DMARDs before ICI initiation as an inclusion criterion for the cohort, few patients with RA (4.2%) received DMARDs after ICI initiation. A history of chronic lung disease was present in 45.9% of patients. Based on the Elixhauser score, patients had a median of 2 (IQR 1.26, 2.6) comorbidities. In 2015, 5% of patients with mNSCLC initiated ICI treatment when it was first approved for metastatic/stage 4 NSCLC, increasing to 26.5% in 2016, 30.5% in 2017, 29.9% in 2018, and 7.5% in 2019 (the "drop" in 2019 reflects the fact that we excluded patients started on an ICI after it became FDA approved for earlier-stage NSCLC). A majority (60.8%) had ICI treatment as second-line therapy. Most of the patients, 78.3%, died during follow-up, and median time from ICI initiation to death was 217 (IQR 75, 452) days (Table 1).

Comparing glucocorticoid users versus nonusers. Among the 663 patients with RA, 368 (55.5%) were treated with glucocorticoids in the first 91 days after ICI initiation. Of these, 70% (258 of 368) were on glucocorticoids before ICI initiation and continued them, suggesting that glucocorticoids were being used to treat RA. The remainder (110 of 368) initiated glucocorticoids after ICI initiation. Similar to the overall RA cohort, glucocorticoid users had a mean age of 74.7 (SD 7) years, 88.6% were White, and 61.1% were female (Table 1). The median average daily glucocorticoid dose in the 91 days after ICI initiation among glucocorticoid users was 6.59 (IQR 3.30, 12.31) mg/day. Comparing patients with RA prescribed versus not prescribed glucocorticoids, there were no difference in demographics (except sex), DMARD use, chronic lung disease, and number of comorbidities using the Elixhauser score. There was no significant difference in the year of ICI initiation between glucocorticoid users and nonusers. However, glucocorticoid-treated patients had a significantly longer time from ICI initiation to death (median 247.5 [IQR 106, 482] days) compared to patients who did not take glucocorticoids (median 175 [IQR 48, 386] days) ($P < 0.001$; Table 1).

Time-varying model of glucocorticoid use and survival. To evaluate the association between glucocorticoid use in the first 91 days after ICI initiation and overall survival, a time-varying adjusted Cox model was performed. In this model, glucocorticoid use at any dose was not associated with overall survival (Table 2). Specifically, compared to no glucocorticoids, 0 to 4.9 mg (adjusted hazard ratio [aHR] 1.00; 95% confidence interval [CI] 1.00, 1.00; $P = 0.683$), 5 to 9.9 mg (aHR 1.00; 95% CI 1.00, 1.00; $P = 0.590$), and ≥10 mg (aHR 1.00; 95% CI 1.00, 1.00; $P = 0.640$) were not associated with survival. Female sex (aHR 0.81; 95% CI 0.68, 0.98) and lung disease (aHR 0.74; 95% CI 0.62, 0.89) were associated with better overall survival, and Elixhauser score (aHR 1.22; 95% CI 1.11, 1.34) was associated with worse overall survival (Table 2).

91-day landmark analysis. Figure 1 displays the Kaplan–Meier analysis of overall survival comparing glucocorticoid use (defined as yes/no) in the first 91 days of ICI treatment. There is no significant relationship between glucocorticoid use in the first 91 days after ICI initiation and overall survival after 91 days (log rank $P = 0.47$). Supplemental Table 1 displays the characteristics of the cohort that survived at least 91 days (n = 495). Other than female sex and ICI duration, there were no statistically significant differences between the no glucocorticoid and glucocorticoid groups. In the 91-day landmark multivariable Cox proportional hazard model, there was no association between average daily steroid dose and overall survival (aHR 1.01; 95% CI 0.93, 1.10). However, Elixhauser score was associated with worse overall

Table 1. Demographic and clinical characteristics in patients with rheumatoid arthritis and nonsmall cell lung cancer treated with ICIs from Medicare fee-for-service claims data*

Factor	Total n (%)	No glucocorticoids in the first 91 days n (%)	Glucocorticoids in the first 91 days n (%)	*P* value
n	663	295 (44.5)	368 (55.5)	
Age, mean (SD), y	75 (7)	75.3 (6.9)	74.7 (7)	0.23
White race	576 (86.9)	250 (84.7)	326 (88.6)	0.15
Hispanic ethnicity	23 (3.5)	11 (3.7)	12 (3.3)	0.31
Female	429 (64.7)	204 (69.2)	225 (61.1)	0.032
Chronic lung disease[a]	304 (45.9)	131 (44.4)	173 (47)	0.5
DMARDs in the 91 days after ICI initiation	28 (4.2)	<11	Redacted[b]	0.18
Modified Elixhauser score, median (IQR)	2 (1.2, 2.6)	2 (1.2, 2.6)	1.8 (1.2, 2.6)	0.57
Radiation ever	430 (64.9)	195 (66.1)	235 (63.9)	0.55
Second-line therapy	403 (60.8)	169 (57.3)	234 (63.6)	0.099
ICI plus chemotherapy	84 (12.7)	48 (16.3)	36 (9.8)	0.013
ICI duration, median (IQR), days	91 (21, 247)	94 (0, 265)	91 (29, 243)	0.19
Death	519 (78.3)	236 (80)	283 (76.9)	0.34
Time from ICI initiation to death, median (IQR), days	217 (75, 452)	175 (48, 386)	247.5 (106, 482)	<0.001
Glucocorticoid use in the 91 days *after* ICI initiation				
Any glucocorticoid use	363 (55.5)	N/A	363 (100)	N/A
Average glucocorticoid dose, median (IQR)	6.59 (3.30, 12.31)	N/A	6.59 (3.30, 12.31)	N/A

* Unknown or missing values: race n = 36 (4.7%); Hispanic ethnicity n = 70 (9%). COPD, chronic obstructive pulmonary disease; DMARD, disease-modifying antirheumatic drug; ICI, immune checkpoint inhibitor; ILD, interstitial lung disease; IQR, interquartile range.
[a] Chronic lung disease is defined as ILD or COPD.
[b] Per the data use agreement with the Centers for Medicare and Medicaid, values less than 11 are not reported.

survival (aHR 1.25; 95% CI 1.08, 1.44; Table 3). In two additional 91-day landmark Cox models, we found no association between overall survival and glucocorticoid dose above 10 mg or glucocorticoid dose categorized by quartiles (Supplemental Tables 2 and 3).

We investigated the physician specialty that prescribed the glucocorticoids after ICI initiation and found that 37.8% were prescribed by oncologists, 22.7% by rheumatologists, 18.6% by internal medicine/hospitalist/general medicine, 14% by nurses or physician assistants, and 6.9% by other specialties including cardiology, endocrinology, geriatrics, gastroenterology, dermatology, critical care, urology, nephrology, and others.

Table 2. Time-varying Cox proportional hazard model for overall survival in ICI-treated patients with rheumatoid arthritis and nonsmall cell lung cancer in the first 91 days after ICI initiation*

Variable	Hazard ratio (95% confidence interval)
Glucocorticoid dose[a]	
None	Reference
0–4.9 mg	1.00 (1.00, 1.00)
5–9.9 mg	1.00 (1.00, 1.00)
≥10 mg	1.00 (1.00, 1.00)
Age (5-y interval)	0.99 (0.93, 1.05)
Female sex	**0.81 (0.68, 0.98)**
Lung disease (COPD or ILD)	**0.74 (0.62, 0.89)**
ICI + chemotherapy	1.23 (0.92, 1.63)
Elixhauser score (5-point interval)	**1.22 (1.11, 1.34)**
Second-line ICI therapy	1.17 (0.97, 1.41)

* Glucocorticoids dose was assessed in 4 different 30 day time periods and varied over time. Race, Hispanic ethnicity, radiation, year of ICI initiation, ILD, and COPD were removed from the model as they were not statistically significant. Bolded values indicate statistical significance at the 0.05 level. COPD, chronic obstructive pulmonary disease; ICI, immune checkpoint inhibitor; ILD, interstitial lung disease.
[a] Time-varying covariate: *P* values were not statistically significant for 0–4.9 mg (*P* = 0.683), 5–9.9 mg (*P* = 0.590), and ≥10 mg (*P* = 0.640).

Sensitivity analysis including all glucocorticoid users (dexamethasone included). In a sensitivity analysis, we included the n = 116 patients who were treated with dexamethasone in the glucocorticoid cohort. Supplemental Table 4 displays comparisons between the dexamethasone users and nonusers. Compared to non-dexamethasone–treated patients, dexamethasone users were slightly younger, had a mean age of 73 years versus 74.98 years (*P* = 0.008), had fewer comorbidities (median 1.6 [IQR 1, 2.4] vs median 2 [IQR 1.2, 2.6]; *P* = 0.004), were less likely to have ICIs as second-line therapy (47.4% vs 60.8%; *P* = 0.007), and were more likely to be receiving concomitant chemotherapy (30.2% vs 12.7%; *P* < 0.001) (Supplemental Table 5). Dexamethasone users had a 48% shorter time to death (median 153 [IQR 85, 347] vs 217 [IQR75, 452] days).

In a Kaplan-Meier curve, glucocorticoid use (including dexamethasone and defined as yes/no) in the first 91 days of ICI treatment was associated with a nonsignificant trend toward worse overall survival (Supplemental Figure 1). In a separate, 91-day landmark Kaplan-Meier curve, dexamethasone use was associated with significantly worse survival compared to nonusers (log rank *P* = 0.02; Supplemental Figure 2). In an adjusted landmark Cox proportional hazard model, dexamethasone use (defined as yes/no) was associated with worse overall survival (aHR 1.48; 95% CI [1.09, 2.02]; Supplemental Table 4).

We investigated the physician specialty that prescribed dexamethasone and found that 76.1% of prescriptions were from

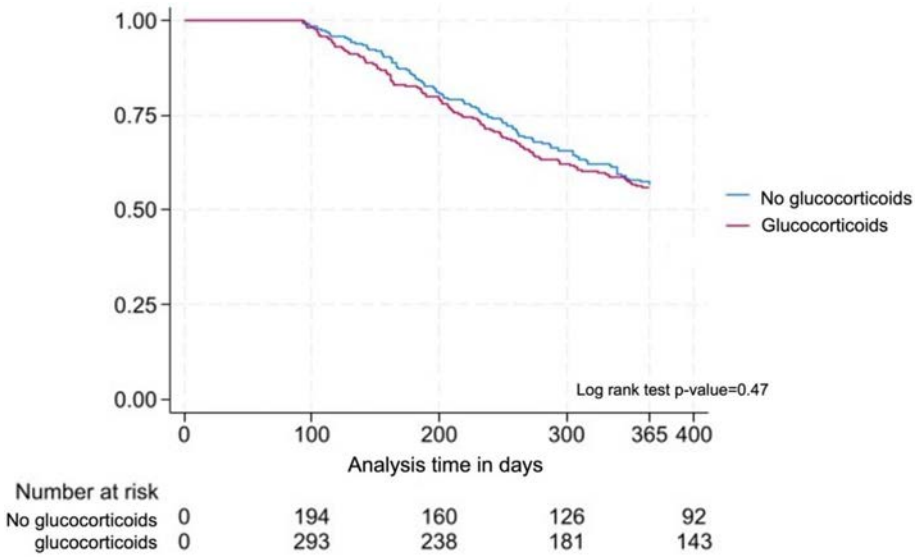

Figure 1. 91-day landmark Kaplan–Meier curve by glucocorticoid exposure in the first 91 days after ICI initiation. ICI, immune checkpoint inhibitor.

oncologists, 10.3% from physician assistants/nurse practitioners, 9.3% from internal medicine/hospitalist/general medicine, 2.6% from rheumatologists, and 1.4% from a hospice provider, lending credence to the idea that dexamethasone was being prescribed for cancer palliation.

DISCUSSION

In this observational study of 663 ICI-treated patients with pre-existing RA and mNSCLC, we demonstrated that glucocorticoids (exclusive of dexamethasone) had no adverse effect on overall survival after controlling for covariates. Of note, the dose of non-dexamethasone glucocorticoids used in these patients with RA was low, a median of only 6.6 mg/day.

Table 3. 91-day landmark Cox proportional hazard model for overall survival in ICI-treated patients with rheumatoid arthritis and nonsmall-cell lung cancer*

Variable	Hazard ratio [95% confidence interval]
Age (5-y interval)	0.92 (0.84, 1.01)
Female sex	0.78 (0.59, 1.04)
Lung disease (COPD or ILD)	0.83 (0.63, 1.10)
DMARD use in 91 days after ICI initiation	0.83 (0.43, 1.59)
ICI + chemotherapy	0.98 (0.57, 1.68)
Elixhauser score (5-point interval)	**1.25 (1.08, 1.44)**
Second-line ICI therapy	1.16 (0.86, 1.55)
Average daily glucocorticoid dose (5-mg increments)	1.01 (0.93, 1.10)

* Values are the hazard ratio (95% confidence interval). Race, Hispanic ethnicity, radiation, year of ICI initiation, ILD, and COPD were removed from the model as they were not statistically significant. Bolded values indicate statistical significance at the 0.05 level. COPD, chronic obstructive pulmonary disease; DMARD, disease-modifying antirheumatic drug; ICI, immune checkpoint inhibitor; ILD, interstitial lung disease. Dexamethasone users were excluded from this model.

There is concern that the use of glucocorticoids could diminish the positive effect of ICI treatment. Glucocorticoids induce apoptosis of T cells, which could lead to a reduction in T lymphocytes generally, and of CD8 positive T cells specifically, potentially reducing the effect of ICI treatment.[11–13] Skribek et al found that glucocorticoids prescribed for irAEs were not associated with death, whereas glucocorticoids prescribed for palliation were.[14] There is some evidence that irAEs are associated with better survival[15] and that steroids may blunt that benefit[15,16]; however in our study, the median glucocorticoid dose was 6.6 mg, suggesting that it was being used to treat RA rather than an irAE. Although we cannot determine from the data the reason for the glucocorticoid prescription, the prescriber specialty could give us some insight. We found that 37.8% of prescriptions were from oncologists, 22.7% from rheumatologists, and 6.9% from various specialties that included small portion of critical care and palliative medicine. In studies of glucocorticoids used to treat irAEs, high doses (eg, 160 mg vs 40 mg) have been shown to be associated with worse overall survival.[17] In patients with RA, lower doses of glucocorticoids are typically used, and the rheumatologist may have other treatment options, even in the ICI setting (eg, conventional or biologic DMARDs). In our study the median glucocorticoid dose was only 6.59 mg/day (IQR 3.29, 12.25) in prednisone equivalents, which supports the theory that glucocorticoids were being used to treat RA flares. Thirty percent of patients with RA initiated glucocorticoids after ICI initiation, which corresponds to the rate of RA flares after ICI initiation identified by McCarter et al.[18]

Some studies suggest that timing of glucocorticoid administration may influence their association with overall survival.[11,19,20] For example, one study found that patients had worse overall

survival if they initiated glucocorticoids within the first 30 days after ICI initiation.[21] Similarly, Arbour et al found that baseline (at the time of ICI initiation) glucocorticoid use was associated with worse progression-free survival and overall survival.[12] These studies did not distinguish between the type of glucocorticoids or the indication for their use. These results differ from ours, as we found no association between glucocorticoid use in the first 91 days after ICI initiation and overall survival (after excluding dexamethasone).

Previously, we demonstrated that few patients with RA in this cohort were on DMARDs before ICI initiation.[22] In this study, we found that only 4.4% of patients with RA were treated with DMARDs in the first 91 days after ICI initiation. This may explain why 54.8% of the patients were on glucocorticoids, a much higher percentage than among patients with RA outside the cancer context.[23] Presumably, glucocorticoids could have been used for their RA or potentially for new-onset irAEs.

Our study has several limitations. As we used Medicare claims data, patients were older, which could reduce generalizability. However, based on population-based data for NSCLC, 71.6% of patients with NSCLC are 65 years of age or older.[2] With this in mind, we believe that usage of the Medicare data reflects the experience of a majority of patients with NSCLC in the United States. Cancer specific information, such as cancer stage or cancer type, is not included in Medicare claims data; however, we only included people who initiated ICIs during the time that the FDA approved ICIs for metastatic/stage IV disease to homogenize these factors. As an alternative data source, the Surveillance, Epidemiology, and End Results Program–Medicare 5% database does include information about cancer stage, but the Medicare 5% sample does not have enough patients with pre-existing RA and mNSCLC to adequately power this study.[24] Another limitation is the potential for misclassification of glucocorticoid use in the time-varying Cox proportional hazard models. All available prescription data from Medicare part D were used to minimize misclassification. Patients could also have been prescribed non-dexamethasone glucocorticoids for palliation or for management of cancer manifestations, for example, brain metastases, dyspnea, or fatigue,[11,12,14,21] which even if occurring in sizable numbers of patients, likely would not have changed our results. Our study did include patients who were already on glucocorticoids before ICI initiation (median 10 [IQR 5, 16.7] mg); however, we have previously demonstrated that non-dexamethasone glucocorticoids in the three months before ICI initiation are not associated with worse survival in patients with NSCLC.[22] Finally, we could not account for smoking in our cohort as identification of tobacco use is difficult in claims data.[25] In conclusion, glucocorticoids, which were largely prescribed at low doses, were not associated with worse overall survival in ICI-treated patients with NSCLC and RA.

AUTHOR CONTRIBUTIONS

All authors contributed to at least one of the following manuscript preparation roles: conceptualization AND/OR methodology, software, investigation, formal analysis, data curation, visualization, and validation AND drafting or reviewing/editing the final draft. As corresponding author, Dr Jannat-Khah confirms that all authors have provided the final approval of the version to be published and takes responsibility for the affirmations regarding article submission (eg, not under consideration by another journal), the integrity of the data presented, and the statements regarding compliance with institutional review board/Declaration of Helsinki requirements.

REFERENCES

1. Remon J, Vilariño N, Reguart N. Immune checkpoint inhibitors in non-small cell lung cancer (NSCLC): approaches on special subgroups and unresolved burning questions. Cancer Treat Rev 2018;64:21–29.
2. Cancer Stat Facts: Lung and Bronchus Cancer. SEER. Accessed October 20, 2022. https://seer.cancer.gov/statfacts/html/lungb.html
3. Khan SA, Pruitt SL, Xuan L, et al. Prevalence of autoimmune disease among patients with lung cancer: implications for immunotherapy treatment options. JAMA Oncol 2016;2(11):1507–1508.
4. Byeon S, Cho JH, Jung HA, et al. PD-1 inhibitors for non-small cell lung cancer patients with special issues: real-world evidence. Cancer Med 2020;9(7):2352–2362.
5. McCarter KR, Arabelovic S, Wang X, et al. Immunomodulator use, risk factors and management of flares, and mortality for patients with pre-existing rheumatoid arthritis after immune checkpoint inhibitors for cancer. Semin Arthritis Rheum 2024;64:152335.
6. Pan EY, Merl MY, Lin K. The impact of corticosteroid use during anti-PD1 treatment. J Oncol Pharm Pract 2020;26(4):814–822.
7. FDA approves nivolumab plus ipilimumab for first-line mNSCLC (PD-L1 tumor expression ≥1%). FDA. Published May 15, 2020. Accessed July 3, 2024. https://www.fda.gov/drugs/resources-information-approved-drugs/fda-approves-nivolumab-plus-ipilimumab-first-line-mnsclc-pd-l1-tumor-expression-1
8. FDA approves nivolumab plus ipilimumab and chemotherapy for first-line treatment of metastatic NSCLC. FDA. Updated May 27, 2020. Accessed July 3, 2024. https://www.fda.gov/drugs/resources-information-approved-drugs/fda-approves-nivolumab-plus-ipilimumab-and-chemotherapy-first-line-treatment-metastatic-nsclc
9. Chung CP, Rohan P, Krishnaswami S, et al. A systematic review of validated methods for identifying patients with rheumatoid arthritis using administrative or claims data. Vaccine 2013;31(suppl 10):K41–K61.
10. Quan H, Sundararajan V, Halfon P, et al. Coding algorithms for defining comorbidities in ICD-9-CM and ICD-10 administrative data. Med Care 2005;43(11):1130–1139.
11. Passiglia F, Cetoretta V, De Filippis M, et al. Exploring the immune-checkpoint inhibitors' efficacy/tolerability in special non-small cell lung cancer (NSCLC) populations: focus on steroids and autoimmune disease. Transl Lung Cancer Res 2021;10(6):2876–2889.
12. Arbour KC, Mezquita L, Long N, et al. Impact of baseline steroids on efficacy of programmed cell death-1 and programmed death-ligand 1 blockade in patients with non-small-cell lung cancer. J Clin Oncol 2018;36(28):2872–2878.
13. Svaton M, Zemanova M, Zemanova P, et al. Impact of concomitant medication administered at the time of initiation of nivolumab therapy on outcome in non-small cell lung cancer. Anticancer Res 2020;40(4):2209–2217.
14. Skribek M, Rounis K, Afshar S, et al. Effect of corticosteroids on the outcome of patients with advanced non-small cell lung cancer treated with immune-checkpoint inhibitors. Eur J Cancer 2021;145:245–254.
15. Wolchok JD, Chiarion-Sileni V, Rutkowski P, et al; CheckMate 067 Investigators. Final, 10-year outcomes with nivolumab plus ipilimumab in advanced melanoma. N Engl J Med 2025;392(1):11–22.

16. Verheijden RJ, van Eijs MJM, May AM, et al. Immunosuppression for immune-related adverse events during checkpoint inhibition: an intricate balance. NPJ Precis Oncol 2023;7(1):41.
17. Verheijden RJ, de Groot JS, Fabriek BO, et al. Corticosteroids for immune-related adverse events and checkpoint inhibitor efficacy: analysis of six clinical trials. J Clin Oncol 2024;42(31):3713–3724.
18. McCarter KR, Wolfgang T, Arabelovic S, et al. Mortality and immune-related adverse events after immune checkpoint inhibitor initiation for cancer among patients with pre-existing rheumatoid arthritis: a retrospective, comparative, cohort study. Lancet Rheumatol 2023;5(5):e274–e283.
19. Fucà G, Galli G, Poggi M, et al. Modulation of peripheral blood immune cells by early use of steroids and its association with clinical outcomes in patients with metastatic non-small cell lung cancer treated with immune checkpoint inhibitors. ESMO Open 2019;4(1):e000457.
20. Ricciuti B, Dahlberg SE, Adeni A, et al. Immune checkpoint inhibitor outcomes for patients with non-small-cell lung cancer receiving baseline corticosteroids for palliative versus nonpalliative indications. J Clin Oncol 2019;37(22):1927–1934.
21. Scott SC, Pennell NA. Early use of systemic corticosteroids in patients with advanced NSCLC treated with nivolumab. J Thorac Oncol 2018;13(11):1771–1775.
22. Jannat-Khah DP, Xie F, Saxena A, et al. Survival in immune checkpoint inhibitor-treated patients with rheumatoid arthritis and non-small cell lung cancer: an observational cohort study. Arthritis Care Res (Hoboken) 2025;77(10):1214–1221.
23. Burmester GR, Pope JE. Novel treatment strategies in rheumatoid arthritis. Lancet 2017;389(10086):2338–2348.
24. SEER-Medicare: Brief Description of the SEER-Medicare Database. National Cancer Institute. Updated May 16, 2019. Accessed July 3, 2024. https://healthcaredelivery.cancer.gov/seermedicare/overview/
25. Desai RJ, Solomon DH, Shadick N, et al. Identification of smoking using Medicare data–a validation study of claims-based algorithms. Pharmacoepidemiol Drug Saf 2016;25(4):472–475.

Arthritis & Rheumatology
Vol. 78, No. 5, May 2026, pp 1045–1061
DOI 10.1002/art.70020

American College of Rheumatology
Empowering Rheumatology Professionals

Plasma Proteomics Identifies Thousand-and-One–Amino Acid Kinase 3 as a Potential Biomarker of Rheumatoid Arthritis Activity and a Novel Therapeutic Target

Pengfei Xin,[1,2,3] Wenzhen Li,[4] Xinyu A,[1,2] Jun Shen,[1,2] Xiaohui Meng,[5] Yanqin Bian,[1,2] Haihui Han,[5] Zheng Xiang,[1,2] Lei Ran,[1] Songtao Sun,[1] Jun Xie,[1] Tao Yue,[1] Qi Zhu,[1] Xiaoming Zhang,[6] Lu Xie,[4] and Lianbo Xiao[1,2]

Objective. Bone destruction associated with active rheumatoid arthritis (RA) remains a major therapeutic challenge, with a lack of reliable molecular markers reflecting bone injury. This study aims to identify novel biomarkers linked to bone destruction in active RA through proteomic analysis, providing new strategies for precise monitoring and targeted therapy.

Methods. Data-independent acquisition mass spectrometry was used for proteomic quantification and bioinformatic analysis on plasma samples from 160 patients with RA and 40 healthy controls. Key proteins associated with bone destruction were screened by integrating Sharp scores with synovial single-cell RNA sequencing data and subsequently validated in two independent cohorts (N_1 = 50 and N_2 = 10) using enzyme-linked immunosorbent assay and multiplex immunohistochemistry. Functional studies were conducted using fibroblast-like synoviocytes (FLSs) in vitro and a collagen-induced arthritis (CIA) mouse model in vivo.

Results. A total of 4,998 plasma proteins were identified, with 506 showing significant differential expression between active and remitted RA. Thousand-and-one–amino acid kinase 3 (TAOK3) levels were positively associated with Sharp scores and markedly elevated in patients with active RA. Combining TAOK3 with C-reactive protein improved diagnostic accuracy for active RA (area under the curve = 0.915). High TAOK3 expression was also associated with increased relapse frequency. Functional studies showed that TAOK3 knockdown suppressed the tumor-like phenotype of FLSs and down-regulated matrix metalloproteinase 1/2/3 and cathepsin K, whereas TAOK3 overexpression promoted pannus cell–mediated bone erosion, mitigated by TAOK3-targeted inhibitor. In vivo, its inhibition showed therapeutic effects in CIA mice.

Conclusion. TAOK3 serves as a potential biomarker for bone destruction in active RA and as a therapeutic target for precision monitoring and intervention.

INTRODUCTION

Rheumatoid arthritis (RA) is a chronic autoimmune disease with a global prevalence of approximately 0.25% to 1%,[1,2] characterized by systemic inflammation and joint destruction. Without standardized treatment, RA can lead to severe joint deformities, functional disabilities, and significantly reduced quality of life.[2–4] Bone destruction, including bone erosion and periarticular osteoporosis, is a hallmark pathologic feature of RA, causing irreversible joint damage with profound clinical consequences.[5] Although early diagnosis and the use of disease-modifying antirheumatic drugs (DMARDs) have shown potential to control

Supported by the National Natural Science Foundation of China (grants 82474302 and 92474203), the Shanghai Science and Technology Commission Support Project (grants 23Y11921900, 22490760100, and 23XD1404300), the Key Specialty Construction Project of the Changning District Health Commission of Shanghai (project 20231003), and the Changning National Master of Traditional Chinese Medicine Studio.

[1]Guanghua Hospital Affiliated to Shanghai University of Traditional Chinese Medicine, Shanghai, China; [2]The Research Institute for Joint Diseases, Shanghai Academy of Traditional Chinese Medicine, Shanghai, China; [3]Longhua Hospital Shanghai University of Traditional Chinese Medicine, Jiangxi Hospital, Nanchang, China; [4]Shanghai-MOST Key Laboratory of Health and Disease Genomics, Shanghai Institute for Biomedical and Pharmaceutical Technologies, Fudan University, Shanghai, China; [5]Wuxi Affiliated Hospital of Nanjing University of Chinese Medicine, Wuxi, China; [6]National Key Laboratory of Immune Response and Immunotherapy, Shanghai Institute of Immunity and Infection, Chinese Academy of Sciences, Shanghai, China.

Drs Xin, Li, A, and Shen contributed equally to this work.

Additional supplementary information cited in this article can be found online in the Supporting Information section (https://acrjournals.onlinelibrary.wiley.com/doi/10.1002/art.70020).

Author disclosures are available at https://onlinelibrary.wiley.com/doi/10.1002/art.70020.

Address correspondence via email to Lianbo Xiao, PhD, at xiao_lianbo@163.com; to Xiaoming Zhang, PhD, at xmzhang@siii.cas.cn; or to Lu Xie, MD, at xielu@sibpt.cn.

Submitted for publication June 12, 2025; accepted in revised form November 5, 2025.

disease progression and prevent long-term complications,[6,7] approximately 30% of patients respond poorly to current therapies because of the heterogeneity of RA pathogenesis, and effective predictors of treatment response are still lacking.[5,8] Therefore, developing novel strategies for the prevention and treatment of bone destruction remains an urgent need.

Fibroblast-like synoviocytes (FLSs), the main cellular component of synovial tissue, are recognized as key drivers of bone destruction in RA.[9–11] Under inflammatory conditions, FLSs adopt a tumor-like aggressive phenotype upon activation.[12] They promote cartilage and bone erosion directly by secreting matrix metalloproteinases (MMPs), inflammatory cytokines, and chemokines and indirectly by sustaining synovial inflammation through interactions with immune cells.[5,13] Additionally, FLSs are characterized by enhanced proliferation, resistance to apoptosis, and increased migratory and invasive behavior.[9,13] Targeting FLSs has emerged as a promising therapeutic approach for RA intervention.[13] Our previous single-cell RNA sequencing (scRNA-seq) study revealed significant heterogeneity among FLSs in active synovial tissues, identifying specific subsets with high bone-destructive potential.[14] However, molecular targets in the blood associated with bone destruction during active RA remain poorly defined. Given the invasive nature of synovial tissue biopsy, discovering reliable blood-based biomarkers for precise monitoring and intervention of RA-related bone damage is critically important.

The rapid advancement of plasma proteomics has opened new avenues for disease research and clinical translation.[15] Hu et al[16] identified ORM1 as significantly up-regulated in the serum of patients with RA compared with healthy individuals and correlated with disease activity. Similarly, Liu et al[17] proposed FGL1 as a novel biomarker for predicting RA disease activity and prognosis. However, plasma proteomic studies specifically focusing on bone destruction in RA are still extremely limited, necessitating further exploration to uncover underlying mechanisms and novel therapeutic targets.

Although treat-to-target strategies have significantly improved RA management, reliable molecular signatures to accurately reflect remission, active disease, and disease cure are still lacking.[18,19] Therefore, our team has been dedicated to profiling proteomic features across different stages of RA to better evaluate disease status. By analyzing molecular differences between the active and remission phases, we aim to elucidate the mechanisms driving disease progression and provide insights into novel targets to prevent bone destruction.

In this study, we employed high-resolution data-independent acquisition (DIA) mass spectrometry to systematically analyze 200 plasma samples, mapping the proteomic landscapes of RA in active and remission phases. For the first time, we identified and validated thousand-and-one–amino acid kinase 3 (TAOK3) as a novel biomarker and potential therapeutic target for RA-related bone destruction by integrating plasma proteomic profiling, scRNA-seq data, and functional validation both in vitro and in vivo.

PATIENTS AND METHODS

Ethical approval and informed consent

This study was approved by the Ethics Committee of Shanghai Guanghua Hospital of Integrative Medicine (approval no. 2023-K-44) and conducted in accordance with the principles of the Declaration of Helsinki. Written informed consent was obtained from all participants. All animal experiments were approved by the Laboratory Animal Ethics Committee of Shanghai University of Traditional Chinese Medicine (approval no. PZSHUTCM2503070001) and were performed in strict accordance with the "Guide for the Care and Use of Laboratory Animals in China."

Participant recruitment

This study included a discovery cohort and two independent validation cohorts. A total of 160 patients with RA were recruited between August 2023 and February 2024 at Shanghai Guanghua Hospital of Integrative Medicine, according to the 2010 American College of Rheumatology/EULAR classification criteria for RA.[20] The inclusion criteria were as follows: (1) aged between 20 and 75 years, (2) diagnosed with RA based on established diagnostic criteria; and (3) signed the informed consent. The exclusion criteria were (1) the presence of severe diseases or malignancies involving the heart, liver, brain, kidneys, or hematopoietic system; (2) long-term use of glucocorticoids within the past 6 months in patients with sustained remission; (3) psychiatric disorders that impaired the ability to participate; (4) pregnancy or breastfeeding; and (5) the coexistence of other rheumatic or autoimmune diseases, such as systemic lupus erythematosus, ankylosing spondylitis, or systemic sclerosis. Additionally, 40 healthy controls (HCs) matched for age, sex, and body mass index (BMI), and without a history of autoimmune diseases, were recruited.

To ensure balanced representation of disease states and enable robust comparative analysis, we employed a predefined stratified recruitment strategy. Disease activity was evaluated based on the Disease Activity Score 28 with erythrocyte sedimentation rate (DAS28-ESR) score. Patients with DAS28-ESR scores < 2.6 maintained for >6 months were prospectively assigned to the remission group ($n = 80$), whereas those with DAS28-ESR scores > 3.2 were assigned to the active disease group ($n = 80$).[14,21] For independent validation, an additional 50 patients with RA (25 with active RA and 25 with remission RA) were recruited from the same hospital under identical criteria. In addition, synovial tissues and matched plasma samples were collected from 10 patients with RA at the same institution for further validation. All patients with RA were receiving stable DMARD therapy (details in Supplementary Tables S1 and S2).

Clinical data and sample collection

Clinical information and laboratory data of all enrolled participants were collected (Supplementary Tables S1 and S2). In the discovery cohort, all patients underwent hand x-ray imaging, and bone erosion and joint space narrowing were evaluated at the metacarpophalangeal, proximal interphalangeal, and wrist joints using the Sharp/van der Heijde scoring method.[22] Two experienced radiologists independently scored the images, and discrepancies were resolved by averaging their scores.

Fasting blood samples were collected from all participants. Plasma was separated by centrifugation at 3,000 rpm for 10 minutes at room temperature, aliquoted into Eppendorf tubes, and stored at –80°C for long-term preservation.

Plasma proteomics sample preparation

Protein concentrations were measured using the bicinchoninic acid (BCA) assay (Beyotime, P0012). For each sample, 15 μg of protein was mixed with 5X loading buffer and boiled for 5 minutes. Proteins were separated on 4% to 20% sodium dodecyl sulfate–polyacrylamide gel electrophoresis (SDS-PAGE) gels (constant voltage 180V, 45 minutes) and visualized by Coomassie brilliant blue R-250 staining. Equal amounts of protein from each sample were pooled for quality control (QC). Dithiothreitol (Bio-Rad, #161-0404) was added to reduce disulfide bonds at 37°C for 1.5 hours, followed by alkylation with iodoacetamide (Bio-Rad, #163-2109) in the dark at room temperature for 30 minutes. Trypsin (Promega, #V5111) was added at a 1:50 enzyme-to-protein ratio, and samples were incubated at 37°C for 15 to 18 hours. Digested peptides were desalted using an MCX desalting column (Omicsolution, OS-MCX-1ML), concentrated by vacuum centrifugation, and reconstituted in 20 μL of 0.1% formic acid (Fluka, #06450) in water. Peptide concentrations were estimated by UV absorbance at 280 nm. Indexed retention time calibration peptides were spiked into each sample for DIA analysis.

DIA mass spectrometry analysis

Peptides were analyzed using an Orbitrap Astral mass spectrometer (Thermo Scientific) coupled with a Vanquish Neo ultra-high–performance liquid chromatography system (Thermo Scientific) in DIA mode. Precursor ions were scanned over an m/z range of 380 to 980; MS1 resolution was set at 240,000 at 200 m/z, with a normalized automatic gain control (AGC) target of 500% and a maximum injection time of 5 ms. MS2 scans in DIA mode used 299 isolation windows with a width of 2 m/z, a collision energy of 25 eV, a normalized AGC target of 500%, and a maximum injection time of 3 ms.

DIA raw data were processed using DIA-NN version 1.8.1. Major parameters included trypsin as the proteolytic enzyme, maximum of one missed cleavage allowed, carbamidomethylation (C) as a fixed modification, and oxidation (M) and acetylation (protein N-terminus) as variable modifications. Protein identification was based on a 99% confidence threshold with a false discovery rate ≤ 1%.

Differential protein analysis and enrichment analysis

Proteins expressed in >50% of samples were selected for differential expression analysis. One-way analysis of variance (ANOVA) was used to compare protein expression levels among the remission, active, and HC groups. *P* values were not adjusted for multiple testing; instead, proteins with a P value < 0.05 and a fold change > 1.5 or <0.67 were considered differentially expressed proteins (DEPs). Pairwise comparisons between groups were performed using two-sample *t*-tests. DEPs were subjected to Gene Ontology (GO) annotation and Kyoto Encyclopedia of Genes and Genomes (KEGG) pathway enrichment analysis using Blast2GO (https://www.blast2go.com/)[23] and KEGG databases,[24] with a significance threshold of $P < 0.05$.

Protein trend clustering analysis

To characterize protein expression trends specific to active RA, fuzzy c-means clustering analysis was performed using the Mfuzz package in R,[25] based on the proteomic profiles of HCs, patients with remission RA, and patients with active RA.

Random forest analysis

To explore the potential value of bone destruction–related proteins in distinguishing active from remission RA, we performed feature importance analysis using a random forest classifier implemented in the randomForest package (v4.7-1.1) in R. The input features were Z score–normalized expression levels of bone destruction–related proteins within profile 3, and the outcome variable was clinical disease status (active vs remission RA). Given the exploratory aim of identifying important features rather than building a predictive model, the random forest was trained on the full cohort without a training-validation split. The model was run with default parameters (ntree = 500 and mtry = $\sqrt{p}$, where p is the number of input proteins). To ensure robustness, the model was repeated five times, and the mean Gini-based importance scores (IncNodePurity) across runs were calculated for each protein. The top 20 proteins were ranked and visualized for interpretation. The Gini impurity at a node is defined as follows:

$$G = 1 - \sum_{i=1}^{C} p_i^2$$

where C is the number of classes and p_i is the proportion of samples belonging to class i. A greater reduction in Gini impurity when splitting on a feature indicates higher importance.

Followed-up information

All 160 patients in the discovery cohort were prospectively observed for 1 year. Follow-up was primarily conducted through outpatient visits every 3 to 6 months, which included clinical assessments and laboratory testing. When patients were unable to attend scheduled visits, follow-up data were supplemented by review of electronic medical records to ensure complete documentation of disease status. Disease relapse during follow-up was defined as DAS28-ESR scores > 3.2.

scRNA-seq data acquisition and analysis

scRNA-seq data of RA synovial tissues were obtained from the National Genomics Data Center (https://ngdc.cncb.ac.cn; accession number PRJCA013514), based on our previous study. After QC, normalization, and feature gene selection, a total of 22,925 cells from patients with active RA (n = 3) and 32,236 cells from patients with remission RA (n = 3) were used for downstream analysis.[14]

Dimensionality reduction (t-distributed stochastic neighbor embedding and uniform manifold approximation and projection) and clustering analyses were conducted using the Seurat R package, with further cell-type annotation based on marker genes. Given the crucial role of FLSs in RA bone destruction, differentially expressed genes between active and remission pannus FLSs were analyzed, and violin plots were generated. Potential targets related to bone destruction were further screened by intersecting differentially expressed genes with bone destruction–related proteins.

Multiplex immunohistochemistry

Tissue sections were deparaffinized with xylene, followed by rehydration, antigen retrieval, and blocking of nonspecific binding. Multiplex staining was performed according to the manufacturer's instructions (PerkinElmer, Opal Kit) using primary antibodies against CD90 (Abcam, #ab16449) and TAOK3 (Proteintech, #67451-1-Ig). After washing, sections were incubated with horseradish peroxidase (HRP)–conjugated secondary antibodies at room temperature for 30 minutes. Nuclei were counterstained with DAPI, and sections were scanned and analyzed using the PerkinElmer Vectra3 platform. The proportion of positive cells was quantified using ImageJ software.

Enzyme-linked immunosorbent assay

In the independent validation cohorts, plasma levels of selected proteins were quantified using commercial enzyme-linked immunosorbent assay (ELISA) kits (Mlbio). In validation cohort 1, concentrations of C-reactive protein (CRP) and TAOK3 were measured, whereas in validation cohort 2, TAOK1, TAOK2, and TAOK3 were assessed to further determine the specificity of TAOK3. To investigate the mechanism of TAOK3 release in FLSs, primary pannus FLSs were stimulated with lipopolysaccharide (LPS; 1 μg/mL; MedChemExpress [MCE]) or tumor necrosis factor α (TNF-α; 10 ng/mL; MCE) for 0, 24, 48, and 72 hours.[26] At each time point, both culture supernatants and cell lysates were collected. Cell lysates were prepared by resuspending 2×10^5 cells in 1 mL of phosphate-buffered saline (PBS) followed by sonication for 1 minute. Total protein concentrations were determined using the BCA method to ensure equal loading, and TAOK3 levels were then quantified with ELISA according to the manufacturer's instructions.

Isolation and culture of primary pannus FLSs

Primary pannus FLSs were isolated from synovial pannus tissues of patients with RA undergoing knee synovectomy at Shanghai Guanghua Hospital of Integrative Medicine, as previously described by our group.[14] Tissues were digested with 100 U/mL type II collagenase at 37°C, and $CD45^-/CD31^-$ fibroblasts were sorted using the Miltenyi system. Cells were cultured in Dulbecco's Modified Eagle Medium (DMEM; Gibco, #11965092) with 10% fetal bovine serum (FBS; Gibco, #10091148) and 1% penicillin/streptomycin (Gibco, #15140148) at 37°C in 5% CO_2. When the cells reached approximately 80% to 90% confluence, they were passaged using trypsin (Gibco, #25300062). Pannus FLSs between passages 3 and 6 were used for all experiments.[10]

Cell transfection

Pannus fibroblasts were seeded into six-well plates at a density of 1×10^5 cells/well and cultured in DMEM containing 10% FBS for 24 hours. At approximately 50% confluence, cells were transfected with Lipofectamine 2000 (Invitrogen, #11668030) following the manufacturer's protocol. Briefly, small interfering RNA (siRNA; 50 nM) or plasmid DNA was diluted in Opti-MEM (Gibco, #31985070), mixed with Lipofectamine 2000, and incubated at room temperature for 20 minutes to form complexes, which were then added to the cells. After 6 hours at 37°C, the medium was replaced with complete DMEM containing 10% FBS. Cells were transfected with TAOK3 siRNA (Si-TAOK3) or negative-control siRNA (Si-NC) (GenePharma). For overexpression, cells were transfected with a TAOK3 overexpression plasmid (CV702; GeneChem) or empty vector. Cells were harvested 48 hours after transfection for downstream experiments.

Quantitative real-time polymerase chain reaction assay

Total RNA was extracted from FLSs using Trizol reagent (Invitrogen, USA) and reverse-transcribed into cDNA using the PrimeScript RT kit (Takara, Japan). Quantitative real-time polymerase chain reaction (qRT-PCR) was performed using a T100 PCR system (Bio-Rad) according to the manufacturer's protocol to measure TAOK3 expression levels. GAPDH was used as an internal control, and relative messenger RNA levels were calculated using the $2^{-\Delta\Delta Ct}$ method. Primer sequences are listed in Supplementary Table S3.

Cell Counting Kit-8 assay

Cell proliferation after TAOK3 knockdown was assessed using a Cell Counting Kit-8 (CCK8, Beyotime). FLSs transfected with Si-TAOK3 or Si-NC were seeded into 96-well plates at a density of 1×10^5 cells per well. At 0, 24, and 48 hours, 10 μL of CCK8 solution was added to each well and incubated at 37°C in a 5% CO_2 incubator for 2 hours. Absorbance at 450 nm was measured using a microplate reader to evaluate cell proliferation.

Flow cytometry

Cells were harvested, washed twice with PBS, and stained with an Annexin V-FITC apoptosis detection kit (Beyotime) according to the manufacturer's protocol. Briefly, cells were incubated with Annexin V-FITC and propidium iodide (PI) at room temperature for 15 minutes in the dark. Apoptotic cells were analyzed by flow cytometry, and data were processed using CytExpert software.

Wound healing assay

Pannus fibroblasts were seeded into six-well plates and allowed to grow beyond 80% confluence. A straight scratch was made in the monolayer using a 200-μL pipette tip. Detached cells and debris were removed by washing with culture medium. Phase-contrast images were acquired at 0 hours and 24 hours using an inverted microscope (Leica DMI3000) at identical magnification. Wound closure was quantified using ImageJ software by consistently segmenting the wound area (cell-free region) at each time point. The migration area rate (%) was calculated as ([wound area at 0 hours – wound area at 24 hours] / wound area at 0 hours) × 100%.

Transwell migration and invasion assays

Transwell chambers with 8.0-μm pores (Corning, #3422) were used to assess pannus FLSs migration and invasion. For migration assays, transfected FLSs were suspended in serum-free DMEM and seeded into the upper chamber at a density of 1×10^5 cells per well, whereas the lower chamber was filled with 600 μL of DMEM supplemented with 20% FBS. After incubation at 37°C for 48 hours, nonmigrated cells on the upper side of the membrane were removed with a cotton swab, and migrated cells on the lower side were fixed with 4% paraformaldehyde and stained with crystal violet. For invasion assays, the upper chamber was precoated with 100 μL of Matrigel (ABW, #082701) and incubated at 37°C for 2 hours before cell seeding. The remaining steps were identical to those of the migration assay. Migrated and invaded cells were imaged using an inverted microscope (Leica DMI3000) and quantified with ImageJ software.

Western blot assay

Total proteins were extracted from pannus fibroblasts and synovial tissues of collagen-induced arthritis (CIA) mice using radioimmunoprecipitation assay lysis buffer (Beyotime, #P0013B) supplemented with protease and phosphatase inhibitors. Protein samples were separated by SDS-PAGE and transferred onto polyvinylidene fluoride membranes (Millipore, #IPVH00010). Membranes were blocked with 5% nonfat milk for 1 hour, followed by overnight incubation at 4°C with primary antibodies. After washing, membranes were incubated with HRP-conjugated secondary antibodies (Proteintech, #SA00001-1 and #SA00001-2) at room temperature for 1 hour. Signals were developed using an enhanced chemiluminescence kit (Tanon, #180-501) and imaged using a GelView 6000 Plus imaging system. Band intensities were quantified using ImageJ software. Primary antibodies included MMP1 (Abcam, #ab134184), MMP2 (CST, #40994S), MMP3 (Abcam, #ab52915), P38 MAPK (Abclonal, #A4771), Phospho-p38 MAPK (Abclonal, #AP1311), cathepsin K (CTSK; Proteintech, #11239-1-AP), receptor activator of nuclear factor κB ligand (RANKL; Proteintech, #23408-1-AP), TAOK3 (Abcam, #ab150388), and β-Actin (Proteintech, #66009-1-Ig).

Bone slice invasion assay

Bone slice invasion assays were performed as previously described.[14] Sterile bovine cortical bone slices (IDS, DT-1BON1000-96) were placed in 96-well plates. Primary pannus cells were seeded at a density of 1×10^5 cells per slice and cultured in DMEM supplemented with 10% FBS for 72 hours to allow adhesion and invasion. Experimental groups included (1) a blank control group (bone slices without cells or interventions), (2) Si-TAOK3 or Si-NC, (3) TAOK3 overexpression plasmid or empty vector, and (4) TAOK3 inhibitor SBI-581 (100 nM; MCE, HY-139439).[27] Rescue experiments with SBI-581 were performed only in the TAOK3-overexpression group. After an additional 72 hours of culture, bone slices were collected, rinsed with chloroform/isopropanol (24:1), treated with diluted sodium hypochlorite to remove adherent cells, dehydrated through a graded

ethanol series, and stained with 0.1% toluidine blue. Resorption pits were visualized using bright-field microscopy (Leica DMI3000), and resorption areas were quantified in ImageJ with consistent thresholding.

CIA mouse model

Male DBA/1 mice (aged 8–10 weeks) were purchased from Beijing Vital River Laboratory Animal Technology Co., Ltd, and housed in the Animal Center of Shanghai University of Traditional Chinese Medicine under standard conditions (22°C, 12-hour light/dark cycle) with free access to food and water. After a 1-week acclimatization period, mice were randomly divided into four groups (initial n = 8 per group): control group, CIA model group, CIA + SBI-581 treatment group, and positive treatment group. The CIA model was established as follows: for the primary immunization, bovine type II collagen (2 mg/mL, dissolved in 0.05 M acetic acid; Chondrex) was emulsified with an equal volume of complete Freund adjuvant (Chondrex) on ice. Successful emulsification was confirmed when a drop remained intact on the water surface, and the emulsion was then subcutaneously injected at the base of the tail. Twenty-one days after the primary immunization, a booster injection was administered using bovine type II collagen emulsified with an equal volume of incomplete Freund adjuvant (Chondrex).[28] Mice were assessed for arthritis severity before treatment. On day 35, mice with a total arthritis score ≥ 1 (scored 0–4 per paw; maximum total = 16) were considered arthritic and included in the analysis (final n = 6 per group).[11] Drug interventions then began as follows: the CIA + SBI-581 group received intraperitoneal injections of SBI-581 (10 mg/kg/day),[27,29] and the positive treatment group received intraperitoneal injections of methotrexate (MTX, 2 mg/kg every 3 days),[28] continuing for 28 days. From the second immunization onwards, two independent, blinded observers assessed arthritis severity until the end of the experiment (day 63).[11] Treatment and assessments were randomized, and cage positions were rotated weekly to minimize environmental confounders.

Micro-computed tomography

Ankle joints were analyzed by micro-computed tomography (micro-CT; PINGSENG SCIENTIFIC). Scanning parameters were set at 90 kV tube voltage and 40 μA tube current, with a nominal voxel size of 15 μm. Image reconstruction and analysis were performed using Avatar3 software, and radiographic joint destruction scores were evaluated according to previously established methods.[14,30]

Histologic analysis

Ankle joints were fixed in 10% neutral-buffered formalin for 48 hours, decalcified in 10% EDTA solution (Pasitong, China), embedded in paraffin, and sectioned at a thickness of 5 μm. Sections were stained with hematoxylin and eosin (H&E) and safranin O/fast green (SO/FG) according to the manufacturers' standard protocols. Histopathologic scoring was performed according to the Standardised Microscopic Arthritis Scoring of Histological sections guidelines.[31,32] Briefly, synovitis was graded based on synovial lining thickness and inflammatory infiltrates (0–3), cartilage damage was graded according to the extent of structural loss and surface irregularities in the articular cartilage (0–3), and bone erosion was graded based on the depth and extent of cortical bone destruction (0–3). All evaluations were performed independently by two blinded observers.

Statistical analysis

Statistical analyses and data visualization were conducted using SPSS software (version 25.0) and R software (version 4.1.2). For variables requiring standardization, *Z* score normalization was applied so that each continuous variable had a mean of 0 and an SD of 1. For normally distributed variables, comparisons between two groups were performed using Student's *t*-test, and multiple-group comparisons were analyzed by one-way ANOVA followed by the least significant difference post hoc test. When the assumption of homogeneity of variances was violated, the Brown-Forsythe test was applied. For nonnormally distributed variables, the Mann-Whitney U test or the Kruskal-Wallis test followed by the Dunn post hoc test was used. Categorical variables were compared using the chi-square test or Fisher exact test, as appropriate. Correlation analyses were conducted using Pearson or Spearman correlation coefficients according to data distribution. Relapse-free survival between the high- and low-TAOK3 expression groups was evaluated using Kaplan-Meier survival analysis with the log-rank test. *P* values <0.05 were considered statistically significant.

Data availability

The original contributions presented in the study are detailed in the article and Supplementary Materials. For further inquiries, please direct them to the corresponding authors.

RESULTS

Study design, characteristics of patients with RA, and overview of proteomic analysis

In this study, we applied DIA-based plasma proteomics to analyze samples from 80 patients with RA in sustained remission, 80 patients with active RA, and 40 HCs (discovery cohort). Additionally, two independent validation cohorts were included: 50 patients with RA from the outpatient department (validation cohort 1) and 10 from the inpatient department (validation

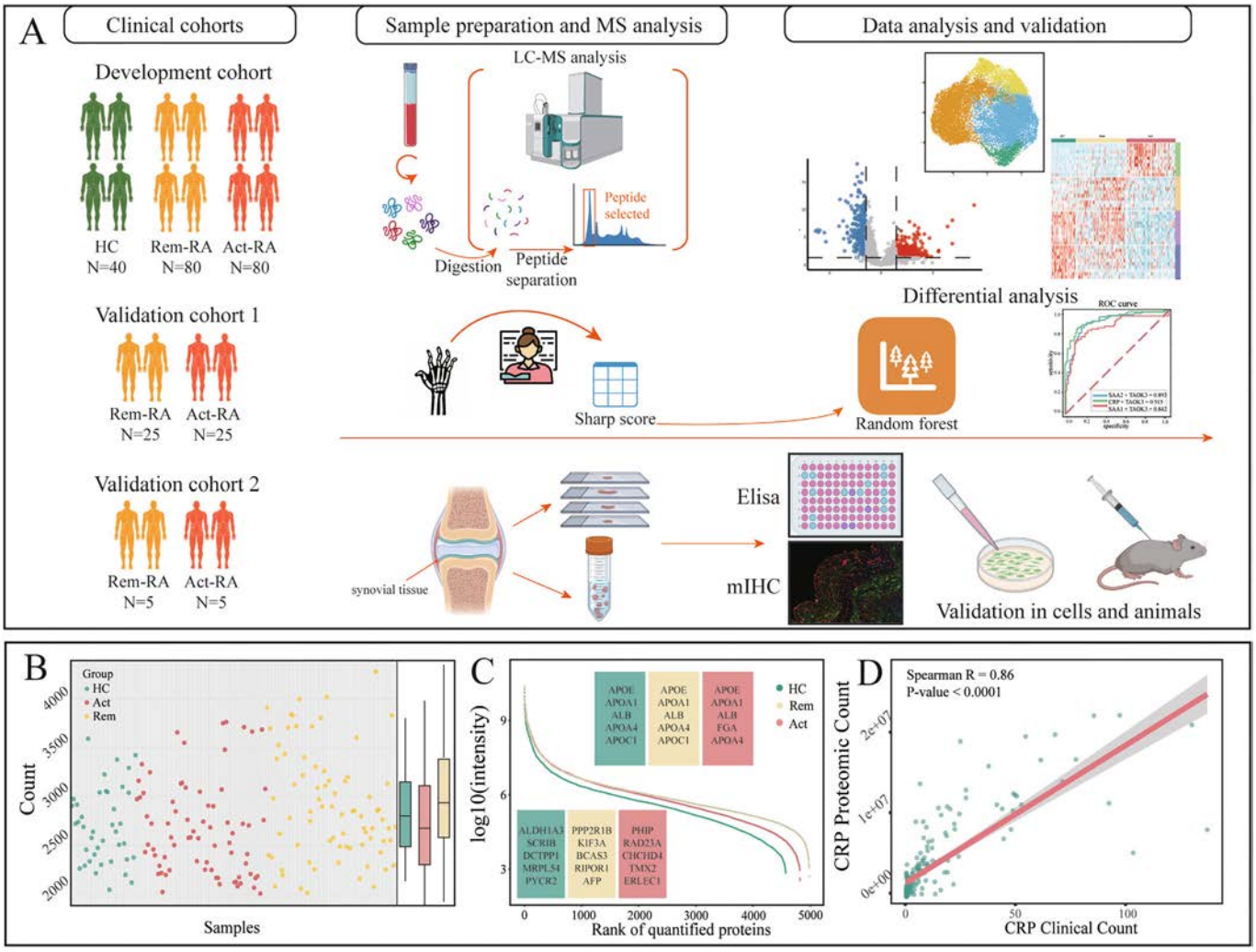

Figure 1. Overview of study design and proteomic analysis. (A) Schematic of the study design, including cohort construction (discovery and validation cohorts), plasma proteomic profiling, identification, and validation of bone destruction–related proteins; and subsequent functional validation in cellular and animal models. (B) Distribution of the number of proteins identified per plasma sample. (C) Dynamic range of protein abundance based on mass spectrometry signal intensity across the HC, Rem-RA, and Act-RA cohorts, with high- and low-abundance proteins annotated. (D) Spearman correlation between CRP levels measured by mass spectrometry and clinical assays in 200 paired samples. The shaded area represents the 95% confidence interval. Act-RA, active rheumatoid arthritis; CRP, C-reactive protein; HC, healthy control; LC-MS, liquid chromatography–mass spectrometry; mIHC, multiplex immunohistochemistry; RA, rheumatoid arthritis; Rem-RA, remission rheumatoid arthritis; ROC, receiver operating characteristic; TAOK3, thousand-and-one–amino acid kinase 3.

cohort 2). The overall study design is illustrated in Figure 1A. In the discovery cohort, participants ranged in age from 36 to 75 years, with women accounting for 80.5% (n = 177). The mean DAS28-ESR score in patients with active RA was 4.78, significantly higher than the 1.94 observed in patients in sustained remission ($P < 0.001$). Detailed demographic and clinical characteristics of participants are summarized in Supplementary Table S1. No significant differences were observed among groups regarding age, sex, BMI, total cholesterol, triglycerides, or aspartate aminotransferase levels.

A total of 4,998 plasma proteins were identified across all samples. The average number of proteins identified per group was 2,697 for HCs, 2,858 for patients with remission RA, and 2,618 for patients with active RA (Figure 1B). Protein quantification was based on the intensity-based absolute quantification algorithm and normalized using the fraction of total method as previously described.[33] The dynamic range of protein abundance spanned approximately six orders of magnitude, demonstrating a significantly deeper detection capability compared with previous studies (Figure 1C).[16,17,34] Protein abundance distributions across samples showed high consistency within each group, confirming the stability of the mass spectrometry platform (Supplementary Figure S1A). Analysis of all QC plasma samples yielded an average Pearson correlation coefficient of

0.97, further supporting the high stability and reproducibility of the mass spectrometry platform (Supplementary Figure S1B). Moreover, CRP levels measured by mass spectrometry showed a strong correlation with clinical test results (R = 0.86, $P < 0.05$; Figure 1D), validating the reliability of the proteomic data. Subcellular localization prediction using CELLO (http://cello.life.nctu.edu.tw)[35] indicated that most identified proteins were located in the nucleus and cytoplasm, with no significant differences observed among the three groups (Supplementary Figure S1C).

Collectively, through large-scale plasma proteomic profiling using high-depth and high-coverage detection technology, we established a solid foundation for characterizing RA-specific proteomic features and discovering novel bone destruction–related proteins.

Proteomic profiling reveals distinct features of active versus remission RA

Proteomic analysis of the discovery cohort revealed significant differences in quantitative protein expression among HCs, patients with remission RA, and patients with active RA (Figure 2A, $P < 0.05$). A total of 1,235 DEPs were identified across the three groups (Figure 2B; Supplementary Table S4A). Comparison between patients with active and remission RA identified 506 DEPs, comprising 306 up-regulated and 200 down-regulated proteins. Several previously reported active-associated markers were validated, including CRP, serum amyloid A (SAA), MMP3, FGL1, PLA2G2A, ORM1, and ORM2.[16,17,26,36] Notably, novel DEPs such as AKAP1 and TAOK3 were identified for the first time in active RA (Figure 2C; Supplementary Table S4B).

GO and KEGG enrichment analyses revealed that DEPs between remission and active RA were predominantly associated with inflammation, immune response, angiogenesis, metabolic processes, and cell proliferation (Figures 2D and E). Interestingly, beyond the activation of classical RA pathways, active RA exhibited significant up-regulation of key regulators in lipid metabolism, particularly the phospholipase D (PLD) signaling cascade (Figure 2F and G), suggesting a potential link between active and lipid metabolic dysregulation.

Furthermore, pairwise GO and KEGG enrichment analyses were conducted among all comparison groups (Supplementary Figures S2A–F; Supplementary Table S4C and D). Of note, the comparison between patients with remission RA and HCs revealed 86 DEPs, of which 30 were significantly up-regulated. Enrichment analysis showed that these up-regulated proteins were exclusively involved in the interleukin-17 signaling pathway and fatty acid degradation. This observation suggests that even during clinical remission, patients with RA may exhibit mild immune activation and disturbances in lipid metabolism.

Identification of bone destruction–related proteins in active RA

To identify potential targets mediating bone destruction and to monitor disease progression in active RA, trend clustering analysis was performed on DEPs between patients with remission RA and active RA. All DEPs were categorized into eight distinct expression patterns (Supplementary Figure S3). Of particular interest, proteins in profile 3 were markedly up-regulated in patients with active RA but showed no significant changes in patients with remission RA or HCs (Figure 3A and B). KEGG enrichment analysis indicated that profile 3 proteins were primarily involved in key signaling pathways associated with RA-related bone destruction,[37,38] suggesting that these proteins may play critical roles in the bone erosion process (Figure 3C). To further identify key bone destruction–related proteins, we analyzed the correlation between protein expression levels in profile 3 and Sharp bone erosion scores in 160 patients with RA. A total of 114 proteins were found to be associated with bone destruction, including SAA2, ATE1, SYNCRIP, and TAOK3 ($P < 0.001$; Figure 3D; Supplementary Table S5).

To explore the relationship between bone destruction–related proteins and active disease, and to evaluate their potential diagnostic value, we employed a random forest model to assess feature importance and selected the top 20 key features. The analysis revealed that SAA2, CRP, SAA1, and TAOK3 exhibited markedly higher importance scores compared with other features, indicating their critical roles within the predictive model, and the importance scores of the remaining features were relatively evenly distributed (Figure 3E and F). Of note, CRP and SAA are widely used clinical biomarkers for diagnosing active RA.[39,40] Our study revealed that combining TAOK3 with CRP significantly enhanced predictive performance (area under the curve [AUC] = 0.915), outperforming either marker alone (Figures 3G and H). These findings suggest that TAOK3 may serve as a novel biomarker that, in combination with existing markers, improves the accuracy of active prediction in RA. To validate these results, we measured plasma levels of CRP and TAOK3 by ELISA in the independent validation cohort 1. Consistent with the discovery cohort, both CRP and TAOK3 were significantly elevated in patients with active RA, and their combination further improved diagnostic performance (AUC = 0.894; Figures 3I and J).

TAOK3 as a potential protein associated with bone destruction in active RA

Given the critical role of FLSs in RA-related bone destruction,[9,10] we further sought to identify potential cellular targets linked to bone erosion in active RA. To this end, we integrated our previously obtained scRNA-seq data of synovial tissues from patients with active RA, for whom FLSs were classified into four subpopulations: $CD55^+$ lining fibroblasts (FB Ling), $CXCL12^+$ sublining fibroblasts (FB Subling), $MFAP5^+$ sublining

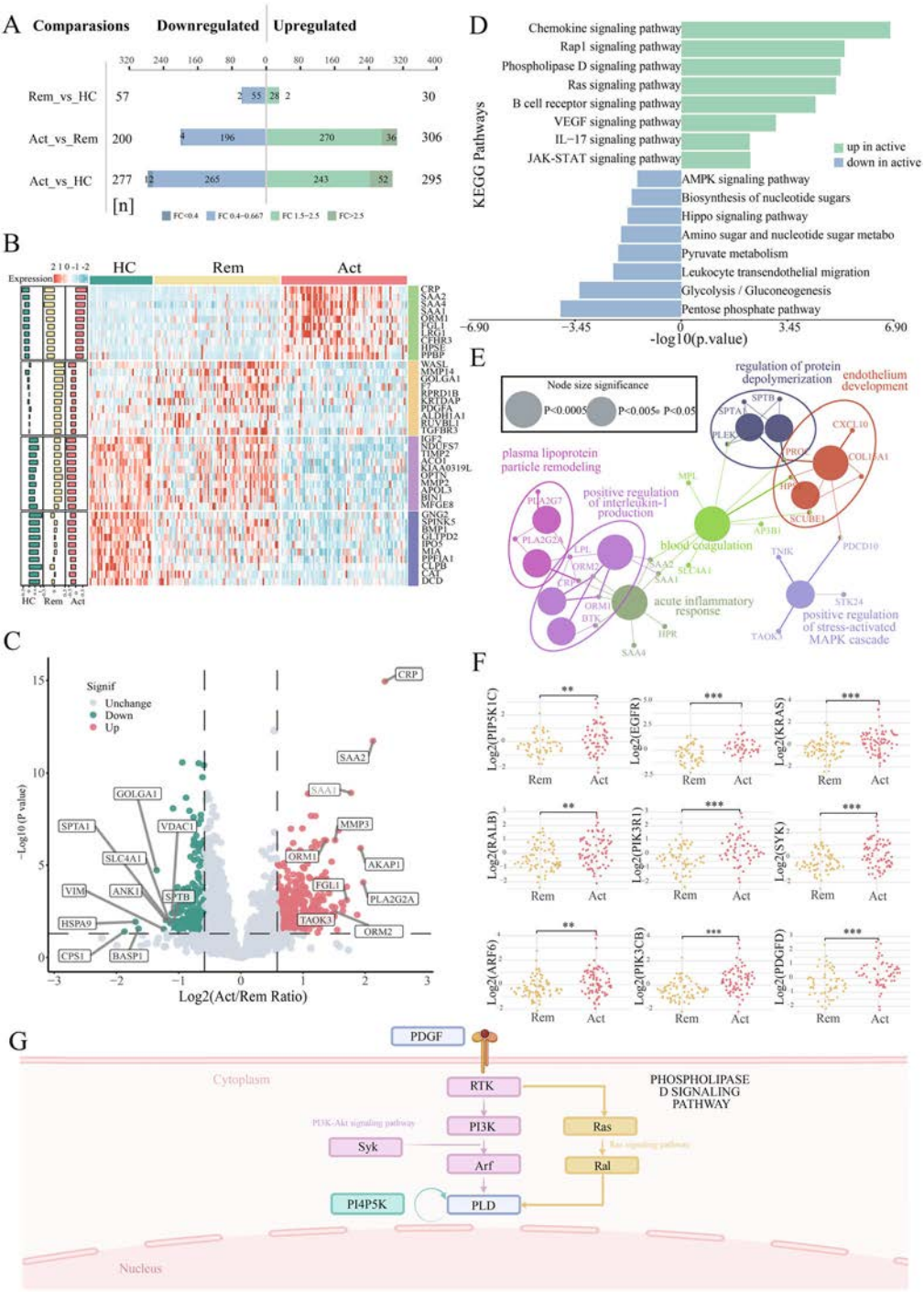

Figure 2. Proteomic features distinguishing Act-RA from sustained Rem. (A) Comparative analysis of DEPs among HC, Rem, and Act patients. (B) Heatmap showing the expression patterns of DEPs across the three groups. Each row represents a protein biomarker, and each column represents a sample. Hierarchical clustering identified four distinct protein clusters. (C) Volcano plot of DEPs between patients with RA in the Act and Rem phases. (D) KEGG pathway enrichment analysis of DEPs between the Act and Rem-RA groups. (E) Functional enrichment analysis of DEPs between the Act-RA and Rem-RA groups using the ClueGO plugin. Each circle represents a biologic process, and node size reflects enrichment significance. Colors indicate functional categories. For clarity, only top representative nodes are labeled. (F and G) In patients with Act-RA, multiple key proteins involved in the PLD signaling pathway were significantly up-regulated, including PDGFD (PDGF family), EGFR (RTK family), KRAS (Ras family), RALB (Ral family), PIK3R1 and PIK3CB (PI3K family), ARF6 (Arf family), and PIP5K1C (PI4P5K family), all of which are family members annotated in the KEGG pathway database. Data in part F are $\log_2$-transformed. Group comparisons used Student's *t*-test. $^{*}P < 0.05$; $^{**}P < 0.01$; $^{***}P < 0.001$. Act, active; AMPK, AMP-activated protein kinase; CRP, C-reactive protein; DEP, differentially expressed protein; FC, fold change; HC, healthy control; IL, interleukin; KEGG, Kyoto Encyclopedia of Genes and Genomes; MAPK, mitogen-activated protein kinase; PLD, phospholipase D; RA, rheumatoid arthritis; Rem, remission; TAOK3, thousand-and-one–amino acid kinase 3; VEGF, vascular endothelial growth factor. Color figure can be viewed in the online issue, which is available at http://onlinelibrary.wiley.com/doi/10.1002/art.70020/abstract.

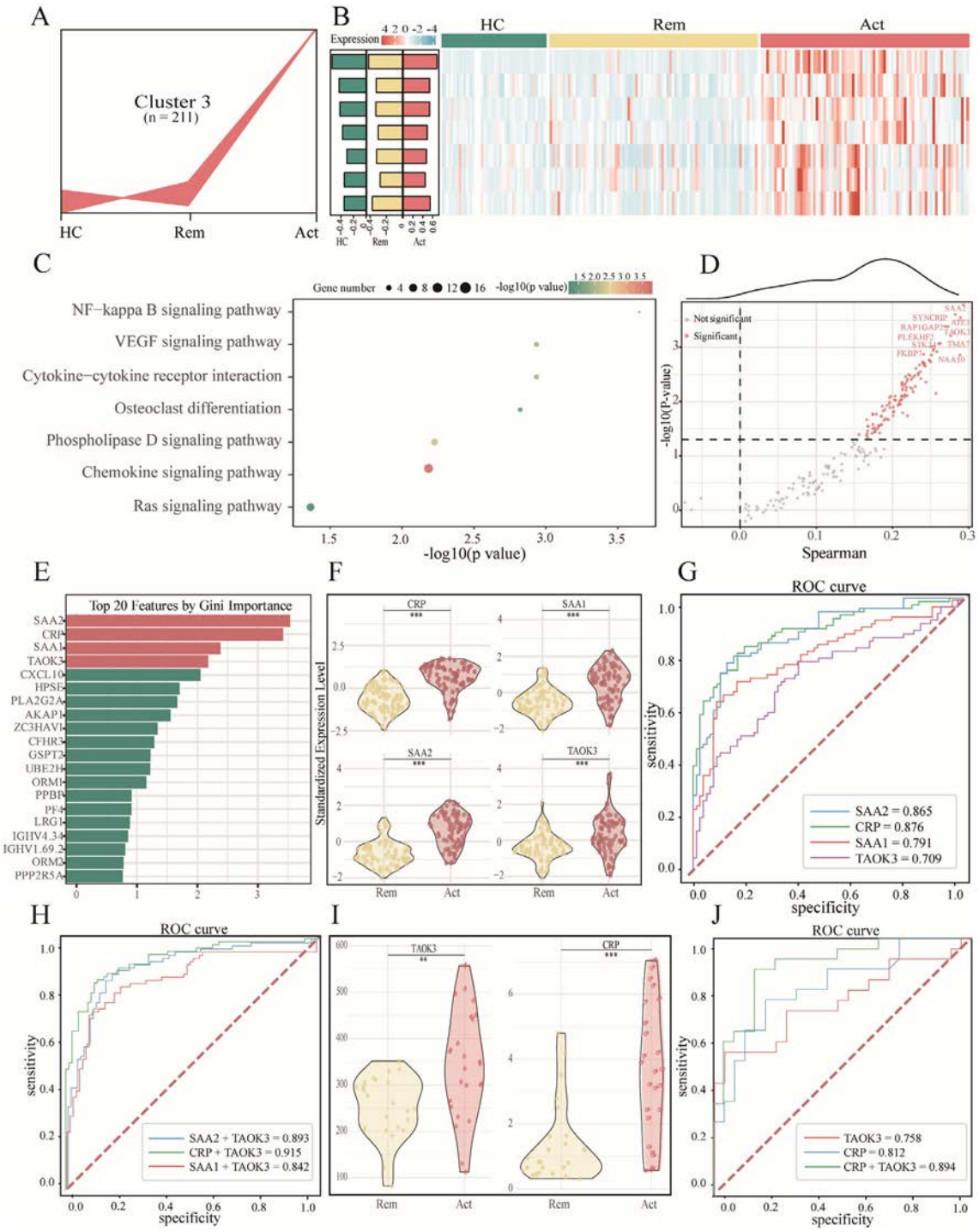

Figure 3. Identification of bone destruction–related proteins in Act-RA. (A and B) Heatmaps showing the expression patterns of proteins in profile 3, highlighting those with high membership scores. (C) Kyoto Encyclopedia of Genes and Genomes enrichment analysis of the 211 differentially expressed proteins in profile 3. (D) Volcano plot showing the Spearman correlation between protein abundance in profile 3 and Sharp bone destruction scores in 160 patients with RA. Bone destruction–related proteins with statistically significant correlations (n = 114, $P < 0.05$) are highlighted in red, and the top 10 most strongly correlated proteins are labeled. (E) Top 20 key protein features identified by random forest feature selection. (F–H) Relative abundance and ROC curve analysis of CRP, SAA1, SAA2, and TAOK3 in plasma samples from patients with RA in the Act and Rem phases in the development cohort. (I and J) TAOK3 and CRP expression levels and corresponding ROC curve analysis in the first independent validation cohort. Concentration units are pg/mL and mg/L, respectively. Data in part F are standardized expression levels. Group comparisons used Student's *t*-test or the Mann-Whitney U test. $^{*}P < 0.05$; $^{**}P < 0.01$; $^{***}P < 0.001$. Act, active; CRP, C-reactive protein; HC, healthy control; RA, rheumatoid arthritis; Rem, remission; ROC, receiver operating characteristic; SAA1, serum amyloid A1; SAA2, serum amyloid A2; TAOK3, thousand-and-one–amino acid kinase 3; VEGF, vascular endothelial growth factor. Color figure can be viewed in the online issue, which is available at http://onlinelibrary.wiley.com/doi/10.1002/art.70020/abstract.

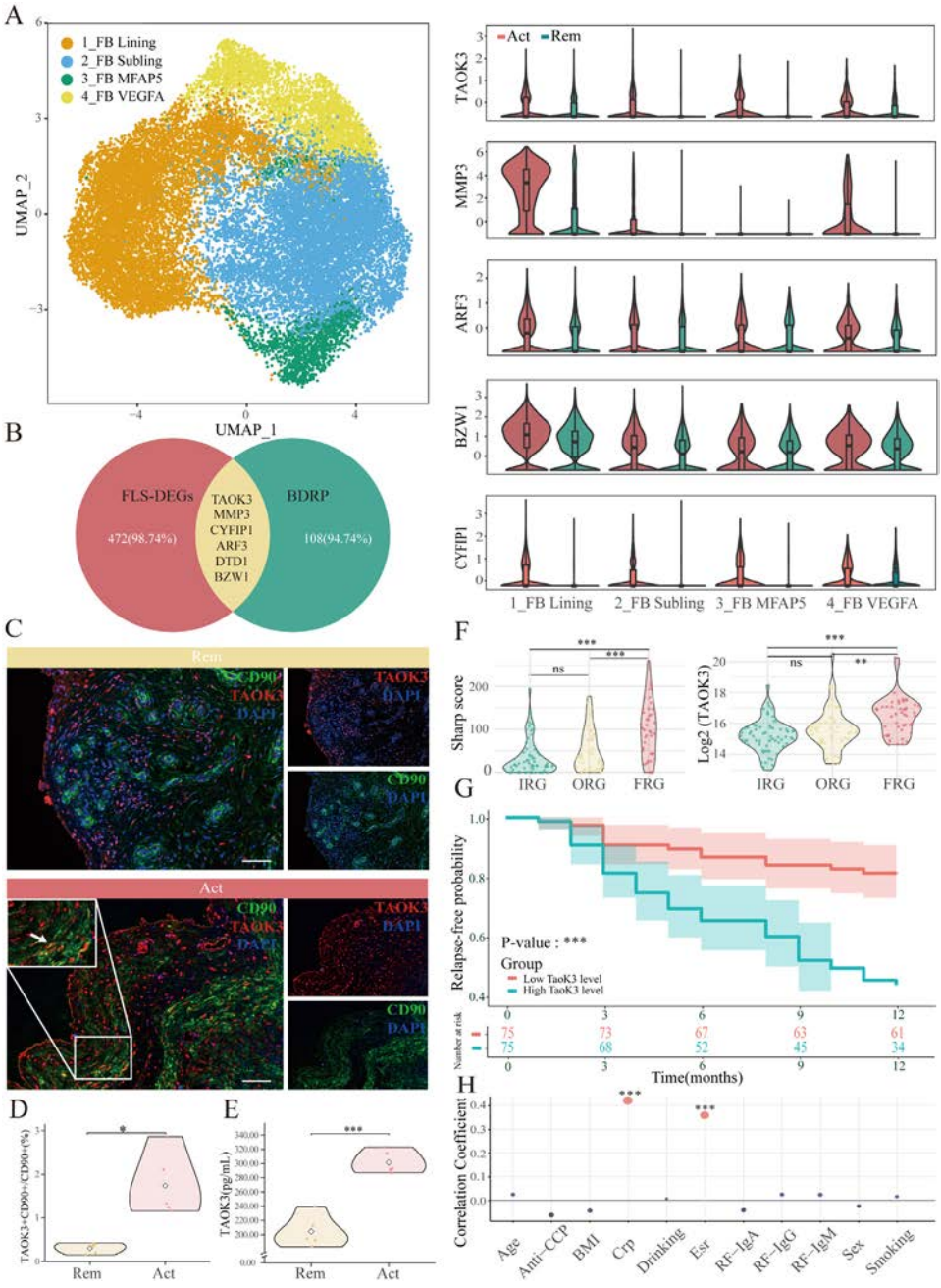

Figure 4. TAOK3 as a key biomarker of bone destruction and poor prognosis in active RA. (A) Single-cell transcriptomic landscape of FLSs in synovial tissues from patients with RA in the Act and Rem phases. UMAP analysis identified four distinct FLS subpopulations. (B) Integrated analysis of differentially expressed genes in active FLSs and bone destruction–related plasma proteins. Venn diagram shows six overlapping targets. (Right) Violin plots display their expression in FLS subsets (Act vs Rem). (C) Multiplex immunohistochemistry shows that $CD90^{+}TAOK3^{+}$ FLSs are distributed in both the lining and sublining areas of the synovial tissue. White arrows indicate $CD90^{+}TAOK3^{+}$ FLSs. Nuclei are counterstained with DAPI. Scale bar = 100 μm. (D and E) Semiquantitative analysis of $CD90^{+}TAOK3^{+}$ FLSs by (left) multiplex immunohistochemistry and (right) paired plasma TAOK3 levels in synovial tissues from patients with Act and Rem-RA in independent validation cohort 2. (F) Radiographic Sharp scores and baseline proteomic expression levels of TAOK3 across relapse frequency subgroups (quartiles) in the discovery cohort. (G) Kaplan-Meier analysis of relapse-free survival in patients with RA stratified by median plasma TAOK3 levels (low vs high expression). (H) Spearman correlation matrix of TAOK3 levels with clinical parameters. TAOK3 expression data in part F were $\log_2$-transformed. Group comparisons used Student's *t*-test or one-way analysis of variance. Data in part G were analyzed by Kaplan-Meier survival analysis with the log-rank test. $^{*}P < 0.05$; $^{**}P < 0.01$; $^{***}P < 0.001$. Act, active; ARF3, ADP-ribosylation factor 3; BDRP, bone destruction–related protein; BMI, body mass index; BZW1, basic leucine zipper and W2 domains 1; CCP, cyclic citrullinated peptide; CRP, C-reactive protein; CYFIP1, cytoplasmic FMR1-interacting protein 1; DEGs, differentially expressed genes; ESR, erythrocyte sedimentation rate; FB, fibroblast; FLS, fibroblast-like synoviocyte; FRG, frequent relapse group; IRG, infrequent relapse group; MMP, matrix metalloproteinase; ns, not significant; ORG, occasional relapse group; RA, rheumatoid arthritis; Rem, remission; RF, rheumatoid factor; TAOK3, thousand-and-one–amino acid kinase 3; UMAP, uniform manifold approximation and projection. Color figure can be viewed in the online issue, which is available at http://onlinelibrary.wiley.com/doi/10.1002/art.70020/abstract.

fibroblasts (FB MFAP5), and VEGFA$^+$ sublining fibroblasts (FB VEGFA)[14] (Figure 4A). Intersecting the 114 plasma proteins associated with bone destruction and the differentially expressed genes of FLSs revealed five commonly up-regulated targets in both the plasma and FLSs of patients with active RA, including TAOK3, MMP3, ARF3, CYFIP1, and BZW1 (Figure 4B). The protein DTD1, which exhibited opposite expression trends between plasma and FLSs, was excluded (Supplementary Figure S4A and B). Interestingly, the identification of classical bone destruction markers such as MMP3 supported the robustness of our screening strategy. Among the identified candidates, TAOK3 exhibited the strongest association with bone erosion. Therefore, we propose that TAOK3 may play a pivotal role in bone destruction associated with active RA and may represent a promising therapeutic target.

To further validate this finding, we analyzed TAOK3 expression levels in synovial tissues and plasma samples from 10 patients with RA in validation cohort 2. Detailed clinical information of the patients is provided in Supplementary Table S2. Multiplex immunohistochemistry analysis revealed a significant increase in the proportion of CD90$^+$TAOK3$^+$ FLSs in the synovial tissues of patients with active RA, distributed in both the lining and sublining areas (Figures 4C and D). Consistently, ELISA results showed a significant elevation of plasma TAOK3 levels in patients with active RA, whereas no significant changes were observed in TAOK1 or TAOK2 expression (Figure 4E; Supplementary Figure S4C and D), suggesting a specific role for TAOK3 in the progression of bone destruction in active RA.

Previous studies have reported that elevated TAOK3 expression is associated with tumor resistance and poor prognosis.[41] To investigate the relationship between TAOK3 and RA prognosis, patients with RA in the discovery cohort were stratified into three groups based on the number of relapses over a 3-year period: infrequent relapse (no more than one time), occasional relapse (two times), and frequent relapse (at least three times). Sharp scores and DAS28-ESR scores progressively increased with the number of relapses (Figure 4F; Supplementary Figure S4E), indicating a strong association between frequent relapses and disease progression. Furthermore, TAOK3 expression levels were significantly higher in the frequent relapse group compared with the infrequent and occasional relapse groups, reinforcing the potential link between TAOK3 and RA bone destruction progression. We observed 160 patients with RA in the discovery cohort for 1 year, with 10 patients lost to follow-up. Based on the median plasma TAOK3 expression level, patients were divided into high- and low-expression groups. Kaplan-Meier survival analysis revealed that patients with low TAOK3 expression had significantly prolonged relapse-free survival (Figure 4G). Spearman correlation analysis further demonstrated that TAOK3 levels positively correlated with ESR and CRP but not with other baseline clinical parameters (Figure 4H). Cumulatively, these findings suggest that TAOK3 is a potential protein associated with bone destruction in active RA and may serve as a prognostic indicator for RA progression.

TAOK3 inhibition suppresses tumor-like phenotypes of FLSs and ameliorates bone destruction in CIA mice

As a key member of the MAPK cascade, TAOK3 has recently attracted attention as a potential therapeutic target in cancer.[27,42] To explore its functional role in RA, we evaluated the effects of TAOK3 knockdown (Si-TAOK3) on FLS proliferation, apoptosis, migration, and invasion. CCK-8 assays showed that Si-TAOK3 significantly inhibited FLS proliferation compared with Si-NC (Supplementary Figure S5A). Annexin V-FITC/PI staining indicated that Si-TAOK3 markedly increased FLS apoptosis (Supplementary Figure S5B). Furthermore, transwell assays demonstrated that Si-TAOK3 significantly reduced the migratory and invasive capacities of FLSs (Figure 5A), which was further confirmed by wound healing assays (Figure 5B).

To explore the underlying mechanisms, Western blot analysis showed that Si-TAOK3 markedly reduced the level of phosphorylated p38 MAPK (p-p38), as reflected by the decreased ratio of p-p38 to total p38, whereas RANKL expression remained unchanged (Supplementary Figure S5C). In addition, Si-TAOK3 decreased the expression of bone resorption–related proteins, including MMP1, MMP2, MMP3, and CTSK (Figure 5C and D). In pannus cell–mediated bone resorption assays, TAOK3 knockdown significantly reduced bone resorption, whereas TAOK3 overexpression enhanced bone-invasive activity. Importantly, treatment with the TAOK3 inhibitor SBI-581 attenuated bone erosion induced by TAOK3 overexpression (Figures 5E and F; Supplementary Figure S5D). Collectively, these findings indicate that TAOK3 plays a critical role in regulating the tumor-like phenotype of FLSs and in pannus cell–mediated bone destruction.

To further evaluate the therapeutic potential of TAOK3 targeting, we examined the effects of the TAOK3 inhibitor SBI-581 in a murine CIA model. SBI-581 is a promising small molecule inhibitor that has been recently reported to exert significant antitumor effects.[27,29] In vivo, CIA mice were treated with intraperitoneal injections of PBS, SBI-581, or MTX (Figure 6A). After 28 days of treatment, SBI-581 significantly attenuated arthritis progression compared with the untreated group (Figures 6B and C). Micro-CT analysis revealed that SBI-581 treatment markedly reduced bone erosion (Figure 6D). Histologic examination by H&E staining and SO/FG staining further confirmed that SBI-581 effectively ameliorated pathologic damage in the ankle joints, including synovial hyperplasia, bone erosion, and cartilage degradation (Figure 6E and F). Moreover, Western blotting of synovial tissues showed elevated TAOK3 expression in CIA mice, which was significantly decreased by MTX or SBI-581 treatment (Supplementary Figure S6A). Taken together, both in vitro and in vivo experiments demonstrate that TAOK3 is critically involved

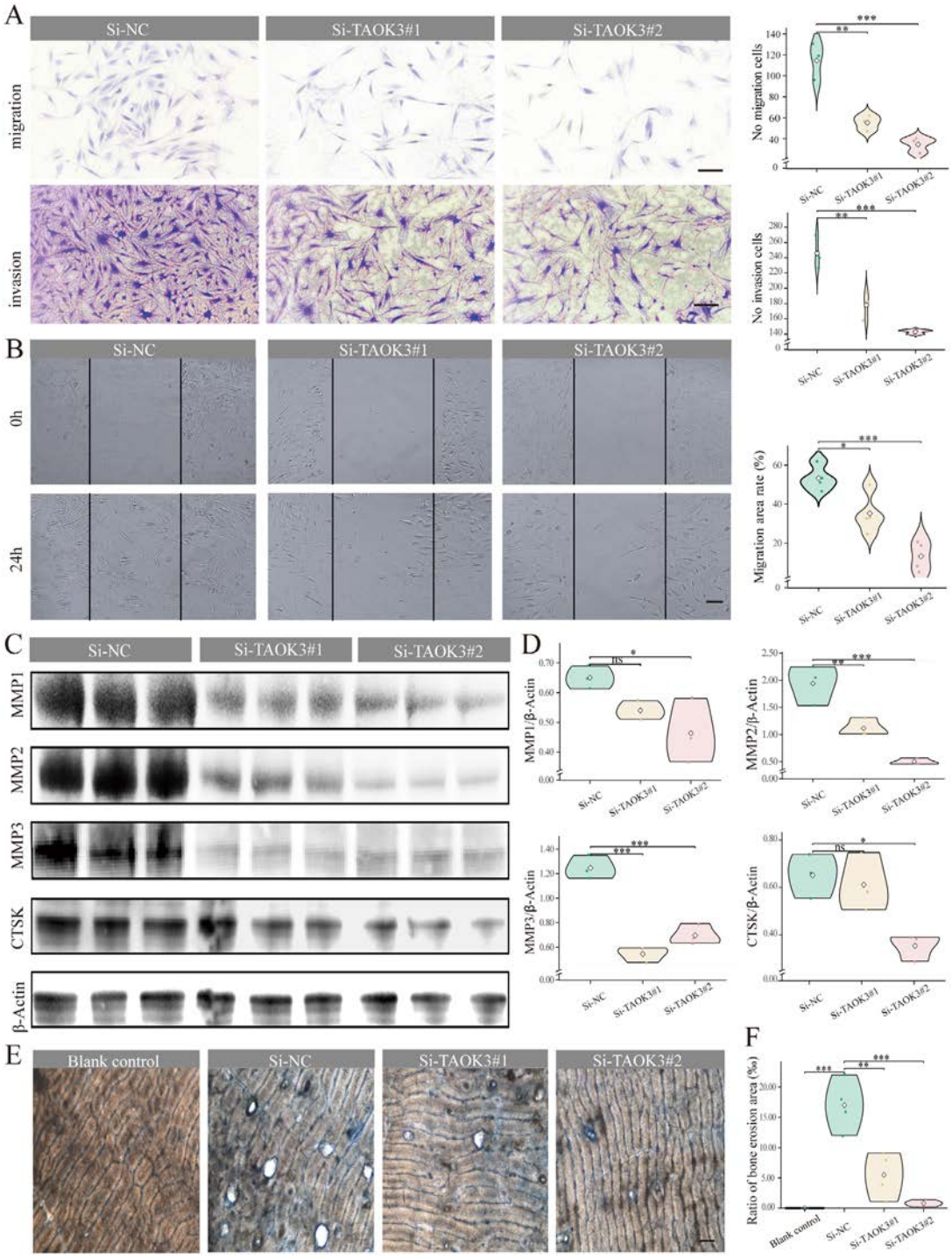

Figure 5. TAOK3 knockdown in vitro attenuates the tumor-like properties of FLSs and mitigates bone erosion induced by pannus cells. (A) Transwell migration and invasion assays evaluating the effects of TAOK3 knockdown by small interfering RNA on pannus FLSs after 2 days of culture. Scale bar = 200 μm. (B) Wound healing assay assessing the migratory capacity of pannus FLSs 24 hours after TAOK3 knockdown. Scale bar = 200 μm. Migration area rate (%) = [(wound area at 0 hours – wound area at 24 hours) / wound area at 0 hours] × 100%. (C) Western blot analysis of MMP1, MMP2, MMP3, and CTSK protein levels in pannus FLSs 48 hours after TAOK3 silencing. (D) Semiquantitative analysis based on the ratio of average band intensity to β-actin. (E) Representative images of bone slice resorption assays showing bone erosion in each group. Scale bar = 100 μm. (F) Quantification of bone resorption area across groups (‰). Data are shown as individual values with group means from at least three biologic replicates using primary FLSs or pannus cells derived from independent patients with rheumatoid arthritis. Group comparisons were performed using one-way analysis of variance. $^{*}P < 0.05$; $^{**}P < 0.01$; $^{***}P < 0.001$. CTSK, cathepsin K; FLS, fibroblast-like synoviocyte; MMP, matrix metalloproteinase; Si-NC, negative-control small interfering RNA; ns, not significant; Si-TAOK3, thousand-and-one–amino acid kinase 3 small interfering RNA. Color figure can be viewed in the online issue, which is available at http://onlinelibrary.wiley.com/doi/10.1002/art.70020/abstract.

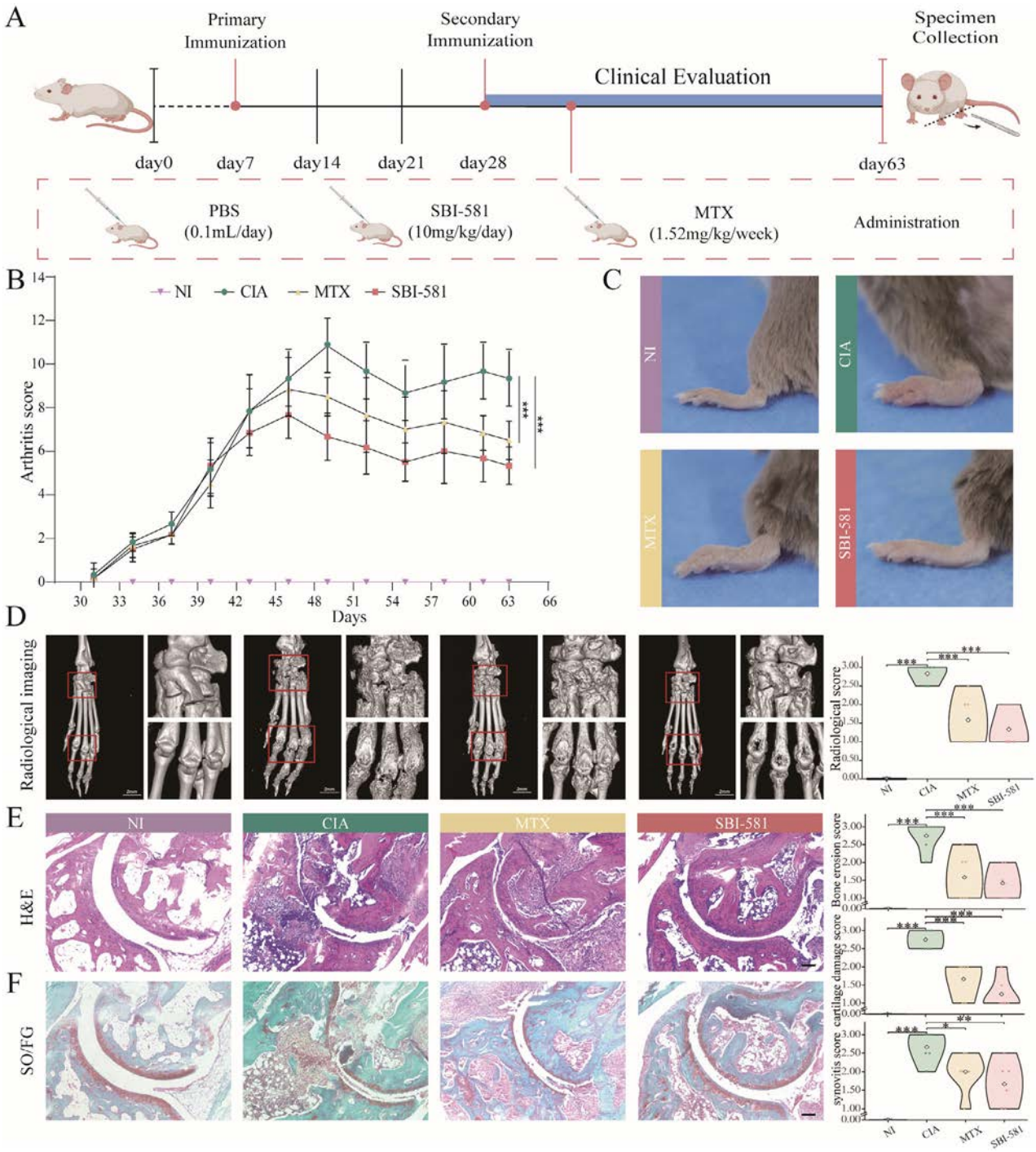

Figure 6. In vivo inhibition of TAOK3 alleviates bone destruction in CIA mice. (A) Schematic diagram of the CIA mouse experimental design. After a 7-day acclimatization period, mice were immunized with bovine type II collagen for 28 days to establish the CIA model followed by intraperitoneal injection of sterile PBS (n = 6), MTX (n = 6), or SBI-581 (n = 6) for 28 consecutive days. (B and C) Arthritis scores of hind paws and representative images from NI mice and CIA mice treated with different interventions. (D) Representative micro-computed tomography images of hind paws and quantitative analysis of bone destruction scores across treatment groups. (E and F) Representative (E) H&E and (F) SO/FG-stained sections from hind paw joints, with histologic scores for bone erosion, cartilage damage, and synovitis assessed according to Standardised Microscopic Arthritis Scoring of Histological sections guidelines (scale 0–3). Scale bar = 50 μm. In part B, data are presented as mean ± SD; in parts D–F, data are presented as individual values with group means indicated. Group comparisons were conducted using one-way analysis of variance. $^{*}P < 0.05$; $^{**}P < 0.01$; $^{***}P < 0.001$. CIA, collagen-induced arthritis; H&E, hematoxylin and eosin; MMP, matrix metalloproteinase; MTX, methotrexate; NI, nonimmunized; PBS, phosphate-buffered saline; SO/FG, safranin O/fast green; TAOK3, thousand-and-one–amino acid kinase 3. Color figure can be viewed in the online issue, which is available at http://onlinelibrary.wiley.com/doi/10.1002/art.70020/abstract.

in the pathologic phenotypes and bone destruction associated with RA and that targeting TAOK3 may represent a promising new therapeutic strategy for RA-related bone erosion.

DISCUSSION

Despite significant advances in RA treatment—particularly with the widespread use of DMARDs—bone destruction in active RA remains a major clinical challenge.[14,43] FLSs are central to disease pathogenesis, driving chronic inflammation and contributing to bone erosion.[11] However, blood-based biomarkers reflecting FLS pathogenic activity are still lacking, limiting accurate assessment and early intervention. In this study, we performed high-depth plasma proteomic profiling in a clinical cohort and mapped the proteomic landscape of active RA. By integrating Sharp scores and previously published single-cell transcriptomic data of synovial tissue, we identified and validated TAOK3 for the first time as a bone destruction–associated biomarker. Functional experiments in vitro and in vivo confirmed TAOK3's critical role in RA-related bone erosion, highlighting its potential as a target for precision monitoring and therapy.

The application of proteomic technology offers new perspectives for understanding the molecular mechanisms underlying different stages of RA. In this study, comparative analysis of plasma proteomic profiles between patients with active and remission RA revealed substantial differences in protein expression. In addition to classical inflammation- and immunity-related pathways, enrichment analysis highlighted significant activation of lipid metabolism–associated signaling in active RA, suggesting that lipid dysregulation may play a key role in active disease and joint damage. This notion is supported by previous findings, including our earlier observation of increased arachidonic acid and linoleic acid metabolism in synovial tissues during active RA.[14,44] Similarly, Ye et al[45] reported enhanced activity of arachidonic acid–regulated calcium-selective channels in $CD4^+$ T cells from patients with RA, promoting T cell hypersensitivity and persistent inflammation. Gan et al[46] further demonstrated a positive correlation between triglyceride levels and markers of inflammation such as CRP and ESR in RA. In the present study, we also found that the PLD signaling pathway was significantly up-regulated in active RA. As a key lipid metabolism pathway, PLD regulates cell proliferation and apoptosis by generating phosphatidic acid and activating MAPK signaling.[47,48] These findings collectively suggest that lipid metabolic dysfunction may serve as a potential driver of active RA, although the precise mechanisms remain to be elucidated.

In addition, we observed significantly elevated levels of several inflammation-related proteins in the plasma of patients with active RA, including CRP, SAA1, and SAA2. Among these, CRP showed the most prominent differential expression; its elevated levels were positively correlated with disease activity (DAS28 score) and are widely used in clinical practice to assess RA activity.[2] However, genetic polymorphisms can introduce substantial interindividual variability in CRP levels, potentially limiting its reliability for disease monitoring.[49] Accordingly, some studies have advocated for the combined use of multiple biomarkers to improve assessment accuracy.[50] In our study, frequent relapse in patients with RA was strongly associated with progressive bone destruction. To identify biomarkers with the potential for monitoring both disease activity and bone destruction, we applied a random forest model and found that TAOK3 ranked among the top features in importance. Notably, combining TAOK3 with CRP significantly enhanced the accuracy of active prediction, highlighting its promise as a dual-purpose biomarker for disease monitoring and prognosis in RA.

TAOK3, a serine/threonine kinase belonging to the TAO kinase family, modulates key signaling pathways such as MAPK, JNK/SAPK, and Hippo.[42,51] Aberrant TAOK3 expression has been implicated in diverse diseases, particularly malignancies, autoimmune disorders, and neurodegenerative conditions. Most current studies have focused on its oncogenic roles; TAOK3 is reportedly overexpressed in several solid tumors, including breast and esophageal cancers, where it facilitates cellular invasion and metastatic spread.[27,29,41] These observations align well with our findings, wherein TAOK3 knockdown markedly suppressed FLS proliferation, migration, and invasion while enhancing apoptosis. Moreover, single-nucleotide polymorphisms in TAOK3 have been associated with increased susceptibility to systemic lupus erythematosus,[52] highlighting its broader relevance in autoimmune pathology.

Although the role of TAOK3 in RA pathogenesis has not been clearly defined, our study provides novel insights into its potential functions. We found that TAOK3 knockdown significantly reduced the expression of MMP1, MMP2, MMP3, and CTSK, accompanied by a marked attenuation of pannus cell–mediated bone resorption. MMPs are well-established mediators of joint destruction in RA, contributing to cartilage degradation, cytokine-driven disruption of intra-articular homeostasis, and enhanced cell migration and angiogenesis.[53] Similarly, CTSK, a critical osteolytic enzyme, promotes bone erosion by regulating osteoclast differentiation and amplifying inflammatory signaling.[54] These downstream pathways may represent mechanisms through which TAOK3 influences FLS pathogenicity. In contrast, TAOK3 overexpression further augmented pannus cell–induced bone resorption, underscoring its pathogenic role in RA-associated bone destruction. Building on these findings, we further investigated the therapeutic potential of TAOK3 inhibition in a CIA mouse model. Treatment with the TAOK3-targeted inhibitor SBI-581 significantly alleviated bone destruction. These findings underscore the pivotal role of TAOK3 in RA-associated bone damage and highlight its potential as a therapeutic target in bone-destructive RA.

To further investigate the mechanisms underlying elevated plasma TAOK3, we assessed TAOK3 expression in FLSs

stimulated with inflammatory cytokines. LPS or TNF-α treatment markedly increased intracellular TAOK3 protein levels, whereas no significant changes were detected in culture supernatants (Supplementary Figure S6B and C). Combined with our apoptosis assays showing that TAOK3 knockdown promotes FLS apoptosis, these findings suggest that increased plasma TAOK3 may be linked to inflammatory stimulation and FLS apoptosis. Nevertheless, the precise mechanisms remain to be elucidated in future studies.

This study has several limitations. First, all participants were recruited from a single center and were exclusively of Han Chinese descent, which may constrain the extrapolation of findings to broader populations. Second, although independent validation cohorts were included, heterogeneity in treatment regimens might have affected plasma protein profiles. Although medication usage was adjusted for in baseline analyses, further studies are needed to delineate its influence on biomarker expression. Third, although our proteomic screening identified several candidate proteins associated with RA-related bone destruction, only TAOK3—the most prominent candidate—underwent systematic functional validation. The roles of other potential targets remain unexplored and warrant further investigation to establish a more comprehensive molecular framework of RA-associated bone damage. Finally, the downstream signaling cascades of TAOK3 in RA pathogenesis remain incompletely defined.

In conclusion, this study identified and validated TAOK3 as a potential plasma biomarker for bone destruction in patients with active RA. We further demonstrated its critical role in promoting the pathogenic phenotype and bone-invasive behavior of synovial cells. With both prognostic and therapeutic relevance, TAOK3 represents a promising target for the precision diagnosis and treatment of RA-associated bone damage.

ACKNOWLEDGMENTS

We sincerely thank the Department of Laboratory Medicine, the Department of Radiology, and all members of Dr Lianbo Xiao's research group at Shanghai Guanghua Hospital of Integrative Medicine for their generous support and valuable contributions to this study.

AUTHOR CONTRIBUTIONS

All authors contributed to at least one of the following manuscript preparation roles: conceptualization AND/OR methodology, software, investigation, formal analysis, data curation, visualization, and validation AND drafting or reviewing/editing the final draft. As corresponding author, Dr Xiao confirms that all authors have provided the final approval of the version to be published and takes responsibility for the affirmations regarding article submission (eg, not under consideration by another journal), the integrity of the data presented, and the statements regarding compliance with institutional review board/Declaration of Helsinki requirements.

REFERENCES

1. Finckh A, Gilbert B, Hodkinson B, et al. Global epidemiology of rheumatoid arthritis. Nat Rev Rheumatol 2022;18(10):591–602.
2. Di Matteo A, Bathon JM, Emery P. Rheumatoid arthritis. Lancet 2023; 402(10416):2019–2033.
3. Sokka T, Kautiainen H, Pincus T, et al; QUEST-RA. Work disability remains a major problem in rheumatoid arthritis in the 2000s: data from 32 countries in the QUEST-RA study. Arthritis Res Ther 2010; 12(2):R42.
4. Ma Y, Chen H, Lv W, et al. Global, regional and national burden of rheumatoid arthritis from 1990 to 2021, with projections of incidence to 2050: a systematic and comprehensive analysis of the Global Burden of Disease study 2021. Biomark Res 2025;13(1):47.
5. Komatsu N, Takayanagi H. Mechanisms of joint destruction in rheumatoid arthritis - immune cell-fibroblast-bone interactions. Nat Rev Rheumatol 2022;18(7):415–429.
6. Aletaha D, Smolen JS. Diagnosis and management of rheumatoid arthritis: a review. JAMA 2018;320(13):1360–1372.
7. Kerschbaumer A, Sepriano A, Bergstra SA, et al. Efficacy of synthetic and biological DMARDs: a systematic literature review informing the 2022 update of the EULAR recommendations for the management of rheumatoid arthritis. Ann Rheum Dis 2023;82(1):95–106.
8. Nagy G, Roodenrijs NMT, Welsing PMJ, et al. EULAR points to consider for the management of difficult-to-treat rheumatoid arthritis. Ann Rheum Dis 2022;81(1):20–33.
9. Németh T, Nagy G, Pap T. Synovial fibroblasts as potential drug targets in rheumatoid arthritis, where do we stand and where shall we go? Ann Rheum Dis 2022;81(8):1055–1064.
10. Liu D, Kuang Y, Chen S, et al. NAT10 promotes synovial aggression by increasing the stability and translation of N4-acetylated PTX3 mRNA in rheumatoid arthritis. Ann Rheum Dis 2024;83(9):1118–1131.
11. Qiu F, Xie D, Chen H, et al. Generation of cytotoxic aptamers specifically targeting fibroblast-like synoviocytes by CSCT-SELEX for treatment of rheumatoid arthritis. Ann Rheum Dis 2025;84(5):726–745.
12. Chu CQ. Fibroblasts in rheumatoid arthritis. N Engl J Med 2020; 383(17):1679–1681.
13. Nygaard G, Firestein GS. Restoring synovial homeostasis in rheumatoid arthritis by targeting fibroblast-like synoviocytes. Nat Rev Rheumatol 2020;16(6):316–333.
14. Meng X, Chen Z, Li T, et al. Role and therapeutic potential for targeting fibroblast growth factor 10/FGFR1 in relapsed rheumatoid arthritis. Arthritis Rheumatol 2024;76(1):32–47.
15. Qu Y, Yao Z, Xu N, et al. Plasma proteomic profiling discovers molecular features associated with upper tract urothelial carcinoma. Cell Rep Med 2023;4(9):101166.
16. Hu C, Dai Z, Xu J, et al. Proteome profiling identifies serum biomarkers in rheumatoid arthritis. Front Immunol 2022;13:865425.
17. Liu S, Guo Y, Lu L, et al. Fibrinogen-like protein 1 is a novel biomarker for predicting disease activity and prognosis of rheumatoid arthritis. Front Immunol 2020;11:579228.
18. Winthrop KL, Isaacs JD, Mease PJ, et al. Unmet need in rheumatology: reports from the Advances in Targeted Therapies meeting, 2022. Ann Rheum Dis 2023;82(5):594–598.
19. Schett G, Tanaka Y, Isaacs JD. Why remission is not enough: underlying disease mechanisms in RA that prevent cure. Nat Rev Rheumatol 2021;17(3):135–144.
20. Aletaha D, Neogi T, Silman AJ, et al. 2010 Rheumatoid arthritis classification criteria: an American College of Rheumatology/European League Against Rheumatism collaborative initiative. Arthritis Rheum 2010;62(9):2569–2581.

21. Smolen JS, Landewé RBM, Bergstra SA, et al. EULAR recommendations for the management of rheumatoid arthritis with synthetic and biological disease-modifying antirheumatic drugs: 2022 update. Ann Rheum Dis 2023;82(1):3–18.
22. Gessl I, Hana CA, Deimel T, et al. Tenderness and radiographic progression in rheumatoid arthritis and psoriatic arthritis. Ann Rheum Dis 2023;82(3):344–350.
23. Götz S, García-Gómez JM, Terol J, et al. High-throughput functional annotation and data mining with the Blast2GO suite. Nucleic Acids Res 2008;36(10):3420–3435.
24. Kanehisa M, Goto S, Sato Y, et al. KEGG for integration and interpretation of large-scale molecular data sets. Nucleic Acids Res 2012;40-(Database issue):D109–D114.
25. Kumar L, E Futschik M. Mfuzz: a software package for soft clustering of microarray data. Bioinformation 2007;2(1):5–7.
26. Kim KM, Lee KG, Lee S, et al. The acute phase reactant orosomucoid-2 directly promotes rheumatoid inflammation. Exp Mol Med 2024;56(4):890–903.
27. Sun M, Li Z, Wang X, et al. TAOK3 facilitates esophageal squamous cell carcinoma progression and cisplatin resistance through augmenting autophagy mediated by IRGM. Adv Sci (Weinh) 2023;10(29): e2300864.
28. Han Y, Liu C, Chen S, et al. Columbianadin ameliorates rheumatoid arthritis by attenuating synoviocyte hyperplasia through targeted vimentin to inhibit the VAV2/Rac-1 signaling pathway. J Adv Res 2025;74:609–620.
29. Iizuka S, Quintavalle M, Navarro JC, et al. Serine-threonine kinase TAO3-mediated trafficking of endosomes containing the invadopodia scaffold TKS5α promotes cancer invasion and tumor growth. Cancer Res 2021;81(6):1472–1485.
30. Chen J, Cheng W, Li J, et al. Notch-1 and Notch-3 mediate hypoxia-induced activation of synovial fibroblasts in rheumatoid arthritis. Arthritis Rheumatol 2021;73(10):1810–1819.
31. Hayer S, Vervoordeldonk MJ, Denis MC, et al. 'SMASH' recommendations for Standardised Microscopic Arthritis Scoring of Histological sections from inflammatory arthritis animal models. Ann Rheum Dis 2021;80(6):714–726.
32. Johnson WT, McBride D, Kerr M, et al. Immunomodulatory nanoparticles for modulating arthritis flares. ACS Nano 2024;18(3):1892–1906.
33. Ge S, Xia X, Ding C, et al. A proteomic landscape of diffuse-type gastric cancer. Nat Commun 2018;9(1):1012.
34. Escal J, Neel T, Hodin S, et al. Proteomics analyses of human plasma reveal triosephosphate isomerase as a potential blood marker of methotrexate resistance in rheumatoid arthritis. Rheumatology (Oxford) 2024;63(5):1368–1376.
35. Yu CS, Lin CJ, Hwang JK. Predicting subcellular localization of proteins for Gram-negative bacteria by support vector machines based on n-peptide compositions. Protein Sci 2004;13(5):1402–1406.
36. Lerner A, Neidhöfer S, Reuter S, et al. MMP3 is a reliable marker for disease activity, radiological monitoring, disease outcome predictability, and therapeutic response in rheumatoid arthritis. Best Pract Res Clin Rheumatol 2018;32(4):550–562.
37. Niu Q, Gao J, Wang L, et al. Regulation of differentiation and generation of osteoclasts in rheumatoid arthritis. Front Immunol 2022;13: 1034050.
38. Ding Q, Hu W, Wang R, et al. Signaling pathways in rheumatoid arthritis: implications for targeted therapy. Signal Transduct Target Ther 2023;8(1):68.
39. Hwang YG, Balasubramani GK, Metes ID, et al. Differential response of serum amyloid A to different therapies in early rheumatoid arthritis and its potential value as a disease activity biomarker. Arthritis Res Ther 2016;18(1):108.
40. Chambers RE, MacFarlane DG, Whicher JT, et al. Serum amyloid-A protein concentration in rheumatoid arthritis and its role in monitoring disease activity. Ann Rheum Dis 1983;42(6):665–667.
41. Lai TC, Fang CY, Jan YH, et al. Kinase shRNA screening reveals that TAOK3 enhances microtubule-targeted drug resistance of breast cancer cells via the NF-κB signaling pathway. Cell Commun Signal 2020;18(1):164.
42. Li J, Wei X, Dong Z, et al. Research progress on anti-tumor mechanism of TAOK kinases. Cell Signal 2024;124:111385.
43. Yoshimura Y, Yamanouchi M, Mizuno H, et al. Efficacy and safety of first-line biological DMARDs in rheumatoid arthritis patients with chronic kidney disease. Ann Rheum Dis 2024;83(10):1278–1287.
44. Lei Q, Yang J, Li L, et al. Lipid metabolism and rheumatoid arthritis. Front Immunol 2023;14:1190607.
45. Ye Z, Shen Y, Jin K, et al. Arachidonic acid-regulated calcium signaling in T cells from patients with rheumatoid arthritis promotes synovial inflammation. Nat Commun 2021;12(1):907.
46. Gan L, He Y, Liu L, et al. Association of serum lipids with autoantibodies and inflammatory markers in rheumatoid arthritis patients. Clin Chim Acta 2018;486:282–290.
47. Kang DW, Choi KY, Min DS. Functional regulation of phospholipase D expression in cancer and inflammation. J Biol Chem 2014;289(33): 22575–22582.
48. Song D, Lim SH, Kim Y, et al. Development and evaluation of indole-based phospholipase D inhibitors for lung cancer immunotherapy. J Med Chem 2025;68(5):5170–5189.
49. Riley TR, Wheeler AM, Cannon GW, et al. Genetically-determined variation in C-reactive protein impacts disease activity assessment in rheumatoid arthritis. Rheumatology (Oxford) 2025;64(6):3921–3928.
50. Ke L, He Q, Qu J, et al. Bone-protective effects of neutralizing angiopoietin-like protein 4 monoclonal antibody in rheumatoid arthritis. Mol Ther 2024;32(12):4497–4513.
51. Fang CY, Lai TC, Hsiao M, et al. The diverse roles of TAO kinases in health and diseases. Int J Mol Sci 2020;21(20):7463.
52. Wang YF, Wei W, Tangtanatakul P, et al. Identification of shared and Asian-specific loci for systemic lupus erythematosus and evidence for roles of type III interferon signaling and lysosomal function in the disease: a multi-ancestral genome-wide association study. Arthritis Rheumatol 2022;74(5):840–848.
53. Bian Y, Xiang Z, Wang Y, et al. Immunomodulatory roles of metalloproteinases in rheumatoid arthritis. Front Pharmacol 2023;14: 1285455.
54. Pan W, Yin W, Yang L, et al. Inhibition of Ctsk alleviates periodontitis and comorbid rheumatoid arthritis via downregulation of the TLR9 signalling pathway. J Clin Periodontol 2019;46(3):286–296.

American College of Rheumatology
Empowering Rheumatology Professionals

Arthritis & Rheumatology
Vol. 78, No. 5, May 2026, pp 1062–1075
DOI 10.1002/art.70028

Tumor Necrosis Factor–Induced Neuropilin-2 in Fibroblast-Like Synoviocytes Exacerbates Rheumatoid Arthritis

Ke Jin, PhD,[1,2] Jingjing Ran, PhD,[1,2] Yuxin Deng, BS,[1,2] Zhiyong Miao, BS,[1,2] Ling Wei, MS,[3] Ying Yang, BS,[4] Min Yang, MD,[1] Tong Li, PhD,[5,6] Haitao Niu, PhD,[7] Geng Yin, MD,[1,8] and Qibing Xie, MD[1]

Objective. We investigated tumor necrosis factor (TNF)-induced neuropilin-2 (NRP2) in rheumatoid arthritis (RA) and focused on its role in inflammation and disease progression and its potential as a therapeutic target in fibroblast-like synoviocytes (FLS).

Methods. Serum and synovial fluid (SF) samples were collected from healthy volunteers (serum, n = 30), patients with osteoarthritis (OA) (SF, n = 20), and patients with RA (serum, n = 76; SF, n = 21) for NRP2 quantification. Synovial tissues from patients with OA (n = 6) and RA (n = 6) were obtained to analyze NRP2 expression and its clinical relevance. Systemic or conditional NRP2 knockout mice were generated, and disease severity was evaluated in serum–transfer-induced arthritis (STIA) models. RA-FLS were transfected with NRP2-specific small interfering RNA to assess the effects on proliferation, apoptosis, and pro-inflammatory cytokine secretion. Chromatin immunoprecipitation sequencing (ChIP-seq) was performed to identify p65-binding sites in the NRP2 locus.

Results. NRP2 levels in RA serum (n = 76) were elevated and correlated with disease activity. TNF up-regulated NRP2 expression in FLS via the transcription factor p65, and elevated NRP2 in turn, amplified local inflammation and tissue damage by increasing FLS proliferation and promoting the release of cytokines, chemokines, and matrix metalloproteinases (MMPs). Both systemic and conditional knockout of NRP2 alleviated joint inflammation and damage in STIA models. The inflammatory regulation mediated by NRP2 was derived primarily from $\alpha^{+}THY1^{+}$ subset within the synovial sublining layer.

Conclusion. TNF-induced NRP2 drives inflammatory persistence in RA and serves as a promising diagnostic biomarker. Targeting the TNF-p65-NRP2 axis in FLS may offer a novel strategy for mitigating arthritis progression.

INTRODUCTION

The hallmark features of rheumatoid arthritis (RA) include synovial hyperplasia with persistent inflammation, accompanied by articular cartilage destruction and bone erosion.[1,2] Sustained inflammatory proliferation of synovial tissue, immune cell infiltration, and inflammatory pannus formation confer tumor-like properties to the synovial microenvironment.[3,4] Despite emerging evidence revealing spatially distinct cell subpopulations with autonomous biologic functions within the synovium, the mechanisms by which these cellular subsets remodel the immunoinflammatory microenvironment via inflammatory signaling, thereby

Supported by National Natural Science Foundation of China (82372789 to Dr Jin, 81902947 to Dr Jin, and 82572070 to Dr Xie), Sichuan Science and Technology Program (2025ZNSFSC0638 to Dr Yin and 2024YFFK0062 to Dr Xie), Natural Science Foundation of Sichuan Province (2024NSFSC1760 to Dr Li), and Individual Matching Funds of West China Hospital (141212012 to Dr Jin).

[1]Department of Rheumatology and Immunology, Laboratory of Human Diseases and Immunotherapies, Frontiers Science Center for Disease-related Molecular Network, West China Hospital, Sichuan University, Chengdu, China; [2]Institute of Immunology and Inflammation, West China Hospital, Sichuan University, Chengdu, China; [3]Hospital of Chengdu Office of People's Government of Xizang Autonomous Region, Chengdu, China; [4]Institute of Respiratory Health, Precision Medicine Key Laboratory of Sichuan Province, Sichuan Provincial Engineering Laboratory of Precision Medicine, West China Hospital, Sichuan University, Chengdu, China; [5]State Key Laboratory of Biotherapy and Cancer Center, West China Hospital, Sichuan University and Collaborative Innovation Center for Biotherapy, Chengdu, China; [6]West China Medical Publishers, West China Hospital of Sichuan University, Chengdu, China; [7]Key Laboratory of Viral Pathogenesis and Infection Prevention and Control, Ministry of Education, School of Medicine, Jinan University, Guangzhou, China; [8]Department of General Practice, General Practice Medical Center, West China Hospital, Sichuan University, Chengdu, China.

Additional supplementary information cited in this article can be found online in the Supporting Information section (https://acrjournals.onlinelibrary.wiley.com/doi/10.1002/art.70028).

Author disclosures and graphical abstract are available at https://onlinelibrary.wiley.com/doi/10.1002/art.70028.

Address correspondence via email to Ke Jin, PhD, at jinke@wchscu.edu.cn; to Haitao Niu, PhD, at htniu@jnu.edu.cn; to Geng Yin, MD, at yingeng1975@163.com; or to Qibing Xie, MD, at xieqibing1971@163.com.

Submitted for publication May 27, 2025; accepted in revised form November 17, 2025.

perpetuating the self-reinforcing cycle of inflammation–proliferation–inflammation, remain poorly characterized.

During the progression of RA, the release of pro-inflammatory cytokines initiates the remodeling of the synovial inflammatory microenvironment, in which necrosis factor-α (tumor necrosis factor [TNF]) plays a central role.[5,6] Within synovial tissues, fibroblast-like synoviocytes (FLS) serve as primary effector cells for TNF. TNF amplifies pro-inflammatory cascades through FLS, promotes FLS proliferation by inhibiting ferroptosis, and induces the sustained activation of arthritogenic genes in these cells.[7,8] Consequently, early intervention with TNF-blocking biologic agents significantly improves patient prognosis and prevents RA-related disability.[9,10] However, a substantial proportion of patients exhibit a primary nonresponse to anti-TNF therapy and fail to achieve clinical remission.[11,12] Notably, systemic TNF blockade in RA increases the risk of venous thromboembolism and serious infections, particularly during the initial six-month treatment period.[13,14] These limitations highlight the need to identify key TNF-inducible effector proteins within FLS that amplify inflammatory cascades. Targeted inhibition of such mediators may mitigate the adverse events associated with global TNF blockade while providing novel therapeutic strategies for FLS-directed precision therapy.

Neuropilin-2 (NRP2) is a single-pass transmembrane non-tyrosine kinase receptor that regulates the development and physiologic functions of blood vessels, lymphatic vessels, and the nervous system.[15–18] As a tumor biomarker and driver of metastasis, NRP2 plays a critical role in tumor progression.[19–23] Recent studies highlight its immunomodulatory functions: Efzofitimod, an NRP2-targeting immunomodulator, has demonstrated efficacy against pulmonary sarcoidosis and is currently in phase III clinical trials.[24,25] A striking finding was the sustained high expression of NRP2 in FLS. Although it is only transiently induced in macrophages, its expression in FLS not only escaped repression but also reached levels dozens of times higher than the peak observed in macrophages.[8] Our previous research identified NRP2 as a TNF-induced immunoregulatory protein in myeloid cells, which has an expression that is sensitive to TNF stimulation and suppressed by inhibiting the TNF-activated NF-κB signaling pathway.[26] However, the clinical relevance of TNF-induced NRP2 expression in RA progression and its specific role in RA pathogenesis remain unknown. Clarifying these questions will elucidate the mechanisms of NRP2-mediated immune microenvironment regulation in synovial tissues and provide novel insights into FLS-targeted therapeutic strategies for RA.

Here, we show that NRP2 expression is positively correlated with RA disease activity and is predominantly localized to the pro-inflammatory $FAP\alpha^{+}THY1^{+}$ FLS subset in the synovial sublining layer. In FLS, TNF promotes NRP2 transcription and translation via the transcription factor p65, which in turn enhances the release of inflammatory cytokines, chemokines, and matrix metalloproteinases (MMPs). Genetic ablation of NRP2 alleviated synovial inflammation and joint damage in a murine arthritis model. Collectively, our findings reveal that TNF-induced NRP2 amplification of inflammatory cascades in synovial tissue drives a self-sustaining inflammatory–proliferative feedback loop. These results identify NRP2 as a potential fibroblast-specific therapeutic target for RA synovitis.

METHODS

Human samples

All human clinical samples used in this study were approved by the Ethics Committee on Biomedical Research, West China Hospital of Sichuan University (Ethical Approval Number: 2020-1151), and participants involved in the study voluntarily signed informed consent forms. In this study, patients with RA met the American College of Rheumatology (ACR) 1986 or EULAR 2010 classification criteria,[9,14] and patients with osteoarthritis (OA) met the ACR classification criteria. Clinical history, signs, and serologic test results were used to ensure that the samples used in this study were RA or OA, rather than other diseases that could also cause arthritis or arthralgia. The basic information of the study participants is summarized in Supplementary Table 1.

Mice

Rosa26-SA-CreERT2 mice and *Nrp2*$^{fl/fl}$ transgenic mice based on C57BL/6J background were purchased from Gempharmatech Co., Ltd (Nanjing, China). DBA/J1 mice purchased from Beijing HFK Bioscience were used for collagen-induced arthritis (CIA) modeling. All the mice were housed in the Animal Experimentation Center of West China Hospital of Sichuan University under specific pathogen-free conditions, following institutional guidelines. All animal experiments were approved by the Animal Ethics Committee, West China Hospital of Sichuan University (Ethical Approval Number: 20240621015). To generate systemic knockout mice, *Nrp2*$^{fl/fl}$ mice were crossed with *Rosa26-SA-CreERT2* mice.

CIA and serum–transfer-induced arthritis (STIA) murine models

The CIA murine model was constructed via the immune response of 8- to 10-week-old male DBA/J1 mice to chick type II collagen. To prepare the chick type II collagen immunogen, chick type II collagen (Chondrex, 20011) (2 mg/mL) was mixed with complete Freund's adjuvant (Chondrex, 7023) (5 mg/mL) in equal volume, and chick type II collagen was slowly dripped into the stirred complete Freund's adjuvant on ice and emulsified for 60 to 90 minutes, until the emulsion added to the water did not

disperse. The mice were immunized twice with this immunogen. For the first immunization (day 0), mice were anesthetized with pentobarbital sodium, and 100 μL of the emulsion was slowly injected at 1.5 to 2 cm from the root of each mice's tails. The second immunization was performed on day 21, with care taken to replace the adjuvant with incomplete Freund's adjuvant, and other procedures were performed identically. On days 35 through 49, the model was successfully constructed if the knee joints, ankle joints, paws, and toe joints of the mice were inflamed.

To induce the STIA murine model, *Nrp2*$^{fl/fl}$ (control) and *Nrp2*$^{fl/fl}$ *Rosa26-SA-CreERT2* (NRP2 knockout, KO) mice were used. In addition, knee, and ankle joint-specific NRP2 conditional knockout (cKO) mice generated via adeno-associated virus (AAV) infection were subjected to a local NRP2-deficient STIA model. The virus was purchased from Nanjing Gausia Biotechnology Co., Ltd. To obtain cKO mice, 20 seven-week-old *Nrp2*$^{fl/fl}$ mice were divided into two groups. The AAV9-GFP group had bilateral intra-articular injections of AAV9-GFP (titer: 4.24 × 1,013 vg/mL) that were administered into both knee and ankle joints. The AAV9-Cre group had bilateral intra-articular injections of AAV9-Cre (titer: 2.63 × 1,013 vg/mL) that were delivered into the knee and ankle joints. The injection volumes, 6 μL per knee joint (via a medial patellar ligament approach) and 2 μL per ankle joint (via a dorsal tibiotalar joint approach), were determined and optimized during preliminary studies. Three weeks after the injection, the mice were used for modeling. *Nrp2*$^{fl/fl}$ and *Nrp2*$^{fl/fl}$ *Rosa26-SA-CreERT2* mice were injected intraperitoneally with 150 μL of K/BxN serum (day 0), and the ankle joints of the mice were noticeably inflamed on day 9. In addition, AAV-GFP and AAV-Cre mice were injected intraperitoneally with 150 μL of K/BxN serum, and arthritis was evident on day 9.

Multiple immunohistochemical staining (tyramide signal amplification)

The tissue slides were baked, deparaffinized, and hydrated, after which the slides were immersed in 10% neutral formalin for 20 minutes. After antigen repair and cooling, the slides were blocked at room temperature for 10 minutes with sealing solution. The samples were incubated with the corresponding primary and secondary antibodies listed in Supplementary Table 2 at room temperature; then, the samples were stained at room temperature for 10 minutes. After that, the cells were subjected to nuclear staining with DAPI. Finally, the slides were washed with saline–sodium citrate buffer and sealed with an anti-quench sealer. A multispectral automated quantitative tissue system (Perkin Elmer) was used to scan the slides, and the data were analyzed with Quapth software.

Flow cytometry

P3 generation of FLS were stained with a phycoerythrin-conjugated anti-human-FAPα antibody (R&D Systems) to assess the purity of FLS. In this study, P3-P8 generation of FLS were used to construct an in vitro model. In addition, heterogeneous subpopulations and infiltrating immune cell numbers and frequencies in mouse synovial tissue were also detected with the antibodies listed in Supplementary Table 2 via flow cytometry. The data were analyzed by Flow Jo software.

Statistical analysis

All experiments were performed with at least three biologic replicates, and the data used in this study were statistically analyzed and graphed via Graph Prism 9.0.0 software. If the data were normally distributed, two-tailed Student's *t*-test or one-way analysis of variance was used. The detailed sample size and statistical methods used for each analysis are specified in the figure legends, and $P < .05$ was considered statistically significant. More details of the materials and methods are available in the Supplementary Materials.

RNA sequencing and chromatin immunoprecipitation followed sequencing (ChIP-seq) raw data are deposited in Science Data Bank (ScienceDB, https://www.scidb.cn/en) under the DOIs 10.57760/sciencedb.24014 and 10.57760/sciencedb.24038. All data are available in the paper and/or the Supplementary Materials. Additional data related to this paper may be obtained from the corresponding author upon reasonable request.

RESULTS

NRP2 functions as a TNF-induced inflammation-sensing protein and an inflammation-sustaining protein in synovial tissues

Unlike synovial tissue from patients with OA, synovial tissue from patients with RA exhibited abnormal hyperplasia and a greater than 5-fold upregulation of NRP2 expression (Figure 1A and B). Compared with healthy controls, patients with RA showed a two-fold increase in mean serum NRP2 protein level (Figure 1C). Furthermore, higher disease activity (Disease Activity Score in 28 joints [DAS28] > 5.1) in patients with RA correlated with increased serum NRP2, whereas patients in clinical remission (DAS28 ≤ 2.6) presented NRP2 levels comparable with those of healthy controls (Figure 1D). Additionally, the mean NRP2 protein level in synovial fluid (SF) of RA patients was approximately three-fold higher than that in the patients with OA (Figure 1E). These findings demonstrate a strong clinical correlation between NRP2 expression in serum or synovial tissue and RA. To validate this correlation, we examined NRP2 expression in the synovial tissue and front paws of STIA mice. NRP2 expression was significantly greater in both synovial tissue and front paws than in controls (Figure 1F and G). Similarly, CIA mice exhibited elevated NRP2 expression in hind paws relative to controls (Figure 1H).

Based on the observed upregulation of NRP2 in RA synovium, we isolated and purified FAPα^{+} FLS from RA synovial tissue

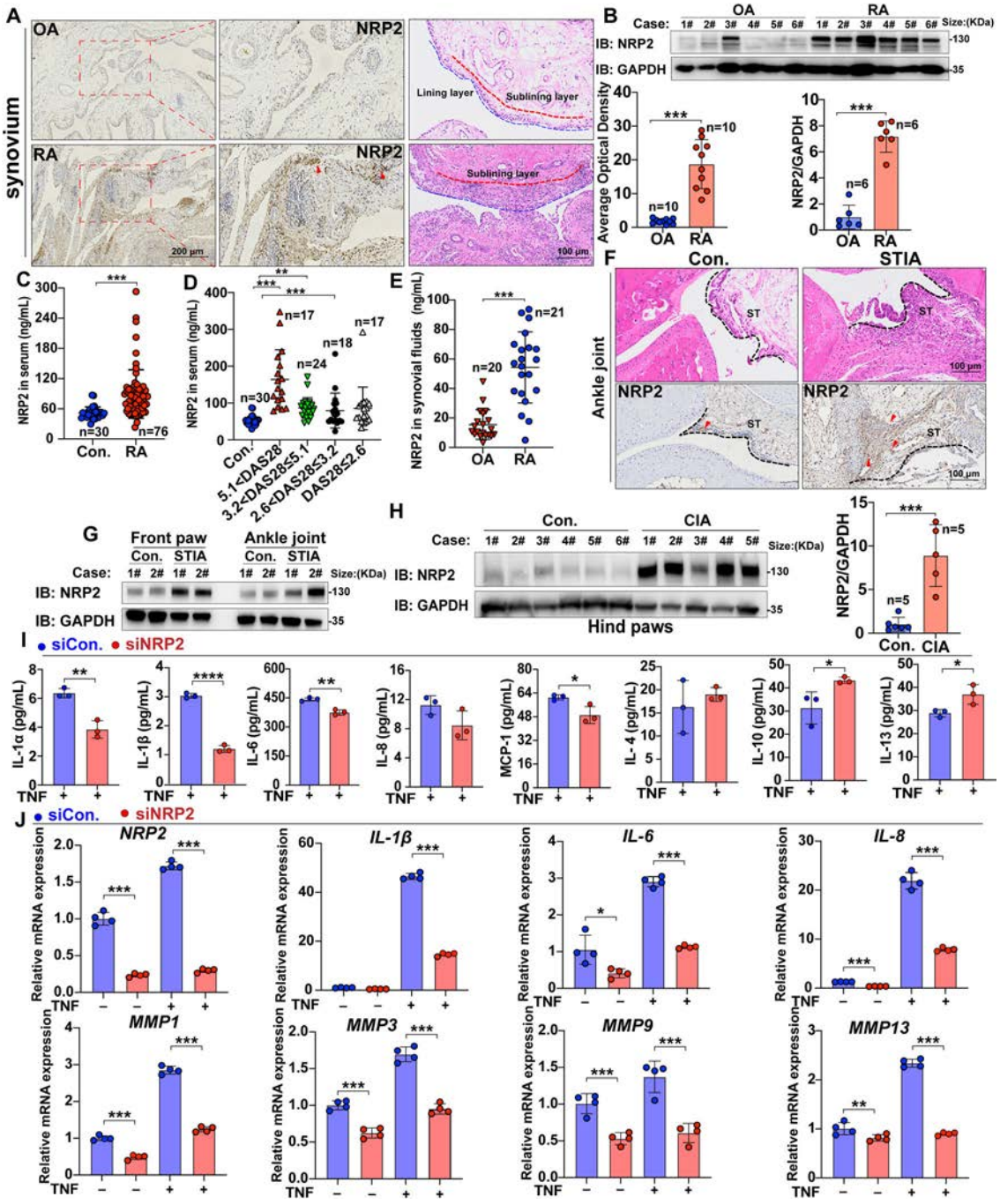

Figure 1. NRP2 acts as a TNF-induced inflammation-sensing and inflammation-sustaining protein in synovial tissues: (A) NRP2 expression (left/middle) and histology of synovial tissues (right) from patients with OA/RA were analyzed by IHC and H&E staining. (B) Western blot analysis of NRP2 expression in synovial tissues. (C–E) NRP2 concentrations in serum from healthy controls and patients with RA (C–D) and in SF from patients with OA/RA (E) by ELISA. (F) Upper: representative histology images of ankle joints of control and STIA mice; lower: NRP2 expression in ankle joints of control and STIA mice. (G–H) Western blot analysis of NRP2 expression in front paws and hind ankle joints from control and STIA mice (G), and in hind paws from control and CIA mice (H). (I) Cytokines in supernatant of RA-FLS were analyzed by Luminex assay. (J) Relative expression of *NRP2*, *IL-1β*, *IL-6*, *IL-8*, *MMP1*, *MMP3*, *MMP9*, and *MMP13* in RA-FLS was detected by qRT-PCR. RA-FLS were transfected with control *siRNA* or *siNRP2* for 24 hours, followed by treatment with or without TNF for 20 hours (I–J). Data are presented as mean ± SD. Statistical significance was determined by one-way ANOVA (D) or two-tailed Student's *t* test (C), (E), (I), and (J), (*$P < 0.05$, **$P < 0.01$, ***$P < 0.001$). ANOVA, analysis of variance; CIA, collagen-induced arthritis; ELISA, enzyme-linked immunosorbent assay; FLS, fibroblast-like synoviocyte; H&E, hematoxylin and eosin; IHC, immunohistochemistry; IL, interleukin; MCP, monocyte chemoattractant protein; MMP, matrix metalloproteinase; mRNA, messenger RNA; NRP2, neuropilin-2; OA, osteoarthritis; qRT-PCR, quantitative reverse-transcription polymerase chain reaction; RA, rheumatoid arthritis; SD, standard deviation; SF, synovial fluid; siRNA, small interfering RNA; STIA, serum–transfer-induced arthritis; TNF, tumor necrosis factor.

(Supplementary Figure 1A and B) to investigate NRP2 expression and its role in inflammatory responses. RA-derived FLS presented higher basal NRP2 expression than OA-derived FLS did (Supplementary Figure 1C). The pro-inflammatory cytokines TNF and interleukin (IL)-1β significantly induced both NRP2 messenger RNA (mRNA) and protein expression in RA-FLS, with TNF exerting a stronger inductive effect (Supplementary Figure 1D and E). Notably, TNF rapidly up-regulated NRP2 protein expression in FLS in a time-dependent manner, and this increase persisted for over 72 hours without significant attenuation (Supplementary Figure 1F–H), indicating that TNF could sustain long-term NRP2 overexpression in FLS.

Knockdown of NRP2 in RA-FLS attenuated the TNF-induced increase in the NRP2 protein level (Supplementary Figure 2A and B). Compared with controls, NRP2 knockdown suppressed the release of pro-inflammatory factors (IL-1, IL-6, and IL-8) and the chemokine monocyte chemoattractant protein-1 (MCP-1) in response to TNF or IL-1β-stimulation and promoted the secretion of anti-inflammatory cytokines IL-10 and IL-13 (Figure 1I and Supplementary Figure 2C). Similarly, regardless of TNF or IL-1β stimulation, NRP2 knockdown reduced mRNA levels of pro-inflammatory cytokines (*IL-1*, *IL-6*, and *IL-8*) and metalloproteinases (*MMP1*, *MMP3*, and *MMP9*) (Figure 1J and Supplementary Figure 2D). These results demonstrate that NRP2 in synovial tissue acts both as a TNF-induced inflammation-sensing protein and a key mediator that sustains inflammatory responses.

Systemic and conditional knockout of NRP2 attenuates synovial inflammation and damage in STIA mice

On day nine post-STIA induction, littermate *Nrp2*$^{fl/fl}$ mice exhibited pronounced swelling in the ankles, hind paws, and toe joints, whereas *Nrp2*$^{fl/fl}$*Rosa26-SA-CreERT2* mice displayed only mild swelling or complete resolution (Figure 2A). Furthermore, *Nrp2*$^{fl/fl}$*Rosa26-SA-CreERT2* mice showed approximately 50% reductions in ankle/hind paw thickness and clinical arthritis scores compared with *Nrp2*$^{fl/fl}$ mice (Figure 2B–D).

Histopathological evaluation of ankle and knee joints revealed elevated osteoclast activity, varying degrees of cartilage erosion, and structural degradation in *Nrp2*$^{fl/fl}$ mice, in contrast with the preserved joint integrity in *Nrp2*$^{fl/fl}$*Rosa26-SA-CreERT2* mice (Figure 2E–F and Supplementary Figure 3A–B). Quantification of the severity of synovitis, pannus formation, and inflammatory cell infiltration via hematoxylin and eosin staining confirmed that scores of the *Nrp2*$^{fl/fl}$*Rosa26-SA-CreERT2* mice were approximately half of those in controls (Figure 2G and Supplementary Figure 3C). Micro-computed tomography (CT) imaging highlighted bone erosion, articular surface roughness, and joint deformity in *Nrp2*$^{fl/fl}$ mice, whereas *Nrp2*$^{fl/fl}$*Rosa26-SA-CreERT2* mice maintained smooth articular surfaces and minimal subchondral bone destruction (Figure 2H). Trabecular bone loss was exacerbated in *Nrp2*$^{fl/fl}$ mice compared with *Nrp2*$^{fl/fl}$*Rosa26-SA-CreERT2* mice (Supplementary Figure 3D). *Nrp2*$^{fl/fl}$*Rosa26-SA-CreERT2* mice exhibited superior bone metrics, including increased bone mineral density (BMD), bone volume (BV), BV/total volume (TV), trabecular thickness (Tb.Th), and trabecular number (Tb.N), alongside reduced trabecular separation (Tb.Sp) in femurs and tibiae (Figure 2I and Supplementary Figure 3D). STIA-challenged *Nrp2*fl/fl*Rosa26-SA-CreERT2* mice showed significant downregulation of the levels of pro-inflammatory cytokines (TNF, IL-1β, and IL-6) in serum and of synovial mRNA (*Tnf*, *Il-1β*, and *Il-6*) levels vs *Nrp2*$^{fl/fl}$ counterparts (Figure 2J and Supplementary Figure 3F). Flow cytometry further revealed reduced infiltration of myeloid cells in the synovial tissues of *Nrp2*$^{fl/fl}$*Rosa26-SA-CreERT2* mice (Figure 2K and Supplementary Figure 3G and H). Collectively, these data indicate that systemic *Nrp2* knockout alleviates synovitis and joint damage in the STIA model.

To further delineate the tissue-specific effects of NRP2 on knee/ankle joint inflammation and tissue injury in the STIA model, we constructed an STIA mouse model with conditional NRP2 knockout localized to the knee/ankle joints. On day nine post-modeling, compared with *Nrp2*$^{fl/fl}$+AAV9-GFP controls, the *Nrp2*$^{fl/fl}$+AAV9-Cre group exhibited reduced swelling in the ankle joints, hind paws, and digit joints, with only mild edema (Supplementary Figure 4A). The *Nrp2*$^{fl/fl}$+AAV9-Cre group exhibited an approximately 30% reduction in ankle/hind paw thickness and clinical arthritis scores vs the *Nrp2*$^{fl/fl}$+AAV9-GFP group (Supplementary Figure 4B-D). Histopathological analysis revealed that *Nrp2*$^{fl/fl}$+AAV9-GFP mice displayed pronounced joint destruction in ankle/knee joints, characterized by bone erosion at articular cartilage and increased periarticular osteoclasts, whereas *Nrp2*$^{fl/fl}$+AAV9-Cre mice showed preserved joint integrity (Supplementary Figure 4E–F and 5A–B). Quantitative assessments of synovitis severity, pannus formation, and inflammatory cell infiltration confirmed significantly lower pathologic scores in *Nrp2*$^{fl/fl}$+AAV9-Cre mice than in *Nrp2*$^{fl/fl}$+AAV9-GFP mice (Supplementary Figure 4G and 5C). *Nrp2*$^{fl/fl}$+AAV9-GFP joints exhibited rough, irregular articular surfaces with overt bone erosion, whereas *Nrp2*$^{fl/fl}$+AAV9-Cre joints maintained near-normal bone architecture (Supplementary Figure 4H). Micro-CT analysis revealed increased trabecular number (Supplementary Figure 5D) and elevated BMD, BV, and BV/TV in *Nrp2*$^{fl/fl}$+AAV9-Cre femurs/tibiae vs *Nrp2*$^{fl/fl}$+AAV9-GFP femurs/tibiae (Supplementary Figure 4I and 5E). Furthermore, *Nrp2*$^{fl/fl}$+AAV9-Cre mice showed greater Tb.Th and Tb.N with reduced Tb.Sp (Supplementary Figure 4I and 5E).

Compared with *Nrp2*$^{fl/fl}$+AAV9-GFP control, local NRP2 knockout significantly decreased the mRNA levels of pro-inflammatory cytokines (*Il-1β*, *Il-6*, and *Tnf*) in synovial tissue and reduced serum protein levels of these cytokines (Supplementary Figure 4J and 5F). Flow cytometry revealed a decreased

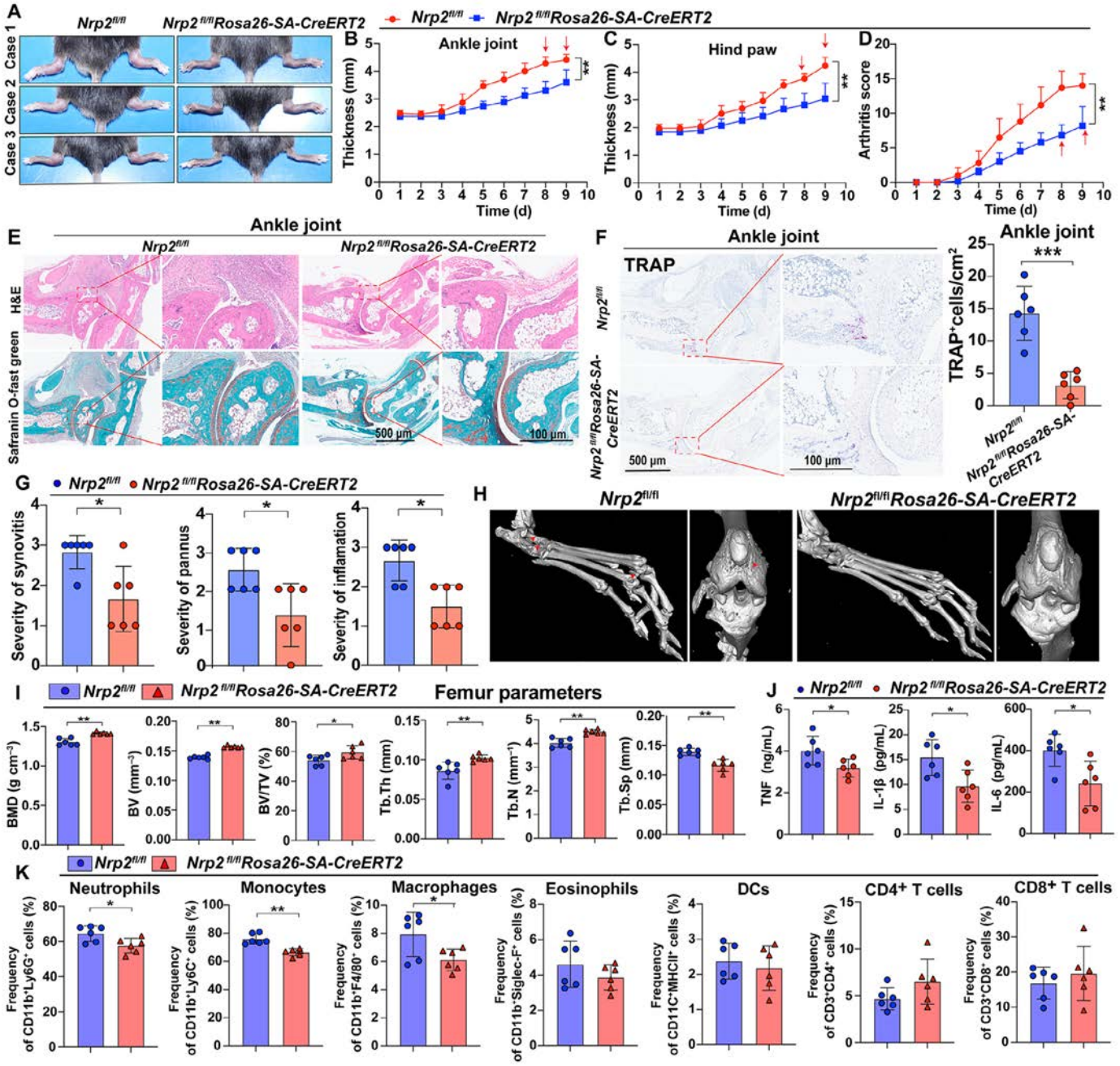

Figure 2. Systemic NRP2 knockout alleviates synovitis and joint damage in STIA mice: (A) Representative images of ankle joints from NRP2-deleted (left) and control (right) STIA mice. (B–C) The thickness of ankle joints (B) and hind paws (C) in NRP2-deleted and control STIA mice was measured at indicated time. (D) Arthritis score of NRP2-deleted and control STIA mice. (E) Histologic analysis: H&E staining (top), safranin O-fast green staining (bottom). (F) Representative images of TRAP staining. Magnified views are shown on the right (E–F). (G) Pathologic scoring of synovial hyperplasia of ankle joints, pannus formation, and inflammatory infiltration in ankle joints (NRP2-deleted vs control STIA mice). (H) Micro-CT images of ankle and knee joints; arrows indicate damaged areas. (I) Quantitative femoral parameters. (J) Serum levels of TNF, IL-1b, and IL-6 in NRP2-deleted and control STIA mice was measured by ELISA. (K) Flow cytometry analysis of frequency of immune cell subsets in synovial tissue of NRP2-deleted and control STIA mice. Data are presented as mean ± SD. (n = 6 mice per group); $^{*}P < 0.05$, $^{**}P < 0.01$. Statistical analysis was performed by using two-tailed Student's *t*-test (B–D, F–G, and I–K). CT, computed tomography; ELISA, enzyme-linked immunosorbent assay; H&E, hematoxylin and eosin; IL, interleukin; micro-CT, micro–computed tomography; NRP2, neuropilin-2; STIA, serum–transfer-induced arthritis; TNF, tumor necrosis factor; TRAP, tartrate-resistant acid phosphatase. Color figure can be viewed in the online issue, which is available at http://onlinelibrary.wiley.com/doi/10.1002/art.70028/abstract.

frequency and absolute counts of infiltrating neutrophils, monocytes, and macrophages in *Nrp2*$^{fl/fl}$+AAV9-Cre synovium (Supplementary Figure 4K and 5G). Overall, we confirmed that both systemic and joint-specific NRP2 ablation robustly mitigated synovitis and osteoarticular damage in STIA mice. These findings substantiate the conclusion that NRP2 functions as an

inflammation-sustaining protein induced during inflammatory processes.

NRP2 in FLS promotes TNF-induced inflammation via the chemokines CCL2 and CCL5

Given that NRP2 is a TNF-induced inflammation-sensing protein and that FLS represents the primary effector cells in synovial tissue responsive to TNF, we further investigated how NRP2 modulates TNF-driven inflammatory responses in FLS. Compared with controls, NRP2-knockdown in FLS (siNRP2 FLS) exhibited substantial downregulation of inflammation-related genes (eg, *CCL5*, *RIPK3*, *FOS*, *NR4A1*, *TEK*, *CXCL2/3/6*, and *MMP1*) within two hours of TNF stimulation (Figure 3A). Most of these down-regulated genes were enriched in TNF- and RA-associated signaling pathways (Figure 3B). Similarly, after 20 hours of TNF stimulation, siNRP2 FLS markedly suppressed the expression of inflammatory genes (eg, *CCL5*, *FOSB*, *CXCL9/10/11*, and *TEK*) (Figure 3C), which were also predominantly enriched in TNF/RA-related pathways (Figure 3D). We selected several genes (*CCL2*, *CCL5*, *FOS*, *LIF*, *TEK*, and the necrosis-related gene *RIPK3*) that were consistently downregulated in siNRP2 groups under both 2-hour and 20-hour TNF stimulation for quantitative reverse-transcription polymerase chain reaction (qRT-PCR) validation. This analysis confirmed their reduced expression across all the TNF exposure conditions compared with that of the controls. The most pronounced downregulation was observed for CCL2 and CCL5 (Figure 3E and F and Supplementary Figure 6A and B). Further analysis confirmed that NRP2 knockdown significantly inhibited CCL2 and CCL5 secretion after 20 hours of TNF stimulation (Figure 3G and H). Conversely, NRP2-overexpressing FLS exhibited increased CCL2 and CCL5 secretion following TNF stimulation (Supplementary Figure 6C–F).

The focus on CCL2 and CCL5 is highly relevant to RA pathogenesis. CCL5 is abundant in the serum and synovium of patients with RA, whereas CCL2 is a master regulator of immune cell recruitment, inflammation, angiogenesis, and osteoclastogenesis.[27–29] Consistent with these findings, we found that the SF levels of CCL2 and CCL5 were approximately six-fold and one-fold greater, respectively, in patients with RA than in controls with OA (Figure 3I and J), underscoring their clinical relevance and revealing that the TNF–NRP2–CCL2/CCL5 axis is a potential contributor to RA inflammation.

THY1$^+$ cells serve as the primary inflammatory regulators in the sublining layer of RA synovial tissue.[2,30] Compared with synovial tissue from patients with OA, RA synovium contained a greater number of THY1$^+$ cells. Furthermore, among RA synovial tissues, those with high NRP2 expression demonstrated more extensive infiltration of CD68$^+$ macrophages and CD4$^+$/CD8$^+$ T cells than those with low NRP2 expression did (Figure 3K), indicating a positive correlation between NRP2 expression levels and the degree of synovial inflammation in RA. Collectively, these results demonstrate that NRP2 in FLS promotes TNF-induced synovitis through the chemokines CCL2 and CCL5.

The TNF-induced inflammation-sensing protein NRP2 is predominantly enriched in the FAPα$^+$THY1$^+$ cell subset localized within the sublining layer of synovial tissues

Podoplanin (PDPN) and thymus cell antigen 1 (THY1, also known as CD90) are established biomarkers of RA-FLS, whereas FAPα has also been implicated in the pathologic progression of RA synovial tissues.[2,30,31] To further characterize these markers, we examined their expression in synovial tissues from patients with OA and RA. Compared with OA synovial tissues, RA synovial tissues exhibited higher FAPα expression in the lining layer, and PDPN was expressed in both the lining and sublining layers. Notably, THY1 expression was elevated in the sublining layer of RA synovial tissues, and its expression regions significantly overlapped with those of NRP2 (Figure 4A). We then sorted FAPα$^+$PDPN$^+$ FLS from RA synovial tissues and analyzed the proportions of THY1$^-$NRP2$^+$ and THY1$^+$NRP2$^+$ cell subsets. The results indicated that cells with high THY1 positivity also displayed increased NRP2 positivity (Figure 4B). In both CIA and STIA murine models, NRP2 expression was predominantly localized to THY1$^+$ sublining cells rather than to THY1$^-$ lining cells, as assessed by the cell proportions and absolute cell counts (Figure 4C–F). These findings further support the predominant enrichment of NRP2 in THY1$^+$ sublining cells. We also performed long-term culture of FAPα$^+$THY1$^-$ and FAPα$^+$THY1$^+$ RA-FLS isolated by fluorescence-activated cell sorting. After extended culture, baseline NRP2 expression levels were comparable between the two FLS subsets, likely because of diminished inflammatory signaling under culture conditions. However, after TNF stimulation, the FAPα$^+$THY1$^+$ subset exhibited significantly higher NRP2 expression than did the FAPα$^+$THY1$^-$ subset. These results indicate that NRP2 is predominantly expressed in the sublining layer of RA synovial tissues, specifically within the FAPα$^+$THY1$^+$ subset, and its expression in this subset is more sensitive to TNF stimulation.

TNF-induced NRP2 promotes the proliferation of FLS and enhances their resistance to apoptosis

Synovial thickening in patients with RA, driven by FLS hyperplasia, underlies bone erosion, joint destruction, and disability.[1,2] We therefore investigated whether TNF-induced NRP2 promotes FLS proliferation. Knockdown of NRP2 in FLS significantly attenuated their proliferative capacity compared with controls (Figure 5A). TNF stimulation enhanced FLS proliferation, yet NRP2-deficient FLS still exhibited markedly reduced proliferation relative to controls (Figure 5A and Supplementary Figure 7A and B).

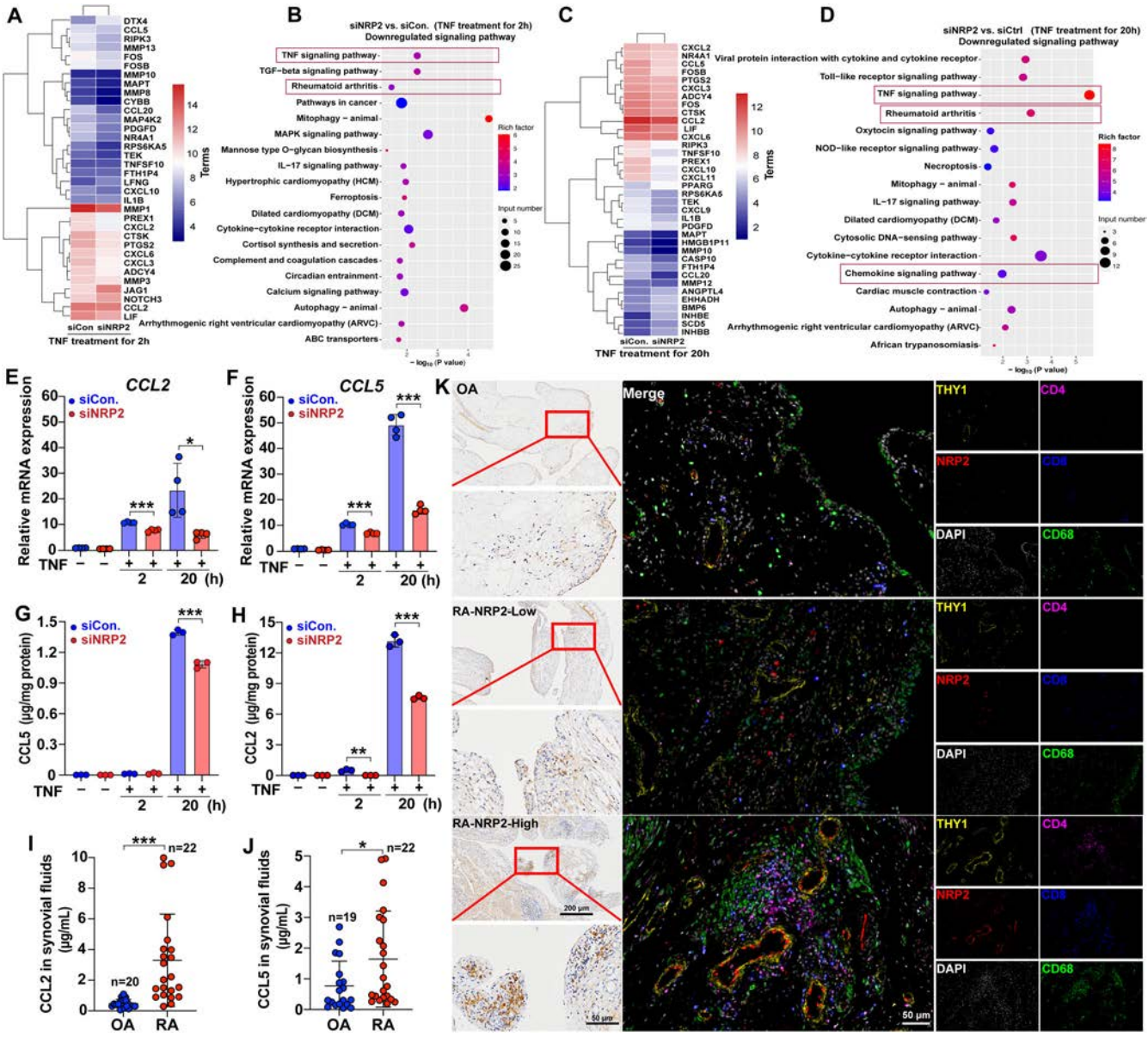

Figure 3. NRP2 in FLS promotes TNF-induced inflammation through CCL2 and CCL5: (A) Heatmap of inflammation-associated genes expression in FLS after 2 hours TNF treatment. (B) KEGG enrichment of down-regulated pathways (*siNRP2* vs *siCon*.) in FLS treated with TNF for two hours. (C) Heatmap of differentially expressed inflammation-associated genes in FLS after 20 hours TNF treatment. (D) KEGG enrichment analysis of down-regulated pathways (*siNRP2* vs *siCon*.) in FLS treated with TNF for 20 hours. (E–F) qRT-PCR of *CCL2* E, and *CCL5*. (F) mRNA in *siRNA*-transfected FLS following TNF stimulation. (G–H) ELISA of CCL2 (G) and CCL5 (H) levels in the supernatant of *siRNA*-transfected FLS after TNF treatment. (I–J) ELISA of CCL2 I, and CCL5 J, levels in SFs from patients with OA/RA. (K) Histologic analysis of synovial tissues from patients with OA/RA. Left: NRP2 expression was detected by IHC (zoomed area in red box); middle (merged images) and right (separate images): multiplex staining for THY1, CD4, NRP2, CD8, CD68, and DAPI. FLS were transfected with control *siRNA* or *siNRP2* via electroporation for 24 hours before TNF treatment (A–H). Data are presented as mean ± SD; $^{*}P < 0.05$, $^{***}P < 0.001$. Statistical analysis was performed by using two-tailed Student's *t*-test (E–J). CCL, C-C motif chemokine ligand; CD, cluster of differentiation; DAPI, 4′,6-diamidino-2-phenylindole; ELISA, enzyme-linked immunosorbent assay; FLS, fibroblast-like synoviocyte; IHC, immunohistochemistry; IL, interleukin; KEGG, Kyoto Encyclopedia of Genes and Genomes; mRNA, messenger RNA; NRP2, neuropilin-2; OA, osteoarthritis; qRT-PCR, quantitative reverse-transcription polymerase chain reaction; RA, rheumatoid arthritis; SF, synovial fluid; siCon, small interfering RNA control; siNRP2, small interfering RNA targeting NRP2; siRNA, small interfering RNA; THY1, thymocyte differentiation antigen 1; TNF, tumor necrosis factor. Color figure can be viewed in the online issue, which is available at http://onlinelibrary.wiley.com/doi/10.1002/art.70028/abstract.

Because TNF is known to induce Caspase-3/Gasdermin E (GSDME)-mediated pyroptosis in RA, we hypothesized that NRP2 might promote proliferation by suppressing cell death. Immunoblot analysis revealed increased levels of GSDME cleavage fragments in RA synovial tissues compared with those in OA synovial tissues, suggesting the occurrence of GSDME-

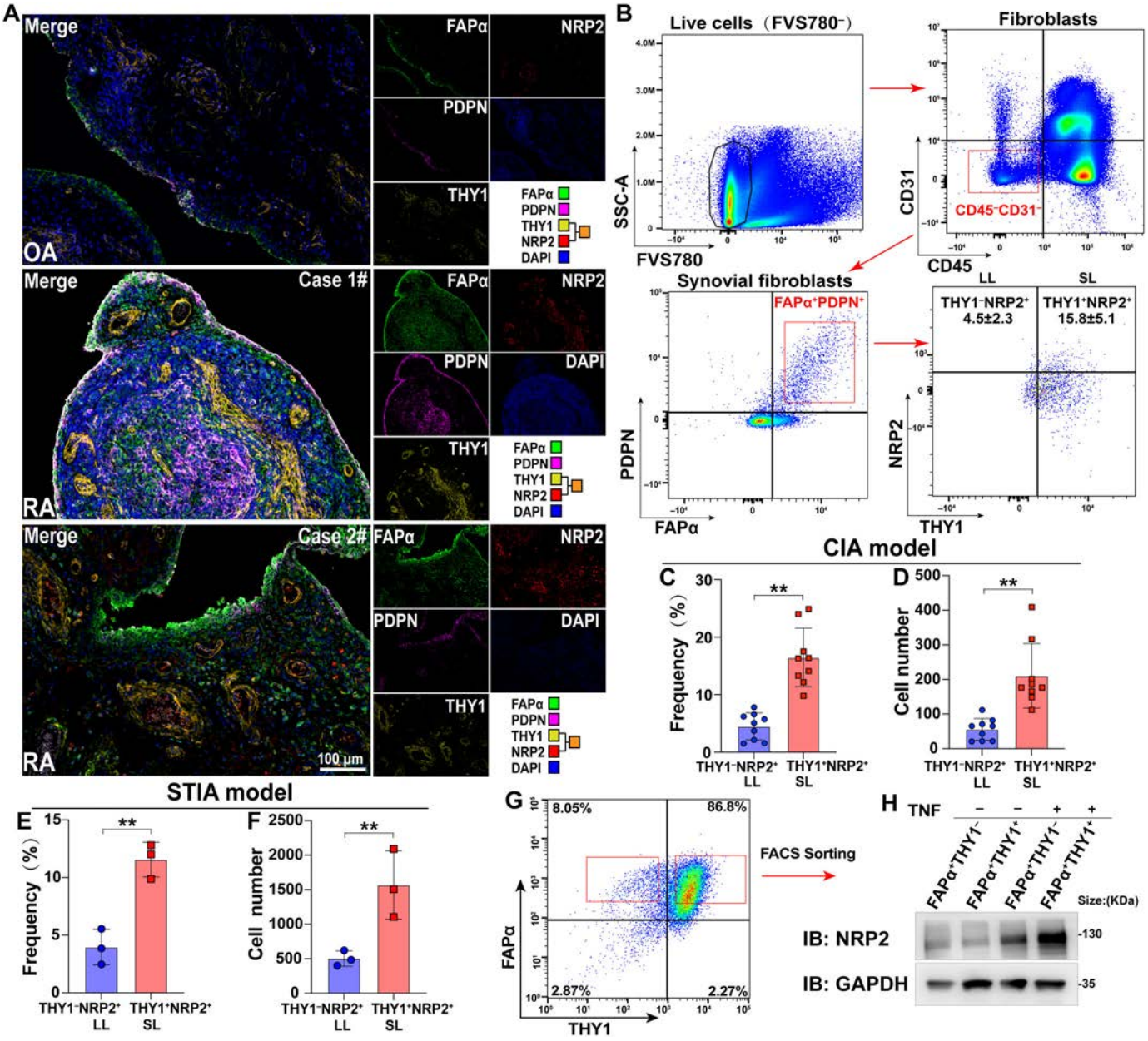

Figure 4. The TNF-induced inflammation-sensing protein NRP2 is predominantly enriched in the FAPα^{+}THY1^{+} cell subset localized within the sublining layer: (A) Multiplex immunohistochemical staining of synovial tissues from patients with OA and RA for FAPα, NRP2, THY1, PDPN, and DAPI. Representative merged images (upper) and individual channel images (lower) are shown. (B) Gating strategy for the flow cytometric analysis of cell subsets in FLS. (C–F) Flow cytometry was performed to determine the frequency and cell number of the THY1^{-}NRP2^{+} cell subset (lining layer) and the THY1^{+}NRP2^{+} cell subset (sublining layer) in CIA model (C–D) and STIA model (E–F). (G) FAPα^{+}THY1^{-} and FAPα^{+}THY1^{+} cell subsets in RA-FLS were isolated by flow cytometry. (H) Western blot analysis of NRP2 expression in the FACS-isolated FAPα^{+}THY1^{-} and FAPα^{+}THY1^{+} cell subsets in FLS treated with or without TNF for 20 hours. Data are presented as mean ± SD (n = 9 mice per group for [C], [D]; n = 3 mice per group for [E], [F]); $^{**}P < 0.01$. Statistical analysis was performed by using two-tailed Student's *t*-test (C–F). CIA, collagen-induced arthritis; DAPI, 4′,6-diamidino-2-phenylindole; FACS, fluorescence-activated cell sorting; FAPα, fibroblast activation protein alpha; FLS, fibroblast-like synoviocyte; NRP2, neuropilin-2; OA, osteoarthritis; PDPN, podoplanin; RA, rheumatoid arthritis; STIA, serum–transfer-induced arthritis; THY1, thymocyte differentiation antigen 1; TNF, tumor necrosis factor. Color figure can be viewed in the online issue, which is available at http://onlinelibrary.wiley.com/doi/10.1002/art.70028/abstract.

dependent pyroptosis in RA (Figure 5B). Activated Caspase-3, triggered by granzyme B and perforin from NK cells, cleaves GSDME to execute pyroptosis.[32,33] In an NK-92MI/RA-FLS coculture system (4 × 10^{5} NK cells), TNF stimulation induced prominent Caspase-3 and GSDME cleavage (Supplementary Figure 7C). However, NRP2 knockdown neither altered cleavage patterns (Figure 5C) nor affected Caspase-3/7 enzymatic activity (Figure 5D). Similarly, NRP2 overexpression failed to modulate

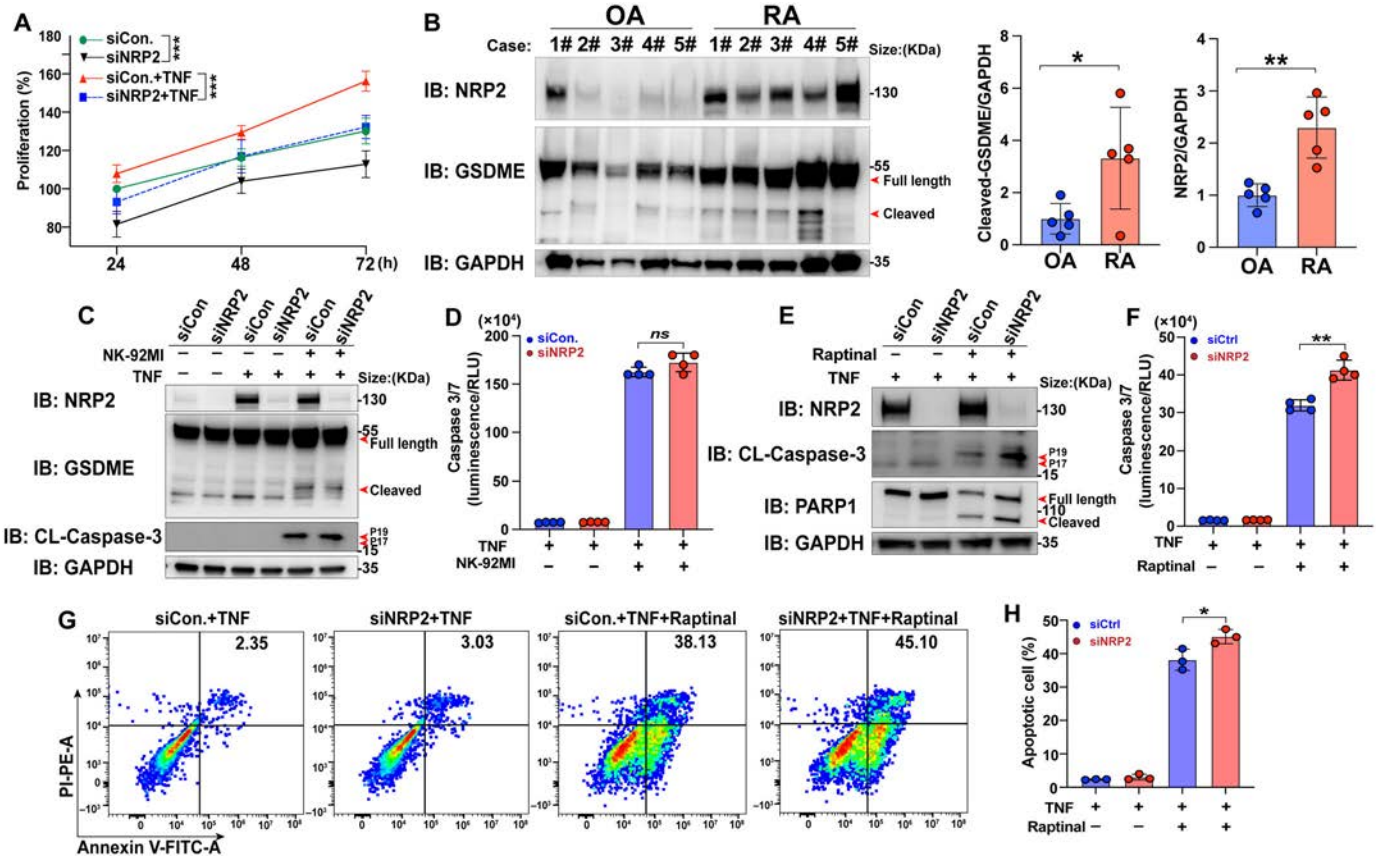

Figure 5. TNF-induced NRP2 promotes proliferation of FLS and enhances their resistance to apoptosis: (A) Proliferative capacity of RA-FLS with or without TNF stimulation was assessed by using CCK-8 at indicated time points. (B) Western blot analysis of NRP2 and GSDME expression in synovial tissues from patients with OA and RA. (C–D) RA-FLS, co-cultured with or without NK-92MI cells were treated with TNF for four hours. (C) Western blot analysis of NRP2, GSDME, and cleaved-Caspase-3 in RA-FLS. (D) Caspase 3/7 Activity Assay. (E–H) RA-FLS were transfected with control *siRNA* or *siNRP2* for 24 hours, followed by treatment with TNF in the presence or absence of Raptinal for four hours. (E) Western blot analysis of NRP2, cleaved-Caspase-3, and PARP1. (F) Caspase 3/7 activity assay. (G) Apoptosis of RA-FLS was analyzed by flow cytometry following Annexin V/PI staining. (H) The quantitative analysis of apoptosis proportion shown in (G). Data are presented as mean ± SD; $^{*}P < .05$, $^{**}P < .01$, $^{***}P < .001$. Statistical analysis was performed by using two-tailed Student's *t*-test (A, D, F, and H). CCK-8, Cell Counting Kit-8; FLS, fibroblast-like synoviocyte; GSDME, gasdermin E; NK-92MI, natural killer-92MI cell line; NRP2, neuropilin-2; OA, osteoarthritis; PARP1, poly(ADP-ribose) polymerase 1; PI, propidium iodide; RA, rheumatoid arthritis; siNRP2, small interfering RNA targeting NRP2; siRNA, small interfering RNA; TNF, tumor necrosis factor. Color figure can be viewed in the online issue, which is available at http://onlinelibrary.wiley.com/doi/10.1002/art.70028/abstract.

GSDME cleavage under TNF stimulation (Supplementary Figure 7D), indicating that NRP2 does not play a significant role in TNF-induced pyroptosis.

We next investigated apoptosis-related mechanisms. When Raptinal was used to induce apoptosis in TNF-stimulated FLS, NRP2-knockdown cells showed elevated cleavage of Caspase-3 and PARP-1 and higher Caspase-3/7 activity compared with those in control cells (Figure 5E and F). The increased apoptosis of NRP2-deficient FLS under TNF challenge was further confirmed by Annexin V/PE staining and cell morphology analysis (Figure 5G and H and Supplementary Figure 7E). Together, these results demonstrate that TNF-induced NRP2 expression promotes inflammatory hyperplasia of FLS through two mechanisms: increasing proliferation and conferring resistance to apoptosis, independent of pyroptosis regulation.

TNF upregulates NRP2 in FLS through p65-mediated NF-κB activation

TNF plays dual roles in regulating cell fate by promoting both cell survival and cell death. Its pro-survival effects typically depend on activation of the canonical NF-κB signaling pathway.[34,35] In our previous studies, we observed that TNF significantly enhanced the proliferation of FLS, and we identified NRP2 as a TNF-induced inflammation-sensing protein. To elucidate the molecular mechanism underlying the role of NRP2 as a TNF-inducible inflammatory mediator in FLS, we first investigated whether NRP2 overexpression in FLS was correlated with NF-κB pathway activation. Notably, inhibitors targeting the canonical NF-κB pathway—including the IKK1/2 inhibitor BMS-345541 (which blocks IKK complex activity), the p-IκBα inhibitor BAY 11-7082 (which inhibits IκBα phosphorylation), and QNZ (EVP4593, an inhibitor that triggers

TNF production through off-target effects)—all suppressed TNF-induced NRP2 expression in FLS. BMS-345541 and BAY 11-7082 exhibited particularly potent inhibitory effects (Figure 6A). These results suggest that TNF-induced NRP2 expression is regulated by the canonical NF-κB pathway.

However, co-immunoprecipitation assays revealed no direct interaction between NRP2 and core components of the NF-κB pathway (eg, IKK, IκBα, p50, or p65) (Figure 6B). To explore alternative regulatory mechanisms, we analyzed DNA methylation levels at the NRP2 promoter in TNF-stimulated RA-FLS. BiSeq-uencing PCR (BSP) revealed comparable methylation levels (Me-CpG = 2.7%) between TNF-treated and untreated groups after 24 hours (Figure 6C), indicating that epigenetic methylation is unlikely to mediate TNF-driven NRP2 upregulation.

Given that TNF elevates both NRP2 mRNA and protein levels, we hypothesized that it is transcriptionally regulated. Small interfering RNA (siRNA)-mediated knockdown of the NF-κB subunit *p50* in FLS had no significant effect on TNF-induced NRP2 expression (Supplementary Figure 8A–C). In contrast, *p65* knockdown markedly reduced TNF-induced NRP2 mRNA and protein expression (Supplementary Figure 8D–F), implicating *p65*-dependent transcriptional activation. Intriguingly, NRP2 knockdown itself attenuated TNF-induced nuclear translocation of p65 (Supplementary Figure 8G), suggesting a feedforward loop that sustains the inflammatory microenvironment. ChIP-seq analysis of p65-bound DNA regions revealed direct binding of p65 to the NRP2 promoter (Figure 6D and E). Peak annotation confirmed specific p65-binding motifs within the NRP2 promoter (Figure 6F). Collectively, these findings demonstrate that TNF upregulates NRP2 expression in FLS via p65-dependent transcriptional activation within the canonical NF-κB pathway (Figure 6G).

DISCUSSION

RA is an immune-mediated chronic inflammatory disease. Its pathologic features include both autoimmune responses (mediated by autoantibodies) and nonspecific inflammatory responses (mediated by inflammatory cytokines and immune cells). Antibodies that mediate RA autoimmune responses primarily include rheumatoid factor (RF) and anti-citrullinated protein antibodies (ACPAs) (Specifically antibodies that target cyclic citrullinated peptide). The combined detection of these antibodies in serological assays results in high sensitivity and specificity, significantly improving the accuracy of early RA diagnosis.[36,37] Notably, protein biomarkers that indicate the extent of nonspecific inflammation remain scarce in RA diagnosis. Additionally, a significant proportion (at least 30%) of patients with RA are seronegative for both RF and ACPAs.[38] Therefore, identifying inflammation-sensitive biomarkers to monitor RA disease progression is of substantial clinical significance. In this study, we discovered that NRP2 expression in patients with RA was rapidly induced and highly sensitive to TNF stimulation. Its serum levels were markedly elevated compared with those of patients with OA and were positively correlated with RA disease activity. Correspondingly, NRP2 expression in SF and synovial tissue of patients with RA was significantly higher than that in patients with OA. These findings indicate that NRP2 is consistently associated with RA progression at both serological and histologic levels, suggesting its potential as a novel biomarker for the auxiliary diagnosis of RA.

FLS are a specialized subset of mesenchymal-derived cells within synovial tissue that exhibit heightened sensitivity to proliferative signaling pathways, including the IL-6-Yap-Snail signaling axis and Notch3 signaling pathway.[39–41] The inflammatory microenvironment of the synovium is established by pro-inflammatory cells, cytokines, and chemokines. Within this milieu, FLS serve as critical signaling hubs that orchestrate these pro-inflammatory components through coordinated molecular interactions, thereby triggering sustained inflammation and tissue hyperplasia. This pathologic cascade ultimately culminates in articular cartilage destruction and bone erosion.[42,43] Consequently, identifying key proteins that promote FLS inflammatory proliferation may reveal promising therapeutic targets. Although epigenetic studies have revealed sustained NRP2 overexpression in FLS, the molecular mechanisms underlying this persistent expression and the specific biologic functions of NRP2 in FLS remain uncharacterized. Our study demonstrated that TNF-enhanced NRP2 expression in FLS through the transcription factor p65. Elevated NRP2 exerted multiple pathobiological effects:

1. Sustaining inflammatory microenvironment: NRP2 maintained the capacity of FLS to secrete pro-inflammatory cytokines (IL-1α/β, IL-6, and IL-8).
2. Amplifying inflammatory responses: NRP2 promoted the secretion of chemokines (CCL2 and CCL5), facilitating the recruitment of pro-inflammatory immune cells (particularly myeloid-lineage cells) to exacerbate local inflammation.
3. Promoting bone erosion: NRP2 maintained FLS production of MMPs, accelerating articular cartilage degradation.
4. Driving inflammatory hyperplasia: NRP2 enhanced FLS survival through anti-apoptotic mechanisms and stimulated proliferative activity.

In STIA murine models, both systemic and conditional NRP2 knockout significantly attenuated synovial inflammation and joint damage. These findings collectively demonstrate that TNF-induced NRP2 in FLS establishes a self-perpetuating inflammatory circuit linking proliferation and inflammation, thereby promoting RA initiation and progression (Figure 6G).

Research on the inflammation-related functions of NRP2 protein remains in its nascent stage, and we have noted several paradoxical findings. For example, NRP2 has been shown to alleviate airway inflammatory responses. Both our work and studies by Mucka et al demonstrated that NRP2 knockout exacerbates

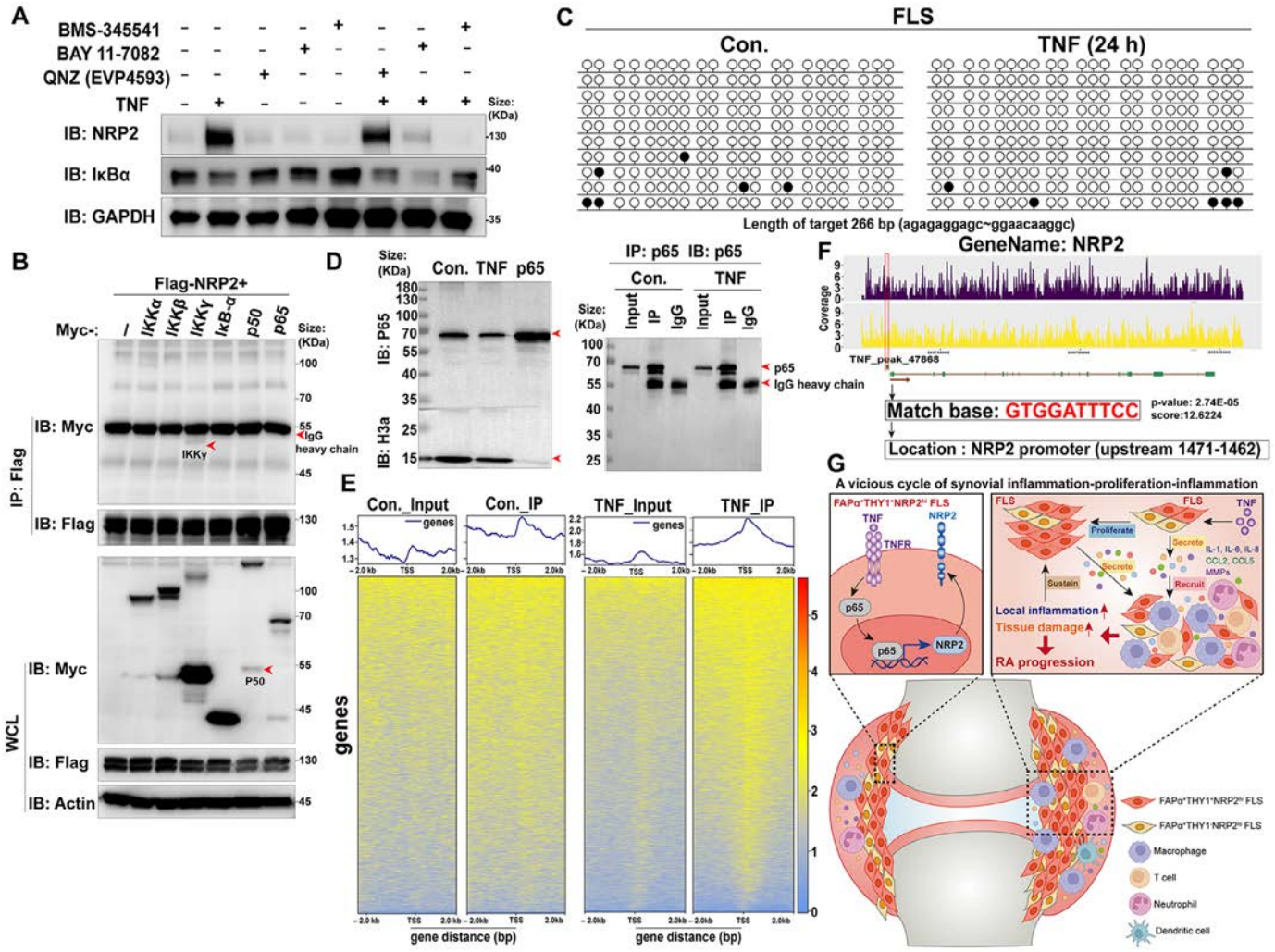

Figure 6. TNF upregulates NRP2 in FLS through p65-mediated NF-κB activation: (A) Western blot analysis of NRP2 and IκBα in FLS treated with or without TNF for 20 hours, in the presence or absence of the IKK1/2 inhibitor BMS-345541, the IκBα phosphorylation inhibitor BAY 11-7082, or the NF-κB inhibitor QNZ (EVP4593). (B) Co-immunoprecipitation assay detecting interactions between NRP2 and components of the canonical NF-κB signaling pathway. (C) Methylation status of the NRP2 promoter region was analyzed by BSP in FLS with or without TNF stimulation for 24 hours. (D) Preprocessing of ChIP-seq: enrichment of p65-bound DNA fragments by immunoprecipitation. (E) Heatmap of ChIP-seq peaks for p65 binding in FLS stimulated with or without TNF for 24 hours. (F) Nucleotide sequences of p65-bound peaks annotated to the NRP2 promoter region. (G) A schematic diagram summarizing the mechanism by which NRP2 in FLS drives inflammatory arthritis. BAY 11-7082, IκBα phosphorylation inhibitor; BMS-345541, IKK1/2 inhibitor; BSP, bisulfite sequencing PCR; ChIP-seq, chromatin immunoprecipitation sequencing; FLS, fibroblast-like synoviocyte; IκBα, inhibitor of κB alpha; IKK, IκB kinase; IL, interleukin; NF-κB, nuclear factor kappa-light-chain-enhancer of activated B cells; NRP2, neuropilin-2; QNZ (EVP4593), NF-κB inhibitor; TNF, tumor necrosis factor. Color figure can be viewed in the online issue, which is available at http://onlinelibrary.wiley.com/doi/10.1002/art.70028/abstract.

inflammatory reactions, suggesting its anti-inflammatory role.[26,44–46] Conversely, NRP2 blockade has proven effective in treating pulmonary sarcoidosis, indicating its pro-inflammatory potential.[25] This dual functionality of NRP2 in inflammation may be partially attributed to its association with chromatin states. A key outcome of TNF-enhanced chromatin accessibility in FLS is the establishment of a persistent "immune memory." This leads to the sustained high expression of certain TNF-induced pro-inflammatory genes, such as NRP2, whereas in macrophages, the expression of these same genes is both transient and significantly weaker.[8,47] In this study, we identified NRP2 as a TNF-induced inflammatory sensitizer. TNF-triggered NRP2 expression promoted pro-inflammatory microenvironment remodeling through FLS, with predominant localization in THY1$^+$ sublining cells. Under TNF stimulation, NRP2 overexpression was predominantly enriched in FAPα$^+$THY1$^+$ cell populations. Intriguingly, the FAPα$^+$THY1$^+$ subset has been implicated in driving severe and persistent arthritis, whereas the FAPα$^+$THY1$^-$ subset contributes to articular cartilage damage.[30] These findings collectively substantiate the pivotal role of NRP2 in mediating the pro-inflammatory functions of FLS.

In summary, NRP2 promotes the initiation and progression of RA by remodeling the synovial pro-inflammatory microenvironment

and serves as a promising biomarker for RA auxiliary diagnosis. The TNF–p65–NRP2 axis in FLS may represent a potential therapeutic target for synovitis modulation.

ACKNOWLEDGMENTS

We gratefully acknowledge patients, rheumatologists, and orthopedic surgeons for providing the biologic samples used in this study. We thank the technical contributions of Mr. Shengqiang Mao, Research Technologist, for bioinformatics data analysis; Ms. Xiaoting Chenand; Jiehao Chen, Senior Research Technologists, for micro-CT experimental support; Ms. Mengli Zhu, Ms. Tingting Guo, and Ms. Yan Wang, Certified Flow Cytometry Specialists, for assistance with flow cytometry; Ms. Yue Liand; and Yaping Wu, Assistant Research Technologists, for histopathological technique optimization.

AUTHOR CONTRIBUTIONS

All authors contributed to at least one of the following manuscript preparation roles: conceptualization AND/OR methodology, software, investigation, formal analysis, data curation, visualization, and validation AND drafting or reviewing/editing the final draft. As corresponding author, Dr Jin confirms that all authors have provided the final approval of the version to be published and takes responsibility for the affirmations regarding article submission (eg, not under consideration by another journal), the integrity of the data presented, and the statements regarding compliance with institutional review board/Declaration of Helsinki requirements.

REFERENCES

1. Marsh LJ, Kemble S, Reis Nisa P, et al. Fibroblast pathology in inflammatory joint disease. Immunol Rev 2021;302(1):163–183.
2. Komatsu N, Takayanagi H. Mechanisms of joint destruction in rheumatoid arthritis - immune cell-fibroblast-bone interactions. Nat Rev Rheumatol 2022;18(7):415–429.
3. Chen H, Fu X, Wu X, et al. Gut microbial metabolite targets HDAC3-FOXK1-interferon axis in fibroblast-like synoviocytes to ameliorate rheumatoid arthritis. Bone Res 2024;12(1):31.
4. Gravallese EM, Firestein GS. Rheumatoid arthritis - common origins, divergent mechanisms. N Engl J Med 2023;388(6):529–542.
5. Zhai Z, Yang F, Xu W, et al. Attenuation of rheumatoid arthritis through the inhibition of tumor necrosis factor-induced caspase 3/gasdermin e-mediated pyroptosis. Arthritis Rheumatol 2022;74(3):427–440.
6. Smolen JS. Insights into the treatment of rheumatoid arthritis: a paradigm in medicine. J Autoimmun 2020;110:102425.
7. Wu J, Feng Z, Chen L, et al. TNF antagonist sensitizes synovial fibroblasts to ferroptotic cell death in collagen-induced arthritis mouse models. Nat Commun 2022;13(1):676.
8. Loh C, Park SH, Lee A, et al. TNF-induced inflammatory genes escape repression in fibroblast-like synoviocytes: transcriptomic and epigenomic analysis. Ann Rheum Dis 2019;78(9):1205–1214.
9. Aletaha D, Smolen JS. Diagnosis and management of rheumatoid arthritis: a review. JAMA 2018;320(13):1360–1372.
10. Bennett JL, Pratt AG, Dodds R, et al. Rheumatoid sarcopenia: loss of skeletal muscle strength and mass in rheumatoid arthritis. Nat Rev Rheumatol 2023;19(4):239–251.
11. Alivernini S, Laria A, Gremese E, et al. ACR70-disease activity score remission achievement from switches between all the available biological agents in rheumatoid arthritis: a systematic review of the literature. Arthritis Res Ther 2009;11(6):R163.
12. Zhang F, Jonsson AH, Nathan A, et al; Accelerating Medicines Partnership: RA/SLE Network. Deconstruction of rheumatoid arthritis synovium defines inflammatory subtypes. Nature 2023;623(7987):616–624.
13. Winthrop KL, Cohen SB. Oral surveillance and JAK inhibitor safety: the theory of relativity. Nat Rev Rheumatol 2022;18(5):301–304.
14. Brown P, Pratt AG, Hyrich KL. Therapeutic advances in rheumatoid arthritis. BMJ 2024;384:e070856.
15. Chen DY, Sun NH, Chen X, et al. Endothelium-derived semaphorin 3G attenuates ischemic retinopathy by coordinating β-catenin-dependent vascular remodeling. J Clin Invest 2021;131(4):e135296.
16. Roy S, Bag AK, Singh RK, et al. Multifaceted role of neuropilins in the immune system: potential targets for immunotherapy. Front Immunol 2017;8:1228.
17. Fernández-Nogales M, López-Cascales MT, Murcia-Belmonte V, et al. Multiomic analysis of neurons with divergent projection patterns identifies novel regulators of axon pathfinding. Adv Sci (Weinh) 2022;9(29):e2200615.
18. Xu Y, Yuan L, Mak J, et al. Neuropilin-2 mediates VEGF-C-induced lymphatic sprouting together with VEGFR3. J Cell Biol 2010;188(1):115–130.
19. Caunt M, Mak J, Liang WC, et al. Blocking neuropilin-2 function inhibits tumor cell metastasis. Cancer Cell 2008;13(4):331–342.
20. Xu Z, Goel HL, Burkart C, et al. Inhibition of VEGF binding to neuropilin-2 enhances chemosensitivity and inhibits metastasis in triple-negative breast cancer. Sci Transl Med 2023;15(694):eadf1128.
21. Islam R, Mishra J, Bodas S, et al. Role of neuropilin-2-mediated signaling axis in cancer progression and therapy resistance. Cancer Metastasis Rev 2022;41(3):771–787.
22. Wang M, Silva CA, Xiong C, et al. Therapeutic blocking of VEGF binding to neuropilin-2 diminishes PD-L1 expression to activate antitumor immunity in prostate cancer. Sci Transl Med 2023;15(694):eade5855.
23. Elaimy AL, Guru S, Chang C, et al. VEGF-neuropilin-2 signaling promotes stem-like traits in breast cancer cells by TAZ-mediated repression of the Rac GAP β2-chimaerin. Sci Signal 2018;11(528):11.
24. Culver DA, Aryal S, Barney J, et al. Efzofitimod for the treatment of pulmonary sarcoidosis. Chest 2023;163(4):881–890.
25. Nangle LA, Xu Z, Siefker D, et al. A human histidyl-tRNA synthetase splice variant therapeutic targets NRP2 to resolve lung inflammation and fibrosis. Sci Transl Med 2025;17(789):eadp4754.
26. Li T, Ran J, Miao Z, et al. Deficiency of inflammation-sensing protein neuropilin-2 in myeloid-derived macrophages exacerbates colitis via NF-κB activation. J Pathol 2024;262(2):175–188.
27. Haringman JJ, Smeets TJ, Reinders-Blankert P, et al. Chemokine and chemokine receptor expression in paired peripheral blood mononuclear cells and synovial tissue of patients with rheumatoid arthritis, osteoarthritis, and reactive arthritis. Ann Rheum Dis 2006;65(3):294–300.
28. Kuan WP, Tam LS, Wong CK, et al. CXCL 9 and CXCL 10 as sensitive markers of disease activity in patients with rheumatoid arthritis. J Rheumatol 2010;37(2):257–264.
29. Moadab F, Khorramdelazad H, Abbasifard M. Role of CCL2/CCR2 axis in the immunopathogenesis of rheumatoid arthritis: latest evidence and therapeutic approaches. Life Sci 2021;269:119034.
30. Croft AP, Campos J, Jansen K, et al. Distinct fibroblast subsets drive inflammation and damage in arthritis. Nature 2019;570(7760):246–251.
31. Nygaard G, Firestein GS. Restoring synovial homeostasis in rheumatoid arthritis by targeting fibroblast-like synoviocytes. Nat Rev Rheumatol 2020;16(6):316–333.
32. Zhang Z, Zhang Y, Xia S, et al. Gasdermin E suppresses tumour growth by activating anti-tumour immunity. Nature 2020;579(7799):415–420.

33. Zhou Z, He H, Wang K, et al. Granzyme A from cytotoxic lymphocytes cleaves GSDMB to trigger pyroptosis in target cells. Science 2020; 368(6494):eaaz7548.

34. Gao C, Deng J, Zhang H, et al. HSPA13 facilitates NF- κB-mediated transcription and attenuates cell death responses in TNFα signaling. Sci Adv 2021;7(41):eabh1756.

35. Mifflin L, Ofengeim D, Yuan J. Receptor-interacting protein kinase 1 (RIPK1) as a therapeutic target. Nat Rev Drug Discov 2020;19(8): 553–571.

36. Lend K, Lampa J, Padyukov L, et al. Association of rheumatoid factor, anti-citrullinated protein antibodies and shared epitope with clinical response to initial treatment in patients with early rheumatoid arthritis: data from a randomised controlled trial. Ann Rheum Dis 2024;83(12): 1657–1665.

37. Pertsinidou E, Saevarsdottir S, Manivel VA, et al. In early rheumatoid arthritis, anticitrullinated peptide antibodies associate with low number of affected joints and rheumatoid factor associates with systemic inflammation. Ann Rheum Dis 2024;83(3):277–287.

38. Bugatti S, De Stefano L, Gandolfo S, et al. Autoantibody-negative rheumatoid arthritis: still a challenge for the rheumatologist. Lancet Rheumatol 2023;5(12):e743–e755.

39. Wei K, Korsunsky I, Marshall JL, et al; Accelerating Medicines Partnership Rheumatoid Arthritis & Systemic Lupus Erythematosus (AMP RA/SLE) Consortium. Notch signalling drives synovial fibroblast identity and arthritis pathology. Nature 2020;582(7811):259–264.

40. Perretti M. Switching on resolution to treat RA moves closer to reality. Nat Rev Rheumatol 2021;17(2):73–74.

41. Symons RA, Colella F, Collins FL, et al. Targeting the IL-6-Yap-Snail signalling axis in synovial fibroblasts ameliorates inflammatory arthritis. Ann Rheum Dis 2022;81(2):214–224.

42. Zhang F, Wei K, Slowikowski K, et al; Accelerating Medicines Partnership Rheumatoid Arthritis and Systemic Lupus Erythematosus (AMP RA/SLE) Consortium. Defining inflammatory cell states in rheumatoid arthritis joint synovial tissues by integrating single-cell transcriptomics and mass cytometry. Nat Immunol 2019;20(7):928–942.

43. Chen J, Cheng W, Li J, et al. Notch-1 and notch-3 mediate hypoxia-induced activation of synovial fibroblasts in rheumatoid arthritis. Arthritis Rheumatol 2021;73(10):1810–1819.

44. Wang B, Guo W, Qiu C, et al. Alveolar macrophage-derived NRP2 curtails lung injury while boosting host defense in bacterial pneumonia. J Leukoc Biol 2022;112(3):499–512.

45. Mucka P, Levonyak N, Geretti E, et al. Inflammation and lymphedema are exacerbated and prolonged by neuropilin 2 deficiency. Am J Pathol 2016;186(11):2803–2812.

46. Immormino RM, Lauzier DC, Nakano H, et al. Neuropilin-2 regulates airway inflammatory responses to inhaled lipopolysaccharide. Am J Physiol Lung Cell Mol Physiol 2018;315(2):L202–L211.

47. Sohn C, Lee A, Qiao Y, et al. Prolonged tumor necrosis factor α primes fibroblast-like synoviocytes in a gene-specific manner by altering chromatin. Arthritis Rheumatol 2015;67(1):86–95.

Arthritis & Rheumatology
Vol. 78, No. 5, May 2026, pp 1076–1087
DOI 10.1002/art.70026

American College of Rheumatology
Empowering Rheumatology Professionals

Per- and Polyfluoroalkyl Substances and Hand Osteoarthritis: Data From the Osteoarthritis Initiative

Jeffrey B. Driban, PhD,[1] Lisa B. Rokoff, PhD,[2] Bing Lu, MD, DrPH,[3] Timothy E. McAlindon, MD, MPH,[4] Charles B. Eaton, MD, MS,[5,6] Mary B. Roberts, MS,[5,6] Diana Mathes, BS,[7] Colleen Lestician, BS,[7] Zhijin Carrie Xu, PhD,[7] Zhihua Tina Fan, PhD,[7] Shawn P. O'Leary, BS,[7] Ida K. Haugen, MD, PhD,[8] Jérémie Sellam, MD, PhD,[9] Alice Courties, MD, PhD,[9] and Abby F. Fleisch, MD, MPH[2,10]

Objective. To explore whether biologic levels of specific per- and polyfluoroalkyl substances (PFAS) and a mixture of PFAS—reflecting the overall effect and accounting for correlations among PFAS—relate to incident hand osteoarthritis (HOA) and progression.

Methods. Among a case-cohort sample from the Osteoarthritis Initiative (n = 1,878), we examined associations of eight PFAS in serum with odds of developing over the subsequent 4 years (1) symptomatic HOA and (2) an increased number of joints with radiographic osteoarthritis (Kellgren-Lawrence ≥2; yes/no). We used weighted logistic regression to assess single PFAS (continuous and quartiles) and quantile g-computation to assess the PFAS mixture in relation to our primary outcomes.

Results. Participants were primarily female (58%) and on average aged 62 years and overweight (mean body mass index = 28.6 kg/m^2). Participants with higher perfluorodecanoic acid (PFDA) and perfluorononanoic acid (PFNA; continuous variables) had greater odds of incident symptomatic HOA (odds ratio [OR] [95% confidence interval (CI)] per interquartile range increment: PFDA 1.12 [1.05–1.20]; PFNA 1.07 [1.00–1.13]), but associations were not monotonic when these PFAS were represented in quartiles. Participants with higher perfluorohexane sulfonic acid had lower odds of incident HOA (eg, OR 0.94 [95% CI 0.88–1.00] per interquartile range increment). We observed no other consistent associations between PFAS and either outcome.

Conclusion. We observed possible associations of PFDA and PFNA serum concentrations with symptomatic HOA incidence, but we otherwise found no consistent evidence that greater PFAS concentrations relate to a greater chance of developing HOA incidence or progression.

INTRODUCTION

Hand osteoarthritis (OA) is a painful disorder that impairs an individual's ability to perform activities of daily life.[1] The prevalence of hand OA has doubled in the United States over the past half century,[2] a finding that cannot be solely explained by increases in longevity,[2] raising the possibility that environmental factors may play a role.[3]

This article was prepared using an Osteoarthritis Initiative (OAI) public use data set and does not necessarily reflect the opinions or views of the OAI investigators, the National Institutes of Health (NIH), or the private funding partners. The funding sources had no role in study design; in the collection, analysis, and interpretation of data; in the writing of the report; or in the decision to submit the article for publication.

Supported by grants from the National Institute of Arthritis and Musculoskeletal and Skin Diseases, NIH (awards R01-AR-081791 and R24-AR-085006). The OAI is a public-private partnership comprised of five contracts (grants N01-AR-2-2258; N01-AR-2-2259; N01-AR-2-2260; N01-AR-2-2261; N01-AR-2-2262) funded by the NIH, a branch of the Department of Health and Human Services, and conducted by the OAI Study Investigators. Private funding partners include Merck Research Laboratories; Novartis Pharmaceuticals Corporation; GlaxoSmithKline; and Pfizer, Inc. Private sector funding for the OAI is managed by the Foundation for the National Institutes of Health. Dr Fleisch's work was supported by the National Institutes of Environmental Health Sciences (grant R01-ES30101).

[1]Department of Population and Quantitative Health Sciences, UMass Chan Medical School, Worcester, Massachusetts; [2]Center for Interdisciplinary and Population Health Research, MaineHealth Institute for Research, Westbrook, Maine; [3]Department of Public Health Sciences, UConn Health, Farmington, Connecticut; [4]Division of Rheumatology, Department of Medicine, UMass Chan Medical School, Worcester, Massachusetts; [5]Center for Primary Care and Prevention, Kent Hospital, Pawtucket, Rhode Island; [6]Department of Family Medicine, Warren Alpert Medical School Brown University, Department of Epidemiology, Brown University School of Public Health, Providence, Rhode Island; [7]Environmental and Chemical Laboratory Services, Public Health & Environmental Laboratories, New Jersey Department of Health, Ewing; [8]Center for Treatment of Rheumatic and Musculoskeletal Diseases (REMEDY), Diakonhjemmet Hospital, Oslo, Norway; [9]Department of Rheumatology, Saint-Antoine Hospital, Assistance Publique–Hôpitaux de Paris (AP-HP), Centre de Recherche Saint-Antoine (CRSA) Inserm UMRS-938, Sorbonne Université, Paris, France; [10]Pediatric Endocrinology and Diabetes, Maine Medical Center, Portland.

Additional supplementary information cited in this article can be found online in the Supporting Information section (https://acrjournals.onlinelibrary.wiley.com/doi/10.1002/art.70026).

Author disclosures are available at https://onlinelibrary.wiley.com/doi/10.1002/art.70026.

Address correspondence via email to Jeffrey B. Driban, PhD, at jeffrey.driban@umassmed.edu.

Submitted for publication June 3, 2025; accepted in revised form November 17, 2025.

Per- and polyfluoroalkyl substances (PFAS) are synthetically produced water-, grease-, or stain-resistant chemicals in a wide range of products (eg, food packaging and water-resistant fabric). These compounds are universally detectable in the US population[4,5] and may exacerbate OA development.[6,7] PFAS, endocrine-disrupting chemicals with long biologic half-lives of 3 to 8 years,[8,9] elicit numerous responses pivotal to OA pathophysiology, including bone loss,[10,11] insulin resistance,[12,13] adiposity,[14,15] and inflammation.[16–18] Specifically, PFAS increase the production of inflammatory mediators (eg, interleukin-1β) by mast cells and macrophages,[16,17] which exacerbate inflammation of articular structures (eg, synovitis), a driving factor in the pathogenesis of hand OA.[19–21] In cross-sectional studies, exposure to PFAS has been associated with self-reported OA diagnosis.[6,7]

Given the ongoing use of PFAS and the scale of contamination, there is an urgent need for longitudinal studies to clarify the relationship between PFAS serum levels and specific OA phenotypes (eg, symptomatic hand OA) to inform public health policies and clinical monitoring. Hand OA is particularly interesting because it is influenced by systemic factors and less susceptible to local biomechanical risk factors (eg, knee trauma and hip shape). Hence, we explored whether specific PFAS and a mixture of PFAS, reflecting the overall effect and accounting for the correlations among each PFAS, relate to hand OA incidence and progression.

MATERIAL AND METHODS

Study sample. We leveraged a case-cohort sample of 1,900 participants from the OA Initiative (OAI) cohort. We used the case-cohort design because it is an efficient and cost-effective study design that enables us to investigate multiple outcomes using the same data framework.

The original OAI cohort comprised 4,796 individuals aged 45 to 79 years, recruited from 2004 to 2006 at four clinical sites in the United States. The OAI staff recruited participants who had or were at high risk for symptomatic knee OA and 122 participants without symptomatic knee OA and at low risk. The OAI participants underwent hand radiographs at baseline and 48-month visits.

Participants in the case-cohort sample had (1) hand radiographs at baseline and 48 months (n = 3,604), (2) no radiographic evidence suggestive of pathology other than OA (eg, psoriatic arthritis or ankylosis; n = 3,588), and (3) no evidence of symptomatic erosive hand OA at baseline (because they could not develop any incident outcomes; n = 3,467) (Supplementary Figure S1). From these participants, we selected a random sample of 1,351 participants to represent the eligible cohort. We then selected an additional 549 "cases" based on the development of at least one of seven outcomes at the 48-month follow-up visit: radiographic hand OA, symptomatic hand OA, radiographic erosive hand OA, symptomatic erosive hand OA, radiographic thumb-base OA, symptomatic thumb-base OA, and erosive thumb-base OA (not considered in analyses because of sample size, n = 14).

By design, the case-cohort sample includes people who meet the baseline criteria for one or more of the seven case definitions above (excluding symptomatic erosive hand OA). If a case status was prevalent at baseline, then we excluded that person from analyses for that outcome (Supplementary Table S1). Among the 1,900 participants in the original case-cohort sample, 1,878 had sufficient baseline serum samples to perform the PFAS assays.

PFAS measurement. We measured PFAS in archived serum from the OAI baseline examination. We sent serum samples that had not undergone a freeze-thaw cycle to the New Jersey Department of Health's Environmental and Chemical Laboratory Service for PFAS measurement.

The laboratory performed analysis of the serum specimens in singlicate for 12 PFAS, using a high-throughput online solid phase extraction (Spark Holland, Emmen, the Netherlands) system and a highly sensitive tandem mass spectrometer (Sciex QTrap 6500, Framingham, MA; iChromQtrap). The PFAS included: perfluorooctanoic acid (PFOA), perfluorooctane sulfonic acid (PFOS), perfluorodecanoic acid (PFDA), perfluorohexane sulfonic acid (PFHxS), 2-(N-methyl-perfluorooctane sulfonamido) acetic acid (MeFOSAA), perfluorononanoic acid (PFNA), perfluoroundecanoic acid (PFUnA), perfluorododecanoic acid, perfluoro-2-proproxypropanoic acid, 4,8-dioxa-3H-perfluorononanoic acid, 9-chlorohexadecafluoro-3-oxanone-1-sulfonic acid, and perfluoroheptanesulfonic acid (PFHpS). The laboratory established the validity of their methods[22,23] and reported the limits of detection (LODs; ranging from 0.001 to 0.025 ng/mL).[22,23]

Radiographic readings. At the baseline and 48-month visits, participants had posteroanterior radiographs of the dominant hand. Although hand OA is often present bilaterally, the OAI focused on the dominant hand because most people with unilateral interphalangeal OA are affected in the dominant hand.[24] Details about determining hand dominance and radiographic acquisition have been described in detail.[25,26]

A trained reader performed the radiographic readings, blinded to chronology and clinical information for radiographic severity using a modified Kellgren-Lawrence (KL) scale,[27] which had excellent intrarater agreements (weighted $\kappa > 0.84$ across 16 joints). A second trained reader reviewed paired radiographs in known chronologic order and provided semiquantitative readings, including the presence of central erosions (dichotomous variable) via a validated approach that expanded the OA Research Society International atlas[28] and had good reproducibility (κ = 0.79–1.00 across 70 hands). The readers focused on 16 joints: 4 distal interphalangeal joints, 4 proximal interphalangeal joints, 5 metacarpophalangeal joints, thumb interphalangeal joint, and

thumb-base joints (first carpometacarpal joint and scaphotrapeziotrapezoidal joint).

Primary outcomes. *Incident symptomatic hand OA.* We classified a participant as having incident symptomatic hand OA if at the 48-month visit, but not at baseline, they had at least two distal or proximal interphalangeal joints on at least two separate digits with at least a small osteophyte or mild joint space narrowing (modified KL grade ≥2) *and* self-reported hand symptoms (hand/finger pain, aching, or stiffness on more than half of the 30 days before the radiograph). It is common practice to require OA in more than one joint[29–32] to reduce misclassification because of prior trauma. This definition is consistent with the American College of Rheumatology criteria for classifying hand OA.[29]

Change in disease burden (number of joints with OA). We measured disease burden as change in the number of hand joints (excluding thumb-base joints) with radiographic OA at 48 months versus baseline using established criteria for radiographic OA (modified KL grade ≥ 2).[27] The advantage of this outcome compared with studying OA progression is the inclusion of people with and without radiographic hand OA, reducing concerns about index event (collider) bias that may be introduced by conditioning on baseline disease severity.[33,34]

Secondary outcomes. As an alternative strategy to define change in disease burden from baseline to 48 months, we assessed change in the sum of KL grades across hand joints (including thumb-base joints). We also examined the odds of developing each of five hand OA phenotypes at the 48-month visit: radiographic hand OA, radiographic thumb-base OA, symptomatic thumb-base OA, radiographic erosive hand OA, and symptomatic erosive hand OA. We classified radiographic hand OA as having a hand with at least two finger joints (digits two to five) on at least two separate digits with a modified KL grade ≥2; radiographic thumb-base OA as KL grade ≥2 in either thumb-base joint; symptomatic thumb-base OA as KL grade ≥2 in either thumb-base joint *and* ipsilateral self-reported hand symptoms; radiographic erosive hand OA as having radiographic hand OA and at least one central erosion; and symptomatic erosive hand OA as having radiographic erosive hand OA *and* self-reported hand symptoms.

Covariates. At baseline, participants reported date of birth, and race (open-ended question). The OAI questionnaire asked, "What is your gender, male or female?" Participants also reported education using six categories (ranging from less than high school graduate to graduate degree). At baseline, study staff measured weight and height, which were used to calculate body mass index (BMI; kg/m^2). For participants who identified as female, we estimated menopause status at baseline based on self-reported last natural period or age at hysterectomy: last natural period within past 12 months (premenopause), last natural period 1 to 4 years ago or hysterectomy <5 years before baseline (perimenopause), and last natural period or hysterectomy ≥5 years before baseline (postmenopause).

Statistical analyses. For analyses, we a priori included PFAS with 60% detectability in samples, ensuring consistency with prior studies.[5,35] Eight PFAS met this threshold (Tables 1 and 2). In cases where PFAS were less than the LOD, we replaced "<LOD" with the LOD/$\sqrt{2}$.[5,35] We assessed distributions and Spearman correlations of serum PFAS concentrations.

Next, we evaluated the proportion of incident symptomatic hand OA and distributions of continuous outcomes (eg, change in number of dominant hand joints with radiographic OA). In a small number of participants with improved radiographic severity at the 48-month follow-up compared with baseline, we assumed no change and imputed the value as zero (n = 10 for number of joints with OA and n = 43 for the sum of KL grades across joints). Because of the high proportions of participants without a change in the number of hand joints with OA (81%) and sum of KL grades (56%), and for consistency across primary and secondary outcomes, we dichotomized both disease burden outcomes (change of ≥1 vs not).

We then examined the linearity of associations of single PFAS with hand OA using generalized additive models. As some of these models indicated possible nonlinear associations, we represented PFAS in our analyses in two ways: (1) a continuous variable per interquartile range (IQR) increment and (2) a categorical variable by quartiles.

We first ran unadjusted logistic models. Then, we ran adjusted models using prior literature on PFAS[6,7,36,37] and hand OA[25,26,38,39]; we a priori adjusted for gender/menopause status (male; female, premenopause; female, perimenopause; or female, postmenopause), race (Black, yes/no), education (college graduate, yes/no), and age at baseline (continuous). In a further adjusted model, we included BMI at baseline (continuous). We avoided adjusting for other metabolic comorbidities (eg, hypertension, diabetes, or dyslipidemia) because they may be mediators on the causal pathway between PFAS and hand OA. We did not explicitly account for other racial categories because of small sample sizes. With sparse missingness of values for the adjustment covariates (<0.5%), we used single imputation to replace missing values with the overall mode (for race and education), age group–specific mode (for menopause status), or gender-specific median (for BMI). For all models, we used sampling weight to account for case-cohort study design. Specifically, cases received a weight equal to 1, and noncases received a weight equal to 1/sampling fraction.[40]

As humans are not exposed to PFAS in isolation but rather multiple PFAS at a time, we also evaluated the joint effect of the PFAS mixture on our primary outcomes. We used quantile-based

Table 1. Descriptive statistics of serum PFAS concentrations among 1,878 Osteoarthritis Initiative participants in this subcohort study*

	Minimum	25th percentile	Median	75th percentile	Maximum	% detected	LOD
PFAS, ng/mL							
PFOS	0.10	9.0	12.7	17.9	85.5	100	0.008
PFOA	0.33	3.9	5.2	6.9	66.3	100	0.025
PFNA	0.07	0.8	1.1	1.5	13.4	100	0.010
PFHxS	0.10	2.0	3.0	4.6	66.7	100	0.012
MeFOSAA	0.03	0.3	0.4	0.7	16.3	100	0.019
PFHpS	<LOD	0.2	0.4	0.6	3.0	97	0.005
PFDA	<LOD	0.1	0.3	0.4	3.5	96	0.024
PFUnA	<LOD	0.1	0.2	0.3	3.4	92	0.006
PFDoA	<LOD	<LOD	<LOD	0.03	0.39	44	0.011
HFPO-DA (GenX)	<LOD	<LOD	<LOD	<LOD	0.02	2	0.009
ADONA	<LOD	<LOD	<LOD	<LOD	0.13	5	0.013
9Cl-PF3ONS	<LOD	<LOD	<LOD	<LOD	0.54	5	0.008

* 9Cl-PF3ONS, 9-chlorohexadecafluoro-3-oxanone-1-sulfonic acid; ADONA, 4,8-dioxa-3H-perfluorononanoic acid; HFPO-DA (GenX), perfluoro-2-proproxypropanoic acid; LOD, limit of detection; MeFOSAA, 2-(N-methyl-perfluorooctane sulfonamido) acetic acid; PFAS, per- and polyfluoroalkyl substances; PFDA, perfluorodecanoic acid; PFDoA, perfluorododecanoic acid; PFHpS, perfluoroheptanesulfonic acid; PFHxS, perfluorohexane sulfonic acid; PFNA, perfluorononanoic acid; PFOA, perfluorooctanoic acid; PFOS, perfluorooctane sulfonic acid; PFUnA, perfluoroundecanoic acid.

g-computation, a mixtures approach that (1) allows for estimation of the joint effect of an exposure mixture on a given outcome and (2) generates output of individual weights for each component in the mixture, which represents the relative contribution of that exposure component to either the positive or negative scaled effect size, taking into account collinearity with other exposures.[41] The estimates reflect the overall effect of a quartile increase of all PFAS in the mixture simultaneously on the odds of hand OA outcome.

Female gender, older age, and higher BMI are risk factors for hand OA, and PFAS may have a more pronounced impact on hand OA among individuals with these risk factors. Hence, we ran separate adjusted models stratified by gender, age group (greater than or equal to or less than the median of 61 years), and BMI category (greater than or equal to or less than 30 kg/m^2 [ie, obese vs nonobese]) at baseline to explore whether associations of individual PFAS with the two primary hand OA outcomes differed by these strata. Among women, we also ran an exploratory analysis restricted to postmenopausal women; we did not restrict to premenopausal and perimenopausal women because of small sample sizes.

In secondary analyses, we used weighted logistic regression to evaluate covariate-adjusted associations of single PFAS with incidence (vs not) of each hand OA phenotype at 48 months. Participants with that hand OA phenotype at baseline were excluded (eg, n = 149 people with prevalent symptomatic hand OA at baseline) (Supplementary Table S1). In secondary analyses, we also used weighted logistic regression to examine associations of PFAS with an increase (vs not) in the sum of KL grade across joints.

Lastly, we conducted a post hoc covariate-adjusted analysis of single PFAS and baseline symptomatic hand OA to examine whether cross-sectional associations were more closely aligned with prior literature than longitudinal analyses within the OAI. We used SAS for data management and performed all statistical analyses in R (version 4.4.1; Core Team, 2018). For continuous PFAS exposures, the sample size for the incident symptomatic hand OA analysis provides 80% power at a conservative 0.01 significance

Table 2. Spearman correlations[a] of serum per- and polyfluoroalkyl substances concentrations among 1,878 Osteoarthritis Initiative participants in this subcohort study*

	PFOA	PFNA	PFHxS	MeFOSAA	PFHpS	PFDA	PFUnA
PFOS	0.64	0.67	0.46	0.24	0.76	0.61	0.44
PFOA	–	0.52	0.48	0.22	0.61	0.43	0.21
PFNA	–	–	0.27	0.22	0.55	0.86	0.73
PFHxS	–	–	–	0.16	0.52	0.17	0.07
MeFOSAA	–	–	–	–	0.21	0.18	0.13
PFHpS	–	–	–	–	–	0.42	0.30
PFDA	–	–	–	–	–	–	0.82

* All correlations had *P* values < 0.05. MeFOSAA, 2-(N-methyl-perfluorooctane sulfonamido) acetic acid; PFDA, perfluorodecanoic acid; PFHpS, perfluoroheptanesulfonic acid; PFHxS, perfluorohexane sulfonic acid; PFNA, perfluorononanoic acid; PFOA, perfluorooctanoic acid; PFOS, perfluorooctane sulfonic acid; PFUnA, perfluoroundecanoic acid.
[a] Correlation coefficients among eight per- and polyfluoroalkyl substances with >60% detectability.

level to detect an odds ratio (OR) of 1.26 per one IQR increase in exposure, using logistic regression models and accounting for the case-cohort design. The data and codebook will be shared by the corresponding author upon request.

RESULTS

Participant characteristics. Participants were mostly female (58%) and White (83%). On average, participants were aged 62 years with a mean BMI of 28.6 kg/m^2. The 519 participants who developed symptomatic hand OA (ie, "cases") tended to be older (65 vs 60 years) and more commonly female (63% vs 54%) than peers without incident symptomatic hand OA (Table 3).

Tables 1 and 2 report the distribution of the 12 measured PFAS and the correlations among the eight PFAS included in analyses. Serum PFAS concentrations were all positively correlated, with weak to moderately strong correlations (Spearman coefficients: 0.07–0.76). PFAS concentrations among participants in the OAI were generally comparable to those in the general US population during overlapping years (participants aged ≥45 years in the National Health and Nutrition Examination Survey [NHANES] 2005–2006 cycle). However, serum PFOS concentrations were lower in OAI versus NHANES participants (geometric mean: 12.4 vs 20.0 ng/mL), and PFHxS concentrations were slightly higher in the OAI (geometric mean: 3.0 vs 1.7 ng/mL) (Supplementary Table S2).

Symptomatic hand OA. Higher serum PFDA and PFNA were associated with greater odds of incident symptomatic hand OA (adjusted OR [aOR] [95% confidence interval (CI)] per IQR increment: 1.12 [1.05–1.20] for PFDA and 1.07 [1.00–1.13] for PFNA) when we represented each PFAS as a continuous measure. When we represented each PFAS in categories, the highest quartile of PFDA (vs quartile 1) was also associated with greater odds of hand OA; however, the quartile estimates were nonmonotonic and PFNA was not associated with hand OA. Additionally, higher PFHxS was associated with lower odds of incident symptomatic hand OA (eg, aOR [95% CI] per PFHxS IQR increment: 0.94 [0.88–1.00]) when represented as a continuous measure. The highest quartile of PFHpS (vs quartile 1) was also associated with lower odds of hand OA (Table 4). Otherwise, we observed no consistent associations between individual PFAS (Table 4) or the mixture of PFAS with incident symptomatic hand OA (Figure 1). Consistent with the single PFAS models, PFDA had the strongest weight in the positive scaled direction (ie, higher odds) after accounting for co-exposures in the quantile g-computation model (Figure 1) and was the PFAS with the largest magnitude estimate in relation to the outcome of incident symptomatic hand OA (Table 4).

Change in disease burden (number of joints with OA). In unadjusted and adjusted models, individual PFAS were not monotonically associated with an increased number of hand joints with radiographic OA over the follow-up (Table 5). Similarly, the mixture of PFAS was not associated with an increase in the number of hand joints with radiographic OA (Figure 1).

Exploratory analyses (stratification by gender, age, and BMI). As in the overall cohort, women with higher PFDA had higher odds of incident symptomatic hand OA. However, women with higher PFHpS had lower odds of incident symptomatic hand OA. Men with higher MeFOSAA had higher odds of incident symptomatic hand OA. There were no other statistically significant monotonic associations of PFAS with hand OA in men

Table 3. Participant characteristics of those included in the analytic dataset, overall and stratified by whether they had developed symptomatic hand OA at the 48-month follow-up visit*

Characteristics	Case-cohort sample (N = 1,878)[a]	Symptomatic hand OA incidence (n = 1,729)[a,b]	
		Yes (n = 519)	No (n = 1,210)
Age, mean ± SD, y	61.5 ± 9.0	65.1 ± 8.0	59.5 ± 8.9
Gender and menopause status, n (%)			
Male	789 (42)	193 (37)	558 (46)
Female, premenopause	149 (8)	17 (3)	128 (11)
Female, perimenopause	150 (8)	28 (5)	112 (9)
Female, postmenopause	790 (42)	281 (54)	412 (34)
Race, n (%)			
White	1,555 (83)	444 (86)	979 (81)
Black	284 (15)	66 (13)	205 (17)
Other reported races[c]	39 (2)	9 (2)	26 (2)
Body mass index, mean ± SD, kg/m^2	28.6 ± 4.7	28.4 ± 4.7	28.7 ± 4.8
College graduate, n (%)	1,198 (64)	306 (59)	808 (67)

* OA, osteoarthritis.
[a] Values reflect descriptive statistics from a single imputation dataset.
[b] A total of 149 participants had symptomatic hand OA at baseline.
[c] Self-reported Asian or "Other" as race.

Table 4. Associations (odds ratio [95% confidence interval]) of baseline serum per- and polyfluoroalkyl substances concentration with symptomatic hand osteoarthritis incidence among the cohort without baseline hand osteoarthritis (n = 1,729)*

	Model 1[a]	Model 2[b]	Model 3[c]
PFOS			
IQR (8.90 ng/mL)	1.01 (0.93–1.09)	0.97 (0.89–1.06)	0.97 (0.89–1.06)
Q1 (0.10–9.00 ng/mL)	Reference	Reference	Reference
Q2 (9.01–12.73 ng/mL)	0.98 (0.79–1.21)	0.87 (0.69–1.10)	0.87 (0.69–1.10)
Q3 (12.74–17.90 ng/mL)	1.08 (0.87–1.34)	1.04 (0.83–1.31)	1.03 (0.82–1.30)
Q4 (17.91–85.50 ng/mL)	0.92 (0.74–1.14)	0.81 (0.64–1.03)	0.81 (0.64–1.03)
PFOA			
IQR (3.01 ng/mL)	0.99 (0.92–1.06)	0.95 (0.88–1.02)	0.95 (0.87–1.02)
Q1 (0.33–3.87 ng/mL)	Reference	Reference	Reference
Q2 (3.88–5.18 ng/mL)	0.86 (0.69–1.07)	0.81 (0.64–1.02)	0.80 (0.64–1.01)
Q3 (5.19–6.88 ng/mL)	0.86 (0.69–1.07)	**0.74 (0.59–0.93)**	**0.74 (0.59–0.93)**
Q4 (6.89–66.30 ng/mL)	1.00 (0.81–1.23)	0.90 (0.72–1.12)	0.88 (0.70–1.11)
PFNA			
IQR (0.74 ng/mL)	1.03 (0.98–1.09)	**1.07 (1.01–1.13)**	**1.07 (1.00–1.13)**
Q1 (0.07–0.76 ng/mL)	Reference	Reference	Reference
Q2 (0.77–1.05 ng/mL)	1.18 (0.95–1.46)	1.20 (0.95–1.50)	1.19 (0.95–1.49)
Q3 (1.06–1.50 ng/mL)	1.00 (0.80–1.24)	0.99 (0.79–1.25)	0.98 (0.78–1.24)
Q4 (1.51–13.40 ng/mL)	1.08 (0.87–1.34)	1.18 (0.93–1.50)	1.17 (0.92–1.48)
PFHxS			
IQR (2.62 ng/mL)	0.99 (0.93–1.04)	**0.94 (0.88–1.00)**	**0.94 (0.88–1.00)**
Q1 (0.10–1.96 ng/mL)	Reference	Reference	Reference
Q2 (1.97–2.97 ng/mL)	1.09 (0.88–1.36)	0.90 (0.71–1.14)	0.91 (0.72–1.15)
Q3 (2.98–4.58 ng/mL)	1.11 (0.90–1.38)	0.92 (0.73–1.17)	0.93 (0.74–1.18)
Q4 (4.59–66.70 ng/mL)	1.04 (0.84–1.29)	0.83 (0.65–1.04)	0.84 (0.66–1.06)
MeFOSAA			
IQR (0.46 ng/mL)	1.03 (0.98–1.08)	1.01 (0.96–1.06)	1.01 (0.96–1.06)
Q1 (0.03–0.25 ng/mL)	Reference	Reference	Reference
Q2 (0.26–0.43 ng/mL)	1.13 (0.91–1.41)	1.10 (0.87–1.38)	1.10 (0.87–1.38)
Q3 (0.44–0.72 ng/mL)	**1.25 (1.00–1.55)**	1.18 (0.94–1.48)	1.18 (0.94–1.49)
Q4 (0.73–16.30 ng/mL)	1.23 (0.99–1.53)	1.10 (0.88–1.38)	1.10 (0.87–1.38)
PFHpS			
IQR (0.34 ng/mL)	1.02 (0.93–1.12)	0.91 (0.82–1.00)	0.90 (0.82–1.00)
Q1 (<LOD–0.21 ng/mL)	Reference	Reference	Reference
Q2 (0.22–0.36 ng/mL)	0.92 (0.73–1.14)	**0.75 (0.59–0.95)**	**0.75 (0.59–0.95)**
Q3 (0.37–0.55 ng/mL)	1.20 (0.97–1.49)	0.93 (0.74–1.17)	0.92 (0.73–1.16)
Q4 (0.56–2.97 ng/mL)	1.00 (0.80–1.24)	**0.75 (0.59–0.95)**	**0.74 (0.58–0.94)**
PFDA			
IQR (0.25 ng/mL)	1.05 (0.99–1.11)	**1.12 (1.05–1.20)**	**1.12 (1.05–1.20)**
Q1 (<LOD–0.15 ng/mL)	Reference	Reference	Reference
Q2 (0.16–0.25 ng/mL)	1.10 (0.89–1.36)	**1.26 (1.00–1.58)**	1.25 (1.00–1.57)
Q3 (0.26–0.40 ng/mL)	0.89 (0.72–1.11)	1.06 (0.84–1.34)	1.06 (0.84–1.33)
Q4 (0.41–3.54 ng/mL)	1.07 (0.86–1.32)	**1.30 (1.03–1.64)**	**1.30 (1.03–1.64)**
PFUnA			
IQR (0.24 ng/mL)	1.01 (0.94–1.07)	1.05 (0.97–1.12)	1.05 (0.98–1.12)
Q1 (<LOD–0.08 ng/mL)	Reference	Reference	Reference
Q2 (0.09–0.16 ng/mL)	0.90 (0.72–1.12)	0.93 (0.74–1.16)	0.93 (0.74–1.16)
Q3 (0.17–0.32 ng/mL)	1.02 (0.83–1.27)	1.15 (0.92–1.44)	1.15 (0.92–1.44)
Q4 (0.33–3.41 ng/mL)	0.95 (0.77–1.18)	1.04 (0.82–1.31)	1.05 (0.83–1.32)

* The analyses had inverse probability weighting to account for oversampling of cases with the case-cohort study design. Bolded estimates indicate $P < 0.05$. IQR, interquartile range; LOD, limit of detection; MeFOSAA, 2-(N-methyl-perfluorooctane sulfonamido) acetic acid; PFDA, perfluorodecanoic acid; PFHpS, perfluoroheptanesulfonic acid; PFHxS, perfluorohexane sulfonic acid; PFNA, perfluorononanoic acid; PFOA, perfluorooctanoic acid; PFOS, perfluorooctane sulfonic acid; PFUnA, perfluoroundecanoic acid; Q, quartile.
[a] Model 1 is unadjusted.
[b] Model 2 is adjusted for gender/menopause status (male, premenopausal female, perimenopausal female, or postmenopausal female), race (Black, yes/no), education level (college graduate, yes/no), and age at baseline.
[c] Model 3 is model 2 with additional adjustment for body mass index at baseline.

or with odds of an increase in the total number of hand joints with radiographic OA among women or men (Supplementary Table S3).

Higher continuous PFNA, PFDA, and PFUnA were associated with higher odds of incident symptomatic hand OA in older participants (aged ≥61 years). In contrast, higher PFOS, PFHxS,

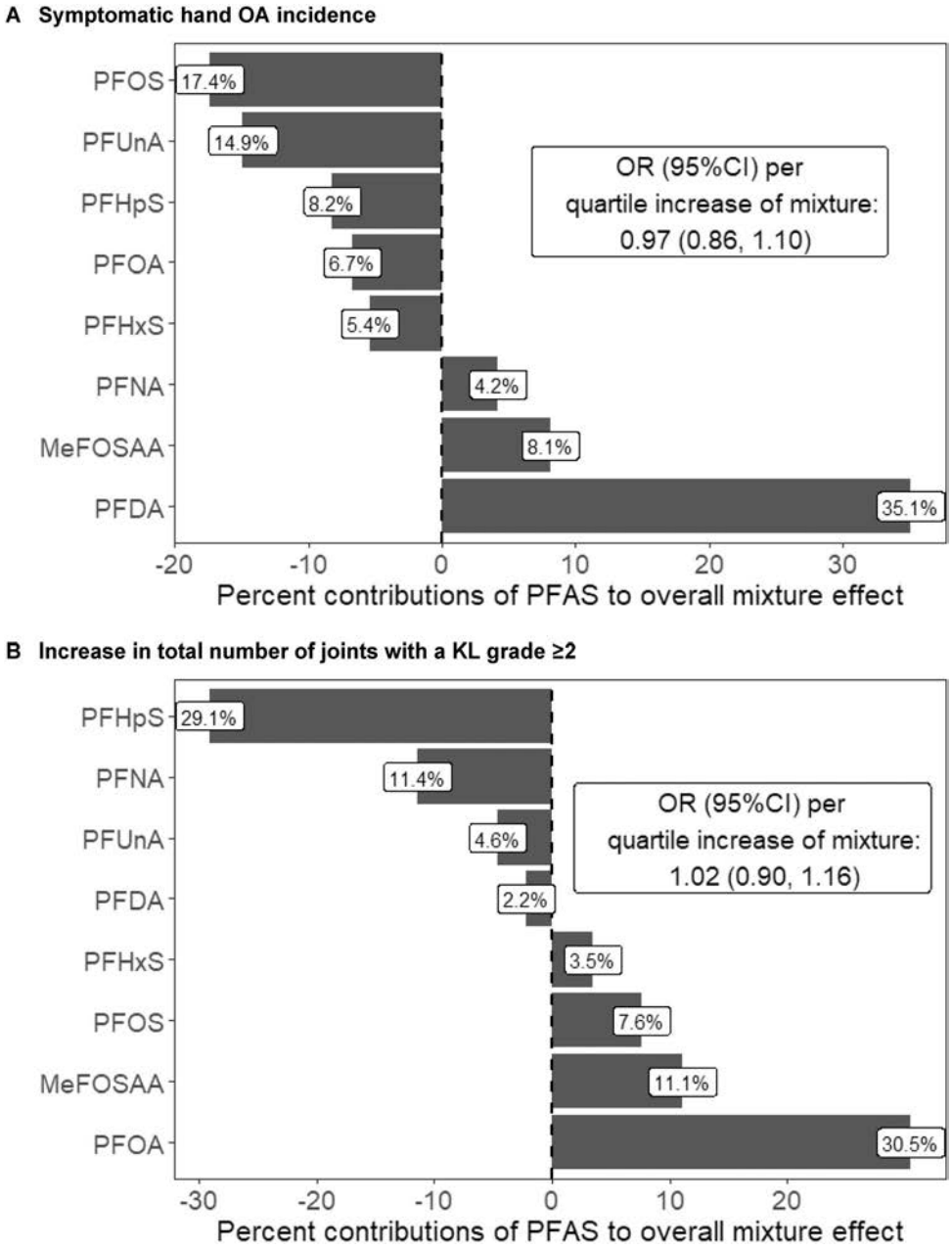

Figure 1. Odds of (A) symptomatic hand OA incidence and (B) an increase (vs not) in total number of joints with a KL grade ≥2 per quartile increase of all PFAS in the mixture simultaneously, and the percent contribution of each PFAS to the overall mixture (calculated using quantile g-computation output and accounting for the scaled effect size in each direction, ie, [absolute value of scaled directional effect/sum of the absolute values of scaled positive and negative effects] × PFAS weight × 100). Models are adjusted for gender/menopause status (male, premenopausal female, perimenopausal female, or postmenopausal female), race (Black, yes/no), education level (college graduate, yes/no), age at baseline, and body mass index at baseline. Models incorporated inverse probability weighting to account for oversampling of cases with the case-cohort study design. CI, confidence interval; KL, Kellgren-Lawrence; MeFOSAA, 2-(N-methyl-perfluorooctane sulfonamido) acetic acid; OA, osteoarthritis; OR, odds ratio; PFAS, per- and polyfluoroalkyl substances; PFDA, perfluorodecanoic acid; PFHpS, perfluoroheptanesulfonic acid; PFHxS, perfluorohexane sulfonic acid; PFNA, perfluorononanoic acid; PFOA, perfluorooctanoic acid; PFOS, perfluorooctane sulfonic acid; PFUnA, perfluoroundecanoic acid.

and PFHpS were associated with lower odds of hand OA in younger participants (aged <61 years) (Supplementary Table S4). In older participants, higher PFHxS quartiles (vs quartile 1) were associated with higher odds of an increase in the total number of hand joints with radiographic OA. There were no other monotonic associations between PFAS and an increase in total number of hand joints with radiographic OA in either age stratum (Supplementary Table S5).

Higher PFOA, PFOS, PFHxS, and PFUnA were associated with lower odds of incident symptomatic hand OA in participants

Table 5. Associations (odds ratio [95% confidence interval]) of baseline serum per- and polyfluoroalkyl substances concentration with having an increase (vs not) in the total number of joints with a Kellgren-Lawrence grade ≥2 between baseline and the 48-month follow-up visit (N = 1,878)*

	Model 1[a]	Model 2[b]	Model 3[c]
PFOS			
IQR (8.90 ng/mL)	0.96 (0.88–1.05)	0.98 (0.89–1.08)	0.98 (0.90–1.08)
Q1 (0.10–9.00 ng/mL)	Reference	Reference	Reference
Q2 (9.01–12.73 ng/mL)	1.05 (0.83–1.32)	1.03 (0.81–1.30)	1.03 (0.81–1.31)
Q3 (12.74–17.90 ng/mL)	0.98 (0.77–1.24)	1.02 (0.80–1.30)	1.02 (0.80–1.30)
Q4 (17.91–85.50 ng/mL)	0.95 (0.75–1.21)	1.01 (0.79–1.30)	1.01 (0.79–1.30)
PFOA			
IQR (3.01 ng/mL)	1.04 (0.96–1.11)	1.03 (0.96–1.11)	1.04 (0.96–1.12)
Q1 (0.33–3.87 ng/mL)	Reference	Reference	Reference
Q2 (3.88–5.18 ng/mL)	0.84 (0.66–1.08)	0.84 (0.65–1.08)	0.84 (0.65–1.08)
Q3 (5.19–6.88 ng/mL)	**1.29 (1.03–1.63)**	**1.31 (1.03–1.66)**	**1.32 (1.04–1.67)**
Q4 (6.89–66.30 ng/mL)	1.03 (0.81–1.31)	1.05 (0.82–1.34)	1.06 (0.83–1.36)
PFNA			
IQR (0.74 ng/mL)	0.98 (0.92–1.04)	0.99 (0.93–1.05)	0.99 (0.93–1.05)
Q1 (0.07–0.76 ng/mL)	Reference	Reference	Reference
Q2 (0.77–1.05 ng/mL)	0.79 (0.63–1.01)	0.79 (0.62–1.01)	0.80 (0.63–1.01)
Q3 (1.06–1.50 ng/mL)	1.08 (0.87–1.36)	1.07 (0.85–1.35)	1.08 (0.86–1.36)
Q4 (1.51–13.40 ng/mL)	**0.77 (0.61–0.98)**	0.80 (0.62–1.03)	0.81 (0.63–1.04)
PFHxS			
IQR (2.62 ng/mL)	1.01 (0.95–1.06)	1.01 (0.95–1.06)	1.01 (0.95–1.06)
Q1 (0.10–1.96 ng/mL)	Reference	Reference	Reference
Q2 (1.97–2.97 ng/mL)	**1.28 (1.01–1.62)**	**1.31 (1.02–1.67)**	**1.31 (1.02–1.67)**
Q3 (2.98–4.58 ng/mL)	1.06 (0.83–1.35)	1.12 (0.87–1.44)	1.11 (0.87–1.43)
Q4 (4.59–66.70 ng/mL)	1.13 (0.89–1.44)	1.18 (0.92–1.52)	1.17 (0.91–1.50)
MeFOSAA			
IQR (0.46 ng/mL)	0.99 (0.93–1.05)	0.99 (0.92–1.04)	0.98 (0.92–1.04)
Q1 (0.03–0.25 ng/mL)	Reference	Reference	Reference
Q2 (0.26–0.43 ng/mL)	1.27 (1.00–1.61)	1.24 (0.97–1.58)	1.24 (0.97–1.58)
Q3 (0.44–0.72 ng/mL)	**1.27 (1.00–1.62)**	1.27 (1.00–1.62)	1.27 (1.00–1.62)
Q4 (0.73–16.30 ng/mL)	1.17 (0.92–1.50)	1.13 (0.88–1.44)	1.13 (0.89–1.45)
PFHpS			
IQR (0.34 ng/mL)	0.94 (0.85–1.04)	0.95 (0.85–1.06)	0.96 (0.86–1.07)
Q1 (<LOD–0.21 ng/mL)	Reference	Reference	Reference
Q2 (0.22–0.36 ng/mL)	1.17 (0.93–1.47)	1.13 (0.89–1.43)	1.13 (0.90–1.44)
Q3 (0.37–0.55 ng/mL)	0.91 (0.71–1.16)	0.90 (0.70–1.15)	0.91 (0.70–1.17)
Q4 (0.56–2.97 ng/mL)	0.92 (0.73–1.18)	0.94 (0.73–1.21)	0.95 (0.74–1.23)
PFDA			
IQR (0.25 ng/mL)	0.98 (0.91–1.04)	0.99 (0.92–1.07)	0.99 (0.92–1.06)
Q1 (<LOD–0.15 ng/mL)	Reference	Reference	Reference
Q2 (0.16–0.25 ng/mL)	1.10 (0.87–1.39)	1.12 (0.89–1.42)	1.13 (0.89–1.43)
Q3 (0.26–0.40 ng/mL)	0.96 (0.76–1.22)	1.00 (0.79–1.27)	1.01 (0.80–1.28)
Q4 (0.41–3.54 ng/mL)	0.91 (0.72–1.16)	0.95 (0.74–1.21)	0.94 (0.73–1.21)
PFUnA			
IQR (0.24 ng/mL)	0.98 (0.91–1.04)	0.99 (0.91–1.06)	0.98 (0.91–1.06)
Q1 (<LOD–0.08 ng/mL)	Reference	Reference	Reference
Q2 (0.09–0.16 ng/mL)	1.19 (0.94–1.49)	1.18 (0.93–1.49)	1.18 (0.93–1.49)
Q3 (0.17–0.32 ng/mL)	0.94 (0.74–1.19)	0.96 (0.75–1.22)	0.96 (0.75–1.22)
Q4 (0.33–3.41 ng/mL)	0.94 (0.74–1.20)	0.95 (0.74–1.22)	0.94 (0.74–1.21)

* The analyses had inverse probability weighting to account for oversampling of cases with the case-cohort study design. Bolded estimates indicate $P < 0.05$. IQR, interquartile range; LOD, limit of detection; MeFOSAA, 2-(N-methyl-perfluorooctane sulfonamido) acetic acid; PFDA, perfluorodecanoic acid; PFHpS, perfluoroheptanesulfonic acid; PFHxS, perfluorohexane sulfonic acid; PFNA, perfluorononanoic acid; PFOA, perfluorooctanoic acid; PFOS, perfluorooctane sulfonic acid; PFUnA, perfluoroundecanoic acid; Q, quartile.
[a] Model 1 is unadjusted.
[b] Model 2 is adjusted for gender/menopause status (male, premenopausal female, perimenopausal female, or postmenopausal female), race (Black, yes/no), education level (college graduate, yes/no), and age at baseline.
[c] Model 3 is model 2 with additional adjustment for body mass index at baseline.

with higher BMI (≥30 kg/m^2). In contrast, higher PFDA and PFNA were associated with higher odds of hand OA in participants with lower BMI (<30 kg/m^2) (Supplementary Table S4). There were no statistically significant associations of PFAS with an increase in the total number of hand joints with radiographic OA in either stratum of BMI, except for nonmonotonic associations of quartiles of

PFOS and PFOA with higher odds of an increase in the total number of hand joints with radiographic OA among those with higher BMI (Supplementary Table S5).

In postmenopausal women, higher PFDA was associated with higher odds of incident symptomatic hand OA, and higher PFHpS was associated with lower odds of hand OA when represented as a continuous variable but not when represented in quartiles. Other PFAS were not monotonically associated with incident symptomatic hand OA or an increase in the total number of hand joints with radiographic OA (Supplementary Table S6).

Secondary outcomes. We found no consistent associations of PFAS concentrations with an increase in the sum of KL grades during the follow-up (Supplementary Table S7). Participants with higher PFOS, PFHxS, and PFHpS had lower odds of incident central erosive OA. PFAS were not consistently and monotonically associated with other OA phenotypes (Supplementary Table S8).

Post hoc analyses. In cross-sectional analyses, higher PFNA and PFUnA were associated with higher odds of baseline symptomatic hand OA. There were no other associations between PFAS and symptomatic hand OA at baseline (Supplementary Table S9).

DISCUSSION

Investigators have hypothesized ubiquitous risk factors that have emerged within the last 70 years to explain the increase in OA prevalence.[2] We observed possible associations of PFDA and PFNA with symptomatic hand OA incidence but otherwise found no consistent evidence that higher PFAS concentrations relate to greater risk of hand OA incidence or progression.

By employing a prospective evaluation and objective OA measures, our work advances the prior literature, which examined self-reported OA cross-sectionally. Our findings contrast with a cross-sectional 2003 to 2008 NHANES study, which found that US adults with higher serum concentrations of PFOA and PFOS had greater odds of self-reported OA,[6] and a study of individuals in the mid-Ohio Valley (2005–2006) with high drinking water exposure to PFOA from a chemical plant, which found that although adults with higher PFOA had higher likelihood of self-reported OA, adults with higher PFOS had lower likelihood.[7] Cross-sectional analyses are susceptible to reverse causation (eg, if PFAS are released more readily from osteoarthritic bone), but this does not appear to explain the discordance in results from our study versus prior studies, as neither PFOS nor PFOA were associated with baseline symptomatic hand OA in our cross-sectional analyses. Although PFAS concentrations in the OAI are lower than in the mid-Ohio Valley, they are similar to those of NHANES. Rather than differences in variability of serum PFAS concentrations, a more likely reason for the discordant results may be that we examined associations of PFAS with well-characterized hand OA versus self-reported OA in the prior studies. Self-reported OA is strongly influenced by knee OA, the most prevalent OA phenotype.[42] PFAS may relate more strongly to knee OA than hand OA, and this is an important topic for future investigation.

By looking at multiple PFAS, individually and as a mixture, our work also advances prior literature, which focused only on PFOS and PFOA. We found that adults with higher concentrations of PFDA and PFNA had higher odds of incidence of symptomatic hand OA in single PFAS models. These associations are biologically consistent because PFDA and PFNA are longer-chain perfluorinated carboxylic acids, and their binding may differ from PFAS with different functional groups or carbon chain lengths.[43–45] We confirmed these associations in each age stratum and among those without obesity. Evidence for PFDA was further corroborated by the mixture models in which it had the strongest weight in the positive scaled direction after accounting for co-exposures. Notably, associations of PFDA and PFNA with incident symptomatic hand OA were nonmonotonic when represented as quartiles, and we observed these signals for incident symptomatic hand OA but not the other phenotypes or radiographic outcomes, suggesting the association may be phenotype specific or related to hand OA symptoms. Unfortunately, the OAI lacks joint-specific and other validated patient-reported outcomes (eg, Australian/Canadian OA Hand Index), which could offer greater insights into the relationship between PFAS and hand OA symptoms. Few population-based studies have examined PFDA or PFNA, and serum PFDA had relatively low variability in concentrations in the OAI. Thus, additional research is needed on the potential role of these lesser studied perfluorinated carboxylic acids in OA.

Our results infer that some PFAS may exhibit a protective effect for incident symptomatic hand OA (eg, PFHpS), especially among women (PFHpS), younger participants (PFHpS and PFOS), or those with obesity (PFHpS, PFOS, PFOA, and PFUnA). The negative relationship complements prior results from the cross-sectional mid-Ohio Valley study, which showed a negative association of PFOS with self-reported OA.[7] Innes and colleagues hypothesized that although PFOS has pro-inflammatory effects, it can also elicit anti-inflammatory effects by activating peroxisome proliferator-activated receptor γ (PPAR-γ), which could reduce the risk of incident OA.[7,46,47] Indeed, there is evidence that the extent and potency of PPAR-γ activation differ by PFAS compound.[48] However, we must be cautious in interpreting these results because they primarily emerged from numerous exploratory analyses within strata of the overall case-control sample.

The OAI offered an unprecedented opportunity to explore the associations between PFAS and OA in a well-characterized study sample with longitudinal data. Our study is the first to examine PFAS and hand-specific OA outcomes. Despite these strengths, our study had limitations. First, the purposeful

recruitment of people aged 45 to 79 years with risk factors for OA could influence the generalizability of our results. The age of this cohort enabled us to observe a high rate of incidence and progression during a 4-year observation period (eg, 30% had incident symptomatic hand OA) and allowed us to generalize results to ages when the incidence of hand OA is greatest.[49] This age range was also ideal because only 8% of the study sample had prevalent symptomatic hand OA at baseline, which reduced the risk of selection (index event) bias. Although the OAI purposefully recruited participants at high risk for knee OA (eg, participants with knee symptoms, repetitive knee bending, or history of knee injury or surgery), it has generated similar estimates for the prevalence of hand OA as population-based cohorts[25,27,50] and offers a more diverse population than population-based cohorts, along with a rich dataset of covariates.

We also performed numerous analyses without correction for multiple comparisons; however, we a priori identified two primary outcomes. We focused on those results and used the results from secondary outcomes to help identify consistent patterns of association. Findings of secondary outcome analyses should be interpreted with caution, as we cannot rule out the risk of selection bias for outcomes with high baseline prevalences (eg, incident radiographic hand [47%] or thumb-base [45%] OA). Future studies investigating these secondary outcomes may be warranted in younger populations with lower baseline prevalence. We also cannot generalize our findings to people exposed to high PFAS concentrations, because the OAI lacked participants with very high PFAS exposure. We also focused on hand OA because OA development in these joints is more likely attributable to systemic exposures, unlike the knee, which can be heavily influenced by local risk factors (eg, knee injury or aberrant joint loading). However, it is unclear how PFAS may relate to other OA phenotypes. Finally, although PFAS concentrations in blood samples represent only part of the total body burden of PFAS, measuring PFAS in other tissues is not feasible in large cohort studies. Therefore, as in other epidemiologic studies of PFAS, we used blood PFAS concentrations as a proxy of overall exposure. Furthermore, we were unable to analyze short-chain PFAS because they tend to have shorter half-lives and are not detectable on routine biomonitoring.[51] Future studies using animal models could help us better understand the health impacts of total PFAS body burden, PFAS in specific tissues (eg, articular cartilage, subchondral bone), and short-chain PFAS.

In conclusion, our findings suggest that individuals with higher PFDA and PFNA may have a greater risk of developing incident symptomatic hand OA. However, we found no other consistent evidence that greater PFAS concentrations relate to a greater likelihood of developing hand OA incidence or progression. The field will benefit from future studies investigating the potential associations of elevated levels of PFDA and PFNA with symptomatic hand OA incidence or hand OA symptomatic progression.

AUTHOR CONTRIBUTIONS

All authors contributed to at least one of the following manuscript preparation roles: conceptualization AND/OR methodology, software, investigation, formal analysis, data curation, visualization, and validation AND drafting or reviewing/editing the final draft. As corresponding author, Dr Driban confirms that all authors have provided the final approval of the version to be published and takes responsibility for the affirmations regarding article submission (eg, not under consideration by another journal), the integrity of the data presented, and the statements regarding compliance with institutional review board/Declaration of Helsinki requirements.

REFERENCES

1. Zhang W, Doherty M, Leeb BF, et al; ESCISIT. EULAR evidence-based recommendations for the diagnosis of hand osteoarthritis: report of a task force of ESCISIT. Ann Rheum Dis 2009;68(1):8–17.
2. Wallace IJ, Worthington S, Felson DT, et al. Knee osteoarthritis has doubled in prevalence since the mid-20th century. Proc Natl Acad Sci U S A 2017;114(35):9332–9336.
3. Deprouw C, Courties A, Fini JB, et al. Pollutants: a candidate as a new risk factor for osteoarthritis-results from a systematic literature review. RMD Open 2022;8(2):e001983.
4. Sunderland EM, Hu XC, Dassuncao C, et al. A review of the pathways of human exposure to poly- and perfluoroalkyl substances (PFASs) and present understanding of health effects. J Expo Sci Environ Epidemiol 2019;29(2):131–147.
5. Botelho JC, Kato K, Wong LY, et al. Per- and polyfluoroalkyl substances (PFAS) exposure in the U.S. population: NHANES 1999-March 2020. Environ Res 2025;270:120916.
6. Uhl SA, James-Todd T, Bell ML. Association of osteoarthritis with perfluorooctanoate and perfluorooctane sulfonate in NHANES 2003-2008. Environ Health Perspect 2013;121(4):447–452.
7. Innes KE, Ducatman AM, Luster MI, et al. Association of osteoarthritis with serum levels of the environmental contaminants perfluorooctanoate and perfluorooctane sulfonate in a large Appalachian population. Am J Epidemiol 2011;174(4):440–450.
8. Olsen GW, Burris JM, Ehresman DJ, et al. Half-life of serum elimination of perfluorooctanesulfonate, perfluorohexanesulfonate, and perfluorooctanoate in retired fluorochemical production workers. Environ Health Perspect 2007;115(9):1298–1305.
9. Li Y, Fletcher T, Mucs D, et al. Half-lives of PFOS, PFHxS and PFOA after end of exposure to contaminated drinking water. Occup Environ Med 2018;75(1):46–51.
10. Khosrojerdi MA, Lotfi H, Babaei Z, et al. Exposure to per- and polyfluoroalkyl substances and bone health: a systematic review and meta-analysis. Int J Environ Health Res 2024;34(12):4074–4095.
11. Tao K, Zeng B, Deng L, et al. Associations between per- and polyfluoroalkyl substances exposures and bone mineral: a systematic review and best evidence synthesis. Environ Health (Wash) 2024;3(4):363–372.
12. Cardenas A, Gold DR, Hauser R, et al. Plasma concentrations of per- and polyfluoroalkyl substances at baseline and associations with glycemic indicators and diabetes incidence among high-risk adults in the Diabetes Prevention Program trial. Environ Health Perspect 2017;125(10):107001.
13. Fleisch AF, Rifas-Shiman SL, Mora AM, et al. Early-life exposure to perfluoroalkyl substances and childhood metabolic function. Environ Health Perspect 2017;125(3):481–487.
14. Cardenas A, Hauser R, Gold DR, et al. Association of perfluoroalkyl and polyfluoroalkyl substances with adiposity. JAMA Netw Open 2018;1(4):e181493.

15. Qi W, Clark JM, Timme-Laragy AR, et al. Per- and polyfluoroalkyl substances and obesity, type 2 diabetes and non-alcoholic fatty liver disease: a review of epidemiologic findings. Toxicol Environ Chem 2020; 102(1-4):1–36.
16. Qazi MR, Bogdanska J, Butenhoff JL, et al. High-dose, short-term exposure of mice to perfluorooctanesulfonate (PFOS) or perfluorooctanoate (PFOA) affects the number of circulating neutrophils differently, but enhances the inflammatory responses of macrophages to lipopolysaccharide (LPS) in a similar fashion. Toxicology 2009; 262(3):207–214.
17. Singh TS, Lee S, Kim HH, et al. Perfluorooctanoic acid induces mast cell-mediated allergic inflammation by the release of histamine and inflammatory mediators. Toxicol Lett 2012;210(1):64–70.
18. Zhang L, Louie A, Rigutto G, et al. A systematic evidence map of chronic inflammation and immunosuppression related to per- and polyfluoroalkyl substance (PFAS) exposure. Environ Res 2023;220: 115188.
19. van Beest S, Damman W, Liu R, et al. In finger osteoarthritis, change in synovitis is associated with change in pain on a joint-level; a longitudinal magnetic resonance imaging study. Osteoarthritis Cartilage 2019;27(7):1048–1056.
20. Damman W, Liu R, Bloem JL, et al. Bone marrow lesions and synovitis on MRI associate with radiographic progression after 2 years in hand osteoarthritis. Ann Rheum Dis 2017;76(1):214–217.
21. Haugen IK, Slatkowsky Christensen B, Bøyesen P, et al. Increasing synovitis and bone marrow lesions are associated with incident joint tenderness in hand osteoarthritis. Ann Rheum Dis 2016;75(4): 702–708.
22. Yu CH, Patel B, Palencia M, et al. A sensitive and accurate method for the determination of perfluoroalkyl and polyfluoroalkyl substances in human serum using a high performance liquid chromatography-online solid phase extraction-tandem mass spectrometry. J Chromatogr A 2017;1480:1–10.
23. Yu CH, Riker CD, Lu SE, et al. Biomonitoring of emerging contaminants, perfluoroalkyl and polyfluoroalkyl substances (PFAS), in New Jersey adults in 2016-2018. Int J Hyg Environ Health 2020;223(1): 34–44.
24. Wilder FV, Barrett JP, Farina EJ. Joint-specific prevalence of osteoarthritis of the hand. Osteoarthritis Cartilage 2006;14(9):953–957.
25. Eaton CB, Schaefer LF, Duryea J, et al. Prevalence, incidence, and progression of radiographic and symptomatic hand osteoarthritis: the Osteoarthritis Initiative. Arthritis Rheumatol 2022;74(6):992–1000.
26. McAlindon TE, Driban JB, Roberts MB, et al. Erosive hand osteoarthritis: incidence and predictive characteristics among participants in the Osteoarthritis Initiative. Arthritis Rheumatol 2021;73(11):2015–2024.
27. Haugen IK, Englund M, Aliabadi P, et al. Prevalence, incidence and progression of hand osteoarthritis in the general population: the Framingham Osteoarthritis Study. Ann Rheum Dis 2011;70(9):1581–1586.
28. Altman RD, Gold GE. Atlas of individual radiographic features in osteoarthritis, revised. Osteoarthritis Cartilage 2007;15 Suppl A: A1–56.
29. Altman R, Alarcón G, Appelrouth D, et al. The American College of Rheumatology criteria for the classification and reporting of osteoarthritis of the hand. Arthritis Rheum 1990;33(11): 1601–1610.
30. Kloppenburg M, Maheu E, Kraus VB, et al; OARSI Hand Clinical Trial Recommendations Work Group. OARSI clinical trials recommendations: design and conduct of clinical trials for hand osteoarthritis. Osteoarthritis Cartilage 2015;23(5):772–786.
31. McAlindon T, Roberts M, Driban J, et al. Incident hand OA is strongly associated with reduced peripheral blood leukocyte telomere length. Osteoarthritis Cartilage 2018;26(12):1651–1657.
32. Scherzer ZA, Alvarez C, Renner JB, et al. Effects of comorbid cardiovascular disease and diabetes on hand osteoarthritis, pain, and functional state transitions: the Johnston County Osteoarthritis Project. J Rheumatol 2020;47(10):1541–1549.
33. Zhang Y, Neogi T, Hunter D, et al. What effect is really being measured? An alternative explanation of paradoxical phenomena in studies of osteoarthritis progression. Arthritis Care Res (Hoboken) 2014; 66(5):658–661.
34. Zhang Y, Niu J, Felson DT, et al. Methodologic challenges in studying risk factors for progression of knee osteoarthritis. Arthritis Care Res (Hoboken) 2010;62(11):1527–1532.
35. Rokoff LB, Rifas-Shiman SL, Aris IM, et al. Mid-childhood plasma concentrations of per- and polyfluoroalkyl substances, modifiable lifestyle factors, and bone mineral density through late adolescence. Environ Sci Technol 2024;58(45):19970–19980.
36. Pomazal R, Malecki K, Stanton N, et al. Determinants of per- and polyfluoroalkyl substances (PFAS) exposure among Wisconsin residents. Environ Res 2024;254:119131.
37. Lin PD, Cardenas A, Hauser R, et al. Temporal trends of concentrations of per- and polyfluoroalkyl substances among adults with overweight and obesity in the United States: results from the Diabetes Prevention Program and NHANES. Environ Int 2021;157: 106789.
38. Nelson AE, Renner JB, Schwartz TA, et al. Differences in multijoint radiographic osteoarthritis phenotypes among African Americans and Caucasians: the Johnston County Osteoarthritis project. Arthritis Rheum 2011;63(12):3843–3852.
39. Qin J, Barbour KE, Murphy LB, et al. Lifetime risk of symptomatic hand osteoarthritis: the Johnston County Osteoarthritis Project. Arthritis Rheumatol 2017;69(6):1204–1212.
40. Prentice RL. A case-cohort design for epidemiologic cohort studies and disease prevention trials. Biometrika 1986;73(1):1–11.
41. Keil AP, Buckley JP, O'Brien KM, et al. A quantile-based g-computation approach to addressing the effects of exposure mixtures. Environ Health Perspect 2020;128(4):47004.
42. Steinmetz JD, Culbreth GT, Haile LM, et al; GBD 2021 Osteoarthritis Collaborators. Global, regional, and national burden of osteoarthritis, 1990-2020 and projections to 2050: a systematic analysis for the Global Burden of Disease Study 2021. Lancet Rheumatol 2023;5(9): e508–e522.
43. Zhang L, Ren XM, Wan B, et al. Structure-dependent binding and activation of perfluorinated compounds on human peroxisome proliferator-activated receptor γ. Toxicol Appl Pharmacol 2014; 279(3):275–283.
44. Wolf CJ, Schmid JE, Lau C, et al. Activation of mouse and human peroxisome proliferator-activated receptor-alpha (PPARα) by perfluoroalkyl acids (PFAAs): further investigation of C4-C12 compounds. Reprod Toxicol 2012;33(4):546–551.
45. Wolf CJ, Takacs ML, Schmid JE, et al. Activation of mouse and human peroxisome proliferator-activated receptor alpha by perfluoroalkyl acids of different functional groups and chain lengths. Toxicol Sci 2008;106(1):162–171.
46. Kirk AB, Michelsen-Correa S, Rosen C, et al. PFAS and potential adverse effects on bone and adipose tissue through interactions with PPARγ. Endocrinology 2021;162(12):bqab194.
47. Zhang Y, Hannan MT, Chaisson CE, et al. Bone mineral density and risk of incident and progressive radiographic knee osteoarthritis in women: the Framingham Study. J Rheumatol 2000;27(4):1032–1037.

48. Evans N, Conley JM, Cardon M, et al. In vitro activity of a panel of per- and polyfluoroalkyl substances (PFAS), fatty acids, and pharmaceuticals in peroxisome proliferator-activated receptor (PPAR) alpha, PPAR gamma, and estrogen receptor assays. Toxicol Appl Pharmacol 2022;449:116136.
49. Hunter DJ, Bierma-Zeinstra S. Osteoarthritis. Lancet 2019; 393(10182):1745–1759.
50. Dahaghin S, Bierma-Zeinstra SM, Ginai AZ, et al. Prevalence and pattern of radiographic hand osteoarthritis and association with pain and disability (the Rotterdam study). Ann Rheum Dis 2005;64(5): 682–687.
51. Centers for Disease Control and Prevention. National Exposure Report [Internet]. Accessed November 20, 2025. https://www.cdc.gov/environmental-exposure-report/

American College of Rheumatology
Empowering Rheumatology Professionals

Arthritis & Rheumatology
Vol. 78, No. 5, May 2026, pp 1088–1101
DOI 10.1002/art.70004

Myeloid-Derived Suppressor Cell–Derived Interferon-β Promotes T Follicular Helper Cell Response and Exacerbates Lupus Development

Ke Rui,[1] Zixiang Chen,[1,2] Jun Liu,[1,2] Wei Huang,[1,2] Xiaomeng Wang,[1,2] Fan Xiao,[3] Yingbo Zhou,[3] Xiaoqiu Dai,[4] Yuan Tang,[3] Mengna Zhao,[3] Na Peng,[5] Xiaoran Wang,[5] Bo Zhu,[1] Shengjun Wang,[1] Liwei Lu,[3] and Jie Tian[1,2]

Objective. Increasing evidence highlights a critical role of T follicular helper (Tfh) cells in autoimmune pathogenesis. This study aimed to identify inflammatory cytokines involved in driving Tfh cell responses in systemic lupus erythematosus (SLE).

Methods. The circulating Tfh frequencies and interferon (IFN)-β levels were analyzed for correlations with disease activities in patients with SLE. Both lupus mice with IFN-β treatment and Ifnar1$^{-/-}$ mice with lupus induction were assessed for Tfh cell responses and disease progression. Sorting-purified naive CD4^{+}T cells from Ifnar1$^{-/-}$ mice were adoptively transferred to lupus mice for monitoring Tfh cell differentiation in vivo. In culture, mouse CD4^{+}T cells treated with IFN-β were examined for Tfh cell differentiation and intracellular signaling pathway. The underlying mechanism for IFN-β secretion by myeloid-derived suppressor cells (MDSCs) was investigated by co-immunoprecipitation and Western blotting.

Results. We found that increased Tfh cells with IFN-I–inducible gene signatures correlated with disease activities in patients with SLE. Consistently, IFN-β treatment markedly enhanced Tfh cell response and exacerbated disease progression in lupus mice. Moreover, mice with IFNAR1 deficiency exhibited attenuated lupus progression with significantly decreased Tfh response. Mechanistically, IFN-β activated the indoleamine 2,3-dioxygenase/kynurenine/aryl hydrocarbon receptor (IDO/Kyn/AhR) axis to promote Tfh cell differentiation. Notably, expanded MDSCs in lupus were found to produce high levels of IFN-β. Further studies showed that the autoantigen activated lymphocyte-derived DNA stimulated IFN-β production by MDSCs via the cyclic GMP-AMP synthase–stimulator of IFN genes (cGAS-STING)–dependent pathway.

Conclusion. These results have demonstrated a novel function of IFN-β in promoting Tfh cell response during lupus progression, which may facilitate the identification of new therapeutic targets for the treatment of SLE.

INTRODUCTION

Systemic lupus erythematosus (SLE) is a chronic autoimmune disease affecting multiple organs and systems.[1,2] Dysregulated T cell responses have been implicated in the pathogenesis of SLE. Numerous studies, including our previous findings, have demonstrated a pivotal role of interleukin (IL)-17–producing CD4^{+} T helper (Th17) cells in promoting plasma cell response and autoantibody production, a hallmark feature of SLE development.[3,4] Increasing evidence has indicated the critical

Supported by the National Natural Science Foundation of China (grants 82572074, 82171771, 82271854, 82471821, U25A6004 and 82572073), the Jiangsu Provincial Key Research and Development Program (grant BE2023758), Major Project of Basic Science Research in Higher Education Institutions of Jiangsu Province (grant 23KJA320001), Jiangsu Association for Science and Technology's Young Talents Nurturing Program (grant TJ-2023-027), Hubei Province Science and Technology Bureau (grant 2023AFB1049), and the Centre for Oncology and Immunology under the Health@InnoHK Initiative funded by the Innovation and Technology Commission, The Government of Hong Kong SAR, China.

[1]Department of Laboratory Medicine, Affiliated Hospital of Jiangsu University, Zhenjiang, China; [2]Department of Immunology, Jiangsu Key Laboratory of Laboratory Medicine, School of Medicine, Jiangsu University, Zhenjiang, China; [3]Department of Pathology, Faculty of Medicine, The University of Hong Kong, Centre for Oncology and Immunology, Hong Kong Science Park, Hong Kong, China; [4]Institute of Biology and Medical Sciences, School of Biology and Basic Medical Sciences, Soochow University, Suzhou, China; [5]Department of Rheumatology, The Second People's Hospital of Three Gorges University, Yichang, China.

Drs Rui, Chen, and Liu are co–first authors and contributed equally to this work.

Additional supplementary information cited in this article can be found online in the Supporting Information section (https://acrjournals.onlinelibrary.wiley.com/doi/10.1002/art.70004).

Author disclosures and graphical abstract are available at https://onlinelibrary.wiley.com/doi/10.1002/art.70004.

Address correspondence via email to Liwei Lu, PhD, at liweilu@hku.hk or Jie Tian, PhD, at tianjie@ujs.edu.cn.

Submitted for publication April 14, 2025; accepted in revised form October 29, 2025.

involvement of enhanced CD4$^+$ T follicular helper (Tfh) cell response in promoting B cell activation for autoantibody overproduction.[5,6] Tfh cells are characterized by the expression of specific transcription factor Bcl6 and surface expression of CXCR5, which allows their localization into the germinal centers (GCs) to facilitate follicular B cell differentiating into antibody-secreting plasma cells.[7] Several studies have shown that aberrant differentiation of Tfh cells induces lupus-like autoimmunity in mice, whereas inhibition of Tfh cell expansion alleviates the severity of murine lupus.[8,9] However, it remains poorly understood how inflammatory cytokines promote Tfh cell differentiation and exacerbate lupus pathogenesis.

Recent studies have revealed a pathogenic role of type I interferons (IFNs) during the development of SLE.[10] In patients with SLE, elevated serum level of type I IFNs and up-regulated expression profile of type I IFN–induced gene transcripts in leukocytes are observed, which are positively correlated with SLE disease activity.[11–13] The type I IFN family includes IFN-α, IFN-β, and several other subtypes. It is recognized that the production of type I IFN subtypes is regulated by distinct cell types and microenvironment milieu.[14] Currently, blocking the type I IFN pathway has been demonstrated as an effective therapeutic approach for the treatment of SLE. Recent reports from clinical trials showed that an IFNAR-specific monoclonal antibody (anifrolumab) has been approved for the treatment of SLE[15] although the anti–IFN-α antibody failed,[16] suggesting a role of other type I IFNs in SLE, such as IFN-β. To date, it remains largely unclear whether IFN-β plays a role in regulating T cell response and promotes lupus pathogenesis. Thus, further investigation may facilitate the identification of new therapeutic targets for the effective treatment of patients with SLE.

Early studies have reported that the main cellular source of type I IFNs is plasmacytoid dendritic cells (pDCs). However, a recent study revealed that pDCs were not effector cells in SLE and were not associated with disease activity and blood IFN signaling. Keratinocyte-derived IFN-κ was found to be a major source of type I IFNs in the skin of patients with lupus.[17] Additionally, increasing evidence shows that myeloid cells can also produce high levels of type I IFNs.[18] Myeloid-derived suppressor cells (MDSCs) are a heterogeneous population of immature myeloid cells with immunosuppressive activity, which are expanded during the development of various autoimmune diseases,[19] including multiple sclerosis,[20,21] rheumatoid arthritis,[22,23] primary Sjögren disease,[24–26] and SLE.[27,28] Our previous studies have demonstrated that dysregulation of MDSCs contributes to the development of primary Sjögren disease.[26] However, it is unclear whether MDSCs produce IFN-β and modulate Tfh cell response during lupus development.

In this study, we identified a novel function and the underlying effector mechanism of IFN-β in promoting Tfh cell differentiation during lupus development. Moreover, we demonstrated that MDSCs were the major cellular source of IFN-β during lupus development whereas IFN-β played a pivotal role in driving Tfh cell response via activating aryl hydrocarbon receptor (AhR) and exacerbated lupus progression, suggesting that targeting IFN-β may provide a promising therapeutic strategy for the treatment of SLE.

PATIENTS AND METHODS

Human samples

Blood samples were collected from patients with SLE (n = 32) and healthy controls (n = 41). Serum samples were collected from 35 patients with SLE and 30 healthy individuals. All patients were diagnosed according to the 2019 EULAR/American College of Rheumatology (ACR) classification criteria for SLE.[29] Age-matched healthy donors without a personal history of cancer or autoimmune diseases were enrolled as controls. The study protocols and consent forms were approved by the ethics committee of the Affiliated Hospital of Jiangsu University (approval number: KY2022K0602). The characteristics of the patients with SLE and healthy controls are shown in Supplementary Tables S1 and S2.

Mice

C57BL/6 (CD45.2) mice and B6.SJL-Ptprca Pepcb /BoyJ (CD45.1) mice were obtained from Cavens Laboratory Animal Co., Ltd (Jiangsu, China), and *Ifnar1*-deficient (Ifnar1$^{-/-}$) C57BL/6 mice were obtained from Cyagen Biosciences Co., Ltd (Guangzhou, China). All mice were maintained in the Animal Center of Jiangsu University (Jiangsu, China). All experiments were approved by the Committee on the Use of Live Animals in Research and Teaching of Jiangsu University. Female MRL/MpJ-Fas^{lpr}/J (MRL/Lpr) mice were purchased from The Jackson Laboratory (Bar Harbor, Maine, USA) and maintained at the Laboratory Animal Unit of the University of Hong Kong. The animal experiments using MRL/Lpr mice were approved by the Committee on the Use of Live Animals in Teaching and Research (no: 3392-14) at the University of Hong Kong. Methods in all experiments, statistics, and related references are described in the Supplementary Methods (Supplementary Tables S3 and S4).

Data availability. The authors verify that all other data supporting the findings of this study are provided in the article and its Supplementary Materials.

RESULTS

Increased Tfh cells with IFN-I–inducible gene signatures correlate with disease activity in patients with SLE and lupus mice

To determine the role of Tfh cells in lupus pathogenesis, we first examined the circulating Tfh cells in peripheral blood

mononuclear cells (PBMCs) of patients with SLE by flow cytometric analysis (Figure 1A). It was found that the frequencies of circulating Tfh cells were significantly increased in patients with SLE. To further examine the correlation of circulating Tfh cells with disease activity, we divided patients with SLE into active (SLE Disease Activity Index [SLEDAI] ≥ 6) and inactive groups (SLEDAI < 6).[4] When compared with patients with inactive SLE, patients with active SLE exhibited a significantly higher percentage of Tfh cells in PBMCs. Moreover, the single-cell transcriptome analysis detected increased circulating Tfh cells in patients with SLE when compared with healthy controls (Figure 1B). The dot plots displaying canonical marker genes for distinct CD4$^+$ T cell subsets were shown in Supplementary Figure S1A.

Interestingly, the gene expression profile of Tfh cells in patients with SLE markedly differed from that in healthy controls at a genome-wide level, among which IFN-I–inducible genes including ISG15, ISG20, IFITM3, and IFITM2 were profoundly enriched in Tfh cells from patients with SLE (Figure 1C). Moreover, gene ontology terms analysis revealed

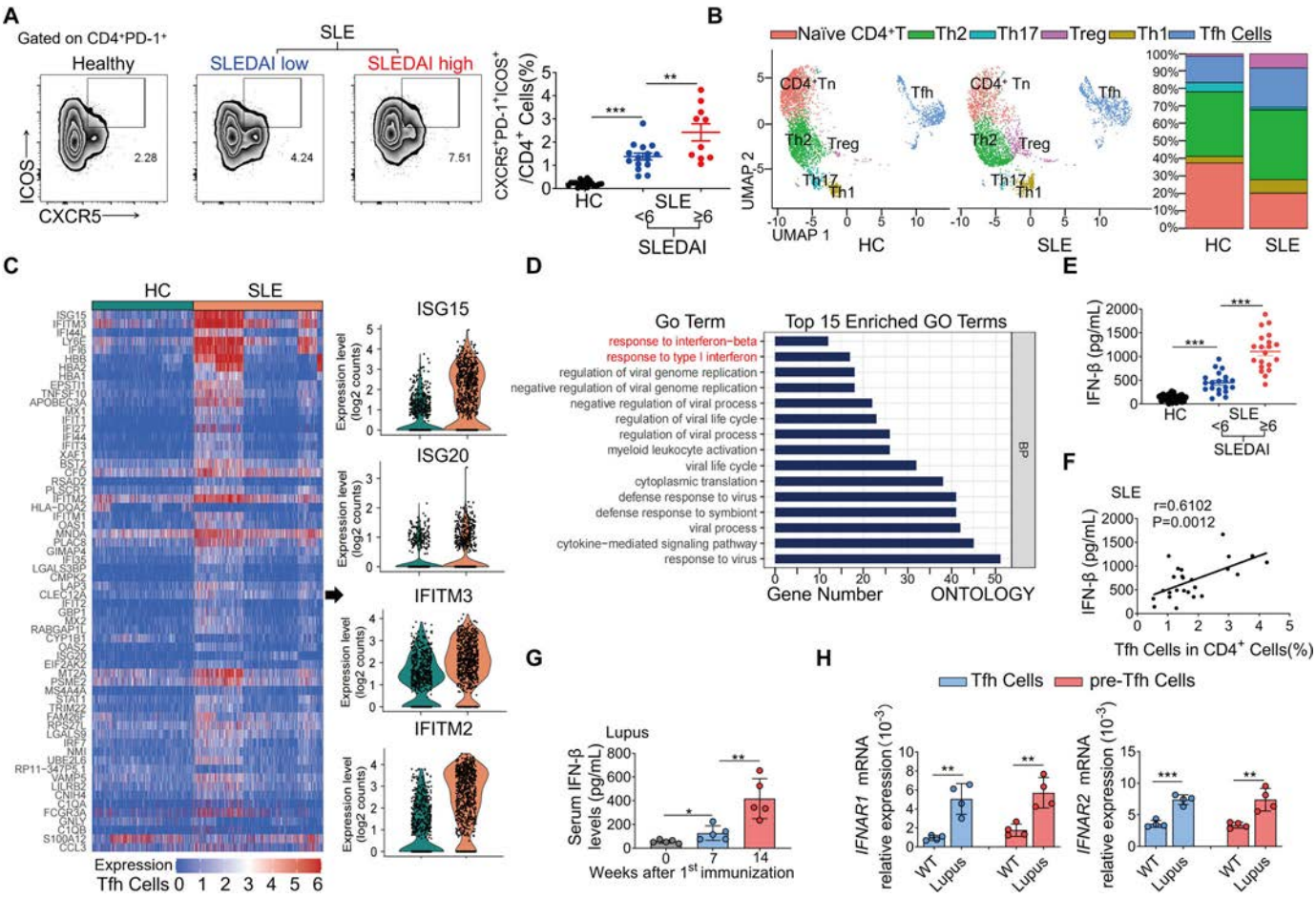

Figure 1. Increased IFN-β correlates with expanded Tfh cells in patients with SLE. (A) Representative flow cytometric profiles show frequencies of CD4$^+$CXCR5$^+$ICOS$^+$PD-1$^+$ Tfh cells in peripheral blood mononuclear cells (PBMCs) from patients with active SLE (SLEDAI ≥ 6, n = 10), inactive SLE (SLEDAI < 6, n = 15) and healthy individuals (n = 20). (B) UMAP visualization and percentages of CD4$^+$ T cell clusters in healthy individuals and patients with SLE by single-cell RNA sequencing. (C) Heatmaps showing the differential expression of genes in Tfh cell cluster between HCs and patients with SLE. Violin plot comparing the expression of ISG15, ISG20, IFITM3, and IFITM2 in each group. (D) GO categories enriched for differentially expressed genes in Tfh cells from PBMCs of patients with SLE. (E) The serum level of IFN-β in patients with SLE (n = 35) and healthy controls (n = 30) by enzyme-linked immunosorbent assay. (F) Correlation of serum levels of IFN-β with Tfh cells in PBMCs from patients with SLE. (G) Concentrations of IFN-β in the serum of lupus mice during the disease development (n = 4 per group). (H) *IFNAR1* and *IFNAR2* mRNA expression were measured in Tfh cells and pro-Tfh cells (CD4$^+$CXCR5$^+$ and CCR7^{lo}PD-1^{hi}) from WT mice and lupus mice by reverse transcription quantitative polymerase chain reaction (n = 4 per group). Data are shown as mean ± SD of three independent experiments. Statistical analysis was determined by one-way analysis of variance in parts A, E, and G; the Pearson correlation coefficient in part F; and Student's *t*-test in part H. ***$P < 0.001$; **$P < 0.01$; *$P < 0.05$. GO, Gene Ontology; HC, healthy control; IFN, interferon; mRNA, messenger RNA; SLE, systemic lupus erythematosus; SLEDAI, SLE Disease Activity Index; Tfh, T follicular helper; UMAP, Uniform Manifold Approximation and Projection; WT, wild-type.

a significant enrichment for genes encoding molecules associated with type I IFN–mediated response (Figure 1D). However, other T cell subsets, including Th1, Th17, and Treg cells, did not show pronounced enrichment of the IFN-β–mediated response or upregulation of IFN-I–inducible genes in patients with SLE (Supplementary Figure S2). We further detected the expression of IFN-β in both patients with SLE and lupus mice. Notably, the serum level of IFN-β was significantly increased in patients with SLE and positively correlated with increased frequencies of circulating Tfh cells (Figure 1E and F). Consistently, IFN-β expression was also increased during the disease development in lupus mice (Figure 1G). Moreover, both Tfh cells and CCR7^{lo}PD-1^{hi}CXCR5^{+}Tfh precursors (pre-Tfh) from lupus mice expressed higher levels of IFNAR1 and IFNAR2 transcripts (Figure 1H), suggesting a potential role of IFN-β signaling in mediating Tfh cell response.

IFN-β enhances Tfh cell response and exacerbates disease progression in lupus mice

To identify the role of IFN-β in regulating Tfh cell response, lupus mice were treated with recombinant IFN-β and monitored for disease progression. It was found that IFN-β treatment markedly increased the serum levels of anti–double-stranded DNA (dsDNA) autoantibody, creatinine, and urea, as well as protein levels in the urine (Figure 2A). Moreover, histologic analysis showed pronounced glomerular damage and renal IgG deposition in IFN-β–treated lupus mice (Figure 2B and C). Both the

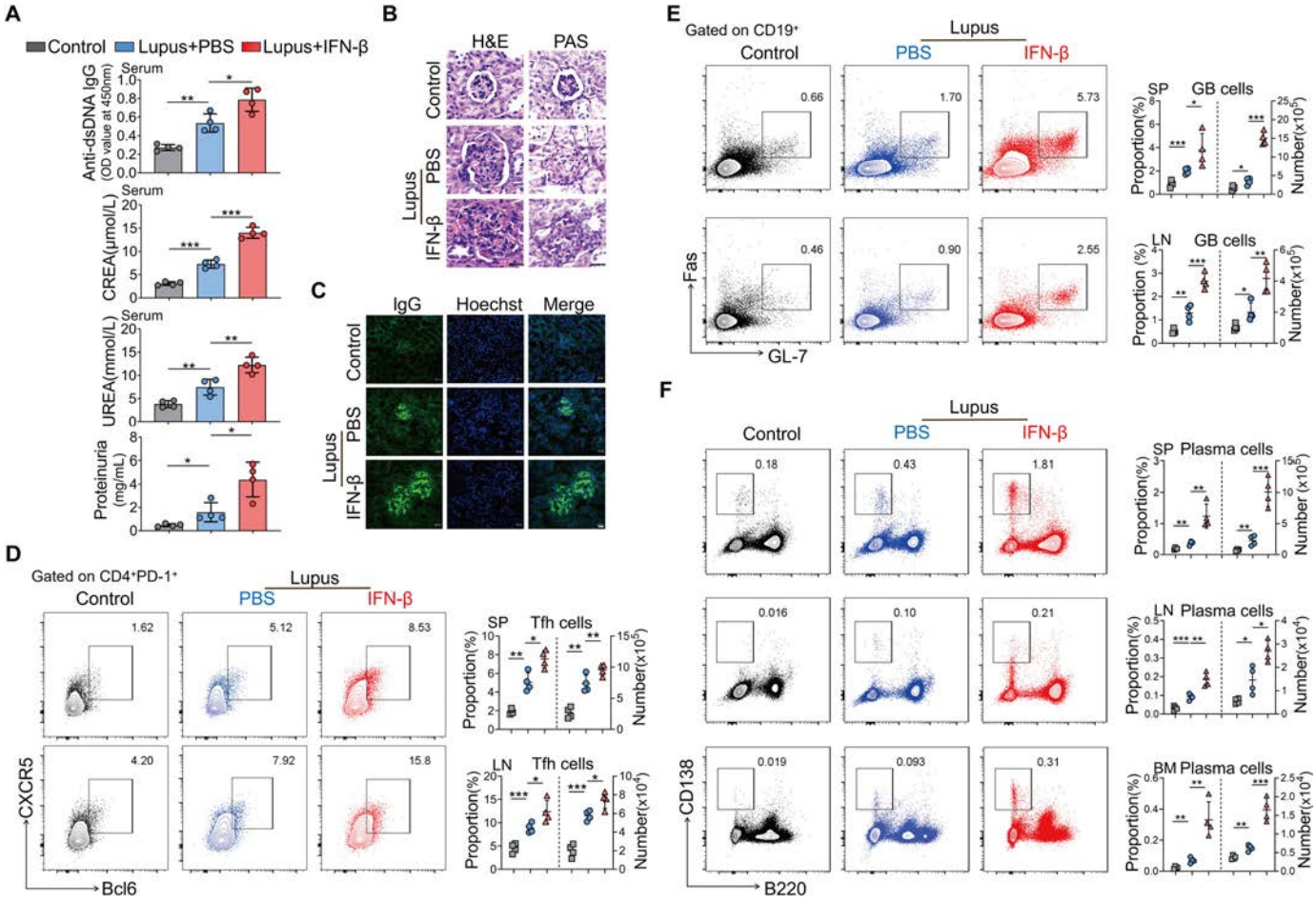

Figure 2. IFN-β enhances Tfh cell response and promotes the development of murine lupus. C57BL/6 mice were subjected to induce lupus, and recombinant IFN-β (1,000 U per mice) or control was intravenously administered at 5, 6, and 7 weeks after the first immunization. Mice were euthanized at 8 weeks (n = 4 per group). The histologic evaluation was conducted at 15 weeks. (A) Concentrations of serum anti-dsDNA IgG, urea, and creatinine, as well as protein levels in the urine, were detected in different groups. Representative images show kidney sections with H&E staining, (B) PAS staining, and (C) immunofluorescent staining of IgG. Scale bar = (B) 20 μm and (C) 20 μm. (D–F) Representative flow cytometric profiles and data plots show the frequencies and numbers of (D) CD4^{+}CXCR5^{+}PD-1^{+} Tfh cells, (E) GB cells, and (F) plasma cells in SP, LNs, and BM from each group. Data are shown as mean ± SD of three independent experiments. Statistical analysis was determined by one-way analysis of variance. ***$P < 0.001$; **$P < 0.01$; *$P < 0.05$. BM, bone marrow; CREA, creatinine; dsDNA, double-stranded DNA; GB, germinal center B; H&E, hematoxylin and eosin; IFN, interferon; LN, lymph node; PAS, Periodic acid-Schiff; PBS, phosphate-buffered saline; SP, spleen; Tfh, T follicular helper. Color figure can be viewed in the online issue, which is available at http://onlinelibrary.wiley.com/doi/10.1002/art.70004/abstract.

percentages and numbers of Tfh cells, GC B cells, and plasma cells were greatly increased in the spleens (SPs), lymph nodes (LNs), and bone marrow (BM) from IFN-β–treated lupus mice (Figure 2D–F). Similar results were also observed in lupus-prone MRL/Lpr mice, among which IFN-β treatment led to significantly increased percentages of Tfh cells and IL-21$^+$ CD4$^+$CXCR5$^+$PD-1$^+$ cells in SPs and LNs when compared with the control group without IFN-β treatment (Supplementary Figure S3A–C). These data suggest that IFN-β may play a pathogenic role in lupus development, possibly by promoting Tfh cell-mediated immune response.

To further determine the function of IFN-β signaling in regulating Tfh cell response during lupus development in vivo, purified naive CD4$^+$T cells from Ifnar1$^{-/-}$ or wild-type (WT; CD45.2) mice were adoptively transferred into Boy/J (CD45.1) recipient mice, followed with lupus induction (Figure 3A). Compared with control groups transferred with WT CD4$^+$ T cells, lupus mice transferred with Ifnar1$^{-/-}$ CD4$^+$ T cells showed significantly reduced frequencies of Tfh cells and IL-21$^+$CD4$^+$CXCR5$^+$PD-1$^+$ cells in the SPs and LNs (Figure 3B and C), indicating that IFN-β signaling is critical for the differentiation and homeostatic maintenance of Tfh cells in vivo. Furthermore, mice receiving WT CD4$^+$ T cells exhibited greater disease severity than those receiving Ifnar1$^{-/-}$ CD4$^+$ T cells, which was manifested as elevated levels of serum anti-dsDNA autoantibody, creatinine, urea, and urinary protein, along with pronounced glomerular damage (Supplementary Figure S4). In addition, the sizes of SPs and LNs from Ifnar1$^{-/-}$ mice were markedly smaller than those from WT mice during lupus development (Figure 3D and E).

Compared with the control group, Ifnar1$^{-/-}$ mice displayed greatly reduced levels of serum anti-dsDNA autoantibody, creatinine, and urea, as well as protein levels in the urine (Figure 3F). Compared with WT lupus mice, Ifnar1$^{-/-}$ mice did not show any obvious glomerular damage as revealed by histologic examination (Figure 3G). Notably, Ifnar1$^{-/-}$ mice showed markedly reduced Tfh cells, IL-21$^+$CD4$^+$CXCR5$^+$PD-1$^+$ cells (Figure 3H and I), GC B cells, and plasma cells (Supplementary Figure S5A and B) in SPs, LNs, and BM. In contrast, the frequencies of Th17 and Treg cells remained largely unchanged, and only a mild decrease was observed in Th1 cells from the SPs of Ifnar1$^{-/-}$ mice (Supplementary Figure S5C and D). To determine whether IFN-β is directly involved in inducing Tfh cell differentiation, naive CD4$^+$T cells from normal mice were cultured with recombinant IFN-β. In culture, IFN-β potently promoted the differentiation of Tfh cells (Figure 3J), and the expression level of key transcript factor Bcl-6 was significantly increased (Figure 3K). Moreover, we also measured the capacity of IFN-α to drive Tfh cell differentiation. In contrast to IFN-β, IFN-α with a 10-fold higher concentration only induced a slight increase in the proportion of Tfh cells, suggesting a much weaker capacity of IFN-α in promoting Tfh cell differentiation (Supplementary Figure S6).

IFN-β promotes Tfh cell differentiation via AhR activation

Upon IFN-β stimulation, naive CD4$^+$T cells exhibited significantly up-regulated AhR-related genes, including AHR, AHRR, CYP1A1, and CYP1B1, as revealed by reverse transcription quantitative polymerase chain reaction (RT-qPCR) analysis (Figure 4A). AhR is a critical cytoplasmic transcription factor that can sense multiple xenobiotics and endogenous metabolites, which has been found to regulate various biologic processes.[30] AHRR, cytochrome P450 1A1 (CYP1A1), and CYP1B1 are the main target genes of AhR.[31] Upon IFN-β treatment in culture, we detected substantial AhR translocation from the cytoplasm to the nucleus in CD4$^+$ T cells by Western blotting and flow cytometric analysis (Figure 4B–D), indicating that IFN-β could activate AhR signaling in T cells. Furthermore, AhR activation was also increased in Tfh cells from patients with SLE, which was correlated with disease activity (Supplementary Figure S7). As an endogenous ligand for AhR, kynurenine (Kyn) is a major metabolic intermediate of indoleamine 2,3-dioxygenase 1 (IDO1)–catalyzed tryptophan. To assess whether the IDO-Kyn-AhR axis was involved in IFN-β–mediated Tfh cell differentiation, we detected the expression of IDO1 and Kyn in vitro. Notably, both IDO1 and Kyn expression levels were significantly increased after IFN-β treatment at the messenger RNA and protein levels (Figure 4E–G). To further verify the role of AhR in IFN-β–mediated differentiation, AhR inhibitors CH-223191 and 3′,4′-dimethoxyflavone (DMF) were used in T cell culture. Indeed, treatment with either CH-223191 or DMF led to the decreased Tfh cell differentiation in culture (Figure 4H), and the expression levels of Bcl6, Ascl2, CD40L, and IL-21 were also significantly decreased (Figure 4I).

Expanded MDSCs express a high level of IFN-β during lupus development

During lupus development in mice, we found a marked expansion of CD11b$^+$Gr-1$^+$MDSCs. The frequencies of MDSCs in the SP, LN, and peripheral blood were significantly increased during lupus progression, reaching the peak value at 5 weeks (Figure 5A and B). RT-qPCR analysis showed that levels of IFN-β transcripts in MDSCs were higher than other immune cells. Flow cytometric analysis further confirmed the high level of IFN-β expression in CD11b$^+$Gr-1$^+$MDSCs (Figure 5C and D), and the monocytic MDSC (M-MDSC) and polymorphonuclear MDSC subsets expressed similar levels of IFN-β (Supplementary Figure S8). Moreover, the immunofluorescent microscopic examination revealed that most MDSCs were located at the T-B cell borders, indicating that accumulated MDSCs may support the differentiation of Tfh cells (Figure 5E). Furthermore, after depleting MDSCs in MRL/lpr lupus mice, the serum levels of anti-dsDNA autoantibody, creatinine, and urea, as well as protein levels in urine in lupus mice were significantly decreased. In addition,

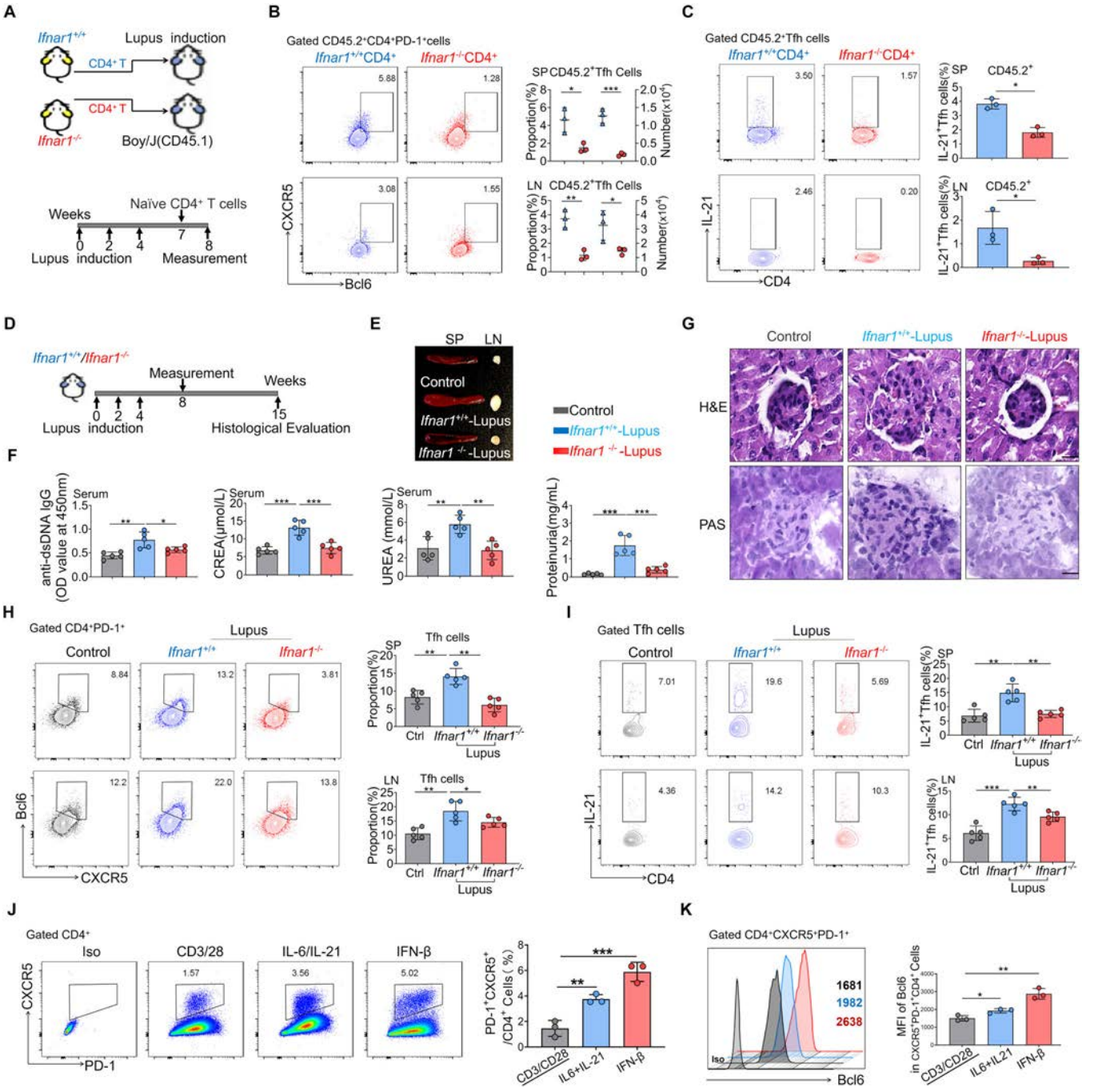

Figure 3. IFN-β induces the differentiation of Tfh cells both in vitro and in lupus mice. (A) Naive $CD4^+$T cells from WT or $IFNAR^{-/-}$ mice were transferred into Boy/J (CD45.1) mice, which were immunized for systemic lupus erythematosus induction (n = 3 per group). Frequencies and numbers of (B) $CD45.2^+$Tfh cells and (C) $CD45.2^+IL\text{-}21^+$Tfh cells in spleens and LNs were analyzed by flow cytometry. (D) WT and $IFNAR^{-/-}$ mice were subjected to activated lymphocyte-derived DNA–induced lupus (n = 5 per group). (E) Representative images show the sizes of SPs and LNs. (F) Concentrations of serum anti-dsDNA IgG, creatinine, and urea as well as protein levels in the urine were detected in different groups. (G) Representative images show the kidney sections with H&E staining and PAS staining. Scale bar = 20 μm. Representative flow cytometric profiles and data plots show the frequencies of (H) $CD4^+CXCR5^+PD\text{-}1^+Bcl\text{-}6^+$Tfh cells and (I) $IL\text{-}21^+$Tfh cells in SPs and LNs from each group. A total of 2×10^6 murine naive $CD4^+$T cells were cultured under anti-CD3 monoclonal antibody (1 μg/mL) and anti-CD28 monoclonal antibody (1 μg/mL) stimulation. IL-6 (25 ng/mL) together with IL-21 (20 ng/mL), or different concentrations of IFN-β (100 U/mL) were added to culture for 3 days. (J) Representative flow cytometric profiles and data plots show the frequencies of $CD4^+CXCR5^+PD\text{-}1^+$ Tfh cells. (K) The expression of Bcl6 in each group was analyzed by flow cytometric analysis. Data are shown as mean ± SD of three independent experiments. Statistical analysis was determined by Student's *t*-test in parts B and C and one-way analysis of variance in parts F, H, I, J, and K. $^{***}P < 0.001$; $^{**}P < 0.01$; $^{*}P < 0.05$. CREA, creatinine; dsDNA, double-stranded DNA; H&E, hematoxylin and eosin; IFN, interferon; IL, interleukin; LN, lymph node; MFI, mean fluorescence intensity; OD, optical density; PAS, Periodic acid-Schiff; SP, spleen; Tfh, T follicular helper. Color figure can be viewed in the online issue, which is available at http://onlinelibrary.wiley.com/doi/10.1002/art.70004/abstract.

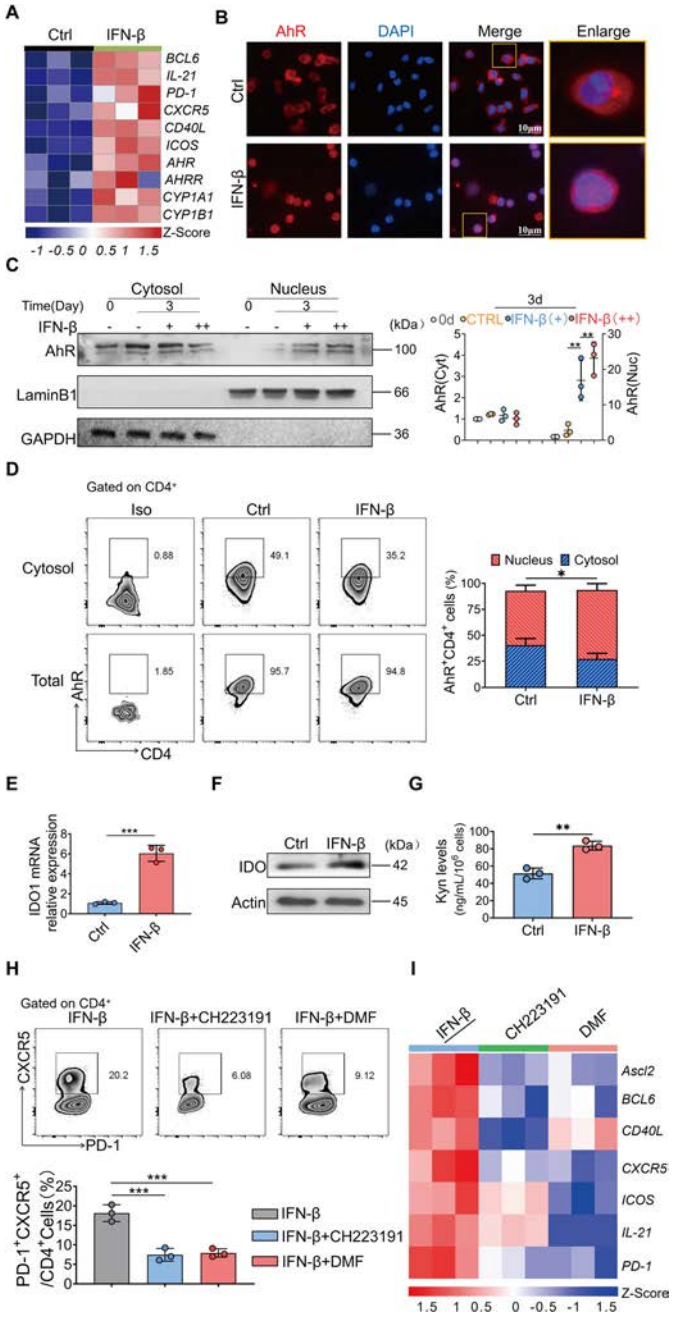

Figure 4. IFN-β activates AhR to promote T follicular helper (Tfh) cell differentiation. A total of 2 × 10^6 murine naive $CD4^+$T cells were cultured under anti-CD3 monoclonal antibody (mAb; 1 μg/mL) and anti-CD28 mAb (1 μg/mL) stimulation. IFN-β (500 U/mL) was added to culture for 3 days and induced Tfh cell differentiation. (A) The gene expression profiles in the IFN-β–treated group and control group were analyzed by reverse transcription quantitative polymerase chain reaction (RT-qPCR) analysis. (B) Immunofluorescence staining showed the localization of AhR in the IFN-β–treated group and control group by confocal microscopy (AhR in red and DAPI in blue; scale bar = 10 μm). (C) Western blot was used to detect the AhR expression in cytosol and the nucleus after different concentrations of IFN-β (100 U/mL and 500 U/mL) treatment for 3 days. The data plot shows the quantitation of AhR. (D) Representative flow cytometric profiles show the AhR level in cytosol and whole cells after IFN-β (500 U/mL) treatment. The data plot shows the AhR expression in cytosol and nucleus in each group. Both mRNA and protein levels of IDO were measured after IFN-β treatment by (E) RT-qPCR and (F) Western blot, respectively. (G) The Kyn level was detected by a kit in each group. Murine naive $CD4^+$T cells were cultured under anti-CD3 mAb and anti-CD28 mAb stimulation. $CD4^+$T cells were pretreated with AhR inhibitors (CH223191 or DMF) for 1.5 hours, and then IFN-β was added to culture for 3 days. (H) The percentage of Tfh cells was measured by flow cytometry. (I) The gene expression profiles in each group were analyzed by RT-qPCR analysis. Data are shown as mean ± SD of three independent experiments. Statistical analysis was determined by one-way analysis of variance in parts C and H and Student's *t*-test in parts D, E, and G. ***$P < 0.001$; **$P < 0.01$; *$P < 0.05$. AhR, aryl hydrocarbon receptor; DMF, 3′,4′-dimethoxyflavone; IDO1, indoleamine 2,3-dioxygenase 1; IFN, interferon; IL, interleukin; Kyn, kynurenine; mRNA, messenger RNA. Color figure can be viewed in the online issue, which is available at http://onlinelibrary.wiley.com/doi/10.1002/art.70004/abstract.

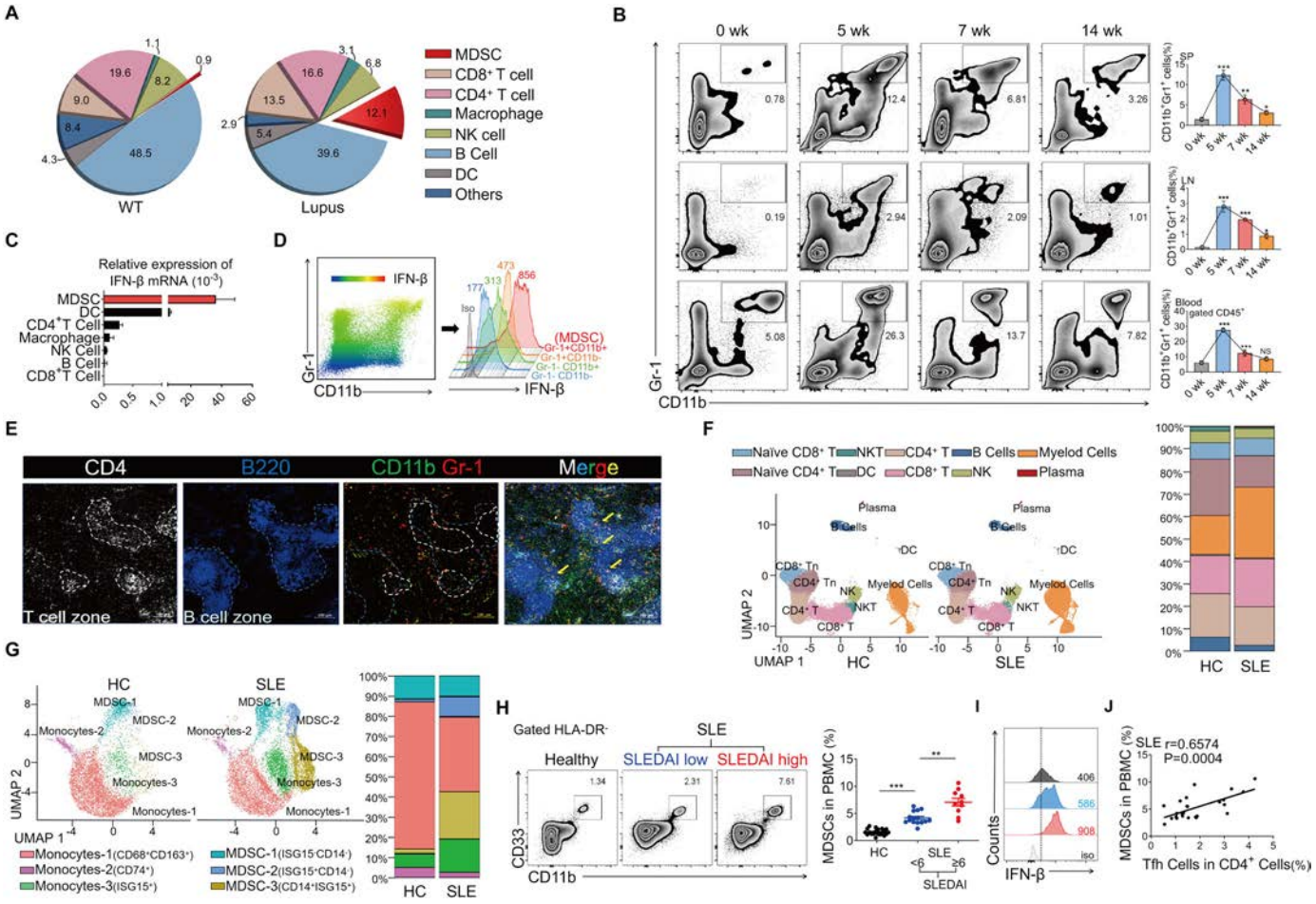

Figure 5. Accumulated MDSCs express plenty of IFN-β in lupus mice. (A) Frequencies of different immune cells in SPs from WT C57BL/6 mice and lupus mice. (B) Kinetic changes of $CD11b^{+}Gr\text{-}1^{+}$ MDSCs in SPs, LNs, and blood during lupus development in mice. The (C) mRNA and (D) protein levels of IFN-β in different cell populations from the SP of lupus mice were analyzed by reverse transcription quantitative polymerase chain reaction and flow cytometry, respectively. (E) Immunofluorescence staining of an SP section from lupus mice, showing the localization of MDSCs (CD4, white; B220, blue; CD11b, green; and Gr-1, red) in the T cell zone (white dashed line) and B cell zone (blue dashed line) by confocal microscopy (scale bar = 100 μm). (F) UMAP visualization and percentages of immune cell clusters in healthy individuals and patients with SLE by single-cell RNA sequencing. (G) UMAP visualization and percentages of myeloid cell clusters in HCs and patients with SLE. Representative flow cytometric profiles and data plots show (H) frequencies and (I) IFN-β levels of $HLA\text{-}DR^{-}CD11b^{+}CD33^{+}$ MDSCs in PBMCs from patients with inactive SLE (SLEDAI < 6, n = 15), with active SLE (SLEDAI ≥ 6, n = 10), and in healthy individuals (n = 20). (J) The correlation of MDSCs and Tfh cells was analyzed. Data are shown as mean ± SD of three independent experiments (n = 4 per group for parts A–E). Statistical analysis was determined by one-way analysis of variance for parts B and H and the Pearson correlation coefficient for part J. $^{***}P < 0.001$; $^{**}P < 0.01$; $^{*}P < 0.05$. DC, dendritic cell; HC, healthy control; IFN, interferon; LN, lymph node; MDSC, myeloid-derived suppressor cell; mRNA, messenger RNA; NK, natural killer; NS, no significance; PBMC, peripheral blood mononuclear cell; SLE, systemic lupus erythematosus; SLEDAI, SLE Disease Activity Index; SP, spleen; Tfh, T follicular helper; UMAP, Uniform Manifold Approximation and Projection; WT, wild-type. Color figure can be viewed in the online issue, which is available at http://onlinelibrary.wiley.com/doi/10.1002/art.70004/abstract.

histologic analysis showed ameliorated glomerular damage and immune complex deposition. Notably, the frequencies of Tfh cells and $IL\text{-}21^{+}CD4^{+}CXCR5^{+}PD\text{-}1^{+}$ cells in SPs and LNs were also decreased. These results demonstrated that the depletion of MDSCs led to the reduced Tfh cells and attenuated lupus development in mice (Supplementary Figure S9A–F).

To further characterize the phenotypic and functional features of the increased MDSCs in murine lupus, we examined the expression pattern of costimulatory molecules and the suppressive capacity of MDSCs on T cell proliferation. During the disease progression, the suppressive effect of MDSCs on $CD4^{+}$T cell proliferation was gradually decreased with diminished levels of arginase and nitric oxide (NO) expression (Supplementary Figure S10A and B). However, up-regulated levels of CD40, CD80, CD86, and major histocompatibility complex II expression on MDSCs were detected, indicating a mature phenotype (Supplementary Figure S10C). Together, these results showed increased IFN-β production by MDSCs with decreased immunosuppressive capacity during murine lupus development.

Next, we analyzed the circulating MDSCs in PBMCs from patients with SLE by flow cytometry. Compared with healthy controls, the frequencies of myeloid cells were significantly

increased in patients with SLE (Figure 5F). To further analyze the transcriptomic profiles of myeloid populations in SLE, we reclustered myeloid cells into six clusters, including MDSC 1–3 and monocytes 1–3. The dot plots displaying canonical marker genes for distinct cell subsets were shown in Supplementary Figure S1B. The dataset analysis showed increased frequencies of MDSCs in SLE (Figure 5G). Flow cytometric analysis showed an increased percentage of MDSCs in patients with SLE, especially those with active disease. Moreover, the expanded MDSCs secreted significantly higher levels of IFN-β, which were positively correlated with increased circulating Tfh cells (Figure 5H–J).

MDSC-derived IFN-β promotes Tfh cell differentiation and lupus progression

To elucidate whether MDSCs promote the differentiation of Tfh cells in lupus mice, MDSCs under different treatment were adoptively transferred into lupus mice (Supplementary Figure S11A). Compared with the control lupus mice, adoptive transfer of MDSCs led to exacerbated disease severity, displaying bigger sizes of the SP and LN; elevated serum levels of anti-dsDNA autoantibody, creatinine, and urea; and elevated protein levels in urine samples, accompanied by increased glomerular damage and immune complex deposition in kidneys. Furthermore, the frequencies and numbers of Tfh cells, GC B cells, and plasma cells in SPs, LNs and BM were profoundly increased. However, the effects of transferred MDSCs with IFN-β gene knockdown in aggravating the disease severity was almost abrogated. When compared with the MDSC-transferred control group, the transfer of MDSCs with silenced IFN-β showed markedly decreased serum levels of anti-dsDNA autoantibody, creatinine, urea, and protein levels in urine in lupus mice. The histologic analysis showed ameliorated glomerular damage, whereas the frequencies and numbers of Tfh cells, GC B cells, and plasma cells in SPs, LNs, and BM were also decreased in mice transferred with IFN-β knockdown MDSCs (Supplementary Figure S11B–H). Furthermore, to determine if MDSCs can promote the Tfh cell differentiation via producing IFN-β, we cocultured MDSCs with naive $CD4^+$T cells under Tfh polarization conditions. Notably, MDSCs potently promoted the Tfh cell differentiation whereas MDSCs with IFN-β gene silenced showed no significant effect in coculture (Supplementary Figure S11I). Taken together, these data demonstrated that MDSCs play a critical role in enhancing Tfh cell response via producing IFN-β.

Activated lymphocyte-derived DNA stimulates MDSCs to produce IFN-β via cyclic GMP-AMP synthase–stimulator of IFN genes pathway

To elucidate the molecular mechanism mediating IFN-β upregulation in MDSCs, we found a significant increase of IFN-I–inducible genes (eg, the *Isg15* and *Ifi* gene families) in MDSCs from patients with SLE by single-cell transcriptome analysis. We further conducted pairwise comparison of gene expression levels in the MDSC2 and 3 clusters vs the MDSC1 cluster. Gene ontology analysis revealed a significant upregulation of IFN-I–inducible genes in the MDSC2 and 3 clusters (Figure 6A and B). It has been reported that activated lymphocyte-derived DNA (ALD-DNA) can modulate the innate immune response mediated by myeloid cells.[32] To investigate whether ALD-DNA can regulate the function of MDSCs, the gene expression files in MDSCs from lupus mice with or without ALD-DNA treatment were determined by RNA sequencing (RNA-seq) analysis. Interestingly, IFN-I (*Ifnb1*) and IFN-I–inducible genes (eg, *Isg15*, *Ifi* gene families, and *Irf* gene families) were strikingly up-regulated (Figure 6C) after ALD-DNA stimulation, which was confirmed by RT-qPCR analysis, showing that ALD-DNA up-regulated expression of IFN-β and IFN-I–inducible genes (*Isg15*, *Irf7*, *Mx*, *Oas1*, and *Ifi* gene families) in MDSCs. Moreover, the protein level of IFN-β was also increased after ALD-DNA stimulation, which was blocked by stimulator of IFN genes (STING) inhibition (Figure 6D–F).

These data suggest that ALD-DNA induces the production of IFN-β in MDSCs whereas IFN-β may probably further act on MDSCs. Notably, ALD-DNA treatment significantly impaired the immunosuppressive activity of MDSCs, accompanied by a pronounced maturation phenotype. Conversely, upon the blockade of IFN-I signaling, ALD-DNA failed to modulate the function of MDSCs (Figure 6G–I), suggesting that ALD-DNA affects the function of MDSCs in an IFN-I–mediated autocrine pattern. It is known that upon binding with dsDNA, cyclic GMP-AMP synthase (cGAS) is activated and initiates the cGAS-STING-IFN-I pathway.[33] As expected, phosphorylated TBK1 and IRF3 increased after ALD-DNA stimulation whereas STING was ubiquitinated in MDSCs, showing primarily K63-linked ubiquitination (Figure 6J–L). Together, these results demonstrated that ALD-DNA impaired the immunosuppressive capacity of MDSCs via the cGAS-STING-IFN-I axis in an IFN-I–mediated autocrine pattern.

DISCUSSION

In this study, we have identified the role of accumulated MDSCs in promoting Tfh cell differentiation and function via IFN-β production in lupus pathogenesis. We showed that IFN-β secreted by MDSCs drives Tfh cell responses via activating AhR. Moreover, MDSCs with the IFN-β gene silenced showed no significant effect on Tfh cell differentiation. Notably, the transfer of MDSCs with silenced IFN-β showed markedly decreased serum levels of anti-dsDNA autoantibody, creatinine, urea, and urine protein levels in lupus mice. Together, these results suggest that targeting IFN-β may serve as a promising therapeutic strategy for the treatment of patients with SLE.

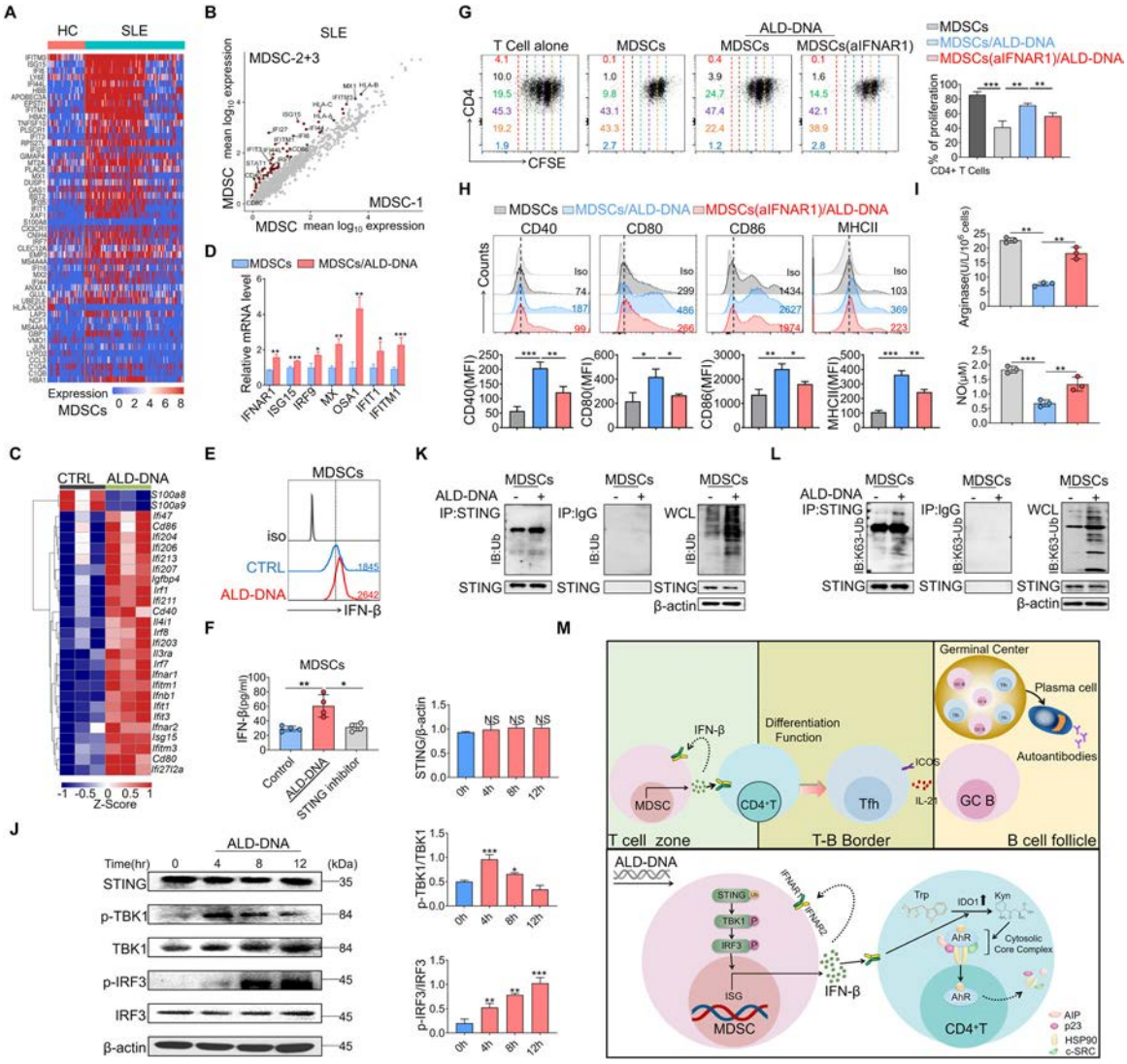

Figure 6. ALD-DNA stimulates MDSCs to produce IFN-β via cyclic GMP-AMP synthase–STING pathway. (A and B) Peripheral blood mononuclear cells from patients with SLE and HCs were collected for single-cell RNA sequencing analysis. (A) Heatmaps show the differential expression of genes in MDSC clusters between HCs and patients with SLE. (B) Pairwise comparison of gene expression levels in MDSC1 versus MDSC2 and MDSC3 clusters from patients with SLE (mean $\log_{10}$ of biologic duplicates). Genes showing more than a two-fold overexpression with false discovery rate < 0.05 in MDSC2 and MDSC3 clusters are highlighted in red; select gene names are indicated. (C) MDSCs from the spleen of lupus mice (7 weeks) were stimulated with ALD-DNA (8 μg/mL) for 24 hours, RNA sequencing was performed to analyze the differential expression of IFN-I target genes. (D) The expression of IFN-I targeted genes in MDSCs treated with ALD-DNA for 24 hours was detected by reverse transcription quantitative polymerase chain reaction. (E) Flow cytometric analysis and (F) enzyme-linked immunosorbent assay were used to measure IFN-β released by MDSCs stimulated with or without ALD-DNA for 48 hours, and the STING inhibitor (H-151; 2 μM) was added in some cases. MDSCs isolated from lupus mice (7 weeks) were pretreated with anti-IFNAR1 monoclonal antibody (mAb; 1 μg/mL) to block the IFN-I signaling and then followed by ALD-DNA stimulation for 48 hours. (G) $CD4^+$ T cells were isolated from the spleen of C57BL/6 mice. MDSCs under different treatments were then collected to co-culture with $CD4^+$ T cells (MDSC/T cell ratio of 1:1) in the presence of anti-CD3 mAb (1 μg/mL) and anti-CD28 mAb (1 μg/mL) for 72 hours. $CD4^+$ T cell proliferation was evaluated by staining with Carboxyfluorescein Succinimidyl Ester (CFSE, 5 μM). (H) Expression of CD40, CD80, CD86, and major histocompatibility complex II on MDSCs were analyzed by flow cytometry. (I) The activity of arginase and NO level were measured in MDSCs. (J) MDSCs were treated with ALD-DNA for different times as indicated; cells were harvested to analyze STING, p-TBK1, and p-IRF3 by Western blot. (K) Immunoblot analysis of Ub and STING in lysate and immunoprecipitated samples from MDSCs treated with or without ALD-DNA. (L) Endogenous K63-linked poly-Ub chains were immunoprecipitated using anti-Ub (linkage-specific K63) antibody. (M) Schematic illustrations of IFN-β secreted by MDSCs drive Tfh cell responses via activating AhR. Data are shown as mean ± SD of three independent experiments. Statistical analysis was determined by Student's *t*-test in part D and one-way analysis of variance in parts F, G, H, I, and J. $^{***}P < 0.001$; $^{**}P < 0.01$; $^{*}P < 0.05$. AhR, aryl hydrocarbon receptor; AIP, AhR-interacting protein; ALD-DNA, activated lymphocyte-derived DNA; GC, germinal center; HC, healthy control; IB, immunoblotting; IDO1, indoleamine 2,3-dioxygenase 1; IFN, interferon; IL, interleukin; IP, immunoprecipitation; Kyn, kynurenine; MDSC, myeloid-derived suppressor cell; MFI, mean fluorescence intensity; MHCII, major histocompatibility complex II; mRNA, messenger RNA; NO, nitric oxide; NS, no significance; SLE, systemic lupus erythematosus; STING, stimulator of IFN genes; Tfh, T follicular helper; Trp, tryptophan; Ub, ubiquitin; WCL, whole cell lysate. Color figure can be viewed in the online issue, which is available at http://onlinelibrary.wiley.com/doi/10.1002/art.70004/abstract.

Extensive evidence indicates that type I IFNs are closely associated with lupus pathogenesis, but the effector mechanisms by which IFN-I contributes to enhanced T cell dysregulation and autoantibody overproduction are not fully understood. Here, we find that IFNAR-deficient mice are resistant to lupus induction and exhibit significantly decreased Tfh cells when compared with WT controls. Notably, adoptive transfer of IFNAR-deficient $CD4^+$T cells into lupus mice showed greatly diminished capability in differentiating into Tfh cells, which supports the notion that IFN-I plays a key role in promoting Tfh cell responses during lupus development. Currently, blocking the IFN-I pathway has been considered a new therapeutic application for the treatment of patients with SLE.[18] However, further investigations are needed to characterize the differential roles played by IFN-α or IFN-β in lupus pathogenesis.[34]

Currently, the available data from clinical trials of blocking IFN-Is have shown varying efficacy in the treatment of SLE.[35] Several clinical trials of blocking IFN-α failed to achieve the desired effect, but the anti–IFN-I receptor monoclonal antibody anifrolumab has shown positive outcome for SLE treatment,[16,36] indicating a potential involvement of IFN-β in lupus pathogenesis. Interestingly, IFN-β has been demonstrated to exhibit higher affinity with IFN receptors, leading to different receptor trafficking, phosphorylation, and signaling kinetics. In addition, it has been reported that IFN-β can uniquely ligate to IFNAR1 independently of IFNAR2.[37] Because IFN-β appears more potent in activating signal transduction than IFN-α,[38,39] we have sought to determine a role of IFN-β in lupus pathogenesis. In 2021, a randomized, double-blind, placebo-controlled, first-in-human, dose-escalation study (NCT02766795) indicated that the anti–IFN-β monoclonal antibody (PF-06823859) exhibited an acceptable safety, tolerability, and pharmacokinetic profile.[40] Based on these findings, the subsequent Phase II trial evaluating PF-06823859 in adult participants with active cutaneous lupus erythematosus or SLE with cutaneous manifestations has reached primary completion. Notably, the potential benefits must be tempered by the consideration that modulating the type I IFN pathway may disrupt vital antiviral defenses, potentially increasing susceptibility to viral infections or tumors and triggering systemic side effects. Nevertheless, further investigation is required for a comprehensive risk-benefit assessment.

Here, we show that Tfh cells from patients with SLE are potentially regulated by IFN-β as revealed by single-cell sequencing analysis. Moreover, we provide strong evidence that IFN-β can regulate the differentiation and function of Tfh cells both in vitro and in vivo. In addition, we also explored whether other T cell populations could be regulated by IFN-β. The human single-cell RNA-seq data showed that the Tfh cell subset is most significantly modulated by IFN-I, although only several IFN-I–inducible genes were modestly increased in Th1 and Treg cells. Furthermore, $Ifnar1^{-/-}$ lupus mice exhibited no significant changes in the proportions of Th17 and Treg cells, and only a mild decrease in Th1 cells from the SPs. Nevertheless, the minor changes in other T cell subsets require further investigation to determine if they are affected directly by IFN-I or indirectly by other effectors during the disease progression. Early studies have suggested pDCs as the main source of IFN-α.[18] Increasing evidence indicates that IFN-β can be produced by various cells, including lymphocytes, natural killer cells, fibroblasts, and macrophages.[41] However, the source of increased IFN-β has not been systematically investigated in lupus development. In this study, we found that MDSCs accumulated in the murine lupus expressed plenty of IFN-β, much more than other myeloid cells, T cells, and B cells.

For decades, MDSC accumulation has been described in diverse pathologic conditions.[42] In recent years, clinical observations and animal model studies have shown that MDSCs accumulate during the development of various autoimmune diseases.[42] However, the current evidence suggests the diverse functions of MDSCs in different autoimmune diseases.[19] For example, MDSCs have been shown to induce the expansion of Breg cells through inducible NO synthase and ameliorate autoimmunity in murine lupus.[28] Intriguingly, Tan et al found that low FoxO1 expression was predominantly expressed in M-MDSCs from both patients with SLE and lupus mice and that M-MDSC–specific FoxO1 deficiency enhanced aberrant B cell function in aggressive SLE.[43] A clinical study proposed that MDSCs from patients with SLE were highly potent in promoting Th17 cell differentiation and disease progression in an arginase-1–dependent manner.[27] Additionally, lupus MDSCs were demonstrated to promote TLR7 pathway activation and lupus pathogenesis through the S100A8/9–IFN-γ axis.[44] These data indicate the diverse functions of MDSCs during SLE development, which is probably because of their extraordinary heterogeneity and functional plasticity.

Here, we observed a population of MDSCs accumulated at the T-B cell border, implying they might assist the differentiation of Tfh cells. MDSCs from lupus can promote Tfh cell differentiation both in vitro and in vivo, whereas IFN-β–silenced MDSCs almost lost the corresponding effect, indicating the critical role of IFN-β in regulating Tfh cells. Interestingly, MDSCs from lupus also expressed increased IFNAR with the disease progression, which further received IFN-β signal in an autocrine pattern, resulting in the impaired suppressive function and enhanced maturation. In view of this, MDSCs in lupus appears to be extremely different from those in cancer, as MDSCs from the tumor microenvironment exhibited reduced levels of IFNAR, thus maintaining their immunosuppressive capacity.[45] Just because of the distinct expression of IFNAR in different pathologic conditions, MDSCs displayed different functions and phenotypes, which might be the predominant reason for their failure in controlling the autoimmune response in lupus. Nonetheless, we cannot exclude the possibility that MDSCs may mediate Tfh cell responses through

the production of other cytokines, which remains to be investigated in future studies.

In recent years, it has been reported that apoptosis-derived membrane vesicles in the serum of patients with SLE could drive the cGAS-STING pathway to enhance IFN-I production and eventually lead to the damage of multiple organs and tissues.[46] It is known that dsDNA fragments are mainly derived from the apoptotic cells and exist in SLE. Previous studies have demonstrated that ALD-DNA is immunogenic and can induce lupus-like manifestations in mice.[47] Here, we show that ALD-DNA could activate the STING-TBK1-IRF3 pathway in MDSCs, thus inducing the production of IFN-β. STING activity is tightly regulated by posttranslational modifications, particularly ubiquitination. K63-linked polyubiquitination at specific STING residues promotes its signaling by triggering dimerization and aggregation. This facilitates the recruitment of TBK1 and IRF3, ultimately enhancing the activity of the cGAS-STING pathway and subsequent IFN-β production. Notably, PBMCs from patients with SLE have been identified to exhibit significantly elevated levels of K63-linked ubiquitination on STING.[48] Here, we also show that ALD-DNA could induce the K63-linked ubiquitination of STING in MDSCs and activate the downstream signaling, thus inducing the production of IFN-β.

Classical IFNAR signaling depends on JAK1, tyrosine kinase 2, signal transducers and activators of transcription (STAT) 1, STAT2, and IFN regulatory factor 9.[41] An early study showed that type I IFNs could induce Bcl6 and promote CXCR5 and PD-1 expression, and the ability of IFN-α/β to drive these Tfh cell features was entirely dependent on STAT1.[49] Recently, IFN-I signaling was identified to drive the production of IL-21 and IFN-γ by Tfh cells in murine and human lupus, which is dependent on STAT4 activation.[50] However, unlike other members of the IFN-I family, the IFN-β signaling pathway has attracted attention because of its unique activation of the STAT1/STAT2-AhR pathway. It has been reported that IFN-β activates AhR to regulate the activity of astrocytes and alveolar epithelial cells and the dormancy of tumor regenerative cells.[51–53]

In this study, we revealed that IFN-β activated the IDO1/Kyn/AhR pathway to induce the differentiation of Tfh cells and blocking the AhR activation effectively reversed IFN-β–mediated Tfh cell differentiation. Indeed, several studies have clarified the role of AhR in SLE pathogenesis. Clinical data from patients with SLE showed that AhR expression was significantly increased in Th17 cells, and the AhR-overexpressing Th17 cells were correlated with SLE activity. In addition, UV light is known to trigger LE, and patients with LE exhibited cutaneous AhR activation, which correlated with the increase of proinflammatory cytokines and skin lesions. Thus, AhR has been considered an independent predictor of skin lesions in patients with SLE.[54] Besides, a potential drug that can induce lupus, propranolol, was identified to activate AhR, thus mediating a significant increase of proinflammatory cytokine secretion.[55] However, there are some contrasting findings about the effect of blocking AhR in a lupus animal model.[56,57] Knocking out AhR strikingly increased the levels of autoantibodies and proinflammatory cytokines in lupus mice.[58]

Interestingly, an imbalance in $CD4^+$ T cell subsets with increased $CXCL13^+$ T cells and reduced IL-22^+ T cells is observed in patients with SLE. IFN-I was further identified to oppose AhR and Jun to promote $CXCL13^+$ T cells and inhibit IL-22^+ T cells, therefore driving the progression of SLE.[59] Because AhR is a nuclear receptor and ligand-dependent transcription factor that can be activated by ligands with diverse structure and different sources, AhR may play a double-edged sword role that can drive or inhibit inflammation, depending on the site of AhR activation and the ligand triggering the response.

In sum, our study identifies a novel function of MDSC-derived IFN-β in driving Tfh cell response, which subsequently promotes the humoral immune response during SLE progression and further exacerbates disease severity. Therefore, inhibition of the MDSC/Tfh axis in lupus may attenuate disease progression. Furthermore, blockade of MDSC-secreted IFN-β represents a new therapeutic option for patients with SLE.

AUTHOR CONTRIBUTIONS

All authors contributed to at least one of the following manuscript preparation roles: conceptualization AND/OR methodology, software, investigation, formal analysis, data curation, visualization, and validation AND drafting or reviewing/editing the final draft. As corresponding authors, Drs Lu and Tian confirm that all authors have provided the final approval of the version to be published and take responsibility for the affirmations regarding article submission (eg, not under consideration by another journal), the integrity of the data presented, and the statements regarding compliance with institutional review board/Declaration of Helsinki requirements.

REFERENCES

1. Tsokos GC. Autoimmunity and organ damage in systemic lupus erythematosus. Nat Immunol 2020;21(6):605–614.
2. Jenks SA, Cashman KS, Woodruff MC, et al. Extrafollicular responses in humans and SLE. Immunol Rev 2019;288(1):136–148.
3. Ma K, Du W, Xiao F, et al. IL-17 sustains the plasma cell response via p38-mediated Bcl-xL RNA stability in lupus pathogenesis. Cell Mol Immunol 2021;18(7):1739–1750.
4. Ma K, Li J, Wang X, et al. $TLR4^+CXCR4^+$ plasma cells drive nephritis development in systemic lupus erythematosus. Ann Rheum Dis 2018;77(10):1498–1506.
5. Crotty S. Follicular helper CD4 T cells (TFH). Annu Rev Immunol 2011;29(1):621–663.
6. He J, Tsai LM, Leong YA, et al. Circulating precursor CCR7(lo)PD-1(hi) $CXCR5^+$ $CD4^+$ T cells indicate Tfh cell activity and promote antibody responses upon antigen reexposure. Immunity 2013;39(4):770–781.
7. Crotty S. T follicular helper cell biology: a decade of discovery and diseases. Immunity 2019;50(5):1132–1148.
8. Kim SJ, Schätzle S, Ahmed SS, et al. Increased cathepsin S in $Prdm1^{-/-}$ dendritic cells alters the T_{FH} cell repertoire and contributes to lupus. Nat Immunol 2017;18(9):1016–1024.

9. Lin M, Huang L, Huang J, et al. Modulation of PKM2 inhibits follicular helper T cell differentiation and ameliorates inflammation in lupus-prone mice. J Autoimmun 2024;145:103198.
10. Rönnblom L, Alm GV. An etiopathogenic role for the type I IFN system in SLE. Trends Immunol 2001;22(8):427–431.
11. Crow MK, Olferiev M, Kirou KA. Targeting of type I interferon in systemic autoimmune diseases. Transl Res 2015;165(2):296–305.
12. Hooks JJ, Moutsopoulos HM, Geis SA, et al. Immune interferon in the circulation of patients with autoimmune disease. N Engl J Med 1979; 301(1):5–8.
13. Hua J, Kirou K, Lee C, et al. Functional assay of type I interferon in systemic lupus erythematosus plasma and association with anti-RNA binding protein autoantibodies. Arthritis Rheum 2006;54(6):1906–1916.
14. Pestka S, Krause CD, Walter MR. Interferons, interferon-like cytokines, and their receptors. Immunol Rev 2004;202(1):8–32.
15. Deeks ED. Anifrolumab: first approval. Drugs 2021;81(15):1795–1802.
16. Khamashta M, Merrill JT, Werth VP, et al; CD1067 study investigators. Sifalimumab, an anti-interferon-α monoclonal antibody, in moderate to severe systemic lupus erythematosus: a randomised, double-blind, placebo-controlled study. Ann Rheum Dis 2016;75(11):1909–1916.
17. Psarras A, Alase A, Antanaviciute A, et al. Functionally impaired plasmacytoid dendritic cells and non-haematopoietic sources of type I interferon characterize human autoimmunity. Nat Commun 2020; 11(1):6149.
18. Psarras A, Wittmann M, Vital EM. Emerging concepts of type I interferons in SLE pathogenesis and therapy. Nat Rev Rheumatol 2022; 18(10):575–590.
19. Rui K, Peng N, Xiao F, et al. New insights into the functions of MDSCs in autoimmune pathogenesis. Cell Mol Immunol 2023;20(5):548–550.
20. Yi H, Guo C, Yu X, et al. Mouse CD11b+Gr-1+ myeloid cells can promote Th17 cell differentiation and experimental autoimmune encephalomyelitis. J Immunol 2012;189(9):4295–4304.
21. Ioannou M, Alissafi T, Lazaridis I, et al. Crucial role of granulocytic myeloid-derived suppressor cells in the regulation of central nervous system autoimmune disease. J Immunol 2012;188(3):1136–1146.
22. Guo C, Hu F, Yi H, et al. Myeloid-derived suppressor cells have a pro-inflammatory role in the pathogenesis of autoimmune arthritis. Ann Rheum Dis 2016;75(1):278–285.
23. Fujii W, Ashihara E, Hirai H, et al. Myeloid-derived suppressor cells play crucial roles in the regulation of mouse collagen-induced arthritis. J Immunol 2013;191(3):1073–1081.
24. Tian J, Zhang B, Yuan Q, et al. GITRL impairs the immunosuppressive function of MDSCs via PTEN-mediated signaling pathway in experimental Sjögren syndrome. Inflamm Res 2022;71(12):1577–1588.
25. Rui K, Hong Y, Zhu Q, et al. Olfactory ecto-mesenchymal stem cell-derived exosomes ameliorate murine Sjögren's syndrome by modulating the function of myeloid-derived suppressor cells. Cell Mol Immunol 2021;18(2):440–451.
26. Tian J, Rui K, Hong Y, et al. Increased GITRL impairs the function of myeloid-derived suppressor cells and exacerbates primary Sjögren syndrome. J Immunol 2019;202(6):1693–1703.
27. Wu H, Zhen Y, Ma Z, et al. Arginase-1-dependent promotion of TH17 differentiation and disease progression by MDSCs in systemic lupus erythematosus. Sci Transl Med 2016;8(331):331ra40.
28. Park MJ, Lee SH, Kim EK, et al. Myeloid-derived suppressor cells induce the expansion of regulatory B cells and ameliorate autoimmunity in the Sanroque mouse model of systemic lupus erythematosus. Arthritis Rheumatol 2016;68(11):2717–2727.
29. Aringer M, Costenbader K, Daikh D, et al. 2019 European League Against Rheumatism/American College of Rheumatology classification criteria for systemic lupus erythematosus. Arthritis Rheumatol 2019;71(9):1400–1412.
30. Dean JW, Zhou L. Cell-intrinsic view of the aryl hydrocarbon receptor in tumor immunity. Trends Immunol 2022;43(3):245–258.
31. Rothhammer V, Quintana FJ. The aryl hydrocarbon receptor: an environmental sensor integrating immune responses in health and disease. Nat Rev Immunol 2019;19(3):184–197.
32. Zhao H, Wen Z, Xiong S. Activated lymphocyte-derived DNA drives glucose metabolic adaptation for inducing macrophage inflammatory response in systemic lupus erythematosus. Cells 2023;12(16):2093.
33. Zhang X, Bai XC, Chen ZJ. Structures and mechanisms in the cGAS-STING innate immunity pathway. Immunity 2020;53(1):43–53.
34. Crow MK. Autoimmunity: interferon α or β: which is the culprit in autoimmune disease? Nat Rev Rheumatol 2016;12(8):439–440.
35. Chaichian Y, Wallace DJ, Weisman MH. A promising approach to targeting type 1 IFN in systemic lupus erythematosus. J Clin Invest 2019; 129(3):958–961.
36. Kalunian KC, Merrill JT, Maciuca R, et al. A phase II study of the efficacy and safety of rontalizumab (rhuMAb interferon-α) in patients with systemic lupus erythematosus (ROSE). Ann Rheum Dis 2016;75(1): 196–202.
37. Jaitin DA, Roisman LC, Jaks E, et al. Inquiring into the differential action of interferons (IFNs): an IFN-alpha2 mutant with enhanced affinity to IFNAR1 is functionally similar to IFN-beta. Mol Cell Biol 2006; 26(5):1888–1897.
38. Moraga I, Harari D, Schreiber G, et al. Receptor density is key to the alpha2/beta interferon differential activities. Mol Cell Biol 2009; 29(17):4778–4787.
39. de Weerd NA, Vivian JP, Nguyen TK, et al. Structural basis of a unique interferon-β signaling axis mediated via the receptor IFNAR1. Nat Immunol 2013;14(9):901–907.
40. Neelakantan S, Oemar B, Johnson K, et al. Safety, tolerability, and pharmacokinetics of PF-06823859, an anti-interferon β monoclonal antibody: a randomized, phase I, single- and multiple-ascending-dose study. Clin Pharmacol Drug Dev 2021;10(3): 307–316.
41. Jiang J, Zhao M, Chang C, et al. Type I interferons in the pathogenesis and treatment of autoimmune diseases. Clin Rev Allergy Immunol 2020;59(2):248–272.
42. Veglia F, Sanseviero E, Gabrilovich DI. Myeloid-derived suppressor cells in the era of increasing myeloid cell diversity. Nat Rev Immunol 2021;21(8):485–498.
43. Tan L, Kong W, Zhou K, et al. FoxO1 deficiency in monocytic myeloid-derived suppressor cells exacerbates B cell dysfunction in systemic lupus erythematosus. Arthritis Rheumatol 2025;77(4):423–438.
44. Yang Y, Zhang X, Jing L, et al. MDSC-derived S100A8/9 contributes to lupus pathogenesis by promoting TLR7-mediated activation of macrophages and dendritic cells. Cell Mol Life Sci 2024; 81(1):110.
45. Alicea-Torres K, Sanseviero E, Gui J, et al. Immune suppressive activity of myeloid-derived suppressor cells in cancer requires inactivation of the type I interferon pathway. Nat Commun 2021;12(1):1717.
46. Kato Y, Park J, Takamatsu H, et al. Apoptosis-derived membrane vesicles drive the cGAS-STING pathway and enhance type I IFN production in systemic lupus erythematosus. Ann Rheum Dis 2018; 77(10):1507–1515.
47. Wen Z, Xu L, Xu W, et al. Production of anti-double-stranded DNA antibodies in activated lymphocyte derived DNA induced lupus model was dependent on CD4+ T cells. Lupus 2012;21(5): 508–516.
48. Tian M, Liu W, Zhang Q, et al. MYSM1 represses innate immunity and autoimmunity through suppressing the cGAS-STING pathway. Cell Rep 2020;33(3):108297.

49. Nakayamada S, Poholek AC, Lu KT, et al. Type I IFN induces binding of STAT1 to Bcl6: divergent roles of STAT family transcription factors in the T follicular helper cell genetic program. J Immunol 2014; 192(5):2156–2166.
50. Dong X, Antao OQ, Song W, et al. Type I interferon-activated STAT4 regulation of follicular helper T cell-dependent cytokine and immunoglobulin production in lupus. Arthritis Rheumatol 2021;73(3): 478–489.
51. Rothhammer V, Mascanfroni ID, Bunse L, et al. Type I interferons and microbial metabolites of tryptophan modulate astrocyte activity and central nervous system inflammation via the aryl hydrocarbon receptor. Nat Med 2016;22(6):586–597.
52. Liu Y, Lv J, Liu J, et al. Mucus production stimulated by IFN-AhR signaling triggers hypoxia of COVID-19. Cell Res 2020;30(12):1078–1087.
53. Liu Y, Lv J, Liu J, et al. STAT3/p53 pathway activation disrupts IFN-β-induced dormancy in tumor-repopulating cells. J Clin Invest 2018; 128(3):1057–1073.
54. Huang W, Rui K, Wang X, et al. The aryl hydrocarbon receptor in immune regulation and autoimmune pathogenesis. J Autoimmun 2023;138:103049.
55. Dorgham K, Amoura Z, Parizot C, et al. Ultraviolet light converts propranolol, a nonselective β-blocker and potential lupus-inducing drug, into a proinflammatory AhR ligand. Eur J Immunol 2015;45(11): 3174–3187.
56. Gutierrez F, Murphy QM, Swartwout BK, et al. TCDD and CH223191 alter T cell balance but fail to induce anti-inflammatory response in adult lupus mice. Immunohorizons 2024;8(2): 172–181.
57. Mustafa A, Holladay SD, Witonsky S, et al. Gestational exposure to 2,3,7,8-tetrachlorodibenzo-p-dioxin disrupts B-cell lymphopoiesis and exacerbates autoimmune disease in 24-week-old SNF1 mice. Toxicol Sci 2009;112(1):133–143.
58. Shinde R, Hezaveh K, Halaby MJ, et al. Apoptotic cell-induced AhR activity is required for immunological tolerance and suppression of systemic lupus erythematosus in mice and humans. Nat Immunol 2018;19(6):571–582.
59. Law C, Wacleche VS, Cao Y, et al; Accelerating Medicines Partnership: RA/SLE Network. Publisher correction: interferon subverts an AHR-JUN axis to promote CXCL13^{+} T cells in lupus. Nature 2024; 632(8025):E6.

Arthritis & Rheumatology
Vol. 78, No. 5, May 2026, pp 1102–1113
DOI 10.1002/art.70010

American College of Rheumatology
Empowering Rheumatology Professionals

Defining Optimally Safe and Effective Blood Levels of Hydroxychloroquine in Lupus: An Important Step Toward Precision Drug Monitoring

Shivani Garg,[1,2] Benoît Blanchet,[3] Yann Nguyen,[4] Fauzia Hollnagel,[1] Ada Clarke,[4] Michelle Petri,[5] Murray B. Urowitz,[6] John G. Hanly,[7] Caroline Gordon,[8] Sang-Cheol Bae,[9] Juanita Romero-Diaz,[10] Jorge Sanchez-Guerrero,[11] Ann E. Clarke,[12] Sasha Bernatsky,[13] Daniel J. Wallace,[14] David A. Isenberg,[15] Anisur Rahman,[15] Joan T. Merrill,[16] Paul R. Fortin,[17] Dafna D. Gladman,[6] Ian N. Bruce,[18,19] Ellen M. Ginzler,[20] Mary Anne Dooley,[21] Rosalind Ramsey-Goldman,[22] Susan Manzi,[23] Andreas Jönsen,[24] Graciela S. Alarcón,[25] Ronald F. Van Vollenhoven,[26] Cynthia Aranow,[27] Véronique Le Guern,[4] Meggan Mackay,[27] Guillermo Ruiz-Irastorza,[28] S. Sam Lim,[29] Murat Inanc,[30] Kenneth C. Kalunian,[31] Søren Jacobsen,[32] Christine A. Peschken,[33] Diane L. Kamen,[34] Anca Askanase,[35] Jill Buyon,[36] Julie Chezel,[37] Alicja Puszkiel,[38] and Nathalie Costedoat-Chalumeau[4]

Objective. Using a hydroxychloroquine (HCQ) dose of 5 mg/kg/day in systemic lupus erythematosus (SLE) is associated with a higher risk of flares; HCQ blood level monitoring could be a better way to adjust the HCQ dose. We studied the upper threshold for a reference range of HCQ levels to inform routine monitoring.

Methods. This observational study included patients (N = 2,010) across the Systemic Lupus International Collaborating Clinics, Wisconsin, international, and French studies who underwent HCQ blood level measurements. Using adjusted spline and logistic regression analyses on the cross-sectional data, we first identified an HCQ blood level associated with higher HCQ toxicity. Next, we tested if this upper threshold level was supratherapeutic (no further risk reduction for the Systemic Lupus Erythematosus Disease Activity Index 2000 [score ≥6]). Finally, we examined associations between chronic kidney disease (CKD) stage and supratherapeutic (toxic) HCQ blood levels.

Results. Among 1,842 patients (excluding 168 patients with very low HCQ blood levels), 4.9% had HCQ-related toxicity. Odds of toxicity were 2.1-fold higher with blood levels ≥1,150 ng/mL and 1.7-fold higher with the cumulative HCQ dose per 1,000-g increase. Blood levels ≥1,150 ng/mL were associated with a saturation in therapeutic effect, indicating supratherapeutic levels. Patients with CKD stage ≥3 had 2.3-fold higher odds of having supratherapeutic levels (≥1,150 ng/mL).

Conclusion. The therapeutic reference range for HCQ blood level monitoring is 750 to <1,150 ng/mL. HCQ level monitoring could optimize HCQ use, particularly in patients with CKD stage ≥3. Future longitudinal studies are needed to validate the use of HCQ blood level monitoring in optimizing dosing.

INTRODUCTION

Hydroxychloroquine (HCQ) is a foundational therapy in the systemic lupus erythematosus (SLE or lupus) therapeutic armamentarium, as it prolongs disease-free and damage-free survival in patients.[1] However, committing a patient to long-term HCQ use can be challenging due to concerns, although rare, of eye and cardiac toxicity. Concerns for irreversible eye or cardiac

The views expressed herein are those of the authors and do not necessarily represent those of the NHS, the NIHR, or the Department of Health.

Supported by a grant sponsored by the Lupus Foundation of America, Wisconsin Chapter, Research Award, and the Rheumatology Research Foundation Innovation Research Award. Dr Garg's work was supported by the NIH (grant 5K23-AR-084608-02). The content is solely the responsibility of authors and does not necessarily represent the official views of the funders or the NIH. Dr Gordon's work was supported by Lupus UK, Sandwell and West Birmingham Hospitals NHS Trust, and the NIHR/Wellcome Trust Birmingham Clinical Research Facility. Dr Bae's work was supported in part by the Basic Science Research Program through the National Research Foundation of Korea, funded by the Ministry of Education (NRF-2021R1A6A1A03038899). Dr Bruce is an NIHR Senior Investigator, and his work was supported by the NIHR Manchester Biomedical Research Centre (NIHR203308).

[1]University of Wisconsin School of Medicine and Public Health, Madison; [2]Yale University, New Haven, Connecticut; [3]Biologie du Médicament-Toxicologie, Hôpital Cochin, Institut du Cancer Paris CARPEM, AP-HP Centre and Université de Paris, CNRS, INSERM, CiTCoM, U1268, Paris, France; [4]National Referral Centre for Rare Autoimmune and Systemic Diseases, Hôpital Cochin, AP-HP Centre and Université Paris Cité and Centre de Recherche en Epidémiologie et Statistiques, Unité Inserm 1153, Université de Paris Cité, Paris, France; [5]Johns Hopkins University School of Medicine, Baltimore, Maryland; [6]Division of Rheumatology, University of Toronto and Schroeder Arthritis Institute, Krembil Research Institute, Toronto Western Hospital, Toronto,

toxicity exacerbate patient fears, leading to early discontinuation of medicine and nonadherence, which increases the risk of lupus flares and hospitalizations.[2–4] Moreover, clinicians' and patients' concerns for toxicity are further amplified in patients with kidney disease given that over 60% of HCQ is cleared by the kidneys and HCQ is primarily dosed based on body weight.[2,5] Without clear guidance on adjusting HCQ doses in patients with chronic kidney disease (CKD), doses are either not adjusted or arbitrarily reduced, which could accelerate toxicity risk or increase the risk of SLE flares.[4,6,7] Balancing efficacy and toxicity for HCQ is particularly difficult, especially amid an ongoing debate regarding the optimal dose.[8–10]

The conundrum to identify an optimal HCQ dose that minimizes harms and maximizes efficacy could be addressed by therapeutic HCQ blood level monitoring, which bypasses clinical variables affecting HCQ absorption or clearance and could guide optimal HCQ dosing in SLE.[10–15] Studies, including a global meta-analysis, have established the clinical significance of using HCQ blood levels as an objective measure to monitor severe nonadherence and also clinical efficacy (lower risk of active lupus or flares).[10–18] The proposed cutoffs to monitor for clinical efficacy are 750 and 1,000 ng/mL.[11,16–18] These cutoffs have a 96% negative predictive value (NPV) for active lupus with levels at or above these thresholds. However, cutoffs for HCQ blood levels associated with higher toxicity risk need further elucidation, as the published literature is conflicted. For instance, one population-based cohort study reported significant associations between HCQ whole blood level tertiles (>1,183 ng/mL) and eye toxicity, whereas another cohort study of more adherent patients noted no associations between blood levels and systemic toxicity risk.[19,20] Clarity on HCQ whole blood levels associated with toxicity and the saturation of therapeutic effect, defined as no further clinical benefits in lowering SLE activity, is needed. These data are vital to inform the upper threshold of the therapeutic reference range for HCQ blood level monitoring to guide optimal HCQ use in SLE, balancing efficacy versus safety, delaying toxicity, and potentially alleviating patient worries regarding toxicity.[21] Finally, having a defined therapeutic range for HCQ whole blood levels could enhance clinical uptake and guide clinicians with precise HCQ dosing based on individual patient risk factors, such as CKD.

In this study, we leveraged cross-sectional data from diverse cohorts—including one cohort from the United States, data from two French studies and one international prospective study centralized in France, and data from a multicenter lupus cohort, the Systemic Lupus International Collaborating Clinics (SLICC) Inception Cohort—to clarify the upper threshold of HCQ blood levels associated with toxicity. Finally, we used recurrent visit data from the US cohort to examine the thresholds of kidney function associated with supratherapeutic HCQ levels to guide safe HCQ dosing in patients with lupus and CKD.

PATIENTS AND METHODS

Population. Cross-sectional data were pooled from different sources: three cross-sectional studies (n = 1,081), one longitudinal registry (n = 269), and one multinational cohort (n = 660) for a total of 2,010 patients. Three previously published cross-sectional studies (n = 1,081) were centralized in Paris, France, and measured HCQ whole blood levels. These three studies included 203, 573, and 305 individuals from a single-center study conducted in France, a multicentric study conducted in France, and a multicentric international study, respectively.[17,18,22] A few patients could have been included in more than one study over the years, but the numbers were small.[17,18,22] The next data source was a longitudinal registry from Madison, Wisconsin

Ontario, Canada; [7]Queen Elizabeth II Health Sciences Centre and Dalhousie University, Halifax, Nova Scotia, Canada; [8]Department of Inflammation and Ageing, College of Medicine and Health, University of Birmingham, Birmingham, United Kingdom; [9]Hanyang University Hospital for Rheumatic Diseases, Hanyang University Institute for Rheumatology, and Hanyang Institute of Bioscience and Biotechnology, Seoul, Korea; [10]Instituto Nacional de Ciencias Médicas y Nutrición, Mexico City, Mexico; [11]Mount Sinai Hospital and University Health Network, University of Toronto, Toronto, Ontario, Canada; [12]Cumming School of Medicine, University of Calgary, Calgary, Alberta, Canada; [13]McGill University Health Centre, Montreal, Quebec, Canada; [14]University of California, Los Angeles; [15]University College London, London, United Kingdom; [16]Oklahoma Medical Research Foundation, Oklahoma City; [17]Centre ARThrite-UL, CHU de Québec–Université Laval, Quebec City, Quebec, Canada; [18]Centre for Musculoskeletal Research, The University of Manchester, Manchester Academic Health Science Centre, Manchester, United Kingdom; [19]Centre for Public Health, Faculty of Medicine, Health and Life Sciences, Queen's University Belfast, Belfast, Northern Ireland, United Kingdom; [20]State University of New York Downstate Medical Center, Brooklyn, New York City; [21]Thurston Arthritis Research Center, University of North Carolina at Chapel Hill; [22]Northwestern University Feinberg School of Medicine, Chicago, Illinois; [23]Allegheny Health Network, Pittsburgh, Pennsylvania; [24]Lund University, Lund, Sweden; [25]University of Alabama at Birmingham Marnix E. Heersink School of Medicine; [26]University of Amsterdam, Amsterdam, the Netherlands; [27]Feinstein Institute for Medical Research, Manhasset, New York; [28]Biobizkaia Health Research Institute, University of the Basque Country, Barakaldo, Spain; [29]Emory University School of Medicine, Atlanta, Georgia; [30]Istanbul University, Istanbul, Turkey; [31]University of California San Diego School of Medicine, La Jolla; [32]Rigshospitalet, Copenhagen University Hospital, Copenhagen, Denmark; [33]University of Manitoba, Winnipeg, Manitoba, Canada; [34]Medical University of South Carolina, Charleston; [35]Hospital for Joint Diseases and Seligman Centre for Advanced Therapeutics, New York University, New York City; [36]New York University School of Medicine, New York City; [37]Bichat University Hospital, AP-HP, Paris, France; [38]Biologie du Médicament – Toxicologie, Cochin University Hospital, AP-HP and Université Paris Cité, INSERM, Optimisation thérapeutique en neuropharmacologie U1144, Paris, France.

Additional supplementary information cited in this article can be found online in the Supporting Information section (https://acrjournals.onlinelibrary.wiley.com/doi/10.1002/art.70010).

Author disclosures and graphical abstract are available at https://onlinelibrary.wiley.com/doi/10.1002/art.70010.

Address correspondence via email to Shivani Garg, MD, PhD, at shivanigargup@gmail.com and shivani.garg@yale.edu or to Nathalie Costedoat-Chalumeau, MD, PhD, at nathalie.costedoat@aphp.fr.

Submitted for publication May 22, 2025; accepted in revised form November 3, 2025.

(institutional review board [IRB]: UW 2019-0942), that included 269 patients with SLE. The final data source consisted of 660 patients from the SLICC Inception Cohort.[16] Although the SLICC cohort was recruited between 1999 and 2011 from 33 centers in 11 countries within North America, Europe, and Asia (parent IRB: Toronto, IRB# 00-0279),[23,24] HCQ serum levels were measured retrospectively at the laboratory of Cochin Hospital (Paris, France).[16] For the current study, the validated published hematocrit-based adjustment described by Blanchet et al was used to estimate whole blood concentrations from serum values.[16,25] Per the 2020 study, the ratio of serum to whole blood HCQ levels was 0.53 ± 0.15.[16,25] This method accounts for the distribution of analytes between plasma and red blood cells and has been shown to yield accurate and reproducible results across a range of hematocrit values. Therefore, for the current study, the validated 0.53 conversion factor was used to extrapolate equivalent levels of HCQ in whole blood from the serum levels in the SLICC cohort, similar to other studies.

Because we were interested in testing the upper limits of therapeutic blood levels, we excluded 168 patients with HCQ whole blood levels <200 ng/mL, as such very low levels have been associated with severe nonadherence,[16] and included the remaining 1,842 patients in the main analysis. All patients (N = 2,010) were included in the sensitivity analyses.

Variables. We abstracted key variables for each patient, including age, sex, and race or ethnicity, from the baseline or enrollment visit (T0). For the analysis, the weight-based HCQ dose (T0) was categorized as ≤5 versus >5 mg/kg/day at the enrollment visit when HCQ blood levels (T0) were collected.[26] Additionally, the duration of HCQ use was abstracted to calculate the cumulative HCQ dose (HCQ dose × duration of HCQ use). Cumulative HCQ dose was calculated until the last visit or the visit when HCQ-related toxicity was noted ($T_{last\ visit}$). Kidney function and the Systemic Lupus Erythematosus Disease Activity Index 2000 (SLEDAI-2K) score were abstracted on the day of the baseline study visit (T0), when HCQ whole blood levels (T0) were measured. Kidney function (estimated glomerular filtration rate [eGFR]) was calculated using the 2021 Chronic Kidney Disease Epidemiology Collaboration equation. Active SLE on the study visit (T0) was defined as an SLEDAI-2K score ≥6. Data on other variables such as steroid dose and other immunosuppressives at study visit (T0) were not uniformly available for all cohorts. HCQ levels from the baseline study visit (T0) were included and measured using a validated high-performance liquid chromatography mass spectrometry assay. The assays were done in a research laboratory but are now commercially available through leading national laboratories (Exagen, Labcorp, ARUP, Mayo Clinic, Hopkins)[27,28] and covered by major payers under the *Current Procedural Terminology* (CPT) code 80020 in the United States. Again, as previously stated, HCQ levels measured in serum (SLICC cohort) were converted to whole blood levels using the following formula: HCQ serum levels/0.53.[16] Finally, data on systemic irreversible HCQ toxicity (eg, eye [abnormal macular examination], heart, or muscle per biopsy findings; skin per clinical observation) over time ($T_{last\ visit}$) were abstracted and categorized as present or absent. It is important to note that analyses included HCQ levels at T0 for all data sources, and HCQ levels at HCQ toxicity and the time to HCQ toxicity were not available. Only data on retinal toxicity were available for the SLICC cohort. One study (n = 305)[17] did not have toxicity data. We performed a single condition imputation analysis using median HCQ toxicity incidence rates per our cohorts and literature.[29–32] This analysis revealed similar results when data from that single study were excluded.[17,32] Given similar results, we used the single imputation analysis for the final models to avoid sample size reduction.

Primary analysis: HCQ blood levels (T0) and HCQ-related toxicity ($T_{last\ visit}$). We used a validated three-step approach to define the upper threshold for HCQ whole blood levels that are supratherapeutic and/or associated with a higher risk of systemic toxicity in 1,842 patients.[11] First, we used the cut point analysis in R to identify an optimal HCQ blood level cutoff with a high NPV for toxicity. Additionally, the NPV of other cutoffs was tested in R as part of the sensitivity analysis. Next, we performed adjusted restricted cubic spline regression analysis to compare the estimated odds ratio (OR) of toxicity at higher HCQ blood levels (eg, 1,000 to <1,050 ng/mL, 1,050 to <1,100 ng/mL, 1,100 to <1,150 ng/mL, 1,150 to <1,200 ng/mL, 1,200 to <1,250 ng/mL, and 1,250 to <1,300 ng/mL) versus the upper cutoff for HCQ blood levels obtained from the optimal cut point analysis. This spline analysis informed the upper threshold for HCQ blood levels associated with higher toxicity odds. Finally, using multivariable logistic regression models, we tested different cutoffs for HCQ whole blood levels to identify the threshold significantly associated with higher toxicity risk. All models were adjusted for variables known to increase HCQ toxicity risk, including age, sex, cumulative HCQ dose, weight-based HCQ dosing ≤5 versus >5 mg/kg/day, and eGFR. A separate sensitivity analysis was performed including all patients (N = 2,010). Finally, given heterogeneity between HCQ serum levels (data from SLICC cohort) and blood levels (other data sources), we performed a sensitivity analysis by separately analyzing associations in the SLICC cohort reporting HCQ serum levels and other data sources (US cohort and data from French studies) reporting HCQ whole blood levels.

Secondary analysis: HCQ blood levels (T0) and active SLE (defined as SLEDAI-2K score ≥6 at T0) to define supratherapeutic levels. Given low toxicity rates with HCQ, we completed optimal cut point, adjusted restricted spline regression, and multivariable logistic regression analyses to test if the upper threshold level was also supratherapeutic. Supratherapeutic levels were defined if levels beyond the upper threshold for HCQ blood levels led to no further change in odds of active SLE

(a ceiling/saturation effect in response). All models were adjusted for variables known to increase active SLE risk, including age, sex, weight-based HCQ dosing ≤5 versus >5 mg/kg/day, and eGFR. Finally, as described previously, additional sensitivity analyses were performed in all patients (N = 2,010) and separately in the SLICC cohort and data from other sources.

Subgroup analysis to identify associations between weight-based HCQ dose categories (≤5 and >5 mg/kg/day) at T0 and supratherapeutic levels (T0). A plot was generated to summarize frequency of subtherapeutic, therapeutic, and supratherapeutic HCQ blood levels (T0) by weight-based HCQ dose categories (T0). Next, we used the chi-square test to check if counts were statistically significant and if HCQ level monitoring would be useful in the weight-based dose categories.

Identifying kidney function thresholds associated with supratherapeutic levels. Using data from all patients (n = 1,842), we first performed a restricted spline analysis to examine associations between HCQ blood levels (T0) and eGFR thresholds (T0), adjusting for age, sex, weight-based HCQ dosing, and SLEDAI-2K (T0). Next, significant eGFR thresholds were used in logistic regression analyses to estimate the odds of having supratherapeutic HCQ blood levels by eGFR thresholds (eg, >90 vs ≤90 mL/min/1.73 m^2 or >60 vs ≤60 mL/min/1.73 m^2). Additionally, regression plots were created to estimate changes in HCQ blood levels across a range of weight-based dosing increments in patients with significant eGFR thresholds.

Finally, for longitudinal mixed-effects modeling, we included patients in the Wisconsin registry with recurrent visits and eGFR ≤60 mL/min/1.73 m^2 (CKD stage ≥3) and who had data on eGFR and HCQ blood levels at each visit (n = 32 unique patients, median visit frequency = 2). Using these longitudinal (recurrent visit) data, we performed a linear mixed-effects model analysis with random intercepts to estimate the change in HCQ blood levels per unit eGFR decline relative to HCQ dose category (>5 vs ≤5 mg/kg/day). These models were adjusted for age, sex, and weight-based HCQ dose.

RESULTS

Baseline characteristics of population. Among 2,010 total patients, 168 patients with very low HCQ levels <200 ng/mL were excluded, and a total of 1,842 patients were included in the main analysis (238 patients from the Wisconsin registry [United States], 1,002 patients from three different published studies centralized in France, and 602 patients from the SLICC cohort). Forty-six percent of the study population was from the multicenter international SLICC cohort and the US cohort. The mean ± SD age was 39 ± 14, 90.4% were female, 56% were White, 29% were Black, 10% were from other ethnic groups, the mean ± SD weight was 68 ± 17 kg, the mean ± SD HCQ dose was 349 ± 88 mg/day, and 44% of patients were taking a ≤5-mg/kg/day HCQ dose. On the day of HCQ blood level measurement (T0), 559 patients had active SLE (SLEDAI-2K score ≥6). Baseline characteristics are shown in Table 1 (all cohorts) and Supplementary Table 1 (by data sets/cohorts).

HCQ blood levels and systemic toxicity. The overall HCQ-related toxicity rate was 4.9% (1% in Wisconsin cohort, 6.2% in data from three previously published studies [France and international], 4.7% in the SLICC cohort). After excluding data from 305 patients without toxicity data, the HCQ-related toxicity rate was 5.1%. Given similar results, we show the results from the single conditional imputation analysis. The overall HCQ

Table 1. Baseline characteristics of the participants*

	Value
Baseline characteristics (baseline visit = T0)	
Participants included in analysis, N	1,842[a]
Age in years, mean ± SD	39 ± 14
Sex, n (%)	
Female	1,665 (90.4)
Male	177 (8.6)
Race and ethnicity, n (%)	
Asian	54 (3)
Black	541 (29)
Hispanic	31 (2)
Other racial and ethnic groups	189 (10)
White	1,027 (56)
Weight in kg, mean ± SD	68 ± 17
eGFR in mL/min/1.73 m^2, mean ± SD	102 ± 33
eGFR ≥60 mL/min/1.73 m^2, n (%)	1,738 (94.4)
eGFR ≥45 and <60 mL/min/1.73 m^2, n (%)	55 (3.0)
eGFR <45 mL/min/1.73 m^2, n (%)	49 (2.6)
HCQ dose in mg/day, mean ± SD	349 ± 88
HCQ dose ≤5 mg/kg/day, n (%)	781 (42)
HCQ dose >5 mg/kg/day, n (%)	1,061 (58)
Cumulative HCQ dose in g, mean ± SD	2,068 ± 1,053
Total HCQ duration in years, mean ± SD	16.0 ± 6.8
HCQ blood levels at T0 in ng/mL, mean ± SD[b]	916 ± 424
Outcome variables	
SLEDAI at baseline visit (T0), mean ± SD	4.1 ± 4.6
Active lupus (SLEDAI score ≥6) at baseline visit (T0), n/N (%)	559/1,842 (30)
Systemic[c] HCQ-related toxicity[d] at $T_{lastvisit}$, n/N (%)	91/1,842 (4.9)

* eGFR was calculated using the race-neutral Chronic Kidney Disease Epidemiology Collaboration 2021 equation. eGFR, glomerular filtration rate; HCQ, hydroxychloroquine; SLEDAI, Systemic Lupus Erythematosus Disease Activity Index; SLICC, Systemic Lupus International Collaborating Clinics; T0, at the time of enrollment; $T_{lastvisit}$, at the time of the last follow-up visit.

[a] One hundred sixty-eight patients with very low HCQ whole blood levels <200 ng/mL (shown to be associated with severe nonadherence) were excluded from analysis.

[b] HCQ blood levels were extrapolated from serum levels for the SLICC cohort using a conversion factor of 0.53.

[c] Includes all systemic toxicity, 85% retinopathy, 9% cardiomyopathy, and 6% skin or muscle toxicity.

[d] One cohort (SLICC) only reported retinopathy as HCQ-related systemic toxicity, one study (multicentric international, n = 305 patients) did not report long-term toxicity data, and a single condition imputation analysis was used to impute toxicity for this cohort using the median HCQ toxicity incidence rate (4.7%).

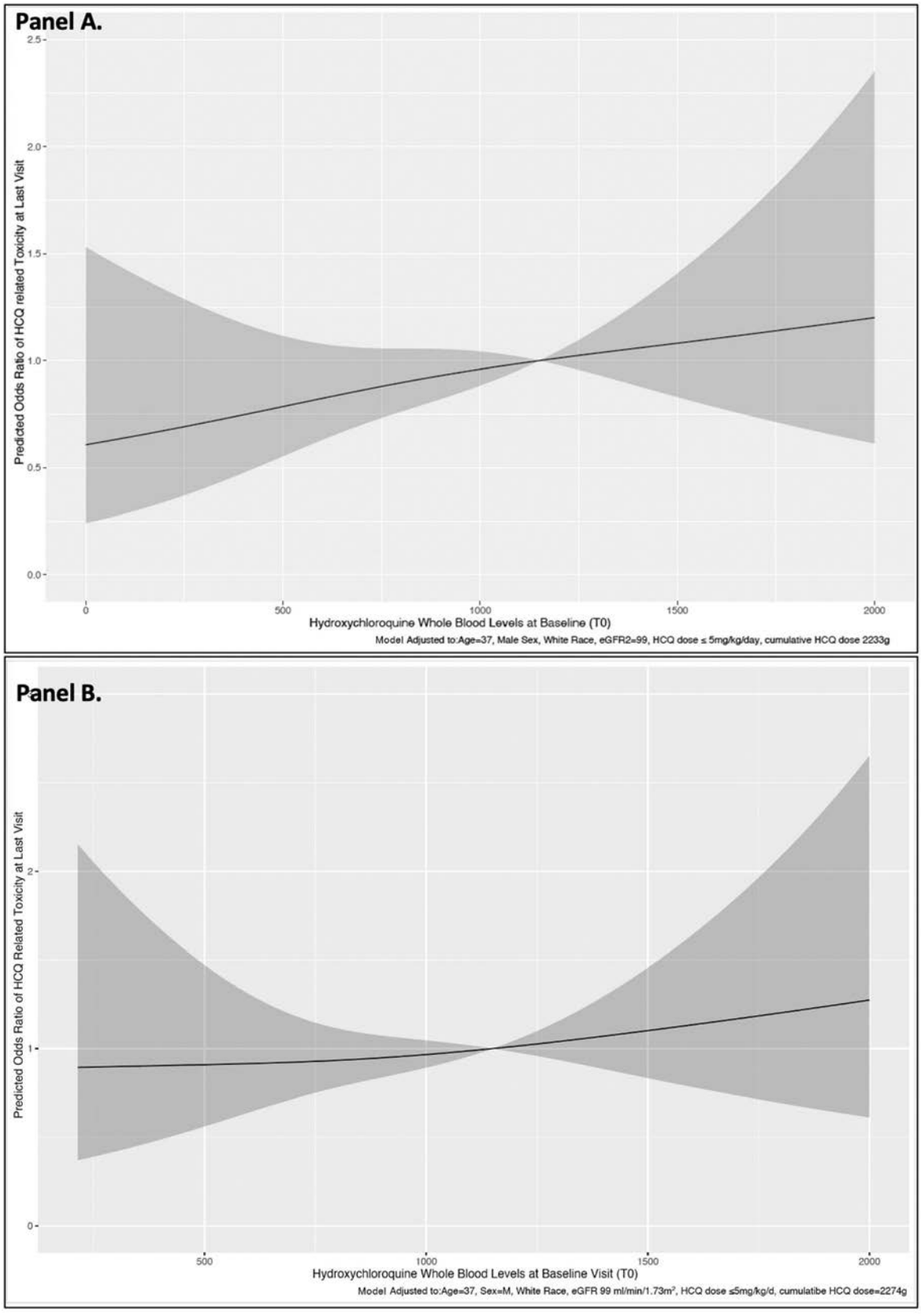

Figure 1. Adjusted restricted cubic splines to show associations between HCQ whole blood levels at baseline and HCQ-related toxicity over time using data from (A) 1,842 patients (not including 168 patients with very low HCQ blood levels <200 ng/mL) and (B) all patients (N = 2,010). eGFR, estimated glomerular filtration rate; HCQ, hydroxychloroquine.

retinopathy was 4.2%. Using the cut point analysis, we found that levels ≥1,150 ng/mL had a ≥93% NPV of identifying toxicity, indicating a potential optimal cut point or upper threshold for HCQ blood levels that could be associated with higher toxicity. Next, the estimated OR of toxicity using 1,150 ng/mL as a reference point revealed a linear increase in estimated OR of toxicity for levels ≥1,150 ng/mL (Figure 1A). Finally, comparing levels informed by the aforementioned analysis, levels ≥1,150 ng/mL were associated with 2.1-fold higher odds of toxicity compared to levels of 750 to <1,150 ng/mL (Table 2), even after adjusting for covariables. These analyses underscored 1,150 ng/mL as an optimal upper threshold for HCQ blood levels linked with toxicity. Similar associations were noted when all patients were included (N = 2,010) in sensitivity analyses (Supplementary Table 2A and Figure 1B). Similar results were noted when serum levels in the SLICC cohort and blood levels from the Wisconsin registry and three published studies (France and international) were analyzed separately (Supplementary Figures 1A and 2A). Finally, even after excluding data from one study that did not have HCQ toxicity information, similar odds of toxicity 1.9-fold (95% confidence interval [CI] 1.2–3.1) were noted with HCQ whole blood levels ≥1,150 ng/mL. Likewise, even after including only HCQ retinopathy, 1.3-fold higher odds of HCQ retinopathy were noted with HCQ whole blood levels ≥1,150 ng/mL (adjusted OR = 1.3, 95% CI 1.2–3.3, $P = 0.007$).

Table 2. Multivariable logistic regression analysis showing factors at baseline visit (T0) associated with HCQ toxicity over time using data from different populations (n = 1,842)*

Variables	Adjusted OR[a] (95% CI)	*P* value
Age per 10-y increase	**1.02 (1.01–1.05)**	**0.02**
Female	0.80 (0.42–1.67)	0.53
White race	Ref	–
Black race	0.97 (0.59–1.57)	0.90
Asian race	0.90 (0.14–3.13)	0.89
Other race or ethnicity	1.67 (0.73–3.50)	0.19
Hispanic ethnicity	NA[b]	0.98
Weight-based HCQ dose, >5 mg/kg/day	0.82 (0.47–1.43)	0.48
Cumulative HCQ dose per 1,000-g increase	**1.74 (1.34–2.30)**	**<0.0001**
eGFR per 10-mL/min/1.73 m^2 increase	0.93 (0.85–1.01)	0.10
Therapeutic HCQ blood levels 750 to <1,150 ng/mL	Ref[c]	–
Subtherapeutic HCQ blood levels <750 ng/mL	1.40 (0.80–2.51)	0.24
Supratherapeutic HCQ blood levels ≥1,150 ng/mL	**2.09 (1.22–3.67)**	**0.01**

* One hundred sixty-eight patients with very low HCQ whole blood levels <200 ng/mL (shown to be associated with severe nonadherence) were excluded from analysis. Statistically significant *P* values (<0.05) are shown in bold. CI, confidence interval; eGFR, estimated glomerular filtration rate; HCQ, hydroxychloroquine; NA, not applicable; OR, odds ratio.
[a] The model was adjusted for age (continuous, T0), sex (patient reported, T0), race or ethnicity, weight-based HCQ dose (>5 vs ≤5 [reference group] mg/kg/day at T0), eGFR (continuous at T0), HCQ whole blood level categories (750 to <1,150 [reference group] vs <750 vs ≥1,150 ng/mL at T0), and cumulative HCQ dose (continuous and calculated between baseline visit and last visit or day of HCQ toxicity [$T_{\text{last visit}}$]).
[b] Unreliable estimates due to small sample size.
[c] The therapeutic range for HCQ blood levels of 750 to <1,150 ng/mL was used as a reference group to demonstrate the ceiling or saturation effect in clinical response with levels >1,150 ng/mL and to demonstrate higher odds of active systemic lupus erythematosus with levels below the therapeutic range.

Supratherapeutic HCQ whole blood levels. We then tested if this HCQ blood level threshold linked with higher toxicity was associated with any additional benefits in reducing odds of active SLE, defined as an SLEDAI-2K score ≥6. Using cut point analysis, levels 1,150 ng/mL had an NPV of 96% for active lupus (SLEDAI-2K score ≥6). Next, we completed a restricted cubic spline analysis using 1,150 ng/mL as the reference point. We noted only a slight change in estimated active lupus (SLEDAI-2K scores ≥6) odds with levels above 1,150 ng/mL (Figure 2A). These findings highlighted a ceiling effect at 1,150 ng/mL. Thus, in our multivariable analysis, we used the HCQ levels categories <750 versus 750 to <1,150 versus ≥1,150 ng/mL, informed by the aforementioned findings and published literature, including a global meta-analysis. In logistic regression analysis adjusted for variables that could potentially lead to active lupus and using 750 to <1,150 ng/mL as the reference category, no significant reduction in odds of active lupus was noted with levels ≥1,150 ng/mL (Table 3), whereas subtherapeutic levels of <750 ng/mL were associated with 1.36-fold higher odds of active lupus (Table 3). This finding suggests that levels beyond this threshold (≥1,150 ng/mL) were indeed supratherapeutic and potentially associated with higher risk of toxicity. Finally, an HCQ dose >5 mg/kg/day was associated with 0.54-fold lower odds of active lupus (Table 3). Similar associations were noted when all patients were included (N = 2,010) in sensitivity analyses (Supplementary Table 2B and Figure 2B) and when serum levels in the SLICC cohort and blood levels from the Wisconsin registry and three published studies (France and international) were analyzed separately (Supplementary Figures 1B and 2B).

Associations between weight-based HCQ dosing, kidney function thresholds, and supratherapeutic HCQ blood levels. We noted a significant number of patients (n = 142 [18%]) had supratherapeutic and potentially toxic levels ≥1,150 ng/mL despite weight-based dosing (Supplementary Figure 3A), whereas 37% had supratherapeutic levels with doses >5 mg/kg/day (Supplementary Figure 3B). Next, adjusted logistic regression analyses noted an eGFR threshold of <60 mL/min/1.73 m^2 was associated with 2.3-fold higher odds of having supratherapeutic HCQ blood levels (Supplementary Table 3). In the CKD Stage 3a (eGFR 45–59 mL/min/1.73 m^2) and CKD Stage 3b or above (eGFR <45 mL/min/1.73 m^2) subgroups, a positive association was noted between weight-based HCQ daily dose (mg/kg/day) and predicted HCQ whole blood levels (ng/mL),

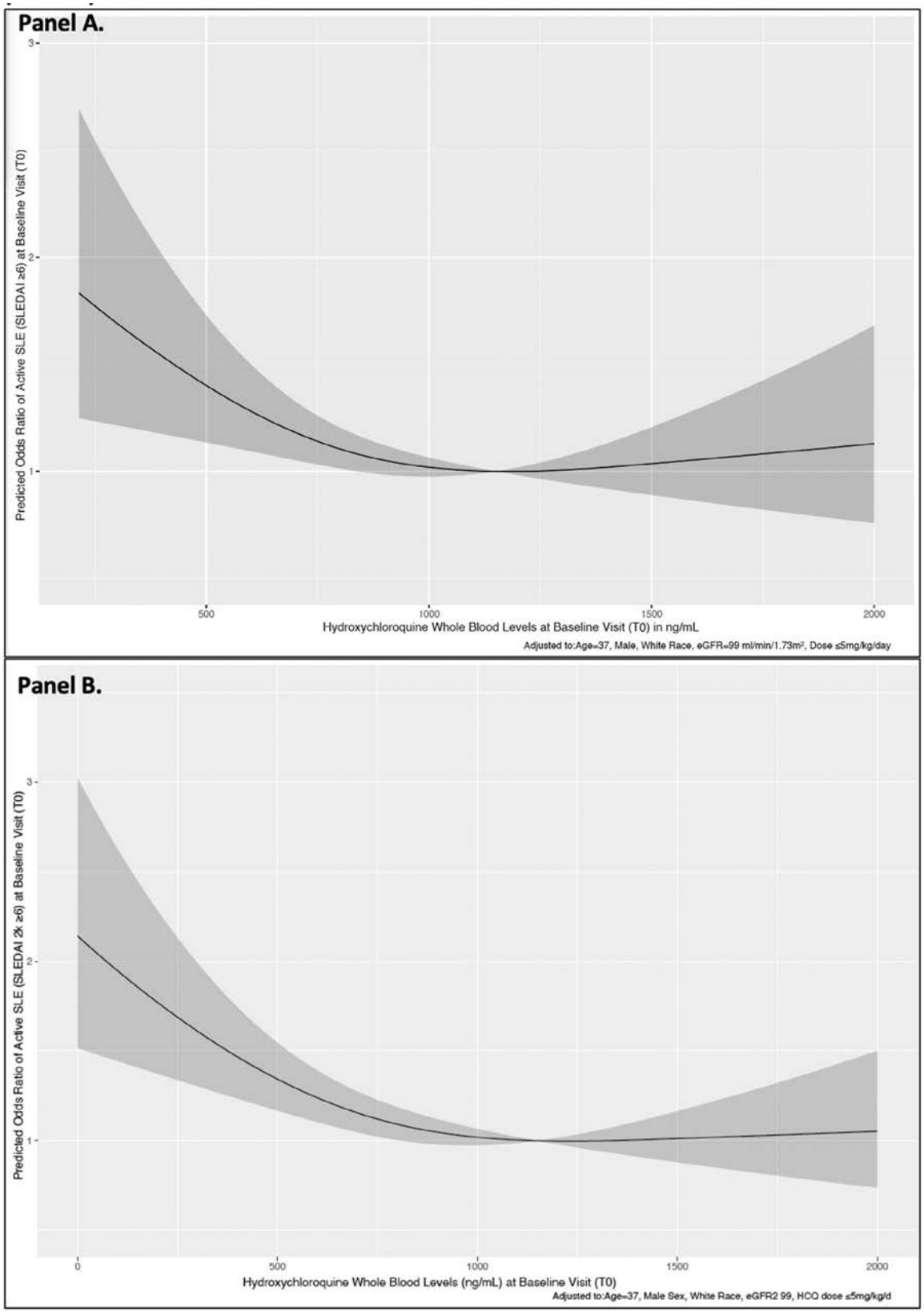

Figure 2. Adjusted restricted cubic splines to show associations between HCQ whole blood levels at baseline visit (T0) and active SLE (SLEDAI score ≥6) at baseline visit (T0) using data from (A) 1,842 patients (not including 168 patients with very low HCQ blood levels <200 ng/mL) and (B) all patients (N = 2,010). eGFR, estimated glomerular filtration rate; HCQ, hydroxychloroquine; SLE, systemic lupus erythematosus; SLEDAI, Systemic Lupus Erythematosus Disease Activity Index.

Table 3. Multivariable logistic regression analysis showing factors at baseline visit (T0) associated with active SLE (SLEDAI-2K score ≥6) at baseline visit (T0) using data from different populations (n = 1,842)*

Variables	Adjusted OR[a] (95% CI)	*P* value
Age per 10-y increase	**0.99 (0.98–1.00)**	**0.02**
Female	1.44 (1.00–2.09)	0.05
White race	Ref	–
Black race	0.95 (0.74–1.21)	0.68
Asian race	**4.12 (2.32–7.55)**	**<0.0001**
Other race or ethnicity	**2.17 (1.56–3.03)**	**<0.0001**
Hispanic ethnicity	1.87 (0.88–3.89)	0.10
Weight-based HCQ dose, >5 mg/kg/day	**0.54 (0.44–0.68)**	**<0.0001**
eGFR per 10-mL/min/1.73 m^2 increase	1.01 (0.97–1.05)	0.72
Therapeutic HCQ blood levels 750 to <1,150 ng/mL	Ref[b]	–
Subtherapeutic HCQ blood levels <750 ng/mL	**1.33 (1.05–1.70)**	**0.02**
Supratherapeutic HCQ blood levels ≥1,150 ng/mL	0.94 (0.71–1.24)	0.67

* One hundred sixty-eight patients with very low HCQ whole blood levels <200 ng/mL (shown to be associated with severe nonadherence) were excluded from analysis. Statistically significant *P* values (<0.05) are shown in bold. CI, confidence interval; eGFR, estimated glomerular filtration rate; HCQ, hydroxychloroquine; OR, odds ratio; SLE, systemic lupus erythematosus; SLEDAI-2K, Systemic Lupus Erythematosus Disease Activity Index 2000.
[a] The model was adjusted for covariables at baseline visit (T0), including age (continuous, T0), sex (patient reported, T0), race or ethnicity (T0), weight-based HCQ dose (>5 vs ≤5 [reference group] mg/kg/day at T0), eGFR (continuous at T0), and HCQ whole blood level categories (750 to <1,150 [reference group] vs <750 vs ≥1,150 ng/mL at T0). SLEDAI-2K scores at baseline visit (T0) were used as the outcome and categorized as active SLE (SLEDAI-2K score ≥6).
[b] The therapeutic range for HCQ blood levels of 750 to <1,150 ng/mL was used as a reference group to demonstrate the ceiling or saturation effect in clinical response with levels >1,150 ng/mL and to demonstrate higher odds of active SLE with levels below the therapeutic range.

with an estimated mean ± SD slope of 136 ± 59 ng/mL and 166 ± 59 ng/mL per 1-mg/kg/day increase, respectively (Supplementary Figure 4). In patients with CKD Stage 3a and CKD Stage 3b or above, even with weight-based dosing of 5 mg/kg/day, the predicted HCQ blood levels were near the supratherapeutic (toxic) threshold. A slight increase in the dose or decline in eGFR would tip levels over to the supratherapeutic threshold, risking toxicity over time in patients with CKD Stage 3 or above (Supplementary Figure 4). This was validated in our adjusted linear longitudinal mixed-effects model, which showed a steeper slope of change in HCQ blood levels relative to eGFR decline in patients with an eGFR <60 mL/min/1.73 m^2 and taking an HCQ dose >5 mg/kg/day (mean ± SD 6.11 ± 2.04 ng/mL) versus those taking a dose of ≤5 mg/kg/day (mean ± SD 4.82 ± 2.72 ng/mL) (Figure 3). Per these slope estimates, significant changes in eGFR, such as a 20-unit decrease, would result in a 122-ng/mL (95% CI 82–162 ng/mL) and 96-ng/mL (95% CI 42–150 ng/mL) increase in HCQ blood levels with doses of >5 and ≤5 mg/kg/day, respectively.

DISCUSSION

In this study leveraging cross-sectional data from diverse SLE cohorts, HCQ whole blood levels ≥1,150 ng/mL at T0 (baseline) were associated with a 2.1-fold higher risk of systemic HCQ-related toxicity. HCQ-related systemic toxicity was infrequent, and only 4.9% of the population experienced toxicity; therefore, we tested the therapeutic effect of having levels ≥1,150 ng/mL. We noted that levels ≥1,150 ng/mL did not significantly reduce the odds of active SLE, indicating a ceiling effect in clinical response with levels ≥1,150 ng/mL and qualifying levels ≥1,150 ng/mL as supratherapeutic levels. Finally, our findings highlight that CKD stage ≥3 was associated with 2.3-fold higher odds of having supratherapeutic levels (≥1,150 ng/mL), and not adjusting HCQ dose in this group could significantly increase levels by 122 ng/mL, with eGFR decline of 20 units. Together these findings establish the clinical significance of HCQ blood level monitoring in not only assessing for severe nonadherence but also guiding clinicians with optimal HCQ use to balance treatment efficacy and safety. Finally, a 2020 single-center prospective cohort study led by Dr Petri[19] highlighted that HCQ whole blood levels ≥1,200 ng/mL were associated with higher risk of retinopathy. Those findings are consistent with this study's findings. These findings suggest that careful HCQ dose adjustments via HCQ blood level monitoring, particularly in high-risk groups (eg, CKD stage ≥3), could be beneficial in personalizing HCQ dosing. Additional multicenter longitudinal studies are needed in the future to establish a roadmap for dose adjustments based on individual patient risk factors.

Following the first study published in 2006 showing that low HCQ levels predict disease exacerbations in patients with SLE,[33] studies from other lupus cohorts[11,13,25,34] and a global meta-analysis[9] confirmed 750 or 1,000 ng/mL as a lower threshold for the reference range for HCQ blood levels associated with better efficacy. In 2020, evidence on the upper threshold of the reference range for HCQ blood level monitoring was reported, and levels >1,183 ng/mL were associated with higher retinopathy risk (incidence of retinopathy = 4.3%).[19] Consistent with prior findings, the current study highlights the reliability of the upper threshold (≥1,150 ng/mL) of the reference range for HCQ blood levels by establishing associations with higher toxicity risk without additional clinical benefits across global SLE populations (N = 2,010). Although a portion of the data was derived from French cohorts, over 46% of the study population was drawn from the multicenter international SLICC cohort and a US-based registry, enhancing the generalizability of our findings. The demographic characteristics of the cohort, including a mean ± SD age of 39 ± 14 years, 90.4% female representation, and racial and ethnic diversity with 56% White, 29% Black, and 10% from other racial or ethnic groups, are consistent with the known epidemiology of SLE. Additionally, the mean ± SD body weight (68 ± 17 kg) and HCQ dosing patterns reflect real-world clinical practice, supporting the applicability of our findings to broader SLE populations.

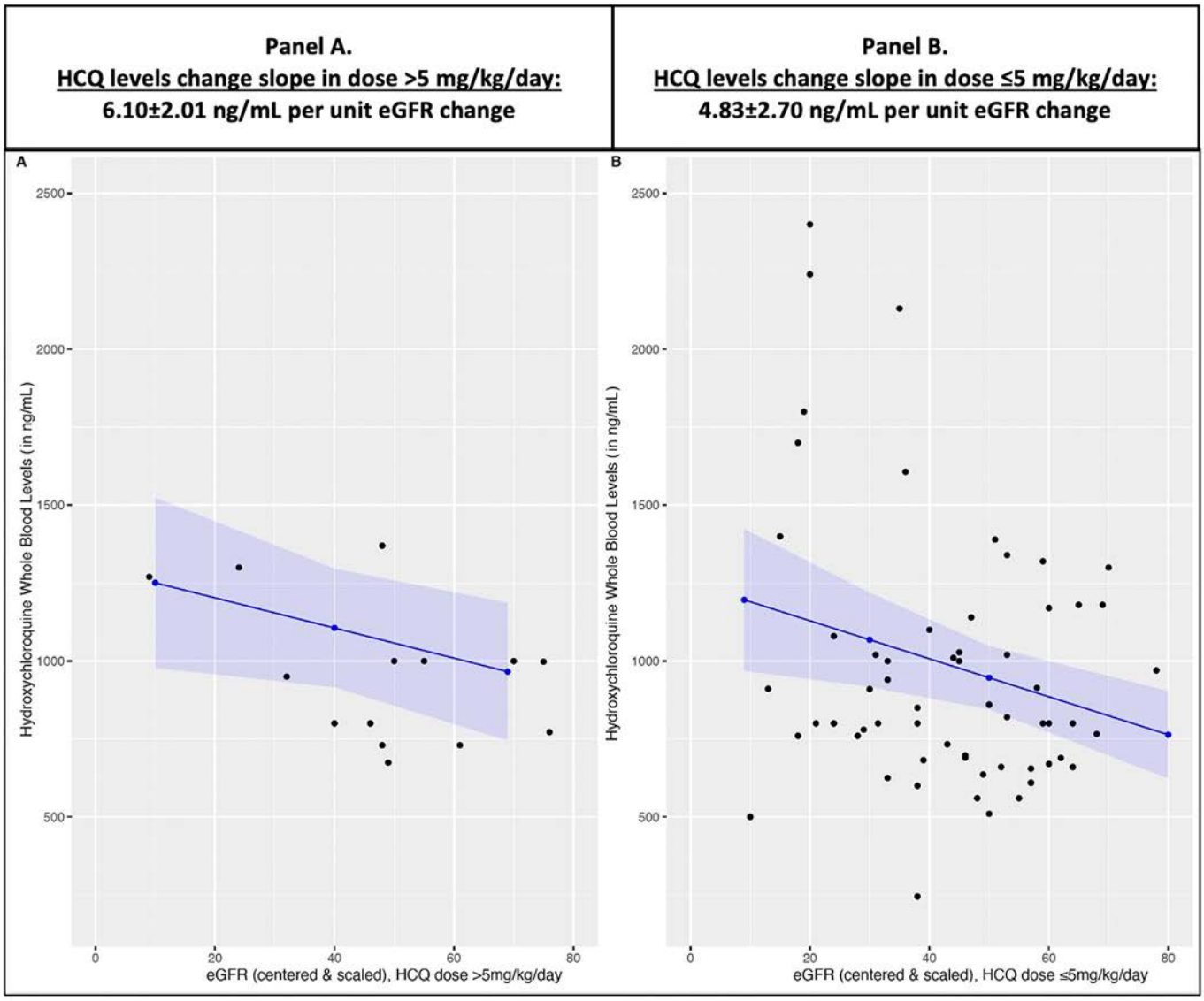

Estimates on HCQ Whole Blood levels change with eGFR decline by HCQ dose category

eGFR change	Change in HCQ whole blood levels (in ng/mL)	
	HCQ dose >5 mg/kg/day	HCQ dose ≤5 mg/kg/day
10 mL/min/1.73m^2	61±20	48±27
15 mL/min/1.73m^2	92±30	73±41
20 mL/min/1.73m^2	122±41	96±54
25 mL/min/1.73m^2	153±50	121±68
30 mL/min/1.73m^2	183±61	145±81
35 mL/min/1.73m^2	214±70	169±95
40 mL/min/1.73m^2	244±80	192±108

Figure 3. Longitudinal modeling showing change in HCQ whole blood levels with kidney function decline over time in patients with CKD (32 patients with CKD stage ≥3 had two or more follow-up visits) by HCQ daily dose category: (A) >5 mg/kg/day versus (B) ≤5 mg/kg/day. CKD, chronic kidney disease; eGFR, estimated glomerular filtration rate; HCQ, hydroxychloroquine.

Routine HCQ whole blood level monitoring bypasses clinical variables (eg, absorption, clearance) that can drive interindividual variability in drug levels, is easier to collect, and guides clinicians in adjusting HCQ doses when levels are supratherapeutic, particularly in patients at higher risk of HCQ toxicity, such as those with CKD.[30] This study provides important data highlighting that 18% of patients had supratherapeutic and potentially toxic levels despite taking ≤5 mg/kg/day of HCQ (44% of the total population). This finding underscores a role of HCQ blood level monitoring even in patients with weight-based dosing. This study sheds new evidence on thresholds of kidney function (eGFR <60 mL/min/1.73 m^2) associated with a 2.3-fold higher risk of supratherapeutic (or toxic) HCQ blood levels. This threshold highlights the need to adjust HCQ doses or perform closer monitoring in patients with low kidney function (eGFR <60 mL/min/1.73 m^2).

Additionally, our study highlights a dose-dependent relationship in patients with impaired renal function (CKD Stage 3a or above) and may have implications for individualized dosing strategies in the CKD subgroup. Although data on how HCQ dose should be reduced in patients with CKD to balance efficacy versus toxicity are lacking, our study delivers preliminary data on changes in HCQ blood levels with eGFR decline relative to weight-based HCQ dose over time. In patients with CKD stage ≥3 taking HCQ doses >5 mg/kg/day, a clinically significant increase in HCQ blood levels by 122 ng/mL was noted with an eGFR decline of 20 units. Despite HCQ dosing (>5 or ≤5 mg/kg/day), variations in HCQ blood levels with eGFR decline of 20 units were above the diurnal variation threshold of <80 ng/mL. Moreover, we noted that patients with eGFR <60 mL/min/1.73 m^2 had higher chances of having supratherapeutic (toxic) levels even if they were receiving weight-based dosing of ≤5 mg/kg/day, as shown in Figure 3. Thus, close monitoring of HCQ blood levels to guide HCQ dose adjustments could prevent toxicity[29] and maximize efficacy in patients with SLE and CKD stage ≥3. Our preliminary findings, along with recent interpretation of HCQ blood levels offered by Balevic et al, provide essential data to design a future clinical trial leveraging HCQ blood level monitoring to inform dose or formulation changes in patients with SLE and CKD.[14] However, given the variability in HCQ blood levels, especially in case of variation in adherence to treatment or even eGFR fluctuations,[14] a decision to adjust HCQ dose, particularly when the dose is weight based, should not be made based on a single HCQ blood level measurement. We recommend repeat measurement of HCQ levels to obtain a better estimate on the median levels and inform clinical decision-making.

The feasibility of HCQ blood level monitoring in the target population is an important consideration. In our view, incorporating HCQ blood level monitoring into clinical care is feasible and is already being routinely implemented in France, other parts of Europe, and some US centers. Supporting this, qualitative studies reported that patients are generally receptive to drug level monitoring, particularly when clinicians initiate open, empathetic conversations during visits.[35–37] Moreover, HCQ level testing is covered by the public health system in France (cost <€30) and by most insurance providers in the United States (copay cost $0–200) and has an established CPT code (80220) in the United States, which supports its practical implementation. Furthermore, drug level monitoring is already a standard practice in other specialties, such as gastroenterology, nephrology, and transplantation medicine, in which patient acceptance has been high. It is also close to the monitoring of international normalized ratio in patients taking warfarin. Finally, HCQ level testing should guide nonjudgmental communication and support physicians and patients in optimizing HCQ dosing.[38] Indeed, in addition to giving important information on adherence to treatment, HCQ level monitoring can offer clinicians the opportunity to optimize HCQ dosing based on each patient's factors, such as CKD and absorption, which are otherwise not accounted for when routinely dosing HCQ. This approach, already used in France for more than 20 years, could shift from traditional "one-size-fits-all" dosing toward a more precise, personalized approach to HCQ management in SLE. Two US longitudinal, prospective mixed-methods studies are currently under way (SHIELD and EMS-HCQ), and a French study is currently being designed to compare both strategies (weight-based HCQ dosing vs personalized HCQ dosing per HCQ blood levels). These ongoing studies will provide valuable insights on HCQ blood level monitoring frequency, cost-effectiveness, and patient–clinician engagement to develop best practices. Additionally, a shared decision-making tool that guides clinicians and patients in decisions to continue HCQ dose with or without changes could be a vital resource for clinical use and should be a research priority.

Despite several strengths of this study, including a large study with diverse populations and appropriate testing of HCQ levels, study limitations include the retrospective design and the inability to control for all confounders affecting outcomes, such as other immunosuppressive medications and steroid dose. Additionally, whole blood levels in the primary population were assayed in each local laboratory as part of routine practice. We cannot demonstrate the interchangeability of all bioanalytical methods due to the lack of an external quality assessment system between laboratories, which is a limitation of our analysis. Besides, HCQ serum levels in the SLICC cohort were measured retrospectively, and whole blood levels were extrapolated from serum levels, which can represent a bias in our analysis because there could be stability issues of HCQ serum levels over time and potential variability introduced by individual hematocrit differences, and the implications for interpreting our findings. Third, the data on the time to HCQ toxicity and HCQ levels at the time of HCQ toxicity were not available. Given the goal of HCQ levels is to determine the chance of future toxicity, these findings remain significant. Moreover, the supratherapeutic effect of the upper threshold for HCQ levels (≥1,150 ng/mL) was tested using HCQ levels and SLEDAI-2K measurements done on the same day

(T0). This bolsters the fact that the upper threshold is supratherapeutic and potentially toxic. However, given that our study shows that HCQ levels could vary with significant kidney function decline and given that our models' testing associations with HCQ toxicity assumed that HCQ levels remain stable over time, we need to test the upper threshold in longitudinal studies, particularly in patients with CKD stage ≥3. Additionally, longitudinal studies should test if a single HCQ blood level measurement versus an average of two or more HCQ blood level measurements should be used to guide HCQ dose adjustments. Fourth, one cohort did not report on long-term eye toxicity; therefore, a single condition imputation was performed to avoid sample size reduction. Results from the single condition imputation analysis and sensitivity analysis excluding data from this cohort were similar. Additionally, our study might underestimate the overall HCQ-related side effects rate given that data on preclinical HCQ toxicity (abnormal eye examination) might not have been abstracted. Finally, only a few patients with CKD stage ≥3 had recurrent visit data (n = 32). Thus, a prospective study is needed to test the efficacy of HCQ blood level monitoring in guiding safe and optimal HCQ use in patients with CKD and SLE, and similar analyses in patients with hepatic dysfunction and gastric bypass are needed.

In conclusion, this study is the first to define a potential therapeutic reference range for HCQ whole blood levels (750–1,150 ng/mL) in SLE, using data from diverse multinational cohorts. It also identifies key patient-specific factors, particularly CKD stage ≥3, that significantly increase the risk of supratherapeutic levels, despite weight-based dosing. By providing quantitative estimates of how HCQ levels change with dose and kidney function decline, our findings offer clinicians a practical framework for safer and more individualized, data-driven dosing decisions. Although our data are cross-sectional, they still lay a strong foundation for future longitudinal studies to evaluate the clinical effectiveness of routine HCQ blood level monitoring. Ultimately, this work supports a shift from traditional "one-size-fits-all" dosing toward a more balanced, precise, and personalized approach to dose HCQ in SLE, potentially bypassing the current issues with weight-based dosing.

AUTHOR CONTRIBUTIONS

All authors contributed to at least one of the following manuscript preparation roles: conceptualization AND/OR methodology, software, investigation, formal analysis, data curation, visualization, and validation AND drafting or reviewing/editing the final draft. As corresponding authors, Drs Garg and Costedoat-Chalumeau confirm that all authors have provided the final approval of the version to be published and take responsibility for the affirmations regarding article submission (eg, not under consideration by another journal), the integrity of the data presented, and the statements regarding compliance with institutional review board/Declaration of Helsinki requirements.

REFERENCES

1. Ruiz-Irastorza G, Ramos-Casals M, Brito-Zeron P, et al. Clinical efficacy and side effects of antimalarials in systemic lupus erythematosus: a systematic review. Ann Rheum Dis 2010;69(1):20–28. doi:https://doi.org/10.1136/ard.2008.101766
2. Garg S, Chewning B, Gazeley D, et al. Patient and healthcare team recommended medication adherence strategies for hydroxychloroquine: results of a qualitative study informing intervention development. Lupus Sci Med 2022;9(1):e000720. doi:https://doi.org/10.1136/lupus-2022-000720
3. Feldman CH, Collins J, Zhang Z, et al. Dynamic patterns and predictors of hydroxychloroquine nonadherence among Medicaid beneficiaries with systemic lupus erythematosus. Semin Arthritis Rheum 2018;48(2):205–213. doi:https://doi.org/10.1016/j.semarthrit.2018.01.002
4. Nguyen NV, Svenungsson E, Dominicus A, et al. Hydroxychloroquine in lupus or rheumatoid arthritis pregnancy and risk of major congenital malformations: a population-based cohort study. Rheumatology (Oxford) 2025;64(1):117–125. doi:https://doi.org/10.1093/rheumatology/keae168
5. Rovin BH, Ayoub IM, Chan TM, et al. Executive summary of the KDIGO 2024 clinical practice guideline for the management of lupus nephritis. Kidney Int 2024;105(1):31–34. doi:https://doi.org/10.1016/j.kint.2023.09.001
6. Petri M, Li J. Time to renal insufficiency based on prior hydroxychloroquine blood levels. [abstract]. Arthritis Rheumatol 2020;72(suppl 10). Accessed August 21, 2025. https://acrabstracts.org/abstract/time-to-renal-insufficiency-based-on-prior-hydroxychloroquine-blood-levels/
7. Durcan L, Clarke WA, Magder LS, et al. Hydroxychloroquine blood levels in systemic lupus erythematosus: clarifying dosing controversies and improving adherence. J Rheumatol 2015;42(11):2092–2097. doi:https://doi.org/10.3899/jrheum.150379
8. Lenfant T, Costedoat-Chalumeau N. Hydroxychloroquine dose: balancing toxicity and SLE flare risk. Nat Rev Rheumatol 2023;19(1):6–7. doi:https://doi.org/10.1038/s41584-022-00868-3
9. Garg S, Unnithan R, Hansen KE, et al. Clinical significance of monitoring hydroxychloroquine levels in patients with systemic lupus erythematosus: a systematic review and meta-analysis. Arthritis Care Res (Hoboken) 2021;73(5):707–716. doi:https://doi.org/10.1002/acr.24155
10. Petri M. Drug monitoring in systemic lupus erythematosus. Curr Opin Pharmacol 2022;64:102225. doi:https://doi.org/10.1016/j.coph.2022.102225
11. Garg S, Chewning B, Hutson P, et al. Reference range of hydroxychloroquine blood levels that can reduce odds of active lupus and prevent flares. Arthritis Care Res (Hoboken) 2024;76(2):241–250. doi:https://doi.org/10.1002/acr.25228
12. Costedoat-Chalumeau N, Pouchot J, Guettrot-Imbert G, et al. Adherence to treatment in systemic lupus erythematosus patients. Best Pract Res Clin Rheumatol 2013;27(3):329–340. doi:https://doi.org/10.1016/j.berh.2013.07.001
13. Garg S, Astor BC, Saric C, et al. Therapeutic hydroxychloroquine blood levels are associated with fewer hospitalizations and possible reduction of health disparities in lupus. Arthritis Care Res (Hoboken) 2024;76(12):1606–1616. doi:https://doi.org/10.1002/acr.25422
14. Balevic S, Sun K, Rogers JL, et al. Interpreting hydroxychloroquine blood levels for medication non-adherence: a pharmacokinetic study. Lupus Sci Med 2024;11(1):e001090. doi:https://doi.org/10.1136/lupus-2023-001090
15. Costedoat-Chalumeau N, Tamirou F, Le Guern V, et al. Blood concentration of hydroxychloroquine in systemic lupus erythematosus care: usefulness and limits. Article in French. Rev Med Interne 2017;38(2):77–80. doi:https://doi.org/10.1016/j.revmed.2016.07.001
16. Nguyen Y, Blanchet B, Urowitz MB, et al. Association between severe nonadherence to hydroxychloroquine and systemic lupus erythematosus flares, damage, and mortality in 660 patients from the SLICC

inception cohort. Arthritis Rheumatol 2023;75(12):2195–2206. doi: https://doi.org/10.1002/art.42645

17. Costedoat-Chalumeau N, Houssiau F, Izmirly P, et al. A prospective international study on adherence to treatment in 305 patients with flaring SLE: assessment by drug levels and self-administered questionnaires. Clin Pharmacol Ther 2019;106(2):374–382. doi:https://doi.org/10.1002/cpt.1194
18. Costedoat-Chalumeau N, Galicier L, Aumaître O, et al; Group PLUS. Hydroxychloroquine in systemic lupus erythematosus: results of a French multicentre controlled trial (PLUS Study). Ann Rheum Dis 2013;72(11):1786–1792. doi:https://doi.org/10.1136/annrheumdis-2012-202322
19. Petri M, Elkhalifa M, Li J, et al. Hydroxychloroquine blood levels predict hydroxychloroquine retinopathy. Arthritis Rheumatol 2020;72(3): 448–453. doi:https://doi.org/10.1002/art.41121
20. Lenfant T, Leroux G, Costedoat-Chalumeau N. Different control populations may lead to different understanding of hydroxychloroquine blood levels as a risk factor for retinopathy: comment on the article by Petri et al. Arthritis Rheumatol 2021;73(4):715. doi:https://doi.org/10.1002/art.41588
21. Yazdany J, Shiboski S, Schmajuk G. The hydroxychloroquine conundrum: striking the right balance between safety and efficacy in rheumatology practice. Arthritis Rheumatol 2024;76(10):1467–1470. doi: https://doi.org/10.1002/art.42930
22. Costedoat-Chalumeau N, Amoura Z, Hulot JS, et al. Very low blood hydroxychloroquine concentration as an objective marker of poor adherence to treatment of systemic lupus erythematosus. Ann Rheum Dis 2007;66(6):821–824. doi:https://doi.org/10.1136/ard.2006.067835
23. Bruce IN, O'Keeffe AG, Farewell V, et al. Factors associated with damage accrual in patients with systemic lupus erythematosus: results from the Systemic Lupus International Collaborating Clinics (SLICC) inception cohort. Ann Rheum Dis 2015;74(9):1706–1713. doi:https://doi.org/10.1136/annrheumdis-2013-205171
24. Petri M, Orbai AM, Alarcón GS, et al. Derivation and validation of the Systemic Lupus International Collaborating Clinics classification criteria for systemic lupus erythematosus. Arthritis Rheum 2012;64(8): 2677–2686. doi:https://doi.org/10.1002/art.34473
25. Blanchet B, Jallouli M, Allard M, et al; PLUS Group. Hydroxychloroquine levels in patients with systemic lupus erythematosus: whole blood is preferable but serum levels also detect non-adherence. Arthritis Res Ther 2020;22(1):223. doi:https://doi.org/10.1186/s13075-020-02291-z
26. Marmor MF, Kellner U, Lai TYY, et al; American Academy of Ophthalmology. Recommendations on screening for chloroquine and hydroxychloroquine retinopathy (2016 Revision). Ophthalmology 2016;123(6):1386–1394. doi:https://doi.org/10.1016/j.ophtha.2016.01.058
27. Exagen Clinical Utility. AVISE HCQ test report. Accessed May 19, 2025. https://avisetest.com/wp-content/uploads/AVISE_HCQ_STR_11-24.pdf
28. Qu Y, Noe G, Breaud AR, et al. Development and validation of a clinical HPLC method for the quantification of hydroxychloroquine and its metabolites in whole blood. Future Sci OA 2015;1(3):FSO26. doi: https://doi.org/10.4155/fso.15.24
29. Jorge AM, Melles RB, Marmor MF, et al. Risk factors for hydroxychloroquine retinopathy and its subtypes. JAMA Netw Open 2024;7(5): e2410677. doi:https://doi.org/10.1001/jamanetworkopen.2024.10677
30. Melles RB, Jorge AM, Marmor MF, et al. Hydroxychloroquine dose and risk for incident retinopathy: a cohort study. Ann Intern Med 2023;176(2):166–173. doi:https://doi.org/10.7326/M22-2453
31. Almeida-Brasil CC, Hanly JG, Urowitz M, et al. Retinal toxicity in a multinational inception cohort of patients with systemic lupus on hydroxychloroquine. Lupus Sci Med 2022;9(1):e000789. doi:https://doi.org/10.1136/lupus-2022-000789
32. Groenwold RH, Donders AR, Roes KC, et al. Dealing with missing outcome data in randomized trials and observational studies. Am J Epidemiol 2012;175(3):210–217. doi:https://doi.org/10.1093/aje/kwr302
33. Costedoat-Chalumeau N, Amoura Z, Hulot JS, et al. Low blood concentration of hydroxychloroquine is a marker for and predictor of disease exacerbations in patients with systemic lupus erythematosus. Arthritis Rheum 2006;54(10):3284–3290. doi:https://doi.org/10.1002/art.22156
34. Cunha C, Alexander S, Ashby D, et al. Hydroxycloroquine blood concentration in lupus nephritis: a determinant of disease outcome? Nephrol Dial Transplant 2018;33(9):1604–1610. doi:https://doi.org/10.1093/ndt/gfx318
35. Schesing KB, Chia R, Elwood B, et al. Assessment of patient and provider attitudes towards therapeutic drug monitoring to improve medication adherence in low-income patients with hypertension: a qualitative study. BMJ Open 2020;10(11):e039940. doi:https://doi.org/10.1136/bmjopen-2020-039940
36. Feyz L, Bahmany S, Daemen J, et al. Therapeutic drug monitoring to assess drug adherence in assumed resistant hypertension: a comparison with directly observed therapy in 3 nonadherent patients. J Cardiovasc Pharmacol 2018;72(2):117–120. doi:https://doi.org/10.1097/FJC.0000000000000602
37. Pagès-Puigdemont N, Mangues MA, Masip M, et al. Patients' perspective of medication adherence in chronic conditions: a qualitative study. Adv Ther 2016;33(10):1740–1754.
38. Garg S, Plantinga LC. A bitter pill to swallow: the challenge of medication nonadherence in systemic lupus erythematosus. J Rheumatol 2024;51(9):841–844. doi:https://doi.org/10.3899/jrheum.2024-0654

American College of Rheumatology
Empowering Rheumatology Professionals

Arthritis & Rheumatology
Vol. 78, No. 5, May 2026, pp 1114–1123
DOI 10.1002/art.70022

Weighing Dose-Related Benefits and Risks of Hydroxychloroquine Treatment in Patients With Systemic Lupus Erythematosus

Brian Meng-Hsun Li, MClinPharm,[1,2] Jia-Horung Hung, MD,[2,3,4] Po-Cheng Yang,[5] Swu-Jane Lin, PhD,[6] Edward Chia-Cheng Lai, PhD,[1,2] and Meng-Yu Weng, MD, PhD[7]

Objective. To weigh higher-dose hydroxychloroquine (HCQ; ≥400 mg/day) and lower-dose HCQ (<400 mg/day) for effectiveness and safety among patients with systemic lupus erythematosus (SLE).

Methods. This nationwide study retrieved data from Taiwan's National Health Insurance Research Database from 2010 to 2021. We included patients with SLE aged over 10 years and initiating HCQ who had no other systemic autoimmune disease at baseline and no historical outcomes of interest. Patients were classified into higher-dose (≥400 mg/day) or lower-dose (<400 mg/day) treatment strategies based on the dosage of their first HCQ prescription. The outcomes were coronary artery disease (CAD), ischemic stroke, venous thromboembolism (VTE), end-stage renal disease, malignancy, and HCQ retinopathy.

Results. Eight hundred seventy-eight (3.77%) patients taking higher-dose HCQ and 22,405 (96.22%) taking lower-dose HCQ were included. After inverse probability weighting, higher-dose HCQ was associated with lower risks of CAD (hazard ratio [HR] 0.86, 95% confidence interval [CI] 0.80–0.93) and VTE (HR 0.40, 95% CI 0.33–0.49). We found no dose-related difference in the risk of ischemic stroke, end-stage renal disease, malignancy, and HCQ retinopathy through a mean follow-up of six years, except for the HCQ retinopathy among patients with SLE aged over 45 years (HR 1.87, 95% CI 1.45–2.42).

Conclusion. For patients with SLE, higher-dose HCQ improves effectiveness, with reduced risks of CAD and VTE. There was no dose-related difference in the risk of HCQ retinopathy for patients with SLE aged younger than 45 years. Our study emphasizes the need for weighing the benefits and risks of optimal HCQ dosage in managing SLE.

INTRODUCTION

Hydroxychloroquine (HCQ) is an established immunomodulator for systemic lupus erythematosus (SLE).[1–3] The medication can improve survival and reduce SLE activity.[4–6] HCQ is recommended in the treatment of every patient when there is no contraindication for SLE, according to American College of Rheumatology and EULAR guidelines.[1,7] In a new era of targeted therapies, HCQ continues to be used as the initial pharmacotherapy for SLE.

The estimated overall risk of retinopathy induced after taking HCQ was 0.65%, according to a study published in 2010 that included data from the National Data Bank for Rheumatic Diseases on 3,995 patients with SLE or rheumatoid arthritis (RA) treated with HCQ.[8] This study concluded that HCQ toxicity is uncommon but increases markedly with the duration of therapy, rising about 1% after five to seven years. However, modern advanced modalities, including spectral domain optical coherence tomography (SD-OCT) combined with automated 10-2 visual field assessment (VFA) as well as multifocal

Supported in part by the National Science and Technology Council of Taiwan (NSTC 113-2628-B-006-009 to Dr Lai and MOST 111-2341-B-006-066 to Dr Weng). The funder had no role in considering the study design or in the collection, analysis, interpretation of data, writing of the report, or decision to submit the article for publication.

[1]School of Pharmacy, Institute of Clinical Pharmacy and Pharmaceutical Sciences, College of Medicine, National Cheng Kung University, Tainan, Taiwan; [2]Population Health Data Center, National Cheng Kung University, Tainan, Taiwan; [3]Spencer Center for Vision Research, Byers Eye Institute, Stanford University School of Medicine, Palo Alto, California; [4]Department of Ophthalmology, National Cheng Kung University Hospital, College of Medicine, National Cheng Kung University, Tainan, Taiwan; [5]School of Medicine, College of Medicine, National Cheng Kung University, Tainan, Taiwan; [6]Department of Pharmacy Systems, Outcomes and Policy, College of Pharmacy, University of Illinois at Chicago; [7]Department of Internal Medicine, Division of Allergy, Immunology, and Rheumatology, National Cheng Kung University Hospital, College of Medicine, National Cheng Kung University, Tainan, Taiwan.

Additional supplementary information cited in this article can be found online in the Supporting Information section (https://acrjournals.onlinelibrary.wiley.com/doi/10.1002/art.70022).

Author disclosures and graphical abstract are available at https://onlinelibrary.wiley.com/doi/10.1002/art.70022.

Address correspondence via email to Meng-Yu Weng, MD, PhD, at maggieweng69@gmail.com.

Submitted for publication March 20, 2025; accepted in revised form November 3, 2025.

electroretinography (mfERG) and fundus autofluorescence, have enabled detection of the early signs of HCQ retinopathy, which in turn increased estimated overall prevalence of HCQ retinopathy. A 2010 study using modern standard screening modalities (detection by SD-OCT or VFA) reported that the overall prevalence of HCQ retinopathy was 7.5%, which was nearly 10 times higher than a preceding report.[9] Guidelines from the American Academy of Ophthalmology (AAO) proposed a baseline fundus examination and annual screening with automated visual fields and SD-OCT after five years of HCQ treatment. Both mfERG and fundus autofluorescence can also be used to improve the accuracy of diagnosis.

In a recent cohort with active surveillance retinopathy screening, the cumulative incidences of retinopathy at 15 years were 21.6% for higher than 6 mg/kg/day, 11.4% for 5 to 6 mg/kg/day, and 2.7% for 5 mg/kg/day or lower.[10] To prevent HCQ retinopathy, the AAO and updated EULAR recommendations suggested a maximum daily HCQ use of ≤5.0 mg/kg real weight.[1,10] However, studies have suggested that an HCQ dose of less than 6.5 mg/kg/day (400 mg or less daily) may not be able to prevent SLE activity and organ damage.[11–13] Moreover, low HCQ blood levels are associated with thrombotic events in SLE.[14]

The optimal daily dose that balances efficacy and safety remains a topic of debate. A maximum daily dosage of ≤5.0 mg/kg may reflect a prioritization of concerns about HCQ retinopathy over managing SLE activity and the complications of SLE. Recent case-crossover studies revealed an association between higher-dose HCQ and decreased risk of lupus flare–related hospitalization among patients with SLE.[15,16] Balancing the effectiveness of managing SLE disease severity against the safety of HCQ retinopathy is crucial. The objective of our study is to weigh the dose-response relationship of HCQ for both effectiveness and safety in patients with SLE, using a target trial emulation study framework.[12]

METHODS

Data source. This nationwide study retrieved data from Taiwan's National Health Insurance Research Database (NHIRD) from 2010 to 2021. The NHIRD includes demographic information and medical claims for outpatient, inpatient, and emergency care services of about 23 million people (nearly 99.9% of the entire population of Taiwan).[17,18] Several diagnosis codes for major diseases in the claims database have been validated by previous studies.[19,20] We linked the NHIRD and Taiwan Cancer Registry to capture the diagnosis of malignancy.[21] We also used catastrophic illness certification (CIC) to capture the current diagnosis of SLE; CIC is necessarily reviewed by experts, ensuring high accuracy in the diagnosis.[18] The National Cheng Kung University Human Research Ethics Committee approved this study (NCKUH IRB no. B-ER-110-524).

Specification of the target trial. We hypothesized an open-labeled, randomized, pragmatic trial to evaluate safety and effectiveness outcomes relating to coronary artery disease (CAD), ischemic stroke, venous thromboembolism (VTE), end-stage renal disease (ESRD), malignancy, and retinopathy among patients with SLE receiving different doses of HCQ. The key components of the trial emulation are presented in Supplementary Table 1. Specifically, we included patients with SLE aged 10 years and older who were receiving their first dose of HCQ and had no history of outcomes of interest and no other systemic autoimmune disease at baseline. The average body weight for patients with SLE in Taiwan was 60 kg, as the majority were young women. Each HCQ tablet contained 200 mg, and the typical clinical dose was either one tablet per day (ie, 200 mg/day) or two tablets per day (ie, 400 mg/day). We selected at random patients who were receiving either a higher dose (≥400 mg per day) or a lower dose (<400 mg per day) of HCQ. The causal contrasts of interest were the intention-to-treat effect.[22]

Emulation of the target trial. We emulated the trial using Taiwan's NHIRD. The study design diagram is provided in Supplementary Figure 1. All eligibility criteria were analogous to the target trial. Specifically, the index date was defined as the first prescription date of HCQ. We retrieved data covering one year before the index date to ensure patients were new users of HCQ, had no outcome-of-interest history, and had no other systemic autoimmune disease at baseline. We confirmed the patients' diagnosis of SLE by using the *International Classification of Diseases, Ninth Revision, Clinical Modification* (ICD-9-CM) codes 710.0 or ICD-10-CM codes M32 together with CIC.

We classified patients into higher- or lower-dose treatment strategies based on the dosage of their first HCQ prescription. To emulate the randomization of the target trial with the two comparison treatment strategies sharing the same probability of treatment assignment, we implemented a propensity score with inverse probability weighting. We estimated the target of inference as the average treatment effect for the entire SLE population. Briefly, we calculated the propensity score using logistic regression based on the measured covariates listed in Supplementary Tables 2 to 5. These covariates were identified based on a literature review and expert opinions, including patient age at index date, sex, insurance premium, and index year. We also considered patients' comorbidities and medication use based on the medical records from one year before the index date (Supplementary Figure 1).

Study outcomes and follow-up period. In parallel with a target trial, the effectiveness outcomes of interest were CAD, ischemic stroke, VTE, ESRD, and malignancy. The safety outcome of interest was HCQ retinopathy. The definitions of these outcomes, validated by previous studies with positive predictive values of 92.0% for CAD, 97.9% for ischemic stroke, and 93.6%

for malignancy, are provided in Supplementary Table 6.[19,23] We employed as-started analysis, an analogue of intention-to-treat effect, and observed patients from the index date until the occurrence of study outcomes, loss to follow-up, death, or end of the study period (December 31, 2021), whichever occurred first.

Statistical analysis. We calculated the standardized mean differences (SMDs) to assess differences in the covariates between the two groups. An SMD value of less than 0.1 was considered as indicating no difference between the groups.[24] We estimated the cumulative incidence curves for each study outcome using the Kaplan-Meier function. We applied the Cox proportional hazards models to estimate the hazard ratio (HR) and 95% confidence interval (CI) for each outcome. We conducted a Bonferroni correction across all analyses to address multiplicity. All statistical analyses were conducted with SAS software, version 9.4 (SAS Institute, Inc).

Sensitivity analyses. We conducted a series of sensitivity analyses to test the robustness of the analysis. First, we reported the rate of patients receiving eye examinations within one and five years after initiating HCQ to determine if the probability of detecting HCQ retinopathy differs between two treatment strategies. Second, to minimize extreme weighting, we calculated the propensity score and stabilized weights by the prevalence of higher-dose HCQ. Third, to avoid undue influence of outliers, we truncated the weights at the 99.5th percentile. Fourth, to estimate the target of inference separately from the main analysis in the entire SLE population, we implemented a propensity score with matching and determined the average treatment effect among patients initiating a higher dose of HCQ. Fifth, to evaluate the per-protocol effect among patients fully adhering to treatment strategies, we repeated the analyses using on-treatment causal contrasts of interest. In the on-treatment analysis to emulate the per-protocol effect, follow-up began at the index date and ended at either the occurrence of study outcomes, loss to follow-up, death, the censoring of patients whose treatments changed or discontinued, or end of the study period. Sixth, we conducted a series of sensitivity analyses with alternative dose thresholds for higher- and lower-dose treatment to assess robustness to dose definition.

Subgroup analyses. To examine if the risk profiles changed, we repeated the analyses for different patient subgroups by patient age (<45 or ≥45 years), sex (male or female), and index year (2010–2013, 2014–2017, or 2018–2021). Furthermore, to examine if other systemic autoimmune diseases had resulted in effect modification impacting the risk of study outcomes, we included patients with systemic autoimmune diseases

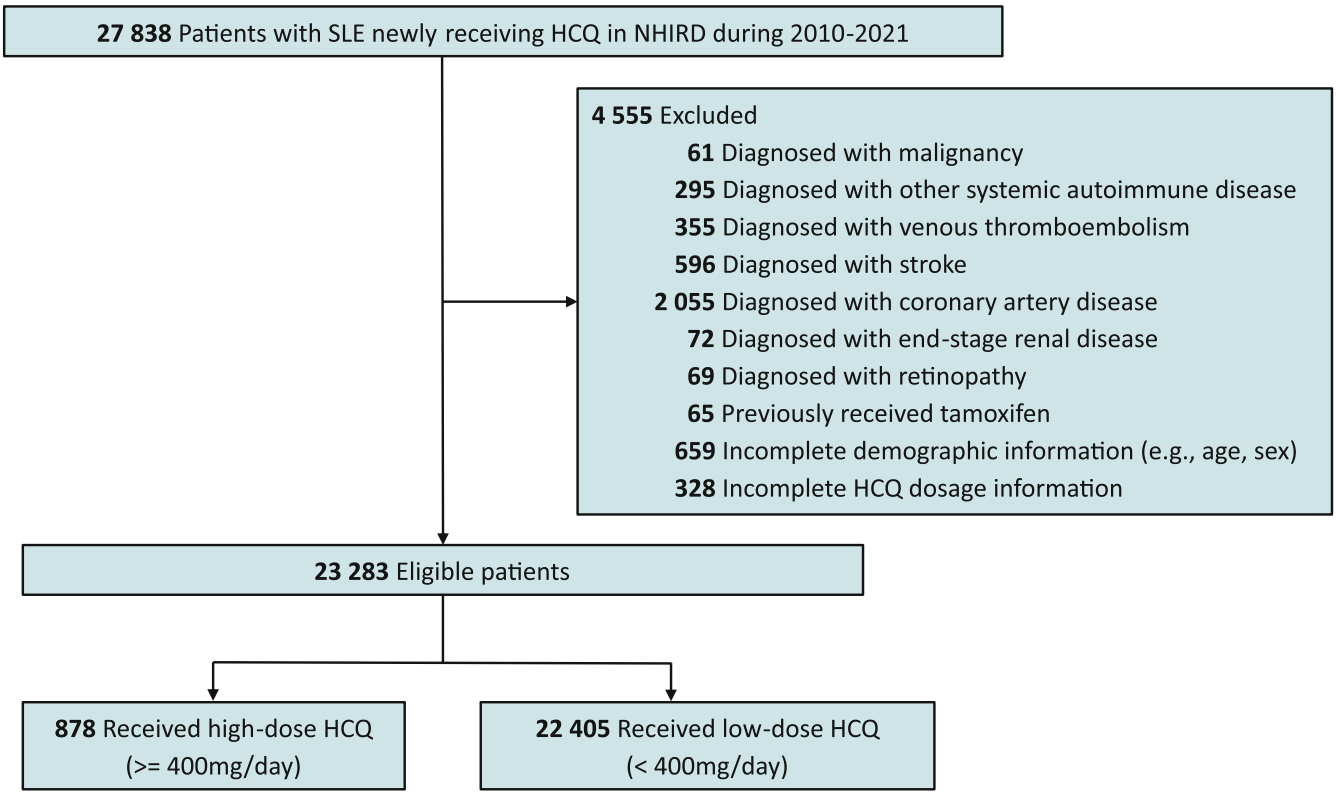

Figure 1. Flowchart of study population selection. HCQ, hydroxychloroquine; NHIRD, National Health Insurance Research Database; SLE, systemic lupus erythematosus. Color figure can be viewed in the online issue, which is available at http://onlinelibrary.wiley.com/doi/10.1002/art.70022/abstract.

Table 1. Baseline characteristics before and after weighting*

Baseline characteristics[a,b]	Original population			Weighted cohort with IPTW		
	Higher-dose HCQ (n = 878)	Lower-dose HCQ (n = 22,405)	SMD	Higher-dose HCQ (n = 21,963)	Lower-dose HCQ (n = 23,293)	SMD
Age, mean (SD), y	39 (18.9)	43.7 (17.2)	−0.259	43.1 (18.4)	43.5 (17.6)	−0.005
Sex, n (%)						
Male	155 (17.7)	3,261 (14.6)	0.084	3,305 (15)	3,406 (14.6)	0.012
Female	723 (82.3)	19,144 (85.4)	−0.084	18,658 (85)	19,888 (85.4)	−0.012
Insurance premium level, n (%)						
<30,000 NTD	387 (44.1)	10,463 (46.7)	−0.053	10,332 (47)	10,853 (46.6)	0.009
30,001–45,000 NTD	107 (12.2)	3,819 (17)	−0.138	3,447 (15.7)	3,927 (16.9)	−0.031
>45,000 NTD	80 (9.1)	2,649 (11.8)	−0.089	2,419 (11)	2,729 (11.7)	−0.022
Dependent	304 (34.6)	5,474 (24.4)	0.225	5,765 (26.2)	5,785 (24.8)	0.032
Index year, n (%)						
2010–2013	313 (35.6)	8,776 (39.2)	−0.073	8,443 (38.4)	9,147 (39.3)	−0.017
2014–2017	309 (35.2)	7,621 (34)	0.025	7,601 (34.6)	7,933 (34.1)	0.012
2018–2021	256 (29.2)	6,008 (26.8)	0.052	5,920 (27)	6,213 (26.7)	0.006
Lupus nephritis, n (%)	286 (32.6)	2,309 (10.3)	0.564	3,079 (14)	2,607 (11.2)	0.085
Daily dose of steroids, n (%)[c]						
≤7.5 mg/day	127 (14.5)	4,017 (17.9)	−0.094	5,234 (23.8)	6,141 (26.4)	−0.058
7.5–15 mg/day	186 (21.2)	5,957 (26.6)	−0.127	2,905 (13.2)	2,901 (12.5)	0.023
15–30 mg/day	163 (18.6)	2,739 (12.2)	0.176	3,345 (15.2)	4,143 (17.8)	−0.069
>30 mg/day	316 (36.0)	2,116 (9.4)	0.668	2,912 (13.3)	2,446 (10.5)	0.085
Physical comorbidities, n (%)						
Antiphospholipid syndrome	21 (2.4)	382 (1.7)	0.049	382 (1.7)	404 (1.7)	0.000
Anxiety disorders	63 (7.2)	2,407 (10.7)	−0.125	2,520 (11.5)	2,471 (10.6)	0.028
Cataract	51 (5.8)	1,587 (7.1)	−0.052	1,221 (5.6)	1,638 (7)	−0.061
Chronic kidney disease	83 (9.5)	1,171 (5.2)	0.163	1,250 (5.7)	1,256 (5.4)	0.013
Liver disorders	80 (9.1)	1900 (8.5)	0.022	1,519 (6.9)	1979 (8.5)	−0.059
Congestive heart failure	51 (5.8)	491 (2.2)	0.185	743 (3.4)	545 (2.3)	0.063
Depressive disorders	40 (4.6)	1,229 (5.5)	−0.043	1,051 (4.8)	1,270 (5.5)	−0.03
Diabetes mellitus	65 (7.4)	1,534 (6.8)	0.022	1,185 (5.4)	1,600 (6.9)	−0.061
Fibromyalgia	14 (1.6)	768 (3.4)	−0.117	834 (3.8)	782 (3.4)	0.024
Glaucoma	16 (1.8)	474 (2.1)	−0.021	624 (2.8)	491 (2.1)	0.047
Hypertension	124 (14.1)	2,568 (11.5)	0.08	2,679 (12.2)	2,696 (11.6)	0.019
Hyperlipidemia	94 (10.7)	2,812 (12.6)	−0.058	2,320 (10.6)	2,907 (12.5)	−0.06
Osteoporosis	31 (3.5)	841 (3.8)	−0.012	1,164 (5.3)	873 (3.7)	0.075
Medication use, n (%)						
Immunosuppressants	118 (13.4)	2,352 (10.5)	0.091	3,207 (14.6)	2,474 (10.6)	0.12
Antacids	305 (34.7)	7,963 (35.5)	−0.017	7,844 (35.7)	8,272 (35.5)	0.004
Antiarrhythmic drugs	39 (4.4)	534 (2.4)	0.114	576 (2.6)	574 (2.5)	0.01
Antidepressants	22 (2.5)	681 (3)	−0.033	553 (2.5)	703 (3)	−0.03
Antiosteoporotic drugs	116 (13.2)	2,669 (11.9)	0.039	2,938 (13.4)	2,788 (12)	0.042
Antiplatelet drugs	120 (13.7)	2,693 (12)	0.049	2,462 (11.2)	2,817 (12.1)	−0.027
Anxiolytics	304 (34.6)	6,660 (29.7)	0.105	6,627 (30.2)	6,970 (29.9)	0.006
Beta-blockers	169 (19.2)	3,787 (16.9)	0.061	3,759 (17.1)	3,961 (17)	0.003
Calcium-channel blockers	204 (23.2)	3,233 (14.4)	0.227	3,430 (15.6)	3,444 (14.8)	0.023
Glucocorticoids	792 (90.2)	14,829 (66.2)	0.608	14,395 (65.5)	15,631 (67.1)	−0.033
Diuretics	359 (40.9)	3,378 (15.1)	0.6	4,319 (19.7)	3,751 (16.1)	0.093
H_2 blockers	459 (52.3)	9,145 (40.8)	0.231	9,225 (42)	9,610 (41.3)	0.015
Hypnotics and sedatives	163 (18.6)	3,590 (16)	0.067	3,792 (17.3)	3,755 (16.1)	0.031
Hypoglycemic agents	83 (9.5)	1,298 (5.8)	0.138	1,221 (5.6)	1,383 (5.9)	−0.016
Nonsteroidal anti-inflammatory drugs	728 (82.9)	17,750 (79.2)	0.094	17,249 (78.5)	18,485 (79.4)	−0.02
Proton pump inhibitors	175 (19.9)	2,715 (12.1)	0.214	3,094 (14.1)	2,896 (12.4)	0.049
Renin system inhibitors	211 (24)	3,501 (15.6)	0.212	3,680 (16.8)	3,720 (16)	0.021
Statins	72 (8.2)	1,857 (8.3)	−0.003	1,860 (8.5)	1932 (8.3)	0.006

* HCQ, hydroxychloroquine; IPTW, inverse probability of treatment weighting; NTD, new taiwan dollar; SMD, standardized mean difference.
[a] All covariates listed in the table were used to calculate the propensity score with inverse probability of treatment weighting.
[b] Type 1 diabetes and the use of medications for lupus nephritis were included as covariates in the propensity score model. The number of prevalent cases of these covariates was less than 3, considered identifiable. Due to privacy protection, these numbers were not reported.
[c] The daily dose of steroids is calculated by prednisolone-equivalent dose.

as a distinct target population separate from the main analysis, and we repeated the analyses.

Patient and public involvement. Taiwan's NHIRD contained anonymized patient-related data to enhance confidentiality. The research questions and study design were independently determined without the involvement of patients. We intend to share the findings of this study with all participants and to make them available to relevant communities upon request.

RESULTS

Patient characteristics. We included a total of 878 (3.77%) patients initiating higher-dose HCQ and 22,405 (96.22%) patients initiating lower-dose HCQ, with a mean age of 39 years (SD 18.9) and 43.7 years (SD 17.2), respectively (Figure 1). The median doses of HCQ were 453.37 mg/day and 350.00 mg/day in the higher-dose HCQ and lower-dose HCQ groups, respectively. After applying inverse probability weighting of propensity score methods, the weighted population comprised 21,963 patients in the higher-dose HCQ group and 23,293 patients in the lower-dose HCQ group (Supplementary Figure 2). Table 1 shows the baseline characteristics of the weighted cohort with the average treatment effects among the entire population. All measured covariates were well balanced between the two treatment groups (Supplementary Figure 3). The overall median follow-up durations in the higher-dose HCQ and lower-dose HCQ groups were 5.35 and 6.15 years, respectively.

Effectiveness outcomes. For CAD, the incidence rates for the higher- and lower-dose groups were 1.48 (95% CI 1.42–1.55) and 1.73 (95% CI 1.67–1.81) per 100 person-years, with an HR of 0.86 (95% CI 0.80–0.93). For ischemic stroke, the incidence rates for the higher- and lower-dose groups were 0.48 (95% CI 0.45–0.52) and 0.45 (95% CI 0.42–0.49) per 100 person-years, with an HR of 1.06 (95% CI 0.91–1.23). For VTE, the incidence rates for the higher- and lower-dose groups were 0.13 (95% CI 0.11–0.15) and 0.32 (95% CI 0.29–0.35) per 100 person-years, with an HR of 0.40 (95% CI 0.33–0.49). For ESRD, the incidence rates for the higher- and lower-dose groups were 0.35 (95% CI 0.32–0.38) and 0.36 (95% CI 0.33–0.39) per 100 person-years, with an HR of 0.99 (95% CI 0.84–1.17). For malignancy, the incidence rates for the higher- and lower-dose groups were 0.64 (95% CI 0.60–0.68) and 0.66 (95% CI 0.61–0.70) per 100 person-years, with an HR of 1.02 (95% CI 0.93–1.12) (Table 2).

HCQ retinopathy. For HCQ retinopathy, the incidence rates for the higher- and lower-dose groups were 0.12 (95% CI 0.11–0.14) and 0.14 (95% CI 0.12–0.16) per 100 person-years, with an HR of 0.92 (95% CI 0.70–1.21) (Table 2). We further performed subgroup analyses and found that in patients aged ≥45 years, the HR of retinopathy for higher-dose HCQ versus lower-dose HCQ was 1.87 (95% CI 1.45–2.42). Additionally, the rates of patients receiving eye examinations within one year after initiating HCQ were 14.4% and 14.8% in the higher-dose HCQ and lower-dose HCQ groups, respectively. The rates slightly increased within three and five years after initiating HCQ but did

Table 2. Study outcomes in patients newly receiving higher-dose HCQ and lower-dose HCQ*

	Original population			Weighted cohort with IPTW		
Study outcomes	Events, n	Incidence rate[a] (95% CI)	HR (95% CI)	Events, n	Incidence rate[a] (95% CI)	HR (95% CI)[b]
Coronary artery disease						
Higher-dose HCQ	55	1.17 (0.88–1.52)	0.67 (0.51–0.87)	1,854	1.48 (1.42–1.55)	0.86 (0.80–0.93)
Lower-dose HCQ	2,295	1.74 (1.67–1.82)	1.00 (reference)	2,376	1.73 (1.67–1.81)	1.00 (reference)
Ischemic stroke						
Higher-dose HCQ	29	0.61 (0.41–0.87)	1.34 (0.92–1.94)	626	0.48 (0.45–0.52)	1.06 (0.91–1.23)
Lower-dose HCQ	623	0.45 (0.42–0.49)	1.00 (reference)	651	0.45 (0.42–0.49)	1.00 (reference)
Venous thromboembolism						
Higher-dose HCQ	10	0.21 (0.10–0.38)	0.65 (0.35–1.21)	167	0.13 (0.11–0.15)	0.40 (0.33–0.49)
Lower-dose HCQ	435	0.31 (0.28–0.34)	1.00 (reference)	455	0.32 (0.29–0.35)	1.00 (reference)
End-stage renal disease						
Higher-dose HCQ	33	0.58 (0.39–0.84)	1.85 (1.26–2.71)	461	0.35 (0.32–0.38)	0.99 (0.84–1.17)
Lower-dose HCQ	470	0.32 (0.29–0.35)	1.00 (reference)	514	0.36 (0.33–0.39)	1.00 (reference)
Malignancy						
Higher-dose HCQ	26	0.43 (0.27–0.66)	0.69 (0.45–1.06)	1,087	0.64 (0.60–0.68)	1.02 (0.93–1.12)
Lower-dose HCQ	952	0.66 (0.62–0.70)	1.00 (reference)	982	0.66 (0.61–0.70)	1.00 (reference)
HCQ retinopathy						
Higher-dose HCQ	6	0.12 (0.05–0.27)	0.88 (0.39–1.97)	164	0.12 (0.11–0.14)	0.92 (0.70–1.21)
Lower-dose HCQ	196	0.14 (0.12–0.16)	1.00 (reference)	205	0.14 (0.12–0.16)	1.00 (reference)

* CI, confidence interval; HCQ, hydroxychloroquine; HR, hazard ratio; IPTW, inverse probability of treatment weighting.
[a] Per 100 person-years.
[b] The HRs with 95% CIs were adjusted by using a Bonferroni correction to address multiplicity.

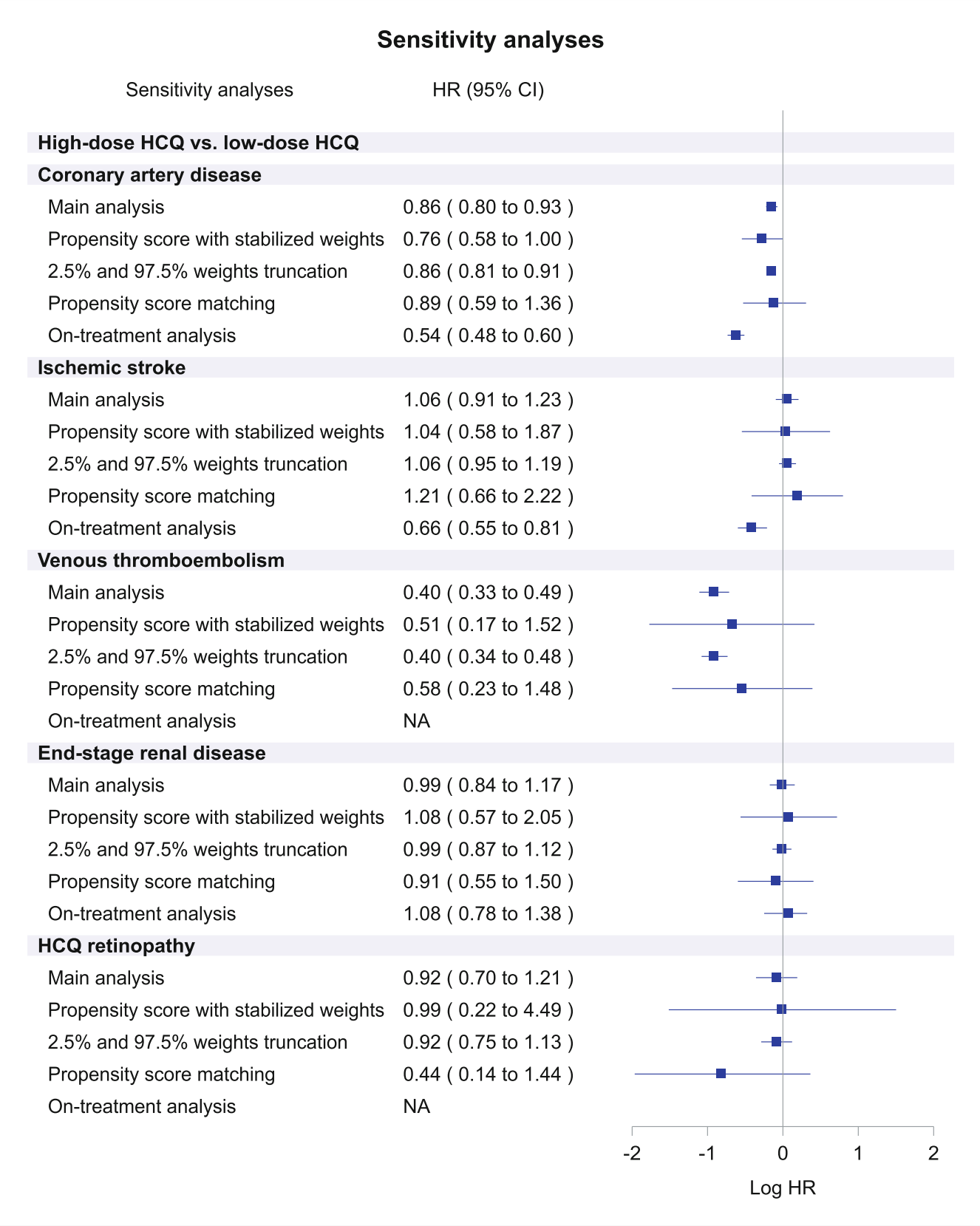

Figure 2. Hazard ratios of study outcomes in sensitivity analyses. The solid line indicates no difference between the two groups (HR = 1). Due to the limited number of events in the on-treatment analyses, we did not report the HRs for venous thromboembolism and HCQ retinopathy. CI, confidence interval; HCQ, hydroxychloroquine; HR, hazard ratio; NA, not applicable.

not differ between the two treatment strategies (23.3% vs 24.1% within three years and 27.4% vs 29.5% within five years).

Sensitivity analyses. All sensitivity analyses yielded results consistent with the main analyses, summarized in Figure 2, Supplementary Figure 4, Table 7 and 8. After we included antiphospholipid syndrome as a covariate, the HRs for both effectiveness and safety outcomes remained consistent with the main analyses. Although the CIs from propensity score matching analyses are wide due to the limited sample size, the trends in effectiveness and safety outcomes were similar. Furthermore, the on-treatment analyses also showed consistent HRs for effectiveness outcomes. Due to the limited number of events in the on-treatment analyses, we did not report HRs for VTE and HCQ retinopathy.

Subgroup analyses. We did not find significant interactions between patient subgroups in the stratified analyses by patients' baseline age, sex, or index year, as summarized in Figure 3. Additionally, the stratified analyses of rare outcomes, such as VTE and HCQ retinopathy, did not reach sufficient statistical power within patient subgroups.

DISCUSSION

Our findings suggested that different doses of HCQ did have distinct therapeutic effects among patients with SLE. We found higher-dose HCQ was associated with a reduced risk of CAD and VTE, but there was no associated risk of ischemic stroke, ESRD, and malignancy compared to lower-dose HCQ in patients with SLE. Additionally, we observed no dose-related difference in the risk of HCQ retinopathy, except for patients with SLE aged over 45 years.

Our findings suggested around a 15% reduction in risk of CAD and a 60% reduction in risk of VTE in patients receiving higher-dose HCQ. In a recent nested case-control study including patients with SLE and RA, researchers found that reduced risks of combined cardiovascular events and VTE were associated with current HCQ use.[23] Randomized clinical trials have demonstrated that treatment with 400 mg/day of HCQ resulted in a significant improvement of lipid metabolism, with a decrease in total cholesterol and serum low-density lipoprotein levels and an increase in high-density lipoprotein cholesterol.[25,26] Some prospective cohort studies also showed improvement of proinflammatory cytokine profiles in SLE treated with HCQ.[27,28] HCQ might reduce the risk of antiphospholipid syndrome.[14,29] The previous studies showed decreased risk of CAD and VTE among patients with SLE treated with HCQ.[30–33] Further to this, our study results confirmed that HCQ dosage also affects efficacy.

Antimalarials may have antineoplastic properties, as assessed in a previous study.[34] Results from a meta-analysis showed that HCQ might be a protective factor for cancer in patients with SLE.[35] Our findings indicate no difference in the risk of malignancy and ESRD between patients with SLE in the higher-dose HCQ group and those in the lower-dose HCQ group. The cancer protection effect of HCQ may not be influenced by the dose.

In recent years, due to advancements in ophthalmic examination methods, the detection rate of HCQ retinopathy has increased. This has brought considerable attention to the side effects of this drug. The daily dose of HCQ and how best to compromise between efficacy and safety is a matter of debate. Our study showed no significant risk of HCQ retinopathy among patients receiving higher-dose HCQ compared to those receiving lower-dose HCQ, which contrasts with previous studies.[10,36,37] However, we observed an increased risk of HCQ retinopathy in patients with SLE aged over 45 years receiving higher-dose HCQ compared to lower-dose HCQ. Two possible explanations could account for these differences. First, our database predominantly consists of Asian populations, which may have unique genetic backgrounds that could theoretically influence drug susceptibility differently when compared to Western populations.[38] Second, the mean age of our study population was less than 45 years. Retinal thickness is known to decrease with age; thus, patients with SLE aged over 45 years may be more vulnerable to the retinal effects of HCQ.[37,39] A previous study has shown that older age at the time of initiating HCQ treatment was associated with retinopathy risk.[37] In our subgroup analyses, we observed an increased risk of HCQ retinopathy in patients with SLE aged over 45 years receiving higher-dose HCQ compared to lower-dose HCQ.

Previous studies related to HCQ retinal toxicity have mostly focused on whether HCQ was taken, the duration of HCQ use, and the cumulative dose of HCQ that leads to the risk of retinal toxicity. Recent case-crossover studies found that a higher HCQ weight-based dose (>5 vs ≤5 mg/kg/day) and a non–weight-based dose (≥400 vs <400 mg/day) were each associated with decreased risk of lupus flares and hospitalization for active SLE.[15,16] However, there has been little discussion on whether different doses affect both the treatment effectiveness and side effects at the same time.

We have several strengths in our study. First, we conducted the research using the NHIRD, which allowed us to include the largest number of participants to evaluate this relatively rare outcome. Second, we pursued a target trial emulation framework to explicitly specify the protocol of the target trial and its observational emulation. This can align the time of eligibility criteria and treatment strategy assignment to avoid potential selection bias.[40]

There are some limitations to our study. First, residual confounding cannot be ruled out. We did not have information on smoking status, obesity, contraceptive use, or laboratory test values or detailed information on SLE disease activity, which prevented a detailed evaluation of SLE disease activity using the national database. However, we have considered the daily dose of steroids and comorbidities and medication as a proxy for SLE

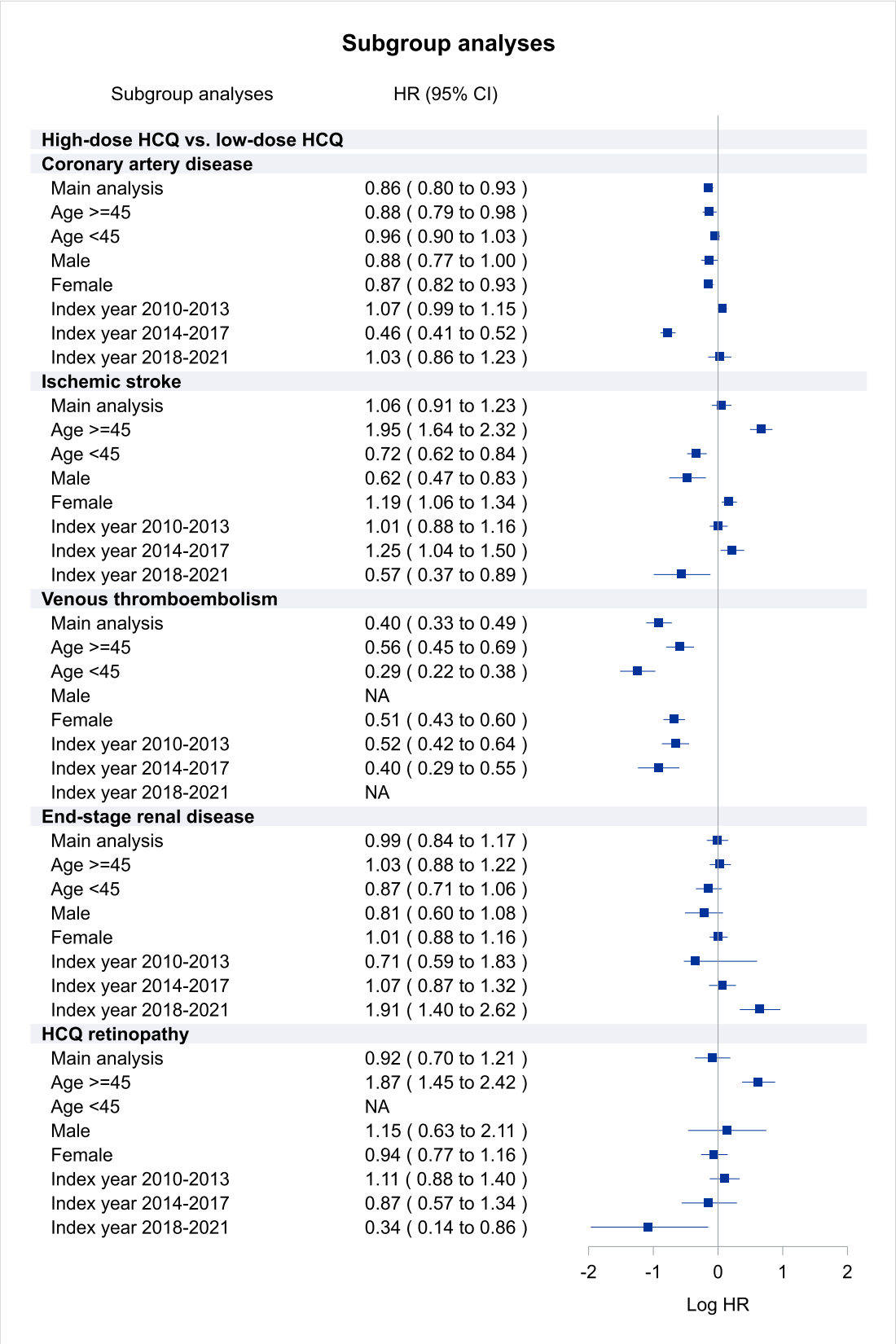

Figure 3. Harzard ratios of study outcomes in subgroup analyses. The solid line indicates no difference between the two groups (HR = 1). Due to the limited number of events in the subgroup analyses, we did not report the HRs for venous thromboembolism and HCQ retinopathy in patients aged less than 45 years old and index date 2018 to 2021. CI, confidence interval; HCQ, hydroxychloroquine; HR, hazard ratio; NA, not applicable. Color figure can be viewed in the online issue, which is available at http://onlinelibrary.wiley.com/doi/10.1002/art.70022/abstract.

disease activity in different groups to avoid potential confounding by indication. Additionally, the dose of HCQ depended on the clinician's preference, with no recommendations for higher-dose HCQ for patients with specific indications, such as SLE disease activity. Second, the screening rates for HCQ retinopathy were relatively low. Our findings indicate the clinical need to increase screening rates among patients with SLE receiving HCQ. As the screening rates were nondifferential between the two treatment strategies in our study, this may cause underestimation of the risk of HCQ retinopathy. Third, because the number of patients receiving higher-dose HCQ was small, the weighted population was larger than the actual study population. To address this issue, we conducted sensitivity analyses by stabilizing weights according to the prevalence of higher-dose HCQ. This approach ensured that the sum of the stabilized weights reflected the actual sample size, and the result remained consistent. Fourth, our study may have underestimated the risk of HCQ retinopathy due to a limited follow-up duration of up to 6.15 years. A previous study using the Rochester Epidemiology Project found that the cumulative incidence rate of HCQ retinopathy at year 5 was 0%, which increased to 3.9% by 10 years.[41] Fifth, the average body weight in the Taiwanese population (approximately 60 kg) may limit the generalizability of our findings to countries with higher rates of excess weight and obesity. Although the lower-dose group had a median of 350 mg/day, which is higher than lower-dose definitions in previous studies, sensitivity analyses comparing ≥400 mg/day versus ≤300 mg/day showed results consistent with the main analyses. Sixth, the small sample size of patients using higher-dose HCQ may limit our ability to evaluate certain rare study outcomes, including ischemic stroke, malignancy, ESRD, and HCQ retinopathy.

For patients with SLE, higher-dose HCQ improves effectiveness, with reduced risks of CAD and VTE. We observed no dose-related difference in the risk of HCQ retinopathy, except for patients with SLE aged over 45 years. Our study emphasizes the need for weighing the benefits and risks of optimal HCQ dosage in managing SLE.

AUTHOR CONTRIBUTIONS

All authors contributed to at least one of the following manuscript preparation roles: conceptualization AND/OR methodology, software, investigation, formal analysis, data curation, visualization, and validation AND drafting or reviewing/editing the final draft. As corresponding author, Dr Weng confirms that all authors have provided the final approval of the version to be published and takes responsibility for the affirmations regarding article submission (eg, not under consideration by another journal), the integrity of the data presented, and the statements regarding compliance with institutional review board/Declaration of Helsinki requirements.

REFERENCES

1. Fanouriakis A, Kostopoulou M, Alunno A, et al. 2019 update of the EULAR recommendations for the management of systemic lupus erythematosus. Ann Rheum Dis 2019;78(6):736–745. doi:https://doi.org/10.1136/annrheumdis-2019-215089
2. Gordon C, Amissah-Arthur MB, Gayed M, et al; British Society for Rheumatology Standards, Audit and Guidelines Working Group. The British Society for Rheumatology guideline for the management of systemic lupus erythematosus in adults. Rheumatology (Oxford) 2018;57(1):e1–e45. doi:https://doi.org/10.1093/rheumatology/kex286
3. Pons-Estel BA, Bonfa E, Soriano ER, et al; Grupo Latino Americano de Estudio del Lupus (GLADEL) and Pan-American League of Associations of Rheumatology (PANLAR). First Latin American clinical practice guidelines for the treatment of systemic lupus erythematosus: Latin American Group for the Study of Lupus (GLADEL, *Grupo Latino Americano de Estudio del Lupus*)-Pan-American League of Associations of Rheumatology (PANLAR). Ann Rheum Dis 2018;77(11):1549–1557. doi:https://doi.org/10.1136/annrheumdis-2018-213512
4. Alarcón GS, McGwin G, Bertoli AM, et al; LUMINA Study Group. Effect of hydroxychloroquine on the survival of patients with systemic lupus erythematosus: data from LUMINA, a multiethnic US cohort (LUMINA L). Ann Rheum Dis 2007;66(9):1168–1172. doi:https://doi.org/10.1136/ard.2006.068676
5. Pons-Estel GJ, Alarcón GS, McGwin G Jr, et al; Lumina Study Group. Protective effect of hydroxychloroquine on renal damage in patients with lupus nephritis: LXV, data from a multiethnic US cohort. Arthritis Rheum 2009;61(6):830–839. doi:https://doi.org/10.1002/art.24538
6. Clowse ME, Magder L, Witter F, et al. Hydroxychloroquine in lupus pregnancy. Arthritis Rheum 2006;54(11):3640–3647. doi:https://doi.org/10.1002/art.22159
7. Hahn BH, McMahon MA, Wilkinson A, et al; American College of Rheumatology. American College of Rheumatology guidelines for screening, treatment, and management of lupus nephritis. Arthritis Care Res (Hoboken) 2012;64(6):797–808. doi:https://doi.org/10.1002/acr.21664
8. Wolfe F, Marmor MF. Rates and predictors of hydroxychloroquine retinal toxicity in patients with rheumatoid arthritis and systemic lupus erythematosus. Arthritis Care Res (Hoboken) 2010;62(6):775–784. doi:https://doi.org/10.1002/acr.20133
9. Melles RB, Marmor MF. The risk of toxic retinopathy in patients on long-term hydroxychloroquine therapy. JAMA Ophthalmol 2014;132(12):1453–1460. doi:https://doi.org/10.1001/jamaophthalmol.2014.3459
10. Marmor MF, Kellner U, Lai TY, et al; American Academy of Ophthalmology. Recommendations on screening for chloroquine and hydroxychloroquine retinopathy (2016 revision). Ophthalmology 2016;123(6):1386–1394. doi:https://doi.org/10.1016/j.ophtha.2016.01.058
11. Durcan L, Clarke WA, Magder LS, et al. Hydroxychloroquine blood levels in systemic lupus erythematosus: clarifying dosing controversies and improving adherence. J Rheumatol 2015;42(11):2092–2097. doi:https://doi.org/10.3899/jrheum.150379
12. Feldman CH, Yazdany J, Guan H, et al. Medication nonadherence is associated with increased subsequent acute care utilization among Medicaid beneficiaries with systemic lupus erythematosus. Arthritis Care Res (Hoboken) 2015;67(12):1712–1721. doi:https://doi.org/10.1002/acr.22636
13. Shaharir SS, Ghafor AH, Said MS, et al. A descriptive study of the factors associated with damage in Malaysian patients with lupus nephritis. Lupus 2014;23(4):436–442. doi:https://doi.org/10.1177/0961203313518624
14. Petri M, Konig MF, Li J, et al. Association of higher hydroxychloroquine blood levels with reduced thrombosis risk in systemic lupus erythematosus. Arthritis Rheumatol 2021;73(6):997–1004. doi:https://doi.org/10.1002/art.41621
15. Jorge AM, Mancini C, Zhou B, et al. Hydroxychloroquine dose per ophthalmology guidelines and the risk of systemic lupus

erythematosus flares. JAMA 2022;328(14):1458–1460. doi:https://doi.org/10.1001/jama.2022.13591

16. Nestor J, Choi H, Mancini C, et al. Hydroxychloroquine dose and hospitalizations for active lupus. Arthritis Rheumatol 2024;76(10):1512–1517. doi:https://doi.org/10.1002/art.42924
17. Hsing AW, Ioannidis JP. Nationwide population science: lessons from the Taiwan National Health Insurance Research Database. JAMA Intern Med 2015;175(9):1527–1529. doi:https://doi.org/10.1001/jamainternmed.2015.3540
18. Hsieh CY, Shao SC, Sung SF, et al. Taiwan's National Health Insurance Research Database (NHIRD): in the Era of Artificial Intelligence, Causal Inference, and Data Security. Clin Epidemiol 2025;17:967–981. Published 2025 Nov 25. doi:https://doi.org/10.2147/CLEP.S553894
19. Hsieh CY, Chen CH, Li CY, et al. Validating the diagnosis of acute ischemic stroke in a National Health Insurance claims database. J Formos Med Assoc 2015;114(3):254–259. doi:https://doi.org/10.1016/j.jfma.2013.09.009
20. Sung SF, Hsieh CY, Lin HJ, et al. Validation of algorithms to identify stroke risk factors in patients with acute ischemic stroke, transient ischemic attack, or intracerebral hemorrhage in an administrative claims database. Int J Cardiol 2016;215:277–282. doi:https://doi.org/10.1016/j.ijcard.2016.04.069
21. Chiang CJ, Wang YW, Lee WC. Taiwan's Nationwide Cancer Registry System of 40 years: past, present, and future. J Formos Med Assoc 2019;118(5):856–858. doi:https://doi.org/10.1016/j.jfma.2019.01.012
22. Hernán MA, Hernández-Díaz S. Beyond the intention-to-treat in comparative effectiveness research. Clin Trials 2012;9(1):48–55. doi:https://doi.org/10.1177/1740774511420743
23. Cheng CL, Lee CH, Chen PS, et al. Validation of acute myocardial infarction cases in the National Health Insurance Research Database in Taiwan. J Epidemiol 2014;24(6):500–507. doi:https://doi.org/10.2188/jea.JE20140076
24. Austin PC. Balance diagnostics for comparing the distribution of baseline covariates between treatment groups in propensity-score matched samples. Stat Med 2009;28(25):3083–3107. doi:https://doi.org/10.1002/sim.3697
25. Babary H, Liu X, Ayatollahi Y, et al. Favorable effects of hydroxychloroquine on serum low density lipid in patients with systemic lupus erythematosus: a systematic review and meta-analysis. Int J Rheum Dis 2018;21(1):84–92. doi:https://doi.org/10.1111/1756-185X.13159
26. Kavanaugh A, Adams-Huet B, Jain R, et al. Hydroxychloroquine effects on lipoprotein profiles (the HELP trial): a double-blind, randomized, placebo-controlled, pilot study in patients with systemic lupus erythematosus. J Clin Rheumatol 1997;3(1):3–8. doi:https://doi.org/10.1097/00124743-199702000-00002
27. Willis R, Seif AM, McGwin G Jr, et al. Effect of hydroxychloroquine treatment on pro-inflammatory cytokines and disease activity in SLE patients: data from LUMINA (LXXV), a multiethnic US cohort. Lupus 2012;21(8):830–835. doi:https://doi.org/10.1177/0961203312437270
28. Monzavi SM, Alirezaei A, Shariati-Sarabi Z, et al. Efficacy analysis of hydroxychloroquine therapy in systemic lupus erythematosus: a study on disease activity and immunological biomarkers. Inflammopharmacology 2018;26(5):1175–1182. doi:https://doi.org/10.1007/s10787-018-0512-y
29. Wallace DJ. Does hydroxychloroquine sulfate prevent clot formation in systemic lupus erythematosus? Arthritis Rheum 1987;30(12):1435–1436. doi:https://doi.org/10.1002/art.1780301219
30. Jorge A, Lu N, Choi H, et al. Hydroxychloroquine use and cardiovascular events among patients with systemic lupus erythematosus and rheumatoid arthritis. Arthritis Care Res (Hoboken) 2023;75(4):743–748. doi:https://doi.org/10.1002/acr.24850
31. Haugaard JH, Dreyer L, Ottosen MB, et al. Use of hydroxychloroquine and risk of major adverse cardiovascular events in patients with lupus erythematosus: a Danish nationwide cohort study. J Am Acad Dermatol 2021;84(4):930–937. doi:https://doi.org/10.1016/j.jaad.2020.12.013
32. Yang DH, Leong PY, Sia SK, et al. Long-term hydroxychloroquine therapy and risk of coronary artery disease in patients with systemic lupus erythematosus. J Clin Med 2019;8(6):796. doi:https://doi.org/10.3390/jcm8060796
33. Grimaldi L, Duchemin T, Hamon Y, et al. Hydroxychloroquine and cardiovascular events in patients with systemic lupus erythematosus. JAMA Netw Open 2024;7(8):e2432190. doi:https://doi.org/10.1001/jamanetworkopen.2024.32190
34. Ruiz-Irastorza G, Ugarte A, Egurbide MV, et al. Antimalarials may influence the risk of malignancy in systemic lupus erythematosus. Ann Rheum Dis 2007;66(6):815–817. doi:https://doi.org/10.1136/ard.2006.067777
35. Li XB, Cao NW, Chu XJ, et al. Antimalarials may reduce cancer risk in patients with systemic lupus erythematosus: a systematic review and meta-analysis of prospective studies. Ann Med 2021;53(1):1687–1695. doi:https://doi.org/10.1080/07853890.2021.1981547
36. Melles RB, Jorge AM, Marmor MF, et al. Hydroxychloroquine dose and risk for incident retinopathy: a cohort study. Ann Intern Med 2023;176(2):166–173. doi:https://doi.org/10.7326/M22-2453
37. Jorge AM, Melles RB, Marmor MF, et al. Risk factors for hydroxychloroquine retinopathy and its subtypes. JAMA Netw Open 2024;7(5):e2410677. doi:https://doi.org/10.1001/jamanetworkopen.2024.10677
38. Ortega VE, Meyers DA. Pharmacogenetics: implications of race and ethnicity on defining genetic profiles for personalized medicine. J Allergy Clin Immunol 2014;133(1):16–26. doi:https://doi.org/10.1016/j.jaci.2013.10.040
39. Alamouti B, Funk J. Retinal thickness decreases with age: an OCT study. Br J Ophthalmol 2003;87(7):899–901. doi:https://doi.org/10.1136/bjo.87.7.899
40. Hernán MA, Sauer BC, Hernández-Díaz S, et al. Specifying a target trial prevents immortal time bias and other self-inflicted injuries in observational analyses. J Clin Epidemiol 2016;79:70–75. doi:https://doi.org/10.1016/j.jclinepi.2016.04.014
41. Dabit JY, Hocaoglu M, Moder KG, et al. Risk of hydroxychloroquine retinopathy in the community. Rheumatology (Oxford) 2022;61(8):3172–3179. doi:https://doi.org/10.1093/rheumatology/keab844

Arthritis & Rheumatology
Vol. 78, No. 5, May 2026, pp 1124–1133
DOI 10.1002/art.70021

American College of Rheumatology
Empowering Rheumatology Professionals

Molecular Stratification of Antiphospholipid Syndrome Through Integrative Analysis of the Whole-Blood RNA Transcriptome

Amala Ambati,[1,2] Feiyang Ma,[1,3] Katarina Kmetova,[1] Sherwin Navaz,[1] Claire K. Hoy,[1] Cyrus Sarosh,[1] Ajay Tambralli,[1] Erika Navarro-Mendoza,[4] Johann E. Gudjonsson,[1,3] J. Michelle Kahlenberg,[1,3] Jacqueline A. Madison,[1,5] Alí Duarte-García,[4] Jason S. Knight,[1] and Yu Zuo[1]

Objective. Antiphospholipid syndrome (APS) is a thromboinflammatory disorder characterized by clinical and mechanistic heterogeneity that complicates early diagnosis and hinders targeted treatment. We aimed to identify distinct molecular endotypes among antiphospholipid antibody (aPL)–positive patients using whole-blood transcriptomics.

Methods. Whole-blood RNA sequencing was performed on 174 aPL-positive patients, including those with primary APS (n = 102), secondary APS (n = 29), and aPL positivity without classifiable APS (n = 43). Unsupervised machine learning and immune cell deconvolution defined transcriptomic clusters and immune landscapes.

Results. Four transcriptionally distinct clusters were identified. At one end of the spectrum, cluster 1 showed up-regulation of ribosomal and metabolic pathways and down-regulation of mechanistic target of rapamycin (mTOR), NETosis, and Hippo/interleukin-6 (IL-6) signaling. In contrast, cluster 4 exhibited the opposite pattern, with strong up-regulation of mTOR, NETosis, and Hippo/IL-6 signaling. Cluster 2 demonstrated modest enrichment in messenger RNA processing and amino acid metabolism, and cluster 3 showed biosynthetic suppression with mild Hippo/IL-6 activation. Clinically, cluster 4 stood out with higher IgG anticardiolipin and anti–β_2-glycoprotein I positivity, elevated neutrophil counts, and increased urine protein-to-creatinine ratios. Immune deconvolution revealed distinct cell type profiles: cluster 1 was lymphoid predominant; cluster 2 had a balanced composition; cluster 3 was enriched in Treg cells, natural killer cells, macrophages, mast cells, and memory B cells; and cluster 4 was dominated by myeloid cells, including neutrophils, eosinophils, and dendritic cells. Distinct immune pathway activations were linked to clinical features, including white matter lesions, seizures, and cardiac valve disease.

Conclusion. This study reveals four endotypes of aPL-positive patients, a step toward personalized medicine for APS through pathway-informed stratification and therapy.

INTRODUCTION

Antiphospholipid syndrome (APS) is a thromboinflammatory, multisystem autoimmune disorder characterized by persistently positive antiphospholipid antibodies (aPL). These aPL are detected by positive testing for IgG/IgM anti–β_2 glycoprotein I (anti-β_2GPI), IgG/IgM anticardiolipin (aCL), or lupus anticoagulant, the latter a functional assay that screens for various aPL.[1] APS may occur as a standalone condition, referred to as primary APS, or it may occur alongside other systemic autoimmune diseases (typically systemic lupus erythematosus [SLE]), which is sometimes referred to as secondary APS. The clinical presentations of APS are highly diverse. Although APS was classically considered in the setting of thrombotic events and

Work in the Zuo Lab has been supported by the National Institute of Arthritis and Musculoskeletal and Skin Diseases, NIH (grant K08-AR-080205); the Rheumatology Research Foundation Investigator Award; the Arthritis National Research Foundation; the Frankel Cardiovascular Center at the University of Michigan; and the Alfred Taubman Medical Research Institute. This work was also supported by the generosity of the Driscoll Family.

[1]Division of Rheumatology, Department of Internal Medicine, University of Michigan, Ann Arbor; [2]ProMedica Rheumatology, ProMedica Toledo Hospital, Sylvania, Ohio; [3]Department of Dermatology, University of Michigan, Ann Arbor; [4]Department of Rheumatology, Mayo Clinic, Rochester, Minnesota; [5]Division of Pediatric Rheumatology, Department of Pediatrics, University of Michigan, Ann Arbor.

Drs Ambati and Ma contributed equally to this work.

Additional supplementary information cited in this article can be found online in the Supporting Information section (https://acrjournals.onlinelibrary.wiley.com/doi/10.1002/art.70021).

Author disclosures are available at https://onlinelibrary.wiley.com/doi/10.1002/art.70021.

Address correspondence via email to Yu Zuo, MD, MS, at yzu@med.umich.edu.

Submitted for publication June 1, 2025; accepted in revised form November 5, 2025.

recurrent first-trimester or late-term pregnancy complications as defined by the 2006 APS classification criteria,[1] additional clinical manifestations of APS were incorporated into the newest iteration of classification criteria by the American College of Rheumatology (ACR)/EULAR[2] in 2023. These clinical manifestations include livedo reticularis/racemosa, aPL nephropathy, pulmonary hemorrhage, cardiac valve abnormalities, thrombocytopenia, and others. Furthermore, though not included in the classification criteria, patients sometimes experience other nonthrombotic clinical manifestations, such as white matter lesions, movement disorders, and cognitive dysfunction. Additionally, some individuals may have persistently positive aPL without any classifiable APS manifestations. This clinical heterogeneity presents significant challenges for both effective management and accurate risk stratification.

The pathogenesis of key aPL-mediated clinical manifestations has been shown to involve the interplay of endothelial cells, neutrophils, monocytes, platelets, coagulation factors, and complement proteins.[3] These findings suggest that the pathophysiology of APS is characterized by disruptions in a complex mosaic of molecular pathways, converging into overlapping clinical phenotypes.

Although the 2023 ACR/EULAR classification criteria have highlighted the clinical heterogeneity of APS, it can be challenging to achieve the precise early patient subtyping needed for proactive management and reliable outcome prediction.[2] Leveraging modern high-throughput "omics" technologies offers the potential to define distinct molecular endotypes—subgroups of APS driven by specific pathophysiologic mechanisms—that might inform earlier and more personalized interventions.[4,5] Advances in this area of research are essential for transforming the diagnosis, treatment, and long-term outcomes of patients with APS.

The goal of our study was to apply integrative whole-blood RNA transcriptomic analyses to cluster aPL-positive patients according to their gene expression profiles. Our design focused on characterizing within-disease heterogeneity—stratifying aPL-positive patients—rather than defining APS-specific transcriptional signatures relative to healthy controls. By identifying potentially pathogenic pathways, we seek to advance precision diagnosis, reveal novel therapeutic targets, and inform more personalized management strategies for APS.

METHODS

This study complied with all relevant ethical regulations and was approved by the University of Michigan Institutional Review Board (HUM00122519, HUM00044257, and HUM00151834) and the Mayo Clinic Institutional Review Board (20-000476).

Human samples. A PAXgene Blood RNA tube by PreAnalytiX (REF 762165) was collected from 102 patients with primary APS, 29 patients with secondary APS, and 43 individuals with persistently positive aPL at least 12 weeks apart but without thrombotic or obstetric manifestations of APS. Our cohort was established before the publication of the 2023 ACR/EULAR criteria. As a result, some patients were classified as having APS based on multiplex aPL testing; however, all met the Sapporo criteria, with persistently positive aPL documented at least 12 weeks apart.[6] In terms of clinical manifestations, we confirmed that all patients designated as having APS fulfilled the clinical requirements for APS classification in the 2023 criteria. However, we were not able to fully capture microvascular or nonthrombotic manifestations as outlined in the 2023 criteria.[2] Lupus was defined according to the 2012 Systemic Lupus International Collaborating Clinics classification criteria.[7] Calprotectin (S100A8/S100A9) levels were measured in citrated plasma using the human S100A8/S100A9 Heterodimer DuoSet enzyme-linked immunosorbent assay (ELISA) (DY8226-05, R&D Systems) per the manufacturer's instructions. Soluble E-selectin and ICAM-1 were quantified in citrated plasma by ELISA (DY724, R&D Systems).

RNA extraction and sequencing. RNA was extracted from the samples, and quality control was performed to ensure a minimum RNA integrity number greater than 6. Whole-blood RNA sequencing was then conducted at the University of Michigan Advanced Genomic Core using an Illumina NovaSeq 6000 sequencer. Each sample was sequenced to a depth of at least 45 million reads, generating 150 bp paired-end reads and libraries. All RNA samples were processed, prepared for sequencing, and sequenced together in a single batch using the same library preparation protocol and sequencing run.

RNA sequencing data analysis. RNA sequencing reads were aligned to the human genome (hg38) using STAR v2.7.11a. Gene-level counts were obtained with quantMode GeneCounts, and all other alignment parameters were set to default. Raw counts were normalized using DESeq2 to account for sequencing depth and library size. Genes expressed in fewer than five samples were excluded as lowly expressed. A $\log2(x + 1)$ transformation was applied to the normalized counts for downstream analyses.

Principal component analysis was performed on the log-transformed data, and the first 50 principal components were used for hierarchical clustering to generate the sample dendrogram. The choice of 50 components was guided by our prior experience and the widely accepted convention in single-cell RNA sequencing analyses—also the default in the commonly used Seurat package—as this number reliably captures the major biologic variation while diminishing noise.[8] Based on dendrogram structure, four distinct clusters were identified. Differential expression analysis among these clusters was conducted using DESeq2 with default parameters. Genes with adjusted P values <0.05

were considered significantly differentially expressed and were subjected to enrichment analysis using Metascape.

To identify coexpression patterns and their associations with sample traits, weighted gene coexpression network analysis (WGCNA) was performed on the log-transformed data. A signed weighted correlation network was constructed using pairwise Pearson correlations, and an adjacency matrix was generated using a soft-thresholding power of 10. This matrix was transformed into a topological overlap matrix (TOM) to quantify network connectivity. Genes were hierarchically clustered based on TOM dissimilarity, and gene modules were identified using dynamic tree cutting with a minimum module size of 50. Similar modules were merged, resulting in 22 distinct modules. Module eigengenes were correlated with clinical traits using Pearson correlation, and functional enrichment of each module was assessed via Metascape.

Pathway enrichment was performed using Metascape (www.metascape.org). For each WGCNA module, the corresponding gene list was uploaded and analyzed with default Metascape settings, which simultaneously query multiple annotation databases, including Gene Ontology (GO) Biological Process, GO Cellular Component, GO Molecular Function, KEGG Pathways, Reactome Gene Sets, and CORUM protein complexes. Metascape applies a false discovery rate correction and defines statistical significance as enrichment $q < 0.05$. Only pathways meeting this built-in false discovery rate threshold were considered significant and are reported. Because some modules share genes and can therefore produce overlapping enriched pathways, Metascape reduces redundancy by clustering enriched terms into nonoverlapping groups based on gene overlap. Enrichment analysis was performed independently for each module, and our interpretation emphasizes robust, recurrent pathways that appeared across multiple modules and remained significant after adjusting for false discovery rates.

Cell type composition was estimated with CIBERSORTx using the LM22 signature matrix to deconvolute immune cell populations in each sample. LM22 reference matrix was used because it is a widely validated immune cell deconvolution panel optimized for peripheral blood transcriptomes.[9,10] Because this was an exploratory study aimed at identifying molecular and cellular heterogeneity in APS, we did not perform a priori power calculations for immune cell deconvolution. To minimize the potential impact of the smaller cluster size, which could reduce sensitivity for detecting subtle shifts in cell proportions, we focused our interpretation on moderate to large changes (≥15%–20%) in immune cell fractions. Pearson correlations were then computed between pathway enrichment scores and cell type abundance estimates. We applied multiple-testing corrections throughout the study using the Benjamini–Hochberg false discovery rate method for differential expression, WGCNA module–trait correlations, immune cell deconvolution correlations, and the built-in false discovery rate adjustment in Metascape for pathway enrichment analyses.

Pathway-specific gene enrichment score calculation. Gene sets for neutrophil extracellular traps (NETs) and Hippo pathways were assembled from published studies, including our own autoimmune transcriptomic work, as well as curated pathway databases and public gene libraries.[11] From these sources, we retained only genes that were reliably detected in our peripheral blood RNA sequencing data set and consistently represented in prior blood-based signatures. For each sample, the pathway gene score was then computed as the mean normalized expression of all genes in the set, yielding a single quantitative measure of relative pathway activity.

Together, these integrative analyses aimed to reveal key transcriptomic signatures and potential biomarkers across primary APS, secondary APS, and persistently aPL-positive individuals without classifiable APS.

Data availability. Transcriptomic data are not publicly available due to privacy and consent restrictions. All other data supporting the findings of this study, including the main text and supplementary materials, are available from the corresponding author upon reasonable request (Yu Zuo, yzu@umich.edu).

RESULTS

Molecularly stratifying aPL-positive patients reveals distinct immune signaling pathways. Whole-blood RNA sequencing was performed on 174 patients, including 102 with primary APS, 29 with secondary APS (all meeting SLE classification criteria[7]), and 43 with persistently positive aPL but without classifiable APS manifestations. Log-transformed whole-blood gene expression data from these patients were subjected to principal component analysis, and the first 50 principal components were used to perform hierarchical clustering. A sample dendrogram was constructed based on this analysis, from which four distinct patient clusters were identified (Figure 1A and B). To validate this four-cluster solution, we performed consensus clustering, which likewise supported the four-cluster structure and demonstrated stable cluster assignments. To further explore transcriptomic differences, we used WGCNA, which identified 22 distinct gene modules. These modules were subsequently analyzed to determine their enrichment in specific biologic pathways and processes, providing insight into the molecular landscape underlying each cluster (Figure 1C). Relative to the other aPL-positive patient clusters, cluster 1 showed the strongest up-regulation of pathways involved in cytoplasmic ribosomal proteins, base excision repair, tyrosine metabolism, and fatty acid biosynthesis. Conversely, it was down-regulated in mammalian target of rapamycin (mTOR) signaling, NET formation, and Hippo/interleukin-6 (IL-6) signaling pathways. Cluster 2 demonstrated modest relative up-regulation of messenger RNA (mRNA) processing and amino acid–metabolism pathways. Cluster 3 exhibited modest relative down-regulation of mRNA processing, amino acid biosynthesis, and fatty acid biosynthesis, accompanied by mild relative

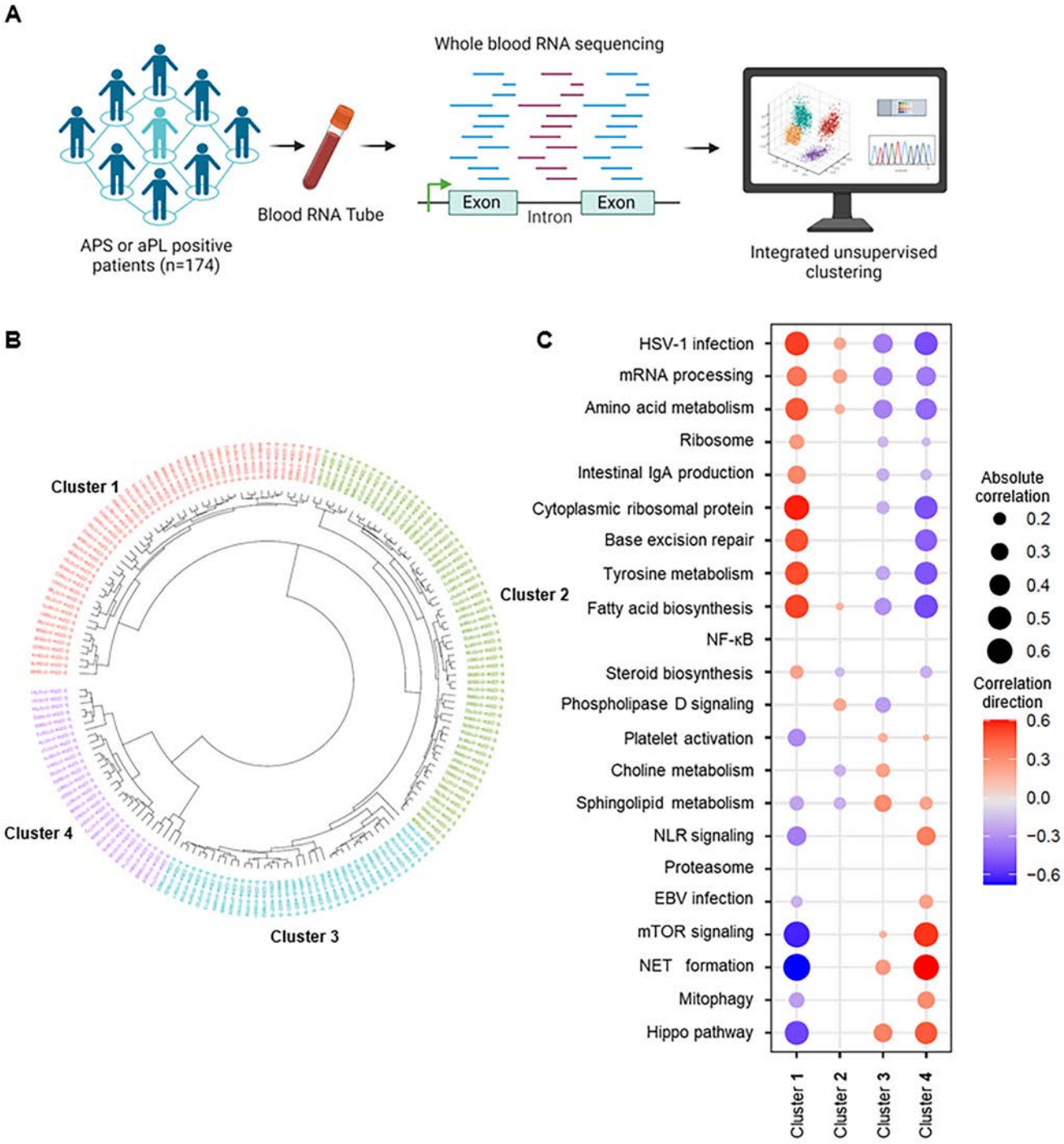

Figure 1. Molecularly stratifying aPL-positive patients. (A) Schematic illustration of study design and whole-blood RNA sequencing. The figure was created at www.biorender.com. (B) Unsupervised hierarchical clustering stratified aPL-positive patients into four distinct clusters, each represented by a different color. Each code within the clusters corresponds to an individual patient's RNA sample. (C) Dot plots illustrate the associations between pathway-specific gene modules and each cluster of aPL-positive patients. Only statistically significant associations are displayed. The specific genes composing each pathway-associated module are detailed in the Supplemental Data. aPL, antiphospholipid antibody; APS, antiphospholipid syndrome; EBV, Epstein-Barr virus; HSV, herpes simplex virus; mRNA, messenger RNA; mTOR, mammalian target of rapamycin; NET, neutrophil extracellular trap; NLR, nucleotide-binding oligomerization domain–like receptor.

up-regulation of the Hippo/IL-6 signaling pathway. Cluster 4 displayed the inverse pattern of cluster 1, with strong relative up-regulation of mTOR signaling, NET formation, and Hippo/IL-6 signaling and relative down-regulation of cytoplasmic ribosomal proteins, base excision repair, tyrosine metabolism, and fatty acid biosynthesis.

We performed sensitivity analyses to ensure our findings were not driven by confounding factors. First, we included immune cell–proportion estimates from CIBERSORTx (LM22) as covariates in the linear models testing the association between each WGCNA module and cluster membership; this adjustment, after correcting for multiple comparisons, did not alter the results, as the NET formation and Hippo/IL-6 signaling gene modules remained highly and significantly associated with cluster 4. To evaluate the influence of APS subtypes (primary APS, secondary APS, or aPL-only without classifiable APS), we added subtype as a covariate and again found both modules were strongly associated with cluster 4; cluster membership also remained unchanged when the analysis was restricted to patients with primary APS. Finally, to test for possible medication effects, we adjusted for hydroxychloroquine (HCQ) use and for a combined indicator of other immunosuppressive therapy (mycophenolate, rituximab, methotrexate, azathioprine, leflunomide, or belimumab). Both the NET formation and Hippo/IL-6 signaling gene modules remained highly significantly associated with cluster 4 after these adjustments (NET formation: adjusted cluster $P = 3.86 \times 10^{-41}$; Hippo/IL-6 signaling: adjusted cluster $P = 4.98 \times 10^{-24}$), and the results were unchanged even after excluding all patients receiving HCQ or any immunosuppressive therapy. These analyses demonstrate that the strong association of these gene modules with cluster 4 is robust and independent of immune cell composition, APS subtype, and medication use.

Table 1 summarizes the clinical and demographic features of these patients across four transcriptomic clusters. Although the clusters showed similar distributions of age and sex, as well as history of thrombosis, obstetric morbidity, thrombocytopenia, livedo reticularis, cardiac valve disease, and APS nephropathy, notable differences still emerged. Cluster 4 had a higher prevalence of IgG aCL and IgG anti-β_2GPI positivity compared to clusters 1 to 3. Individuals in cluster 4 also had elevated absolute neutrophil counts, circulating calprotectin levels—a marker of neutrophil activation and NET formation—and urine protein-to-creatinine ratios. Patients in cluster 4 were also more likely to receive immunosuppressive therapy, whereas circulating E-selectin levels, a marker of endothelial activation, did not differ significantly among clusters.

Across the 22 gene modules, NET formation and Hippo/IL-6 signaling pathways showed some of the most pronounced positive and negative correlations (Figure 1C). To explore this further, we generated pathway-specific enrichment scores by selecting genes ranked by their contribution to NETs pathway enrichment (5 genes) and Hippo pathway activation (11 genes), based on our prior work and public gene libraries (Supplemental Table 1). These NET and Hippo enrichment scores were applied across the patient cohort. We found that both NET and Hippo scores varied significantly among the clusters. Cluster 4 had the highest enrichment scores for both pathways, whereas cluster 1 had the lowest (Table 1). A higher NET score was associated with increased levels of circulating calprotectin (a marker of neutrophil activation and NET formation), elevated absolute neutrophil counts, higher positivity for IgG aCL and IgG anti-β_2GPI, and increased urine protein-to-creatinine ratios (Supplemental Table 2). Similarly, a higher Hippo score correlated with elevated levels of calprotectin, C-reactive protein (CRP), E-selectin (a marker of endothelial activation), absolute neutrophil counts, and urine protein-to-creatinine ratios (Supplemental Table 2).

Immune cell composition across the four clusters. Deconvolution analysis revealed distinct immune cell type distributions among the four clusters (Figure 2A and B). Cluster 1 was enriched in lymphoid cells, including B cells, plasma cells, $CD4^+$ T cells, and $CD8^+$ T cells. Cluster 2 displayed a relatively uniform distribution of all analyzed immune cell types. Cluster 3 showed enrichment in Treg cells, natural killer (NK) cells, macrophages, mast cells, and memory B cells. Cluster 4 was characterized by a predominance of myeloid cells, including neutrophils, eosinophils, dendritic cells, macrophages, NK cells, and T cells. We also observed several significant associations between specific immune cell types and pathway-specific gene modules (Figure 2C). Neutrophils demonstrated strong positive correlations with NET formation, Hippo/IL-6 signaling, and mTOR signaling pathways and significant negative correlations with fatty acid biosynthesis, tyrosine metabolism, and cytoplasmic ribosomal protein pathways. B cells were positively correlated with intestinal IgA production, whereas plasma cells did not show notable associations with any gene modules. Resting T cells exhibited moderate negative correlations with Hippo/IL-6 signaling, sphingolipid metabolism, and choline metabolism, alongside moderate positive correlations with mRNA processing and amino acid metabolism (Figure 2C). To validate our deconvolution estimates, we correlated CIBERSORTx-derived neutrophil proportions with absolute neutrophil counts obtained from clinical complete blood cell counts. The correlation was moderate to strong and highly significant, providing confirmation of the accuracy of our deconvolution results (Supplemental Figure 1).

The association of gene modules with nonthrombotic/nonobstetric clinical manifestations among patients with APS and aPL-positive patients. Analysis of the associations between pathway-specific gene modules and nonthrombotic, nonobstetric clinical manifestations of APS revealed several statistically significant findings (Supplemental Figure 2). White matter lesions were linked to up-regulation of genes involved in NF-κB signaling and cytoplasmic ribosomal proteins. Seizures were associated with increased expression of genes related to choline and sphingolipid metabolism. Cardiac valve disease showed up-regulation of genes associated with Hippo/IL-6 signaling and NET formation,

Table 1. Clinical and demographic characteristics of aPL-positive patients across four clusters (N = 174)*

	Cluster 1 (n = 50)	Cluster 2 (n = 59)	Cluster 3 (n = 36)	Cluster 4 (n = 29)	*P* value
Diagnoses, n (%)					
Primary APS (thrombotic or obstetric manifestations)	30 (60.0)	34 (57.6)	20 (55.6)	18 (62.1)	0.976
aPL positive without classifiable APS	12 (24.0)	10 (17.0)	12 (33.3)	9 (31.0)	0.233
Demographics					
Age, mean ± SD, y	43 ± 13	46 ± 18	46 ± 14	45 ± 17	0.879
Male, n (%)	15 (30.0)	15 (25.4)	12 (33.3)	9 (31.0)	0.859
aPL positivity profile, n (%)					
IgG aCL	26 (52.0)	40 (67.8)	26 (89.7)	22 (75.7)	**0.022**
IgM aCL	27 (54.0)	26 (44.1)	12 (33.3)	11 (37.9)	0.076
IgG anti-β_2GPI	29 (58.0)	42 (71)	26 (72)	26 (90)	**0.005**
IgM anti-β_2GPI	26 (52.0)	26 (44.1)	12 (33.3)	14 (48.3)	0.405
Lupus anticoagulant	20 (40.0)	34 (57.6)	21 (58.3)	16 (55.2)	0.149
Triple positive[a]	12 (24.0)	26 (44.1)	15 (41.7)	12 (41.4)	0.116
Laboratory studies, mean ± SD					
Neutrophil count, $10^3/\mu L$[b]	3.29 ± 1.89	4.48 ± 1.91	4.28 ± 0.35	6.29 ± 2.16	**<0.0001**
CRP, mg/dL	0.32 ± 0.36	0.52 ± 0.54	0.80 ± 0.72	0.69 ± 0.81	0.050
C3, mg/dL	74.35 ± 17.62	77.79 ± 17.08	78.76 ± 15.82	76.76 ± 21.28	0.770
C4, mg/dL	19.85 ± 4.52	20.38 ± 5.07	20.21 ± 4.54	19.39 ± 6.02	0.871
Platelet count, $10^3/\mu L$[b]	241.11 ± 78.25	263.35 ± 90.84	221.68 ± 77.97	216.21 ± 73.85	0.074
Creatinine, mg/dL[b]	1.05 ± 0.65	0.98 ± 0.36	1.03 ± 0.33	1.00 ± 0.47	0.679
Urine protein/creatinine ratio[b]	0.09 ± 0.14	0.41 ± 0.91	0.31 ± 0.52	0.49 ± 0.90	**0.043**
E-selectin, pg/mL	29,530 ± 15,851.60	32,143.89 ± 21,024.42	34,875.52 ± 17,416.36	38,409.11 ± 21,422.65	0.284
Calprotectin, μg/mL	1.28 ± 1.17	1.74 ± 1.54	2.45 ± 1.65	3.15 ± 3.23	**<0.001**
Clinical history, n (%)					
Venous thrombosis	22 (44)	29 (49.2)	22 (61.1)	14 (48.3)	0.386
Arterial thrombosis	10 (20.0)	15 (25.4)	6 (16.7)	5 (17.2)	0.580
Pregnancy morbidity	12 (24.0)	7 (11.9)	5 (13.9)	4 (13.8)	0.234
Cardiac valve disease	5 (10.0)	7 (11.9)	8 (22.2)	6 (20.7)	0.091
Livedo reticularis	18 (36.0)	13 (22.0)	9 (25.0)	12 (41.4)	0.77
APS nephropathy	4 (8.0)	4 (6.8)	2(5.6)	1 (3.4)	0.411
Immunosuppressive medications, n (%)					
Hydroxychloroquine	26 (52.0)	30 (50.8)	20 (55.6)	20 (69.0)	**0.03**
Other immunosuppressive medications[c]	7 (14)	11 (18.6)	8 (22)	9 (31)	**0.03**
NET and Hippo scores, mean ± SD					
NET score	−2.23 ± 0.96	−0.46 ± 1.89	0.47 ± 2.36	4.21 ± 6.67	**<0.0001**
Hippo score	−5.04 ± 3.72	−0.29 ± 4.86	0.15 ± 5.49	9.1 ± 9.52	**<0.0001**

* Intergroup differences for categorical variables were assessed using the Jonckheere–Terpstra trend test, whereas differences for continuous variables were evaluated using one-way analysis of variance for normally distributed data and the Kruskal–Wallis test for skewed distributions. Bold *P* values indicate $p < 0.05$. aCL, anticardiolipin; anti-β_2GPI, anti–β_2 glycoprotein I; aPL, antiphospholipid antibody; APS, antiphospholipid syndrome; CRP, C-reactive protein; NET, neutrophil extracellular trap.
[a] Triple positive includes positive lupus anticoagulant, positive IgG or IgM aCL, and IgG or IgM positive anti-β_2GPI.
[b] Platelet counts, absolute neutrophil counts, and serum creatinine levels were obtained from clinical laboratory test results collected on the same day as the research RNA samples. Among the 174 participants, 123 had these clinical laboratory tests performed on the corresponding date. Similarly, urine protein-to-creatinine ratios were extracted from clinical laboratory data when available on the same day as RNA sample collection; 124 of 174 participants had this measurement.
[c] Other immunosuppressive medications: mycophenolate, rituximab, methotrexate, azathioprine, leflunomide, or belimumab.

alongside down-regulation of genes involved in intestinal IgA production (Supplemental Figure 2).

DISCUSSION

Using whole-blood RNA sequencing integrated with unsupervised machine learning and immune cell deconvolution, our study stratified patients with APS or persistently positive aPL across diverse clinical presentations into four biologically distinct clusters. These clusters were defined by coordinated gene expression modules and predicted immune cell compositions. Cluster 1 was marked by up-regulation of cytoplasmic ribosomal proteins, base excision repair, tyrosine metabolism, and fatty acid biosynthesis pathways, with down-regulation of mTOR signaling, NET formation, and Hippo/IL-6 signaling. In contrast, cluster 4 displayed the inverse pattern, with strong up-regulation of mTOR signaling, NET formation, and Hippo/IL-6 pathways. Cluster 2 showed modest enrichment in mRNA processing and amino acid–metabolism pathways, whereas cluster 3 exhibited relative suppression of similar biosynthetic pathways, alongside mild

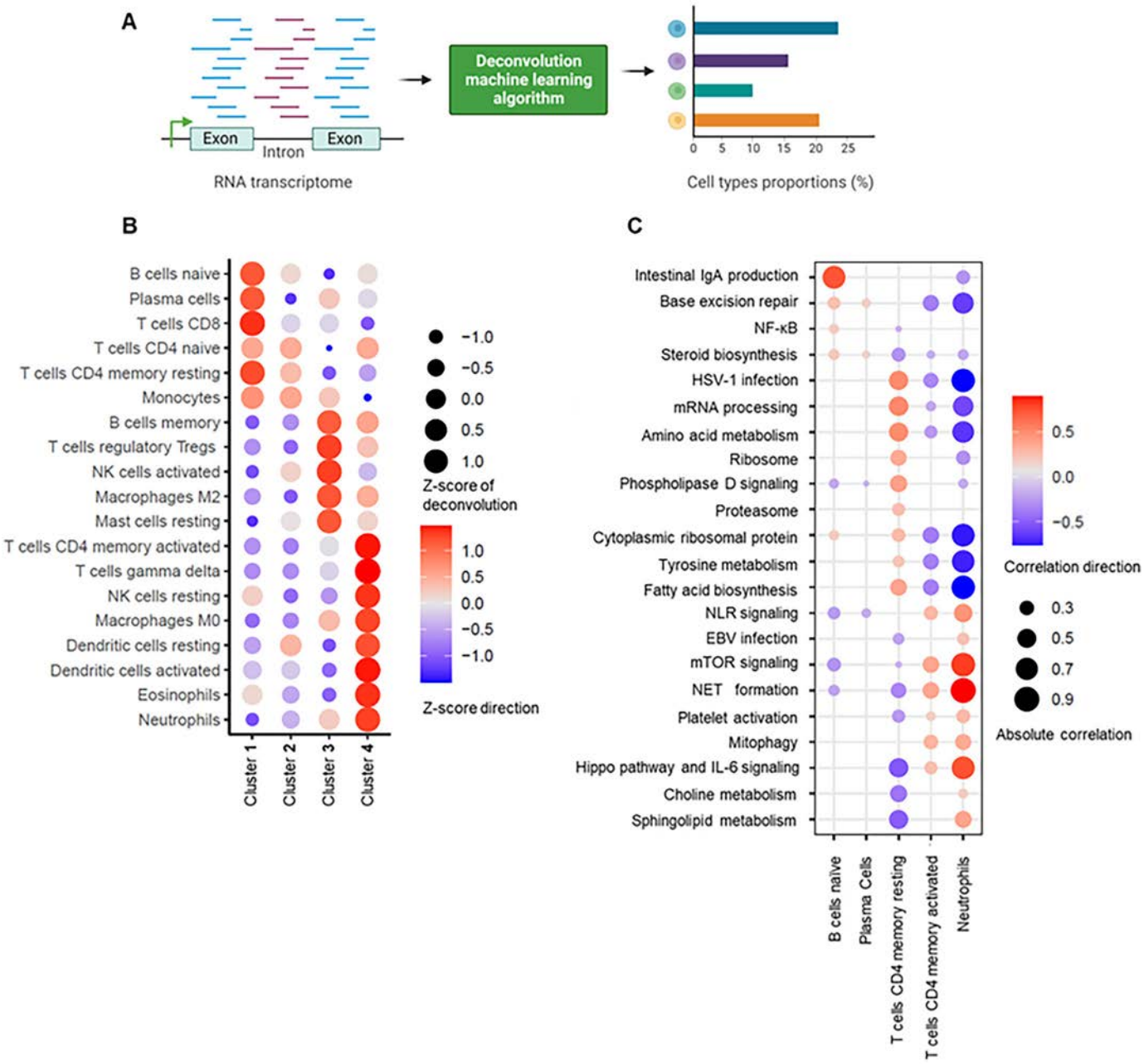

Figure 2. Deconvolution analysis unveils the immune cell composition across four distinct clusters. (A) Schematic illustration of deconvolution analysis of whole-blood transcriptomic data. Cell type deconvolution was performed using CIBERSORTx with the LM22 (22 immune cell types) as the signature matrix. The figure was created at www.biorender.com. (B) Dot plot demonstrating associations between immune cell types and each cluster of aPL-positive patients. (C) Dot plot showing associations between pathway-specific gene modules and immune cell types. Only associations that remain statistically significant after multiple-comparison adjustment are displayed. aPL, antiphospholipid antibody; APS, antiphospholipid syndrome; EBV, Epstein-Barr virus; HSV, herpes simplex virus; IL, interleukin; mRNA, messenger RNA; mTOR, mammalian target of rapamycin; NET, neutrophil extracellular trap; NK, natural killer; NLR, nucleotide-binding oligomerization domain–like receptor.

up-regulation of Hippo/IL-6 signaling. Cluster 4 also stood out for its clinical associations—higher rates of IgG aCL and anti-β_2GPI positivity, elevated neutrophil counts, and increased urine protein-to-creatinine ratios. Immune deconvolution further revealed distinct cellular landscapes: cluster 1 had a lymphoid-predominant profile; cluster 2 displayed a balanced mix; cluster 3 was enriched in Treg cells, NK cells, macrophages, mast cells, and memory B cells; and cluster 4 was myeloid-skewed, with neutrophils, eosinophils, and dendritic cells. Our cohort of 174 aPL-positive patients represents, to our knowledge, the largest whole-blood RNA sequencing study in APS to date. Although cluster 4 included only 29 patients, several analyses confirm

adequate power. Associations of cluster 4 with the NET formation and Hippo/IL-6 signaling modules were exceptionally strong ($P < 1 \times 10^{-40}$) and remained highly significant after 5,000 permutation tests (empirical $P < 1 \times 10^{-3}$). These findings were robust to sensitivity analyses; removing 20% of samples preserved significance in >95% of resamples, and even downsampling cluster 4 to 10 patients retained significance in 100% of runs. A formal one-way analysis of variance power analysis further indicated >0.99 power to detect the observed effect sizes. Thus, despite its smaller size, cluster 4 is sufficiently powered to support the stability of these associations.

Whole-blood RNA sequencing has previously been applied in APS research to compare transcriptomic profiles between patients and healthy controls, consistently revealing marked gene expression changes—particularly in interferon-regulated genes (IRGs).[12–16] For instance, a study of 62 patients with thrombotic primary APS and 29 healthy controls identified 34 differentially expressed genes, 33 of which were up-regulated by at least two-fold, including 14 IRGs—highlighting the prominent role of interferon signaling in APS pathogenesis.[13] Gene expression profiling in that study distinguished patients with APS from controls with 79% accuracy, which improved to 82% when analysis was focused exclusively on IRGs, underscoring their promise as potential biomarkers. In contrast, our study did not detect significant variation in IRGs signatures within the APS cohort. This is likely due to differences in comparison strategies. Although patients with APS typically show elevated baseline interferon activity relative to healthy individuals, the variation within the APS or aPL-positive group is likely more limited, making it difficult to detect statistically significant differences across subgroups. Building on prior work, our study uniquely applies whole-blood RNA sequencing in combination with unsupervised clustering to stratify aPL-positive individuals into four transcriptionally distinct subgroups. This approach moves beyond conventional primary versus secondary APS classification and reveals underlying molecular heterogeneity. The presence of such distinct molecular signatures supports the concept that APS comprises a spectrum of immune and vascular phenotypes. This stratification highlights the need for more personalized approaches to APS care, guided by the dominant immunopathogenic mechanisms in each subgroup.

Our study reinforces the role of neutrophil-driven inflammation in a subset of APS patients, further implicating NETs in disease pathogenesis. Pathway enrichment analysis revealed significant up-regulation of NET formation genes in cluster 4, whereas these pathways were down-regulated in cluster 1. NETs—extracellular DNA and chromatin structures released by activated neutrophils—have been implicated in promoting vascular inflammation, endothelial damage, and hypercoagulability. Prior studies, including our own, have demonstrated that aPL directly trigger NETosis and that increased circulating NET-associated biomarkers are associated with thrombotic risk in APS.[3,17] Transcriptomic analysis of APS neutrophils further supports this link, revealing an activated neutrophil signature that enhances adhesion and NET formation.[18] Our study builds on these findings by showing that patients with APS in cluster 4 have elevated NET enrichment scores, which correlate with increased circulating calprotectin levels—a marker of neutrophil activation and NET formation—as well as a higher protein-to-creatinine ratio, indicating renal damage and potential inflammation. This aligns with a recent transcriptomic study of APS kidneys, which revealed up-regulated NET-related genes in affected kidneys.[19] Additionally, patients in cluster 4 had higher levels of IgG aCL and IgG anti-β_2GPI. Notably, this mirrors a recent lupus transcriptomic study showing that aPL positivity in patients with lupus is associated with up-regulation of neutrophil and myeloid gene modules,[20] further supporting the hypothesis that neutrophil-driven inflammation exacerbates APS autoimmunity.

Beyond NETosis, the up-regulation of Hippo/IL-6 signaling in cluster 4 offers potential insights into APS-associated immune remodeling, particularly in the context of myeloid cell activation and inflammation. The Hippo pathway regulates the transcriptional coactivators YAP and TAZ, which, when activated, translocate to the nucleus and drive proinflammatory gene expression programs, including IL-6 production, and enhance immune cell survival and chemotaxis.[21,22] In myeloid cells such as neutrophils and macrophages, YAP/TAZ activity has been shown to promote inflammatory polarization, prolong cell lifespan, and support tissue infiltration—all features consistent with the innate immune activation observed in APS.[21,22] In our study, elevated expression of Hippo pathway genes in cluster 4 was accompanied by increased calprotectin and CRP levels, supporting a potential mechanistic link between Hippo signaling and systemic inflammation. Additionally, Hippo signaling is known to be activated by mechanical and cellular stress, which is particularly relevant in APS, in which endothelial dysfunction is a key feature of vascular pathology. We observed a positive association between Hippo pathway enrichment and circulating E-selectin levels—a marker of endothelial activation—suggesting that this signaling axis may represent an immune cell response to vascular stress. Taken together, these findings suggest that Hippo pathway activation may contribute to a proinflammatory, myeloid-driven endotype in a subset of patients with APS. This pathway could serve as a potential new therapeutic target to mitigate thromboinflammatory risk, and future studies should investigate its functional role in APS pathogenesis more directly.

Our study further highlights the relationship between immune cell composition and the molecular heterogeneity of APS. Deconvolution analysis of immune cells highlighted variation in immune system involvement across APS subtypes. Patients in cluster 4 exhibited a dominant myeloid signature, characterized by increased neutrophils, eosinophils, and dendritic cells, whereas cluster 1 was enriched in lymphoid cells, including B cells, plasma cells, and $CD8^+$ T cells. These findings reinforce the notion that

APS pathogenesis is associated with distinct immune mechanisms in different patient subsets. Although prior research has focused on B cell–mediated autoantibody production in APS, our data emphasize the critical role of innate immune cells in the disease process. This myeloid-driven inflammatory signature further supports the involvement of neutrophils in APS-related vascular complications and thrombosis, suggesting potential avenues for targeted therapeutic intervention.

Our findings suggest that nonthrombotic APS manifestations are associated with distinct gene expression profiles, providing mechanistic insights that align with prior research. Seizures were linked to up-regulation of genes involved in choline and sphingolipid metabolism—pathways previously implicated in seizure generation, epileptogenesis, and drug-resistant epilepsy across human studies, animal models, and monogenic metabolic disorders.[23–25] Cardiac valve disease was associated with increased expression of genes related to Hippo and IL-6 signaling, consistent with growing evidence that persistent IL-6 elevation plays a direct pathogenic role in vascular and degenerative valve disease rather than serving solely as a marker of inflammation.[26,27] Together, these findings support the biologic relevance of these pathways in APS-related organ damage.

We acknowledge several limitations in our study. Chief among them is the absence of healthy control samples. Because our study was specifically designed to stratify aPL-positive patients and examine within-disease heterogeneity, the study does not directly define APS-specific transcriptional signatures relative to healthy individuals. Next, relying on whole-blood transcriptomics may mask cell-specific contributions to APS pathogenesis. Single-cell RNA sequencing could provide a more precise view of immune cell involvement. Additionally, our cross-sectional design limits the ability to assess dynamic gene expression changes. Longitudinal studies tracking transcriptomic shifts over time and responses to treatment could offer deeper insights into disease progression. We also acknowledge that estimating cell type composition with CIBERSORTx may introduce indirect compositional effects, so correlations between gene modules and cell types should be interpreted with caution. The underlying biologic relationships will require validation using independent experimental approaches. The clinical significance of the four molecular endotypes requires further validation. To gain deeper insight into APS pathogenesis, future studies should investigate the direct contribution of the novel gene expression modules identified in our study. Pathways such as Hippo signaling that have not been previously implicated in APS warrant further investigation to clarify their role in driving the underlying immunologic and vascular abnormalities characteristic of the disease. Finally, the derived NETs and Hippo pathway scores were used solely in an exploratory framework to illustrate relative pathway activity across APS/aPL-positive patient clusters. They are not intended as validated diagnostic tools or definitive pathway signatures. Although these gene sets capture key elements of NETosis and Hippo signaling, they are not comprehensive. Future studies incorporating broader gene panels and orthogonal validation methods—such as protein-level measurements or functional NET assays—will be necessary to confirm these findings and assess their potential clinical utility.

In summary, our study establishes the potential to stratify patients with APS and aPL-positive patients based on whole-blood transcriptomic profiles, uncovering biologically distinct subgroups with diverse immune activation patterns and clinical features. This level of stratification could not have been achieved through clinical or serologic data alone and offers clinicians a previously inaccessible layer of insight into APS heterogeneity. Notably, the identification of NETosis and Hippo pathway activation as key differentiators among patient subgroups points to possible novel therapeutic targets and could lay the groundwork for more personalized approaches to APS management. Looking ahead, integration of single-cell RNA sequencing and proteomic data will be critical to refine these molecular signatures and to delineate the specific cellular drivers of APS immunopathogenesis. Furthermore, longitudinal studies are needed to assess the temporal stability of these transcriptomic clusters and their relationship to disease progression and treatment response. By leveraging transcriptomic profiling to define biologically meaningful APS endotypes, we hope to move the field closer to precision medicine strategies tailored to the underlying immune mechanisms of individual patients.

AUTHOR CONTRIBUTIONS

All authors contributed to at least one of the following manuscript preparation roles: conceptualization AND/OR methodology, software, investigation, formal analysis, data curation, visualization, and validation AND drafting or reviewing/editing the final draft. As corresponding author, Dr Zuo confirms that all authors have provided the final approval of the version to be published and takes responsibility for the affirmations regarding article submission (eg, not under consideration by another journal), the integrity of the data presented, and the statements regarding compliance with institutional review board/Declaration of Helsinki requirements.

REFERENCES

1. Ambati A, Knight JS, Zuo Y. Antiphospholipid syndrome management: a 2023 update and practical algorithm-based approach. Curr Opin Rheumatol 2023;35(3):149–160. doi:https://doi.org/10.1097/BOR.0000000000000932
2. Barbhaiya M, Zuily S, Naden R, et al; ACR/EULAR APS Classification Criteria Collaborators. The 2023 ACR/EULAR antiphospholipid syndrome classification criteria. Arthritis Rheumatol 2023;75(10):1687–1702. doi:https://doi.org/10.1002/art.42624
3. Ambati A, Zuo Y, Knight JS. An update on inflammation in antiphospholipid syndrome. Curr Opin Rheumatol 2023;35(2):89–97. doi:https://doi.org/10.1097/BOR.0000000000000926
4. Barturen G, Babaei S, Català-Moll F, et al. Integrative analysis reveals a molecular stratification of systemic autoimmune diseases. Arthritis Rheumatol 2021;73(6):1073–1085. doi:https://doi.org/10.1002/art.41610

5. Lopez-Pedrera C, Pérez-Sánchez C, Tektonidou MG. Towards precision medicine in antiphospholipid syndrome. Lancet Rheumatol 2025; 7(8):e576–e589. doi:https://doi.org/10.1016/S2665-9913(25)00094-3
6. Miyakis S, Lockshin MD, Atsumi T, et al. International consensus statement on an update of the classification criteria for definite antiphospholipid syndrome (APS). J Thromb Haemost 2006;4(2):295–306. doi:https://doi.org/10.1111/j.1538-7836.2006.01753.x
7. Petri M, Orbai AM, Alarcón GS, et al. Derivation and validation of the Systemic Lupus International Collaborating Clinics classification criteria for systemic lupus erythematosus. Arthritis Rheum 2012;64(8):2677–2686. doi:https://doi.org/10.1002/art.34473
8. Hao Y, Stuart T, Kowalski MH, et al. Dictionary learning for integrative, multimodal and scalable single-cell analysis. Nat Biotechnol 2024; 42(2):293–304. doi:https://doi.org/10.1038/s41587-023-01767-y
9. Hirano M. Cancer immunity and gene expression data: a quick tool for immunophenotype evaluation. Cancer Res 2018;78(23):6536–6538. doi:https://doi.org/10.1158/0008-5472.CAN-18-3288
10. Sun N, Luo Y, Zheng B, et al. A novel immune checkpoints-based signature to predict prognosis and response to immunotherapy in lung adenocarcinoma. J Transl Med 2022;20(1):332. doi:https://doi.org/10.1186/s12967-022-03520-6
11. Ma F, Tsou PS, Gharaee-Kermani M, et al. Systems-based identification of the Hippo pathway for promoting fibrotic mesenchymal differentiation in systemic sclerosis. Nat Commun 2024;15(1):210. doi:https://doi.org/10.1038/s41467-023-44645-6
12. Palli E, Kravvariti E, Tektonidou MG. Type I interferon signature in primary antiphospholipid syndrome: clinical and laboratory associations. Front Immunol 2019;10:487. doi:https://doi.org/10.3389/fimmu.2019.00487
13. Verrou KM, Sfikakis PP, Tektonidou MG. Whole blood transcriptome identifies interferon-regulated genes as key drivers in thrombotic primary antiphospholipid syndrome. J Autoimmun 2023;134:102978. doi:https://doi.org/10.1016/j.jaut.2022.102978
14. Xourgia E, Tektonidou MG. Type I interferon gene expression in antiphospholipid syndrome: Pathogenetic, clinical and therapeutic implications. J Autoimmun 2019;104:102311. doi:https://doi.org/10.1016/j.jaut.2019.102311
15. Cecchi I, Radin M, Barinotti A, et al. Type I interferon pathway activation across the antiphospholipid syndrome spectrum: associations with disease subsets and systemic antiphospholipid syndrome presentation. Front Immunol 2024;15:1351446. doi:https://doi.org/10.3389/fimmu.2024.1351446
16. Knight JS, Tektonidou MG. Can transcriptomics guide the management of SLE-associated APS? Nat Rev Rheumatol 2024;20(8):457–458. doi:https://doi.org/10.1038/s41584-024-01123-7
17. Tambralli A, Gockman K, Knight JS. NETs in APS: current knowledge and future perspectives. Curr Rheumatol Rep 2020;22(10):67. doi:https://doi.org/10.1007/s11926-020-00936-1
18. Knight JS, Meng H, Coit P, et al. Activated signature of antiphospholipid syndrome neutrophils reveals potential therapeutic target. JCI Insight 2017;2(18):e93897. doi:https://doi.org/10.1172/jci.insight.93897
19. Tektonidou MG, Verrou KM, Gakiopoulou H, et al. Kidney whole-transcriptome profiling in primary antiphospholipid syndrome reveals complement, interferons and NETs-related gene expression. Rheumatology (Oxford) 2024;63(11):3184–3190. doi:https://doi.org/10.1093/rheumatology/keae397
20. Nikolopoulos D, Loukogiannaki C, Sentis G, et al. Disentangling the riddle of systemic lupus erythematosus with antiphospholipid syndrome: blood transcriptome analysis reveals a less-pronounced IFN-signature and distinct molecular profiles in venous versus arterial events. Ann Rheum Dis 2024;83(9):1132–1143. doi:https://doi.org/10.1136/ard-2024-225664
21. Meli VS, Veerasubramanian PK, Downing TL, et al. Mechanosensation to inflammation: roles for YAP/TAZ in innate immune cells. Sci Signal 2023;16(783):eadc9656. doi:https://doi.org/10.1126/scisignal.adc9656
22. Mia MM, Cibi DM, Abdul Ghani SAB, et al. YAP/TAZ deficiency reprograms macrophage phenotype and improves infarct healing and cardiac function after myocardial infarction. PLoS Biol 2020;18(12):e3000941. doi:https://doi.org/10.1371/journal.pbio.3000941
23. Kulagina TP, Shevchenko NA, Arkhipov VI. Influence of seizures on lipids of homogenate and neuronal and glial nuclei of rat neocortex. Biochemistry (Mosc) 2004;69(10):1143–1147. doi:https://doi.org/10.1023/B:BIRY.0000046889.60018.8c
24. Wortmann SB, Mayr JA. Choline-related-inherited metabolic diseases-a mini review. J Inherit Metab Dis 2019;42(2):237–242. doi:https://doi.org/10.1002/jimd.12011
25. Ong WY, Herr DR, Farooqui T, et al. Role of sphingomyelinases in neurological disorders. Expert Opin Ther Targets 2015;19(12):1725–1742. doi:https://doi.org/10.1517/14728222.2015.1071794
26. Knopp T, Jung R, Wild J, et al. Myeloid cell-derived interleukin-6 induces vascular dysfunction and vascular and systemic inflammation. Eur Heart J Open 2024;4(4):oeae046. doi:https://doi.org/10.1093/ehjopen/oeae046
27. Wassmann S, Stumpf M, Strehlow K, et al. Interleukin-6 induces oxidative stress and endothelial dysfunction by overexpression of the angiotensin II type 1 receptor. Circ Res 2004;94(4):534–541. doi:https://doi.org/10.1161/01.RES.0000115557.25127.8D

Arthritis & Rheumatology
Vol. 78, No. 5, May 2026, pp 1134–1144
DOI 10.1002/art.70025

American College of Rheumatology
Empowering Rheumatology Professionals

Risk Factors for Relapse in Antineutrophil Cytoplasmic Antibody–Associated Vasculitis Among Patients With Relapse After Induction of Remission With Rituximab

Ellen Romich, MD, MSCE,[1] Joshua F. Baker, MD, MSCE,[1,2] Thomas R. Riley IV MD, MSCE,[1] Ian Green, MD, MPH,[1] Rennie L. Rhee, MD, MSCE,[1] Carol A. McAlear, MA,[1] Ulrich Specks, MD,[3] Rona M. Smith, MD,[4,5] David R. Jayne, MD,[4,5] and Peter A. Merkel, MD, MPH,[1,2] for the RITAZAREM Investigators

Objective. The objective of the study was to determine risk factors for relapse of antineutrophil cytoplasmic antibody (ANCA)–associated vasculitis (AAV) after reinduction of remission with rituximab and discontinuation of maintenance therapy.

Methods. This is a post hoc analysis of the RITAZAREM clinical trial. Patients aged 15 years or older with AAV and a positive test for anti–proteinase-3 or anti-myeloperoxidase-ANCA who achieved remission after reinduction with rituximab and glucocorticoids were randomized at month 4 to receive continued rituximab or azathioprine for a maintenance period up to 24 months, followed by observation until relapse or up to 48 months. Generalized estimating equations logistic regression identified baseline and time-varying risk factors for relapse by the next visit for the two study phases: maintenance (months 4–24) and off-treatment (months 24–48).

Results. Among 170 patients (median [interquartile range] age 59 [48–68] years, disease duration 5 [2–10] years), 99 relapses occurred (46 during maintenance). During maintenance, musculoskeletal involvement (odds ratio [OR]: 2.8, 95% confidence interval [CI]: 1.1–7.2; P = 0.03) and higher patient global assessment (OR: 1.1, 95% CI: 1.0–1.2; P = 0.04) were associated with relapse. During the off-treatment phase, presence of $CD19^+$ B cells (OR: 2.5, 95% CI: 1.2–5.1; P = 0.01) and reappearance of ANCA (OR: 3.2, 95% CI: 1.3–7.7; P = 0.01) were each associated with higher relapse risk. Multivariable analysis identified markers of inflammation (changes in platelets, white blood cells, and IgA) associated with relapse.

Conclusion. Risk factors for relapse in AAV vary by treatment phase. Monitoring markers of inflammation and immune reconstitution may identify patients at risk for relapse, particularly after treatment withdrawal.

INTRODUCTION

Antineutrophil cytoplasmic antibody (ANCA)–associated vasculitis (AAV), including granulomatosis with polyangiitis and microscopic polyangiitis, is a group of multisystem autoimmune diseases that often presents with organ- and life-threatening manifestations and is treated with prolonged use of immunosuppressive medications. Approaches to induction of remission in

Supported by the Penn Vasculitis Center. The RITAZAREM trial was supported by the Arthritis Research UK (now Vs Arthritis; grant 18706) and Roche/Genentech (MA28150). Roche/Genentech also provided rituximab for the study. The Vasculitis Clinical Research Consortium (VCRC) is part of the US Rare Diseases Clinical Research Network, NIH, which is an initiative of the Office of Rare Diseases Research, National Center for Advancing Translational Science (NCATS). Dr Romich's work was supported by National Institute of Arthritis and Musculoskeletal and Skin Diseases, NIH, Rheumatology Research Training Grant (5T32-AR076951-05). Dr Baker's work was supported by two Rehabilitation Research and Development Merit Awards (grants RX003644 and RX004770). Dr Riley's work was supported by the Clinical Pharmacoepidemiology Training Grant (grant 5T32GM075766-17). The VCRC was supported by the NCATS, National Institute of Arthritis and Musculoskeletal and Skin Diseases (grant U54 AR057319), National Center for Research Resources (grant U54 RR019497), and Research Committee on Intractable Vasculitides, the Ministry of Health, Labour and Welfare of Japan. Drs Smith's and Jayne's work was supported by the National Institute for Health Research, Cambridge Biomedical Research Centre, and the Cambridge Clinical Trials Unit.

[1]Division of Rheumatology, Department of Medicine, University of Pennsylvania, Philadelphia; [2]Division of Epidemiology, Department of Biostatistics, Epidemiology, and Informatics, University of Pennsylvania, Philadelphia; [3]Division of Pulmonary and Critical Care Medicine, Mayo Clinic, Rochester, Minnesota; [4]Department of Medicine, University of Cambridge, Cambridge, United Kingdom; [5]Cambridge University Hospitals NHS Foundation Trust, Cambridge, United Kingdom.

Additional supplementary information cited in this article can be found online in the Supporting Information section (https://acrjournals.onlinelibrary.wiley.com/doi/10.1002/art.70025).

Author disclosures are available at https://onlinelibrary.wiley.com/doi/10.1002/art.70025.

Address correspondence via email to Ellen Romich, MD, MSCE, at ellen.romich@pennmedicine.upenn.edu.

Submitted for publication July 15, 2025; accepted in revised form November 17, 2025.

new or relapsing disease and maintenance of remission have advanced considerably, resulting in improved survival.[1,2] Despite these advances, relapses are common during maintenance treatment and particularly once treatment is discontinued.[3,4] However, prolonged immunosuppression carries risks including secondary immunodeficiency, and not all patients experience relapse after completion of an induction and maintenance regimen.[5] Optimal dosing and treatment duration is not known.

Prior studies demonstrated that factors associated with relapse in AAV include disease manifestations such as pulmonary, renal, and sinonasal disease; treatment phase (maintenance vs postmaintenance); return of a positive test for ANCAs or rising ANCA levels; return of detectable $CD19^+$ B cells (peripheral blood); and patient-reported outcomes.[6–15] Genetic polymorphisms may also influence response to treatments, such as response to rituximab with Fcγ receptor or B cell–activating factor variants.[16,17] However, the ability to predict relapses in clinical practice remains limited. Existing studies commonly evaluate relapse risk over a several-year follow-up period, whereas in clinical practice it may be more practical to identify patients at high short-term risk of relapse if such predictions could guide treatment or monitoring strategies.

The RITAZAREM clinical trial enrolled patients with ANCA-positive AAV with clinical relapse. Following reinduction and achievement of remission with rituximab, patients were randomized to rituximab every four months or daily azathioprine, for a total of two years of treatment.[18] Patients were observed off treatment for an additional 12 to 24 months after completion of the maintenance regimen. Compared to azathioprine, rituximab reduced risk of relapse by 60%.[18]

The objective of this post hoc analysis of the RITAZAREM data set was to identify risk factors for short-term relapse in patients with AAV after successful reinduction of remission with rituximab, focusing separately on risk factors for relapse during maintenance treatment and off-treatment observation phases. This approach reflects the clinical scenario of desiring to know a patient's risk of relapse within a few months, which could influence treatment decisions in real time.

METHODS

Study design. This study is a post hoc analysis of the RITAZAREM clinical trial. The primary aim of this analysis was to determine predictors of disease relapse by the next study visit for two study phases as defined in the trial protocol: (1) treatment for maintenance of remission (months 4–24) and (2) off-treatment observation (months 24–48).[19] In RITAZAREM, all patients received rituximab, 375 mg/m^2 per week for four weeks, at month 0 for treatment to re-induce remission, and patients who achieved remission by month 4 were randomized to receive either rituximab or azathioprine with the goal of maintaining remission.[18] During the maintenance phase, patients randomized to rituximab received doses (1,000 mg) at months 4, 8, 12, 16, and 20, and patients randomized to azathioprine (2 mg/kg per day) received this medication from month 4 through 24, with the drug tapered off from month 24 to month 27 (Supplementary Figure S1). For the current study, maintenance and off-treatment phases were analyzed separately to test if there were distinct drivers of relapse for patients during maintenance therapy versus observation off-treatment. Data will be shared upon reasonable request. See Appendix for RITAZAREM Trial Investigators.

Study participants. Major inclusion and exclusion criteria for the RITAZAREM trial were as previously described.[19] Briefly, patients were aged 15 years or older with a diagnosis of AAV, had a current or prior positive test for proteinase-3 (PR3)-ANCA or myeloperoxidase (MPO)-ANCA, and experienced a disease relapse after previously achieving remission. Patients were included in this subanalysis if they completed treatment with rituximab for reinduction of remission in the RITAZAREM trial, achieved remission again by month 4, and moved on to maintenance treatment. All patients gave written, informed consent for trial participation, and de-identified data were used for this study.

Outcomes. The main outcome for this study was relapse, assessed as a binary outcome at each visit and defined as a return of disease activity by or at the subsequent study visit (3- to 6-month interval). This was chosen to reflect the clinical scenario of desiring to know a patient's risk of relapse *before the next follow-up visit*. Relapse was defined as in the RITAZAREM trial as the return or first appearance of at least one item on the Birmingham Vasculitis Activity Score for Wegener's granulomatosis (BVAS/WG).[20]

Covariates. *Variables collected at enrollment.* Data collected at trial enrollment included age; sex; body mass index; disease duration; ANCA type (anti-PR3 or anti-MPO); cumulative disease manifestations by organ system (constitutional, mucous membranes, ear/nose/throat, lung, kidney, musculoskeletal, skin, neurologic, cardiac, gastrointestinal, other); relapse severity at trial entry (severe or nonsevere); prednisone regimen at induction (1 mg/kg or 0.5 mg/kg); prior treatment with rituximab, azathioprine, or cyclophosphamide; and cumulative prior rituximab exposure. Treatment assignment in the maintenance phase, with rituximab or azathioprine, was determined upon randomization at month 4 among patients who achieved remission after induction therapy.

Genotyping was performed for the *FCGR2A* R131H (G>A variant) in a subset of patients with adequate samples available. The A allele corresponds to the missense variant R131H that influences the function of the Fcγ receptor; the AA genotype has been associated with complete remission and earlier time to remission among rituximab-treated patients with AAV.[16] Therefore, R131H genotype (categorical) was evaluated with an interaction with treatment (see Supplementary Methods for further detail).

Variables collected throughout follow-up period (time-varying). Data collected at enrollment and follow-up visits included prednisone dose, body mass index (certain visits only), number of months since last rituximab dose, laboratory measures (white blood cell count, hemoglobin, platelets, creatinine, erythrocyte sedimentation rate, C-reactive protein, alanine aminotransferase, IgG, IgM, and IgA), MPO and PR3 positivity (binary), MPO and PR3 level, $CD19^+$ B cell counts or percentage, BVAS/WG, physician global assessment (0–10, higher is worse), patient global assessment (0–10, higher is worse), EuroQOL five dimensions questionnaire visual analogue Scale (0–100),[21] Patient-Reported Outcomes Measurement Information System (PROMIS) Fatigue (short-form 4a v1.0 T-score[22]), PROMIS Pain Interference (short-form 4a v1.1 T-score[23]), and PROMIS Physical Function (short-form 4a v2.0 T-score[24]). Laboratory values were converted/harmonized to common units. Change in laboratory values and patient-reported outcomes was operationalized as the percentage change relative to the month 4 value (remission). As a sensitivity analysis based on a prior study demonstrating that changes in the patient global were predictive of relapse, absolute change in the patient global assessment from the prior visit was also evaluated.[8]

ANCA values. MPO-ANCA or PR3-ANCA positivity was determined at local sites during the trial. Additionally, MPO-ANCA or PR3-ANCA levels were determined semiquantitatively by a central laboratory (Mayo Clinic) using an automated addressable laser-bead immunoassay (BioPlex 2200, Bio-Rad) after completion of the trial.[25] A positive value was ≥1.0 antibody index unit. ANCA positivity for this study was based on the central laboratory result when available and otherwise was based on the local trial result. This approach minimized missing data (ANCA positivity <1% missing). Because patients were identified to have one ANCA type (MPO or PR3) at trial enrollment and ANCA type was prespecified to be included in the models, ANCA positivity was defined as either MPO or PR3 positive. Change in ANCA positivity during follow-up was categorized as negative to negative, negative to positive, positive to positive, or positive to negative compared to the prior visit.

$CD19^+$ B cell values. $CD19^+$ B cell results were determined at local sites during the trial and reported as cell counts and/or as a percentage of white blood cells. Cell counts were converted to common units (cells per 10^9/L). Test results recorded as less than the lower limit of the assay were recoded as zero (ie, <0.01 cells per 10^9/L was recoded as 0 and <1% recoded as 0). The presence of B cells (binary) was defined as either ≥0.01 cells × 10^9/L or ≥1%, similar to prior studies.[6,13] When B cell presence was missing for a given visit but the preceding and subsequent visits had identical results (ie, both present or both absent), that result was carried forward to replace the missing value. With this approach, data regarding B cell presence were missing in <10% of visits.

Statistical analysis. The statistical approach can be found in the Supplementary Methods. Enrollment characteristics and month 4 (remission) laboratory and outcome measure results were summarized. Characteristics at month 4 were compared among patients who did and did not experience relapse during trial follow-up using *t*-test, Wilcoxon rank-sum test, or chi-square test, as appropriate. To allow comparison of effect sizes across variables with different units of measurement, laboratory values and patient-reported outcome measures were natural log-transformed to fit a normal distribution and then standardized to month 4 remission values by subtracting the mean of the month 4 values and dividing by the SD of the month 4 values.

Logistic regression incorporating generalized estimating equations was used to identify risk factors for relapse by the next visit in each study phase following a prespecified modeling approach and including all available outcomes over time. For the maintenance phase analysis, data from months 4 to 20 were included, whereas for the off-treatment phase analysis, data from months 24 to 42 were included. Regression coefficients from these models can be interpreted as the relative odds of relapse before or at the next study visit among those with the exposure compared to those without the exposure.

Enrollment characteristics (static variables) were assessed first for their association with relapse. Variables associated in univariate analyses ($P < 0.10$) were explored as potential predictors for a multivariable model. Treatment group and ANCA type were prespecified to be included given their clinical relevance. Variables with $P < 0.05$ in the multivariable model were retained to establish a *base model*.

Time-varying predictors were then assessed by evaluating their association with relapse when added to the base model (see Supplementary Table S2 for variable list). Time-varying measures with $P < 0.10$ were included as potential predictors. Finally, the full *multivariable model* retained only variables with $P < 0.05$. Prespecified interactions between treatment and month, between ANCA positivity and B cell presence/return, and between treatment and B cell presence/return were also explored. The inclusion of a treatment and month interaction allows time-effects to vary by treatment, thereby accounting for differences in medication exposure over time between treatment groups.

Generalized estimating equations with logistic link function, robust SEs, and exchangeable correlation structure was used, accounting for repeated measures per patient. Alternative correlation structures were also explored. Variables in the full multivariable models were assessed for collinearity using variable inflation factors, and neither model had variable inflation factors >10. Analyses were conducted using Stata (StataCorp; 2023. *Stata Statistical Software: Release 18*. StataCorp LLC.).

RESULTS

This study included 170 patients with a median (interquartile range) age of 59 (48–68) years and disease duration of 5 (2–10) years who were randomized to rituximab or azathioprine at month 4 after achieving remission (Table 1). During follow-up, there were

Table 1. Enrollment characteristics by relapse status*

	Total (N = 170)	Relapse (n = 99)	No relapse (n = 71)	*P* value
Age at enrollment, y	59 (48–68)	58 (46–67)	61 (53–72)	0.10
Female sex	86 (51)	47 (47)	39 (55)	0.34
Body mass index	28 (24–32)	29 (26–32)	26 (24–32)	0.02
Treatment group				<0.001
Rituximab	85 (50)	38 (38)	47 (66)	
Azathioprine	85 (50)	61 (62)	24 (34)	
Prednisone induction regimen				0.72
0.5 mg/kg/d	122 (72)	70 (71)	52 (73)	
1.0 mg/kg/d	48 (28)	29 (29)	19 (27)	
Relapse type at enrollment				0.38
Nonsevere	64 (38)	40 (40)	24 (34)	
Severe	106 (62)	59 (60)	47 (66)	
ANCA type at enrollment (ever)				0.06
anti-MPO	47 (28)	22 (22)	25 (35)	
anti-PR3	123 (72)	77 (78)	46 (65)	
Disease duration at enrollment, mo	5 (2–10)	4 (2–9)	6 (3–13)	0.04
Organ involvement (ever)				
Constitutional	91 (54)	52 (53)	39 (55)	0.76
Musculoskeletal	125 (74)	79 (80)	46 (65)	0.03
Skin	54 (32)	38 (38)	16 (23)	0.03
Mucous membranes/eyes	58 (34)	37 (37)	21 (30)	0.29
Ear/nose/throat	127 (75)	75 (76)	52 (73)	0.71
Cardiac	6 (4)	5 (5)	1 (1)	0.40
Gastrointestinal tract	3 (2)	2 (2)	1 (1)	1.00
Lungs	103 (61)	57 (58)	46 (65)	0.34
Kidneys	114 (67)	64 (65)	50 (70)	0.43
Nervous system	47 (28)	29 (29)	18 (25)	0.57
Other	40 (24)	28 (28)	12 (17)	0.08
Prior azathioprine treatment	126 (74)	75 (76)	51 (72)	0.56
Prior rituximab treatment	60 (35)	34 (34)	26 (37)	0.76
Cumulative rituximab dose before enrollment, g	3.9 (2.8–6.0)	4.0 (3.0–6.0)	3.0 (2.5–6.0)	0.43
Prior oral or IV cyclophosphamide	133 (78)	75 (76)	58 (82)	0.36
FCGR2A R131H genotype, n	128	50	78	
GG	39 (31)	16 (32)	23 (30)	0.93
AG	59 (46)	23 (46)	36 (46)	
AA	30 (23)	11 (22)	19 (24)	

* Values presented as n (%) or median (interquartile range) unless otherwise specified. ANCA, antineutrophil cytoplasmic antibody; *FCGR2A* R131H, Fcγ receptor IIa R131H variant; IV, intravenous; MPO, myeloperoxidase; PR3, proteinase-3.

99 relapses, with 46 during the maintenance phase (months 4–24) and 53 during the off-treatment phase (months 24–48). Seventeen patients were censored due to death (n = 4), withdrawal (n = 8), or loss to follow-up (n = 5). The probability of relapse by the next study visit by month and treatment increased over time and was higher for the azathioprine group at each time point except for between months 30 and 36 (Figure 1).

Patients who experienced a relapse at any time during follow-up after randomization were more likely to receive azathioprine and have higher body mass index, shorter disease duration, and more frequent involvement of joints and skin (Table 2). They were also more likely to have lower serum creatinine, higher alanine aminotransferase, and higher IgG and IgA levels at month 4 (remission) (Supplementary Table S1).

Maintenance phase. In unadjusted analyses, disease duration, musculoskeletal involvement (includes arthritis and/or arthralgia), cumulative prior rituximab dose, and prior cyclophosphamide treatment were associated with relapse ($P < 0.1$) (Table 2). Within the base model, disease duration at enrollment was associated with lower odds of relapse (odds ratio [OR]: 0.9, 95% confidence interval [CI]: 0.8–1.0; $P = 0.005$), whereas musculoskeletal involvement was associated with 2.8-fold higher odds of relapse (OR: 2.8, 95% CI: 1.1–7.2; $P = 0.029$).

In univariate analyses for follow-up variables, higher (worse) patient global assessment was associated with relapse (Figure 2; Supplementary Table S2). In the multivariable model, musculoskeletal involvement (OR: 2.8, 95% CI: 1.1–7.5; $P = 0.038$) and higher patient global assessment scores (OR: 1.1, 95% CI: 1.0–1.2; $P = 0.043$) were associated with higher odds for relapse, whereas treatment with rituximab (OR: 0.3, 95% CI: 0.2–0.7; $P = 0.001$) and longer disease duration were associated with lower odds for relapse (OR: 0.9, 95% CI: 0.9–1.0; $P = 0.018$) (Table 3). Laboratory values, ANCA status, $CD19^+$ B cells, and *FCGR2A* R131H genotype were not associated with relapse during this phase. Percentage change in patient global assessment

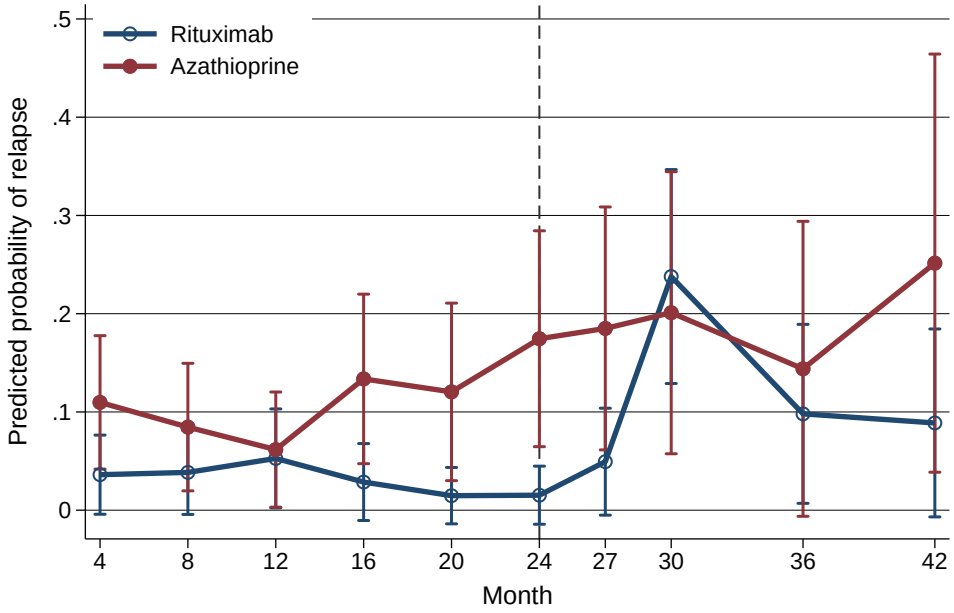

Figure 1. Predicted probability of relapse by month and treatment. Predicted probability of relapse by next visit from unadjusted generalized estimated equations logistic regression including treatment by month interaction. Probability of relapse is higher for the azathioprine group (red) at all time points except for month 30. The last scheduled rituximab maintenance treatment occurred at month 20 in the rituximab group (blue), while azathioprine was tapered off during months 24 to 27. The vertical line at month 24 divides the maintenance and off-treatment phases for the analysis.

from month 4 (remission) and absolute change in patient global from the prior visit were not associated with relapse by next visit during the maintenance phase.

Off-treatment phase. In unadjusted analyses, higher body mass index and skin involvement at enrollment were associated with higher odds of relapse by the next visit. Additionally, relapses were more common at month 30 (OR: 3.3, 95% CI: 1.4–7.8; $P = 0.005$) (Table 2). There was a higher proportion of patients with relapse at month 30 in the rituximab group; therefore, an interaction between treatment and study month was included. The interaction suggested that the risk of flare was higher at month 30 among patients in the rituximab arm, but not in the azathioprine arm ($P = 0.019$ for interaction) (Table 3). Thus, the base model for the off-treatment phase includes treatment assignment, ANCA type (both prespecified), study month, and the interaction between treatment and month.

Time-varying follow-up variables evaluated included laboratory values, patient-reported outcome measures, and the percentage change in these variables compared to month 4 (remission). Results are shown in Figure 2 and Supplementary Table S2. Individually, higher C-reactive protein, IgA, and percentage change in platelet count, white blood cell count, IgA, and C-reactive protein were associated with increased odds of relapse by next visit ($P < 0.05$). Additionally, ANCA positivity (OR: 2.0, 95% CI: 1.1–3.6; $P = 0.028$), change in ANCA from negative to positive compared to the prior visit (OR: 3.2, 95% CI: 1.3–7.7; $P = 0.011$), and $CD19^+$ B cell presence (OR: 2.5, 95% CI: 1.2–5.1; $P = 0.017$) were each associated with two- to three-fold increased risk of relapse by the next visit during the off-treatment phase, independent of treatment arm. The final full multivariable model for the off-treatment phase included variables in the base model (treatment, ANCA type, study month, and treatment and month interaction), along with IgA level and changes (percentage) in IgA, platelet count, and white blood cells from month 4 (Table 3). ANCA status and $CD19^+$ B cell presence were not significant in the full multivariable model. The patient global assessment and percentage change in the global assessment compared to month 4 were not associated with relapse during the off-treatment phase. In a sensitivity analysis, the change in the patient global assessment from the prior visit during the off-treatment phase was associated with relapse in unadjusted analyses (OR: 1.14, 95% CI: 1.02–1.28; $P = 0.019$) but was not significant in the multivariable model.

There was no interaction between treatment and the presence of $CD19^+$ B cells in the off-treatment phase ($P = 0.109$). Similarly, there was no significant interaction between treatment and ANCA positivity (in place of ANCA change) ($P = 0.490$). Replacing ANCA positivity (vs negativity) with ANCA level during the modeling process did not substantially change results.

As a sensitivity analysis, stratification by treatment group for the off-treatment phase was explored. In the rituximab group, adjusting for ANCA type and month, $CD19^+$ B cell presence was associated with relapse by the next visit (OR: 5.3, 95% CI: 1.5–19.4; $P = 0.01$), whereas ANCA positivity was not (OR: 1.6, 95% CI: 0.7–4.1; $P = 0.292$). In contrast, in the azathioprine group,

Table 2. Univariable logistic generalized estimating equations models for odds of relapse by next visit for each phase using enrollment characteristics and study month*

Univariable models	Maintenance phase		Off-treatment phase	
	OR (95% CI)	*P* value	OR (95% CI)	*P* value
Age at enrollment	0.99 (0.97–1.01)	0.30	1.00 (0.98–1.01)	0.71
Male (vs female)	0.90 (0.49–1.65)	0.74	1.58 (0.90–2.78)	0.11
Body mass index at enrollment[a]	1.49 (0.47–4.66)	0.50	3.05 (1.01–9.20)	0.05
Disease duration (years) at enrollment	0.91 (0.85–0.98)	0.01	0.98 (0.94–1.03)	0.50
Lung involvement	0.81 (0.44–1.48)	0.49	0.71 (0.40–1.26)	0.25
Ear, nose, throat involvement	0.94 (0.49–1.80)	0.85	1.17 (0.56–2.42)	0.68
Renal involvement	0.87 (0.46–1.63)	0.66	0.76 (0.42–1.37)	0.36
Musculoskeletal involvement	2.67 (1.12–6.39)	0.03	1.15 (0.61–2.19)	0.66
Skin involvement	1.16 (0.61–2.19)	0.65	1.77 (1.00–3.13)	0.05
Anti-PR3 (vs anti-MPO) at enrollment	0.97 (0.48–1.94)	0.92	1.68 (0.81–3.50)	0.16
Rituximab (vs azathioprine)	0.32 (0.17–0.62)	0.001	0.47 (0.27–0.83)	0.01
1.0 mg/kg/d (vs 0.5 mg/kg/d) induction prednisone regimen	1.27 (0.67–2.41)	0.46	1.03 (0.55–1.95)	0.93
Severe (vs nonsevere) relapse type at enrollment	0.62 (0.34–1.13)	0.13	0.90 (0.49–1.62)	0.72
BVAS/WG score at enrollment	1.00 (0.85–1.18)	0.98	1.10 (0.97–1.24)	0.14
Prior rituximab treatment	0.68 (0.35–1.32)	0.25	1.17 (0.66–2.08)	0.60
Cumulative prior rituximab dose (grams)	0.89 (0.79–1.00)	0.05	1.03 (0.96–1.11)	0.39
Prior azathioprine treatment	1.05 (0.53–2.06)	0.90	1.39 (0.70–2.74)	0.35
Prior oral or IV cyclophosphamide treatment	0.57 (0.29–1.10)	0.10	1.06 (0.50–2.24)	0.88
FCGR2A R131H genotype by treatment				
AG (vs GG), rituximab	1.71 (0.25–11.82)	0.59	2.85 (0.63–12.92)	0.18
AA (vs GG), rituximab[b]	–	–	4.11 (0.77–21.89)	0.10
Study month (vs mo 4)				
8	0.82 (0.33–2.00)	0.66	–	–
12	0.77 (0.30–1.94)	0.57	–	–
16	1.06 (0.44–2.55)	0.89	–	–
20	0.80 (0.31–2.11)	0.66	–	–
Study month (vs mo 24)				
27	–	–	1.29 (0.50–3.32)	0.60
30	–	–	3.33 (1.44–7.75)	0.005
36	–	–	1.47 (0.52–4.16)	0.46
42	–	–	1.89 (0.66–5.39)	0.23

* BVAS/WG, Birmingham Vasculitis Activity Score for Wegener's granulomatosis; CI, confidence interval; *FCGR2A* R131H, Fcγ receptor IIa; IV, intravenous; MPO, myeloperoxidase; OR, odds ratio; PR3, proteinase-3.
[a] Values log-transformed.
[b] Category omitted due to limited data.

ANCA positivity was associated with relapse (OR: 2.4, 95% CI: 1.0–5.9; $P = 0.047$), whereas CD19+ B cell presence was not (OR: 1.5, 95% CI: 0.6–3.5; $P = 0.389$). Due to small sample sizes, treatment-stratified models with additional variables and time interactions were not feasible.

DISCUSSION

This study identified risk factors for relapse after reinduction treatment with rituximab in patients with AAV at high risk of further relapse and identified distinct risk factors that differ according to each treatment phase. Shorter disease duration, musculoskeletal involvement, and higher (worse) patient global assessment were associated with relapse by the next visit during maintenance treatment. Markers of inflammation and immune reconstitution, meaning the presence or reappearance of serologic measures of systemic inflammation (eg, acute phase reactants), autoantibodies, and B cell function, were associated with relapse during the off-treatment phase. In the full multivariable model, these include higher IgA level and an increase in IgA level, platelet count, and white blood cell count compared to remission values. Overall, these findings suggest that monitoring of these laboratory values to identify patients at higher risk of short-term relapse may be most informative after treatment withdrawal.

Notably, there was a much higher risk of relapse by the next visit at study month 30 among patients who had been receiving maintenance rituximab (last maintenance dose administered at month 20) compared to azathioprine (tapered off during months 24–27). Patients receiving rituximab had 27-times higher odds of relapse between month 30 and 36, although the wide CI indicates uncertainty about the true magnitude of increased odds. The potential for relapse may have differed owing to more patients with early relapse in the azathioprine group and continued azathioprine exposure during months 24 to 27. Nevertheless, this finding supports that withdrawal of treatment is significantly associated with relapse and highlights a high-risk timeframe for relapse in patients treated with rituximab for maintenance of remission (approximately 10–16 months after the last infusion).

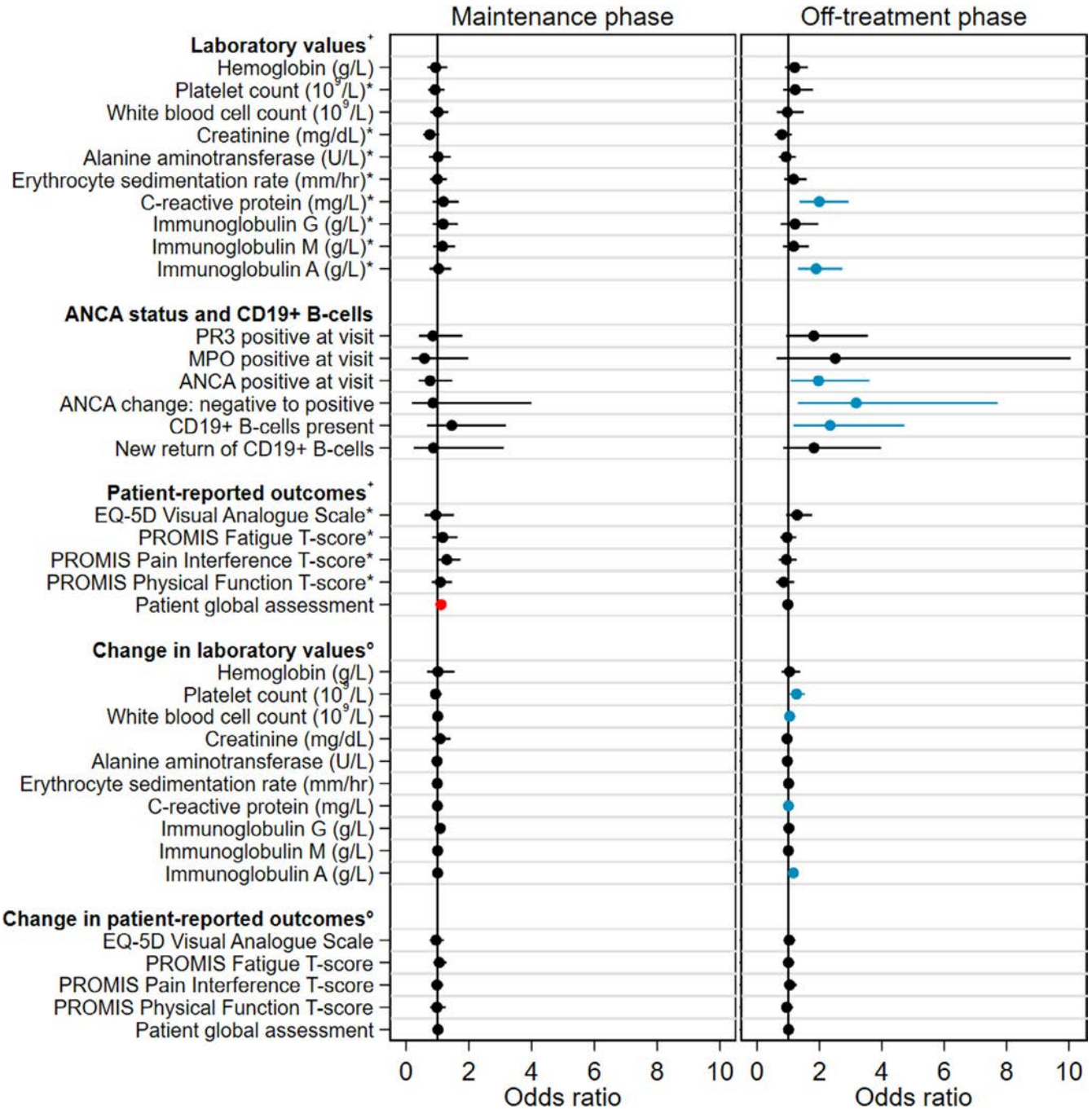

Figure 2. Odds ratios for relapse by next visit during the maintenance and off-treatment phases for individual follow-up variables. Odds ratios and 95% confidence intervals for relapse by next visit for laboratory values, ANCA status, and $CD19^+$ B cells, patient-reported outcomes, and change in these values compared to remission during the maintenance and off-treatment phases. Each follow-up variable was evaluated individually, and models were adjusted for the base model for each phase. Patient global assessment was associated with relapse by next visit during the maintenance phase (red). C-reactive protein, IgA, ANCA positivity, change in ANCA from negative to positive, and $CD19^+$ B cell presence are each associated with relapse by next visit during the off-treatment phase (blue). $^+$Continuous values were standardized to month 4 (remission) values. *Indicates variable is log-transformed. ^{0}Odds ratios for change in laboratory values and patient-reported outcomes are scaled to represent 10% change compared to remission. ANCA, antineutrophil cytoplasmic autoantibody; EQ-5D, EuroQOL five dimensions questionnaire; MPO, myeloperoxidase; PR3, proteinase-3; PROMIS, Patient-Reported Outcomes Measurement Information System.

Table 3. Full multivariable logistic generalized estimating equations model for odds of relapse by next visit during observation and maintenance phases*

	Maintenance phase		Off-treatment phase	
	OR (95% CI)	*P* value	OR (95% CI)	*P* value
Enrollment variables				
Treatment assignment: Rituximab (vs azathioprine)	0.3 (0.2–0.7)	<0.001	0.1 (0.0–0.6)	0.02
ANCA type at enrollment: anti-PR3 (vs anti-MPO)	0.9 (0.4–2.0)	0.80	1.7 (0.8–3.7)	0.20
Disease duration (years) at enrollment	0.9 (0.9–1.0)	0.02	–	–
Musculoskeletal involvement	2.8 (1.1–7.5)	0.04	–	–
Month (vs mo 24)				
27	–	–	1.0 (0.3–3.3)	0.95
30	–	–	0.8 (0.2–3.4)	0.81
36	–	–	0.4 (0.1–2.3)	0.28
42	–	–	0.9 (0.2–4.6)	0.91
Treatment by month interaction				
Rituximab, mo 27	–	–	1.3 (0.1–29.8)	0.88
Rituximab, mo 30	–	–	26.8 (1.7–428.3)	0.02
Rituximab, mo 36	–	–	21.1 (0.9–496.2)	0.06
Rituximab, mo 42	–	–	3.8 (0.2–73.1)	0.37
Follow-up variables				
Patient global assessment (0–10)	1.1 (1.0–1.2)	0.04	–	–
IgA level (g/L)[a]	–	–	1.6 (1.1–2.4)	0.02
Percent change in IgA level (g/L) from month 4[b]	–	–	1.1 (1.0–1.2)	0.004
Percent change in platelet count (10^9/L) from month 4[b]	–	–	1.2 (1.0–1.5)	0.02
Percent change in white blood cells (10^9/L) from month 4[b]	–	–	1.04 (1.0–1.1)	0.04

* ANCA, antineutrophil cytoplasmic antibody; CI, confidence interval; MPO, myeloperoxidase; OR, odds ratio; PR3, proteinase-3.
[a] Values log-transformed and standardized to month 4.
[b] Odds ratio scaled to represent 10% change in value.

This timeframe coincides with B cell repopulation after treatment with rituximab.[26]

The full models in the off-treatment phase also suggest that immune reconstitution is a strong predictor of flare. Several variables were associated with relapse in univariate analyses, including higher C-reactive protein, increases in C-reactive protein compared to remission, presence of detectable $CD19^+$ B cells, ANCA positivity, change in ANCA from negative to positive compared to the prior visit, and change in the patient global assessment from the prior visit. Although not all of these factors were retained in the final multivariable model, likely in part due to the interrelatedness of these measures as markers of inflammation and immune activity and a lack of granular assessments of B cell populations and ANCA levels over time, these findings provide further support that markers of immune reconstitution and inflammation are associated with short-term relapse risk. Thus, multiple approaches to identifying patients with immune reconstitution may be informative.

Prediction of relapse in AAV is an area of considerable interest, with prior attention given to the utility of ANCA levels and $CD19^+$ B cell counts.[9,12,27,28] This study identified associations between each of these measures and relapse in the off-treatment phase but not the maintenance phase. $CD19^+$ B cell repopulation coincides temporally with loss of drug effect. However, these measures did not remain in the final multivariable models, meaning that an independent predictive value was not found for the presence of $CD19^+$ B cells or ANCA positivity above what could be predicted from the timing of dosing. The findings that IgA, C-reactive protein, and white blood cell counts are associated with relapse are consistent with risk factors identified from the MAINRITSAN clinical trials.[29] However, other commonly recognized risk factors for relapse, such as lung involvement, sinonasal disease, and anti-PR3 antibody type, were not redemonstrated.[14] Differences between studies may reflect distinct patient populations. The patient population from the current study was selected to include ANCA-positive individuals with known relapsing disease. By enriching for relapsing disease and ANCA positivity, baseline disease manifestations differ from other trial populations that included patients with relapsing or nonrelapsing disease.[29] The current study also confirms an association between patient global assessment of disease activity and subsequent relapse.[8]

Strengths of this study include standardized prospective data collection at international expert centers within a clinical trial setting, randomized treatment assignment, minimal loss to follow-up, and centralized ANCA testing. A sequential modeling approach identified predictors with incremental benefit in the model while avoiding overfitting. Limitations to consider include generalizability from a clinical trial setting with selective enrollment of patients. Additionally, defining on- and off-treatment phases poses challenges. For this analysis, treatment phases were based on a two-year maintenance treatment period defined by the trial protocol. However, the end of rituximab's biologic effect is challenging to define, and patients receiving azathioprine tapered the medication off over months 24 to 27. Inclusion of a

treatment and month interaction term in the off-treatment phase models allows for time-dependent differences in relapse likelihood between treatment groups, which may help to mitigate confounding arising from differences in medication exposure. Missing data were encountered for some laboratory values, particularly for $CD19^+$ B cell measures, which were available as counts, percentages, or both. This limited the ability to include a single quantitative measure of B cells. Therefore, presence of B cells was defined based on thresholds for cell counts or percentages to accommodate the available data and reflect the ways B cell values are commonly encountered in practice. Similarly, although ANCA status was available from the trial data with minimal missingness, ANCA levels were determined separately at a central laboratory and only available for a subset of patients. However, in a sensitivity analysis, replacing ANCA status with quantitative ANCA binding level in the model building process yielded similar results.

These findings demonstrate that risk factors for short-term relapse in AAV differ by phase of treatment and suggest that laboratory monitoring at regular intervals for markers of immune activity (acute phase reactants, immunoglobulins, ANCA status, $CD19^+$ B cells) may be most informative after withdrawal of maintenance treatment. These results indicate that none of these tests in isolation is highly predictive of relapse. These findings highlight the efficacy of rituximab for maintenance treatment and the increased risk of relapse after treatment withdrawal, which can inform clinical practice. Additional longitudinal studies are needed to develop predictive tools to identify patients with increased risk of relapse over a short period and determine clinically significant thresholds of change in laboratory and immunologic parameters that influence risk of relapse. This may inform treatment and monitoring decisions, particularly after withdrawal of maintenance treatment. A prior study evaluated extended dosing of rituximab after completion of two years of fixed-schedule maintenance rituximab using return of B cells versus rise in ANCA levels to determine when to readminister rituximab and found that administration based on B cell repopulation resulted in fewer clinical relapses but also more frequent infusions of rituximab and COVID-19 infections.[13] Consideration of other markers of immune activity may help to tailor management of individual patients after maintenance treatment. Studies to predict risk of treatment-related infections will also be important to balance the risks and benefits of different approaches to maintenance treatment and observation after treatment withdrawal.

In conclusion, this study identified that among patients with AAV, markers of inflammation and immune reconstitution are associated with disease relapse within three to six months during the period of observation off treatment after completion of a regimen to maintain remission. These data support monitoring of these laboratory tests at regular intervals to help identify patients with AAV at risk for relapse after withdrawal of treatment.

ACKNOWLEDGMENT

The authors thank Phyllis A. Gimotty, PhD for her valuable advice on the approach to this analysis, which aided in refining the methodology and improving the overall rigor of this study.

AUTHOR CONTRIBUTIONS

All authors contributed to at least one of the following manuscript preparation roles: conceptualization AND/OR methodology, software, investigation, formal analysis, data curation, visualization, and validation AND drafting or reviewing/editing the final draft. As corresponding author, Dr Romich confirms that all authors have provided the final approval of the version to be published, and takes responsibility for the affirmations regarding article submission (eg, not under consideration by another journal), the integrity of the data presented, and the statements regarding compliance with institutional review board/Declaration of Helsinki requirements.

ROLE OF THE STUDY SPONSOR

Roche/Genentech had no role in the study design or in the collection, analysis, or interpretation of the data or the decision to submit the manuscript for publication. Publication of this article was not contingent upon approval by Roche/Genentech.

REFERENCES

1. Nelveg-Kristensen KE, Szpirt W, Carlson N, et al. Increasing incidence and improved survival in ANCA-associated vasculitis-a Danish nationwide study. Nephrol Dial Transplant 2021;37(1):63–71.
2. Rhee RL, Hogan SL, Poulton CJ, et al. Trends in long-term outcomes among patients with antineutrophil cytoplasmic antibody-associated vasculitis with renal disease. Arthritis Rheumatol 2016;68(7):1711–1720.
3. He P, Hu JP, Tian XJ, et al. Prevalence and risk factors of relapse in patients with ANCA-associated vasculitis receiving cyclophosphamide induction: a systematic review and meta-analysis of large observational studies. Rheumatology (Oxford) 2021;60(3):1067–1079.
4. King C, Druce KL, Nightingale P, et al. Predicting relapse in anti-neutrophil cytoplasmic antibody-associated vasculitis: a Systematic review and meta-analysis. Rheumatol Adv Pract 2021;5(3):rkab018.
5. Tieu J, Smith RM, Gopaluni S, et al. Rituximab associated hypogammaglobulinemia in autoimmune disease. Front Immunol 2021;12:671503.
6. McClure ME, Zhu Y, Smith RM, et al. Long-term maintenance rituximab for ANCA-associated vasculitis: relapse and infection prediction models. Rheumatology (Oxford) 2021;60(3):1491–1501.
7. Tomasson G, Grayson PC, Mahr AD, et al. Value of ANCA measurements during remission to predict a relapse of ANCA-associated vasculitis-a meta-analysis. Rheumatology (Oxford) 2012;51(1):100–109.
8. Tomasson G, Davis JC, Hoffman GS, et al. Brief report: the value of a patient global assessment of disease activity in granulomatosis with polyangiitis (Wegener's). Arthritis Rheumatol 2014;66(2):428–432.
9. Terrier B, Pagnoux C, Perrodeau É, et al; French Vasculitis Study Group. Long-term efficacy of remission-maintenance regimens for ANCA-associated vasculitides. Ann Rheum Dis 2018;77(8):1150–1156.
10. Alberici F, Smith RM, Jones RB, et al. Long-term follow-up of patients who received repeat-dose rituximab as maintenance therapy for ANCA-associated vasculitis. Rheumatology (Oxford) 2015;54(7):1153–1160.

11. Mehta P, Balakrishnan A, Phatak S, et al. Diagnostic accuracy of antineutrophil cytoplasmic antibodies (ANCA) in predicting relapses of ANCA-associated vasculitis: systematic review and meta-analysis. Rheumatol Int 2023;43(3):437–448.
12. Fussner LA, Hummel AM, Schroeder DR, et al; Rituximab in ANCA-Associated Vasculitis-Immune Tolerance Network Research Group. Factors determining the clinical utility of serial measurements of antineutrophil cytoplasmic antibodies targeting proteinase 3. Arthritis Rheumatol 2016;68(7):1700–1710.
13. Zonozi R, Cortazar FB, Jeyabalan A, et al. Maintenance of remission of ANCA vasculitis by rituximab based on B cell repopulation versus serological flare: a randomised trial. Ann Rheum Dis 2024;83(3): 351–359.
14. Zhou H, Liang W, Hu H, et al. An update on risk factors for relapse in antineutrophil cytoplasmic antibody-associated vasculitis. Clin Exp Immunol 2024;218(2):120–135.
15. Romich E, Banerjee S, Amudala N, et al. Patient-reported sinonasal symptoms and risk of relapse in antineutrophil cytoplasmic antibody-associated vasculitis. Arthritis Care Res (Hoboken) 2024;76(8): 1099–1108.
16. Cartin-Ceba R, Indrakanti D, Specks U, et al; RAVE-Immune Tolerance Network Research Group. The pharmacogenomic association of Fcγ receptors and cytochrome P450 enzymes with response to rituximab or cyclophosphamide treatment in antineutrophil cytoplasmic antibody-associated vasculitis. Arthritis Rheumatol 2017;69(1): 169–175.
17. Alberici F, Smith RM, Fonseca M, et al. Association of a TNFSF13B (BAFF) regulatory region single nucleotide polymorphism with response to rituximab in antineutrophil cytoplasmic antibody-associated vasculitis. J Allergy Clin Immunol 2017;139(5):1684–1687.e10.
18. Smith RM, Jones RB, Specks U, et al; RITAZAREM co-investigators. Rituximab versus azathioprine for maintenance of remission for patients with ANCA-associated vasculitis and relapsing disease: an international randomised controlled trial. Ann Rheum Dis 2023;82(7): 937–944.
19. Gopaluni S, Smith RM, Lewin M, et al; RITAZAREM Investigators. Rituximab versus azathioprine as therapy for maintenance of remission for anti-neutrophil cytoplasm antibody-associated vasculitis (RITAZAREM): study protocol for a randomized controlled trial. Trials 2017;18(1):112.
20. Stone JH, Hoffman GS, Merkel PA, et al; International Network for the Study of the Systemic Vasculitides (INSSYS). A disease-specific activity index for Wegener's granulomatosis: modification of the Birmingham Vasculitis Activity Score. Arthritis Rheum 2001;44(4):912–920.
21. Herdman M, Gudex C, Lloyd A, et al. Development and preliminary testing of the new five-level version of EQ-5D (EQ-5D-5L). Qual Life Res 2011;20(10):1727–1736.
22. Lai J-S, Cella D, Choi S, et al. How item banks and their application can influence measurement practice in rehabilitation medicine: a PROMIS fatigue item bank example. Arch Phys Med Rehabil 2011; 92(10 suppl):S20–S27.
23. Amtmann D, Cook KF, Jensen MP, et al. Development of a PROMIS item bank to measure pain interference. Pain 2010;150(1):173–182.
24. Rose M, Bjorner JB, Gandek B, et al. The PROMIS Physical Function item bank was calibrated to a standardized metric and shown to improve measurement efficiency. J Clin Epidemiol 2014;67(5): 516–526.
25. Kaul R, Johnson K, Scholz H, et al. Performance of the BioPlex 2200 Autoimmune Vasculitis kit. Autoimmun Rev 2009;8(3):224–227.
26. Thiel J, Rizzi M, Engesser M, et al. B cell repopulation kinetics after rituximab treatment in ANCA-associated vasculitides compared to rheumatoid arthritis, and connective tissue diseases: a longitudinal observational study on 120 patients. Arthritis Res Ther 2017;19 (1):101.
27. Charles P, Terrier B, Perrodeau É, et al; French Vasculitis Study Group. Comparison of individually tailored versus fixed-schedule rituximab regimen to maintain ANCA-associated vasculitis remission: results of a multicentre, randomised controlled, phase III trial (MAINRITSAN2). Ann Rheum Dis 2018;77(8): 1143–1149.
28. Specks U, Merkel PA, Seo P, et al; RAVE-ITN Research Group. Efficacy of remission-induction regimens for ANCA-associated vasculitis. N Engl J Med 2013;369(5):417–427.
29. Delestre F, Charles P, Karras A, et al; French Vasculitis Study Group (FVSG). Rituximab as maintenance therapy for ANCA-associated vasculitides: pooled analysis and long-term outcome of 277 patients included in the MAINRITSAN trials. Ann Rheum Dis 2024;83(2): 233–241.

APPENDIX A: RITAZAREM TRIAL INVESTIGATORS

Collaborators of the RITAZAREM Trial Investigators are as follows: Reem Al-jayyousi (Nephrology, University Hospitals of Leicester NHS Trust, Leicester, United Kingdom); Yoshihiro Arimura (Kyorin University School of Medicine, Tokyo, Japan); Jacqueline Andrews (NIHR Leeds Musculoskeletal Biomedical Research Unit, Leeds Teaching Hospitals Trust, Leeds, United Kingdom); Simon Bond and Marianna Nodale (Cambridge Clinical Trials Unit, Cambridge University Hospitals NHS Foundation Trust, Cambridge, United Kingdom); Annette Bruchfeld (Nephrology, Karolinska University Hospital and Karolinska Institute, Stockholm, Sweden); Brian Camilleri (Nephrology, Ipswich Hospital NHS Trust, Ipswich, United Kingdom); Simon Carette (Rheumatology, University of Toronto, Toronto, Ontario, Canada); Chee Kay Cheung (Nephrology, University of Leicester, Leicester, United Kingdom); Michael Clarkson (Cork University Hospital, Cork, Ireland); Janak de Zoysa (North Shore Hospital, Auckland, New Zealand); Vimal Derebail (Medicine, University of North Carolina at Chapel Hill, Chapel Hill, North Carolina); Tim Doulton (Nephrology, East Kent Hospitals University NHS Foundation Trust, Canterbury, United Kingdom); Tomomi Endo, Eri Muso, and Tatsuo Tsukamoto (Kitano Hospital, Osaka, Japan); Alastair Ferraro (Nephrology, Nottingham University Hospitals NHS Trust, Nottingham, United Kingdom); Lindsy Forbess (Rheumatology, Cedars-Sinai Medical Center, Los Angeles, California); Shouichi Fujimoto (Hemovascular Medicine and Artificial Organs, Faculty of Medicine, University of Miyazaki, Miyazaki, Japan); Shunsuke Furuta (Allergy and Clinical Immunology, Chiba University, Chiba, Japan); Ora Gewurz-Singer (Rheumatology, University of Michigan, Ann Arbor, Michigan); Yoshitomo Hamano (Tokyo Metropolitan Geriatric Hospital, Tokyo, Japan); Lorraine Harper (Nephrology, University of Birmingham, Birmingham, United Kingdom); Toshiko Ito-Ihara (The Clinical and Translational Research Center, Kyoto Prefectural University of Medicine, Kyoto, Japan); Rachel B. Jones (Medicine, University of Cambridge, Cambridge, United Kingdom); Nader Khalidi (Medicine, McMaster University, Hamilton, Ontario, Canada); Rainer Klocke (Rheumatology, Dudley Group of Hospitals NHS Trust, Dudley, United Kingdom); Curry L. Koening (Rheumatology, The University of Utah, Salt Lake City, Utah); Yoshinori Komagata (First Department of Internal Medicine, Kyorin University School of Medicine, Tokyo, Japan); Hajime Kono and Shunya Uchida (Teikyo University Hospital, Tokyo, Japan); Carol A. Langford (Rheumatic and Immunologic Diseases, Cleveland Clinic Foundation, Cleveland, Ohio); Peter Lanyon (Rheumatology, Nottingham University Hospital, Nottingham, United Kingdom); Sarah Lawman (Brighton Royal Sussex County Hospital, Brighton, United Kingdom); Raashid Luqmani (Nuffield Department of Orthopaedics, Rheumatology and Musculoskeletal Science, University of Oxford, Oxford, United Kingdom); Larry W. Moreland (Medicine/Rheumatology, University of Pittsburg, Pittsburg, Pennsylvania); Kim Mynard (Vasculitis and lupus clinic, Cambridge University Hospitals NHS Foundation Trust, Cambridge, United Kingdom); Patrick Nachman (UNC Kidney Center, Division of Nephrology and Hypertension, University of North Carolina at Chapel Hill, Chapel Hill, North Carolina); Christian Pagnoux (Mount Sinai Hospital,

University of Toronto, Toronto, Ontario, Canada); Chen Au Peh (Nephrology, Royal Adelaide Hospital, Adelaide, South Australia, Australia); Charles Pusey (Medicine, Imperial College London, London, United Kingdom); Dwarakanathan Ranganathan (Medicine, Royal Brisbane and Women's Hospital, Herston, Queensland, Australia); Ken-ei Sada (Okayama University, Okayama, Japan); Richard Smith and Richard Watts (Ipswich Hospital NHS Trust, Ipswich, United Kingdom); Robert Spiera (Rheumatology, Hospital for Special Surgery, New York, New York); Antoine G. Sreih (Rheumatology, University of Pennsylvania Perelman School of Medicine, Philadelphia, Pennsylvania); Kazuo Suzuki (Teikyo University, Tokyo Japan); Vladamir Tesar (Medicine, Charles University, Praha, Czech Republic); Augusto Vaglio (University of Parma, Parma, Italy); Giles Walters (Nephrology, Australian National University Medical School, Canberra, Australian Capital Territory, Australia); and Caroline Wroe (Nephrology, South Tees Hospitals NHS Foundation Trust, Middlesbrough, United Kingdom).

Arthritis & Rheumatology
Vol. 78, No. 5, May 2026, pp 1145–1151
DOI 10.1002/art.70032

American College of Rheumatology
Empowering Rheumatology Professionals

Antineutrophil Cytoplasmic Antibody–Associated Vasculitides in Systemic Sclerosis: A Unique Clinical Overlap With Significant Implications for Treatment and Outcomes

Deborah Eshagh, MD,[1] Thomas Quéméneur, MD,[2] Alexandre Karras, MD, PhD,[3] Viviane Queyrel, MD,[4] Jean-Francois Augusto, MD, PhD,[5] Christian Agard, MD, PhD,[6] Vincent Audard, MD, PhD,[7] Alexandre Cez, MD,[8] Marion Couderc, MD,[9] Pierre Duffau, MD, PhD,[10] Cécile Audrey Durel, MD,[11] Stanislas Faguer, MD, PhD,[12] Noémie Jourde-Chiche, MD, PhD,[13] Aurélie Lavergne, MD,[14] Christian Lavigne, MD, PhD,[15] Nicolas Limal, MD,[16] Rafik Mesbah, MD,[17] Amélie Servettaz, MD, PhD,[18] Carole Philipponnet, MD,[19] Perrine Smets, MD,[20] Theophile Hubsch, MD,[21] Benjamin Chaigne, MD, PhD,[1] Alexis Régent, MD, PhD,[1] Xavier Puéchal, MD, PhD,[1] Luc Mouthon, MD, PhD,[1] and Benjamin Terrier, MD, PhD,[1] on behalf of the French Vasculitis Study Group

Objective. Systemic sclerosis (SSc) is an autoimmune disease characterized by autoantibody production, fibrosis, and vasculopathy. The coexistence of antineutrophil cytoplasmic autoantibody (ANCA)–associated vasculitides (AAV) in SSc is rare and poorly characterized, with limited data on the impact of treatments, particularly high-dose glucocorticoids (GCs), on both conditions. This study aimed to describe the clinical phenotype, management, and outcomes of patients with overlapping SSc and AAV.

Methods. We conducted a multicenter retrospective study in 18 French centers, including patients who met the 2013 American College of Rheumatology (ACR)/EULAR criteria for SSc and the 2022 ACR/EULAR criteria for AAV. Clinical, biologic, and radiologic data were collected.

Results. We included 30 patients (median age 51.5 years, 83% female). SSc preceded AAV in all cases; 27% had diffuse cutaneous SSc, whereas 73% had limited cutaneous SSc. Anti-Scl70 antibodies were detected in 50%, and interstitial lung disease (ILD) was present in 80%, predominantly with a fibrosing nonspecific interstitial pneumonia pattern (54%). AAV was microscopic polyangiitis in 90%, with myeloperoxidase (MPO)–ANCA positivity in 93%. Renal involvement was common (76%), with a median serum creatinine level of 170 µmol/L (interquartile range [IQR] 120–361 µmol/L) and proteinuria (urine protein to creatinine ratio of 2 g/g creatinine [IQR 0.9–2.3 g/g creatinine]). All patients received GCs in combination with cyclophosphamide (50%) or rituximab (47%). No cases of scleroderma renal crisis were observed. SSc manifestations, including ILD and skin involvement, remained stable during follow-up.

Conclusion. AAV, predominantly microscopic polyangiitis with MPO-ANCA, can occur in SSc, particularly in patients with fibrosing ILD and anti-Scl70. Standard vasculitis treatments appear to be effective and do not worsen outcomes in SSc.

INTRODUCTION

Antineutrophil cytoplasmic autoantibody (ANCA)–associated vasculitides (AAV) are a group of necrotizing vasculitides characterized by inflammation of small blood vessels.[1] The three main entities are microscopic polyangiitis (MPA), granulomatosis with polyangiitis (GPA), and eosinophilic GPA (EGPA). AAV are commonly associated with two major ANCA patterns: anti–

[1]Department of Internal Medicine, Cochin Hospital, AP-HP, Paris, France; [2]Department of Internal Medicine, Centre Hospitalier, Valenciennes, France; [3]Department of Nephrology, Georges Pompidou Hospital, AP-HP, Paris, France; [4]Department of Internal Medicine, Centre Hospitalier Universitaire, Nice, France; [5]Department of Nephrology, Centre Hospitalier Universitaire, Angers, France; [6]Nantes Université, Centre Hospitalier Universitaire Nantes, Service de médecine interne, Nantes, France; [7]Department of Nephrology and Transplantation, Henri Mondor University Hospital, Université Paris Créteil (AP-HP), Institute Mondor of Research Biomedical, Créteil, France; [8]Department of Nephrology, Tenon Hospital, AP-HP, Paris, France; [9]Department of Rheumatology, Centre Hospitalier Universitaire, INSERM, IMosT, UMR 1240, Université d'Auvergne, Clermont-Ferrand, France; [10]Department of Internal Medicine, Centre Hospitalier Universitaire, Bordeaux, France; [11]Department of Internal Medicine, Hôpital Edouard Herriot, Lyon, France; [12]Department of Nephrology and Organ Transplantation and National Referral Centre for Rare Kidney Diseases, University Hospital of Toulouse, Toulouse, France; [13]Department of Nephrology, Centre Hospitalier Universitaire, Marseille, France; [14]Department of Nephrology, Centre Hospitalier

proteinase 3, which is predominantly observed in GPA, and anti-myeloperoxidase (MPO-ANCA), which is more commonly associated with MPA and, to a lesser extent, EGPA.[2,3] Renal involvement, often manifesting as rapidly progressive glomerulonephritis, is a hallmark of AAV. Treatment typically combines high-dose glucocorticoids (GCs) with immunosuppressive agents such as rituximab or cyclophosphamide.[4–6] Although AAV is primarily idiopathic, it can also occur as a result of other conditions, including drug exposure or underlying autoimmune disease. Secondary AAV is most commonly associated with MPO-ANCA.[7,8]

Systemic sclerosis (SSc) is a complex autoimmune disease characterized by autoantibodies production, cutaneous and visceral fibrosis, and widespread vasculopathy.[9] SSc is classified into diffuse cutaneous SSc (dcSSc), in which skin fibrosis extends beyond the elbows and knees, and limited cutaneous SSc (lcSSc), in which fibrosis is restricted to the distal extremities.[10] Interstitial lung disease (ILD) is a common complication in SSc and a leading cause of death, typically presenting as nonspecific interstitial pneumonia (NSIP). Vasculopathy, including Raynaud phenomenon, is often an early manifestation of SSc, whereas scleroderma renal crisis (SRC) is the most severe renal complication, characterized by hypertensive emergency, acute kidney injury, and thrombotic microangiopathy. GC use is a well-established risk factor for SRC.[11–13]

The prevalence of ANCA in SSc ranges from 0% to 12% in published studies,[14–16] with MPO-ANCA being the most commonly reported subtype. The coexistence of AAV and SSc is rare, with only anecdotal reports describing this overlap.[17] Data on how SSc affects the management of AAV, particularly in the context of high-dose GC use, are scarce. Similarly, the impact of AAV treatments on SSc progression, including ILD and vasculopathy, remains poorly understood.

This study aimed to characterize the rare association between SSc and AAV, describe the clinical phenotype and management of this complex overlapping syndrome, and assess the impact of treatments on both diseases.

METHODS

Study design. This retrospective multicenter study was conducted in 18 centers in France. Patients with a diagnosis of SSc and AAV were included. SSc diagnoses were made between 1990 and 2020, whereas AAV diagnoses were made between 2001 and 2021. Patients were eligible for inclusion if they were over 18 years of age and met both the 2013 American College of Rheumatology (ACR)/EULAR classification criteria for SSc[9] and the 2022 ACR/EULAR criteria for AAV.[18]

Data collection. The following clinical and biologic data were collected for each patient: date of SSc diagnosis, clinical manifestations, immunologic biomarkers (additional SSc-related antibodies, including anti–RNA polymerase III and anti-Ku, were assessed in 57% of patients), previous treatment, date of AAV diagnosis, disease duration of SSc at the diagnosis of AAV, type of vasculitis, clinical manifestations, presence of ANCA, histologic confirmation, therapeutic management, and renal and overall outcome. The chest scans of all patients were reviewed by an experienced radiologist and classified according to the American Thoracic Society/European Respiratory International Multidisciplinary Consensus of the Idiopathic Interstitial Pneumonias.[19]

Statistical analysis. Descriptive statistics were used to summarize baseline characteristics. Continuous variables were expressed as medians with interquartile ranges (IQRs) for nonnormally distributed data, and categorical variables were expressed as frequencies (percentages).

Comparisons between subgroups were performed using the Mann–Whitney or Wilcoxon signed rank test for continuous variables and the chi-square test or Fisher's exact test for categorical variables. A two-tailed P value <0.05 was considered statistically significant.

Ethical considerations. The study was conducted in accordance with the tenets of the Declaration of Helsinki and was approved by our local institutional review board. Informed consent was not required due to the retrospective nature of the study. However, patient confidentiality was strictly maintained throughout the study.

RESULTS

Patients' characteristics at the diagnosis of SSc. A total of 30 patients with concurrent SSc and AAV were included in the study (Table 1). The cohort was predominantly female

Universitaire, Rennes, France; [15]Department of Internal Medicine, Centre de référence des Maladies Auto-Immunes et Auto-inflammatoires Systémiques rares de l'Adulte du Nord, Nord-Ouest, Méditerranée et Guadeloupe, site d'Angers Centre Hospitalier Universitaire, Angers, France; [16]Department of Internal Medicine, Henri Mondor Hospital, AP-HP, Créteil, France; [17]Department of Nephrology, Centre Hospitalier, Boulogne sur Mer, France; [18]Department of Internal Medicine, Centre Hospitalier Universitaire, Reims, France; [19]Department of Nephrology, Centre Hospitalier Universitaire, Clermont-Ferrand, France; [20]Department of Internal Medicine, Centre Hospitalier Universitaire, Clermont-Ferrand, France; [21]Department of Internal Medicine, Hôpital d'instruction des Armées Saint Anne, Toulon, France.

Additional supplementary information cited in this article can be found online in the Supporting Information section (https://acrjournals.onlinelibrary.wiley.com/doi/10.1002/art.70032).

Author disclosures are available at https://onlinelibrary.wiley.com/doi/10.1002/art.70032.

Address correspondence via email to Benjamin Terrier, MD, PhD, at benjamin.terrier@aphp.fr.

Submitted for publication May 23, 2025; accepted in revised form November 12, 2025.

Table 1. Patients' characteristics at the time of SSc diagnosis*

Characteristics	Value (n = 30)
Demographics	
Female sex, n (%)	25 (83)
Age at diagnosis (IQR), y	51.5 (46–71)
Clinical manifestation of SSc, n (%)	
Raynaud phenomenon	30 (100)
Calcinosis	2 (7)
Gastroesophageal reflux	21 (70)
Arthralgia	10 (33)
Myalgia	3 (10)
Interstitial lung disease	24 (80)
NSIP with fibrosis	13/24 (54)
NSIP	3/24 (12)
UIP	5/24 (21)
PH	3 (10)
SRC	2 (7)
Myocardial damage	1 (3)
Laboratory tests, n (%)	
Positive ANA	30 (100)
Anti-Scl70	16 (53)
Anticentromere	6 (20)
Anti–RNA polymerase III	1 (3)
Anti-Ku	1 (3)
Nonspecific	6 (20)

* ANA, antinuclear antibody; IQR, interquartile range; NSIP, nonspecific interstitial pneumonia; PH, pulmonary hypertension; SRC, scleroderma renal crisis; SSc, systemic sclerosis; UIP, usual interstitial pneumonia.

(83%), with a median age of 51.5 (IQR 46–71) years at diagnosis of SSc.

In all cases, SSc preceded the diagnosis of AAV. The median interval between the onset of SSc symptoms and the diagnosis of AAV was 6 years (IQR 1–10 years), providing a more accurate estimate of disease chronology.

Nine patients (27%) had dcSSc, whereas the remaining 73% had lcSSc. The median modified Rodnan skin score (mRSS) at diagnosis of AAV was 4 (IQR 4–6) for lcSSc and 24 (IQR 16–29) for dcSSc. Raynaud phenomenon was observed in all patients. ILD was present in 80% of patients, with high-resolution computed tomography (HRCT) showing NSIP with fibrosis in 54%, NSIP without fibrosis in 13%, usual interstitial pneumonia (UIP) in 21%, and an indeterminate pattern in 12%. Two patients had an SRC before the diagnosis of vasculitis.

Antinuclear antibodies (ANAs) were detected in all patients. The most common autoantibody subtype was anti-Scl70, identified in 53% of patients. Anticentromere antibodies were found in six patients (20%), nonspecific ANAs were found in six patients (20%), and anti–RNA polymerase III antibodies were found in one patient (3%).

Previous treatments for SSc included GCs alone in five patients and GCs and immunosuppressive therapy in seven patients. The different immunosuppressants were cyclophosphamide (n = 4), azathioprine (n = 2), methotrexate (n = 2), and mycophenolate mofetil (n = 2); two patients received multiple immunosuppressants: mycophenolate mofetil, cyclophosphamide, azathioprine, and methotrexate for the first patient and cyclophosphamide and mycophenolate mofetil for the second.

Patients' characteristics at diagnosis of AAV. MPA was the predominant AAV subtype, observed in 27 patients (90%), followed by GPA in 2 patients (7%) and EGPA in 1 patient (3%) (Table 2). ANCAs were present in 29 patients (97%), with anti MPO-ANCA specificity in 28 patients (93%).

Renal involvement was the most common manifestation of AAV, affecting 76% of patients. The median serum creatinine level at diagnosis was 170 μmol/L (IQR 120–361 μmol/L), with a median urine protein to creatinine ratio of 2 g/g creatinine (IQR 0.9–2.3 g/g creatinine). Pulmonary involvement was reported in seven patients (23%), including six cases of diffuse alveolar hemorrhage and one case of pulmonary nodules. Peripheral neuropathy and skin involvement were observed in four patients (13%) each.

Histologic confirmation of AAV was available in 25 patients, including 21 renal biopsies, 2 muscle biopsies, 1 skin biopsy, and 1 paranasal sinus biopsy. Pauci-immune glomerulonephritis

Table 2. Characteristics at the time of AAV diagnosis*

Characteristics	Value (n = 30)
AAV subtype, n (%)	
MPA	27 (90)
GPA	2 (7)
EGPA	1 (3)
Baseline clinical characteristics of AAV, n (%)	
Constitutional signs	15 (50)
Arthralgia	6 (20)
Myalgia	3 (10)
Cutaneous involvement	4 (13)
Purpura	2 (7)
Livedo	2 (7)
Ear, nose, and throat involvement	5 (17)
Sinusitis	3 (10)
Otitis	1 (3)
Crusty rhinitis	1 (3)
Ocular involvement	2 (7)
Blepharitis	1 (3)
Scleritis	1 (3)
Pulmonary involvement	7 (23)
Intra-alveolar hemorrhage	6 (20)
Nodules	1 (3)
Peripheral nervous system involvement	4 (13)
Mononeuritis multiplex	3 (10)
Polyneuropathy	1 (3)
Glomerulonephritis	23 (77)
Laboratory tests	
Serum creatinine, median (IQR), μmol/L	170 (120–361)
Proteinuria, urine protein to creatinine ratio, median (IQR), g/g	2 (0.95–2.26)
Positive ANCA, n (%)	29 (97)
MPO-ANCA, n (%)	28/29 (93)
PR3-ANCA, n (%)	1/29 (3)

* AAV, ANCA-associated vasculitis; ANCA, antineutrophil cytoplasm antibody; EGPA, eosinophilic granulomatosis polyangiitis; GPA, granulomatosis with polyangiitis; IQR, interquartile range; MPA, microscopic polyangiitis; MPO, myeloperoxidase; PR3, proteinase 3.

was found in all renal biopsy samples (n = 25). In one patient, the renal biopsy showed concomitant features of pauci-immune vasculitis and SRC. In this patient, the clinical presentation was dominated by AAV with a pulmonary-renal syndrome combining intra-alveolar hemorrhage and rapidly progressive glomerulonephritis, whereas the SRC component appeared to be an incidental finding.

Therapeutic management and progression of AAV. All patients received GCs as part of their induction therapy, with a median initial dose of 0.8 mg/kg/day (IQR 0.5–1.0 mg/kg/day) (Table 3). Fifteen patients (50%) received pulses of methylprednisolone (between 250 and 1,000 mg per day for three days), primarily those with more severe renal impairment (median creatinine level of 322 µmol/L in those receiving pulses vs 120 µmol/L in those not receiving pulses; $P = 0.03$).

Plasma exchanges were performed in five patients: two for rapidly progressive glomerulonephritis, two for peripheral neuropathy, and one for pulmonary-renal syndrome. Induction immunosuppressive regimens included cyclophosphamide in 15 patients (50%) and rituximab in 14 patients (47%). Only one patient received GC monotherapy. This patient had EGPA and a Five-Factor Score of 0, consistent with current therapeutic recommendations for this low-risk form. Patients who received cyclophosphamide were diagnosed with AAV in earlier years compared with those treated with rituximab, whereas age at diagnosis and disease severity were similar between groups.

The GC tapering strategy was intermediate between the standard and reduced-dose regimens described in the PEXIVAS protocol (Figure 1, Supplementary Figure 1). Maintenance immunosuppressive therapy was initiated in 26 patients, with rituximab in 16 patients, azathioprine in 6 patients, and mycophenolate mofetil in 4 patients. All but one patient with kidney involvement were treated with angiotensin-converting enzyme inhibitors at the time of diagnosis.

After a median follow-up of 4 years (IQR 2–10 years), 9 patients achieved durable remission of AAV without sequelae, 17 patients were in durable remission with sequelae (chronic renal failure in 13 patients and neuropathic pain in 2 patients), and 4 patients experienced an AAV relapse, with renal involvement in 3 (median delay of relapse was 24 months).

Table 3. Therapeutic management of AAV*

AAV management	n (%)
Glucocorticoids	30 (100)
Pulse of methylprednisolone	15 (50)
Plasma exchange	5 (17)
Induction therapy	29 (97)
Cyclophosphamide	15 (52)
Rituximab	14 (48)
Maintenance therapy	26 (87)
Rituximab	16 (62)
Azathioprine	6 (23)
Mycophenolate mofetil	4 (15)

* AAV, ANCA-associated vasculitis; ANCA, antineutrophil cytoplasmic antibody.

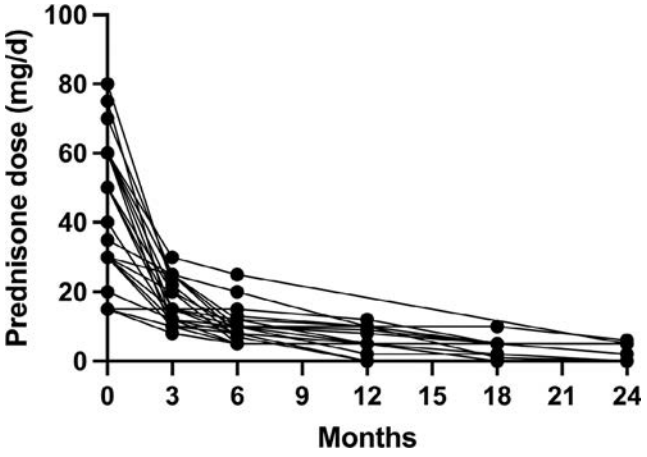

Figure 1. Reduction of glucocorticoids in the treatment of antineutrophil cytoplasmic antibody–associated vasculitis.

SSc evolution after AAV treatment. After a median follow-up of 4 years (IQR 2–10 years), no cases of SRC were observed after the use of high-dose GCs for AAV treatment. SSc manifestations remained stable during follow-up, with no significant progression of skin involvement or ILD (Figure 2). Changes in mRSS were analyzed only in patients with dcSSc, whereas pulmonary function evolution was evaluated exclusively in patients with established ILD.

DISCUSSION

This study sheds light on the rare association between SSc and AAV, highlighting unique clinical phenotypes and critical considerations for diagnosis and management. By characterizing this overlap syndrome, we underscore the importance of heightened vigilance in patients with SSc, especially those with specific risk factors.

Our results show that patients with SSc who develop AAV are predominantly women in their 50s, reflecting the general demographics of SSc.[20] Most patients had lcSSc, which is classically associated with anticentromere antibodies and a lower risk of ILD. However, more than half of the patients in this cohort had anti-Scl70 antibodies and fibrosing ILD, a pattern typically associated with dcSSc.[21] This atypical association is consistent with previous studies, including those by Quéméneur et al[22] and Zanatta et al,[23] which demonstrated that anti-Scl70 antibodies in patients with lcSSc are strongly associated with ILD. Interestingly, the most common HRCT pattern in our cohort was fibrosing NSIP, in contrast to the predominance of UIP in AAV-ILD cases.[24,25] Our data suggest that patients with lcSSc, anti-Scl70 antibodies, and fibrosing ILD represent a unique phenotype at

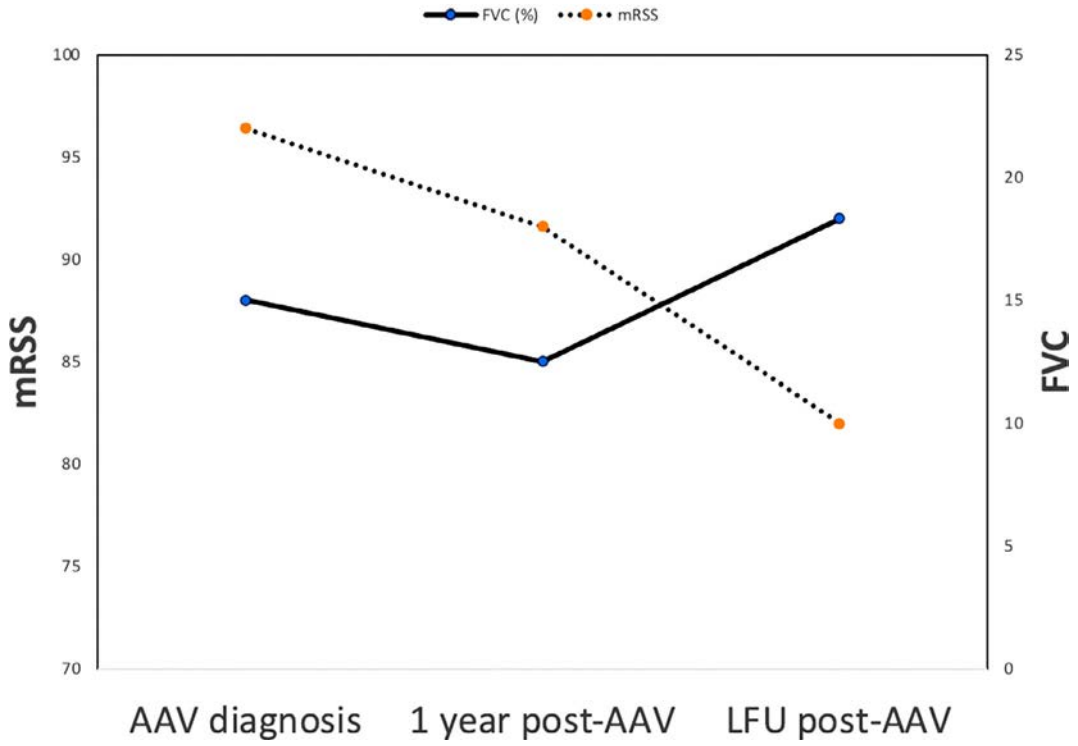

Figure 2. Changes in mRSS in patients with diffuse cutaneous systemic sclerosis and FVC in patients with interstitial lung disease during AAV management. AAV, antineutrophil cytoplasmic antibody–associated vasculitis; FVC, forced vital capacity; LFU, last follow-up; mRSS, modified Rodnan skin score.

increased risk of developing AAV; this observation should be interpreted with caution due to the small sample size and the retrospective design of the study. Early identification of these patients is critical because this overlapping syndrome requires management strategies different from those used for typical SSc or AAV alone. It should be noted because of the long inclusion period that testing for certain SSc-related antibodies, such as anti–RNA polymerase III or anti-Ku, was not systematically performed in earlier cases, which may have introduced a potential selection bias.

In our cohort, AAV occurred relatively early in the disease course, with a median time of five years from SSc diagnosis to AAV onset. Nearly all cases were MPA with MPO-ANCA positivity, a pattern consistent with the known prevalence of MPO-ANCA in secondary AAV. Renal involvement was predominant, affecting more than three-quarters of patients. Clinical presentations were consistent with rapidly progressive glomerulonephritis, and histologic findings revealed pauci-immune extracapillary glomerulonephritis. Distinguishing between AAV and SRC is critical for patients with SSc with renal manifestations. SRC typically occurs in dcSSc and is associated with anti–RNA polymerase III antibodies, severe hypertension, and features of thrombotic microangiopathy in 50% of the cases. In contrast, our study confirms that AAV-associated renal involvement is characterized by higher proteinuria, MPO-ANCA positivity, and a lower prevalence of hypertension. These findings are consistent with those reported by Arad et al,[26] who highlighted the diagnostic and prognostic differences between AAV and SRC in patients with SSc. Differentiating between these two conditions is critical because their management is fundamentally different. AAV treatment requires high-dose GCs and immunosuppressive therapy, whereas SRC management focuses on angiotensin-converting enzyme inhibitors and blood pressure control. In cases of renal involvement among patients with lcSSc with anti-Scl70 antibodies, AAV should be strongly considered, especially in the presence of proteinuria, hematuria, and MPO-ANCA positivity.

The tolerability of AAV treatment in this cohort was favorable. Notably, no cases of SRC were reported despite the use of high-dose GCs. This is a significant finding, given that GCs are a known risk factor for SRC in SSc. Additionally, lung function remained stable, with no significant decline in forced vital capacity, during follow-up. Interestingly, GC tapering followed a pattern closer to the reduced-dose regimen outlined in the PEXIVAS protocol,[27] whereas the vast majority were treated before the publication of the PEXIVAS trial results, likely reflecting the need to mitigate the risk of SRC in patients with SSc. Maintenance therapy was primarily based on rituximab and azathioprine, and after a median follow-up of four years, most patients achieved durable remission, albeit in some cases with sequelae, including chronic kidney disease and neuropathic pain. For patients at high risk of SRC,

avacopan,[28] a C5aR1 antagonist, may be an option for reducing GC therapy. Therefore, tolerance of GC treatment should be analyzed in relation to the time elapsed between SSc and AAV diagnosis. If more than five years have elapsed, the risk of SRC is much lower, making it safer to prescribe GC therapy. If the time is shorter, avacopan could be a better option.

This study is one of the largest to examine the rare overlap between SSc and AAV, using a multicenter design to provide robust and generalizable findings. The rigorous inclusion criteria, requiring validation of both the ACR/EULAR 2013 classification criteria for SSc[9] and the ACR/EULAR 2022 classification criteria for AAV,[18] enhance diagnostic accuracy and reliability. However, the retrospective design may introduce selection and recall bias, and the small sample size inherent to the rarity of this overlap limits statistical power for subgroup analyses. Additionally, the absence of a comparator group prevents a direct evaluation of the impact of AAV on SSc progression and vice versa. Despite these limitations, the study offers valuable insights into the phenotype, management, and outcomes of SSc-AAV overlap. It also underscores the necessity of prospective studies to further elucidate its pathophysiology and optimal management strategies.

In conclusion, AAV is a rare but clinically significant complication of SSc that predominantly manifests as MPO-ANCA MPA with renal involvement. Patients with lcSSc, anti-Scl70 antibodies, and fibrosing ILD seem to be at the highest risk. Treatment for vasculitis, including high-dose GCs and immunosuppressive agents such as rituximab and cyclophosphamide, was well tolerated and did not exacerbate SSc-related manifestations. These findings underscore the necessity of personalized treatment strategies and additional research to improve outcomes in this distinctive overlapping syndrome.

AUTHOR CONTRIBUTIONS

All authors contributed to at least one of the following manuscript preparation roles: conceptualization AND/OR methodology, software, investigation, formal analysis, data curation, visualization, and validation AND drafting or reviewing/editing the final draft. As corresponding author, Dr Terrier confirms that all authors have provided the final approval of the version to be published and takes responsibility for the affirmations regarding article submission (eg, not under consideration by another journal), the integrity of the data presented, and the statements regarding compliance with institutional review board/Declaration of Helsinki requirements.

REFERENCES

1. Jennette JC, Falk RJ, Bacon PA, et al. 2012 revised International Chapel Hill Consensus Conference Nomenclature of Vasculitides. Arthritis Rheum 2013;65(1):1–11. doi:https://doi.org/10.1002/art.37715
2. Westman KW, Selga D, Bygren P, et al. Clinical evaluation of a capture ELISA for detection of proteinase-3 antineutrophil cytoplasmic antibody. Kidney Int 1998;53(5):1230–1236. doi:https://doi.org/10.1046/j.1523-1755.1998.00873.x
3. Guillevin L, Durand-Gasselin B, Cevallos R, et al. Microscopic polyangiitis: clinical and laboratory findings in eighty-five patients. Arthritis Rheum 1999;42(3):421–430. doi:https://doi.org/10.1002/1529-0131(199904)42:3<421:AID-ANR5>3.0.CO;2-6
4. Puéchal X, Pagnoux C, Baron G, et al; French Vasculitis Study Group. Adding azathioprine to remission-induction glucocorticoids for eosinophilic granulomatosis with polyangiitis (Churg-Strauss), microscopic polyangiitis, or polyarteritis nodosa without poor prognosis factors: a randomized, controlled trial. Arthritis Rheumatol 2017;69(11):2175–2186. doi:https://doi.org/10.1002/art.40205
5. Guillevin L, Pagnoux C, Karras A, et al; French Vasculitis Study Group. Rituximab versus azathioprine for maintenance in ANCA-associated vasculitis. N Engl J Med 2014;371(19):1771–1780. doi:https://doi.org/10.1056/NEJMoa1404231
6. Charles P, Terrier B, Perrodeau É, et al; French Vasculitis Study Group. Comparison of individually tailored versus fixed-schedule rituximab regimen to maintain ANCA-associated vasculitis remission: results of a multicentre, randomised controlled, phase III trial (MAINRITSAN2). Ann Rheum Dis 2018;77(8):1143–1149. doi:https://doi.org/10.1136/annrheumdis-2017-212878
7. Ando M, Miyazaki E, Ishii T, et al. Incidence of myeloperoxidase antineutrophil cytoplasmic antibody positivity and microscopic polyangiitis in the course of idiopathic pulmonary fibrosis. Respir Med 2013;107(4):608–615. doi:https://doi.org/10.1016/j.rmed.2013.01.006
8. Kagiyama N, Takayanagi N, Kanauchi T, et al. Antineutrophil cytoplasmic antibody-positive conversion and microscopic polyangiitis development in patients with idiopathic pulmonary fibrosis. BMJ Open Respir Res 2015;2(1):e000058. doi:https://doi.org/10.1136/bmjresp-2014-000058
9. van den Hoogen F, Khanna D, Fransen J, et al. 2013 classification criteria for systemic sclerosis: an American College of Rheumatology/European League Against Rheumatism collaborative initiative. Arthritis Rheum 2013;65(11):2737–2747. doi:https://doi.org/10.1002/art.38098
10. LeRoy EC, Black C, Fleischmajer R, et al. Scleroderma (systemic sclerosis): classification, subsets and pathogenesis. J Rheumatol 1988;15(2):202–205.
11. Steen VD. Renal involvement in systemic sclerosis. Clin Dermatol 1994;12(2):253–258. doi:https://doi.org/10.1016/S0738-081X(94)90329-8
12. Penn H, Howie AJ, Kingdon EJ, et al. Scleroderma renal crisis: patient characteristics and long-term outcomes. QJM 2007;100(8):485–494. doi:https://doi.org/10.1093/qjmed/hcm052
13. Teixeira L, Mahr A, Berezné A, et al. Scleroderma renal crisis, still a life-threatening complication. Ann N Y Acad Sci 2007;1108(1):249–258. doi:https://doi.org/10.1196/annals.1422.027
14. Merkel PA, Polisson RP, Chang Y, et al. Prevalence of antineutrophil cytoplasmic antibodies in a large inception cohort of patients with connective tissue disease. Ann Intern Med 1997;126(11):866–873. doi:https://doi.org/10.7326/0003-4819-126-11-199706010-00003
15. Ruffatti A, Sinico RA, Radice A, et al. Autoantibodies to proteinase 3 and myeloperoxidase in systemic sclerosis. J Rheumatol 2002;29(5):918–923.
16. Moxey J, Huq M, Proudman S, et al. Significance of anti-neutrophil cytoplasmic antibodies in systemic sclerosis. Arthritis Res Ther 2019;21(1):57. doi:https://doi.org/10.1186/s13075-019-1839-5
17. Kao L, Weyand C. Vasculitis in systemic sclerosis. Int J Rheumatol 2010;2010:385938. doi:https://doi.org/10.1155/2010/385938
18. Yazici H, Tascilar K, Yazici Y. 2022 American College of Rheumatology/European Alliance of Associations for Rheumatology classification criteria sets for three types of antineutrophilic cytoplasmic antibody-associated vasculitis. Curr Opin Rheumatol 2023;35(1):1–5. doi:https://doi.org/10.1097/BOR.0000000000000916

19. American Thoracic Society; European Respiratory Society. American Thoracic Society/European Respiratory Society International Multidisciplinary Consensus Classification of the Idiopathic Interstitial Pneumonias. This joint statement of the American Thoracic Society (ATS), and the European Respiratory Society (ERS) was adopted by the ATS board of directors, June 2001 and by the ERS Executive Committee, June 2001. Am J Respir Crit Care Med 2002;165(2):277–304. doi:https://doi.org/10.1164/ajrccm.165.2.ats01
20. Chifflot H, Fautrel B, Sordet C, et al. Incidence and prevalence of systemic sclerosis: a systematic literature review. Semin Arthritis Rheum 2008;37(4):223–235. doi:https://doi.org/10.1016/j.semarthrit.2007.05.003
21. Steen VD. Autoantibodies in systemic sclerosis. Semin Arthritis Rheum 2005;35(1):35–42. doi:https://doi.org/10.1016/j.semarthrit.2005.03.005
22. Quéméneur T, Mouthon L, Cacoub P, et al. Systemic vasculitis during the course of systemic sclerosis: report of 12 cases and review of the literature. Medicine (Baltimore) 2013;92(1):1–9. doi:https://doi.org/10.1097/MD.0b013e31827781fd
23. Zanatta E, Huscher D, Ortolan A, et al; EUSTAR collaborators. Phenotype of limited cutaneous systemic sclerosis patients with positive anti-topoisomerase I antibodies: data from the EUSTAR cohort. Rheumatology (Oxford) 2022;61(12):4786–4796. doi:https://doi.org/10.1093/rheumatology/keac188
24. Bouros D, Wells AU, Nicholson AG, et al. Histopathologic subsets of fibrosing alveolitis in patients with systemic sclerosis and their relationship to outcome. Am J Respir Crit Care Med 2002;165(12):1581–1586. doi:https://doi.org/10.1164/rccm.2106012
25. Maillet T, Goletto T, Beltramo G, et al; French Vasculitis Study Group (FVSG). Usual interstitial pneumonia in ANCA-associated vasculitis: a poor prognostic factor. J Autoimmun 2020;106:102338. doi:https://doi.org/10.1016/j.jaut.2019.102338
26. Arad U, Balbir-Gurman A, Doenyas-Barak K, et al. Anti-neutrophil antibody associated vasculitis in systemic sclerosis. Semin Arthritis Rheum 2011;41(2):223–229. doi:https://doi.org/10.1016/j.semarthrit.2010.11.001
27. Walsh M, Merkel PA, Peh CA, et al; PEXIVAS Investigators. Plasma exchange and glucocorticoids in severe ANCA-associated vasculitis. N Engl J Med 2020;382(7):622–631. doi:https://doi.org/10.1056/NEJMoa1803537
28. Jayne DRW, Merkel PA, Schall TJ, et al; ADVOCATE Study Group. Avacopan for the treatment of ANCA-associated vasculitis. N Engl J Med 2021;384(7):599–609. doi:https://doi.org/10.1056/NEJMoa2023386

American College of Rheumatology
Empowering Rheumatology Professionals

Arthritis & Rheumatology
Vol. 78, No. 5, May 2026, pp 1152–1165
DOI 10.1002/art.70039

Single-Cell Profiling Reveals Divergent Mechanisms of Fibrosis in Localized Scleroderma and Systemic Sclerosis

Junxia Huang, MS,[1] Xue Han, MS,[1] Xiuyuan Wang, MD,[1] Liuting Huang, MS,[1] Manna Lin, MS,[1] Cheng Chen, MS,[1] Linzhu Kang, BS,[1] Yuqing Huang, BS,[1] Feifei Hu, MD,[1] Xinzhi Xu, MD,[2] Xue Yang, MD,[3,4] and Ji Yang, MD[1]

Objective. Localized scleroderma (LoS) and systemic sclerosis (SSc) are both fibrotic diseases, but LoS is limited to the skin, whereas SSc involves systemic organ fibrosis. This study aimed to elucidate the mechanisms underlying these differences.

Methods. Skin biopsies from three healthy controls, three patients with LoS, and three patients with SSc underwent immunofluorescence and single-cell RNA sequencing (scRNA-seq). Key molecular functions were validated using in vitro assays and murine models.

Results. Immunofluorescence revealed a high prevalence of tertiary lymphoid structures (TLS) in LoS lesions (65.7%) compared with SSc (14.3%, $P = 0.0013$). scRNA-seq identified T follicular helper (Tfh) cells enriched within TLS in LoS. Tfh cells likely promote B cell recruitment via the *CXCL13/CXCR5* axis, and integrin α4 may support Tfh cell retention, contributing to TLS stability. These organized immune aggregates, together with elevated transforming growth factor β (*TGF-β*) expression, may drive localized fibroblast activation and skin fibrosis in LoS. In contrast, SSc lesions contained fibroblasts with high CREB3L1 expression. CREB3L1 overexpression increased Type I collagen, fibronectin 1, and periostin levels in fibroblasts, whereas knockdown reduced them. In a SSc mouse model, CREB3L1 upregulation worsened skin and lung fibrosis, whereas knockdown alleviated it.

Conclusion. These findings suggest that LoS fibrosis is driven by TLS-mediated local immune activation, whereas the systemic activation of CREB3L1-expressing fibroblasts plays an important role in SSc fibrosis. Targeting local inflammation may benefit LoS, whereas targeting CREB3L1 offers a promising antifibrotic strategy in SSc.

INTRODUCTION

Localized scleroderma (LoS) and systemic sclerosis (SSc) are rare, chronic autoimmune diseases characterized by inflammatory cell infiltration and fibrosis, yet they exhibit distinct clinical features and outcomes.[1] LoS is typically limited to the skin and subcutaneous tissue, causing localized skin sclerosis without internal organ involvement (eg, pulmonary fibrosis).[2,3] In contrast, SSc is a systemic disorder that affects both the skin and multiple internal organs, including the lungs, heart, kidneys, and gastrointestinal tract.[4] Both diseases share histopathological features in the skin, including collagen deposition, immune cell infiltration, and abnormal vascular intimal hyperplasia that culminates in vascular narrowing. However, LoS demonstrates pronounced inflammation during early disease stages,[2] whereas advanced SSc progresses to vascular occlusion, loss of skin appendages, and visceral fibrosis.[5] This paradoxical overlap in histopathology yet disparity in clinical outcomes underscores the need to identify distinct molecular drivers underlying each disease.

Supported by the National Natural Science Foundation of China (grants 82373463, 82203917, 82073436), National Outstanding Young Physician Program, the Shanghai Municipal Health Commission Traditional Chinese Medicine Research Project (grant 2024PT004), the Oriental Scholar Program, the 2022 Clinical Physician Training Project, the 2023 Clinical Research Special Fund of Zhongshan Hospital, Fudan University (grant ZSLCYJ202323), 2024 Shanghai Oriental Talents Program-Top Talent Project (grant BJKJ2024048), the Flagship Integrated Traditional Chinese and Western Medicine Clinical Department Program, the Shanghai Talent Development Fund, and the Shanghai Health and Wellness Discipline Leader program.

[1]Department of Dermatology, Zhongshan Hospital of Fudan University, Shanghai, China; [2]Department of Dermatology, Minhang Meilong Branch, Zhongshan Hospital, Fudan University, Shanghai, China; [3]Division of Rheumatology, Huashan Hospital, Fudan University, Shanghai, China; [4]Institute of Rheumatology, Immunology and Allergy, Fudan University, Shanghai, China.

Dr Junxia Huang, Xue Han, Xiuyuan Wang, Liuting Huang, and Manna Lin are co-first authors and contributed equally to the text.

Additional supplementary information cited in this article can be found online in the Supporting Information section (https://acrjournals.onlinelibrary.wiley.com/doi/10.1002/art.70039).

Author disclosures are available at https://onlinelibrary.wiley.com/doi/10.1002/art.70039.

Address correspondence via email to Xue Yang, MD, at yangxue21@yeah.net; or to Ji Yang, MD, at yang.ji@zs-hospital.sh.cn.

Submitted for publication July 20, 2025; accepted in revised form November 18, 2025.

Transcriptomic profiling of both skin and blood has highlighted important mechanistic differences between LoS and SSc. LoS shows a predominant contribution of T cell dysregulation with relatively little activation of fibrotic programs. By contrast, SSc exhibits systemic profibrotic transcriptional signatures, even though the two conditions share certain inflammatory components.[6] These findings underscore key differences in fibroproliferative mechanisms underlying LoS and SSc. Tertiary lymphoid structures (TLS) are ectopic, organized lymphoid aggregates that arise in settings of chronic inflammation. They have been observed in both autoimmune diseases and cancer, where they influence local immune activity and inflammatory responses.[7,8] A previous report reported TLS in LoS lesions containing $CD21^+$ follicular dendritic cells,[9] suggesting a potential role in localized immune activation. However, the mechanisms governing TLS formation in LoS and the functional contributions of T follicular helper (Tfh) cells within these structures remain poorly understood.

Patients with SSc commonly develop multiorgan fibrosis, whereas LoS is confined to the skin, indicating disease-specific regulation of fibroblast activity. Single-cell RNA sequencing (scRNA-seq) has revealed considerable heterogeneity among fibroblasts in SSc. In the lung, a subset of myofibroblasts with elevated *COMP*, *POSTN*, and COL1A1 expression is associated with pulmonary fibrosis,[10] whereas in the skin, fibroblast subpopulations correlate with autoantibody profiles.[11] Although both LoS and SSc share core pathogenic features such as immune dysregulation and fibroblast activation, the spatial regulation and extent of fibrotic progression appear to differ, and the cellular mechanisms underlying these differences remain poorly defined. To address this gap, we applied scRNA-seq to directly compare the cellular and molecular landscapes of skin with LoS and SSc and integrated these data with histology, immunofluorescence, and murine models. We aimed to identify molecular determinants that distinguish localized from systemic fibrotic pathways.

METHODS

Patients and healthy donors

Patients with SSc and LoS along with healthy controls (HC) were recruited from Shanghai Zhongshan Hospital. SSc diagnoses adhered to the 2013 American College of Rheumatology/European League Against Rheumatism classification criteria.[12] Clinical metadata for all patients undergoing scRNA-seq, including organ involvement, immunosuppressive therapy at the time of biopsy, and disease progression status, are detailed in Supplementary Table 1. Disease progression was defined as new or worsening skin or internal organ involvement during follow-up, including progressive skin fibrosis (modified Rodnan skin score increase >5 and ≥25% from baseline to 12 ± 3 months[13]), progressive interstitial lung disease (forced vital capacit [FVC] decline ≥10%, or FVC decline 5–9% with diffusing capacity of the lung for carbon monoxide decline ≥15%), or radiographic progression on high-resolution computed tomography.[14] This study protocol was approved by the Institutional Review Board for Clinical Research of Shanghai Zhongshan, Hospital of Fudan University (approval number: B2023-414). scRNA-seq was performed on skin biopsies from three patients per group (LoS, SSc, HC).

scRNA-seq and analysis

Skin biopsies (5 mm) were obtained from the skin of healthy donors and patients with LoS or SSc. Tissues were dissociated using sCelLive Tissue Dissociation Solution (Singleron Biotechnologies, Nanjing, China) on a Singleron PythoN Tissue Dissociation System. Single-cell suspensions were prepared following the GEXSCOPE Single Cell RNA Library Kits protocol.[15] Libraries were sequenced on an Illumina NovaSeq 6000 platform with 150 bp paired-end reads. Samples were sequenced in multiple runs, and batch effects were corrected using Harmony v1.0 with the top 20 principal components from principal component analysis. Cells with fewer than 200 detected genes, cells with the top 2% gene or unique molecular identifier (UMI) counts, and cells with >20% mitochondrial content were excluded. Genes detected in fewer than five cells were also removed. After filtering, 75,283 cells were retained for downstream analyses, with a mean of 1,204 detected genes and 3,995 UMIs per cell; 12.6% of the reads were mitochondrial. Data processing—including quality control, dimensionality reduction, and clustering—was performed using Scanpy v1.8.1 in Python 3.7. Cell clusters were visualized using uniform manifold approximation and projection (UMAP) with Seurat functions (Run UMAP). The enrichment preferences of the cell clusters were evaluated using $R_{o/e}$ values ($R_{o/e}$ >1 indicates enrichment and <1 indicates relative depletion).[16] Differentially expressed genes were identified via Wilcoxon rank-sum test with default parameters, retaining genes expressed in over 10% of cells per group and showing an average log2 (fold change) >1. Gene Ontology (GO) and Kyoto Encyclopedia of Genes and Genomes pathway analyses were conducted with the "clusterProfiler" R package (version 3.16.1), considering pathways with an adjusted *P* value less than 0.05 as significantly enriched. Cell-cell interaction (CCI) among vascular endothelial cells (VECs), capillary endothelial cells (CapECs), Tfh cells, CD8 T cells, B cells, and fibroblasts were predicted using NicheNet in R[17] based on known ligand-receptor pairs. Pseudotemporal trajectories were constructed with Monocle2 (version 2.10.0). Transcription factor regulatory networks were analyzed using pySCENIC (v0.11.0) by integrating scRNA-seq data with transcription factors from AnimalTFDB. GRNBoost2 was used to infer co-expression networks, followed by CisTarget for motif enrichment analysis. Regulon activity scores were quantified with AUCell and visualized as heatmaps.

Immunofluorescence staining

Fresh skin tissues from patients with LoS (n = 35), patients with SSc (n = 34), and healthy donors (n = 6) were fixed,

embedded, and sectioned into 5-μm–thick slices. The three LoS, three SSc, and three HC samples analyzed by scRNA-seq were included within this larger histology cohort. Detailed clinical and histologic information is provided in Supplementary Tables 2 and 3. Sections were deparaffinized in xylene and subjected to antigen retrieval using citrate buffer. Following blocking with 3% goat serum albumin, the sections were incubated overnight at 4°C with primary antibodies (listed in Supplementary Table 4). After phosphate-buffered saline (PBS) washing, sections were incubated with fluorescent secondary antibodies, counterstained with DAPI, and imaged using a confocal microscope. Histologic evaluation of skin biopsies was independently conducted by two dermatopathologists who were both blinded to the patients' clinical diagnoses and disease status.

Primary skin fibroblast isolation and culture

Full-thickness skin samples were obtained from the forearms of patients with SSc or healthy donors. Skin pieces were digested with 0.1% type I collagenase and 0.25% trypsin for 1 hour at 37°C. The resulting cell suspension was filtered through a 70-μm nylon mesh and plated for adherence. Fibroblasts (passages 3 to 6) were cultured in Dulbecco's modified Eagle medium (DMEM) supplemented with 10% to 15% fetal bovine serum, 5 mM glucose, 0.7 mM glutamine, and 1% penicillin-streptomycin.

Cell transfection

For CREB3L1 overexpression, primary skin fibroblasts at 70% confluence were transduced with recombinant lentivirus (Hanbio Biotech) in DMEM containing Polybrene (4 μg/mL) at an multiplicity of infection (MOI) of 80. After 48 hours, the medium was replaced with fresh complete medium, followed by puromycin selection (4 μg/mL) for 72 hours. The expression vector pHBLV-CMV-MCS-3FLAG-EF1-ZsGreen-T2A-PURO was used. For CREB3L1 knockdown, primary skin fibroblasts were transduced with short hairpin RNA (shRNA) lentivirus (MOI = 25) targeting CREB3L1 (sh-CREB3L1: 5′-GCTGAAGAGCTACATCAACAA-3′) or nontargeting control (sh-NC) (Hanbio Biotech) in the presence of Polybrene (8 μg/mL). Puromycin selection (2.5 μg/mL) was performed for 72 hours before analysis by Western blotting (WB).

CREB3L1 modulation in a bleomycin-induced mouse model of SSc

All animal procedures were approved by the Institutional Animal Care and Use Committee of Zhongshan Hospital (Approval No. 2024-016), and the animals were housed in a specific pathogen-free facility at the hospital's experimental animal center. Adeno-associated viruses (AAVs)[18] used in this study, including AAV6-sh*Creb3l1* (*Creb3l1* knockdown) and AAV6-oe*Creb3l1* (*Creb3l1* overexpression), were custom designed by Hanheng Biotechnology Co., Ltd (Shanghai, China).

Eight-week-old male C57BL/6 mice were randomly divided into the following four groups: HC, BLM-ctrl (bleomycin with control virus), BLM-OE (bleomycin with *Creb3l1* overexpression virus), and BLM-sh (bleomycin with *Creb3l1* knockdown virus) (eight mice per group, two independent experiments). Dermal fibrosis was induced by daily intradermal injection of bleomycin (100 μg in 100 μL; Nippon Kayaku, Japan) into a 2 cm^2 dorsal skin area for three weeks. Control mice received equivalent volume PBS injections before bleomycin injection and were anesthetized with sodium pentobarbital and administered intratracheally with AAVs (5×10^{10} vector genomes in 75 μL PBS). Control groups received AAV-mock particles. Skin and lung samples were harvested on day 22 for analysis.

WB

Protein lysates from fibroblasts and mouse tissues were extracted using radioimmunoprecipitation assay buffer containing protease and phosphatase inhibitors. Equal amounts of protein were separated by sodium dodecyl sulfate–polyacrylamide gel electrophoresis, which were transferred to polyvinylidene difluoride membranes and probed with primary antibodies (Supplementary Table 4) followed by horseradish peroxidase-conjugated secondary antibodies. Signals were detected by chemiluminescence, and band intensities were quantified using ImageJ.

Immunohistochemistry and imaging

Skin and lung tissues from mice were fixed in 4% paraformaldehyde, paraffin-embedded, sectioned, and stained with hematoxylin and eosin for histology or Masson's trichrome for collagen deposition assessment. Immunohistochemical staining for collagen I and collagen III was performed using primary antibodies from Servicebio (Wuhan, China).

Statistical analysis

Data are presented as mean ± SD from at least three independent experiments. Statistical comparisons were performed using unpaired Student's *t*-test (two-group comparisons) or one-way analysis of variance (ANOVA) with Tukey's post hoc test (multiple groups), whereas pairwise comparisons involving small sample sizes or zero counts in HCs were assessed by Fisher's exact test. The significance level was set at $P < 0.05$. Statistical analyses were conducted using GraphPad Prism 9.0 (GraphPad Prism Software, Inc., San Diego, CA).

The single-cell sequencing data generated in this study have been deposited in the NCBI Sequence Read Archive (BioProject: PRJNA1280955). A read-only access link can be obtained from the corresponding author on request. Individual-level patient data

are not publicly available because of privacy and ethical considerations.

RESULTS

Histologic identification of TLS in LoS and SSc lesions

Histologic analysis of hematoxylin and eosin (HE)-stained sections revealed distinct pathologic features in skin lesions from patients with LoS and SSc. Both conditions exhibited increased collagen deposition and thickened collagen bundles; however, LoS lesions demonstrated more pronounced perivascular clustering of immune cells compared with those in SSc (Figure 1A). LoS skin lesions exhibited well-organized immune cell aggregates resembling lymphoid follicles, which were often arranged around blood vessels (Figure 1B).

Immunofluorescence staining confirmed these structures as TLS. Multiplex immunolabeling identified the cellular constituents of TLS, including $CD4^+$ T cells, $CD8^+$ T cells, B cells ($CD20^+$), follicular dendritic cells ($CD21^+$), and macrophages ($CD68^+$) (Figure 1C). Fisher's exact test demonstrated significantly higher TLS in LoS (65.7%, 23 of 35) compared with those with SSc (14.3%, 5 of 34, $P = 0.0013$) and HCs (0%, 0 of 6, $P < 0.0001$) (Figure 1D). Subgroup analysis further indicated that TLS were significantly enriched in early-stage LoS (≤1 year: 17 of 20, 85.0% vs >1 year: 6 of 15, 40.0%; $P = 0.01$). Among LoS subtypes, TLS were more frequently observed in plaque (13 of 17, 76.5%) and generalized (6 of 8, 75.0%) forms, compared with linear (3 of 8, 37.5%) and deep (1 of 2, 50.0%) forms, although these differences did not reach statistical significance ($P = 0.12$) (Supplementary Table 2).

These findings raise the question of why TLS formation is markedly more prominent in LoS than in SSc. The perivascular immune niches characteristic of LoS may help elucidate the mechanisms underlying TLS formation in fibrotic skin disorders.

Distinct cellular composition of LoS and SSc lesions

To elucidate mechanisms underlying TLS development in LoS compared with SSc, we employed scRNA-seq of lesional skin complemented by immunofluorescence staining, primary fibroblast functional assays, and in vivo validation (Figure 2A). Clinical metadata for all samples is provided in Supplementary Tables 1 and 3.

Droplet-based scRNA-seq was performed on skin biopsies from three patients with LoS, three patients with SSc, and three HC. After quality filtering, we retained transcriptomes from 26,774 HC skin cells (36.6% of total), 28,621 LoS skin cells (39.1%), and 17,797 SSc skin cells (24.3%). UMAP analysis revealed 11 major clusters: B cells, endothelial cells (ECs), fibroblasts, keratinocytes, mononuclear phagocytes, mast cells, melanocytes, mural cells, Schwann cells, sweat gland cells, and T and NK cells.

Cell-composition analysis using the $R_{o/e}$[16] metric showed enrichment of ECs in both LoS and SSc relative to HC (LoS 1.48 vs 0.47; SSc 1.30 vs 0.80) and a marked enrichment of immune cell clusters, including B cells (1.77 vs 0.15) and T and NK cells (1.36 vs 0.60) in LoS (Figure 2B), consistent with histopathological findings of frequent TLS formation. Group-specific UMAP plots revealed distinct spatial distributions of cell clusters among LoS, SSc, and HC samples, underscoring differences in cellular organization across conditions (Figure 2C). Differential gene expression analysis identified cluster-specific marker genes that further characterized each cell population (Figure 2D).

These findings reveal different cellular compositions in LoS and SSc lesions, characterized by prominent immune cell expansion in LoS and increased endothelial cell proportions in both conditions, highlighting key cell populations potentially involved in TLS formation and fibrosis.

Enhanced TGFβ signaling associated with VEC and CapEC hyperplasia in LoS and SSc

To investigate the mechanisms underlying endothelial expansion observed in LoS and SSc lesions, we performed unsupervised clustering of ECs, identifying four subpopulations: arterial endothelial cells (AECs), CapECs, lymphatic endothelial cells (LECs), and VECs.

CapEC subclusters were increased in LoS (4.2-fold vs HC, $P = 0.025$) and in SSc (3.5-fold vs HC, $P = 0.032$). VECs were increased in LoS (1.9-fold vs HC, $P = 0.040$) but showed no significant change in SSc (1.3-fold vs HC, $P = 0.063$) (Figure 3A), consistent with the vascular remodeling observed in these lesions.[19,20] To assess potential signaling pathways involved, we valuated TGFβ receptor (TGFβR) signaling, a well-established mediator of vascular remodeling and fibrosis.[21,22] Enrichment analysis revealed increased TGFβR pathway activity in CapECs and VECs from both LoS and SSc samples relative to controls (Figure 3B). Additionally, *TGFβR2* expression was consistently elevated across AEC, CapEC, and VEC subclusters in LoS and SSc lesions (Figure 3C).

Immunofluorescence confirmed the upregulation of TGFβR2 and CD31 (pan-endothelial marker) in LoS and SSc lesions (Figure 3D–F). These findings indicate that TGFβ signaling, particularly through TGFβR2, is associated with endothelial cell expansion and contributes to the distinct vascular features observed in LoS and SSc skin lesions.

Tfh cell-enriched interactions with ECs in LoS and their association with TLS development

To investigate mechanisms underlying TLS formation in LoS, we performed unsupervised clustering on T and NK cells, identifying five distinct subpopulations. Analysis of cell proportions

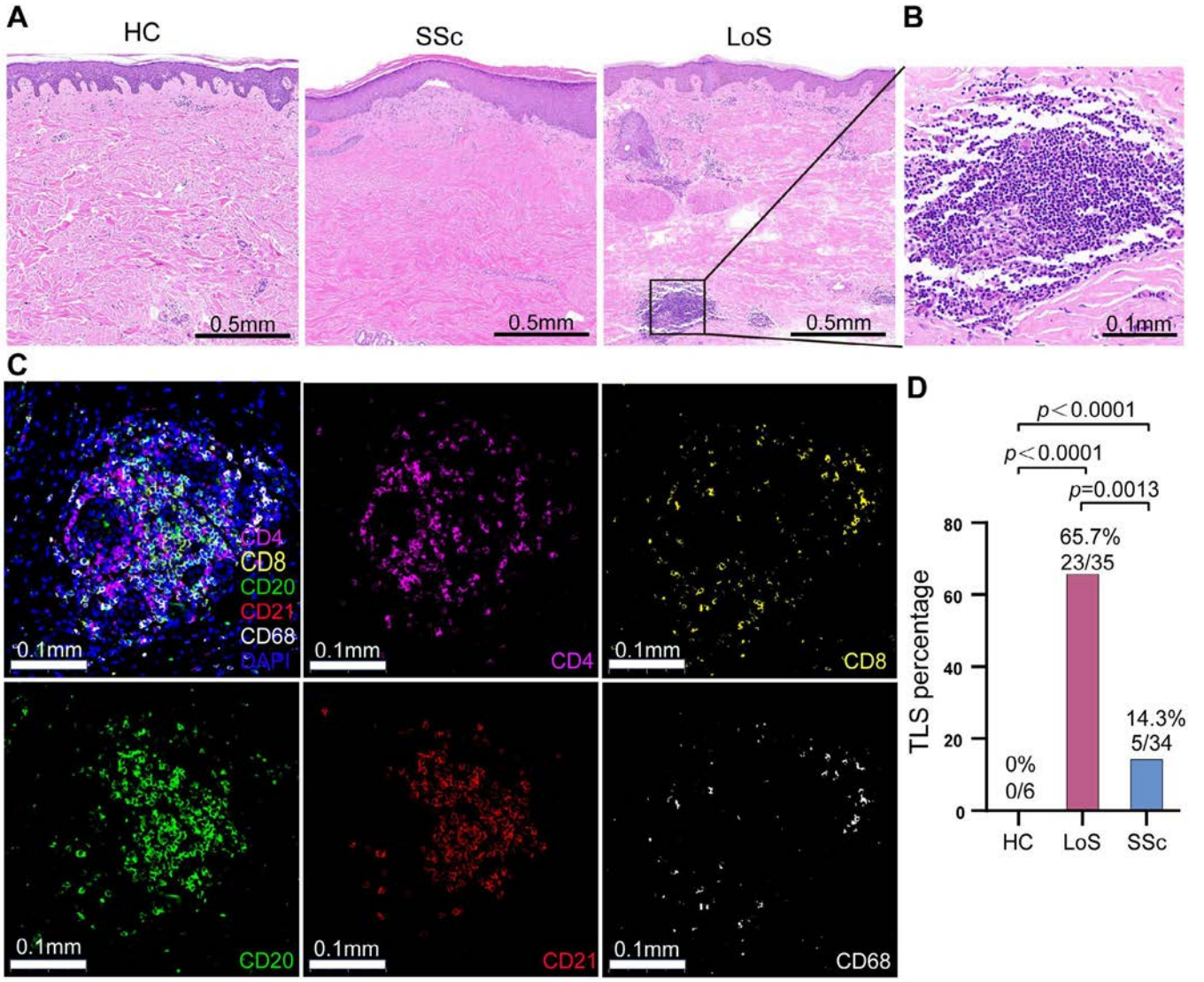

Figure 1. Histologic and immunofluorescence analysis of TLS in LoS and SSc skin lesions: (A) HE-stained sections of skin from HC and patients with LoS and SSc (magnification, 5×). (B) Magnified view of the LoS section, showing lymphocyte clusters forming TLS within the dermis (magnification, 20×). (C) Immunofluorescence staining of LoS skin lesions, displaying clustered $CD4^+$ T cells, $CD8^+$ T cells, $CD20^+$ B cells, and $CD21^+$ follicular dendritic cells and $CD68^+$ macrophages collectively defining the TLS structure (magnification, 20×). (D) Prevalence of TLS in HC, LoS, and SSc groups, identified by the aggregation of CD4, CD8, CD20, CD21, and CD68 positive cells. Pairwise comparisons among groups (HC, LoS, SSc) were conducted using Fisher's exact test. HC, healthy control; HE, hematoxylin and eosin; LoS, localized scleroderma; SSc, systemic sclerosis; TLS, tertiary lymphoid structures.

revealed a marked increase in Tfh cells in both LoS (19.83%) and SSc (19.44%) compared with HC (8.23%) (Figure 4A). Given the established role of Tfh cells in the organization of lymphoid follicles, we examined their interactions within lesional tissues. CCI analysis revealed frequent crosstalk between Tfh cells and ECs in LoS lesions, primarily mediated by ligand-receptor pairs such as *CXCL12-CXCR4*, *SELL-CD34*, and *ICAM1-ITGAL* (Figure 4B). These interactions were infrequent in SSc lesions. Given the frequency of these interactions, Tfh–endothelial crosstalk in LoS lesions may reflect the formation of perivascular immune niches associated with TLS development.

Further analysis demonstrated frequent interactions between Tfh cells and B cells in LoS, indicative of coordinated immune cell clustering (Figure 4C). Key ligand-receptor pairs driving these interactions include *CXCL13-CXCR5*, *IFNGII-IFNR*, *TNFSF9-TNFRSF9*, *TNF-ICOS*, and *TNF-VSIR*, supporting the hypothesis that Tfh cells recruit B cells and promote lymphoid follicle-like structures.

Expression analysis showed that *CXCL13* was predominantly expressed by Tfh cells (Supplementary Figure 1A). In contrast, CXCR5 expression was largely restricted to B cells (Supplementary Figure 1B) and was significantly up-regulated in B cells from LoS compared with HC (Figure 4D), suggesting enhanced chemotactic responsiveness in the LoS immune microenvironment. Functional profiling indicated that B cells in

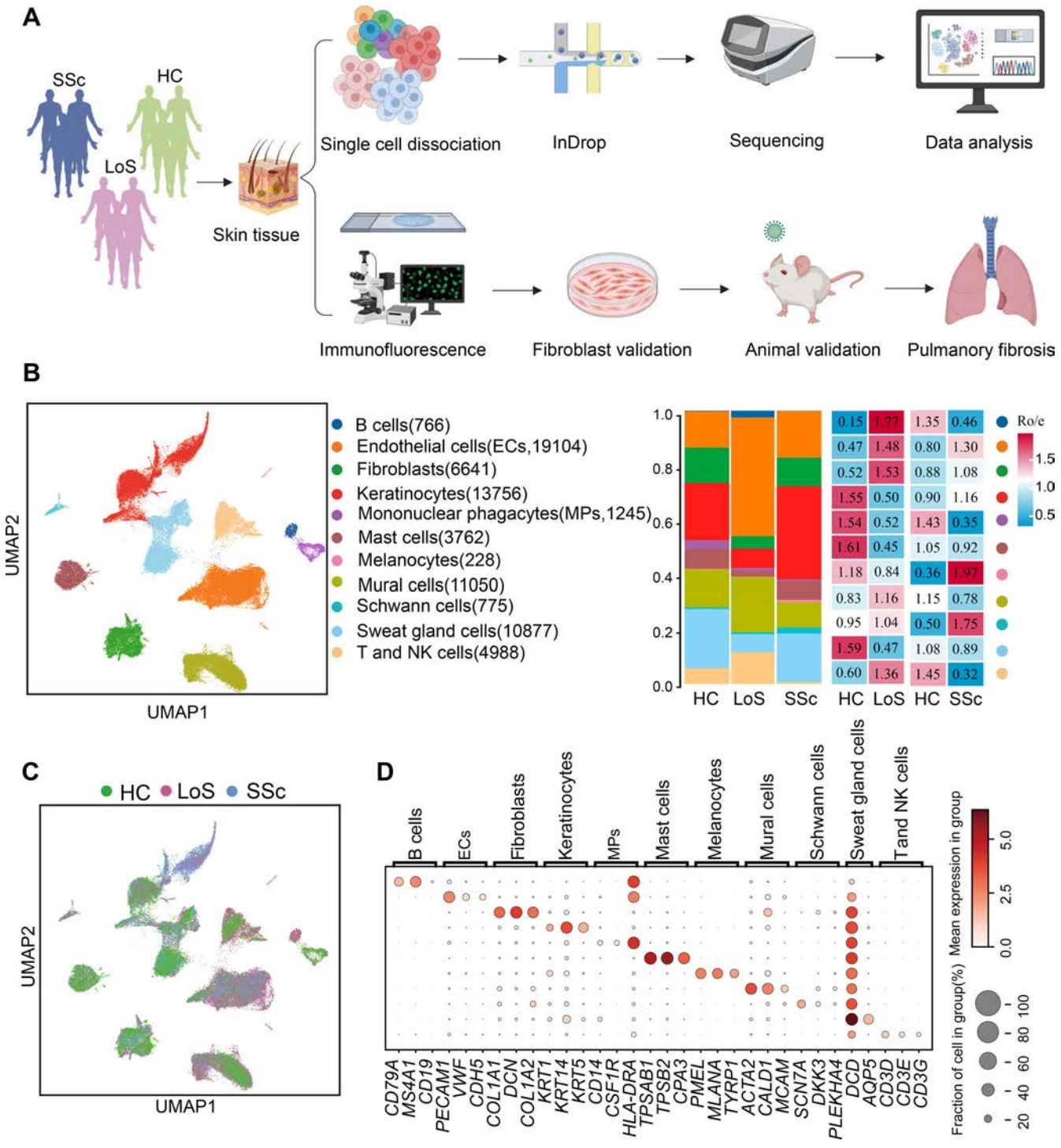

Figure 2. scRNA-seq reveals distinct cellular compositions in LoS and SSc skin lesions: (A) Schematic of the full experimental workflow. (B) UMAP of scRNA-seq data from HC, LoS, and SSc skin, identifying 11 cell clusters; adjacent bar plots show the proportions of major cell types across groups (n = 3 each). Tissue preference of each cluster was assessed by the $R_{o/e}$[16]. (C) UMAP plots showing the distribution of cell clusters within each group (HC, LoS, SSc). (D) Expression profiles of marker genes across cell clusters, indicating genes that define specific subpopulations within the skin lesions. HC, healthy control; LoS, localized scleroderma; NK, natural killer; scRNA-seq, single cell RNA-sequencing; SSc, systemic sclerosis; UMAP, uniform manifold approximation and projection. Color figure can be viewed in the online issue, which is available at http://onlinelibrary.wiley.com/doi/10.1002/art.70039/abstract.

LoS were enriched for immune activation pathways rather than antibody production (Figure 4E), consistent with clinical observations that LoS is generally not associated with autoantibody positivity.

Gene expression analysis further confirmed high expression of major histocompatibility complex class II molecules (*HLA-DMA*, *HLA-DPA1*, *HLA-DPB1*, *HLA-DQB1*, *HLA-DRA*, and *HLA-DQA1*)

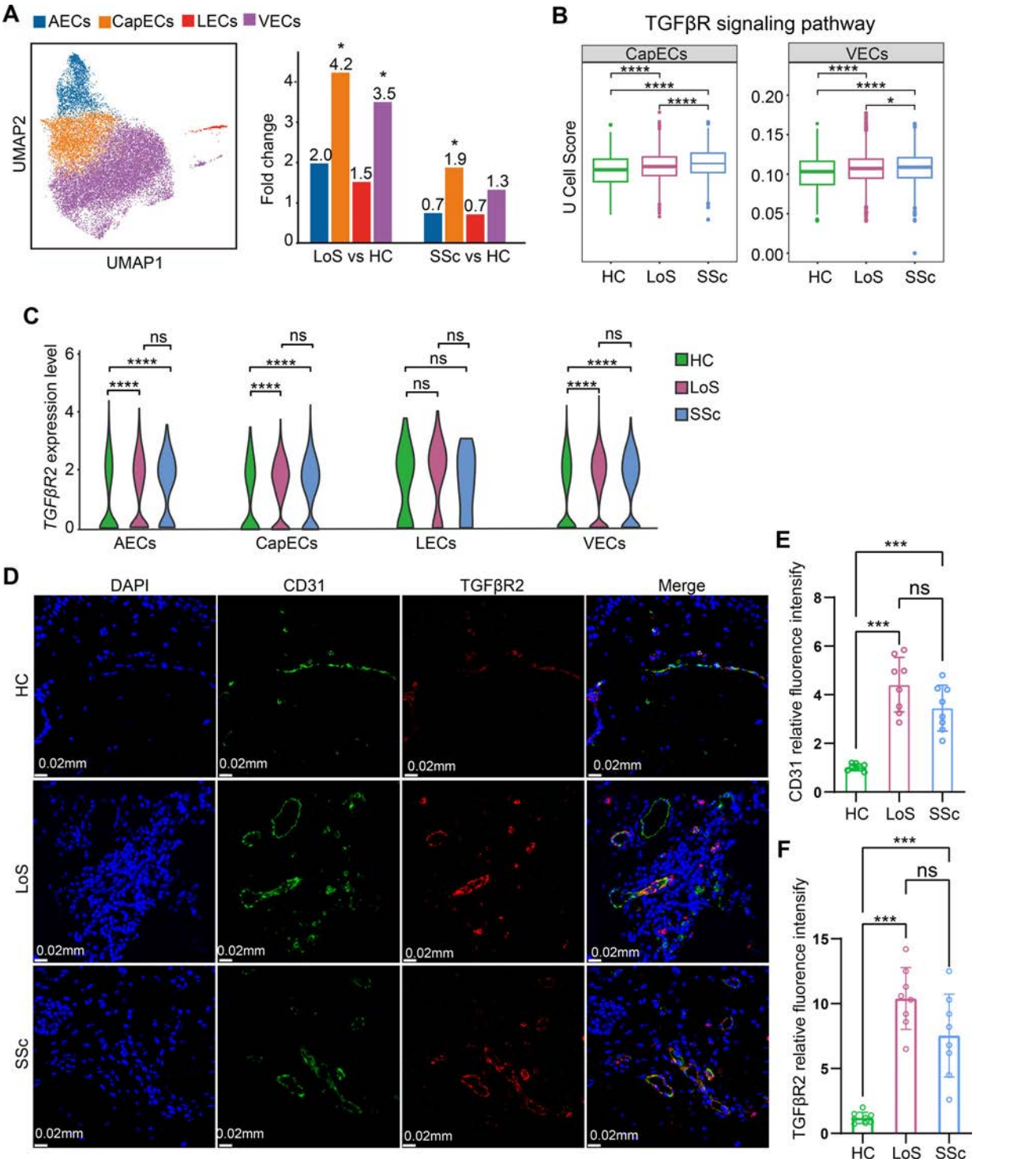

Figure 3. The hyperplasia VECs and CapECs in LoS and SSc skin show a higher TGFβ signal: (A) UMAP plot of endothelial cell clustering, identifying four subpopulations: AECs, CapECs, LECs, and VECs, color-coded by type. Bar plots show fold-change in CapEC and VEC proportions in LoS and SSc compared with HC. (B) TGFβR signaling pathway enrichment scores in CapECs and VECs across HC, LoS, and SSc groups. (C) Violin plot showing *TGFβR2* expression levels in AECs, CapECs, LECs, and VECs across HC, LoS, and SSc groups. (D) Representative immunofluorescence images showing CD31 (green) and TGFβR2 (red) expression in skin lesions from HC (n = 8), LoS (n = 8), and SSc (n = 8) groups. Nuclei were counterstained with DAPI (blue). Images were captured at 63× magnification. (E) Quantification of CD31 fluorescence intensity across HC, LoS, and SSc groups. (F) Quantification of TGFβR2 fluorescence intensity in HC, LoS, and SSc groups. Results are expressed as mean ± SD, using one-way ANOVA. * $P < 0.05$, ** $P < 0.01$, *** $P < 0.001$, **** $P < 0.0001$. AECs, arterial endothelial cells; ANOVA, analysis of variance; CapECs, capillary endothelial cells; HC, healthy control; LoS, localized scleroderma; LECs, lymphatic endothelial cells; ns, not significant; SSc, systemic sclerosis; TGFβR, transforming growth factor β receptor; UMAP, uniform manifold approximation and projection; VECs, vascular endothelial cells. Color figure can be viewed in the online issue, which is available at http://onlinelibrary.wiley.com/doi/10.1002/art.70039/abstract.

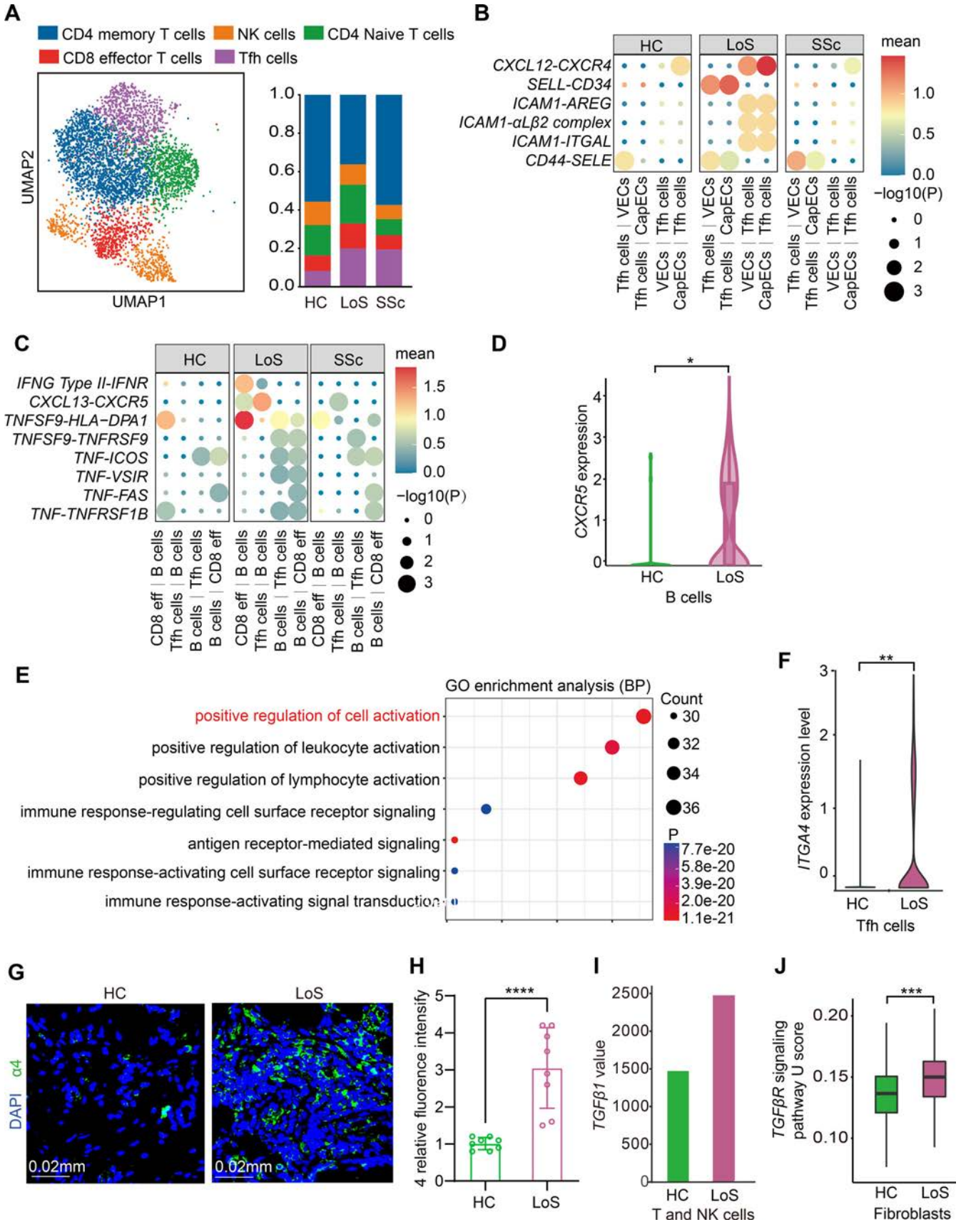

Figure 4. Legend on next page.

(Supplementary Figure 1C), whereas transcripts for Ig isotypes (*IGHA1*, *IGHA2*, *IGHD*, *IGHM*, *IGHG*, *IGHG2*, *IGHG3*, and *IGHG4*) were low (Supplementary Figure 1D). These data suggest that B cells in LoS lesions primarily function as antigen-presenting and immune-coordinating cells, rather than antibody-secreting effectors.

Integrin α4 expression and Tfh cell retention in LoS lesions

Comparison of *ITGA4* gene expression in Tfh cell clusters revealed significantly higher transcript levels in LoS lesions compared with HCs (Figure 4F), suggesting that integrin α4 may contribute to the retention of immune cells within TLS. Immunofluorescence staining confirmed elevated α4 expression within TLS in LoS skin (Figure 4G–H), supporting its potential role in anchoring Tfh cells in situ. In contrast, the expression level of other retention-associated molecules—*TIGAE* (encoding CD103), *CD69* (encoding CD69), and *LTA* and *LTB* (encoding LTα1β2)—did not differ between groups (Supplementary Figure 1E). These integrins have been reported as key molecules mediating the retention of immune cells within TLS,[23,24] but their unchanged expression in LoS suggests they may not play a major role in this context. Collectively, these findings identify integrin α4 as a potentially unique contributor to TLS stabilization in LoS.

To explore the connection between immune–stromal interactions and fibrotic remodeling, we next examined TGFβ signaling in LoS lesions. T and NK cells exhibited elevated total expression of *TGFβ1* (Figure 4I), whereas fibroblasts showed increased enrichment scores for *TGFβR* signaling pathway (Figure 4J). Given the established role of TGFβ's in promoting collagen synthesis,[25] these findings suggest a model in which immune-derived TGFβ activates fibroblast TGFβR signaling, contributing to localized fibrotic responses in LoS skin.

CREB3L1 upregulation drives fibroblast activation and collagen production in SSc skin and lung fibrosis

To investigate the mechanisms contributing to skin fibrosis in SSc and assess potential parallels in pulmonary fibrosis, we analyzed fibroblast differentiation trajectories. Pseudotime reconstruction identified three distinct trajectories among fibroblasts in the HC, LoS, and SSc groups, with SSc fibroblasts predominantly enriched in the Fate1 trajectory (Figure 5A). Regulon specificity score (RSS) analysis of Fate1-associated genes revealed *SOX4* (12g), *HDAC1* (368g), *CREB3L1* (392g), *CREB* (95g), and *NELFE* (340g) as the top five transcription factors (Figure 5B). Among these, *CREB3L1* regulated the largest number of Fate1-specific genes, suggesting it as a key transcriptional driver of this differentiation pathway in SSc fibroblasts. This finding is consistent with previous studies linking CREB3L1 to SSc-related skin and lung fibrosis.[26] Comparative analysis of CREB3L1 expression across groups confirmed its elevated expression in SSc fibroblasts relative to HC and LoS (Figure 5C).

To validate the reproducibility of this observation, we reanalyzed an independent public scRNA-seq data set (GSE138669) comprising skin biopsies from 12 patients with SSc and 10 HCs. Unsupervised clustering identified 14 fibroblast subpopulations (C1–C14) (Supplementary Figure 2A), among which C1, C7, and C14 exhibited high CREB3L1 expression, with markedly higher levels in SSc samples (Supplementary Figure 2B). GO enrichment analysis revealed that all three subclusters (C1, C7, C14) were enriched in extracellular matrix–related pathways, such as "extracellular matrix organization" and "extracellular structure organization" (Supplementary Figure 2C–E). Pseudotime analysis further revealed that the Fate 1 trajectory was predominantly enriched with SSc fibroblasts compared with HC, and this enrichment was largely attributable to the preferential alignment of C1 and C14 subclusters along this path (Supplementary Figure 2F). This independent analysis confirms the reproducibility of our findings and supports an association between CREB3L1 expression and profibrotic fibroblast states in SSc. We next explored whether CREB3L1 upregulation also occurs in lung fibrosis associated with SSc. Analysis of bulk RNA-seq data from lung fibroblasts (GSE215841) revealed significantly higher CREB3L1 expression in SSc samples compared with controls (Figure 5D). This observation was corroborated by single-cell transcriptomic analysis of SSc-interstitial lung disease (ILD) lung tissues (GSE128169), which confirmed CREB3L1 upregulation across multiple lung cell populations, including fibroblasts, with the highest expression observed in alveolar epithelial cells (Figure 5E).

To elucidate the downstream targets of CREB3L1 in SSc fibroblasts, we identified the top 10 regulated genes from pySCENIC regulon analysis, 5 of which are associated with collagen

Figure 4. Increased frequency of Tfh cells cluster in LoS skin lesion induced tertiary lymphoid like structure: (A) Unsupervised clustering of T and NK cells identified five subpopulations—$CD4^+$ memory T, NK, $CD4^+$ naïve T, $CD8^+$ Teff, and Tfh cells—color-coded with bar plots showing their proportions in HC, LoS, and SSc. (B) CCI between Tfh cells and CapEC/VEC clusters in HC, LoS, and SSc. (C) CCI between B cells and Tfh cells/CD8 Teff cells clusters in LoS and HC. (D) *CXCR5* expression in B cell subpopulations from HC and LoS. (E) GO enrichment of B cells showing up-regulated pathways. (F) Violin plot showing *ITGA4* expression in Tfh subcluster in HC and LoS. (G–H) Immunofluorescence staining and quantification for α4 in HC (n = 8) and LoS (n = 8) skin lesions (magnification, 40×40X). (I) *TGFβ1* expression in all T and NK cells from HC and LoS. (J) *TGFβR* signaling pathway U scores in fibroblast clusters in HC and LoS. Data are mean ± SD, with statistical analysis performed using unpaired Student's *t*-test or one-way ANOVA. * $P < 0.05$, ** $P < 0.01$, *** $P < 0.001$, **** $P < 0.0001$. ANOVA, analysis of variance; BP, biological process; CapEC, capillary endothelial cell; CCI, cell-cell interaction; GO, gene ontology; HC, healthy control; LoS, localized scleroderma; NK, natural killer; ns, not significant; SSc, systemic sclerosis; Tfh, T follicular helper; TGFβ, transforming growth factor β; TGFβR, TGFβ receptor; VEC, vascular endothelial cell. Color figure can be viewed in the online issue, which is available at http://onlinelibrary.wiley.com/doi/10.1002/art.70039/abstract.

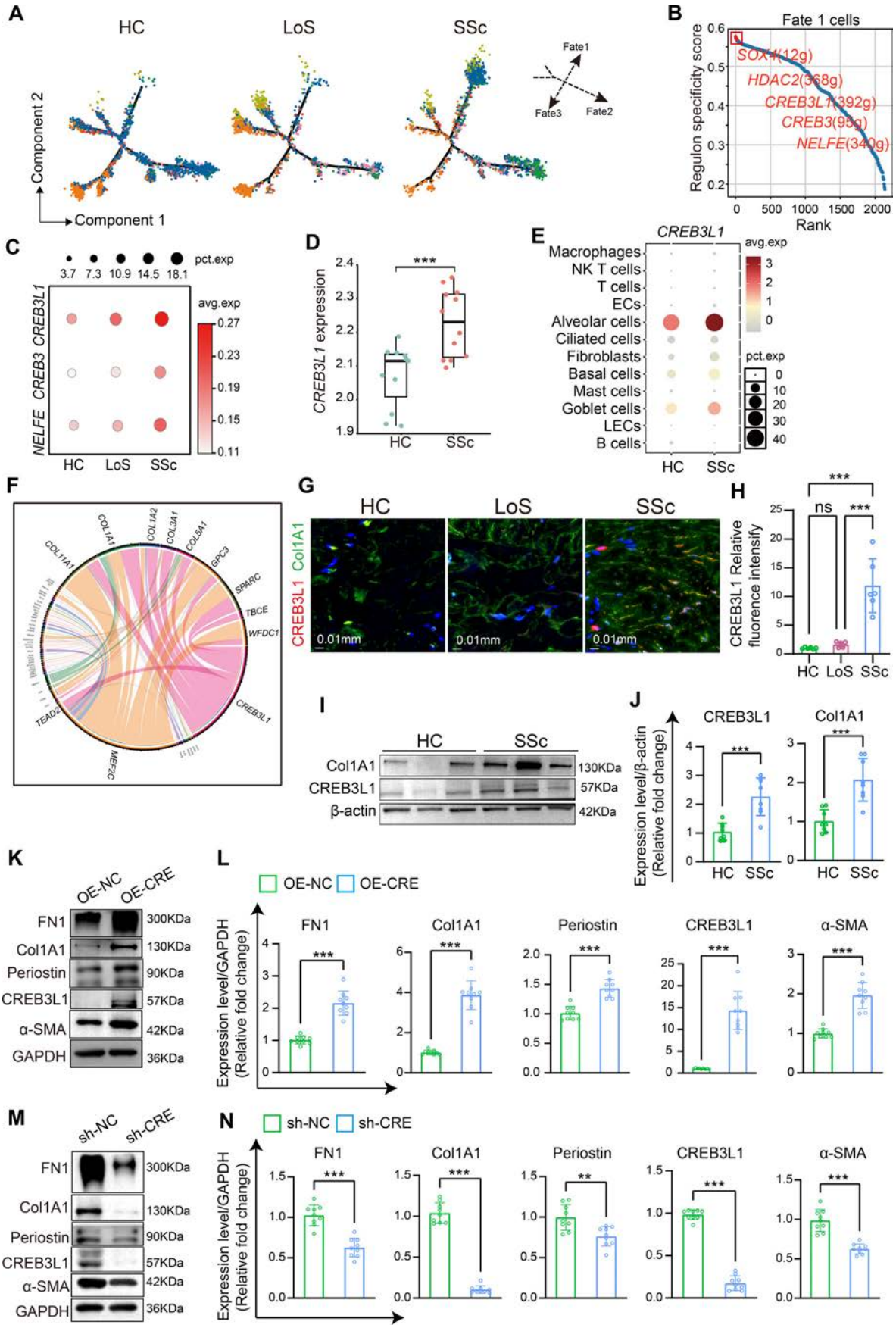

Figure 5. Legend on next page.

synthesis and fibrosis, including *COL1A1*, *COL11A1*, *COL3A1*, *COL5A1*, and *COL1A2* (Figure 5F). Immunofluorescence staining showed co-localization of CREB3L1 and COL1A1 in fibroblasts, with CREB3L1 expression significantly elevated in SSc lesions relative to HC and LoS (Figure 5G–H). WB further validated the co-upregulation of CREB3L1 and COL1A1 in primary fibroblasts from SSc skin (Figure 5I–J).

To functionally validate the role of CREB3L1 in fibrosis, we performed overexpression and knockdown experiments in SSc-derived primary fibroblasts using viral vectors. *CREB3L1* overexpression led to increased expression of fibrosis markers, including FN1, COL1A1, Periostin, and α-smooth muscle actin (α-SMA) (Figure 5K–L), whereas *CREB3L1* knockdown reduced the expression of these markers (Figure 5M–N). In addition, scratch assay results demonstrated that *CREB3L1* overexpression enhanced fibroblast migration, whereas its knockdown impaired motility (Supplementary Figure 3A–B). Together, these findings highlight that CREB3L1 may play a critical role in fibroblast activation and collagen production, contributing to the fibrotic processes observed in both skin and lung tissues of patients with SSc.

CREB3L1 promotes fibrosis in models of SSc

To validate the profibrotic role of CREB3L1 in vivo, we employed bleomycin-induced murine models of SSc. C57BL/6 mice received daily intradermal injections of bleomycin for three weeks. Before induction, mice were administered adeno-associated viral vectors via intratracheal instillation: HC, BLM-ctrl (bleomycin with control virus), BLM-OE (bleomycin with *Creb3l1* overexpression virus), and BLM-sh (bleomycin with *Creb3l1* knockdown virus). On day 22, skin and lung samples were harvested for analysis (Figure 6A). WB analysis of both skin and lung tissues revealed increased expression of the fibrosis markers FN1, COL1A1, and Periostin in BLM-treated mice compared with HC. These markers were further elevated in the BLM-OE group and reduced in the BLM-sh group (Figure 6B–C; quantified in Supplementary Figure 4A–B). Ultrasound imaging demonstrated increased dermal thickness in BLM-OE mice and attenuation in BLM-sh mice relative to BLM-ctrl (Figure 6D and Supplementary Figure 4C). Masson's trichrome staining confirmed enhanced collagen deposition in the skin and lungs of BLM-OE mice and reduced deposition in the BLM-sh group (Figure 6E–F). Immunohistochemical staining showed increased Col1 expression in skin and both Col1 and Col3 in lung tissues of BLM-OE mice, with corresponding reductions in the BLM-sh group (Figure 6G–I). Additionally, body weight monitoring revealed more pronounced weight loss in BLM-OE mice and partial preservation of weight in BLM-sh mice (Supplementary Figure 4D). Together, these findings support a key role for CREB3L1 in driving tissue fibrosis in SSc and show consistent effects in in vivo models. These results further highlight CREB3L1 as a potential therapeutic target for fibrotic diseases.

DISCUSSION

LoS and SSc are fibrotic disorders that share histopathological features, such as dermal fibrosis and immune cell infiltration, but differ markedly in their clinical manifestations. We found that LoS lesions were characterized by the presence of TLS enriched with immune cells, which may drive localized fibroblast activation, whereas fibroblasts with higher CREB3L1 expression in SSc were associated with systemic fibrotic progression.

TLS act as local hubs of immune activation under chronic inflammation. In LoS, they were more frequent and localized near neovascularized regions, where CXCR4–CXCL12 signaling may attract Tfh cells and CXCL13–CXCR5 interactions facilitate B cell clustering and TLS formation.[27–29] Previous studies have shown that integrins such as CD103 and LTα1β2 contribute to immune cell retention and TLS formation in chronic inflammatory settings.[23,24] In our study, we found that integrin α4, but not CD103 or LTα1β2, was specifically up-regulated in LoS, suggesting a disease-specific mechanism of TLS stabilization. These immune cell infiltrates, through upregulation of TGFβ expression, further activate fibroblasts and promote localized fibrosis in LoS skin.[30] In contrast, SSc lesions exhibited weak Tfh interactions and low integrin α4 expression, corresponding to the rare presence of TLS.

SSc fibrosis is characterized by a shift toward extensive fibroblast-driven collagen production. We identified a fibroblast

Figure 5. Pseudotime reconstruction and CREB3L1 expression in fibroblast differentiation and fibrosis in SSc: (A) Pseudotime trajectories of fibroblast differentiation in HC, LoS, and SSc. (B) RSS in Fate1 cells highlighting the top five transcription factors. (C) Bubble plots of *CREB3L1*, *CREB3*, and *NELFE* expression across HC, LoS, and SSc. (D) *CREB3L1* expression in fibroblasts from SSc (n = 12) and HC (n = 11) lungs (GSE215841). (E) *CREB3L1* expression across lung cell subpopulations in SSc-ILD patients (8 samples/4 patients) and HCs (5 samples/4 donors) (GSE128169). (F) Chord diagram of the top 10 CREB3L1 downstream targets in SSc fibroblasts identified by pySCENIC. (G–H) Immunofluorescence and quantification of Col1A1 and CREB3L1 in HC, LoS and SSc (100×). (I–J) WB and quantification of CREB3L1 and Col1A1 in primary skin fibroblasts from HC and SSc. (K–N) WBs of CREB3L1 and fibrosis-associated proteins (FN1, COL1A1, Periostin, α-SMA) in fibroblasts transfected with OE-NC, OE-CRE, sh-NC, or sh-CRE (n = 3/group, 3 independent experiments). Data are mean ± SD; unpaired Student's *t*-test; * $P < 0.05$, ** $P < 0.01$, *** $P < 0.001$. α-SMA, α-smooth muscle actin; EC, endothelial cell; HC, healthy control; ILD, interstitial lung disease; LoS, localized scleroderma; NK, natural killer; ns, not significant; OE-CRE, CREB3L1 overexpression; OE-NC, control lentivirus; RSS, Regulon specificity score; SSc, systemic sclerosis; sh-CRE, short hairpin RNA targeting CREB3L1; sh-NC, nontargeting short hairpin RNA; WB, Western blot. Color figure can be viewed in the online issue, which is available at http://onlinelibrary.wiley.com/doi/10.1002/art.70039/abstract.

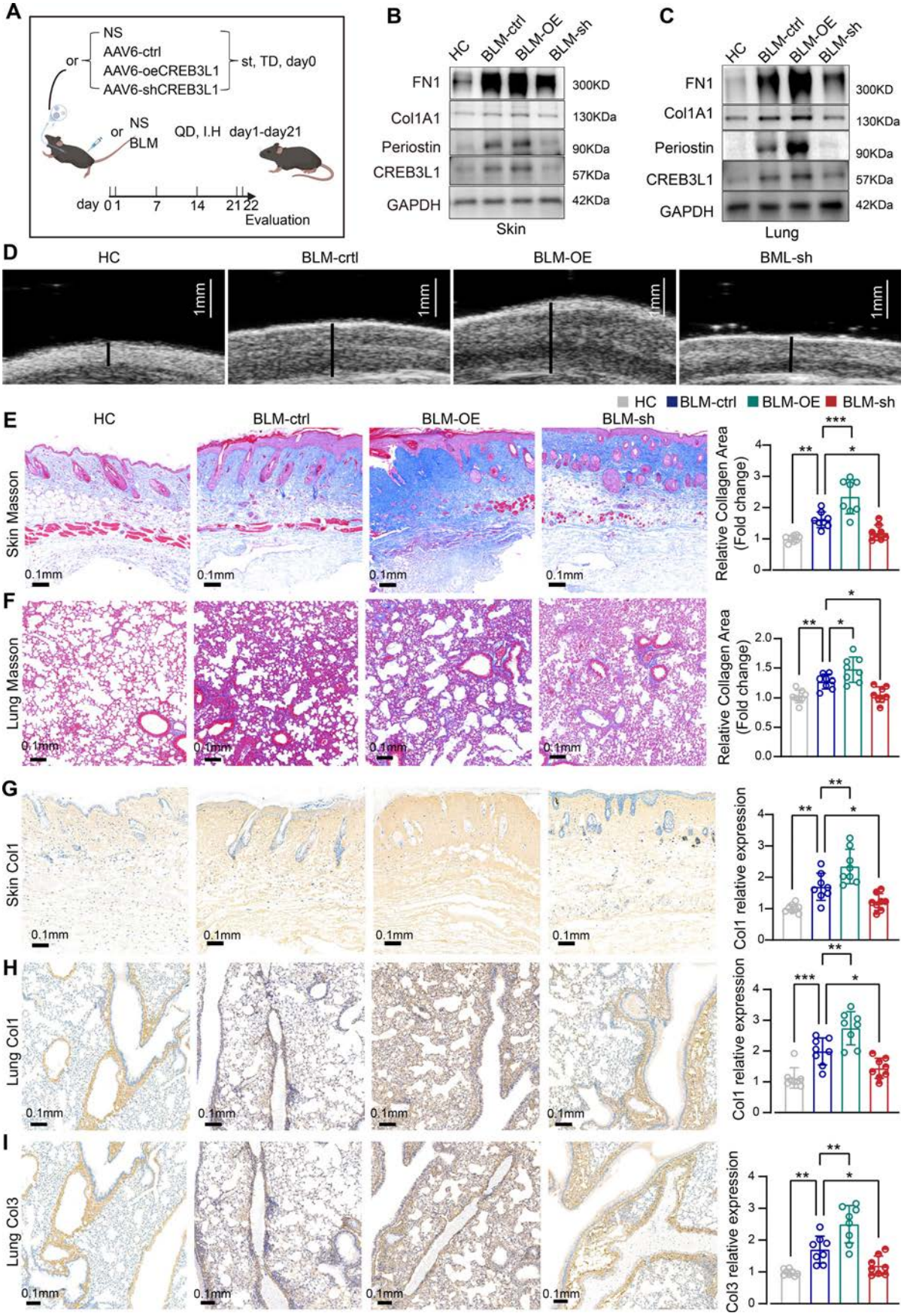

Figure 6. Legend on next page.

trajectory (Fate1) in SSc defined by high CREB3L1 expression and activation of profibrotic genes, supporting its role as a key transcriptional driver of fibrosis. This finding was validated in an independent scRNA-seq data set (GSE138669), where CREB3L1 was similarly elevated in fibroblast subpopulations enriched for extracellular matrix pathways, indicating a convergent profibrotic trajectory across data sets. Consistent with our results, previous studies have shown that CREB3L1 promotes collagen secretion and myofibroblast activation in other fibrotic contexts, such as thyroid and kidney tissues.[26,31,32]

To further assess the role of CREB3L1 in SSc-associated pulmonary fibrosis, we analyzed transcriptomic and single-cell data sets from lung tissues. Bulk RNA-seq (GSE215841[33]) revealed increased CREB3L1 expression in SSc lung fibroblasts compared with controls, and single-cell RNA-seq (GSE128169[10]) confirmed its upregulation across multiple lung cell types, particularly in alveolar cells. This cross-tissue expression pattern supports a role for CREB3L1 in mediating multiorgan fibrosis in SSc, involving both skin and lung compartments. Consistently, in bleomycin-induced mouse models, CREB3L1 overexpression aggravated collagen deposition and fibrosis-related gene expression, whereas CREB3L1 knockdown mitigated fibrotic changes in both skin and lung tissues.

Collectively, our study provides new insights into the divergent fibrotic mechanisms of LoS and SSc. In LoS, fibrosis appears to be driven primarily by local immune activation and TLS formation, leading to immune–fibroblast interactions within lesional skin. In contrast, SSc is characterized by widespread fibroblast activation associated with CREB3L1 upregulation in both skin and lung tissues, reflecting a systemic fibrotic program.

Although both diseases involve immune–stromal crosstalk, their spatial and mechanistic contexts differ: LoS displays localized TLS-rich inflammation, whereas SSc exhibits diffuse CREB3L1-associated fibrosis. Although TLS are rare in SSc, circulating Th17 and Tfh cells have been implicated in systemic fibrotic priming,[34] which suggests that CREB3L1-expressing fibroblasts may sustain a persistent profibrotic state under systemic immune influence.

A limitation of this study is that two patients with SSc in the scRNA-seq cohort were receiving cyclophosphamide at the time of biopsy, which might have affected lymphoid aggregate formation. Future studies with larger, treatment-naïve cohorts are warranted to validate and extend these findings. Together, these results lay the groundwork for targeted therapeutic strategies tailored to the distinct pathophysiologic processes in LoS and SSc—addressing localized immune-mediated fibrosis in LoS and systemic fibroblast activation in SSc.

AUTHOR CONTRIBUTIONS

All authors contributed to at least one of the following manuscript preparation roles: conceptualization AND/OR methodology, software, investigation, formal analysis, data curation, visualization, and validation AND drafting or reviewing/editing the final draft. As corresponding author, Drs X. Yang and J. Yang confirm that all authors have provided the final approval of the version to be published and take responsibility for the affirmations regarding article submission (eg, not under consideration by another journal), the integrity of the data presented, and the statements regarding compliance with institutional review board/Declaration of Helsinki requirements.

REFERENCES

1. Teske N, Fett N. Recent advances in treatment of systemic sclerosis and morphea. Am J Clin Dermatol 2024;25(2):213–226. doi:https://doi.org/10.1007/s40257-023-00831-2
2. Papara C, De Luca DA, Bieber K, et al. Morphea: The 2023 update. Front Med (Lausanne) 2023;10:1108623. doi:https://doi.org/10.3389/fmed.2023.1108623
3. Fett N, Werth VP. Update on morphea: part I. Epidemiology, clinical presentation, and pathogenesis. J Am Acad Dermatol 2011;64(2):217–228. doi:https://doi.org/10.1016/j.jaad.2010.05.045
4. Jerjen R, Nikpour M, Krieg T, et al. Systemic sclerosis in adults. Part I: clinical features and pathogenesis. J Am Acad Dermatol 2022;87(5):937–954. doi:https://doi.org/10.1016/j.jaad.2021.10.065
5. Showalter K, Gordon JK. Skin histology in systemic sclerosis: a relevant clinical biomarker. Curr Rheumatol Rep 2020;23(1):3. doi:https://doi.org/10.1007/s11926-020-00970-z
6. Chen HW, Zhu JL, Martyanov V, et al. Gene expression signatures in inflammatory and sclerotic morphea skin and sera distinguish morphea from systemic sclerosis. J Invest Dermatol 2023;143(10):1886–1895.e10. doi:https://doi.org/10.1016/j.jid.2023.02.036
7. Sato Y, Silina K, van den Broek M, et al. The roles of tertiary lymphoid structures in chronic diseases. Nat Rev Nephrol 2023;19(8):525–537. doi:https://doi.org/10.1038/s41581-023-00706-z
8. Helmink BA, Reddy SM, Gao J, et al. B cells and tertiary lymphoid structures promote immunotherapy response. Nature 2020;577(7791):549–555. doi:https://doi.org/10.1038/s41586-019-1922-8

Figure 6. Effects of CREB3L1 on fibrosis-related protein expression in skin and lung tissues of treated mice: C57BL/6 mice (n = eight per group, two independent experiments) received intratracheal AAV vectors (5×10^{10} vg/75 μL PBS) followed by daily intradermal bleomycin (100 μg/100 μL) injections to a 2 cm^2 dorsal area for three weeks; controls received PBS + AAV-mock. Skin and lung tissues were collected on day 22. (A) Experimental workflow. (B–C) WB of CREB3L1 and fibrosis-related proteins (FN1, Col1A1, and Periostin) in skin and lung tissues. (D) Representative skin ultrasound images of mice from the HC, BLM-ctrl, BLM-OE, and BLM-sh groups. (E–F) Masson staining of skin and lung tissue from different groups and quantitative analysis of collagen area (10×). (G) Immunofluorescence and quantitative analysis of Col1 in skin tissues from different groups (10×). (H–I) Immunofluorescence and quantitative analysis of Col1 and Col3 in lung tissues from different groups (10×). Data shown as mean ± SD; one-way ANOVA; * $P < 0.05$, ** $P < 0.01$, *** $P < 0.001$. AAV, adeno-associated virus; ANOVA, analysis of variance; BLM-ctrl, bleomycin + control virus; BLM-OE, bleomycin + *Creb3l1*-overexpression virus; BLM-sh, bleomycin + *Creb3l1*-knockdown virus; HC, healthy control; ns, not significant; PBS, phosphate-buffered saline; WB, Western blot. Color figure can be viewed in the online issue, which is available at http://onlinelibrary.wiley.com/doi/10.1002/art.70039/abstract.

9. Cassisa A, Vannucchi M. Morphea profunda with tertiary lymphoid follicles: description of two cases and review of the literature. Dermatopathology (Basel) 2022;9(1):17–22. doi:https://doi.org/10.3390/dermatopathology9010003
10. Valenzi E, Bulik M, Tabib T, et al. Single-cell analysis reveals fibroblast heterogeneity and myofibroblasts in systemic sclerosis-associated interstitial lung disease. Ann Rheum Dis 2019;78(10):1379–1387. doi:https://doi.org/10.1136/annrheumdis-2018-214865
11. Clark KEN, Xu S, Attah M, et al. Single-cell analysis reveals key differences between early-stage and late-stage systemic sclerosis skin across autoantibody subgroups. Ann Rheum Dis 2023;82(12):1568–1579. doi:https://doi.org/10.1136/ard-2023-224184
12. van den Hoogen F, Khanna D, Fransen J, et al. 2013 classification criteria for systemic sclerosis: an American College of Rheumatology/European League Against Rheumatism Collaborative initiative. Arthritis Rheum 2013;65(11):2737–2747. doi:https://doi.org/10.1002/art.38098
13. Wu W, Jordan S, Graf N, et al; EUSTAR Collaborators. Progressive skin fibrosis is associated with a decline in lung function and worse survival in patients with diffuse cutaneous systemic sclerosis in the European Scleroderma Trials and Research (EUSTAR) cohort. Ann Rheum Dis 2019;78(5):648–656. doi:https://doi.org/10.1136/annrheumdis-2018-213455
14. Distler O, Assassi S, Cottin V, et al. Predictors of progression in systemic sclerosis patients with interstitial lung disease. Eur Respir J 2020;55(5):1902026. doi:https://doi.org/10.1183/13993003.02026-2019
15. Dura B, Choi JY, Zhang K, et al. scFTD-seq: freeze-thaw lysis based, portable approach toward highly distributed single-cell 3′ mRNA profiling. Nucleic Acids Res 2019;47(3):e16. doi:https://doi.org/10.1093/nar/gky1173
16. Zhang L, Yu X, Zheng L, et al. Lineage tracking reveals dynamic relationships of T cells in colorectal cancer. Nature 2018;564(7735):268–272. doi:https://doi.org/10.1038/s41586-018-0694-x
17. Browaeys R, Saelens W, Saeys Y. NicheNet: modeling intercellular communication by linking ligands to target genes. Nat Methods 2020;17(2):159–162. doi:https://doi.org/10.1038/s41592-019-0667-5
18. Piras BA, Tian Y, Xu Y, et al. Systemic injection of AAV9 carrying a periostin promoter targets gene expression to a myofibroblast-like lineage in mouse hearts after reperfused myocardial infarction. Gene Ther 2016;23(5):469–478. doi:https://doi.org/10.1038/gt.2016.20
19. Muruganandam M, Ariza-Hutchinson A, Patel RA, et al. Biomarkers in the pathogenesis, diagnosis, and treatment of systemic sclerosis. J Inflamm Res 2023;16:4633–4660. doi:https://doi.org/10.2147/JIR.S379815
20. Nicolosi PA, Tombetti E, Maugeri N, et al. Vascular remodelling and mesenchymal transition in systemic sclerosis. Stem Cells Int 2016;2016(1):4636859. doi:https://doi.org/10.1155/2016/4636859
21. Holderfield MT, Hughes CC. Crosstalk between vascular endothelial growth factor, notch, and transforming growth factor-beta in vascular morphogenesis. Circ Res 2008;102(6):637–652. doi:https://doi.org/10.1161/CIRCRESAHA.107.167171
22. Goumans MJ, Ten Dijke P. TGF-β signaling in control of cardiovascular function. Cold Spring Harb Perspect Biol 2018;10(2):a022210. doi:https://doi.org/10.1101/cshperspect.a022210
23. Jiao S, Xiong Q, Yan M, et al. Intratumor expanded T cell clones can be non-sentinel lymph node derived in breast cancer revealed by single-cell immune profiling. J Immunother Cancer 2022;10(1):e003325. doi:https://doi.org/10.1136/jitc-2021-003325
24. Mebius RE. Organogenesis of lymphoid tissues. Nat Rev Immunol 2003;3(4):292–303. doi:https://doi.org/10.1038/nri1054
25. Meng XM, Nikolic-Paterson DJ, Lan HY. TGF-β: the master regulator of fibrosis. Nat Rev Nephrol 2016;12(6):325–338. doi:https://doi.org/10.1038/nrneph.2016.48
26. Tabib T, Huang M, Morse N, et al. Myofibroblast transcriptome indicates $SFRP2^{hi}$ fibroblast progenitors in systemic sclerosis skin. Nat Commun 2021;12(1):4384. doi:https://doi.org/10.1038/s41467-021-24607-6
27. Sati S, Huang J, Kersh AE, et al. Recruitment of CXCR4+ type 1 innate lymphoid cells distinguishes sarcoidosis from other skin granulomatous diseases. J Clin Invest 2024;134(17):e178711. doi:https://doi.org/10.1172/JCI178711
28. Cabrita R, Lauss M, Sanna A, et al. Tertiary lymphoid structures improve immunotherapy and survival in melanoma. Nature 2020;577(7791):561–565. doi:https://doi.org/10.1038/s41586-019-1914-8
29. Chaurio RA, Anadon CM, Lee Costich T, et al. TGF-β-mediated silencing of genomic organizer SATB1 promotes Tfh cell differentiation and formation of intra-tumoral tertiary lymphoid structures. Immunity 2022;55(1):115–128.e9. doi:https://doi.org/10.1016/j.immuni.2021.12.007
30. Lodyga M, Hinz B. TGF-β1 - A truly transforming growth factor in fibrosis and immunity. Semin Cell Dev Biol 2020;101:123–139. doi:https://doi.org/10.1016/j.semcdb.2019.12.010
31. Pan Z, Xu T, Bao L, et al. CREB3L1 promotes tumor growth and metastasis of anaplastic thyroid carcinoma by remodeling the tumor microenvironment. Mol Cancer 2022;21(1):190. doi:https://doi.org/10.1186/s12943-022-01658-x
32. Davis JL, Kennedy C, Clerkin S, et al. Single-cell multiomics reveals the complexity of TGFβ signalling to chromatin in iPSC-derived kidney organoids. Commun Biol 2022;5(1):1301. doi:https://doi.org/10.1038/s42003-022-04264-1
33. Renaud L, Waldrep KM, da Silveira WA, et al. First characterization of the transcriptome of lung fibroblasts of SSc patients and healthy donors of African Ancestry. Int J Mol Sci 2023;24(4):3645. doi:https://doi.org/10.3390/ijms24043645
34. Yang X, Yang J, Xing X, et al. Increased frequency of Th17 cells in systemic sclerosis is related to disease activity and collagen overproduction. Arthritis Res Ther 2014;16(1):R4. doi:https://doi.org/10.1186/ar4430

American College of Rheumatology
Empowering Rheumatology Professionals

Arthritis & Rheumatology
Vol. 78, No. 5, May 2026, pp 1166–1175
DOI 10.1002/art.70019

Decision Tree Analysis as a Preliminary Evidence-Based Tool for Identifying the Syndrome of Undifferentiated Recurrent Fever in Children Compared With Hereditary Recurrent Fevers and Periodic Fever, Aphthosis, Pharyngitis, and Adenitis Syndrome

Riccardo Papa, MD, PhD,[1] Francesca Bovis, PhD,[2] Silvia Federici, MD, PhD,[3] Serena Palmeri, MD,[1,4] Marta Bustaffa, MD, PhD,[5] Giada Recchi, BSc,[1] Roberta Bertelli, BSc,[6] Roberta Caorsi, MD,[1,4] Stefano Volpi, MD, PhD,[1,4] Sabrina Fuehner, PhD,[7] Veysel Cam, MD,[8] Anna Kozáková, MD,[9] Šárka Horáčková Fingerhutová, MD, PhD,[9] Antonella Insalaco, MD,[3] Dirk Foell, MD,[7] Seza Ozen, MD,[8] Isabella Ceccherini, PhD,[10] and Marco Gattorno, MD,[1] on behalf of the Eurofever study group for the classification criteria of recurrent fevers and PerSAID project

Objective. To develop evidence-based criteria to classify patients with syndrome of undifferentiated recurrent fevers (SURF).

Methods. One hundred twelve patients with SURF observed in a single tertiary referral center were analyzed. Patients with genetically confirmed hereditary recurrent fever (HRF) or with periodic fever, aphthosis, pharyngitis, and adenitis (PFAPA) syndrome already analyzed for the Eurofever classification criteria were used as disease controls. A decision tree approach was tested by randomly splitting the available data in a training set and in an internal test set. An alternative model using a classical regression model was also analyzed. An external validation for both approaches was performed on 123 patients recruited from four other centers.

Results. The decision tree model integrating clinical and genetic data identified 91% of patients with SURF. A decision tree model based solely on clinical variables identified up to 88% of patients with SURF. The logistic regression model including genetic tests exhibited an overall accuracy of 89.2% (95% confidence interval [CI] 81.1–94.7). In contrast, the logistic regression model exclusively based on clinical manifestations displayed an overall accuracy of 66.7% (95% CI 56.1–76.1). When the classification criteria including genetic tests were applied to the external validation cohort, the model demonstrated a strong discriminative power, with areas under the receiver operating characteristic curve of 96.3% using the decision tree model and 88.0% with the logistic regression model.

Conclusion. The study shows the possibility of achieving evidence-based criteria that can classify SURF at least with respect to the main HRF and PFAPA syndrome and may be considered as a preliminary tool for the enrollment of more homogeneous cohorts of patients in future studies.

INTRODUCTION

Syndrome of undifferentiated recurrent fevers (SURF) classifies a group of patients affected by stereotypic, usually self-resolving, inflammatory flares of unknown etiology separated by intervals of overall well-being over a period of at least six months. Differential diagnosis includes several monogenic conditions

The funders had no role in study design, data collation, data analysis, data interpretation, writing of the manuscript, and decision to submit. The corresponding author had full access to all of the data and the final responsibility for the decision to submit for publication.

Partially supported by Italian Ministry of Health (Ricerca Corrente 2025). This study was conducted within the framework of PerSAID project (ERAPerMED2021-262) and Eurofever registry (project 2007332). Dr Kozáková's and Dr Fingerhutová's work was supported by the Czech Health Research Council (AZV CR; grant NU21-05-00522). This work is generated in the context of the European Reference Network for Rare Immunodeficiency, Autoinflammatory and Autoimmune Diseases—project 739543.

[1]UOC Reumatologia e Malattie Autoinfiammatorie, IRCCS Istituto Giannina Gaslini, Genoa, Italy; [2]Department of Health Sciences (DISSAL), University of Genoa, Genoa, Italy; [3]Division of Rheumatology, IRCCS Ospedale Pediatrico Bambino Gesù, Rome, Italy; [4]University of Genoa, Department of Neurosciences, Rehabilitation, Ophthalmology, Genetics, Maternal and Child Health (DINOGMI), Genoa, Italy; [5]UOC Medicina d'Urgenza e Pronto Soccorso, IRCCS Istituto Giannina Gaslini, Genoa, Italy; [6]UOC Genetica Umana, IRCCS Istituto Giannina Gaslini, Genoa, Italy;

collectively referred to as hereditary recurrent fevers (HRF). The most common HRF is familial Mediterranean fever (FMF), caused by *MEFV* mutations.[1,2] Other diseases are mevalonate kinase deficiency (MKD), caused by *MVK* mutations[3,4]; tumor necrosis factor receptor–associated periodic fever syndrome (TRAPS), secondary to *TNFSRF1A* mutations[5]; and cryopyrin-associated periodic syndromes (CAPS), caused by *NLRP3* mutations.[6] The emergence of the next-generation sequencing (NGS) technique has revealed a growing number of novel ultrarare monogenic diseases in which recurrent fever episodes may be part of the clinical phenotype.[7] Periodic fever, aphthosis, pharyngitis, and adenitis (PFAPA) syndrome is a multifactorial condition and represents the most common form of recurrent fever in childhood.[8]

Recently, increasing attention has been directed toward a group of patients presenting with recurrent fever in whom genetic analysis does not provide an explanation and who do not fulfill the PFAPA syndrome criteria.[9] These patients have been recently grouped under the term "SURF."[10–14] According to some recent studies, despite a certain degree of variability, patients with SURF display a distinctive clinical presentation, dominated by the presence of abdominal pain and musculoskeletal manifestations and a good response to colchicine.[11] Recent studies have shown a distinct pattern of activation of the pyrin inflammasome in patients with SURF when compared to FMF and PFAPA syndrome.[15]

Evidence-based classification criteria have been recently developed for HRF and PFAPA syndrome.[16] Classification criteria are crucial for the proper identification of patients being recruited into biologic and clinical studies and in therapeutic trials. Some preliminary empirical indications for the clinical suspicion of SURF have been proposed.[11]

The aim of the present study is to compare a homogeneous group of pediatric patients with SURF observed in a single tertiary care center with patients affected by HRF and PFAPA syndrome previously included in the study that developed the Eurofever classification criteria (members of the Eurofever study group are listed in Appendix A) in order to identify the clinical variables associated with SURF by an evidence-based approach.

METHODS

Selection of patients with SURF. One hundred twelve consecutive pediatric patients with SURF observed at Gaslini Institute in Genoa, Italy, since 2012 were included in the study. The inclusion criteria for patients with SURF has already been described[11] and are the following: (1) patients with stereotypic fever episodes separated by a regular or irregular interval of general well-being; (2) absence of an alternative diagnosis achieved during the follow-up; (3) availability of the results of genetic tests for at least the four best known HRF (FMF, MVK, TRAPS, and CAPS); (4) absence of pathogenic variants, likely pathogenic variants, or variants of unknown significance (VUS) in genes associated with HRF (Sanger and/or NGS panel) and pathogenic variants with a compatible inheritance pattern identified in genes tested through an extended autoinflammatory disease panel following whole-exome sequencing (WES); (5) a persistent recurrent disease course for at least 12 months; and (6) negativity of the Eurofever classification criteria for PFAPA syndrome.[12,16] Patients were included in the Eurofever longitudinal registry[17] after informed consent, and this study was approved by the Ethical Review Board of Regione Liguria.

Selection of patients with control diseases from the Eurofever registry. Pediatric patients with HRF (FMF, MVK, TRAPS, and CAPS) or PFAPA syndrome already involved in the development of the Eurofever classification criteria[16] were used as disease controls. The process of classification of the patients has been previously described.[16] Briefly, 60 patients for each disease (FMF, TRAPS, MKD, CAPS, and PFAPA syndrome) were selected from the Eurofever registry. Twenty-five international experienced clinicians/researchers and eight geneticists (total 33 panelists) in the field of systemic autoinflammatory diseases blinded to patients' original diagnoses were invited to participate in a multiround secured web process to classify each of the patients into one of mutually exclusive diagnoses.[16] At the end of the fourth round, consensus was achieved for a total of 188 pediatric patients (56 with MKD, 32 with TRAPS, 32 with FMF, 31 with CAPS, and 37 with PFAPA syndrome).[16]

To assess the generalizability of the SURF classifiers to a broader population, an external validation pediatric cohort was established, comprising 40 patients with SURF, 40 patients with PFAPA syndrome, 35 patients with FMF, and 8 patients with MKD from four centers (Ankara, Münster, Prague, and Rome). Because of the higher degree of clinical similarity of SURF with FMF, PFAPA syndrome, and MKD, we decided to focus the external validation on these four conditions.

[7]Department of Pediatric Rheumatology and Immunology, University of Muenster, Muenster, Germany; [8]Department of Pediatrics Rheumatology, Hacettepe University Faculty of Medicine, Ankara, Turkey; [9]General University Hospital in Prague and Department of Paediatrics and Inherited Metabolic Disorders, Charles University, Prague, Czech Republic; [10]UOSD Area Aggregazione Laboratori della Ricerca, IRCCS Istituto Giannina Gaslini, Genoa, Italy.

Drs Papa and Bovis are co-first authors and contributed equally to this work.

Additional supplementary information cited in this article can be found online in the Supporting Information section (https://acrjournals.onlinelibrary.wiley.com/doi/10.1002/art.70019).

Author disclosures are available at https://onlinelibrary.wiley.com/doi/10.1002/art.70019.

Address correspondence via email to Marco Gattorno, MD, at marcogattorno@gaslini.org.

Submitted for publication June 25, 2025; accepted in revised form November 12, 2025.

Variables description. All demographic and clinical variables recorded in the Eurofever registry have been considered for the diagnostic assessment. Clinical characteristics encompassed all the manifestations, from disease onset to diagnosis and initiation of the proper treatment. The items examined were as follows: (1) nature of the fever episodes (duration, frequency, regular frequency pattern, etc), (2) clinical manifestations associated with fever episodes and presence of the symptoms (always or often/sometimes), and (3) presence of triggers. For the statistical analysis, the PFAPA syndrome–related clinical features (exudative or erythematous tonsillitis, stomatitis, cervical lymph nodes) were also evaluated for their frequency: never, sometimes (less than 50% of episodes), or often/always.[16]

Statistical analysis. Continuous variables were summarized using mean and SD or median (and range or interquartile range) as appropriate, and categorical variables were described as frequencies (and percentage). For group comparisons, standardized mean differences were calculated according to Cohen's d effect size. Cohen's d effect size >0.1 denotes meaningful imbalance in the baseline covariates.[18] No data imputations were performed.

The decision tree approach was tested by randomly splitting the available data in a training set (70%) and in an internal validation set (30%). A decision tree approach was chosen because it produces very clear results and is easy to interpret and apply to everyday clinical practice.

The recursive partitioning (rPART) method[19] was used to identify the optimal split of the data that would best classify patients with autoinflammatory diseases as with or without SURF. All demographic and clinical variables collected in the Eurofever registry were initially considered as candidate predictors. The rPART algorithm automatically selected variables and determined their hierarchy in the decision tree by identifying the splits that maximized discrimination between patients with and without SURF, without prior manual selection or weighting.

Two fully grown decision tree classifiers with no limit on the complexity parameter were developed. In the first decision tree model, demographic and clinical features were combined with the information coming from the genetic analysis (confirmatory, nonconfirmatory, negative). In the second decision tree model, genetic data were not included, and only demographic and clinical features were considered. This approach was performed in an attempt to identify, with an evidence-based approach, the clinical variables possibly associated with SURF, independently of the need to perform a genetic analysis. We then calculated the area under the receiver operating characteristic curve (AUC), accuracy, sensitivity, and specificity of the decision tree classifier for predicting SURF versus non-SURF.

To support the decision tree results, an alternative model was created using a classification methodology previously described[20] and detailed in Supplementary material point 1. Briefly, the score was obtained in the training set by summing all the weights (estimated by a multivariable logistic regression model) associated with the presence or absence of symptoms in each patient. The discriminative ability of the score was assessed by receiver operating characteristic curve analysis, and the optimal cutoff value that provided the best discrimination between patients with and without SURF was identified through the Youden index criterion.

External validation was performed using an independent cohort of patients that was not involved in model training. This allowed for an assessment of the model's generalizability and helped ensure that the observed performance was not a result of overfitting. Software used to analyzed data were SAS (v 9.4) and R version 4.1.3, as well as the packages "rpart," "party," and "r.part plot."

RESULTS

Patient description. A total of 300 patients were included in the study. The demographic and clinical features of patients with SURF are reported in Table 1 and compared with those observed in the disease control patients with HRF and PFAPA syndrome, previously used in developing the Eurofever classification criteria for autoinflammatory recurrent fevers.[16] Patients were randomly split into a training set (n = 207) and a testing set (n = 93) (Supplementary Table 2). The clinical and demographic characteristics were similar between the training and testing cohorts. All patients with SURF were of western European Caucasian origin (Table 1). Eighteen patients with SURF were studied with a 4-gene mini panel for recurrent fevers, 20 patients were studied with an 11-gene NGS panel, 24 patients were studied with exome sequencing with an applied in silico panel for recurrent fevers, and 58 patients were studied with exome sequencing with an applied in silico extended panel for autoinflammatory diseases. Colchicine treatment was used in 82% of patients with SURF, with a partial or complete response in 89% of them. In other patients with SURF, on-demand steroids was the alternative therapeutic approach to colchicine (Table 1).

Diagnostic performance of two statistical models for classifying patients with SURF. *Decision tree classifier.* Figure 1 and Supplementary Table 3 illustrate the decision boundaries of the decision tree, which integrates demographic and clinical information with genetic analysis, classified as positive in case of pathogenic mutations in genes associated with HRF or negative for NGS panels. As expected, the probability of being classified as having SURF with a positive genetic test result is 0%. According to this model, the probability rises to 91% if the genetic test result is negative for pathogenic variants and if the patient does not present with exudative or erythematous pharyngitis or does so only occasionally (Figure 1).

Table 1. Demographic and clinical characteristics of the whole population enrolled*

Characteristics	CAPS	FMF	MKD	PFAPA syndrome	SURF	TRAPS	*P*	SMD[a]
No. of patients	31	32	56	37	112	32	–	–
Sex, n (%)								
Female	12 (38.7)	16 (50.0)	31 (55.4)	19 (51.4)	56 (50.0)	14 (43.8)	0.746	0.143
Male	19 (61.3)	16 (50.0)	25 (44.6)	18 (48.6)	56 (50.0)	18 (56.2)	–	–
Age at onset, median (IQR), y	1.20 (0.45–2.86)	2.68 (1.33–5.95)	0.35 (0.17–0.78)	1.58 (0.67–2.98)	2.42 (0.96–4.53)	1.18 (0.36–4.20)	<0.001	0.387
Age at diagnosis, median (IQR), y	16.61 (6.36–29.24)	6.08 (4.24–9.30)	6.51 (3.68–14.59)	4.83 (3.27–6.41)	6.45 (4.19–9.98)	19.31 (6.23–35.87)	<0.001	0.716
Duration of episodes, median (IQR), days	1.50 (0.75–3.25)	2.00 (2.00–3.00)	5.00 (4.00–7.00)	4.00 (3.00–4.00)	4.00 (3.00–5.00)	10.00 (7.00–13.00)	<0.001	0.907
No. of episodes/year, median (IQR)	15.00 (10.00–30.00)	12.00 (12.0–20.2)	12.00 (10.5–16.5)	12.00 (12.0–18.0)	12.00 (12.0–20.0)	6.00 (3.0–13.5)	0.001	0.443
Positive genetic test result, n (%)	31 (100.0)	32 (100.0)	56 (100.0)	0 (0.0)	0 (0.0)	32 (100.0)	<0.001	–
Positive family history, n (%)	21 (67.7)	12 (37.5)	16 (28.6)	4 (10.8)	21 (18.8)	24 (75.0)	<0.001	0.763
East Mediterranean origin, n (%)	0 (0.0)	12 (37.5)	3 (5.4)	0 (0.0)	0 (0.0)	0 (0.0)	<0.001	0.528
Cold trigger, n (%)	12 (38.7)	2 (6.2)	1 (1.8)	0 (0.0)	0 (0.0)	1 (3.1)	<0.001	0.479
Any trigger, n (%)	17 (54.8)	7 (21.9)	35 (62.5)	4 (10.8)	1 (0.9)	11 (34.4)	<0.001	0.778
Abdominal pain, n (%)	2 (6.5)	25 (78.1)	51 (91.1)	17 (45.9)	72 (64.3)	24 (75.0)	<0.001	0.978
Aphthosis, n (%)	5 (16.1)	1 (3.1)	38 (67.9)	26 (70.3)	44 (39.3)	0 (0.0)	<0.001	1.056
Diarrhea, n (%)	1 (3.2)	8 (25.0)	46 (82.1)	2 (5.4)	26 (23.2)	7 (21.9)	<0.001	0.878
Vomiting, n (%)	0 (0.0)	10 (31.2)	40 (71.4)	4 (10.8)	17 (15.2)	4 (12.5)	<0.001	0.784
Arthralgia, n (%)	28 (90.3)	17 (53.1)	42 (75.0)	16 (43.2)	79 (70.5)	23 (71.9)	<0.001	0.464
Arthritis, n (%)	15 (48.4)	14 (43.8)	17 (30.4)	0 (0.0)	7 (6.2)	2 (6.2)	<0.001	0.694
Oligoarthritis, n (%)	10 (32.3)	10 (31.2)	11 (19.6)	0 (0.0)	3 (2.7)	0 (0.0)	<0.001	0.569
Monoarthritis, n (%)	8 (25.8)	9 (28.1)	6 (10.7)	0 (0.0)	5 (4.5)	2 (6.2)	<0.001	0.448
Myalgia, n (%)	16 (51.6)	11 (34.4)	34 (60.7)	11 (29.7)	59 (52.7)	27 (84.4)	<0.001	0.525
Fasciitis, n (%)	0 (0.0)	0 (0.0)	0 (0.0)	0 (0.0)	0 (0.0)	2 (6.2)	0.005	0.122
Cartilage overgrowth, n (%)	10 (32.3)	0 (0.0)	0 (0.0)	0 (0.0)	0 (0.0)	0 (0.0)	<0.001	0.325
Any lymph node involvement, n (%)	7 (22.6)	6 (18.8)	51 (91.1)	32 (86.5)	49 (43.8)	15 (46.9)	<0.001	0.948
Cervical adenitis, n (%)	6 (19.4)	5 (15.6)	50 (89.3)	32 (86.5)	47 (42.0)	15 (46.9)	<0.001	0.99
Painful lymph nodes, n (%)	1 (3.2)	1 (3.1)	38 (67.9)	10 (27.0)	2 (1.8)	10 (31.2)	<0.001	0.814
Serositis, n (%)	0 (0.0)	5 (15.6)	6 (10.7)	0 (0.0)	1 (0.9)	2 (6.2)	0.001	0.339
Chest pain, n (%)	0 (0.0)	14 (43.8)	7 (12.5)	0 (0.0)	12 (10.7)	3 (9.4)	<0.001	0.536
Aseptic meningitis, n (%)	4 (12.9)	1 (3.1)	0 (0.0)	0 (0.0)	0 (0.0)	0 (0.0)	<0.001	0.237
Hearing loss, n (%)	10 (32.3)	0 (0.0)	0 (0.0)	0 (0.0)	0 (0.0)	0 (0.0)	<0.001	0.325
Headache, n (%)	18 (58.1)	4 (12.5)	23 (41.1)	5 (13.5)	14 (12.5)	8 (25.0)	<0.001	0.509
Fatigue, n (%)	23 (74.2)	15 (46.9)	39 (69.6)	13 (35.1)	39 (34.8)	22 (68.8)	<0.001	0.569
Any skin rash, n (%)	31 (100.0)	2 (6.2)	24 (42.9)	1 (2.7)	15 (13.4)	17 (53.1)	<0.001	1.85
Urticarial rash, n (%)	29 (93.5)	0 (0.0)	6 (10.7)	0 (0.0)	9 (8.0)	3 (9.4)	<0.001	1.538
Conjunctivitis, n (%)	19 (61.3)	2 (6.2)	9 (16.1)	1 (2.7)	1 (0.9)	17 (53.1)	<0.001	0.853
Erysipeloid rash, n (%)	0 (0.0)	2 (6.2)	2 (3.6)	0 (0.0)	0 (0.0)	2 (6.2)	0.068	0.217
Maculopapular rash, n (%)	11 (35.5)	0 (0.0)	21 (37.5)	1 (2.7)	8 (7.1)	11 (34.4)	<0.001	0.609
Migratory rash, n (%)	1 (3.2)	0 (0.0)	1 (1.8)	0 (0.0)	0 (0.0)	12 (37.5)	<0.001	0.445
Any tonsillitis, n (%)	2 (6.5)	4 (12.5)	34 (60.7)	37 (100.0)	55 (49.1)	4 (12.5)	<0.001	1.508
Exudative tonsillitis, n (%)	0 (0.0)	1 (3.1)	19 (33.9)	32 (86.5)	40 (35.7)	1 (3.1)	<0.001	1.224
Erythematous tonsillitis, n (%)	2 (6.5)	4 (12.5)	28 (50.0)	34 (91.9)	39 (34.8)	4 (12.5)	<0.001	1.098
Periorbital edema, n (%)	1 (3.2)	0 (0.0)	1 (1.8)	0 (0.0)	2 (1.8)	12 (37.5)	<0.001	0.441

(Continued)

Table 1. (*Cont'd*)

Characteristics	CAPS	FMF	MKD	PFAPA syndrome	SURF	TRAPS	*P*	SMD[a]
Irregular period fever, n (%)	27 (87.1)	19 (59.4)	35 (62.5)	7 (18.9)	39 (34.8)	25 (78.1)	<0.001	0.749
Amyloidosis, n (%)	0 (0.0)	0 (0.0)	1 (1.8)	0 (0.0)	0 (0.0)	6 (18.8)	<0.001	0.295
Response to steroids, n (%)								
No	1 (3.2)	1 (3.1)	3 (5.4)	1 (2.7)	0 (0.0)	3 (9.4)	<0.001	1.175
Yes	2 (6.5)	5 (15.6)	31 (55.4)	28 (75.7)	10 (8.9)	24 (75.0)	–	–
Not done	28 (90.3)	26 (81.2)	22 (39.3)	8 (21.6)	102 (91.1)	5 (15.6)	–	–
Response to colchicine, n (%)								
No	2 (6.5)	2 (6.2)	5 (8.9)	0 (0.0)	10 (8.9)	7 (21.9)	<0.001	1.695
Yes	0 (0.0)	28 (87.5)	7 (12.5)	3 (8.1)	81 (72.3)	1 (3.1)	–	–
Not done	29 (93.5)	2 (6.2)	44 (78.6)	34 (91.9)	21 (18.8)	24 (75.0)	–	–
Response to interleukin-1 inhibitors, n (%)								
No	0 (0.0)	0 (0.0)	0 (0.0)	1 (2.7)	0 (0.0)	0 (0.0)	<0.001	0.944
Yes	22 (71.0)	1 (3.1)	17 (30.4)	0 (0.0)	7 (6.2)	13 (40.6)	–	–
Not done	9 (29.0)	31 (96.9)	39 (69.6)	36 (97.3)	105 (93.8)	19 (59.4)	–	–
Response to tonsillectomy, n (%)								
No	0 (0.0)	1 (3.1)	10 (17.9)	4 (10.8)	18 (16.1)	1 (3.1)	0.01	0.463
Yes	0 (0.0)	2 (6.2)	3 (5.4)	4 (10.8)	1 (0.9)	1 (3.1)	–	–
Not done	31 (100.0)	29 (90.6)	43 (76.8)	29 (78.4)	93 (83.0)	30 (93.8)	–	–

* CAPS, cryopyrin-associated periodic syndromes; FMF, familial Mediterranean fever; IQR, interquartile range; MKD, mevalonate kinase deficiency; PFAPA syndrome, periodic fever, aphthosis, pharyngitis, and adenitis; SMD, standardized mean difference; SURF, syndrome of undifferentiated recurrent fever; TRAPS, tumor necrosis factor receptor–associated periodic fever syndrome;

[a] SMD was calculated according to Cohen's d effect size (Cohen's d effect size >0.1 denotes meaningful imbalance in the baseline covariates).

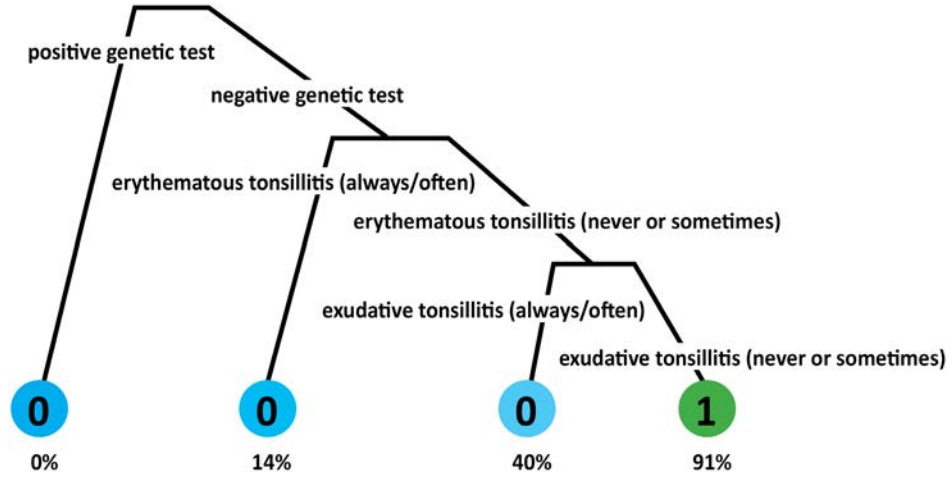

Figure 1. Decision tree to classify syndrome of undifferentiated recurrent fever based on clinical variables and genetic test results.

According to a decision tree model based solely on clinical variables, patients with SURF are classified by the absence of triggers for the fever episodes, conjunctivitis, and constant presence of erythematous tonsillitis. Moreover, the duration of the fever episodes (range three to six days) and the presence of myalgia during flares allow for the correct classification of 81% of patients with SURF (Figure 2). In the same model, the absence of fatigue during attacks, the presence of lymphadenopathy at any site, and fewer than 14 fever episodes per year were additional variables that accurately identified patients with SURF (Figure 2). The likelihood of being classified as having SURF increases with the presence or absence of these specific variables, ranging from 64% to 88% (Figure 2 and Supplementary Table 4). Supplementary Figures 1 and 2 show the number of patients classified as

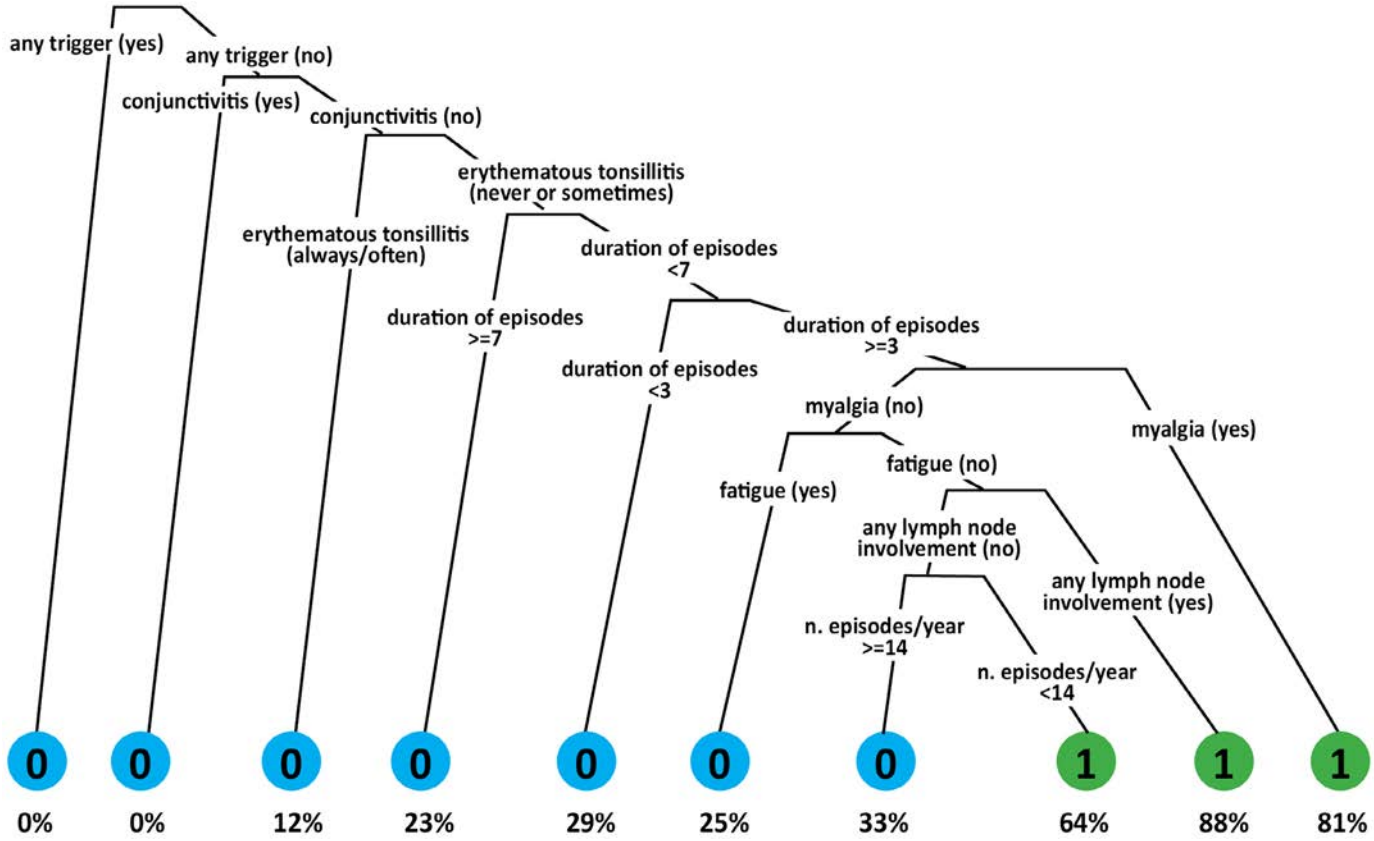

Figure 2. Decision tree to classify syndrome of undifferentiated recurrent fever solely based on clinical variables. Color figure can be viewed in the online issue, which is available at http://onlinelibrary.wiley.com/doi/10.1002/art.70019/abstract.

Table 2. Performance values of classifiers of SURF using the decision tree classifier in the testing set (n = 93)*

Classifier	AUC% (95% CI)	Accuracy% (95% CI)	Sensitivity% (95% CI)	Specificity% (95% CI)
Decision tree with genetic testing	95.7 (92.1–99.3)	92.5 (85.1–96.9)	91.2 (76.3–98.1)	93.2 (83.5–98.1)
Decision tree without genetic testing	87.2 (79.5–94.9)	84.9 (76.0–91.5)	70.6 (52.5–84.9)	93.2 (83.5–98.1)

* AUC, area under the curve; CI, confidence interval; SURF, syndrome of undifferentiated recurrent fever.

having SURF, PFAPA syndrome, or HRF according to the decision trees used for the genetic and clinical classification of SURF in the entire study population (N = 300).

As expected, models that include genetic information demonstrate superior performances compared to those without genetic information (Table 2 and Supplementary Table 5). When genetic data are excluded, the AUC of the decision tree model in the testing set decreases from 96% (95% confidence interval [CI] 92%–99%) to 87% (95% CI 79%–95%), and sensitivity drops from 91% (95% CI 85%–97%) to 71% (95% CI 76%–91.5%). However, specificity remains consistent at 93% in both models (Table 2).

Logistic regression model. Univariable and multivariable logistic regression analyses incorporating all the variables listed in Table 1 and the genetic test results were conducted on the training set, with detailed findings presented in Supplementary Table 1. The logistic regression model that included the genetic test results exhibited high predictive performance. The variables included in the model were the absence of a positive genetic test result with a score of 78, the absence of persistent presence of cervical lymph node involvement with a score of 18, and sporadic enlargement of cervical lymph nodes with a score of 4.

The threshold for predicting a patient with SURF was set at 78, achieving an AUC of 89.7% (95% CI 81.6%–95.0%), indicating excellent discriminative power. The model demonstrated an overall accuracy of 89.2% (95% CI 81.1%–94.7%), with a sensitivity of 91.2% (95% CI 76.3%–98.1%) and a specificity of 88.1% (95% CI 77.1%–95.1%) (Table 3).

In contrast, the logistic regression model exclusively based on clinical manifestations and excluding the results of genetic tests retained in the final model the absence of triggers (score of 72), the sporadic presence of cervical lymph node enlargement with a score of 8, and the absence of a constant presence of lymph node enlargement with a score of 16. The absence of fatigue during attacks had a score of 4. The score threshold for predicting a patient with SURF was set at 76, resulting in an AUC of 71.2% (95% CI 60.9%–80.2%) and indicating a moderate predictive capability. The overall accuracy of the model was 66.7% (95% CI 56.1%–76.1%), with a sensitivity of 88.2% (95% CI 72.5%–96.7%) and a specificity of 54.2% (95% CI 40.7%–67.3%) (Table 3).

Table 3. Performance values of classifiers of SURF using a logistic regression model in the testing set (n = 93)*

	Score	Cutoff	AUC% (95% CI)	Accuracy% (95% CI)	Sensitivity% (95% CI)	Specificity% (95% CI)
Logistic regression with genetic testing[a]						
Positive genetic test result	78 (for absence)	>78	89.7 (81.6–95.0)	89.2 (81.1–94.7)	91.2 (76.3–98.1)	88.1 (77.1–95.1)
Cervical lymph nodes (sometimes vs never)	4 (for presence)					
Cervical lymph nodes (always vs never)	18 (for absence)					
Logistic regression without genetic testing[b]						
Any trigger	72 (for absence)	>76	71.2 (60.9–80.2)	66.7 (56.1–76.1)	88.2 (72.5–96.7)	54.2 (40.7–67.3)
Cervical lymph nodes (sometimes vs never)	8 (for presence)					
Cervical lymph nodes (always vs never)	16 (for absence)					
Fatigue	4 (for absence)					

* AUC, area under the curve; CI, confidence interval; SURF, syndrome of undifferentiated recurrent fever.
[a] Cutoff > 78.
[b] Cutoff > 76.

Table 4. Performance values of classifiers of SURF in the external validation set (n = 123; 40 patients with SURF, 40 patients with PFAPA syndrome, 35 patients with FMF, 8 patients with MKD)*

Classifier	AUC% (95% CI)	Accuracy% (95% CI)	Sensitivity% (95% CI)	Specificity% (95% CI)
Decision tree with genetic test	96.3 (91.3–98.9)	95.9 (90.8–98.7)	97.5 (86.8–99.9)	95.2 (88.1–98.7)
Decision tree without genetic test	77.1 (68.7–84.2)	80.5 (72.4–87.1)	67.5 (50.9–81.4)	86.7 (77.5–93.2)
Logistic regression with genetic test[a]	88.0 (80.9–93.1)	83.7 (76.0–89.8)	100.0 (91.2–100.0)	75.9 (65.3–84.6)
Logistic regression without genetic test[b]	65.0 (55.9–73.3)	54.5 (45.2–63.5)	95.0 (83.1–99.4)	34.9 (24.8–46.2)

* AUC, area under the curve; CI, confidence interval; FMF, familial Mediterranean fever; MKD, mevalonate kinase deficiency; PFAPA syndrome, periodic fever, aphthosis, pharyngitis, and adenitis; SURF, syndrome of undifferentiated recurrent fever.
[a] Cutoff > 78.
[b] Cutoff > 76.

External validation sample. When the classification criteria, including the genetic test, were applied to the external validation cohort, the model demonstrated strong discriminative power, with AUCs of 96.3% using the decision tree model and 88.0% with the logistic regression model (Table 4). The decision tree model based solely on clinical variables showed high specificity (86.7%) but lower sensitivity (67.5%), whereas the logistic regression model achieved high sensitivity (95%) but very low specificity (35%). In the decision tree model based exclusively on clinical variables, sensitivity varied across centers. The Prague center demonstrated the lowest sensitivity (50%), whereas the Turkish center achieved perfect sensitivity (100%). Both the Rome and Münster centers reported a sensitivity of 60%. Specificity was consistently high (>85%) across all centers, with the exception of the Turkish center, where it was reduced to 76%.

DISCUSSION

The present study represents the first attempt to develop an evidence-based approach for the identification and classification of pediatric patients with autoinflammatory recurrent fever lacking a precise genetic etiology or nosological definition (as in the case of PFAPA syndrome), currently grouped under the definition of SURF. A decision tree model was able to identify the clinical variables that may aid in the better definition of this subgroup of patients for future studies (ie, duration of attacks 3–6 days, <14 episodes/year, absence of triggers, conjunctivitis, tonsillitis or fatigue during attacks, and presence of myalgia or lymph node involvement) with a higher accuracy when associated with negative genetic analysis results (Supplementary Table 10).

The definition and even the actual existence of SURF as a distinct clinical group remain under discussion. Over the last decade, several clinical studies have attempted to better characterize this group of patients, who display typical features of recurrent fevers but do not meet the clinical criteria for PFAPA syndrome or have a positive genetic test result for the most common forms of HRF.[10–14] The need for a better definition of this group of patients arises from clinical observations in daily practice, which show that a significant number of these "undefined" patients with recurrent fever visit clinics for autoinflammatory diseases.

The variability in patient selection, including ethnicity, geographic distribution, and the extent of genetic analysis across different cohorts of patients with SURF described in the literature, has led to significant heterogeneity in terms of clinical presentation, treatment response, and outcomes. However, despite these limitations, some general features appear to be shared across all studies: (1) absence or minimal involvement of the classic PFAPA syndrome triad; (2) prevalence of specific clinical features such as arthralgia, myalgia, abdominal pain, and skin rash; (3) negative genetic test results; and (4) a generally good response to colchicine or anti–interleukin-1 (anti–IL-1) treatment.[10–14] In light of this distinctive response to colchicine, the activation pattern of the pyrin inflammasome was recently analyzed, revealing that patients with SURF responsive to colchicine exhibit a different activation pattern compared to those with FMF or PFAPA syndrome and healthy controls.[15] Additionally, a distinctive overexpression of the IL-1 signature was observed in the tonsils of patients with SURF compared to patients with PFAPA syndrome.[12] These data provide the first biologic evidence of a difference in the pathogenic mechanisms leading to these patient subgroups. An extensive analysis of activated pathways during inflammatory response in SURF monocytes may show novel details.

With the aim of obtaining a more homogeneously selected cohort of patients with SURF, we decided to include in the present study only patients coming from a single center, confirming the selective inclusion criteria used in previous studies[10] and thus avoiding excessive heterogeneity in their recruitment. Patients were compared with an historical group of patients already used for the definition of the evidence-based Eurofever criteria, which were validated by a group of international experts.[16]

Our study was able to identify clinical variables that, whenever present in the decision tree, can identify patients with SURF with good accuracy. As expected, a negative genetic test result,

associated with the lack or persistent presence of exudative or erythematous tonsillitis, was the best classifier for patients with SURF. This result is secondary to the higher prevalence of patients with persistent tonsillitis in PFAPA syndrome when compared to SURF. A more detailed definition of the frequency of PFAPA syndrome–related clinical features during the flare could help for a better definition of the actual differences of these manifestations between PFAPA syndrome and SURF for the development of future definitive criteria.

The application of the decision tree model in a purely clinical setting led to the identification of several clinical variables capable of distinguishing, with relatively high accuracy, patients with SURF from those with other forms of recurrent fever. Notably, patients with SURF do not report clear triggers for their fever episodes. In addition, conjunctivitis is generally not observed during these episodes. The median duration of fever episodes in SURF is four days,[13] which is a distinguishing feature compared to FMF. Arthralgia and myalgia are frequently observed in patients with SURF.[13] The present study demonstrates that myalgia more effectively differentiates SURF from PFAPA syndrome, in which arthralgia was reported in nearly 30% of patients, consistent with previous studies.[13] Finally, in the decision tree model, the presence of lymph node involvement at any site was able to distinguish patients with SURF from those with CAPS and FMF, although its prevalence was notably higher still in those with MKD and PFAPA syndrome.

Although the present preliminary classification criteria should not be used for diagnostic purposes in clinical practice, the results of the comparative analysis among different recurrent fevers may help to highlight certain clinical features that can assist clinicians in considering a possible diagnosis of SURF based on clinical evaluation. Overall, the decision tree was able to identify clinical features that accurately predicted the likelihood of a patient being classified as having SURF compared to other recurrent fevers, even in the absence of genetic testing, and performed better than the classic regression tree model. External validation using patients from other pediatric centers demonstrated a generally satisfactory performance, particularly for the decision tree model. However, a certain degree of variability was observed in the prevalence of clinical features associated with SURF across the different centers, possibly related to a different approach in patient selection. This reinforces the need to develop an evidence-based common tool that could help to better classify this group of patients for future clinical studies.

General reduction of costs of genetic analysis and increasing availability of molecular analysis in different countries strongly support the indication to perform a genetic test in patients with recurrent fevers, especially if not consistent with a PFAPA syndrome classic phenotype. However, these tests are still not available in all countries or not covered by different health systems or insurance companies. Therefore, in the absence of a genetic test or while waiting for the results of genetic testing, application of the decision tree could help the physician to identify patients with a higher probability to have SURF and start a trial with colchicine.

The present study has a number of limitations:

1. The use of patients observed in a single center might have introduced a bias of selection of patients with SURF mainly related to their response to colchicine, which in our experience represents one of the most characteristic features of this subgroup of patients.
2. Although most of the patients with SURF underwent extensive exclusion of the most frequent genes associated with recurrent fevers through NGS panels or an in silico panel after WES, it is possible that some of them could carry mutations in genes not yet identified at the time of genetic analysis. In any case, the present study was able to distinguish SURF only from the four main HRF and PFAPA syndrome. For this reason, an extensive investigation via whole-genome sequencing of all patients with SURF in our cohort is currently under analysis, and it would be suggested, whenever possible, in all patients with recurrent fevers.
3. The exclusion of patients carrying VUS of genes associated with HRF in the present study does not allow us to shed light on the actual interpretation of these variants in real life. In this line, it is worth noting that a recent study conducted on a group of patients bearing the R92Q variant of the *TNFRSF1A* gene enrolled in the Eurofever registry showed that this subgroup of patients displayed a high degree of similarity, in terms of clinical manifestations associated with recurrent fevers and colchicine response, with patients with SURF rather than TRAPS and PFAPA syndrome.[21]

Even with these limitations, the present study shows the possibility of achieving evidence-based criteria that can classify SURF, at least with respect to the main HRF and PFAPA syndrome, and may be considered as a preliminary step for the enrollment of more homogenous cohorts of patients in future studies. Moreover, identifying possible patients with SURF may prompt the initiation of colchicine treatment while awaiting the results of genetic analysis. The elaboration of definitive criteria would need the collection of patients with SURF from different centers and blind evaluation with confounding conditions by a panel of experts possibly involving both pediatric and adult patients.

ACKNOWLEDGMENTS

The authors would like to thank Eugenia Mosci and Elisa Patrone for their precious assistance.

AUTHOR CONTRIBUTIONS

All authors contributed to at least one of the following manuscript preparation roles: conceptualization AND/OR methodology, software,

investigation, formal analysis, data curation, visualization, and validation AND drafting or reviewing/editing the final draft. As corresponding author, Dr Gattorno confirms that all authors have provided the final approval of the version to be published and takes responsibility for the affirmations regarding article submission (eg, not under consideration by another journal), the integrity of the data presented, and the statements regarding compliance with institutional review board/Declaration of Helsinki requirements.

REFERENCES

1. Bernot A, Clepet C, Dasilva C, et al; The French FMF Consortium. A candidate gene for familial Mediterranean fever. Nat Genet 1997; 17(1):25–31. doi:https://doi.org/10.1038/ng0997-25
2. The International FMF Consortium. Ancient missense mutations in a new member of the RoRet gene family are likely to cause familial Mediterranean fever. Cell 1997;90(4):797–807. doi:https://doi.org/10.1016/S0092-8674(00)80539-5
3. Drenth JPH, Cuisset L, Grateau G, et al; International Hyper-IgD Study Group. Mutations in the gene encoding mevalonate kinase cause hyper-IgD and periodic fever syndrome. Nat Genet 1999;22(2):178–181. doi:https://doi.org/10.1038/9696
4. Houten SM, Kuis W, Duran M, et al. Mutations in MVK, encoding mevalonate kinase, cause hyperimmunoglobulinaemia D and periodic fever syndrome. Nat Genet 1999;22(2):175–177. doi:https://doi.org/10.1038/9691
5. McDermott MF, Aksentijevich I, Galon J, et al. Germline mutations in the extracellular domains of the 55 kDa TNF receptor, TNFR1, define a family of dominantly inherited autoinflammatory syndromes. Cell 1999;97(1):133–144. doi:https://doi.org/10.1016/S0092-8674(00)80721-7
6. Hoffman HM, Mueller JL, Broide DH, et al. Mutation of a new gene encoding a putative pyrin-like protein causes familial cold autoinflammatory syndrome and Muckle-Wells syndrome. Nat Genet 2001; 29(3):301–305. doi:https://doi.org/10.1038/ng756
7. Poli C, Aksentijevich I, Bousfiha AA, et al. Human inborn errors of immunity: 2024 update on the classification from the International Union of Immunological Societies Expert Committee. J Hum Immun 2025;1(1):e20250003. doi:https://doi.org/10.70962/jhi.20250003
8. Marshall GS, Edwards KM, Butler J, et al. Syndrome of periodic fever, pharyngitis, and aphthous stomatitis. J Pediatr 1987;110(1):43–46. doi:https://doi.org/10.1016/S0022-3476(87)80285-8
9. Broderick L, Hoffman HM. Pediatric recurrent fever and autoinflammation from the perspective of an allergist/immunologist. J Allergy Clin Immunol 2020;146(5):960–966.e2. doi:https://doi.org/10.1016/j.jaci.2020.09.019
10. Papa R, Rusmini M, Volpi S, et al. Next generation sequencing panel in undifferentiated autoinflammatory diseases identifies patients with colchicine-responder recurrent fevers. Rheumatology (Oxford) 2020; 59(2):344–360. doi:https://doi.org/10.1093/rheumatology/kez270
11. Papa R, Penco F, Volpi S, et al. Syndrome of undifferentiated recurrent fever (SURF): an emerging group of autoinflammatory recurrent fevers. J Clin Med 2021;10(9):1963. doi:https://doi.org/10.3390/jcm10091963
12. Luu I, Nation J, Page N, et al. Undifferentiated recurrent fevers in pediatrics are clinically distinct from PFAPA syndrome but retain an IL-1 signature. Clin Immunol 2021;226:108697. doi:https://doi.org/10.1016/j.clim.2021.108697
13. Sutera D, Bustaffa M, Papa R, et al. Clinical characterization, long-term follow-up, and response to treatment of patients with syndrome of undifferentiated recurrent fever (SURF). Semin Arthritis Rheum 2022;55:152024. doi:https://doi.org/10.1016/j.semarthrit.2022.152024
14. Macaraeg M, Baker E, Handorf E, et al. Clinical, immunologic, and genetic characteristics in patients with syndrome of undifferentiated recurrent fevers. Arthritis Rheumatol 2025;77(5):596–605. doi:https://doi.org/10.1002/art.43065
15. Palmeri S, Penco F, Bertoni A, et al. Pyrin inflammasome activation defines colchicine-responsive SURF patients from FMF and other recurrent fevers. J Clin Immunol 2024;44(2):49. doi:https://doi.org/10.1007/s10875-023-01649-7
16. Gattorno M, Hofer M, Federici S, et al; Eurofever Registry and the Paediatric Rheumatology International Trials Organisation (PRINTO). Classification criteria for autoinflammatory recurrent fevers. Ann Rheum Dis 2019;78(8):1025–1032. doi:https://doi.org/10.1136/annrheumdis-2019-215048
17. Vyzhga Y, Frenkel J, Insalaco A, et al; for Eurofever the Paediatric Rheumatology International Trials Organisation (PRINTO). Monitoring of adverse events and safety in autoinflammatory diseases: real-life data from the Eurofever registry. J Clin Immunol 2024;44(5):119. doi:https://doi.org/10.1007/s10875-024-01719-4
18. Jacob C. Statistical Power Analysis for the Behavioral Sciences. 2nd ed. Lawrance Erlbaum Associates; 1988.
19. Breiman L, Friedman JH, Olshen RA, et al. Classification and Regression Trees. Chapman and Hall/CRC; 1984. https://www.researchgate.net/publication/327606791_Classification_and_regression_trees
20. Federici S, Sormani MP, Ozen S, et al; Paediatric Rheumatology International Trials Organisation (PRINTO) and Eurofever Project. Evidence-based provisional clinical classification criteria for autoinflammatory periodic fevers. Ann Rheum Dis 2015;74(5):799–805. doi:https://doi.org/10.1136/annrheumdis-2014-206580
21. Gerritsma AM, Sutera D, Cantarini L, et al; for Eurofever/Eurotraps projects and Paediatric Rheumatology International Trials Organisation (PRINTO). TNFRSF1A-pR92Q variant identifies a subset of patients more similar to systemic undifferentiated recurrent fever than TNF receptor-associated periodic syndrome. Clin Exp Rheumatol 2023;41(10):1998–2007.

APPENDIX A: EUROFEVER STUDY GROUP FOR THE CLASSIFICATION CRITERIA OF RECURRENT FEVERS

Members of the Eurofever study group are as follows: Michael Hofer, Federica Vanoni, Jordi Anton, Juan Ignacio Arostegui, Karyl S. Barron, Eldad Ben-Chetrit, Paul Brogan, Luca Cantarini, Isabella Ceccherini, Fabrizio De Benedetti, Fatma Dedeoglu, Erkan Demirkaya, Joost Frenke, Raphaela Goldbach-Mansky, Ahmet Gul, Veronique Hentgen, Hal M. Hoffman, Tilmann Kallinich, Isabelle Koné-Paut, Jasmin Kuemmerle-Deschner, Helen J. Lachmann, Ronald M. Laxer, Avi Livneh, Laura Obici, Dorota Rowczenio, Ricardo Russo, Yael Shinar, Anna Simon, Natasa Toplak, Isabelle Touitou, Yosef Uziel, Marielle van Gijn, Daniel L. Kastner, Alberto Martini, Maria Pia Sormani, and Nicolino Ruperto.

Arthritis & Rheumatology
Vol. 78, No. 5, May 2026, pp 1176–1183
DOI 10.1002/art.70002

American College of Rheumatology
Empowering Rheumatology Professionals

Romosozumab and Denosumab Combination Therapy After Denosumab in Postmenopausal Osteoporosis

Giovanni Adami, MD, Francesco Pollastri, MD, Angelo Fassio, MD, Filippo Montanari, MD, Anna Piccinelli, MD, Camilla Benini, MD, Emma Pasetto, MSc, Carmen Dartizio, MD, Davide Gatti, MD, Maurizio Rossini, MD, and Ombretta Viapiana, MD

Objective. Transition from long-term denosumab (Dmab) to parathyroid hormone-analogs or romosozumab (Romo) might expose patients to the risk of the so-called rebound phenomenon. Adding Romo to Dmab might represent an option in patients experiencing a fracture while on Dmab. The aim of this study was to investigate the effects of the combination of Romo to Dmab in postmenopausal osteoporosis.

Methods. We did a 36-month combined retrospective and prospective study analyzed with prospective score matching. Postmenopausal women were divided into two groups: patients on Dmab who added Romo to Dmab (Dmab from baseline [M–24] to Romo initiation [M0] → Dmab + Romo from M0 to M+12), and matched controls on Dmab continuing Dmab (Dmab from M–24 to M0 → Dmab from M0 to M+12). Bone mineral density and bone turnover markers (CTX, P1nP) were assessed at follow-up time points.

Results. A total of 50 women were included in the study: 25 patients in the Dmab → Dmab + Romo group and 25 matched controls in the Dmab → Dmab group. The between-group difference at M+12 was 3.3% (95% confidence interval –5.2 to 11.8), indicating a nonsignificant trend toward greater improvement with combination therapy. Adding Romo to Dmab increased P1nP significantly between M0 and M+3 (+22.5 ng/mL, SE = 8.7; $P = 0.028$).

Conclusion. Ongoing treatment with Dmab did not blunt the anabolic response of Romo, indicating sustained modeling-based bone formation activity. Adding Romo in patients failing Dmab might be a valuable option.

INTRODUCTION

Osteoporosis is characterized by decreased bone mass and deterioration of bone microarchitecture, with increased fracture risk. Current approved treatments for postmenopausal osteoporosis include antiresorptive drugs (bisphosphonates and Dmab), anabolic agents (teriparatide and abaloparatide), and romosozumab (Romo), an antisclerostin monoclonal antibody with dual action on bone formation and resorption. Osteoporosis treatment regimens often include sequential therapies involving drugs with complementary mechanisms, and the sequential approach with anabolic first has been proved to be the most effective on bone mineral density (BMD) changes and fracture risk reduction.[1] However, in real life, most patients start with an antiresorptive agent as first line. Switching from bisphosphonates to an anabolic agent is considered safe and effective, albeit with attenuated effects on BMD. However, transitioning from denosumab (Dmab) to teriparatide or Romo may expose patients to increased fracture risk due to the simultaneous activation of multiple bone remodeling units upon treatment cessation, known as the "rebound effect." In such patients, anabolic initiation is usually prompted by treatment failure, defined as significant bone density loss and/or fragility fractures. Sequential therapy with Romo has also shown variable outcomes.[2] Romo after long-term alendronate led to lower BMD gains than observed in treatment-naive patients. Switching from long-term Dmab to Romo yielded only minimal BMD improvements and did not protect against multiple vertebral fractures upon Dmab discontinuation.[3,4] Our preliminary study demonstrated that adding Romo to ongoing Dmab treatment improved lumbar spine BMD significantly in six months.[5] Moreover, we previously showed that Dmab increased circulating sclerostin levels,[6] supporting the hypothesis that adding Romo could exploit this mechanism to enhance BMD responses in patients already on Dmab. In the present study, we aimed to

[1]Rheumatology Unit, University of Verona, Verona, Italy.

Additional supplementary information cited in this article can be found online in the Supporting Information section (https://acrjournals.onlinelibrary.wiley.com/doi/10.1002/art.70002).

Author disclosures and graphical abstract are available at https://onlinelibrary.wiley.com/doi/10.1002/art.70002.

Address correspondence via email to Giovanni Adami, MD, PhD, at giovanni.adami@univr.it

Submitted for publication March 13, 2025; accepted in revised form October 24, 2025.

evaluate the effects of 12 months of combination therapy with Romo and Dmab.

MATERIAL AND METHODS

We designed a combined retrospective and prospective 36-month study analyzed with prospective score matching to evaluate the effects of Romo and Dmab combination therapy on postmenopausal women with severe osteoporosis. We did a 12-month prospective observational study starting at month 0 (M0) (Romo initiation), complemented by retrospective data collection at 24 months before initiation (M–24) and M–12 from the patients' medical records. The study design can therefore be described as a hybrid observational study, with retrospective and prospective components. Figure 1 depicts the study design. If a patient refused or was not eligible to be treated with combination, she was still considered for the Dmab-only group and treated according to clinical practice. The study population was divided into two cohorts based on treatment exposure: (1) combination group, in which patients were treated with Dmab for two years, at which point Romo was added to ongoing Dmab: Dmab (M –24 to M0) → Dmab + Romo (M0 to M+12), and (2) Dmab-only group: patients who were stable on Dmab, and for whom continuing Dmab treatment alone was deemed appropriate by the treating physician: Dmab (M–24 to M0). Patients in the Dmab + Romo group were prospectively enrolled at M0 (when Romo was added to ongoing Dmab therapy). Study protocol is given in the Supplementary Materials. Enrollment occurred between December 2022 and January 2024. For these patients, we also retrieved retrospective data (M–24 to M0) from their charts to ensure longitudinal comparability. Patients were instructed to receive Dmab (60 mg subcutaneously) first, followed by Romo (210 mg subcutaneously) within seven days. This sequence was chosen to maintain the antiresorptive effect of Dmab while initiating the anabolic action of Romo without delay. All administrations were verified by patient report.

Patients in the second group (Dmab only) were selected from the overall pool of postmenopausal women treated with Dmab referring to our outpatient clinic (between January 2016 and March 2024) who had available baseline (M–24) and follow-up dual-energy x-ray absorptiometry (DXA) scans and serum samples collected (n = 388). Patients were then matched through propensity score matching to balance baseline characteristics between the treated and control groups. The propensity scores were estimated using a logistic regression model. The following baseline covariates, selected based on clinical relevance and prior literature, were included in the model: age, sex, T score at femoral neck, total hip and lumbar spine, prior vertebral and nonvertebral fractures, and procollagen I intact N-terminal peptide (P1nP) and C-terminal telopeptide of type I collagen (CTX) serum levels. Patients were matched 1:1 using nearest-neighbor matching without replacement, with a caliper width of 0.2 SDs of the logit of the propensity score to ensure close matches. Matching was performed at M0.

Inclusion and exclusion criteria for the combination treatment (M0 to M+12). The inclusion criteria were as follows: postmenopausal women with severe osteoporosis, defined as 10-year major osteoporotic fracture risk ≥20%, assessed using the deDeFRA tool (a validated fracture risk assessment tool derived from FRAX)[7–9] and T score at the spine or femur of less than –2.5 (or less than –2.0 if there were two or more moderate or severe vertebral fractures or a femoral fracture in the previous two years).

The exclusion criteria were as follows: history of myocardial infarction or stroke, bone diseases other than osteoporosis (eg, Paget disease), history of bone malignancy, severe liver or kidney disease (estimated glomerular filtration rate [eGFR] <30 mL/min or Child-Pugh grade B/C), uncontrolled endocrine disorders (eg, hypocalcemia, primary hyperparathyroidism), treatment with bisphosphonates for more than 6 months in the 12 months preceding Dmab initiation, and prior or active treatment with glucocorticoids or hormone blocking therapy.

Data collection. BMD measurements were taken at baseline (M–24) and at M–12, M0, M+6 and M+12 of therapy, at the femoral neck, total hip, and lumbar spine (L1–L4) using DXA with the QDR Hologic Delphi machine. The variation coefficient for the vertebral site was 1%, whereas it was 1.2% for the femoral neck. Blood samples were collected in the morning after fasting at M0, M+3, M+6, and M+12. The serum samples were aliquoted and stored at –80°C until they were assayed for bone turnover

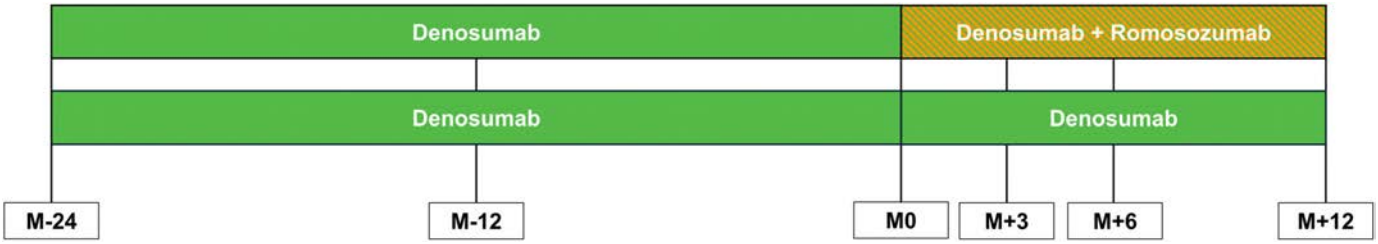

Figure 1. Study design. M, month.

markers (BTMs): CTX (a marker of bone resorption) and P1nP (a marker of bone formation)

To provide a comprehensive analysis of the BTMs trends, we also collected M–24 and M–12 data retrieving the information from electronic medical records (M–24 to M0). These included CTX and P1nP, collected at M–24 and M–12 (ie, 24 and 12 months before M0, ± 1 month). This approach allows for a longitudinal view of BTMs and BMD both before and after the initiation of Romo or continuation of Dmab, enabling the comparison of treatment effects over time. All participants received calcium and vitamin D according to clinical practice (>1,000 IU/day of vitamin D) +1,200 mg/day of calcium (dietary + supplements combined if needed).

Sample size considerations. We previously observed that the difference in lumbar spine BMD between combination of Romo and Dmab versus Dmab alone was around 6% at lumbar spine, which corresponds to an effect size of $|\delta| = 1.5$.[5] We therefore needed a sample size of 11 in each group to reliably (with probability ≥0.9) detect an effect size of $|\delta| \geq 1.5$, assuming a two-sided criterion for detection that allows for a maximum Type I error rate of $\alpha = 0.05$. We finally aimed to conservatively include 25 patients in both groups to account for missing data.

Statistical analysis. Group comparisons were performed with analysis of variance post hoc tests with *P* value adjusted with Holm method. Categorical variables were compared with the chi-squared test. All differences were considered significant when $P < 0.05$. Between-group percentages and absolute changes in BMD and BTMs were assessed with a mixed model for repeated measures (MMRM) using Satterthwaite and restricted maximum likelihood method with treatment sequence, time, treatment-by-time interaction, and baseline BMD as fixed effects and with patients as random effect. Sensitivity analyses missing data (if <5%) were imputed using a random forest algorithm (Orange, version 3.37.0). The imputation process was iterative and used a random forest model with 10 trees; the model allowed for an unlimited number of features and unrestricted tree depth. Splitting of nodes continued until each node contained fewer than five instances. To assess the robustness of the primary propensity score–matched analysis, we conducted a sensitivity analysis using inverse probability of treatment weighting (IPTW) based on the full cohort (n = 388 Dmab only, n = 25 Dmab + Romo). Propensity scores were estimated through logistic regression, including the same covariates used for matching (age, sex, T score at femoral neck, total hip and lumbar spine, prior vertebral and nonvertebral fractures, P1nP and CTX serum levels). Stabilized inverse probability weights were applied to everyone to create a pseudopopulation in which baseline covariates were balanced between the two groups. To reduce the impact of extreme weights, we performed trimming of propensity scores at the first and 99th percentiles. Covariate balance after weighting was assessed by standardized mean differences, with values <0.10 considered indicative of good balance. Weighted analyses were then conducted using MMRM for repeated measures to estimate the treatment effect on BMD and BTMs similarly to the primary analysis. All statistical analyses were performed using SPSS Version 26 (SPSS, Inc.), GraphPad Prism version 9.5.1 (GraphPad Software), JASP (version 0.19.0), and R (version 4.5.1). This study was approved by the University of Verona ethic committee (prot. registration: REUMABANK 1483CESC). All patients provided informed consent to participate in the study and/or retrospective collection of the data. Patients provided consent for publication of anonymized data. Data of the analysis is available upon reasonable request.

RESULTS

Fifty patients were included in the prospective study, and data before inclusion were retrieved from electronic medical records. Supplementary Figure S1 shows the study flowchart. Twenty-five women received Dmab alone, and 25 women received Dmab first and then had Romo added to ongoing Dmab (Dmab + Romo). Characteristics of the population included are shown in Table 1.

Retrospective study results (M−24 to M0). BMD and BTMs changes from M–24 and M0 are shown in Figures 2 and 3, respectively. BMD significantly increased in both groups between M–24 and M0. Lumbar spine increased by 5.2% (95% confidence interval [CI] 3.8–6.6; $P < 0.001$) and 5.5% (95% CI 3.9–7.1; $P < 0.001$), femoral neck increased by 2.1% (95% CI 0.9–3.3; $P = 0.028$) and 2.2% (95% CI 1.0–3.4; $P = 0.027$), and total hip increased by 2.3% (95% CI 1.3–3.3; $P < 0.001$) and 0.8% (95% CI –0.2 to 1.8; *P* = nonsignificant [ns]).

We found a statistically significant decrease in P1nP levels from M–24 to M–12 (–48.5 ng/mL, 95% CI –54.4 to –42.6; $P < .001$ and –52.7 ng/mL, 95% CI –58.2 to –47.2; $P < .001$) and from M–24 to M0 (–49.1 ng/mL, 95% CI –61.8 to –36.4; $P < 0.001$ and –48.3 ng/mL, 95% CI –60.3 to –36.3; $P < 0.001$). CTX decreased significantly in all Dmab users at M –12 (–0.267 ng/mL, 95% CI –0.31 to –0.22; $P < 0.001$ and –0.262 ng/mL, 95% CI –0.32 to –0.21; $P < 0.001$) and remained suppressed thereafter.

Prospective study results (M0 to M+12). BMD and BTMs changes from M–24 and M0 are shown in Figures 2 and 3, respectively.

Dmab-alone continued. BMD slightly increased at all sites between M0 and M+12 but did not reach statistical significance at any site. Between M–24 and M+12, the overall increases in the Dmab-alone group were as follows: lumbar spine, 8.3% (95% CI 1.8–14.8; $P = 0.042$); femoral neck, 2.8% (95% CI –1.9

Table 1. Study population characteristics*

Characteristics	Denosumab to denosumab + romosozumab (n = 25)	Matched denosumab to denosumab (n = 25)	Unmatched denosumab to denosumab (n = 388)	Abs. SMD Pre-matching or Abs. Diff. Pre, %	Abs. SMD Post-matching or Abs. Diff. Post, %
Age, mean ± SD, y	73.5 ± 8.9	74.1 ± 9.1	68.2 ± 10.5	0.51	0.07
BMI, mean ± SD	24.6 ± 2.9	24.4 ± 3.0	24.8 ± 3.2	0.06	0.07
Comorbidities, n (%)					
Rheumatoid arthritis	1 (4)	1 (4)	28 (7)	3	0
MACE	0 (0)	1 (4)	28 (7)	7	4
Hypertension	14 (56)	15 (60)	252 (65)	9	4
VTE	0 (0)	3 (12)	31 (8)	8	12
CKD	2 (8)	3 (12)	58 (15)	7	4
MGUS	0 (0)	1 (4)	12 (3)	3	4
Prevalent vertebral fractures, n (%)	24 (96)	23 (92)	310 (80)	16	4
Recent vertebral fractures (<2 y), n (%)	13 (52)	12 (48)	116 (30)	22	4
Nonvertebral MOF fractures, n (%)	16 (64)	15 (60)	155 (40)	24	4
Hip fractures, n (%)	1 (4)	1 (4)	12 (3)	1	0
M−24 BMD and markers					
Lumbar spine BMD, mean ± SD, g/cm^2	0.811 ± 0.113	0.801 ± 0.120	0.850 ± 0.130	0.3	0.09
Femoral neck BMD, mean ± SD, g/cm^2	0.659 ± 0.169	0.670 ± 0.167	0.700 ± 0.180	0.23	0.07
Total hip BMD, mean ± SD, g/cm^2	0.686 ± 0.187	0.690 ± 0.179	0.720 ± 0.190	0.18	0.02
Lumbar spine T score, mean ± SD	−1.9 ± 0.9	−1.9 ± 1.0	−1.6 ± 1.1	0.28	0.01
Femoral neck T score, mean ± SD	−1.9 ± 1.0	−2.0 ± 1.0	−1.7 ± 1.2	0.17	0.01
Total hip T score, mean ± SD	−2.3 ± 1.2	−2.3 ± 1.1	−2.0 ± 1.3	0.23	0.01
CTX, mean ± SD, ng/mL	0.387 ± 0.195	0.375 ± 0.200	0.410 ± 0.220	0.11	0.06
P1nP, mean ± SD, ng/mL	81.2 ± 22.7	82.5 ± 23.5	75.0 ± 25.0	0.25	0.07
PTH, mean ± SD, pg/mL	44.1 ± 18.1	42.5 ± 18.8	40.0 ± 20.0	0.21	0.09
Vitamin D, mean ± SD, ng/mL	38.1 ± 13.5	39.0 ± 13.8	35.0 ± 15.0	0.21	0.07
M0 BMD and markers					
Lumbar spine BMD, mean ± SD, g/cm^2	0.853 ± 0.123	0.845 ± 0.131	0.891 ± 0.170	0.23	0.06
Femoral neck BMD, mean ± SD, g/cm^2	0.673 ± 0.175	0.685 ± 0.174	0.712 ± 0.190	0.21	0.07
Total hip BMD, mean ± SD, g/cm^2	0.702 ± 0.194	0.696 ± 0.187	0.731 ± 0.201	0.15	0.03
Lumbar spine T score, mean ± SD	−1.4 ± 0.7	−1.4 ± 0.9	−1.1 ± 1.0	0.30	<0.01
Femoral neck T score, mean ± SD	−1.8 ± 1.0	−1.9 ± 1.1	−1.3 ± 0.9	0.55	0.09
Total hip T score, mean ± SD	−2.2 ± 1.1	−2.2 ± 1.1	−1.7 ± 1.2	0.41	<0.01
CTX, mean ± SD, ng/mL	0.120 ± 0.081	0.113 ± 0.078	0.093 ± 0.070	0.38	0.08
P1nP, mean ± SD, ng/mL	32.1 ± 21.4	34.2 ± 22.3	36.6 ± 20.3	0.22	0.09
PTH, mean ± SD, pg/mL	49.1 ± 21.1	48.5 ± 22.8	45.0 ± 20.0	0.20	0.03
Vitamin D, mean ± SD, ng/mL	41.1 ± 16.5	42.0 ± 17.8	35.0 ± 15.0	0.40	0.05

* Abs. diff., absolute difference; BMD, bone mineral density; BMI, body mass index; CKD, chronic kidney disease stages 3a–3b by KDIGO guidelines; CTX, C-terminal telopeptide of type I collagen; Dmab, denosumab; M, month; MACE, major adverse cardiovascular events; MGUS, monoclonal gammopathy of undetermined significance; MOF, major osteoporotic fractures; P1nP, procollagen I intact N-terminal peptide; PTH, parathyroid hormone; Romo, romosozumab; SMD, standardized mean difference; VTE, venous thromboembolism.

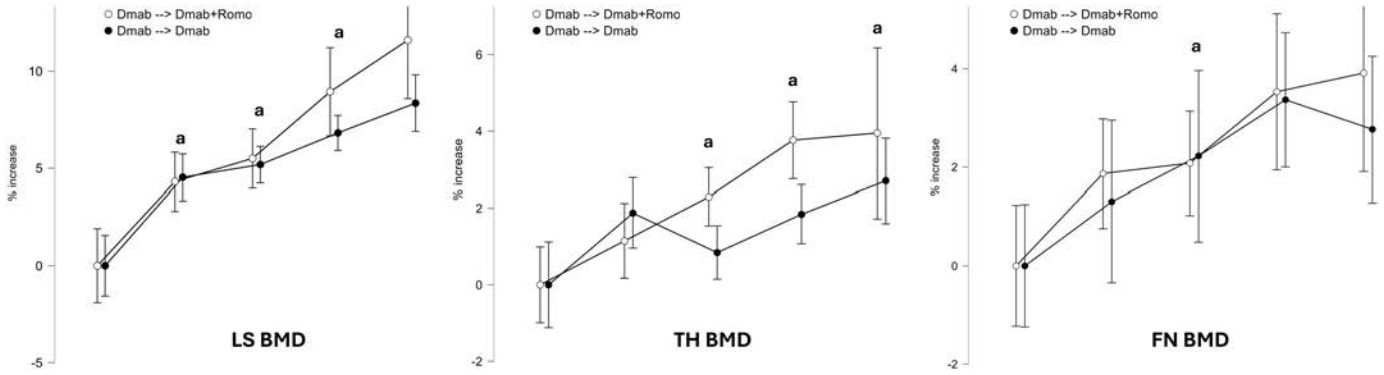

Figure 2. BMD changes over the study period for LS (left), TH (middle), and FN (right). Between-group differences were tested with a mixed model for repeated measures using Satterthwaite and restricted maximum likelihood method with treatment sequence, time, treatment-by-time interaction, and baseline BMD as fixed effects and with patients as random effect. a, $P < 0.05$ versus baseline; b, $P = 0.074$ for Dmab → Dmab versus Dmab → Dmab + Romo. Error bars show 95% confidence interval. BMD, bone mineral density; Dmab, denosumab; FN, femoral neck; LS, lumbar spine; Romo, romosozumab; TH, total hip.

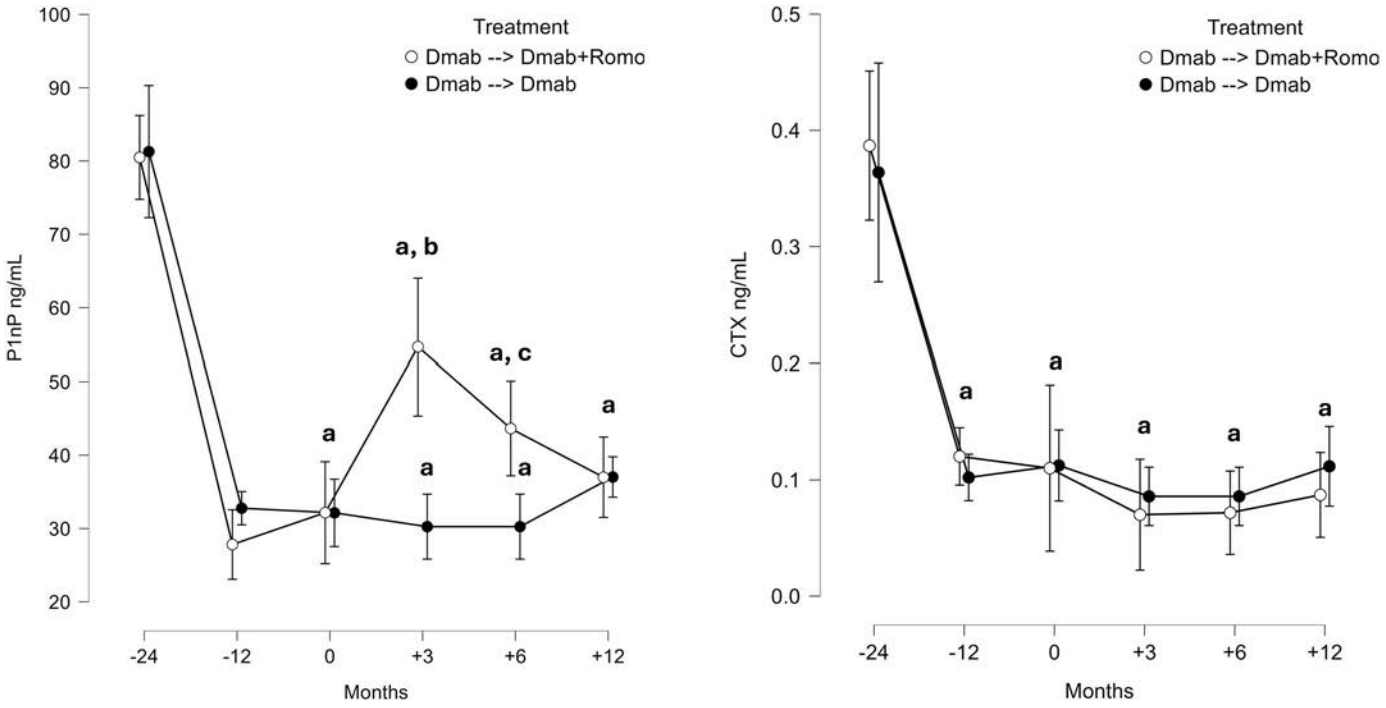

Figure 3. Bone turnover markers changes over the study period. P1np (left) and CTX (right). Between-group differences were tested with a mixed model for repeated measures using Satterthwaite and restricted maximum likelihood method with treatment sequence, time, treatment-by-time interaction, and baseline bone mineral density as fixed effects and with patients as random effect. a, $P < 0.05$ versus baseline; b, $P < 0.001$ for Dmab → Dmab versus Dmab → Dmab + Romo; c, $P = 0.057$ for Dmab → Dmab versus Dmab → Dmab + Romo. Error bars show 95% confidence interval. CTX, C-terminal telopeptide of type I collagen; Dmab, Dmab; P1nP, procollagen I intact N-terminal peptide; Romo, Romo.

to 7.5; P = ns); and total hip, 2.7% (95% CI −1.4 to 6.8; P = ns). P1nP and CTX remained stable between M0 and M+12.

Dmab + Romo. BMD significantly increased at lumbar spine between M0 and M+6 (3.4%; 95% CI 0.1–6.7; $P = 0.034$) and between M0 and M+12 (6.1%; 95% CI 0.6–11.6; $P = 0.028$). Between M−24 and M+12, the overall increases in the Dmab + Romo group were lumbar spine 11.6% (95% CI 5.7–17.5; $P = 0.010$), femoral neck 3.9% (95% CI 0.1–9.6; $P = 0.042$), and total hip 3.9% (95% CI −0.1 to 7.6; $P = 0.054$).

P1nP increased significantly between M0 and M+3 (+22.5 ng/mL, 95% CI 5.4–39.6; $P = 0.028$). P1nP decreased thereafter (−17.6 ng/mL, 95% CI −37.4 to 2.2; P = ns at M+12). CTX did not change between M0 and M+12.

Group comparisons. In the MMRM, we found a trend toward significance at lumbar spine M+12 between the Dmab + Romo and Dmab-alone groups (difference between groups 3.2%, 95% CI −5.4 to 11.8; $P = 0.074$). We did not find any significant difference in femoral neck and total hip between groups at M+12.

We found a significant difference at M+3 in P1nP levels between the Dmab-alone and Dmab + Romo groups (difference between groups 24.4 ng/mL, 95% CI 0.3–49.1; $P = 0.033$). We found a trend toward significance at M+6 in P1nP levels between the Dmab-alone and Dmab + Romo groups (difference between groups 13.4 ng/mL, 95% CI −1.7 to 28.5; $P = 0.057$). In the sensitivity analysis using IPTW, after weighing, baseline characteristics were well balanced (all standardized mean differences <0.1), similar to the propensity score matching.

The weighted analysis confirmed a trend toward greater lumbar spine BMD gain at M+12 in the Dmab + Romo group compared to Dmab alone: mean difference 3.1% (95% CI −1.5 to 7.5; $P = 0.064$). Similar trends were observed at the femoral neck (difference 1.0%, 95% CI −1.8 to 3.9) and total hip (difference 1.2%, 95% CI −1.3 to 3.8). For BTMs, P1nP at M+3 remained significantly higher in the combination group (difference 21.0 ng/mL, 95% CI 5.0–37.0; $P = 0.022$), consistent with the primary analysis.

DISCUSSION

Herein we investigated the effects of Romo in combination with ongoing Dmab treatment in postmenopausal women with severe osteoporosis. In aggregate, we showed that ongoing Dmab did not blunt the anabolic response to Romo.

When evaluating the percentage change from M−24 (24 months before initiation of Romo) to M+12, the final BMD gains were around 11%. In contrast, the Dmab-only group exhibited a

modest, nonsignificant, 3% increase in BMD between M0 and M +12, leading to a total gain of 8% over the 36-month study period. However, the between-group difference at the lumbar spine was modest (3.3%, 95% CI –5.2 to 11.8), and due to the limited sample size, the study was underpowered to detect the expected 6% difference used for sample size estimation. At the femoral neck and total hip, the patterns were similar, albeit of a smaller magnitude, with the combination group showing greater BMD response than the Dmab-only group.

The analysis of BTMs adds another layer of understanding to the anabolic effects of Romo. After the initiation of Romo in the combination group, P1nP increased markedly, with a similar magnitude to what has been reported in patients on Romo naive to treatment,[5,10] indicating a preserved anabolic response despite continued CTX suppression. Interestingly, we previously demonstrated that Dmab and bisphosphonates increased circulating sclerostin levels, supporting the opportunity of a combined approach with Romo to boost the BMD response.[6,11] In aggregate, our finding suggests that Romo can stimulate bone formation through modeling-based mechanisms even in the context of continued Dmab treatment. Indeed, the deep suppression of CTX in this group further indicates a net anabolic effect with new bone mass created. Interestingly, a recently published study showed that, in mice, Dmab did not blunt the anabolic modeling-based effect of Romo, with overall similar BMD findings compared to our study.[12] The greater BMD gains reported in naive patients receiving Romo[10,13] can be attributed to the simultaneous stimulation of modeling-based and remodeling-based bone formation. The latter was indeed not fully engaged in patients who had already experienced remodeling suppression during Dmab therapy. Indeed, the resorptions cavities were already filled during the first period on Dmab (M–24 to M0), and, therefore, the BMD gain, in terms of remodeling-based bone formation, were already accrued in those patients.

In our study we included patients who had been on Dmab for a long time to ensure they were in the fully closed remodeling phase, where the response to ongoing Dmab is consistent, and any additional BMD changes did not reflect remodeling-based bone formation but only modeling-based bone formation as observed in the extension phase of the FREEDOM trial.[14] Moreover, the choice of a two-year prior Dmab exposure was mainly pragmatic, aiming to ensure a homogeneous cohort, and we believe that a longer prior exposure would not have significantly altered the outcomes. Indeed, although the treatment duration's influence is critical in the context of discontinuation (rebound risk), it should not affect the therapeutic response to combination therapy with Romo in this specific study.

Combining Dmab with anabolic treatments has already been done in the literature. Our group previously showed that Romo combined with ongoing Dmab for 6 months increased BMD and P1nP more than Dmab alone[5]; herein we presented the 12-month findings with additional insight on the BMD and BTMs trends before Romo treatment initiation. The efficacy of combining teriparatide and Dmab was reported in the Dmab and Teriparatide Administration (DATA) study.[15,16] However, the results of the DATA study and ours should not be directly compared. Indeed, the DATA study included only Dmab-naive patients. Teriparatide acts primarily through stimulating remodeling-based bone formation and needs opened remodeling units to be maximally effective on BMD. It could be speculated, therefore, that in patients with fully closed remodeling surfaces due to long-term Dmab therapy, the addition of teriparatide would lose part or even most of its efficacy. Another study exploring combination of treatments was conducted by our group in 2016.[17] In that study, teriparatide was introduced three months after Dmab initiation with superimposable results to the DATA study. Nevertheless, the short three-month period on Dmab before teriparatide addition may be not sufficient to fully close all remodeling units, and the reversal phase may still have been incomplete. In contrast, in the present study Dmab was administered for two years, and, therefore, we can speculate that the P1nP and BMD increases were mainly due to modeling-based bone formation, which was not affected by ongoing Dmab treatment. Kumar and colleagues recently published a small case series of three patients in whom Romo was added to Dmab after three months from the last Dmab dose.[18] Romo was then continued for 12 months, and Dmab was restarted after 9 months from the last dose. In this scheme the overlap between the two drugs was shorter, with three months off Dmab between month 3 and month 6 of Romo treatment. Despite the small number of patients included, the authors found somehow similar results to ours, with larger increases at the lumbar spine. The off-Dmab period might permit a reopening of the bone remodeling units with greater efficacy of Romo (ie, overflow remodeling-based bone formation). However, this strategy may not be optimal. First, a slight decrease in BMD for the reopening of remodeling units with subsequent refill would not really increase bone mass but just merely play with the remodeling space. Second, prior studies showed that Romo cannot effectively prevent the rebound associated Dmab withdrawal.[3,4,19–21] Indeed, in the study by Kumar et al, CTX serum levels steeply increased above the normal postmenopausal range despite Romo treatment.[18] More recently, Hong and colleagues showed that the transition from Dmab to Romo resulted in a significant increase in lumbar spine BMD but not total hip BMD.[22] Of note, patients were treated for a median period of two years with Dmab, limiting the generalizability to short-term Dmab users. More importantly, Hong and colleagues reported a significant increase in CTX serum levels (greater than +100% at month 12) that paralleled the somewhat similar P1nP increase, after the transition from Dmab to Romo. Nonetheless, even if the combination might represent an effective strategy, our results should consider broader clinical and economic contexts, as the combination is significantly more costly and might not be fully reimbursed by many health systems.

The more pronounced BMD gains observed at the lumbar spine compared to the femoral neck and total hip likely reflect site-specific differences in bone composition and responsiveness to Romo. The lumbar spine, with its higher trabecular content, is particularly sensitive to modeling-based bone formation, whereas cortical sites such as the femoral neck and hip rely more on remodeling-based bone formation and overflow remodeling-based bone formation with closure of cortical porosity. In our cohort, the prolonged suppression of bone turnover induced by prior Dmab therapy may have attenuated the remodeling response at these cortical-rich sites. Consistently, Kashii et al reported that hip BMD increases with Romo were observed only in patients with normal or elevated baseline P1nP levels, highlighting the role of active bone formation in driving gains at the femoral neck and hip.[23]

Our study should be interpreted in light of the strengths and limitations. The major strength is the detailed collection of data in the prospective phase of the study with single-batch analysis of BTMs and systematic collection of BMD data. Albeit potentially of scientific interest, we did not include a group that switched from Dmab to Romo. Indeed, we felt that this strategy would not have been ethical due to the potential risk of rebound effect upon Dmab discontinuation. It has been shown that Romo does not totally prevent the rebound in BTMs associated with Dmab discontinuation, and there are reports of multiple vertebral fractures in patients transitioning from Dmab to Romo.[3,4] However, Hong et al reported no vertebral fractures in 86 patients who transitioned to Romo after a median of four Dmab doses.[22] Yet, this finding should be interpreted with caution. The absence of fractures in that study could be influenced by factors such as the shorter duration of prior Dmab treatment and chance, rather than providing definitive evidence against the risk of rebound fractures. We also acknowledge that body mass index (BMI) and renal function (eGFR) were not included in the propensity score model or IPTW, although patients with severe chronic kidney disease were excluded and BMI was well balanced between groups; residual confounding from unmeasured variables cannot be completely ruled out. Further adequately powered randomized controlled trials are needed to confirm our findings; however, a randomized controlled trial design was not feasible in our setting due to ethical considerations. Our study may therefore serve as a basis for future sample size estimations. The lack of fracture outcomes is another limitation of our study, and future studies with larger cohorts are needed to evaluate this endpoint.

In conclusion, our data suggest that Romo can retain its anabolic potential when introduced in combination with Dmab. The findings support the combination of Romo and Dmab in patients with severe osteoporosis treated with long-term Dmab in whom the response to treatment is not deemed adequate. Yet, these findings should be interpreted as exploratory and hypothesis-generating, pending confirmation in larger, prospective studies.

ACKNOWLEDGMENT

Open access publishing facilitated by Università degli Studi di Verona, as part of the Wiley - CRUI-CARE agreement.

AUTHOR CONTRIBUTIONS

All authors contributed to at least one of the following manuscript preparation roles: conceptualization AND/OR methodology, software, investigation, formal analysis, data curation, visualization, and validation AND drafting or reviewing/editing the final draft. As corresponding author, Dr Adami confirms that all authors have provided the final approval of the version to be published and takes responsibility for the affirmations regarding article submission (eg, not under consideration by another journal), the integrity of the data presented, and the statements regarding compliance with institutional review board/Declaration of Helsinki requirements.

REFERENCES

1. Cosman F, Kendler DL, Langdahl BL, et al. Romosozumab and antiresorptive treatment: the importance of treatment sequence. Osteoporos Int 2022;33(6):1243–1256.
2. Ramchand SK, Leder BZ. Sequential therapy for the long-term treatment of postmenopausal osteoporosis. J Clin Endocrinol Metab 2024;109(2):303–311.
3. Kashii M, Ebina K, Kitaguchi K, et al. Romosozumab was not effective in preventing multiple spontaneous clinical vertebral fractures after denosumab discontinuation: a case report. Bone Rep 2020;13:100288.
4. Krikelis M, Gazi S, Trovas G, et al. Progression of multiple vertebral fractures after denosumab discontinuation under treatment with romosozumab. A case-report. Joint Bone Spine 2024;91(5):105754.
5. Adami G, Pedrollo E, Rossini M, et al. Romosozumab added to ongoing denosumab in postmenopausal osteoporosis, a prospective observational study. JBMR Plus 2024;8(4):ziae016.
6. Gatti D, Viapiana O, Fracassi E, et al. Sclerostin and DKK1 in postmenopausal osteoporosis treated with denosumab. J Bone Miner Res 2012;27(11):2259–2263.
7. Adami S, Bianchi G, Brandi ML, et al. Validation and further development of the WHO 10-year fracture risk assessment tool in Italian postmenopausal women: project rationale and description. Clin Exp Rheumatol 2010;28(4):561–570.
8. Bonaccorsi G, Fila E, Cervellati C, et al. Assessment of fracture risk in a population of postmenopausal Italian women: a comparison of two different tools. Calcif Tissue Int 2015;97(1):50–57.
9. Bonaccorsi G, Messina C, Cervellati C, et al. Fracture risk assessment in postmenopausal women with diabetes: comparison between DeFRA and FRAX tools. Gynecol Endocrinol 2018;34(5):404–408.
10. Saag KG, Petersen J, Brandi ML, et al. Romosozumab or alendronate for fracture prevention in women with osteoporosis. N Engl J Med 2017;377(15):1417–1427.
11. Gatti D, Viapiana O, Adami S, et al. Bisphosphonate treatment of postmenopausal osteoporosis is associated with a dose dependent increase in serum sclerostin. Bone 2012;50(3):739–742.
12. Bustamante-Gomez C, Fu Q, Goellner JJ, et al. Potent suppression of bone remodeling by denosumab does not blunt the anabolic response to romosozumab in mice. Bone 2025;199:117567.
13. Cosman F, Crittenden DB, Adachi JD, et al. Romosozumab treatment in postmenopausal women with osteoporosis. N Engl J Med 2016;375(16):1532–1543.
14. Bone HG, Wagman RB, Brandi ML, et al. 10 years of denosumab treatment in postmenopausal women with osteoporosis: results from

the phase 3 randomised FREEDOM trial and open-label extension. Lancet Diabetes Endocrinol 2017;5(7):513–523.

15. Leder BZ, Tsai JN, Uihlein AV, et al. Denosumab and teriparatide transitions in postmenopausal osteoporosis (the DATA-Switch study): extension of a randomised controlled trial. Lancet 2015;386(9999):1147–1155.
16. Tsai JN, Nishiyama KK, Lin D, et al. Effects of denosumab and teriparatide transitions on bone microarchitecture and estimated strength: the DATA-Switch HR-pQCT study. J Bone Miner Res 2017;32(10):2001–2009.
17. Idolazzi L, Rossini M, Viapiana O, et al. Teriparatide and denosumab combination therapy and skeletal metabolism. Osteoporos Int 2016; 27(11):3301–3307.
18. Kumar S, Gild ML, McDonald MM, et al. A novel sequential treatment approach between denosumab and romosozumab in patients with severe osteoporosis. Osteoporos Int 2024;35(9):1669–1675.
19. McClung MR, Bolognese MA, Brown JP, et al. Skeletal responses to romosozumab after 12 months of denosumab. JBMR Plus 2021;5(7):e10512.
20. McCarroll K, Fitzpatrick D, Lannon R. Comment on: a novel sequential treatment approach between denosumab and romosozumab in patients with severe osteoporosis. Osteoporos Int 2024;35(10): 1869–1870.
21. Ebina K, Tsuboi H, Nagayama Y, et al. Effects of prior osteoporosis treatment on 12-month treatment response of romosozumab in patients with postmenopausal osteoporosis. Joint Bone Spine 2021; 88(5):105219.
22. Hong N, Shin S, Kim H, et al. Romosozumab following denosumab improves lumbar spine bone mineral density and trabecular bone score greater than denosumab continuation in postmenopausal women. J Bone Miner Res 2025;40(2):184–192.
23. Kashii M, Kamatani T, Nagayama Y, et al. Baseline serum PINP level is associated with the increase in hip bone mineral density seen with romosozumab treatment in previously untreated women with osteoporosis. Osteoporos Int 2023;34(3):563–572.

American College of Rheumatology
Empowering Rheumatology Professionals

Arthritis & Rheumatology
Vol. 78, No. 5, May 2026, pp 1184

DOI 10.1002/art.43438

Clinical Images: Alkaptonuria: a conundrum

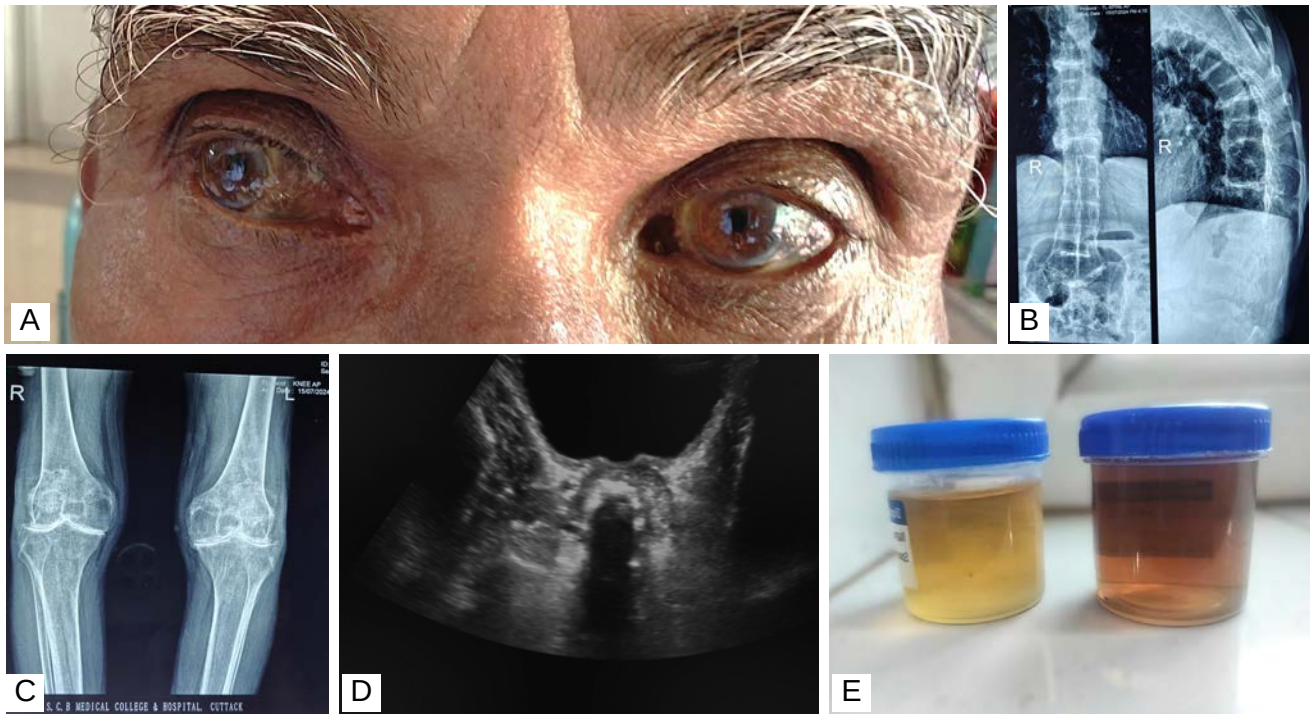

The patient, a 74-year-old hypertensive man, presented with generalized aches and pains, flexor contractures in both palms for five years, and tingling and numbness in both hands and feet for two years. Physical examination revealed blackish pigmentation in the bilateral pinna and sclera of the eyes (A). The patient had synovitis in both knees, with crepitus and restricted range of motion. Thoracic kyphosis with loss of lumbar lordosis was noted (B). Neurologic examination revealed impaired touch sensation below the left knee. Cardiovascular evaluation revealed a grade 3 pansystolic murmur over the apex. Two-dimensional echocardiography revealed thickened calcified anterior and posterior mitral leaflets with mild mitral regurgitation. Nerve conduction study confirmed axonal neuropathy affecting both lower limbs. Radiographs revealed calcification over the intervertebral discs and menisci of the bilateral knee joints (B and C). Pelvic ultrasonography revealed prostatic calcification (D). His urine turned black upon exposure to sunlight (E). His urine homogentisic acid was positive (qualitative), which confirmed the diagnosis. Alkaptonuria (AKU) is characterized by a deficiency of the enzyme homogentisate 1,2-dioxygenase, leading to homogentisic acid deposition in tissue and multiorgan involvement. AKU is a diagnostic dilemma owing to its mimicry of other conditions such as spondylarthritis. The essence of diagnosis is to identify the triad of symptoms: dark urine, ochronosis, and ochronotic arthropathy, corroborated by biochemical or genetic assessment. A new overview map has recently been created that reports 1,233 patients with AKU worldwide.[1] Early intervention with treatments such as nitisinone[2] may help to manage disease progression and improve patient outcomes.

Author disclosures are available at https://onlinelibrary.wiley.com/doi/10.1002/art.43438.

1. Zatkova A, Ranganath L, Kadasi L. Alkaptonuria: current perspectives. Appl Clin Genet 2020;13:37–47. doi:https://doi.org/10.2147/TACG.S186773
2. Ranganath LR, Psarelli EE, Arnoux JB, et al. Efficacy and safety of once-daily nitisinone for patients with alkaptonuria (SONIA 2): an international, multicentre, open-label, randomised controlled trial. Lancet Diabetes Endocrinol 2020;8(9):762–772. doi:https://doi.org/10.1016/S2213-8587(20)30228-X

Sarada Khandual, MBBS, MD, DrNB
Sarit Pattanaik, MBBS, MD, DM
Saumya Tripathy, MBBS, MD, DM
Manoj Parida, MBBS, MD
Kiran Khillare, MBBS, MD, DrNB
Bidyut Das, MBBS, MD, PhD
bidyutdas@hotmail.com
Department of Clinical Immunology and Rheumatology
Srirama Chandra Bhanja Medical College
Cuttack, India

Arthritis & Rheumatology
Vol. 78, No. 5, May 2026, pp 1185–1186

DOI 10.1002/art.43435

Clinical Images: Sevoflurane-induced periostitis

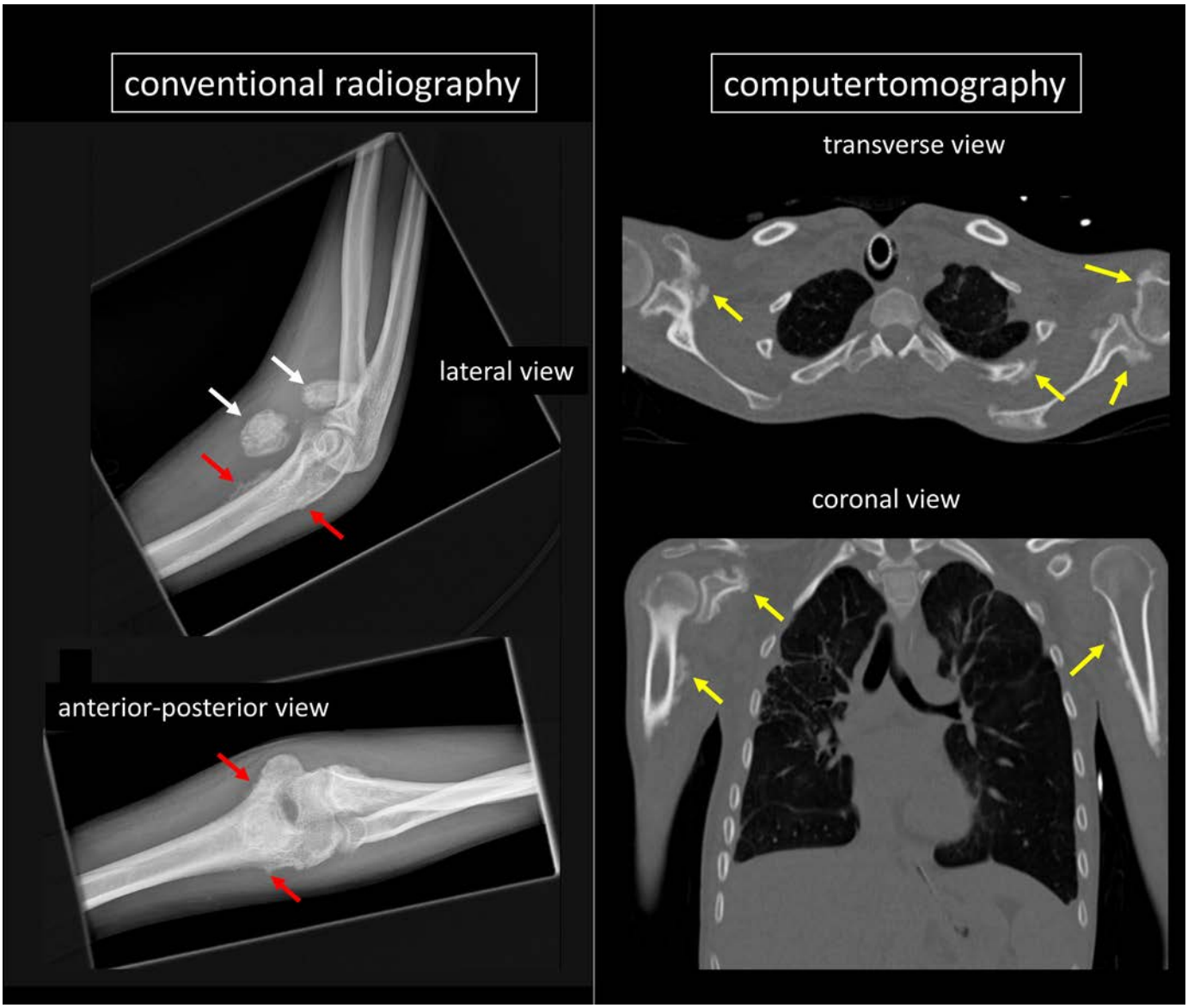

A 25-year-old patient was treated with the volatile anesthetic sevoflurane for approximately three months due to agitation unresponsive to intravenous anesthetics. The patient had septic multiorgan failure resulting from a Bartholin abscess and COVID-19 pneumonia with bacterial superinfection and empyema. Chronic medical conditions included GAD65 antibody–positive autoimmune encephalitis, temporal lobe epilepsy, and Ig deficiency syndrome. The patient developed clinical signs of monoarthritis at the right elbow, raising suspicion for septic or autoimmune arthritis. Arthrosonography revealed severe pericapsulitis without distinct synovitis and joint effusion. Arthrocentesis yielded no fluid. X-ray imaging demonstrated signs of calcifying periostitis (red arrows), amorphous calcifications at the medial aspect of the joint capsule (white arrows), and altered trabeculation in the juxtaarticular distal humerus. A subsequent chest computed tomography identified periostitis with new bone formation of ribs two to eight bilaterally, both scapulae, and both proximal humeri (yellow arrows). Fluoride levels were elevated in serum (1.62 mg/L; normal <0.1 mg/L) and urine (47.0 mg/L; normal <1.0 mg/L). This led to a diagnosis of sevoflurane-induced skeletal fluorosis. Three weeks after discontinuing sevoflurane, clinical and ultrasound signs regressed, and fluoride

levels in serum (0.24 mg/L) and urine (1.7 mg/L) dropped. Unfortunately, the patient died soon thereafter due to refractory septic shock. Approximately 5% of inhaled sevoflurane are metabolized to hexafluoroisopropanol with release of inorganic fluoride and carbon dioxide.[1] Although skeletal fluorosis from environmental exposure[2] and long-term voriconazole exposure[3] is recognized, to our knowledge, this is the first reported case associated with volatile anesthetics. Informed consent could not be obtained because the patient was deceased. All efforts were made to ensure that no personally identifiable information was disclosed.

ACKNOWLEDGMENT

Open Access funding enabled and organized by Projekt DEAL.

Author disclosures are available at https://onlinelibrary.wiley.com/doi/10.1002/art.43435.

1. ULTANE (Sevoflurane). U.S. Food and Drug Administration; 2024. Accessed May 26, 2025. https://www.accessdata.fda.gov/drugsatfda_docs/label/2025/020478s035lbl.pdf
2. Solanki YS, Agarwal M, Gupta AB, et al. Fluoride occurrences, health problems, detection, and remediation methods for drinking water: a comprehensive review. Sci Total Environ 2022;807(Pt 1): 150601.
3. Valor-Méndez L, Wacker J, Schett G, et al. Clinical images: voriconazole-induced synovitis, enthesitis, and periostitis. Arthritis Rheumatol 2022;74(7):1183.

Christian Beyer, MD
christian.beyer@uk-erlangen.de
Marion Ganslmayer, MD
Richard Strauß, MD
Department of Medicine 1
Friedrich-Alexander-University Erlangen-Nuremberg
Erlangen, Germany
Bernhard Manger, MD
Department of Medicine 3,
Friedrich-Alexander-University Erlangen-Nuremberg
Erlangen, Germany

Arthritis & Rheumatology
Vol. 78, No. 5, May 2026, pp 1187–1191

American College of Rheumatology
Empowering Rheumatology Professionals

LETTER

DOI 10.1002/art.43426

Nociplasticity, rather than fibromyalgia, best conceptualizes symptoms not linked to well-defined organ disease in systemic lupus erythematosus: comment on the article by Pisetsky et al

To the Editor:

Pisetsky et al suggest that nociplasticity, rather than fibromyalgia (FM), be adopted as a unifying term and concept to account for the widespread pain, fatigue, cognitive, mood, and sleep disturbances in systemic lupus erythematosus (SLE) that cannot be explained by characteristic immune or inflammatory mechanisms.[1] They comment that "lupus-associated nociplasticity (LAN)" integrates these diverse symptoms within an immunologic framework, providing a mechanistic understanding lacking in FM.

SLE, as the authors note, is the prototypic systemic autoimmune disease. Its pathogenesis, diagnosis, and therapy are based on aberrant autoimmunity driving systemic inflammation. In contrast, FM is the prototypic nociplastic pain condition. Its pathogenesis, diagnosis, and therapy are based on central sensitivity. FM and nociplastic pain, present in 3% to 5% of the general population, is found in 20% to 30% of patients with systemic autoimmune diseases, including SLE, rheumatoid arthritis, and spondyloarthropathies.[2] However, FM is also present in 20% to 30% of a variety of chronic pain conditions, including osteoarthritis and chronic low-back and neck pain, not considered autoimmune in nature.

Pisetsky et al propose that neuroimmune dysfunction integrates classic SLE autoimmunity, including anti-DNA antibodies and tissue inflammation, to nociplastic symptoms, including levels of pain, fatigue, mood, stress, dysautonomia, and interoception.[1] Neuroimmune dysfunction has been evaluated in FM, other chronic pain disorders, and depression.[2] Nonspecific, subtle alterations in cytokines have been detected in FM, but elevated acute phase reactants and characteristic anti-DNA and anti-RNA autoantibodies are absent. There is no evidence of central nervous system inflammation or structural damage, and pain severity correlates with functional changes in neuro-connectivity.

Associating the severity of these nociplastic symptoms in SLE to autoimmunity would result in unwarranted testing and overtreatment. In SLE and rheumatoid arthritis, the severity of pain and fatigue often do not correlate with traditional disease activity measures, and the presence of comorbid FM and nociplastic pain has been associated with failure to respond to immune therapy.[3]

FM and nociplastic pain are firmly established as a chronic illness, characterized by widespread pain, fatigue, and sleep disturbances that cannot be attributed to another disease. The ambiguity, uncertainty, and lack of prestige inherent in FM noted by the authors is no different than that of chronic headaches, low-back pain, and depression. Such symptoms may be aggravated by a comorbid disease, but their pathogenesis and treatment are independent of that disease. LAN fits the illness model of FM but not the autoimmune disease profile of SLE.

Author disclosures are available at https://onlinelibrary.wiley.com/doi/10.1002/art.43426.

Don L. Goldenberg, MD
dongoldenberg44@gmail.com
Tufts University School of Medicine
Boston, MA

1. Pisetsky DS, Rogers JL, Eudy AM, et al. Nociplasticity: a proposed concept to understand the symptomatology of systemic lupus erythematosus. Arthritis Rheumatol 2025;77(8):966–970.
2. Clauw DJ. From fibrositis to fibromyalgia to nociplastic pain: how rheumatology helped get us here and where do we go from here? Ann Rheum Dis 2024;83(11):1421–1427.
3. Chmielewski G, Majewski MS, Kuna J, et al. Fatigue in inflammatory joint diseases. Int J Mol Sci 2023;24(15):12040.

DOI 10.1002/art.70040

Reply

To the Editor:

We thank Dr Goldenberg for his thoughtful comments on our proposal for new terminology for symptoms of systemic lupus erythematosus (SLE).[1] Specifically, we suggested the term "lupus-associated nociplasticity" (LAN) to encompass pain and related symptoms (ie, fatigue, mood disturbance, cognitive dysfunction) that occur prominently in lupus. We suggested that new terminology could increase understanding of lupus symptomatology as well as facilitate both research and clinical care.

At present, three types of pain are now distinguished: nociceptive, neuropathic, and nociplastic.[2] Nociplastic pain, the newest addition to the classification, basically involves pain that cannot be readily categorized as nociceptive (tissue injury) or neuropathic (nerve abnormality). Although the mechanism of nociplastic pain is not known, disturbance in neural processing is likely and is usually denoted as central sensitization.[3] Peripheral sensitization may also occur.

For rheumatologists, fibromyalgia is the most frequent condition linked with sensitization.[4] As Dr Goldenberg correctly indicates, fibromyalgia can occur with a variety of diseases. In this framework, fibromyalgia is a diagnosis, nociplastic pain is a descriptor (or classifier), and central and/or peripheral sensitization is a presumed mechanism. We have proposed the term nociplasticity rather than nociplastic pain as the descriptor to account better for the abnormalities in sensory processing that extend beyond pain and expand symptomatology.

Two main reasons have prompted this proposal. First, the current construct for nociplastic pain includes symptoms other than pain (ie, fatigue). We think that nociplasticity provides a more apt description of the symptom complex. The second reason relates to communication with patients. Many patients consider pain as their "lupus."[5] Identifying this pain as LAN can promote better clinical care by validating symptoms of patients as lupus rather than another diagnosis (ie, fibromyalgia), which can be confusing, leading to discordance between patient and provider and fragmenting care.

Because of the frequency of nociplasticity in SLE, an important issue concerns the role of the immune system.[6] As provocative studies have now demonstrated, antibodies in the blood of patients with fibromyalgia can mediate pain behavior when transferred into mice.[7] These findings, along with the role of immune mediators in brain function (neuroinflammation), raise the possibility that immune disturbances drive nociplasticity.[8]

In contrast to Dr Goldenberg, we think that the use of the term LAN, rather than leading to unwarranted testing, will encourage more diverse and relevant testing (eg, pain maps, inventories for central sensitization) to anchor the determination of nociplasticity in routine care.[9,10] Because assessing disease activity in SLE is challenging, we think that recognition of nociplasticity as a cause of symptoms can potentially limit overtreatment with immunosuppressive agents, whose use may be prompted by patient reports of flare. It may also direct attention to managing symptoms such as depression and use of pharmacologic or nonpharmacologic therapies.

The future will likely see important advances in diagnosis and treatment of pain and other features of nociplasticity wherever they occur. We hope that rheumatologists will be leaders in this advance and look forward to further discussion to improve understanding and treatment of the most common and debilitating symptoms in our field.

Author disclosures are available at https://onlinelibrary.wiley.com/doi/10.1002/art.70040.

David S. Pisetsky, MD, PhD
David.pisetsky@duke.edu
Amanda M. Eudy, PhD
Jennifer L. Rogers, MD
Division of Rheumatology and Immunology, Duke University Medical Center
Durham, NC

Ru-Rong Ji, PhD
Katherine T. Martucci, PhD
Center for Translational Pain Medicine, Department of Anesthesiology, Duke University Medical Center
Durham, NC
Peter E. Lipsky, MD
AMPEL BioSolutions and RILITE Research Institute
Charlottesville, VA

1. Pisetsky DS, Rogers JL, Eudy AM, et al. Nociplasticity: a proposed concept to understand the symptomatology of systemic lupus erythematosus. Arthritis Rheumatol 2025;77(8):966–970.
2. Kosek E, Cohen M, Baron R, et al. Do we need a third mechanistic descriptor for chronic pain states? Pain 2016;157(7):1382–1386.
3. Woolf CJ. Central sensitization: implications for the diagnosis and treatment of pain. Pain 2011;152(3 suppl):S2–S15.
4. Fitzcharles MA, Cohen SP, Clauw DJ, et al. Nociplastic pain: towards an understanding of prevalent pain conditions. Lancet 2021;397(10289):2098–2110.
5. Rogers JL, Clowse MEB, McKenna K, et al. Patient and physician perspectives of systemic lupus erythematosus flare: a qualitative study. J Rheumatol 2024;51(5):488–494.
6. Pisetsky DS, Eudy AM, Rogers JL, et al. Pain in systemic lupus erythematosus: emerging insights and paradigms. Nat Rev Rheumatol 2025;21(10):626–639.
7. Goebel A, Krock E, Gentry C, et al. Passive transfer of fibromyalgia symptoms from patients to mice. J Clin Invest 2021;131(13):e144201.
8. Ji RR, Nackley A, Huh Y, et al. Neuroinflammation and central sensitization in chronic and widespread pain. Anesthesiology 2018;129(2):343–366.
9. Clauw DJ. Why don't we use a body map in every chronic pain patient yet? Pain 2024;165(8):1660–1661.
10. Mayer TG, Neblett R, Cohen H, et al. The development and psychometric validation of the central sensitization inventory. Pain Pract 2012;12(4):276–285.

DOI 10.1002/art.70055

Rituximab versus cyclophosphamide for IgA vasculitis

To the Editor:

Adult-onset IgA vasculitis (IgAV) carries a substantial risk of progressive glomerulonephritis and chronic renal dysfunction.[1] Although cyclophosphamide is frequently prescribed for severe adult IgAV based on evidence from other vasculitides, a small trial failed to demonstrate renal benefit.[1,2] Conversely, promising data on rituximab's efficacy for renal disease are limited to small uncontrolled case series, leaving comparative effects on definitive renal outcomes largely undefined.[3] This study addresses a critical evidence gap by comparing renal outcomes between these therapies, providing data to guide evidence-based treatment selection.

We conducted an emulated trial with patients across 76 health care organizations using electronic medical record data from a deidentified database, TriNetX, from 2017 to 2025. This

study was deemed exempt from approval by the Mass General Brigham Institutional Review Board. This study adhered to Strengthening the Reporting of Observational Studies in Epidemiology guidelines.

Using *International Statistical Classification of Diseases and Related Health Problems, Tenth Revision* (ICD-10) and RxNorm-based algorithms utilized in prior research, we identified a cohort of 1,190 adults diagnosed with IgAV and concurrent glomerular disease who also received a first prescription for rituximab or cyclophosphamide within one year of diagnosis.[4] To emulate an intention-to-treat analysis, patients were analyzed according to their initial treatment assignment. To emulate randomization, propensity score matching (1:1, using a nearest neighbor greedy matching algorithm) was applied to balance treatment groups on demographics, comorbidities, laboratory data, and medication use (Table 1, Supplementary Table S1).

Primary outcomes were five-year incidences of end-stage renal disease (ESRD), dialysis dependence, kidney transplantation, and chronic kidney disease (stage III–V), excluding patients with prior such diagnoses. Varicose vein and trauma (laceration) diagnoses served as negative controls. Outcomes and comorbidities were identified utilizing previously validated ICD-10 codes.[5,6] Hazard ratios (HRs) for all outcomes were estimated using Cox regression models on weighted samples.

After matching, 368 patients were analyzed in each group, with minimal differences in baseline characteristics between groups (standardized mean difference < 0.10) (Table 1). Among 368 matched pairs, those treated with rituximab had lower risks of ESRD (HR 0.65; 95% confidence interval [CI] 0.45–0.93), dialysis dependence (HR 0.66; 95% CI 0.45–0.97), kidney transplantation (HR 0.50; 95% CI 0.29–0.87), and stage III to V chronic kidney disease (HR 0.65; 95% CI 0.49–0.88) compared to those

Table 1. Baseline patient characteristics in patients with IgA vasculitis treated with rituximab versus cyclophosphamide*

Characteristic	Before PSM			After PSM		
	Rituximab cohort (n = 472)	Cyclophosphamide cohort (n = 758)	SMD	Rituximab cohort (n = 368)	Cyclophosphamide cohort (n = 368)	SMD
Age at index, mean (SD), y	50.9 (21.4)	47.8 (23.4)	0.137	50.2 (21.8)	49.6 (21.9)	0.025
Sex, n (%)						
Female	253 (53.7)	347 (50.1)	0.072	187 (50.8)	201 (54.6)	0.076
Male	199 (42.3)	331 (47.8)	0.112	168 (45.7)	156 (42.4)	0.066
Unknown sex	19 (4.0)	14 (2.0)	0.118	13 (3.5)	11 (3.0)	0.031
Race and ethnicity, n (%)						
American Indian or Alaska Native	10 (2.1)	10 (1.4)	0.051	10 (2.7)	10 (2.7)	<0.001
Asian	19 (4.0)	48 (6.9)	0.128	17 (4.6)	18 (4.9)	0.013
Black or African American	48 (10.2)	77 (11.1)	0.030	33 (9.0)	37 (10.1)	0.037
Native Hawaiian or other Pacific Islander	10 (2.1)	10 (1.4)	0.051	10 (2.7)	10 (2.7)	<0.001
Other race	18 (3.8)	34 (4.9)	0.053	18 (4.9)	13 (3.5)	0.068
Unknown race	66 (14.0)	74 (10.7)	0.101	48 (13.0)	47 (12.8)	0.008
White	312 (66.2)	451 (65.2)	0.023	245 (66.6)	247 (67.1)	0.012
Comorbidities, n (%)						
Hypertension	309 (65.6)	385 (55.6)	0.205	226 (61.4)	224 (60.9)	0.011
Hyperlipidemia	190 (40.3)	216 (31.2)	0.191	139 (37.8)	135 (36.7)	0.022
Diabetes mellitus	122 (25.9)	115 (16.6)	0.228	82 (22.3)	81 (22.0)	0.007
Chronic kidney disease	278 (59.0)	307 (44.4)	0.297	199 (54.1)	201 (54.6)	0.011
Sjögren disease	25 (5.3)	13 (1.9)	0.185	10 (2.7)	11 (3.0)	0.016
Rheumatoid arthritis	57 (12.1)	33 (4.8)	0.266	23 (6.3)	30 (8.2)	0.074
Systemic lupus erythematosus	62 (13.2)	97 (14.0)	0.025	45 (12.2)	59 (16.0)	0.109
Smoking status (nicotine dependence)	110 (23.4)	125 (18.1)	0.131	76 (20.7)	86 (23.4)	0.066
Chronic viral hepatitis B without delta agent	10 (2.1)	10 (1.4)	0.051	10 (2.7)	10 (2.7)	<0.001
Chronic viral hepatitis C	22 (4.7)	11 (1.6)	0.178	10 (2.7)	10 (2.7)	<0.001
HIV disease	10 (2.1)	10 (1.4)	0.051	10 (2.7)	0 (0.0)	0.236
Laboratory values						
GFR, mean ± SD, mL/min/1.73 m^2	55.3 ± 39.8	49.4 ± 35.0	0.159	50.8 ± 35.3	49.1 ± 33.2	0.083
GFR 60–90 mL/min/1.73 m^2, n (%)	139 (29.5)	225 (29.7)	0.005	109 (29.5)	109 (29.7)	0.005
GFR ≥90 mL/min/1.73 m^2, n (%)	95 (20.1)	158 (20.8)	0.017	74 (20.1)	77 (20.8)	0.017
Medications, n (%)						
Mycophenolate mofetil	101 (21.4)	75 (10.8)	0.291	63 (17.1)	60 (16.3)	0.022
Tacrolimus	52 (11.0)	17 (2.5)	0.347	20 (5.4)	17 (4.6)	0.037
Azathioprine	52 (11.0)	33 (4.8)	0.234	24 (6.5)	32 (8.7)	0.082

* GFR, glomerular filtration rate; PSM, propensity score matching; SMD, standardized mean difference.

Table 2. Associations of rituximab versus cyclophosphamide for risk of incident renal, cardiac, and thromboembolic complications and negative control outcomes in patients with IgA vasculitis*

Outcome	Rituximab cohort incident cases (n = 368)	Cyclophosphamide cohort incident cases (n = 368)	Hazard ratio (95% CI)	Log-rank *P* value
End-stage renal disease	49	72	0.65 (0.45–0.93)	0.019
Dialysis dependence	42	64	0.66 (0.45–0.97)	0.034
Kidney transplantation	18	36	0.50 (0.29–0.87)	0.014
Stage III–V chronic kidney disease	76	105	0.65 (0.49–0.88)	0.004
Cardiovascular events				
Myocardial infarction	13	22	0.71 (0.36–1.42)	0.33
Stroke	14	17	0.93 (0.46–1.89)	0.84
Thromboembolic events				
Venous thromboembolism	18	19	1.07 (0.47–2.48)	0.87
Pulmonary embolism	15	18	0.89 (0.45–1.77)	0.74
Negative controls				
Trauma (laceration of the head)	14	16	0.99 (0.41–2.35)	0.98
Varicose veins	11	11	1.00 (0.42–2.37)	0.99

* CI, confidence interval.

treated with cyclophosphamide (Table 2). There was no difference in risks of myocardial infarction (HR 0.71; 95% CI 0.36–1.42), stroke (HR 0.93; 95% CI 0.46–1.89), or venous thromboembolism (HR 1.07; 95% CI 0.47–2.48). There was no increased risk of negative control outcomes.

Among patients with IgAV, we found that rituximab compared to cyclophosphamide treatment was associated with a reduced risk of long-term renal complications. Study strengths include its large sample size given disease rarity, extensive covariate matching, and negative control analysis. Study limitations include confounding by indication (though controlling for laboratory data may reduce disease severity–related bias), inability to stratify risk between skin-limited and renal-involved disease, lack of medication dosing and exposure data, generalizability considerations given the large academic center representation, inability to evaluate combination therapy due to limited sample sizes, misclassification risk due to reliance on structured clinical data, and other potential unmeasured confounders. For instance, the lack of urinalysis or histopathologic data may bias estimates toward the null or overstate rituximab's benefit if cyclophosphamide is preferentially used in severe cases.

In the context of scarce high-quality evidence, these findings offer novel real-world evidence to inform therapeutic decision-making in adult patients with IgAV and renal involvement.

Data used in this study were obtained from the TriNetX Research Network, a federated health research network. Due to proprietary restrictions and institutional data sharing agreements, individual-level data cannot be shared publicly. Drs Sparks, LaChance, and Piette contributed equally and should be considered co-senior authors. Mr Mahajan's work was supported by the Rheumatology Research Foundation Future Physician Scientist Award. Dr Sparks' work was supported by the National Institute of Arthritis and Musculoskeletal and Skin Diseases (grants R01-AR-080659, R01-AR-077607, P30-AR-070253, and P30-AR-072577) and the National Heart, Lung, and Blood Institutes, NIH (grantR01-HL-155522); the R. Bruce and Joan M. Mickey Research Scholar Fund; and the Llura Gund Award funded by the Gordon and Llura Gund Foundation. All listed funders had no role in the preparation or decision to publish this article.

Author disclosures are available at https://onlinelibrary.wiley.com/doi/10.1002/art.70055.

Arjun Mahajan, MS
amahajan@hms.harvard.edu
Jeffrey A. Sparks, MD, MMSc
Harvard Medical School and Division of Rheumatology, Inflammation, and Immunity, Brigham & Women's Hospital
Boston, MA
Sharon A. Chung, MD, MAS
Division of Rheumatology, University of California, San Francisco
Jennifer E. Yeh, MD, PhD
Department of Dermatology, Stanford University, Palo Alto, CA
Avery H. LaChance, MD, MPH
Evan W. Piette, MD
Harvard Medical School and Department of Dermatology, Brigham & Women's Hospital
Boston, MA

1. Maritati F, Canzian A, Fenaroli P, et al. Adult-onset IgA vasculitis (Henoch-Schönlein): update on therapy. Presse Med 2020; 49(3):104035. doi:https://doi.org/10.1016/j.lpm.2020.104035

2. Pillebout E, Alberti C, Guillevin L, et al; CESAR study group. Addition of cyclophosphamide to steroids provides no benefit compared with steroids alone in treating adult patients with severe Henoch Schönlein

Purpura. Kidney Int 2010;78(5):495–502. doi:https://doi.org/10.1038/ki.2010.150

3. Xiong Y, Cuevas S, Xu G, et al. The efficacy of rituximab in the treatment of IgA vasculitis nephritis. Clin Exp Med 2024;24(1):213. doi:https://doi.org/10.1007/s10238-024-01461-6
4. Mahajan A, Barbieri JS, Sparks JA, et al. Cancer risk in IgA vasculitis patients. Rheumatology (Oxford) 2025;64(10):5567–5569. doi:https://doi.org/10.1093/rheumatology/keaf358
5. Kuang A, Xu C, Southern DA, et al. Validated administrative data based ICD-10 algorithms for chronic conditions: a systematic review. J Epidemiol Popul Health 2024;72(4):202744. doi:https://doi.org/10.1016/j.jeph.2024.202744
6. Grams ME, Plantinga LC, Hedgeman E, et al; CDC CKD Surveillance Team. Validation of CKD and related conditions in existing data sets: a systematic review. Am J Kidney Dis 2011;57(1):44–54. doi:https://doi.org/10.1053/j.ajkd.2010.05.013